

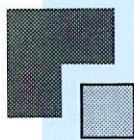
Prepared for:

Rijkswaterstaat - RIKZ

Sensitivity analysis of SWAN for the Amelande Zeegat

Report

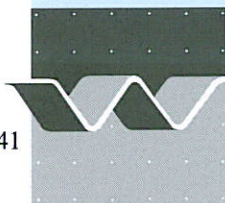
September 2007



Alkyon

Hydraulic Consultancy & Research

H4918.41



wL | delft hydraulics

Prepared for:

Rijkswaterstaat - RIKZ

Sensitivity analysis of SWAN for the Amelanders Zeegat

A. J. van der Westhuysen and G. Ph. van Vledder

Report

September 2007

Contents

List of Tables

List of Figures

List of Symbols

1	Introduction	1-1
2	Simulation conditions and variations.....	2-1
2.1	Choice of base cases.....	2-1
2.2	Sensitivity tests	2-2
2.2.1	Sensitivity to uncertainties in model input.....	2-2
2.2.2	Sensitivity to uncertainties in model physics	2-3
2.2.3	Naming convention and variables analysed.....	2-4
3	Model setup.....	3-1
3.1	Choice of computational grids	3-1
3.2	SWAN version and model settings.....	3-2
3.3	Wave boundary conditions	3-3
3.4	Bathymetry	3-4
3.5	Water level and current fields	3-6
3.5.1	General.....	3-6
3.5.2	WAQUA grids	3-7
3.5.3	Treatment of dry points.....	3-7
3.5.4	Interpolation	3-8
3.6	Wind fields	3-8
4	Simulation results	4-1
4.1	General	4-1
4.2	Base cases.....	4-1
4.2.1	NW storm with flood current	4-1
4.2.2	NW storm at high water.....	4-2
4.2.3	NW storm with ebb current.....	4-3
4.2.4	SW extreme storm	4-3
4.2.5	NW extreme storm.....	4-4
4.3	Sensitivity to wave boundary input.....	4-4
4.3.1	Severe NW storm conditions.....	4-4
4.3.2	Extreme NW storm conditions	4-5
4.4	Sensitivity to current and water level.....	4-5
4.4.1	Flood current	4-6
4.4.2	Ebb current.....	4-6

4.4.3	Increase in water level	4-7
4.5	Sensitivity to wind input.....	4-8
4.5.1	Uniform wind fields.....	4-8
4.5.2	Spatially non-uniform wind field	4-9
4.6	Sensitivity to model physics	4-9
4.6.1	Transfer of energy from wind to waves	4-9
4.6.2	Source terms in shallow water	4-10
4.7	Summary of model sensitivities.....	4-11
5	Conclusions	5-1
6	Recommendations.....	6-1
	References	
	Figures	

List of Tables

- 2.1 Wind, water level and offshore wave conditions for hindcasted storm instants.
- 2.2 Boundary conditions for the two academic storms.
- 2.3 Summary of sensitivity runs considered in this study.
- 2.4 Collection of output parameters analysed in the sensitivity study.

- 3.1 Numerical characteristics of the SWAN computational grids.
- 3.2 Data files with bottom information.

- 4.1 Overview of the changes in model outcomes $(\text{Value}_{\text{Variation}} - \text{Value}_{\text{Base}})/\text{Value}_{\text{Base}}$ per sensitivity test, given as average values along the indicated output ray.

List of Figures

- 3.1 Grid lines of curvi-linear grid GridCL.
- 3.2 Grid lines of curvi-linear grid AZG3A.
- 3.3 Grid lines of curvi-linear grid AK4A.
- 3.4 Effect of wind input limitation on fetch-limited growth curves. Results for $U_{10} = 10$ m/s.
- 3.5 Effect of wind input limitation on fetch-limited growth curves. Results for $U_{10} = 30$ m/s.
- 3.6 Origin of boundary conditions for AZG3A: AZB11 and AZB12 (blue), and NS2 (red).
- 3.7 Outline of bottom data files used for construction of bathymetry for tidal inlet of Ameland.
- 3.8 Outline of bottom data files used for construction of bathymetry for tidal inlet of Ameland, based on AZG2004 data.
- 3.9 Outline of bottom data files used for construction of bathymetry for tidal inlet of Ameland, based on kwelder data.
- 3.10 Bathymetry of computational grid AZG3A.
- 3.11 Bathymetry of computational grid AK4A.
- 3.12 Outline of WAQUA grids.
- 3.13 Spatial variation of current magnitude on AZG grid for 8 Feb. 2004, 20:00 hours.
- 3.14 Spatial variation of current magnitude on WAW grid for 8 Feb. 2004, 20:00 hours.
- 3.15 Spatial variation of current magnitude on WAW grid for 8 Feb. 2004, 20:00 hours and dry falling points.
- 3.16 Spatial variation of current magnitude on WAW grid for 8 Feb. 2004, 20:00 hours after correction of dry points.
- 3.17 Variation of water level and current speed and direction for Grid AZG3A and for event 20040208_2000.
- 3.18 Variation of water level and current speed and direction for Grid AZG3A and for event 20040208_2230.
- 3.19 Variation of water level and current speed and direction for Grid AZG3A and for event 20040209_0130.
- 3.20 HIRLAM wind fields
- 3.21 Downscaled wind fields
- 3.22 Comparison of wind speed variation from downscaling (blue line) and according to Taylor & Lee (red line) using a land roughness of 0.1 along a downwind ray from the island of Ameland (dashed white line)

- 4.1 Location of output curves used in the sensitivity analysis on grid AZG3A (above) and grid AK4A (below).
- 4.2a Simulation results for base case C1XXX. Significant wave height on grids AZG3A (above) and AK4A (below).

- 4.2b Simulation results for base case C1XXX. Mean wave period on grids AZG3A (above) and AK4A (below).
- 4.2c Simulation results for base case C1XXX. Ratio of H_{m0}/Depth on grids AZG3A (above) and AK4A (below).
- 4.2d Simulation results for base case C1XXX. Integral parameters along Curve B
- 4.3a Simulation results for base case C2XXX. Significant wave height on grids AZG3A (above) and AK4A (below).
- 4.3b Simulation results for base case C2XXX. Mean wave period on grids AZG3A (above) and AK4A (below).
- 4.3c Simulation results for base case C2XXX. Ratio of H_{m0}/Depth on grids AZG3A (above) and AK4A (below).
- 4.3d Simulation results for base case C2XXX. Integral parameters along Curve A.
- 4.4a Simulation results for base case C3XXX. Significant wave height on grids AZG3A (above) and AK4A (below).
- 4.4b Simulation results for base case C3XXX. Mean wave period on grids AZG3A (above) and AK4A (below).
- 4.4c Simulation results for base case C3XXX. Ratio of H_{m0}/Depth on grids AZG3A (above) and AK4A (below).
- 4.4d Simulation results for base case C3XXX. Integral parameters along Curve B.
- 4.5a Simulation results for base case C4XXX. Significant wave height (above) and mean wave period (below).
- 4.5b Simulation results for base case C4XXX. Ratio of H_{m0}/Depth .
- 4.5c Simulation results for base case C4XXX. Integral parameters along Curve C.
- 4.6a Simulation results for base case C5XXX. Significant wave height on grids AZG3A (above) and AK4A (below).
- 4.6b Simulation results for base case C5XXX. Mean wave period on grids AZG3A (above) and AK4A (below).
- 4.6c Simulation results for base case C5XXX. Ratio of H_{m0}/Depth on grids AZG3A (above) and AK4A (below).
- 4.6d Simulation results for base case C5XXX. Integral parameters along Curve A.
- 4.7a Sensitivity run C2BH1: Variation in wave height at the boundary. Differences in significant wave height (above) and mean period (below).
- 4.7b Sensitivity run C2BH1: Variation in wave height at the boundary. Differences in mean direction (above) and directional spreading (below).
- 4.7c Sensitivity run C2BH1: Variation in wave height at the boundary. Integral parameters along Curve D.
- 4.7d Sensitivity run C2BH2: Variation in wave height at the boundary. Integral parameters along Curve D.
- 4.8a Sensitivity run C2BT1: Variation in wave period at the boundary. Differences in significant wave height (above) and mean period (below).
- 4.8b Sensitivity run C2BT1: Variation in wave period at the boundary. Differences in mean direction (above) and directional spreading (below).
- 4.8c Sensitivity run C2BT1: Variation in wave period at the boundary. Integral parameters along Curve D.

- 4.8d Sensitivity run C2BT2: Variation in wave period at the boundary. Integral parameters along Curve D.
- 4.9a Sensitivity run C2BD1: Variation in wave direction at the boundary. Differences in significant wave height (above) and mean period (below).
- 4.9b Sensitivity run C2BD1: Variation in wave direction at the boundary. Differences in mean direction (above) and directional spreading (below).
- 4.9c Sensitivity run C2BD1: Variation in wave direction at the boundary. Integral parameters along Curve D.
- 4.9d Sensitivity run C2BD2: Variation in wave direction at the boundary. Integral parameters along Curve D.
- 4.10a Sensitivity run C2BS2: Variation in directional spreading at the boundary. Differences in significant wave height (above) and mean period (below).
- 4.10b Sensitivity run C2BS2: Variation in directional spreading at the boundary. Differences in mean direction (above) and directional spreading (below).
- 4.10c Sensitivity run C2BS2: Variation in directional spreading at the boundary. Integral parameters along Curve D.
- 4.10d Sensitivity run C2BS1: Variation in directional spreading at the boundary. Integral parameters along Curve D.
- 4.11a Sensitivity run C5BH1: Variation in wave height at the boundary. Differences in significant wave height (above) and mean period (below).
- 4.11b Sensitivity run C5BH1: Variation in wave height at the boundary. Differences in mean direction (above) and directional spreading (below).
- 4.11c Sensitivity run C5BH1: Variation in wave height at the boundary. Integral parameters along Curve D.
- 4.11d Sensitivity run C5BH2: Variation in wave height at the boundary. Integral parameters along Curve D.
- 4.12a Sensitivity run C5BT1: Variation in wave period at the boundary. Differences in significant wave height (above) and mean period (below).
- 4.12b Sensitivity run C5BT1: Variation in wave period at the boundary. Differences in mean direction (above) and directional spreading (below).
- 4.12c Sensitivity run C5BT1: Variation in wave period at the boundary. Integral parameters along Curve D.
- 4.12d Sensitivity run C5BT2: Variation in wave period at the boundary. Integral parameters along Curve D.
- 4.13a Sensitivity run C5BD1: Variation in wave direction at the boundary. Differences in significant wave height (above) and mean period (below).
- 4.13b Sensitivity run C5BD1: Variation in wave direction at the boundary. Differences in mean direction (above) and directional spreading (below).
- 4.13c Sensitivity run C5BD1: Variation in wave direction at the boundary. Integral parameters along Curve D.
- 4.13d Sensitivity run C5BD2: Variation in wave direction at the boundary. Integral parameters along Curve D.
- 4.14a Sensitivity run C5BS2: Variation in directional spreading at the boundary. Differences in significant wave height (above) and mean period (below).

- 4.14b Sensitivity run C5BS2: Variation in directional spreading at the boundary. Differences in mean direction (above) and directional spreading (below).
- 4.14c Sensitivity run C5BS2: Variation in directional spreading at the boundary. Integral parameters along Curve D.
- 4.14d Sensitivity run C5BS1: Variation in directional spreading at the boundary. Integral parameters along Curve D.
- 4.15a Sensitivity run C1FC1: Deactivation of flood current. Differences in significant wave height (above) and mean period (below).
- 4.15b Sensitivity run C1FC1: Deactivation of flood current. Differences in mean direction (above) and directional spreading (below).
- 4.15c Sensitivity run C1FC1: Deactivation of flood current. Integral parameters along Curve D.
- 4.15d Sensitivity run C1FC1: Deactivation of flood current. Frequency spectra at various locations along Curve D.
- 4.15e Sensitivity run C1FC1: Deactivation of flood current. Integral parameters along Curve B.
- 4.16a Sensitivity run C3FC2: Deactivation of ebb current. Differences in significant wave height (above) and mean period (below).
- 4.16b Sensitivity run C3FC2: Deactivation of ebb current. Differences in mean direction (above) and directional spreading (below).
- 4.16c Sensitivity run C3FC2: Deactivation of ebb current. Integral parameters along Curve D.
- 4.16d Sensitivity run C3FC2: Deactivation of ebb current. Frequency spectra at various locations along Curve D.
- 4.16e Sensitivity run C3FC2: Deactivation of ebb current. Integral parameters along Curve B.
- 4.17a Sensitivity run C5FL1: Increase in water level. Differences in significant wave height (above) and mean period (below).
- 4.17b Sensitivity run C5FL1: Increase in water level. Differences in mean direction (above) and directional spreading (below).
- 4.17c Sensitivity run C5FL1: Increase in water level. Integral parameters along Curve D.
- 4.17d Sensitivity run C5FL1: Increase in water level. Frequency spectra at various locations along Curve D.
- 4.17e Sensitivity run C5FL1: Increase in water level. Integral parameters along Curve A.
- 4.18a Sensitivity run C2WS1: Variation in spatially uniform wind speed. Differences in significant wave height (above) and mean period (below).
- 4.18b Sensitivity run C2WS1: Variation in spatially uniform wind speed. Differences in mean direction (above) and directional spreading (below).
- 4.18c Sensitivity run C2WS1: Variation in spatially uniform wind speed. Integral parameters along Curve E.
- 4.18d Sensitivity run C2WS1: Variation in spatially uniform wind speed. Integral parameters along Curve F.

- 4.18e Sensitivity run C2WS1: Variation in spatially uniform wind speed. Integral parameters along Curve A.
- 4.19a Sensitivity run C2WS2: Variation in spatially uniform wind speed. Differences in significant wave height (above) and mean period (below).
- 4.19b Sensitivity run C2WS2: Variation in spatially uniform wind speed. Differences in mean direction (above) and directional spreading (below).
- 4.19c Sensitivity run C2WS2: Variation in spatially uniform wind speed. Integral parameters along Curve E.
- 4.19d Sensitivity run C2WS2: Variation in spatially uniform wind speed. Integral parameters along Curve F.
- 4.19e Sensitivity run C2WS2: Variation in spatially uniform wind speed. Integral parameters along Curve A.
- 4.20a Sensitivity run C2WD1: Variation in spatially uniform wind direction. Differences in significant wave height (above) and mean period (below).
- 4.20b Sensitivity run C2WD1: Variation in spatially uniform wind direction. Differences in mean direction (above) and directional spreading (below).
- 4.20c Sensitivity run C2WD1: Variation in spatially uniform wind direction. Integral parameters along Curve E.
- 4.20d Sensitivity run C2WD1: Variation in spatially uniform wind direction. Integral parameters along Curve F.
- 4.20e Sensitivity run C2WD1: Variation in spatially uniform wind direction. Integral parameters along Curve A.
- 4.21a Sensitivity run C2WD2: Variation in spatially uniform wind direction. Differences in significant wave height (above) and mean period (below).
- 4.21b Sensitivity run C2WD2: Variation in spatially uniform wind direction. Differences in mean direction (above) and directional spreading (below).
- 4.21c Sensitivity run C2WD2: Variation in spatially uniform wind direction. Integral parameters along Curve E.
- 4.21d Sensitivity run C2WD2: Variation in spatially uniform wind direction. Integral parameters along Curve F.
- 4.21e Sensitivity run C2WD2: Variation in spatially uniform wind direction. Integral parameters along Curve A.
- 4.22a Sensitivity run C2WH1: Simulation with downscaled HIRLAM wind field. Differences in significant wave height (above) and mean period (below).
- 4.22b Sensitivity run C2WH1: Simulation with downscaled HIRLAM wind field. Differences in mean direction (above) and directional spreading (below).
- 4.22c Sensitivity run C2WH1: Simulation with downscaled HIRLAM wind field. Integral parameters along Curve E.
- 4.2d Sensitivity run C2WH1: Simulation with downscaled HIRLAM wind field. Integral parameters along Curve F.
- 4.22e Sensitivity run C2WH1: Simulation with downscaled HIRLAM wind field. Integral parameters along Curve A.
- 4.23a Sensitivity run C2PW1: Limiting the magnitude of wind energy transfer. Differences in significant wave height (above) and mean period (below).

- 4.23b Sensitivity run C2PW1: Limiting the magnitude of wind energy transfer. Differences in mean direction (above) and directional spreading (below).
- 4.23c Sensitivity run C2PW1: Limiting the magnitude of wind energy transfer. Integral parameters along Curve E.
- 4.23d Sensitivity run C2PW1: Limiting the magnitude of wind energy transfer. Integral parameters along Curve F.
- 4.23e Sensitivity run C2PW1: Limiting the magnitude of wind energy transfer. Integral parameters along Curve A.
- 4.24a Sensitivity run C2PW2: Limiting the magnitude of wind energy transfer. Differences in significant wave height (above) and mean period (below).
- 4.24b Sensitivity run C2PW2: Limiting the magnitude of wind energy transfer. Differences in mean direction (above) and directional spreading (below).
- 4.24c Sensitivity run C2PW2: Limiting the magnitude of wind energy transfer. Integral parameters along Curve E.
- 4.24d Sensitivity run C2PW2: Limiting the magnitude of wind energy transfer. Integral parameters along Curve F.
- 4.24e Sensitivity run C2PW2: Limiting the magnitude of wind energy transfer. Integral parameters along Curve A.
- 4.25a Sensitivity run C2PS5: Reduction in strength of bottom friction. Differences in significant wave height (above) and mean period (below).
- 4.25b Sensitivity run C2PS5: Reduction in strength of bottom friction. Differences in mean direction (above) and directional spreading (below).
- 4.25c Sensitivity run C2PS5: Reduction in strength of bottom friction. Integral parameters along Curve E.
- 4.25d Sensitivity run C2PS5: Reduction in strength of bottom friction. Integral parameters along Curve F.
- 4.25e Sensitivity run C2PS5: Reduction in strength of bottom friction. Integral parameters along Curve A.
- 4.26a Sensitivity run C2PS6: Reduction in strength of depth-induced breaking. Differences in significant wave height (above) and mean period (below).
- 4.26b Sensitivity run C2PS6: Reduction in strength of depth-induced breaking. Differences in mean direction (above) and directional spreading (below).
- 4.26c Sensitivity run C2PS6: Reduction in strength of depth-induced breaking. Integral parameters along Curve E.
- 4.26d Sensitivity run C2PS6: Reduction in strength of depth-induced breaking. Integral parameters along Curve F.
- 4.26e Sensitivity run C2PS6: Reduction in strength of depth-induced breaking. Integral parameters along Curve A.
- 4.27a Sensitivity run C2PS7: Reduction in strength of triad interaction. Differences in significant wave height (above) and mean period (below).
- 4.27b Sensitivity run C2PS7: Reduction in strength of triad interaction. Differences in mean direction (above) and directional spreading (below).
- 4.27c Sensitivity run C2PS7: Reduction in strength of triad interaction. Integral parameters along Curve E.

- 4.27d Sensitivity run C2PS7: Reduction in strength of triad interaction. Integral parameters along Curve F.
- 4.27e Sensitivity run C2PS7: Reduction in strength of triad interaction. Integral parameters along Curve A.
- 4.28a Sensitivity run C4PS5: Reduction in strength of bottom friction. Differences in significant wave height (above) and mean period (below).
- 4.28b Sensitivity run C4PS5: Reduction in strength of bottom friction. Differences in mean direction (above) and directional spreading (below).
- 4.28c Sensitivity run C4PS5: Reduction in strength of bottom friction. Integral parameters along Curve C.
- 4.29a Sensitivity run C4PS6: Reduction in strength of depth-induced breaking. Differences in significant wave height (above) and mean period (below).
- 4.29b Sensitivity run C4PS6: Reduction in strength of depth-induced breaking. Differences in mean direction (above) and directional spreading (below).
- 4.29c Sensitivity run C4PS6: Reduction in strength of depth-induced breaking. Integral parameters along Curve C.
- 4.30a Sensitivity run C4PS7: Reduction in strength of triad interaction. Differences in significant wave height (above) and mean period (below).
- 4.30b Sensitivity run C4PS7: Reduction in strength of triad interaction. Differences in mean direction (above) and directional spreading (below).
- 4.30c Sensitivity run C4PS7: Reduction in strength of triad interaction. Integral parameters along Curve C.
- 4.31a Sensitivity run C5PS5: Reduction in strength of bottom friction. Differences in significant wave height (above) and mean period (below).
- 4.31b Sensitivity run C5PS5: Reduction in strength of bottom friction. Differences in mean direction (above) and directional spreading (below).
- 4.31c Sensitivity run C5PS5: Reduction in strength of bottom friction. Integral parameters along Curve E.
- 4.31d Sensitivity run C5PS5: Reduction in strength of bottom friction. Integral parameters along Curve F.
- 4.31e Sensitivity run C5PS5: Reduction in strength of bottom friction. Integral parameters along Curve A.
- 4.32a Sensitivity run C5PS6: Reduction in strength of depth-induced breaking. Differences in significant wave height (above) and mean period (below).
- 4.32b Sensitivity run C5PS6: Reduction in strength of depth-induced breaking. Differences in mean direction (above) and directional spreading (below).
- 4.32c Sensitivity run C5PS6: Reduction in strength of depth-induced breaking. Integral parameters along Curve E.
- 4.32d Sensitivity run C5PS6: Reduction in strength of depth-induced breaking. Integral parameters along Curve F.
- 4.32e Sensitivity run C5PS6: Reduction in strength of depth-induced breaking. Integral parameters along Curve A.
- 4.33a Sensitivity run C5PS7: Reduction in strength of triad interaction. Differences in significant wave height (above) and mean period (below).

- 4.33b Sensitivity run C5PS7: Reduction in strength of triad interaction. Differences in mean direction (above) and directional spreading (below).
- 4.33c Sensitivity run C5PS7: Reduction in strength of triad interaction. Integral parameters along Curve E.
- 4.33d Sensitivity run C5PS7: Reduction in strength of triad interaction. Integral parameters along Curve F.
- 4.33e Sensitivity run C5PS7: Reduction in strength of triad interaction. Integral parameters along Curve A.

List of Symbols

Symbol	Units	Description
α_{BJ}	-	Proportionality coefficient for surf breaking (APLHA in SWAN)
α_{EB}	-	Proportionality coefficient for triad interaction (TRFAC in SWAN)
C_{JON}	m^2s^{-3}	Proportionality coefficient for bottom friction (CFJON in SWAN)
c	m/s	Wave phase velocity
Dir	$^{\circ}TN$	Mean wave direction
Dspr	$^{\circ}$	Directional spreading
f	Hz	Wave frequency
γ_{BJ}	-	Breaker parameter for surf breaking (GAMMA in SWAN)
H_{m0}	m	Significant wave height
NAP	m	Dutch national levelling datum
$T_{m-1,0}$	s	Mean absolute wave period
T_p	s	Peak absolute wave period
U_{10}	m/s	Wind speed at a height of 10 m
u_*	m/s	Friction velocity of the wind

I Introduction

The spectral wind wave model SWAN (Booij et al. 1999) plays a key role in the estimation of the Hydraulic Boundary Conditions (HBC) for the primary sea defences of The Netherlands. Since some uncertainty remains with respect to the reliability of SWAN for application to the geographically complex area of the Wadden Sea, a number of activities have been initiated under project H4918 'Uitvoering Plan van Aanpak SBW-RVW Waddenzee' (Plan of Action on the Boundary Conditions for the Wadden Sea) to devise a strategy for the improvement of the model. This activity is carried out in parallel with a measurement campaign that is being undertaken in the Wadden Sea to assist in the establishment of the boundary conditions ('SBW-Veldmetingen').

In this context, hindcast studies have recently been carried out with SWAN for the Wadden Sea (WL 2006b, Royal Haskoning 2006 and WL 2007b), in which model results were compared with buoy observations taken in the vicinity of the Amelande Zeegat tidal inlet. The objective of these studies was to determine the predictive skill of SWAN for a number of severe storm conditions, including a range of wind and wave directions, high water levels and strong tidal currents through the Amelande Zeegat tidal inlet. These hindcasts indicated that, at the buoy locations positioned around the tidal inlet, the largest discrepancies between model results and observations are found at short fetches at the lee of the barrier islands, and in the main tidal channel ('Borndiep') where strong wave-current interaction occurs. Since no observations or simulations were made to date in the region of the primary sea defences along the mainland coastline (at Friesland and Groningen), it is at present uncertain how these inaccuracies would affect the quality of model results there.

Sensitivity analysis is a means by which insight can be obtained into the relative importance of the various physical process and model inputs to model outcomes obtained in the Wadden Sea region. In such a sensitivity analysis, which precedes an uncertainty analysis, a first selection between important and less important uncertainty sources can be obtained (Van Vuren 2005). Insight into the model sensitivity is achieved by systematically and deterministically varying the model input values one by one and estimating their impact on the model results. The probability of occurrence of a particular model input value is not taken into account at point. Nonetheless, it benefits the realism of the sensitivity analysis to choose variations in input parameters within a reasonable range of expectation. A sensitivity analysis stands in contrast to an uncertainty analysis, which typically follows the former. In an uncertainty analysis, the input values for a selection of model parameters are determined by varying each variable over its uncertainty band, to obtain an indication of the uncertainty in model outcomes.

Three recent sensitivity studies have been carried out for the Wadden Sea region, in WL/Alkyon (2004), Alkyon (2007a) and Alkyon (2007b) respectively. WL/Alkyon (2004) carried out a sensitivity analysis of the influence of the various source terms in SWAN on the predicted wave conditions at the primary mainland sea defences for the greater Wadden Sea region. It was found that the processes of wind input and bottom friction have the largest influence on wave conditions at the sea defences. In addition, the importance of accurate bathymetrical information and wave refraction were also established. However, the finding that wind input and bottom friction are the most important physical processes may have been biased, since a relatively coarse computational grid (cell size of 100 m x 100 m,

see Alkyon 1999) was used in these simulations. Such a coarse grid does not adequately resolve the surf zone at the mainland, where shallow water processes such as surf breaking and triad interaction are typically dominant.

Alkyon (2007a,b) performed sensitivity analyses of the influence of model settings and input fields on model results in the region of the Amelander Zeegat tidal inlet. A significant finding of this study is that conditions in the tidal inlet are insensitive to small variations in the imposed boundary conditions. In this regard, the outer delta of the tidal inlet works as a filter that blocks most of the waves coming from the North Sea. The degree to which wave energy is shielded off is determined for a large part by the water depth (bathymetry and water level). By contrast, the wave conditions in the tidal inlet prove to be sensitive to variations in wind speed and direction, and also to be strongly affected by local currents. Concerning physical processes, the region on the North Sea side of the ebb tidal delta is affected the most by variations in the strength of depth-induced breaking and triad interactions, whereas the deeper regions in the tidal inlet are rather insensitive to these variations. These results suggest that - at least under the investigated storm conditions - the wave field in the inner Wadden Sea comprises of locally-generated waves and is largely unaffected by wave conditions in the North Sea. These results give important insights into the relative importance of the various wave processes in the Amelander Zeegat tidal inlet. However, for the purpose of the HBC, it remains to be determined how these sensitivities affect the conditions along the mainland coast. Furthermore, it is of interest how these sensitivities would be affected by extreme storm conditions in the Wadden Sea.

The aim of the present study is to extend the scope of the sensitivity analyses discussed above, to determine the effect of a number of variations in model physics and model input on the wave conditions at the primary sea defences on the mainland coast behind the Amelander Zeegat. In this regard, a selection of both observed severe storms as well as hypothetical extreme events are analysed, and the surf zone at the mainland is resolved with a fine computational grid spacing (order of 40 m). The investigated variations to the reference cases include: sensitivity to offshore wave boundary conditions; the effect of currents, sensitivity to wind speed, wind direction and spatial variations in the wind field, the effect of water level on low-frequency waves and sensitivities to source terms dominant in shallow water. In addition to these tests, it was also envisaged to investigate the influence of surf beat along the mainland coast using the Delft3D model, as a small part of the project scope. However, the results of the surf beat module proved insufficiently reliable to be included in the present analysis. We note that the influence of nonstationary calculation with SWAN, including the use of nonstationary wind and current fields, was not considered in the present study. This aspect of sensitivity is considered in a forthcoming study within the greater 'SBW-RVW Waddenzee' project (see WL 2006a).

The following methodology is followed in this study. Firstly, a selection is made of observed severe NW storms in the Amelander Zeegat from recent hindcasts, which is supplemented by two hypothetical extreme storms with return periods of 1/4000 year, from both NW and SW. To these observed and hypothetical conditions, referred to as the base (reference) cases, a series of variations are made. These are grouped into the categories of model input (including the offshore boundary input to SWAN, wind fields and current fields) and of model physics, which included the source terms of wind input, and the shallow water processes of bottom friction, triad interaction and depth-induced breaking. Variations (mostly small) were made to the magnitude, direction or strength of these model inputs and

processes, and the resulting model outcomes were compared with those of the base cases. These comparisons were made in terms of spatial plots (difference maps) and along rays defined along the mainland coastline and along paths of wave field development. Due to the nature of the input variations tested (e.g. the exclusion of current fields and the use of spatially non-uniform wind fields), it was not attempted to produce normalised variables of sensitivity. We note that the sensitivity analysis performed here is to be followed by an uncertainty analysis, in which the probability of occurrence of the studied variations are taken into account (see WL 2007a).

This sensitivity analysis was carried out by André van der Westhuisen, based on model simulations performed by Gerbrant van Vledder (Alkyon). The internal quality assurance and review was carried out by Jacco Groeneweg, and the external review was done by Leo Holthuijsen (Delft University of Technology).

This report is structured as follows. Section 2 presents the conditions on which the sensitivity analysis is based as well as the variations in model input and settings that were investigated. In Section 3 the model setup used in this study is described. In Section 4 the results of the sensitivity runs are presented and analysed. Sections 5 and 6 close the report with conclusions and recommendations.

2 Simulation conditions and variations

In this section a description is given of the basic simulation conditions and sensitivity tests that were considered in this study. Section 2.1 presents the selection of the basic conditions (base cases) that were used in this sensitivity analysis. In Section 2.2, a summary is given of the variations to these base cases that were included in the sensitivity analysis.

2.1 Choice of base cases

In order to determine the effect of model input and model physics of wave condition along the mainland coast of the Wadden Sea, a number of characteristic field situations (base cases) were selected on which sensitivities are tested. In the selection of these base cases, attention was given to both recently observed severe storms, and to hypothetical extreme storms. The former group is included since the environmental input conditions are relatively well known, which increases the realism of the analysis. However, the extension of the study to less well-defined extreme conditions is important, since it is for these conditions that the HBC have to be determined.

For the category of severe storms, the observed storm of 8-9 February 2004 was selected. Based on a statistical analysis of WL (2004), this event has a return period of about 1 year. Three instants during this storm were included in the analysis, namely at flood, slack tide and ebb during the same tidal cycle. These three storm instants are identified with the run codes C1XXX, C2XXX and C3XXX, respectively (see naming convention below). Table 2.1 summarises the conditions during these storm instants in terms of wind velocity at the offshore buoy location AZB11 (from KNMI wind model based on a downscaling technique, see Section 3.6), water level at NES and offshore wave conditions at AZB11.

Run code	Date, time (MET)	Wind dir (°N)	U_{10} (m/s)	Water level (m +NAP)	H_{m0} (m)	$T_{m-1,0}$ (s)	Wave dir (°N)
C1XXX	08/02/2004, 20h00	314	13.5	1.00	4.1	7.4	300
C2XXX	08/02/2004, 22h30	325	16.6	2.60	5.3	9.5	319
C3XXX	09/02/2004, 01h30	328	16.3	1.75	4.8	9.7	338

Table 2.1 Wind, water level and offshore wave conditions for hindcasted storm instants

For the extreme conditions, two hypothetical 4000 year storms were hindcasted, one from the southwest (225° N) and one from the northwest (315° N). These two base cases are identified by the run codes C4XXX and C5XXX respectively. The wind speed U_{10} , wave boundary conditions H_{m0} and T_p , and water level were obtained from the tables provided in Alkyon (1999) and SDU (2006). These conditions are summarised in Table 2.2:

Run code	Wind direction (°N)	U_{10} (m/s)	Water level (m +NAP)	H_{m0} (m)	T_p (s)
C4XXX	225	34.0	4.70	5.8	12.4
C5XXX	315	34.0	4.70	9.4	18.0

Table 2.2 Boundary conditions for the two academic storms

2.2 Sensitivity tests

Having selected the basic conditions on which to perform the analysis, the sensitivity of model output to two classes of variation were investigated, namely variation in model input and variability in the magnitude of source terms (or changes in their formulation). In general, the variations made to these model inputs and settings were small (typically 10%), in order to evoke an approximately linear response from the model. The aspects investigated in each of the two classes of uncertainties are presented in the sections below.

2.2.1 Sensitivity to uncertainties in model input

Offshore boundary conditions of waves

In the studies of Alkyon (2007a,b) it was found that conditions in the tidal inlet are insensitive to small variations in the imposed boundary conditions, since the ebb tidal delta blocks most of the waves coming from the North Sea. However, the degree to which wave energy is shielded off was found to depend for a large part by the water depth (bathymetry and water level). In particular, low frequency energy may enter the inner Wadden Sea region at high water levels. In the present study, this investigation is extended to include, besides an observed severe storm (C2XXX), an hypothetical extreme NW condition, with a higher water level. For these two storm conditions, the sensitivity at the mainland coast to the following variations to the wave boundary conditions are investigated:

- a) A variation in the significant wave height of + and - 10%
- b) A variation in the wave period of + and - 10%
- c) A variation in the mean wave direction of + and - 10°
- d) A variation in the directional spreading of + and - 10°

Current fields and water level

In the studies of Alkyon (2007a,b) and WL (2007b) it has been shown that the inclusion of current fields significantly influences the results of SWAN in the tidal inlet, and even inside the Wadden Sea itself. In the present study, the effect of including currents of the wave conditions at the mainland coast is investigated, by doing sensitivity studies with the current fields deactivated. This is done for the flood and ebb storm instants recorded during the 8-9 February 2004 storm (C1XXX, C3XXX).

As pointed out above, earlier hindcast studies have found that low-frequency wind waves from the North Sea dissipate a significant amount of energy on the ebb tidal delta and on the shoals in the tidal inlet. No storms have been measured yet in which the North Sea waves

have penetrated much beyond the tidal inlet, presumably because the water level has not been high enough yet. To investigate the sensitivity of conditions at the mainland coast to this uncertainty, a sensitivity test is conducted in which the water level of the NW extreme storm is increased by 1 m to +5.7 m NAP.

Wind input

In the hindcast studies of WL (2006b), Royal Haskoning (2006) and WL (2007b), it was found that over short dimensionless fetches, simulated wave heights and period measures are higher than observed values. These inaccuracies may affect simulated conditions at the mainland coast. One possible source of this error is that the wind input to the model is inaccurate. This can be due to an incorrect wind measurement or the omission of sheltering effects of the islands on the wind field. Therefore, the sensitivity of the simulated conditions along the Frisian to the following variations in the wind field was investigated:

- a) A variation in the wind speed of + and - 10%,
- b) A variation in the wind direction of + and - 10°,
- c) The use of a spatially varying wind field, based on a downscaled HIRLAM field

Downscaling of HIRLAM wind fields is a means to include the effect spatial variations in surface roughness on the wind field. This technique was developed by Verkaik et al. (2006).

2.2.2 Sensitivity to uncertainties in model physics

Transfer of energy from wind to waves

A comparison between simulated and observed wave heights and periods at short fetches seems to point to an overestimation of the transfer of energy from the wind to the waves in the model for highly-forced, young wind sea. This has also been reported by Donelan et al. (2007) in experiments at Lake George, Australia, and by Graber (WISE Workshop 2006) and Jensen (WISE Workshop 2007) in simulations of Hurricane Katrina. These authors propose a limitation of the transfer of energy from the wind to the waves under such highly forced conditions. To investigate the effect of such a limitation of the energy transfer on the wave conditions at the Frisian coast, for a NW storm condition the wind input term is capped above a certain level of wind forcing (given by u_*^2/c). Two levels of wind input limitation is investigated. This is described in more detail in Section 3.2.

Source terms in the surf zone

In WL/Alkyon (2004) it was concluded that bottom friction has a relatively dominant effect on simulated conditions at the mainland coast. As discussed in the introduction, this conclusion is based on simulations with a rather coarse computational grid (cross-shore cell size of 100 m), so that the effect of depth-induced breaking could have been over- or underestimated. Therefore, the sensitivity of model results along the mainland coastline to the processes of bottom friction, triad interaction and depth-induced breaking were investigated in the present study on a grid that is significantly finer (cell size of 40 m) than that used in WL/Alkyon (2004).

Following WL/Alkyon (2004), the respective strengths of the three surf zone source terms were reduced in turn, based on the following: The setting used for bottom friction in the reference case is $C_{JON} = CFJON = 0.067 \text{ m}^2\text{s}^{-3}$ (default value for wind sea). The range of uncertainty is considered to extend to $C_{JON} = 0.038 \text{ m}^2\text{s}^{-3}$ (default value for swell), which amounts to a 50% reduction in the strength of bottom friction dissipation. Similarly, the setting used for triad interaction is $\alpha_{EB} = TRFAC = 0.1$, which is the default value in SWAN 40.51, but which has been reduced to $\alpha_{EB} = 0.05$ in SWAN 40.51A. This 50% reduction in the magnitude of triad interaction is again considered to be a reasonable range of uncertainty. Concerning depth-induced breaking, Battjes and Stive (1985) show that the breaker parameter γ_{BJ} (GAMMA in SWAN) can vary between 0.6 and 0.85, depending on the wave steepness. Dingemans (1997) shows that, for a constant bulk dissipation in shallow water, a dependence exists between the breaker parameter and the proportionality coefficient α_{BJ} (ALPHA in SWAN):

$$\alpha_{BJ} \gamma_{BJ}^{-5} = \text{constant} . \quad (2.1)$$

Expression (2.1) implies that the parameter variation $(\alpha_{BJ}, \gamma_{BJ}) = (1, 0.6-0.85)$ is equivalent to the variation $(\alpha_{BJ}, \gamma_{BJ}) = (0.38-2.1, 0.73)$ in which γ_{BJ} is held constant. This indicates that if the default $\gamma_{BJ} = 0.73$ is used, the proportionality coefficient α_{BJ} can vary by more than + and - 50% of its default value, indicating the uncertainty range. We therefore reduce α_{BJ} by 50%, similar to the proportionality coefficients for bottom friction and triad interaction¹.

2.2.3 Naming convention and variables analysed

The various sensitivity tests conducted in this study were organised using a system of run codes comprising five characters. The first two characters denote the basic condition to which the variation is applied, so that 'C1' represents a run based on Condition 1 (storm instant 08/02/2004 at 20h00, see Table 2.1). The base cases presented in Section 2.1 are therefore identified as C1XXX, C2XXX, and so on. The third character denotes the group name of the variation that is being considered. With reference to the sections above, the groups include (B)oundary conditions of waves, (F)low fields and water level, (W)ind input and the (P)hysical formulations, including the formulation of wind input and the surf zone source terms. The fourth and fifth characters identify the specific item that is varied in the simulation (see Table 2.3 below). The character 'X' is used to denote an unspecified variable (a wildcard), by which groups of conditions can be referred to compactly. For example, all conditions with which the sensitivity for the offshore boundary conditions are investigated are referred to as the set CXBXX, or briefly as CXB. Using this system of identification, the sensitivity runs defined above are summarised in Table 2.3.

The tests series presented in Table 2.3 was evaluated in terms of the influence on the wave parameter output of SWAN, and in some cases on the output wave spectra. The collection of output parameters that were analysed are presented in Table 2.4. We note that the spectral mean period $T_{m-1,0}$ was used in the analysis, which is less sensitive to changes at higher spectral frequencies than, say, T_{m01} , since the former is more regularly used in dyke design.

1. In the proposal phase of this project, it was intended to study a reduction of 10% in all the proportionality coefficients, which, as indicated, is much less than the actual uncertainty in the source term strengths.

Category	Condition Code	Group Code	Item Code	Description	Run Code
Offshore waves	C2	(B)oundary	(H)m0	Wave height +10%	C2BH1
			(T)	Wave height -10%	C2BH2
			(D)irection	Wave period +10%	C2BT1
				Wave period -10%	C2BT2
			(S)preading	Mean direction +10°	C2BD1
				Mean direction -10°	C2BD2
			C5	(B)oundary	(H)m0
	(T)	Directional spreading -10°			C2BS2
	(D)irection	Wave height +10%			C5BH1
		Wave height -10%			C5BH2
	(S)preading	Wave period +10%			C5BT1
		Wave period -10%			C5BT2
	(S)preading	Mean direction +10°			C5BD1
		Mean direction -10°	C5BD2		
Flow fields and water level	C1,C2,C3	(F)low	(C)urrent	Flood case, current off	C1FC1
			(L)evel	Ebb case, current off	C3FC2
				Uniform water level +1m	C5FL1
Wind input	C2	(W)ind	(S)peed	Wind speed +10%	C2WS1
			(D)irection	Wind speed -10%	C2WS2
			(H)IRLAM	Wind direction +10%	C2WD1
Physics	C2	(P)hysics	(W)ind	Wind direction -10%	C2WD2
				HIRLAM downscaled	C2WH1
	C2	(P)hysics	(S)urf zone	Wind input function, cut-off 1	C2PW1
				Wind input function, cut-off 2	C2PW2
	C4	(P)hysics	(S)urf zone	Bottom friction -50%	C2PS5
				Depth breaking -50%	C2PS6
				Triad interaction -50%	C2PS7
	C5	(P)hysics	(S)urf zone	Bottom friction -50%	C4PS5
				Depth breaking -50%	C4PS6
				Triad interaction -50%	C4PS7
	C5	(P)hysics	(S)urf zone	Bottom friction -50%	C5PS5
Depth breaking -50%				C5PS6	
Triad interaction -50%				C5PS7	

Table 2.3 Summary of sensitivity runs considered in this study.

Description	SWAN output variable	Unit
Significant wave height H_{m0}	HM0	(m)
Mean absolute period $T_{m-1,0}$	TMM10	(s)
Mean direction	DIR	(° TN)
Directional spreading	DSPR	(°)

Table 2.4 Collection of output parameters analysed in the sensitivity study.

3 Model setup

In this section the model setup is described, including the choice of computational grids, model settings, boundary conditions, bathymetry, water levels, and current and wind fields.

3.1 Choice of computational grids

Following the recommendations of WL/RIKZ/Alkyon/NRL (2007), a dedicated non-uniform computational grid for the tidal inlet of Ameland was developed. This grid is based on the 'Kuststrook' model for the whole Wadden Sea. For the present study a part around the tidal inlet of Ameland was taken and modified to obtain a finer resolution in the mouth of the tidal inlet. This modification was performed in two steps. In the first step the section of the Kuststrook model was refined in both x - and y - direction with a factor 3, followed by a shift of grid points in the mouth of the tidal inlet. Following the terminology introduced in WL/RIKZ/Alkyon/NRL (2007) the code name of this grid is AZG3A. This grid for the tidal inlet is nested in grid NS2 enveloping the Wadden Sea, which provides (part of) the boundary conditions for grid AZG3A (see Section 3.3). Grid NS2 is derived also from the Kuststrook model. The grid NS2 was obtained from the larger GridCL by removing grid cells along its northern and eastern sides. Figure 3.1 shows the outline of these grids and the location of the offshore wave buoys used in the winter season of 2004-2005. For readability every fourth grid line is plotted.

The northern boundary of grid NS2 was chosen such that it touches the locations of the buoys ELD and SON. Similarly, the northern boundary of grid AZG3A touches the locations of the buoys AZB11 and AZB12, which provide the offshore wave boundary conditions, see next section. The southern boundary extends to the Frisian coast. The eastern boundary is located near the eastern tip of Ameland, whereas the western boundary is located just west of the island of Terschelling. We note that the AZG3A grid used in this study slightly deviates from the grid AZG3A used in WL/RIKZ/Alkyon/NRL (2007). The main difference is its larger extent in westward direction. An overview of the grid lines of grid AZG3A is shown in Figure 3.2. The typical resolution of this grid in the mouth of the tidal inlet and near the buoys is 60 m. Further away from this area, the average cell size gradually increases to values of about 150 m near the mainland, which is too coarse for resolving surf zone processes.

To obtain greater resolution at the coast, the grid AK4A is used, which is nested in the AZG3A grid. The AK4A grid is also based on the Kuststrook model. Its generation is performed in two steps. In the first step a section of the Kuststrook model is refined with a factor 4 in cross-shore direction and with a factor 2 in along-shore direction. The typical resolution is 40 m in cross-shore direction and 100 m in along-shore direction. Figure 3.3 shows the outline of the AZG3A and AK4A grids. Every fourth grid line of the AK4A grid is plotted. The numerical characteristics of these computational grids are summarized in Table 3.1, in which N_x and N_y denote the grid dimensions.

Name	Nx	Ny	% active points
GridCL	391	161	79
NS2	381	139	81
AZG3A	286	412	75
AK4A	150	244	26

Table 3.1: Numerical characteristics of the SWAN computational grids.

The simulations on the AZG3A and AK4A grids have typical simulation times in the order of respectively 2.5 hours and 20 minutes on a Pentium 3.4 GHz processor with 1 Gb internal memory. The time required for running on the NS2 grid is in the order of a few hours.

3.2 SWAN version and model settings

The present computations for the tidal inlet of Ameland were performed with SWAN version 40.51 without bug fix A, in order to be consistent with the hindcasts performed by WL(2006b), Royal Haskoning (2006) and WL (2007b)². The frequency range was 0.03 - 1.0 Hz with 38 geometrically-spaced frequencies and 36 directions distributed over the full circle at 10° intervals. Following the recommendations of Alkyon (2007a,b) rather strict convergence criteria were imposed. The following command was applied:

```
NUM STOPC 0.00 0.01 0.001 99.5 STAT mxitst=80 alfa=0.01
```

Following WL (2006b) and Haskoning (2006) the following physical settings were applied:

```
GEN3 WESTH
QUAD
TRIAD TRFAC=0.1
BREAKING ALPHA=1 GAMMA=0.73
FRICTION JONSWAP CFJON=0.067
```

For the CXP series of sensitivity runs, the magnitude of the shallow water source terms were each reduced by 50% in turn. Therefore, for these simulations the following alternative settings were used:

```
CXPS1 series:      FRICTION JONSWAP CFJON=0.0335
CXPS2 series:      BREAKING ALPHA=0.5 GAMMA=0.73
CXPS3 series:      TRIAD TRFAC=0.05
```

The wind input source term used with the above model settings is based on that of Yan (1987), given by:

2. The most significant alteration made in bug fix A with respect to the base version 40.51 is to reduce the proportionality factor of nonlinear triad interaction from TRFAC=0.1 to 0.05, in combination with an increase in the frequency up to which triad interactions are computed.

$$\beta = \frac{1}{\sigma E} S_{in}(\sigma, \theta) = A \left(\frac{u_*}{c} \right)^2 \cos(\theta - \alpha) + B \left(\frac{u_*}{c} \right) \cos(\theta - \alpha) + C \cos(\theta - \alpha) + D$$

where A , B , C and D are fitting coefficients, E the variance density, σ the radian frequency, θ the wave direction, α the wind direction, u_* the wind friction velocity and c the wave phase speed. For the sensitivity runs C2PW1 and C2PW2, the value of the dimensionless wind input β is limited for young wind sea. This is done by limiting the magnitude of β to values of $2 \cdot 10^{-2}/\pi$ and $10^{-2}/\pi$ respectively. The influence of this limitation in wind input on young wind seas is shown in Figures 3.4 and 3.5. Here dimensionless growth curves are presented, which are based on simulations at wind speeds of $U_{10} = 10$ m/s and 30 m/s respectively. It can be seen that the influence of this wind input capping is to reduce wave growth at short dimensionless fetches, and that this effect, expressed in dimensionless terms, is invariant to the wind speed.

3.3 Wave boundary conditions

Following the procedure applied in Haskoning (2006), the wave boundary conditions for the AZG3A grid are, in principle, obtained from the wave buoys AZB11 and AZB12. However, for the storm of 8-9 February 2004 no reliable information was available from the AZB12 buoy, so that the AZB11 buoy was used for the entire northern boundary of grid AZG3A and the North Sea part of the western and eastern boundary. The remaining boundary conditions are obtained from the grid GridCL, which consists of a section of the Kuststrook model enclosing the AZG3A grid. In this way, realistic wave boundary conditions are obtained for all boundaries of the AZG3A grid. Figure 3.6 illustrates the origin of the wave boundary conditions along all boundaries of the AZG3A grid. The eastern and western boundaries receive their information from the overall grid GridCL (red lines), whereas the blue line indicates the area that receives information from wave buoy AZB11. The wave boundary conditions for the AZG3A grid are specified as 2D-wave spectra for all boundary points.

The representation of measured spectral information differed from the representation in SWAN that was required for this study. The measured spectra are provided as energy density, mean wave direction Dir and directional spreading $Dspr$ as a function of frequency. These frequencies are linearly distributed in the interval 0.01 Hz – 0.5 Hz. The SWAN spectra are given as a function of frequency and direction, where the frequencies are geometrically distributed in the interval 0.03 Hz – 1.0 Hz and the directions are steps of 10° distributed over the full circle.

The transformation of the measured spectra to the 2D spectra in SWAN format is performed in a number of steps to account for the above-mentioned differences:

- The measured energy density spectra are extended to 1.0 Hz using an f^{-4} power law. In this way 50 frequencies are added. The mean direction and directional spread at these extra frequencies are taken equal to those at $f=0.50$ Hz.
- The energy densities, mean directions and directional spreadings are interpolated to the frequency domain of the SWAN computations by using an energy conserving method.

- The directional distribution per frequency is reconstructed using a directional distribution: $D(\theta) = A_s \cos^{2s}(\theta - Dir)$, with θ the wave direction and A_s a normalisation coefficient. The spreading factor s depends on the directional spreading $Dspr$. The relation between s and $Dspr$ is approximated as $s = 2/Dspr^2 - 1$ (if $Dspr$ is expressed in radians).
- The normalisation coefficient is computed as: $A_s = 1/(2\sqrt{\pi}) \cdot \Gamma(s+1)/\Gamma(s+1/2)$ with $\Gamma(\cdot)$ the gamma function.

For the CXB series of the sensitivity runs, variations on the incoming wave boundary conditions were imposed. For the historic storm these variations were imposed on the boundary spectra for AZG3A using an option in the wave spectra transformation program. The variations on the mean direction and directional spreading, were imposed on the mean directional and directional spread as obtained from the buoys. To avoid unrealistic spreading values a lower limit of $Dspr = 5^\circ$ and an upper limit of $Dspr = 81^\circ$ were applied. The variation of the significant wave height was achieved by multiplying the energy densities with a factor of either 1.21 (+10% change in wave height) or 0.81 (-10% change in wave height). The variation of wave periods was achieved by transforming all values in the frequency array with a factor of 1.1 (-10% change in wave period, note sign) and 0.9 (+10% change in wave period) followed by a renormalisation to conserve energy (and thus wave height). Next, this transformed spectrum was interpolated to the original frequency array using an energy conserving method. A small correction was needed for the downshifting of the frequency axis since this led to zero energy over 0.9-1.0 Hz. This was solved by specifying an energy density at this frequency based on a f^{-4} power law from the previous energy density. This method of shifting the frequency axis caused all period measures to change with 10%.

For the hypothetical extreme storms, the wave boundary conditions were directly imposed on the boundaries of the NS2 grid using the parametric method of specifying the wave boundary conditions at the buoy locations ELD and SON.

3.4 Bathymetry

The bathymetry for the tidal inlet of Ameland and surrounding area was obtained from depth soundings performed by RIKZ in the period 1999 through 2006. These soundings were processed by RIKZ to obtain a digital representation on regular grids with a resolution of 20 m.

The depth values for the GridCL grid were provided together with the grid information of the Kuststrook model. For the grids AZG3A and AK4A the bathymetry was obtained from various sources in order to cover the complete domain of these grids. The following sources were used:

- *Source 1:* Tidal inlet of Ameland from 2004;
- *Source 2:* Data from a small coastal strip along the 'kwelder' of the Frisian coast on a 5 m grid based on laser altimetry measurements in 2004;
- *Source 3:* Data for the complete Wadden Sea from 1999;
- *Source 4:* Tidal inlet of Vlieland from 2004;
- *Source 5:* Bathymetry of the Kustfijn-V4 model.

The bathymetry on the AZG3A and AK4A computational grids was generated hierarchically, so that for each grid point the most recent bathymetrical data was used. First, the data from Source 1 was used to cover the area around the tidal inlet of Ameland, whereas the data from Source 2 was used to cover a narrow strip along the Frisian mainland. The data from Source 2 was supplemented with 20 m data from the Source 3, despite the fact that these data were obtained in 1999. Next, data from Source 4 was used to fill further gaps. The remaining missing bottom points were taken from Source 5. Figure 3.7 shows the outline of the areas covered by each data file. Figure 3.8 shows the bathymetry obtained from the data from Source 1, and Figure 3.9 shows the bathymetry based on the data from Source 2. The combined bottom topography on the AZG3A grid is shown in Figure 3.10. For grid AK4A the bottom topography is presented in Figure 3.11.

The digital bottom data were provided on grids with a spatial resolution of 20 m. This does not mean that the actual resolution of these data is 20 m, since these data are based on depth soundings usually measured along rays (ship tracks) separated by 100 m at steps of 5 m to 10 m along a track. This implies that the original data have different spatial resolution in x- and y-direction. For comparison, the spatial resolution of the computational grid AZG3A varies from about 60 m in the tidal inlet of Ameland to about 150 m towards the Frisian coast and to the tidal inlets of Vlieland and Schiermonnikoog. These considerations imply that the average spatial resolution of the depth soundings is comparable with the resolution of the computational grid.

The kwelder data were gridded in boxes of 20 m to better reflect the size of the grid cells along the Frisian coast. This gridding consisted of computing the average value of all depth values related to grid points that lie in a box with sizes of 20 m around the point of interest. It could be argued that taking the minimum depth in a box would better reflect depth-limited wave conditions. Inspection of the differences between the minimum and average depth values in a cell revealed that in 90% of the grid cells these differences are less than 0.1 m, which is small compared to the depth values used in this study. Furthermore, taking the average depth value in box would result in a somewhat conservative wave condition in actual computations for determining Hydraulic Boundary Conditions. For the purposes of this study, using average depth values in a box is therefore considered acceptable.

The names of the data files that were used to construct the bottom for the computational grids are summarized in Table 3.2.

Data file	Source of information
KB126-1110_20040701.asc	Source 1
KB127-1110_20040701.asc	Source 1
KB127-1312_20040525.asc	Source 1
KB127-1514_20040525.asc	Source 1
KB128-1110_20050322.asc	Source 1
KB128-1312_20050307.asc	Source 1
KB128-1514_20040612.asc	Source 1
KB129-1110_20050413.asc	Source 1
KB129-1514_20050307.asc	Source 1
KB130-1110_20050420.asc	Source 1
KBc126-1312_20060504.asc	Source 1
KBc129-1312_20060504.asc	Source 1
KBc130-1312_20060504.asc	Source 1
KB124_1312_20020807.asc	Source 4
KB124_1514_20020807.asc	Source 4
KB125_1312_20040325.asc	Source 4
KB125_1514_20040211.asc	Source 4
KB125_1716_20030701.asc	Source 4
KB126_1312_20040211.asc	Source 4
KB126_1514_20040211.asc	Source 4
KB126_1716_20030701.asc	Source 4
KB127_1514_20040211.asc	Source 4
KB126_1716_20030701.asc	Source 4
1241312.int	Source 3
1241514.int	Source 3
1251514.int	Source 3
1251716.int	Source 3
1261716.int	Source 3
1271716.int	Source 3
frkwelders.agr	Source 2

Table 3.2: Data files with bottom information

3.5 Water level and current fields

3.5.1 General

The observed storm instants were simulated with current and water levels that were computed with the WAQUA Kuststrook and Wadden models. For the purposes of this study a selection of these data were provided by RIKZ on two non-overlapping curvi-linear grids covering the Amelander Zeegat. Output fields were written to data files every 30 minutes for a period of a few days around the selected storm events. The information in these files was interpolated to the non-uniform SWAN computational grids. The following sections describe the procedure to prepare these fields for the SWAN model.

The hypothetical extreme events were considered without currents, since these were not available.

3.5.2 WAQUA grids

Existing WAQUA model results for the hindcast periods were available on two non-overlapping grids, which were taken from the Kuststrook model. A fine grid provided the currents in an area around the tidal inlet of Ameland and up to the coast of the Frisian mainland. A coarser grid covering a larger part of the Wadden Sea enveloped this fine grid. The outline of these grids is shown in Figure 3.12. In this figure each fourth grid line is shown.

The current and water level data in the coarser AZG grid were set to zero for the area covered by the fine WAW grid. Next, all data points in the WAW grid were supplemented with the non-zero data points in the AZG grid. In this way a set of data points was obtained that could be used to interpolate to the SWAN computational grids.

However, test computations indicated that along the boundary between the two grids the current and water level data at the boundary points in both grids were interpolated in some way between zero and non-zero data values. This is illustrated in the Figures 3.13 and 3.14, which show the spatial variation of the current velocity and water level on the grids AZG and WAW respectively for the situation of 8 February 2004, 20:00 hours. Evidently, these interpolated data values were introduced in the selection procedure applied by RIKZ to generate WAQUA data for selected output areas.

These interpolated data along the boundary of the two grids were removed by ‘cutting’ small strips of data points from each grid before combining them into one set of points for each selected moment of time.

3.5.3 Treatment of dry points

The WAQUA model has a facility for handling dry points that conflicts with the procedure in SWAN to handle dry points. Some grid points may become dry or wet as the water level changes. In the case a grid point is dry, the u - and v - component of the current velocities are set to zero in the WAQUA computation, and the water level is taken as the land height plus a few centimeters (the actual value depends on the model settings of the WAQUA simulation). Using these water levels as input for a SWAN simulation would cause shallow grid points in a SWAN grid to become wet with a small water depth, whereas they should be treated as dry points. Whenever this happens this will distort the SWAN computation in an unpredictable way. It is therefore needed to identify these points and to replace the water level in such a point with the water level from the nearest non-dry WAQUA grid point.

This was done by means of an automated iterative procedure (coded in MATLAB) to replace the ‘dry’ water levels by the water level in the nearest ‘active’ water level in the WAQUA grid. The first step in this procedure is to identify the dry points in the set of WAQUA grid points on the detailed WAW grid. Such points have zero values for the u - and v -components of the current velocity. This results in blocks and strips of points along the boundaries of the Wadden islands, the Frisian coast and sand banks. An example of such a

set of points is shown in Figure 3.15 for the situation of 8 February 2004, 20:00 hours. The dry points are marked with black circles.

Next, an iterative procedure was applied to replace the water level in the dry points with the nearest ‘active’ water level. This was achieved by first identifying each dry point surrounded by two or three ‘active’ points. Next, a new water level was determined as the average of the water levels in these surrounding ‘active’ points. Subsequently, these grid points were activated such that they can be treated as an ‘active’ point in the next iteration. The iteration procedure was repeated until no dry points could be identified that are surrounded by two or three ‘active’ points. This procedure was applied to all water levels fields needed for the SWAN simulations. An example of such a corrected water level field is shown in Figure 3.16 for the same situation as shown in Figure 3.15.

Application of this procedure resulted in some deviating results along the Frisian coast, where water levels were determined that were considerably higher than the overall water level in the Wadden Sea. Close inspection of the results indicated that this area consists of a high lying pool of water that was emptying its content through a narrow channel. As a consequence these points were treated as active grid points. It could be argued to treat this area as a dry area, which would result in a different (lower) water level for these points. However, it was deemed more conservative with respect to wave conditions at the sea defences to consider these as wet points.

The current speed was set to zero in all dry points.

3.5.4 Interpolation

The conversion of the WAQUA current and water level data to the SWAN grids was performed on the basis of a triangulation of the set of coordinates resulting from the combined WAQUA grid points. Next, for each point in a SWAN computational grid, a search was carried out to find the enveloping triangle. Finally, bi-linear interpolation in each triangle was applied to obtain the u- and v-components and water level in each computational grid point of the SWAN grids AZG3A and AK4A. The spatial variation of the current magnitude and direction, and water level for all three observed storm events are shown in the Figures 3.17 to 3.19. Note that for the instant of assumed slack tide (22:30h) the current speed is still significant.

3.6 Wind fields

The simulations of the three observed storm events were performed with a constant uniform wind speed and direction over the whole computational domain. For the sensitivity run C2WH1 on the effects of the use of a spatially varying wind field, however, more detailed wind information was required.

This spatially varying wind field was derived from HIRLAM data available on a 11 km grid, which was provided by RIKZ. A downscaling technique was applied to improve the spatial resolution of this wind field by including the effect of local surface roughness on wind flow. The downscaling was performed with the KNMI downscaling software version 2.3. The

spatial resolution of the down-scaled wind field was 250 m. Detailed information on the principles behind the downscaling can be found in Verkaik (2006) and Verkaik et al. (2006).

Figures 3.20 and 3.21 show the spatial variation of the wind speed and direction of the HIRLAM and downscaled wind field. The sheltering effect of the Wadden islands under the prevailing NW wind condition can be clearly seen. These figures also show some obvious anomalies in the wind speed as the NW tip of Terschelling and near the town of Harlingen. These anomalies are probably related to some internal correction in the downscaling procedure. For the present study, however, these anomalies are outside the area of interest and will not be considered.

At present no thorough validation of the downscaling of HIRLAM wind fields exists. In developing the downscaling method Verkaik et al. (2006) used wind measurements at a single location to validate their method. Since their method is based on well-established physical considerations, it generally provides plausible results.

To obtain an indication of the accuracy of the downscaled HIRLAM wind field used in the present study, the predicted wind speed variation from the downscaling behind Ameland was compared with the theoretical variation according to Taylor and Lee (1984). The model of Taylor and Lee (1984) describes the development of an internal boundary layer after a land-sea transition. The result of their model is the variation of the wind speed $U(x)$ with fetch x starting from an upwind wind speed U_u . For the comparison, a situation was selected with a wind direction that is more or less perpendicular to the island of Ameland. The time instant of 8 Feb. 2004, 22:30 hours satisfied this criterion and was subsequently selected. The model of Taylor and Lee (1984) was applied with a land surface roughness of 0.1 and the upwind wind speed was taken from the downscaled wind speed. The result of the comparison is shown in Figure 3.22. The results compare rather well and give confidence in the applicability of the downscaling technique. It is nonetheless recommended that the source of the anomalies at Terschelling and Harlingen shown in Figures 3.20 and 3.21 be traced and remedied in newer versions of the downscaling method. In addition, wind speed observations are needed to further validate this technique.

To make the model input to SWAN on the uniform and spatially varying wind fields consistent, the speed and direction obtained from the down-scaled HIRLAM wind field at the location of buoy AZB11 was imposed as a uniform wind field. The wind speed and direction at this location are hardly affected by the relatively high surface roughness of the Wadden islands.

4 Simulation results

4.1 General

In this section, the results of the sensitivity tests defined in the previous sections are presented. First, an overview is given of the simulation results obtained for the five base cases presented in Section 2.1. Thereafter, the results of the sensitivity tests are presented, organised in the groups given in Section 2.2.

The presentation of the sensitivity tests is done by means of spatial difference plots of integral parameter output of a particular sensitivity test and its corresponding base case. In addition, a number of output curves are defined along which the results of both the base case and the variation are plotted. This output is presented mainly in terms of integral parameters, but can also include wave spectra and source terms, depending on the sensitivity test in question.

The collection of output curves that were employed are shown in Figure 4.1, in relation to the bathymetry of the computational domain. The primary output curve for sensitivity results runs along the Frisian coast, at a constant 500 m parallel to the primary sea defence (Curve A). It is noted that due to the complex bathymetry in front of the sea defence – including a land reclamation project ('kwelder') – the water depth varies rather strongly along this output curve. For the conditions C1XXX and C3XXX, which had lower water levels, Curve A fell dry for the most part, so that an additional output curve B was defined running along the 0 m NAP contour of the Frisian coastline. Similarly, for the SW extreme condition (C4XXX), an output curve C was defined around the head of Ameland at a depth of 0 m NAP. It was furthermore found useful to define some extra output curves on which to study sensitivities in the development of the wave field across the Wadden Sea. These include a ray from the ebb tidal delta through the main tidal channel and to the Frisian coast (Curve D), and curves running from the islands of Ameland and Terschelling to the Frisian coast (curves E and F respectively). Selections of these output curves are employed where appropriate in the analysis. A summary of the average model responses along the output curves A, B and C is given in Table 4.1 at the end of this section.

4.2 Base cases

4.2.1 NW storm with flood current

Figures 4.2a-d show the simulation results of the base case C1XXX, which was recorded on 08/02/2004 at 20:00. This condition features an offshore wave condition of $H_{m0} = 4.1$ m and $T_{m-1,0} = 7.4$ s from WNW, with a wind of $U_{10} = 13.5$ m/s from NW (see Table 2.1). The current field for this simulation time, produced by WAQUA, is presented in Figure 3.17. At the time of the observations, the tide was rising (water level at NES was +1.0 m NAP), causing a maximum computed flood current in the main tidal channel of about 2.3 m/s, and a weaker current of about 0.4 m/s over the tidal flats. Figures 4.2a-c show spatial plots of the simulated significant wave height H_{m0} , mean period $T_{m-1,0}$, mean wave direction (vector arrows) and the wave height over depth ratio. The top panels of these figures show the results obtained on the AZG3A grid, the location of the detailed AK4A grid, and also the

output curve along the coast. Considering the relatively low water level for this case, results along the coast are evaluated along Curve B, located on 0m NAP. The bottom panels present the results on the detailed AK4A grid.

Figures 4.2a and 4.2b show that high wave energy is found on the North Sea side of the barrier islands, which is dissipated for the most part either on the coasts of the barrier islands or on the ebb tidal delta. The high periods associated with these waves persist only a short distance beyond the tidal inlet. Moving from the barrier islands to the coast, the prevailing NW wind gives rise to young wind sea, reaching significant wave heights of approximately 0.5 m. Figure 4.2c presents a spatial plot of wave height over depth ratio. North of the barrier islands this ratio exceeds 0.4, and in front of the mainland coast this ratio lies between 0.3 and 0.4. WL (2003) shows that SWAN typically produces H_{m0} over depth values of this order when the shallow water growth limit is reached. Under such conditions, the development of wave heights and periods are limited by the finite water depth and strong depth-induced dissipation (e.g. Bretschneider 1958 and Young and Verhagen 1996). Figure 4.2d presents the variation of integral parameters along Curve B, which was in a water depth of about 0.6 m at the time. Along this contour, the significant wave height is about 0.25 m and the mean period $T_{m-1,0}$ approximately 1.5 s. The bottom panel of Figure 4.2d shows that the ratio of H_{m0} to depth is about 0.4 along the entire contour, testifying to the depth-limited conditions found here.

4.2.2 NW storm at high water

Figures 4.3a-d show the simulation results of the base case C2XXX, recorded on 08/02/2006 at 22:30, features an offshore wave condition of $H_{m0} = 5.3$ m and $T_{m-1,0} = 9.5$ s from NW, with a wind of $U_{10} = 16.6$ m/s, also from NW (see Table 2.1). The current field for this simulation time is presented in Figure 3.18. At the time of the observations it was approximately high tide (water level at NES of +2.6 m NAP), and current velocities reached a maximum of 0.9 m/s. Figures 4.3a-c show spatial plots of the simulated significant wave height, mean period $T_{m-1,0}$, mean wave direction (arrows) and the wave height over depth ratio. As with the condition C1XXX, the wave field on the North Sea side of the barrier islands is characterised by high wave heights and high periods, both being strongly reduced on the coasts of the barrier islands and on the ebb tidal delta. Wind sea is generated over the region behind the barrier islands, reaching significant wave heights of up to about 1 m. Figure 4.3c presents a spatial plot of the wave height over depth ratio, which indicates strongly depth-limited conditions north of the barrier islands and along large parts of the mainland coast.

Figure 4.3d presents the variation of integral parameters along Curve A, running along the primary sea defence. The water depth in front of the primary sea defence varies strongly, as can also be seen from the bathymetry shown in Figure 4.1. The SW half of Curve A lies on a steep foreshore in relatively deep water, whereas the NE half lies on a plateau formed by the land reclamation site, with a water depth of about 0.5 m shoreward of the start of the surf zone. This variation in water depth is reflected in the integral wave parameters. Over the shallow NE half of Curve A, the significant wave height has an average value of about 0.25 m, bringing the wave height over depth ratio to about 0.4. This indicates that the wave field, which reached its shallow water growth limit over the Wadden Sea interior, is limited even further in this surf zone due to the reduction in water depth. Here the wave height is entirely determined by the limited water depth, a situation commonly referred to as a

saturated surf zone. However, over the SW half of Curve A, wave heights increase up to 1 m, and non-saturated surf zone conditions are found ($H_{m0}/\text{depth} < 0.4$). Similarly, the mean period varies by about from 1 s to 3 s over the length of Curve A.

4.2.3 NW storm with ebb current

Figures 4.4a-d show the simulation results of the base case C3XXX, recorded on 09/02/2006 at 01:30, features an offshore wave condition of $H_{m0} = 4.8$ m and $T_{m-1,0} = 9.7$ s from NNW, with a wind of $U_{10} = 16.3$ m/s, also from NNW (see Table 2.1). The current field for this simulation time is presented in Figure 3.19. At the time of the observations, the tide was ebbing (water level at NES of +1.75 m NAP), and the ebb current reached a maximum velocity of 1.6 m/s. Figures 4.4a and 4.4b show spatial plots of the simulated significant wave height, mean period and mean wave direction (arrows). As with the two cases considered above, the wave field on the North Sea side of the barrier islands is characterised by high wave heights and high periods, whereas inside the Wadden Sea wave heights and high periods are significantly lower, indicating the presence of young wind sea. In this region, significant wave heights do not exceed 1 m. Figure 4.4c presents the wave height over depth ratios over the computational domain. As was found above, this ratio indicates that depth-limited conditions prevail north of the barrier islands and in front of the mainland coast. Figure 4.4d presents the variation of integral parameters along Curve B. As indicated by the wave height over depth ratio (constant value of 0.4), wave conditions along this contour are at the shallow water growth limit. This results in a significant wave height of approximately 0.6 m and a mean period $T_{m-1,0}$ of about 2.5 s.

4.2.4 SW extreme storm

Figures 4.5a-c show the simulation results of the base case C4XXX, a hypothetical 1/4000 year storm, which was generated by a wind speed of $U_{10} = 34.0$ m/s from SW (see Table 2.1). The uniform water level used in this simulation is +4.7 m NAP. Current have not been included. Figures 4.5a and 4.5b show the spatial plots of the simulated significant wave height, mean period, mean wave direction (arrows) and the wave height over depth ratio. In the Wadden Sea interior, the mean wave direction is aligned with the SW wind, and wave heights and mean periods are virtually constant. The latter suggests that the shallow water growth limit is reached in this region, which is confirmed by the consistently high values of H_{m0}/depth found here (Figure 4.5b). The wave heights and mean periods north of the barrier islands are significantly higher than those inside the Wadden Sea. These high waves are generated by the SW outside of the ring of barrier islands (on the overall NS2 computational grid), and subsequently refract towards the Ameland Zeegat on the intermediate water depths.

For this SW storm the output curve C is considered, which is located at the 0 m NAP contour around the head of Ameland. Figure 4.5c shows that there is a strong variation of the integral parameters along Curve C. Starting on the North Sea side of Ameland and moving anti-clockwise along this output curve, high westerly waves are found that refract around the head of Ameland. Between 5000 m and 10 000 m along Curve C, at the westernmost tip of Ameland, wave heights increase as the shoreline becomes most exposed to offshore waves, and which also appear to be focussed by refraction. Here the wave height over depth ratio exceeds 0.5. Moving towards the end of Curve C, the local wave conditions inside the Wadden Sea are found. These are characterised by a SW wave direction,

significant wave heights of about 2 m, which are at the shallow water growth limit ($H_{m0}/\text{depth} = 0.4$).

4.2.5 NW extreme storm

Figures 4.6a-d show the simulation results of the base case C5XXX, a hypothetical 1/4000 year storm, which features an offshore wave condition of $H_{m0} = 9.4$ m and $T_p = 18.0$ s from NW, with a wind of $U_{10} = 34.0$ m/s also from NW (see Table 2.1). The uniform water level used in this simulation is +4.7 m NAP. Currents were not included. Figures 4.6a-c show spatial plots of the simulated significant wave height, mean period, mean wave direction (arrows) and the wave height over depth ratio. The North Sea side of the barrier islands is characterised by significant wave heights of 4-9 m and $T_{m-1,0}$ periods of 10-14 s. Although the values of these parameters are strongly reduced on the coasts of the barrier islands and on the ebb tidal delta, waves entering the Wadden Sea through the tidal inlet still have a significant wave height of about 3 m and a mean period of about 5 s. Directly behind the barrier islands, significant wave heights are relatively low, but increase to a constant 3 m at longer fetches, under the combined influence of the strong wind and high water level. Figure 4.6c shows that the wave height over depth ratio is in the range 0.3-0.5 over the entire model domain (except over the tidal channels). This indicates that, even at this extreme water level, wave heights have reached their shallow water growth limit over almost the entire domain.

Figure 4.6d presents the variation of integral parameters along Curve A, running along the primary sea defence. As discussed above, water depths vary rather strongly along this output curve. Nonetheless, the constant wave height over depth ratio of about 0.4 shows that depth-limited conditions exist along the length of Curve A. Therefore, wave heights are seen to increase to the SW, where the water depth is greater. Similarly the mean wave period increases over the steeper, SW part of Curve A.

4.3 Sensitivity to wave boundary input

The first results of the sensitivity study that are considered are those for the variation of wave conditions imposed on the offshore model boundary. In the sections below, the results for the observed severe NW storm C2XXX is considered first, followed by the results of the hypothetical extreme NW storm C5XXX (see Table 2.3).

4.3.1 Severe NW storm conditions

Figures 4.7 to 4.10 present the sensitivity of wave conditions to variations in the wave height ($H_{m0} +$ and $- 10\%$), mean wave period ($T_{m-1,0} +$ and $- 10\%$), mean wave direction ($+ and - 10^\circ$) and directional spreading ($+ and - 10^\circ$) imposed at the North Sea boundary. In this presentation, the figures with subscripts a and b present spatial maps of the difference between a particular sensitivity run and the base case C2XXX, in terms of wave height, mean period, mean direction and directional spreading. For brevity, only a selection of the total list of sensitivities (the ones that could lead to an increase in wave heights at the primary sea defence) are presented. In the figures with subscripts c and d, the results of integral parameters along output curve D is presented for all eight conditions presented in Table 2.3. Curve D runs over the ebb tidal delta, through the main tidal channel and over the

salt marches to the mainland shore, and gives insight in the penetration of offshore waves into the Wadden Sea and to the mainland shore.

Inspection of Figures 4.7 to 4.10 reveals that conditions at the primary sea defence is insensitive to all the variations at the offshore boundary investigated here. This finding is in agreement with a similar finding by Alkyon (2007a,b). It can be seen that neither a variation of the wave height, period measures nor wave directions affect the conditions at the Frisian coast in any noticeable way. None of the results of the sensitivity runs along the output curve A vary significantly from those of the base case presented in Figure 4.3d (see also Table 4.1 below), and are therefore not reproduced here. Regarding the insensitivity to variation in the wave height at the offshore boundary, Figures 4.7c and 4.7d show that at the ebb tidal delta, the wave height over depth ratio reaches a value of 0.4 (see also Figure 4.3c above). Due to the existence of a saturated breaker zone over the ebb tidal delta, both increases and decreases in the significant wave height in the offshore are 'filtered' out of the wave field. The vertical dashed line in these figures indicate the position where this output curve is crossed by Curve A. Regarding variations in mean wave period, Figures 4.8a-d show that the changes made at the boundary persist somewhat further into the Wadden Sea than was the case with the variation in wave height. Nonetheless, after passing through the tidal inlet, the changes made to the mean wave period at the boundary are overshadowed by the decrease in wave period due to local wind sea growth. Similarly, Figures 4.9 and 4.10 show that variations in directional properties at the offshore boundary are overshadowed by the directional properties of the wind sea locally generated in the Wadden Sea. (The white parts in the wet areas of Figure 4.10b indicate that the value of the variation is smaller than -10% or -10° , i.e. a reduction greater than 10% or 10° .)

4.3.2 Extreme NW storm conditions

Figures 4.11 to 4.14 present the sensitivity of wave conditions to variations in the boundary conditions of the extreme storm C5XXX. (It is noted that in these simulations the variation in boundary conditions are imposed on the NS2 grid, for which the offshore boundary is more northerly than that of the AZG3A grid, see Section 3.3. Imposed variations may therefore be diminished upon reaching the AZG3A grid.) The presentation of the results are similar to that used in the section above. It may be expected that for this case, which features an extreme water level of +4.7 m NAP, a greater sensitivity to variations at the offshore boundary would be displayed at the mainland coast. However, Figures 4.11c and 4.11d show that at the ebb tidal delta saturated conditions exist also for this extreme storm (see also Figure 4.6c above), so that variations in wave height do not penetrate into the Wadden Sea. Also, similar to what was found for the observed NW storm C2XXX above, variations in the wave period and directional characteristics do not affect wave conditions inside the Wadden Sea (see Table 4.1).

4.4 Sensitivity to current and water level

The next sensitivity investigated is the influence of tidal currents and water level on wave conditions at the primary sea defence. For this, we consider the base cases C1XXX (flood current), C3XXX (ebb current) and the extreme NW storm C5XXX. The influence of the current fields on conditions at the coast are investigated by deactivating these input fields in

the variations to the base cases. The effect of water level is investigated by increasing the water level in the extreme NW storm.

4.4.1 Flood current

Figure 4.15 presents the effect of deactivating a flood current of the base case C1XXX (and hence, indirectly, the result of including current effects). Figure 4.15a shows, by means of spatial difference plots, that the deactivation of the flood current field in the simulation leads to large increases in significant wave heights and mean periods in the main tidal channel (of the order of 50%, see Figure 4.15c). As above, the white parts in the wet areas of these figures indicate that the value of the variation is below -10% or -10° , i.e. a reduction greater than 10% or 10° . Moving towards the shore, the resulting difference in the wave height reduces, whereas the difference in mean period persists to the coast. Figure 4.15b shows that the mean wave direction and directional spreading are affected by the presence of the current by more than 10° and 10% respectively. Figure 4.15c presents the evolution of integral parameters along the output curve D running through the main tidal channel. This figure confirms the strong increase in significant wave height and mean period and the strong change in mean wave direction in the tidal channel due to the deactivation of the flood current. However, Figure 4.15c shows that at the location of the output curve B (indicated by the vertical dashed line) the significant wave height is insensitive to the presence of the current. In this region, the wave height to depth ratio has a value of 0.3 to 0.4, which reveals that this insensitivity is due to depth limitations.

The strong influence of the current on the wave energy and period is also illustrated in Figure 4.15d, where the frequency spectra (in terms of absolute frequency) are presented at regular intervals along Curve D. It is seen that between 10 000 m and 15 000 m along Curve D, the frequency spectra are strongly affected, presumably due to the combined effect of Doppler shifting and the current-induced refraction of low-frequency waves out of the channel (refer Figure 4.15b). However, this effect is diminished at the coast (at $x = 23\,400$ m). Figure 4.15e presents the sensitivity of the model results at the output curve B to the deactivation of the flood current (Table 4.1). The greatest influence of deactivating the flood current along this contour is an average increase in the mean wave period of 10.7% (Table 4.1). As was shown in Figure 4.2c above, the wave height over depth ratio along Curve B (a constant 0.4) indicates depth-limited conditions along its entire length, which is reflected in an average increase of only 0.12 upon deactivation of the flood current. The mean direction along the mainland is affected by less than one degree, averaged along its length, due to the presence of the flood current (Table 4.1).

4.4.2 Ebb current

Figure 4.16 shows the sensitivity to an ebb current field in the wave simulation. Figures 4.16a and 4.16b show that significant wave heights and mean periods are decreased in the tidal channel by the deactivation of the ebb current in base case C3XXX by up to about 25% (see also Figure 4.16c), and that the mean wave direction and directional spreading are altered by more than 10° and 10% respectively. Figure 4.16c presents the evolution of these quantities along the output curve D through the main tidal channel, showing similar, but opposite effects to the flood current case presented above. Again it is seen that conditions near the coast become saturated (H_{m0}/depth approximately 0.4), explaining the insensitivity of the significant wave heights here (vertical dashed line indicate

location of Curve B). Figure 4.16d presents the progression of frequency spectra (in terms of absolute frequency) along Curve D, showing that at 10 000 m to 15 000 m along this curve the wave period is reduced by the ebb current (presumably due to current-induced refraction of waves towards the channel centre). However, as found above, the frequency spectrum at the coast ($x = 23\,400$ m) is hardly affected by the variation in the current conditions. Figure 4.16e presents the wave parameters along output curve B at the Frisian coastline. Significant wave heights and mean periods are only slightly affected by the deactivation of the current with variations of -0.41% and 2.79% respectively (Table 4.1). This is considered to be due to the saturated conditions found here ($H_{m0}/\text{depth} \approx 0.4$). However, for this case the mean wave direction has changed by up to 15 degrees along this contour.

4.4.3 Increase in water level

The base case of the extreme storm condition C5XXX features a high water level of +4.7 m NAP. Yet, from results presented in Section 4.2.5, it was seen that even at this water level the conditions at the primary sea defence are insensitive to wave conditions north of the barrier islands. It is conceivable that if the water level had been higher still, some significant amount of wave energy may have penetrated from the North Sea into the Wadden Sea. Figure 4.17 presents the sensitivity run C5FL1, in which the water level in the base case C5XXX was increased by 1 m. Figure 4.17a shows that the increase in water level results in an increase in significant wave height in excess of 10% over most of the Wadden Sea and even by more than 20% along the Frisian coast. This significant increase in the wave height is accompanied by an increase in the mean period of more than 8% over large regions in the Wadden Sea. Figure 4.17b shows that the increase in water level also strongly affects the directional characteristics of the wave field.

Figures 4.17c and 4.17d present the integral parameters and frequency spectra along the output curve D. Figure 4.17c shows that along the length of Curve D the wave height to depth ratio remains unaltered (reaching 0.4 at the mainland coast), even though the water depth is increased by a constant 1 m. This indicates that even at this higher water level the shallow water growth limit is reached and conditions at the coast are saturated. Furthermore, Figure 4.17d shows that in the base case C5XXX the low-frequency offshore waves (spectral peak at 0.06 Hz at $x = 0$ m) do not penetrate much beyond $x = 10\,000$ m, and that this result is not altered much with the 1 m increase in water level. Therefore, it can be concluded that the strong increase in wave height found here is due to the greater depth for the locally-generated, depth-limited wind sea, and not due to the greater penetration of North Sea waves into the Wadden Sea. Figure 4.17c also shows that near the coast (vertical dashed line indicates location of Curve A) the mean wave direction is altered somewhat (an average 1.6 degrees, Table 4.1) by the higher water level. This effect is presumably caused by a change in wave refraction due to the greater water depth at the coast. Figure 4.17e presents the considered integral parameters along the output curve A. As mentioned above, the wave height over depth ratio indicates saturated conditions all along Curve A, so that the significant wave height increases proportionately to the increase in water depth (by an average 24.0%, Table 4.1). Correspondingly, the mean wave period increases by an average of 15.2%.

4.5 Sensitivity to wind input

From the results presented in Section 4.3, as well as from studies such as Alkyon (2007a,b), it is apparent that wave conditions in the Wadden Sea are determined by local, (depth-limited) wind sea growth. It may therefore be expected that conditions at the primary sea defence would be sensitive to variations in the wind field over the Wadden Sea. These sensitivities are investigated below, by considering variations to the base case C2XXX. The investigation includes variations to the uniformly imposed wind speed (speed + and - 10%, direction + and - 10°) and the use of a spatially non-uniform wind field (see Table 2.3).

4.5.1 Uniform wind fields

Figures 4.18 to 4.21 present the sensitivity of model outcomes at the mainland coast to variations in the spatially uniform wind field. In this presentation, the figures with subscripts a and b present spatial plots of the difference in output parameters between a particular sensitivity run and the base case C2XXX, whereas those with subscripts c, d and e, present the results of integral parameters along output curves E, F and A. Output curves E and F are selected to be able to follow the growth of wind sea from the lee of the barrier islands to the mainland coast.

Figure 4.18a shows that a 10% increase in wind speed leads to an increase in the significant wave height in excess of 10% and mean period of up to 5% over large areas of the Wadden Sea. The strongest increase in wave height is at the lee of the barrier islands, and the influence decreases towards the mainland coast (see also Figures 4.18c and 4.18d). Figure 4.18e shows the variation in model outcomes along Curve A at the primary sea defence. As was seen in Figure 4.3d above, the wave height to depth ratio over the NE half of Curve A indicates saturated surf zone conditions. Over this stretch, the wave conditions are insensitive to the increase in wind speed. However, over the SW half of Curve A, that is not fully saturated, the higher wind speed results in increases in the significant wave height of up to 10% and in the mean period of up to 4%.

Figure 4.19 shows the corresponding results for the situation in which the spatially uniform wind speed is reduced by 10%. Figure 4.19a shows a decrease in significant wave heights and mean periods of 10% and 5% respectively over a large area of the Wadden Sea. However, as seen above, these differences recede towards the mainland coast (see also Figures 4.19c and 4.19d). Figure 4.19e shows that the conditions along Curve A are somewhat more sensitive to a decrease in the wind speed than what was found for an increase in wind speed above. The reason for this is again found in the wave height to depth ratio: a decrease in wind speed leads to a sufficiently large reduction in this ratio so that conditions are not fully saturated anymore. This leads to an increase in the sensitivity in model results along Curve A.

Figures 4.20 and 4.21 presents the results of a change in the direction of the uniform wind field. Figures 4.20a and 4.20b and Figures 4.21a and 4.21b show that the mean wave direction in the Wadden Sea is strongly effected by the change in the wind direction. Furthermore, at the leese side of the islands the significant wave height and mean period are altered by up to about 10% due to the change in the effective fetch caused by the change in wind direction. However, at the output curve A, the significant wave height and mean period

are changed by less than 0.5% on average (Table 4.1). This is in contrast to the mean wave direction, which changes by just over 10° , in the same direction as the adjustment in the wind direction.

4.5.2 Spatially non-uniform wind field

Figure 4.22 presents the results of a sensitivity run in which the spatially uniform wind field used in the C2XXX base case was replaced by a the downscaled wind field described in Section 3.6 above. To the north of the barrier islands, this downscaled wind field corresponds to the spatially uniform wind field, but at the lee of the barrier islands the wind speeds are significantly lower than those of the uniform wind speed. An exception to this is the area at Harlingen (at the southernmost tip of the AZG3A grid) where a spuriously high wind speed is found, as noted in Section 3.6.

Figure 4.22a shows that behind the islands the significant wave heights and mean periods are about -20% and -5% lower respectively than in the uniform wind case, in accordance with the lower wind speeds behind the islands in the downscaled wind field. However, it can be seen in Figure 4.22a that the effect of the locally reduced wind speed is greatly diminished upon reaching the mainland coast. Figures 4.22c and 4.22d reveal that this effect is not due the reaching of the shallow water growth limit (note the low H_{m0}/depth ratio), but simply that the loss of initial wave growth is caught up over longer fetches. Figure 4.22b shows that the use of the downscaled wind field also alters the wave direction and directional spreading by more than 20% and 20° respectively. In fact, regarding the output curve A, Figure 4.22e shows that the only significant difference in wave model outcomes at the mainland coast is in the mean direction, which is changed by an average of 3 degrees along this curve (the increase in significant wave height at the SW end of Curve A is due to the wind field error at Harlingen, and is not considered here).

4.6 Sensitivity to model physics

Whereas in the sections above the sensitivity of model outcomes was investigated for variations in model input, the remainder of the simulations focus on the sensitivity to the settings of model physics. Here we consider the sensitivity to the capping off of the transfer of energy from wind to the waves for young wind sea, and the sensitivity to the three source terms dominant in shallow water (bottom friction, triad interaction and depth-induced breaking).

4.6.1 Transfer of energy from wind to waves

Figures 4.23 and 4.24 present the sensitivity of model outcomes to the use of two different values for the limitation of energy transfer from the wind to the waves. Figure 4.23 shows that, for the higher capping value for the transfer, there is only a small effect on the results. However, Figure 4.24 shows that for the lower capping value for the transfer, wave heights close to the lee of the barrier islands are reduced by more than 10%. Mean wave periods are increased up to 10% very locally. Also, the mean wave direction and directional spreading are affected close to the lee of the barrier islands. Figures 4.24c and 4.24d confirm that the influence of the wind transfer capping is limited to a fetch close to the barrier island. However, Figure 4.24c shows that due to the limitation in the transfer, the regeneration of

waves over the land reclamation site ('kwelder') after breaking is weaker. These sensitivities are also seen in Figure 4.24e, which presents the integral parameters along output curve A. Here the significant wave height is reduced by an average of 7.7% and the mean period increased by an average of 4.2% (Table 4.1).

4.6.2 Source terms in shallow water

Figures 4.25 to 4.33 present a comparison of the sensitivity of model results to variations in the magnitude of the source terms of bottom friction, triad interaction and depth-induced breaking (see Table 2.3). The analysis focuses on the Frisian sea defences (for NW conditions) and those at the head of Ameland (for SW conditions).

Severe NW storm conditions

Figures 4.25 to 4.27 present the results of the sensitivity tests for the base case C2XXX. Figure 4.25a and 4.25b show that reducing the proportionality coefficient of the bottom friction term has a large influence on integral parameters in the interior of the Wadden Sea for this condition: significant wave height values increase by up to 10%, mean period values increase by more than 10% in places (since bottom friction dissipates lower frequencies most strongly), and the directional spreading changes by more than 10% in the lee of the islands. The shore-normal output curves E and F (Figures 4.25c and 4.25d) show that wave heights and periods increase significantly over regions where the H_{m0}/depth ratio indicates that the shallow water growth limit has not been reached, namely in the interior region of the Wadden Sea (see also Figure 4.3c). At the coast, however, conditions become limited by the depth (especially along Curve E), at which point depth-induced breaking dissipates the excess energy resulting from the reduced bottom friction strength. As a result, the unsaturated SW half of output curve A shows increases in significant wave height and mean period of approximately 6%, but along the saturated NE half of Curve A this response reduces (Figure 4.25e).

Figures 4.26a and 4.26b show that a reduction in the proportionality coefficient of depth-induced breaking only affects the surf zones on the northern sides of the barrier islands and on the ebb tidal delta, and to a lesser degree on the foreshore at the Frisian coast. Figures 4.26c and 4.26d suggest that this insensitivity to depth-induced breaking is due to the fact that the shallow water growth limit is not reached over the whole Wadden Sea interior. Small increases in the significant wave height and mean periods are found within the surf zone, where energy is dissipated over a somewhat longer distance, but shoreward of the surf zone these differences disappear (Figure 4.26c). Figure 4.26e and Table 4.1 show that along Curve A the significant wave height is altered by an average 3.2% and the mean period by an average 1.5%. Lastly, Figures 4.27a and 4.27b show that the reduction in the strength of triad interaction increases the mean period on the north coasts of the barrier islands by up to 5%, but that the Wadden Sea itself is unaffected. Model results along output curve A is virtually unaffected by this alteration, with an increase in the mean period of only 0.22% (Figure 4.27e and Table 4.1).

Extreme SW storm conditions

Figures 4.28 to 4.30 present the results of the sensitivity tests that are based on C4XXX, the hypothetical extreme storm from the SW. Figure 4.28a shows that the reduction in bottom

friction increases wave heights and mean periods north of the barrier islands moderately, where wave periods are relatively high and the water depth relatively great. However, in the Wadden Sea interior, the influence of bottom friction reduction is small. Figure 4.28c presents these results along Curve C (around the head of Ameland), where the North Sea side is shown to be the most sensitive to the altered bottom friction strength. Here the significant wave height increases by 1% and the mean period by 2.3%. By contrast, Figure 4.29a and 4.29b shows a large sensitivity of the significant wave height and mean period over the entire Wadden Sea interior to a reduction in the magnitude of the depth-induced breaking source term. Figure 4.29c reveals that this alteration has increased the H_{m0}/depth ratio along Curve C, whereby larger wave heights (+7.5%) and higher mean periods (+2%) are able to exist in this saturated region. Figures 4.30a - 4.30c and Table 4.1 show a relatively small increase in mean period (1.3%) due to the decrease in the magnitude of triad interactions.

Extreme NW storm conditions

Figures 4.31 to 4.33 present the results of the sensitivity tests that are based on C5XXX, the hypothetical extreme storm from the NW. Figures 4.31a and 4.31b show that decrease in the strength of bottom friction has some influence on model results at the lee of the barrier islands, of which the mean wave period is affected the most (since bottom friction dissipates the low frequency components the strongest). The H_{m0}/depth ratios presented in Figures 4.31c and 4.31d reveal that the insensitivity to the bottom friction setting is due to the fact that the shallow water growth limit prevails in the Wadden Sea interior. As a result, model outcomes along the coastline (Curve A, Figure 4.31e and Table 4.1) are fairly insensitive to the applied change ($H_{m0} + 0.7\%$ and $T_{m-1,0} + 2.3\%$).

By contrast, Figure 4.32a shows that wave heights and periods are significantly affected by the decrease in the proportionality coefficient of the depth-induced breaking. Significant wave heights increase strongly in the surf zone on the northern side of the barrier islands (> 10%), but also increase significantly over the Wadden Sea interior (up to 6%). This increase in wave heights in the Wadden Sea is accompanied by an increase in mean periods in this region (up to 5%). Figures 4.32c and 4.32d show that these increases in wave height and period is linked to an increase in the H_{m0}/depth ratio in this region, which is caused by the reduction in the depth-induced breaking strength. These figures show that the sensitivity to the breaking strength persists to the coast, so that average increases in significant wave height and period of respectively 6.1% and 5.4% are found along output curve A (Figure 4.32e, Table 4.1). Figure 4.33 presents the results obtained by reducing the magnitude of the triad interaction source term. It can be seen in Figures 4.33a and 4.33b that this variation has a significant influence on the mean wave period (increase by more than 10%) and the directional spreading (reduction of more than 10%) north of the barrier islands. However, in the Wadden Sea interior and at the Frisian coastline the influence of the reduction of triad strength is quite low. Along Curve A the mean period is increased by an average of only 0.8%.

4.7 Summary of model sensitivities

To summarise the model sensitivities discussed above, Table 4.1 presents an overview of the changes in model outcomes in terms of the four output parameters, per sensitivity test.

Category	Run code	Variation in input	Ray	H _{m0} (%)	T _{m-1,0} (%)	Dir (deg)	Dspr (%)
Offshore waves	C2BH1	Wave height +10%	A	0.00	-0.01	-0.01	0.01
	C2BH2	Wave height -10%	A	0.00	0.00	0.01	0.00
	C2BT1	Wave period +10%	A	0.00	-0.01	-0.01	0.01
	C2BT2	Wave period -10%	A	0.00	0.01	0.01	-0.02
	C2BD1	Mean direction +10°	A	0.00	-0.02	-0.01	-0.01
	C2BD2	Mean direction -10°	A	0.00	0.01	0.01	0.01
	C2BS1	Directional spreading +10°	A	0.00	-0.01	-0.01	-0.01
	C2BS2	Directional spreading -10°	A	0.00	0.02	0.02	0.01
	C5BH1	Wave height +10%	A	0.00	0.00	0.00	0.00
	C5BH2	Wave height -10%	A	0.00	0.00	0.00	0.00
	C5BT1	Wave period +10%	A	0.00	-0.02	-0.01	0.00
	C5BT2	Wave period -10%	A	0.00	0.02	0.02	0.00
	C5BD1	Mean direction +10°	A	0.00	0.00	0.00	0.00
	C5BD2	Mean direction -10°	A	0.00	-0.01	0.00	0.01
	C5BS1	Directional spreading +10°	A	0.00	0.00	0.00	0.00
	C5BS2	Directional spreading -10°	A	0.00	-0.01	0.00	0.01
Flow fields and water level	C1FC1	Flood case, current off	B	0.12	10.70	0.82	-1.19
	C3FC2	Ebb case, current off	B	-0.41	-2.79	-3.58	0.55
	C5FL1	Uniform water level +1m	A	24.05	15.21	-1.57	1.93
Wind input	C2WS1	Wind speed +10%	A	4.89	0.95	0.45	-0.15
	C2WS2	Wind speed -10%	A	-6.04	-1.98	-0.66	-1.44
	C2WD1	Wind direction +10%	A	-0.08	0.55	10.01	-1.33
	C2WD2	Wind direction -10%	A	0.25	-0.33	-10.25	-0.49
	C2WH1	HIRLAM downscaled	A	0.64	0.25	3.31	-0.61
Physics	C2PW1	Wind input function, cut-off 1	A	-1.05	2.11	0.23	0.73
	C2PW2	Wind input function, cut-off 2	A	-7.65	4.20	1.28	6.62
	C2PS5	Bottom friction -50%	A	4.03	7.27	1.00	0.51
	C2PS6	Depth breaking -50%	A	3.24	1.53	-0.62	-0.60
	C2PS7	Triad interaction -50%	A	0.04	0.22	0.00	-0.02
	C4PS5	Bottom friction -50%	C	1.01	2.30	1.18	-1.19
	C4PS6	Depth breaking -50%	C	7.45	2.01	-0.38	-0.07
	C4PS7	Triad interaction -50%	C	0.20	1.29	0.05	-0.07
	C5PS5	Bottom friction -50%	A	0.68	2.27	2.73	1.13
	C5PS6	Depth breaking -50%	A	6.10	5.44	-0.65	1.59
C5PS7	Triad interaction -50%	A	0.05	0.80	0.82	1.20	

Table 4.1: Overview of the changes in model outcomes $(\text{Value}_{\text{variation}} - \text{Value}_{\text{Base}})/\text{Value}_{\text{Base}}$ per sensitivity test, given as average values along the indicated output ray.

5 Conclusions

In this study, the sensitivity of model outcomes of SWAN were investigated to variations in model input and model settings, with the focus on the primary sea defences along the Frisian coast behind the Ameland Zeegat. Sensitivities were studied both for observed severe NW storms and hypothetical extreme storms from NW and SW. Regarding model input, variations in offshore wave boundary conditions (significant wave height, mean period, mean direction and directional spreading), variations in wind input (speed, direction and spatial variability), and the effect of currents and water level were considered. Regarding model settings, the influence of limiting the amount of wind energy transfer to young waves, and variations in the strength of shallow water source terms were investigated. These sensitivities were studied using spatial difference plots and by comparing integral parameters and wave spectra along output curves. All sensitivity tests were considered in stationary simulation mode, and the model sensitivity to nonstationary input fields was not considered. The average of the computed model responses along the output curves A, B and C are presented in Table 4.1 above.

The following conclusions can be drawn from this investigation, which are limited to the conditions investigated here:

- Analysis of the base cases shows that the wave field in the Wadden Sea behind the Ameland Zeegat is locally generated by wind, under depth-limited conditions. For the historical severe storms, depth limitation is significant at the ebb tidal delta, dissipating a substantial amount of wave energy arriving from the North Sea. Inside the Wadden Sea, locally generated waves dominate, but along the Frisian coast wave conditions are restricted by the shallow water wave growth limit. For the hypothetical extreme storms, for which the wind forcing is more than twice as strong, the shallow water wave growth limit exists over almost the entire Wadden Sea interior. Closer to the coast, saturated surf zone conditions exist, which further limits the simulated wave heights.
- Considering the variations in model input investigated, the sensitivities can be summarised as follows: the largest model responses were observed for an increase in water level, the inclusion of current effects, changes in the uniform wind field (speed and direction) and the modelling of wind input. Concerning shallow water source terms, the model is the most sensitive to bottom friction where the shallow water growth limit has not been reached fully, and the most sensitive to depth-induced breaking where this growth limit has indeed been reached. The analysis showed that conditions at the Frisian coast are not very sensitive to wave conditions imposed at the North Sea boundary, to the use of downscaled HIRLAM wind fields (as opposed to spatially uniform fields) and to triad wave interaction. We note that the outcome that simulated wave conditions at the Frisian coast is more sensitive to local winds than to offshore wave conditions suggests that, in determining wave conditions here, the uncertainty in the wind input dominates over the uncertainty in the offshore wave input.
- Wave conditions along the primary sea defence of the Frisian coast behind the Ameland Zeegat are insensitive to variations in wave boundary conditions

imposed on the North Sea side of the barrier islands. Variations of 10% in the significant wave height and period, and 10° in the mean direction and directional spreading at the boundary leads to changes of only up to 0.02% in the significant wave height, mean period and directional spreading, and up to 0.02° in the mean direction. This insensitivity is due to the saturated conditions that exist in the surf zone on the ebb tidal delta, in which wave energy is significantly dissipated. This result is in agreement with the finding of Alkyon (2007a,b) that the Wadden Sea region forms a separate wave system from that found on the North Sea side of the barrier island, and is largely unaffected by the latter.

- The inclusion of ebb and flood currents strongly influence wave characteristics along the main tidal channel in the tidal inlet. Under flood currents, significant wave heights and mean periods decrease by up to 50% in the model, whereas they increase under ebb current by about 25%. Currents also influence on wave directions and spreading by up to about 15° and 10% respectively, presumably through current-induced refraction. For the conditions considered, the foreshore at the primary sea defence was saturated, strongly reducing the response of the wave heights at the dyke. Here the inclusion of currents results in a difference in the significant wave height of less than 0.5%. However, average changes in the mean period of up to 10.7% and in the wave direction of up to 3.6° are found here.
- Wave conditions at the primary sea defence are very sensitive to an increase in water level during an extreme NW storm. When the water level was increased by 1 m to +5.7 m NAP, wave heights and mean periods were found to increase by 24% and 15.2% respectively. This increase is in no significant way due to the entering of low-frequency energy from the North Sea. Rather, the increase in the values of these parameters is due to the higher asymptote value of the shallow water wave growth limit, and the fact that the saturated conditions along the foreshore allow a higher wave height at the primary sea defence.
- Variations in wind speed and direction by 10% and 10° respectively have a large impact on the wave conditions in the Wadden Sea interior, with H_{m0} increasing in excess of +10%, $T_{m-1,0}$ by up to 5% and mean wave direction by about 10° . However, at the primary sea defence beyond the surf zone, these variations in wave height and period are only felt along those stretches where steep, non-saturated foreshores are found. Where the foreshore is saturated, the resulting variation in significant wave height is mostly removed by depth-induced breaking. By contrast, a variation in the direction of the wind results in an almost equal variation in the mean wave direction, which is also found in the wave conditions at the primary sea defence.
- The use of a spatially varying downscaled wind field results in a reduction of wave height of up to 20% at the lee of the barrier islands, but this influence dies away in the background wind sea growth before the primary sea defence is reached. However, the spatially varying downscaled wind field differs from the uniform wind field also in terms of wind direction. The resulting difference in wave direction alters the wave direction at the sea defence by an average of 3.3° .

- The limitation in the amount of energy transfer from the wind to the waves at young wind seas only significantly affects wave heights and periods at the lee of the barrier islands. This limitation has little influence on conditions at the mainland primary sea defence.
- Regarding shallow water source terms, the proportionality coefficients of all three processes were reduced by 50%, corresponding to their uncertainty range. Given this variation, the model outcomes at the primary sea defences at the Frisian coast and at the head of Ameland are generally the most sensitive to depth-induced breaking, and are insensitive to nonlinear triad interaction. However, the sensitivity of model results along the sea defences depends on the storm condition considered. Where conditions are such that the shallow water growth limit is not reached over the entire Wadden Sea interior (e.g. the NW historical storm), model results are also sensitive to the reduction in bottom friction, which increases significant wave height by 4% and the mean wave period by 7.3%. In situations where the shallow water growth limit is reached (e.g. NW and SW storms), however, model results at the sea defence are the most sensitive to depth-induced breaking. For these situations, a reduction in the depth-induced breaking magnitude increases significant wave height by up to 6.1% and the mean wave period by up to 5.4%.

6 Recommendations

From the results of the sensitivity study, and from the conclusions drawn in Section 5, the following recommendations are made:

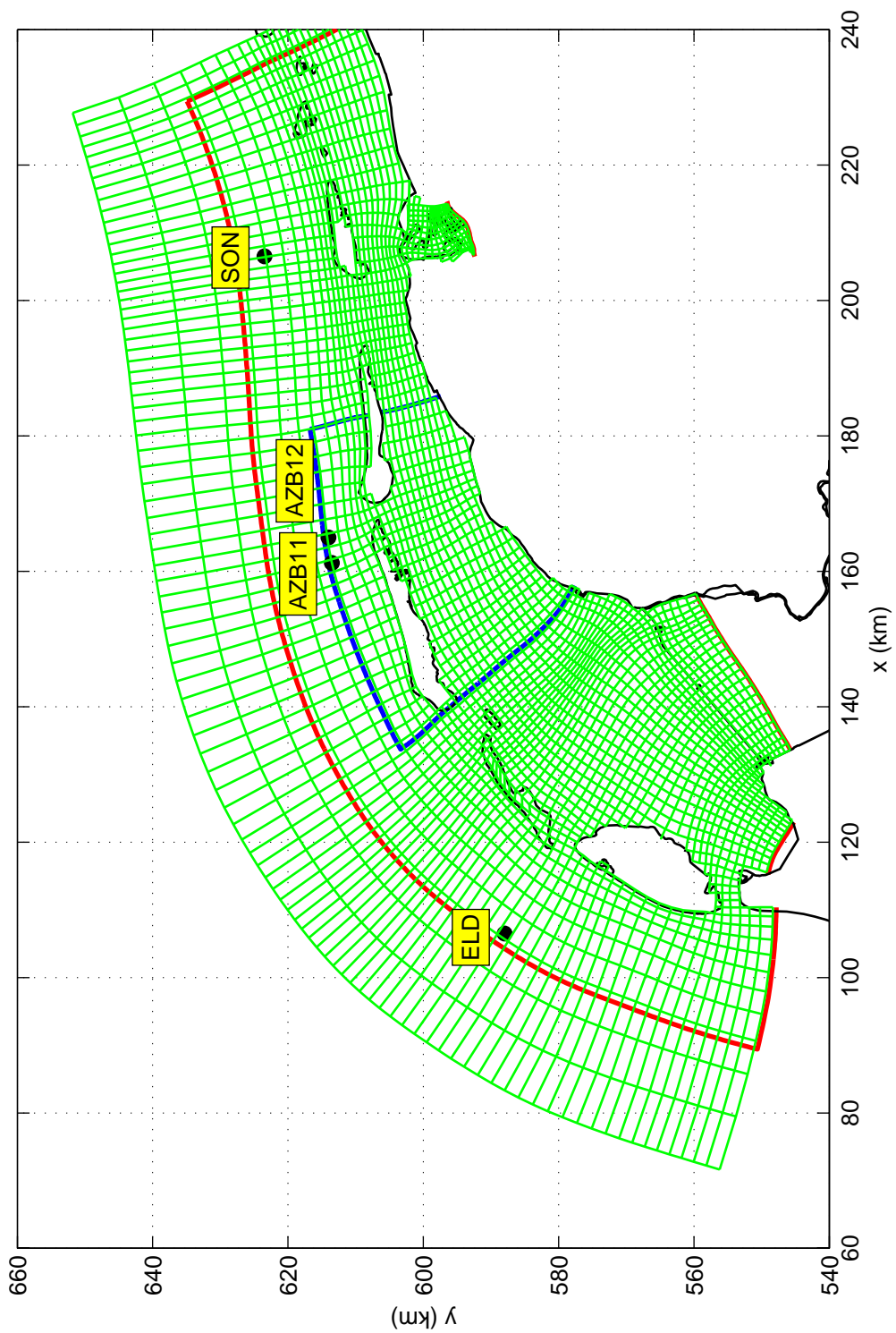
- In this study the sensitivity of SWAN to a number of model inputs and settings were investigated, to obtain a first estimate of the importance of these parameters to model results along the primary sea defences of the Wadden Sea. Although in the variation of model inputs it was attempted to apply physically reasonable values, no account was taken of the probability of occurrence of a particular input value. By combining the sensitivity to each input with its band of uncertainty, a ranking of priority of input values can be compiled. It is therefore recommended to extend this study with an uncertainty analysis in which the stochastic nature of the model inputs is taken into account, as is planned within the greater 'SBW-RVW Waddenzee' project (see WL 2006a).
- Analysis of the base cases considered in this study show that, according to SWAN, the shallow water wave growth limit (e.g. Bretschneider 1958 and Young and Verhagen 1996) is reached over (at least parts of) the Wadden Sea and that saturated surf zone conditions exist along (at least parts of) the Frisian coast. This growth limit was shown to result in an insensitivity of wave conditions, in particular wave heights, in front of the primary sea defences to many model inputs and settings in SWAN. It is therefore important to determine whether the growth limit and saturated conditions that are predicted by SWAN actually do occur in nature. It is therefore recommended to verify the existence of these phenomena along the Frisian coast behind the Ameland tidal inlet, by analysis of wave buoy and water depth observations made during historic storms.
- Given that an analysis of the observations show that growth limit and saturated conditions exist, it is essential to verify the accuracy of SWAN results under these conditions (the shallow water growth limit). De Waal (2002) suggested that SWAN underestimates this growth limit, which would lead to unconservative wave height estimates along the primary sea defences. It is recommended to verify, and if necessary, improve the modelling of the shallow water growth limit in SWAN.
- According to the results of SWAN, the Frisian coast behind the Ameland tidal inlet becomes saturated during severe storms. However, it is plausible that at places in the Wadden Sea where the tidal inlets are wider, and where the foreshore is steeper (e.g. when the tidal channel runs close to the mainland), saturated conditions may not occur and greater model sensitivity, in particular in wave heights, than that demonstrated in this study would be found. It is therefore recommended to verify the existence of saturated areas at other locations along the Wadden Sea coastline, and hence to determine the generality of the sensitivity results presented here.
- Assuming that growth limit and saturated conditions exist in front of large parts of the Wadden Sea coastline during design conditions, accurate estimation of the total water depth in front of the sea defence for these conditions becomes crucial. It is recommended to verify and, where necessary, improve the modelling of water levels and the estimation of the bathymetry for design conditions.

- Under historical severe storm conditions, currents were shown to have an influence on mean wave periods and wave directions at the primary sea defences, even under saturated conditions. It is recommended to extend the sensitivity analysis to also include the effect of currents on wave conditions during extreme storm conditions.
- Given the sensitivity of model results to wave-current interaction, it is recommended to verify and, if necessary, improve the modelling of this process in SWAN.
- This and earlier studies have shown that wave conditions at the primary sea defences are determined by local wave generation in the Wadden Sea. This study demonstrated that simulated wave directions at the sea defences are very sensitive to directional information in the imposed wind fields. It is therefore recommended to ensure high accuracy in the wind directional information used in SWAN, which may necessitate the use of spatially non-uniform wind fields.

References

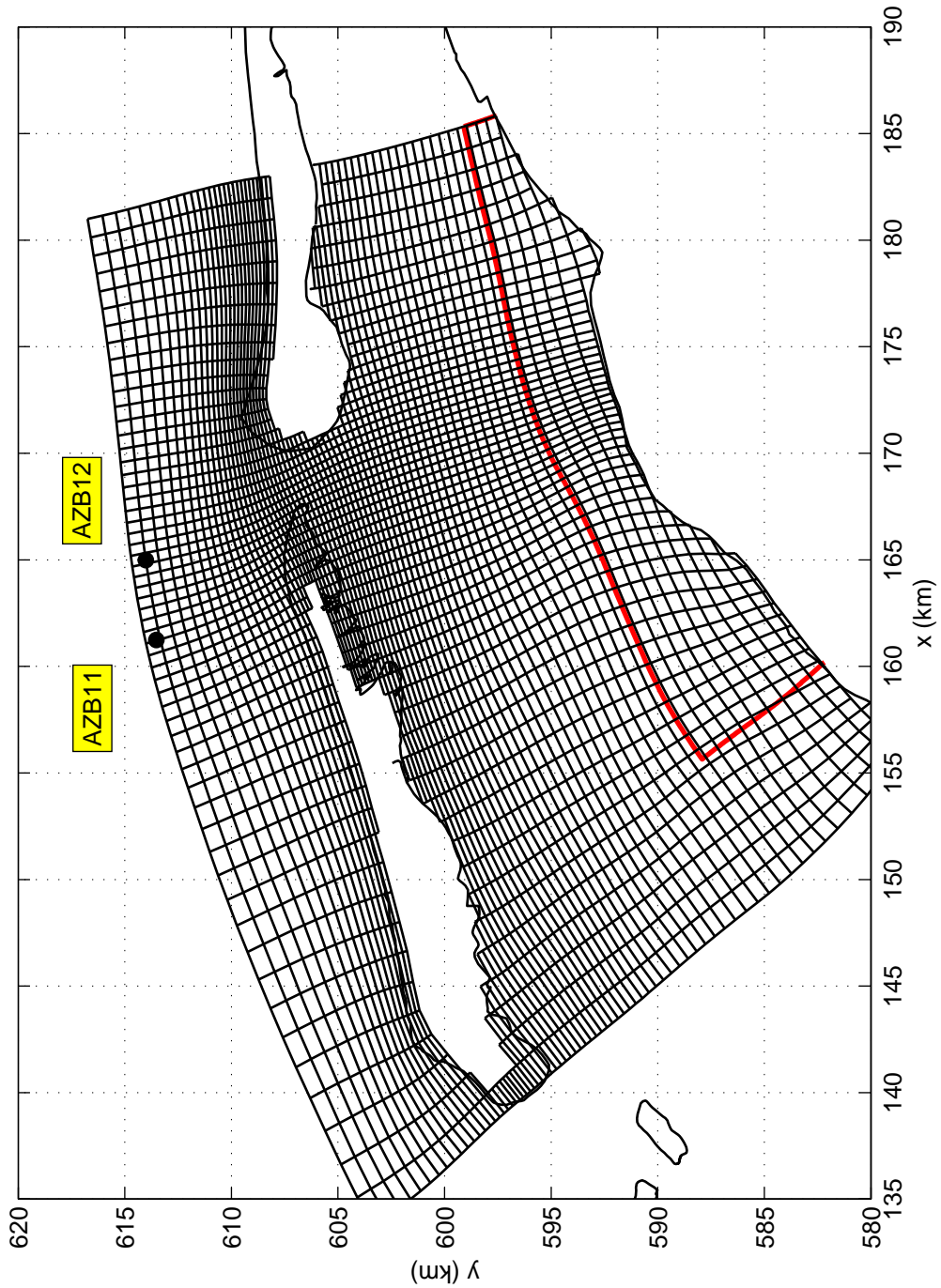
- Alkyon (1999). Wave computations in the Waddenzee. Alkyon report A352, November 1999.
- Alkyon (2007a). Analysis SWAN hindcast tidal inlet of Ameland: Storms of 8 February 2004 and 2, 8 January 2005. Alkyon report A1725, February 2007.
- Alkyon (2007b). Analysis SWAN hindcast tidal inlet of Ameland: Storms of 17 December 2005 and 9 February 2006. Alkyon report A1725, February 2007.
- Bretschneider (1958). Revisions in wave forecasting: Deep and shallow water, Proc. 6th Conf. on Coastal Eng., ASCE, Council on Wave Research.
- Booij, N., R.C. Ris and L.H. Holthuijsen (1999). A third generation wave model for coastal regions, Part I, Model description and validation. *J. Geophys. Res.*, 104, C4, 7649-7666.
- Donelan, M.A., A.V. Babanin, I.R. Young and M.L. Banner (2006). Wave-follower field measurements of the wind-input spectral function. Part II: Parameterization of the wind input. *J. Phys. Oceanogr.*, 36, 1672-1689.
- Royal Haskoning (2006). Hindcast Tidal inlet of Ameland. Storms of 17 December 2005 and 9 February 2006. Report Royal Haskoning 9S2639.A0. December 2006.
- Taylor, P.A., R.J. Lee, (1984). Simple guidelines for estimating wind speed variations due to small-scale topographic features. *Climatol. Bull.*, Vol. 18, 3-32.
- Van Vuren (2005). Stochastic modelling of river morphodynamics, Ph.D. Thesis, Delft University of Technology, the Netherlands.
- Verkaik, J.W. (2006). On wind and roughness over land. Ph.D. Thesis, University of Wageningen, the Netherlands.
- Verkaik, A.W., A.J.M. Jacobs, A.B.C. Tijm, and J.R.A. Onvlee (2006). Local windspeed estimation by physical downscaling of weather model forecasts. Submitted to *J. Wind Engineering and Industrial Aerodynamics*.
- Waal, J.P. de (2002). Wave growth limit in shallow water, Proc. 4th Int. Conf. on Ocean Waves (WAVES2001), San Francisco, 580-589.
- WL (2003). Wave growth limit in shallow water. WL | Delft Hydraulics Report H4173, July 2003.
- WL (2004). Golfstatistiek op relatief diep water 1979-2002 (In Dutch). WL | Delft Hydraulics Report Q3770, November 2004.
- WL/Alkyon (2004). Identification of wave modelling improvements. WL | Delft Hydraulics / Alkyon Hydraulic Consultancy and Research Report H4301/A1183, March 2004.
- WL (2006a). Plan van Aanpak SBW Natuurrandvoorwaarden Waddenzee. WL | Delft Hydraulics Report H4750, March 2006.
- WL (2006b). Storm Hindcasts Norderneyer Seegat and Ameland Zeegat. WL | Delft Hydraulics Report H4803.11, August 2006.
- WL (2007a). Uncertainty analysis of Hydraulic Boundary Conditions of the Wadden Sea. WL | Delft Hydraulics Report H4918.31, June 2007.
- WL (2007b). Storm hindcast for Waddensea. WL | Delft Hydraulics Report H4918.20, August 2007.
- WL/RIKZ/Alkyon/NRL (2007). Sensitivity analysis of numerical aspects of SWAN. WL | Delft Hydraulics Report H4803.60, May 2007.
- Yan, L. (1987). An improved wind input source term for third generation ocean wave modelling. Technical report, Rep. No. 87-8, Royal Dutch Meteor. Inst.
- Young, I. R. and L. A. Verhagen (1996). The growth of fetch-limited waves in water of finite depth. Part 1. Total energy and peak frequency. *Coastal Engineering* 29, 47-78.

Figures



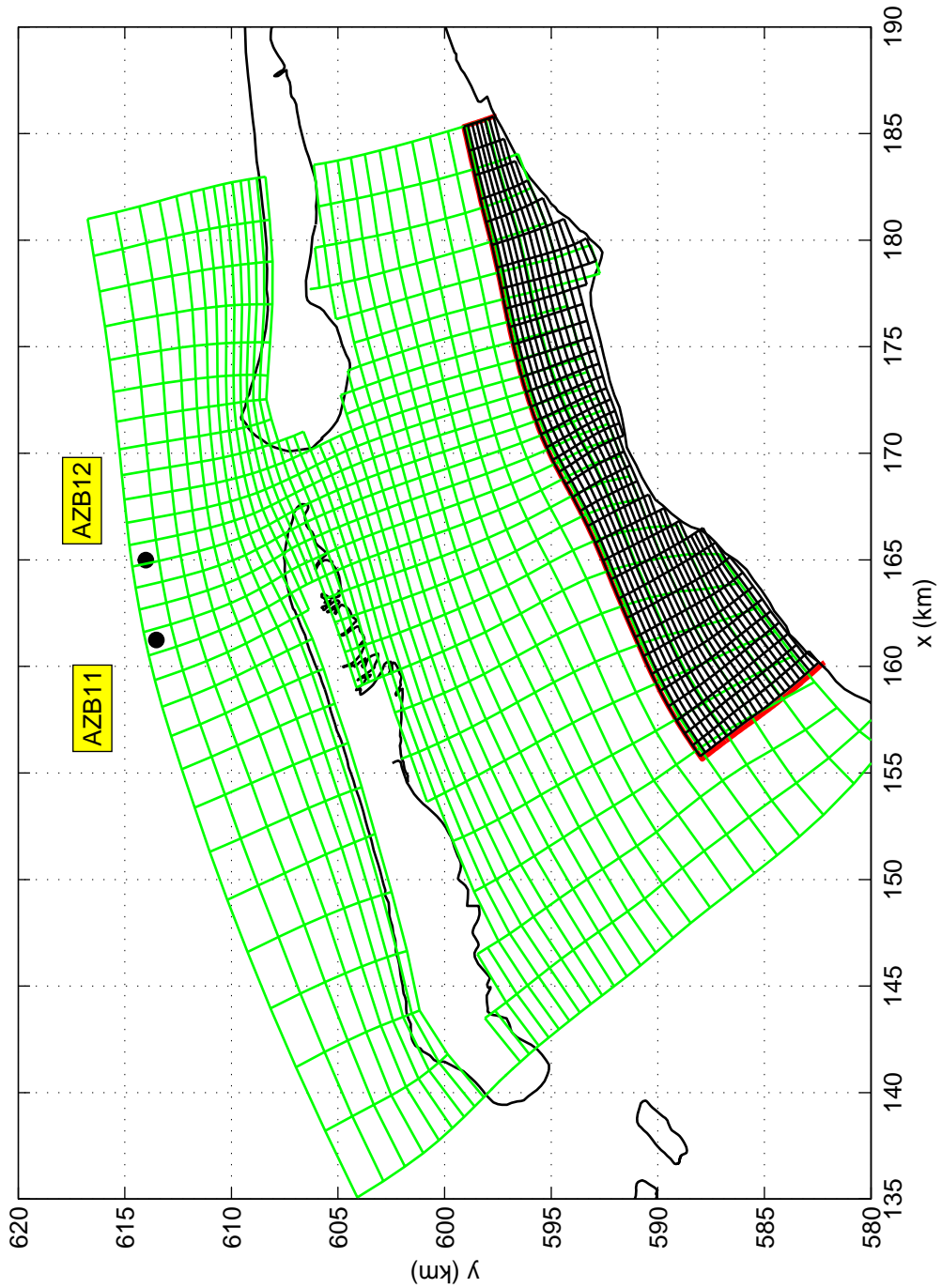
Grid lines of curvi-linear grid GridCL (every fourth line is shown)
 outline of grids NS2 (red) and AZG3A (green)
 Location of wave buoys ELD, SON, AZB11 and AZB12

Ameland



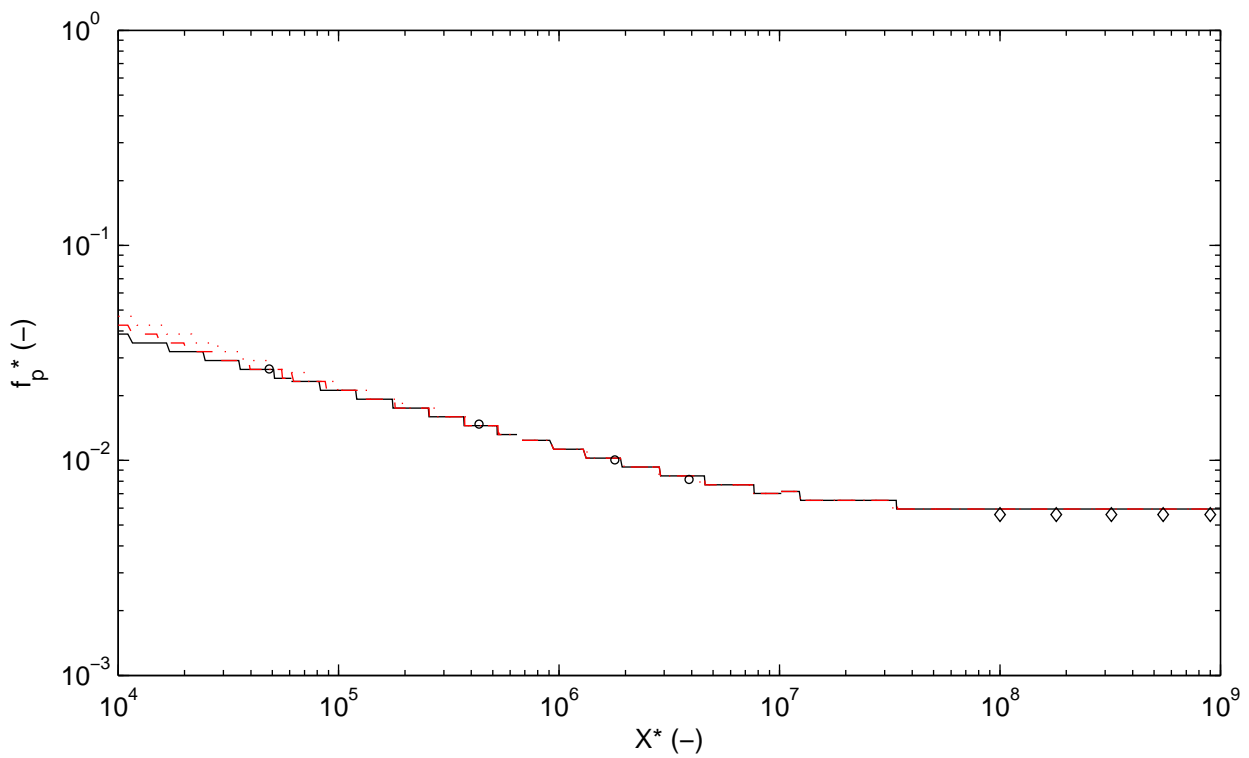
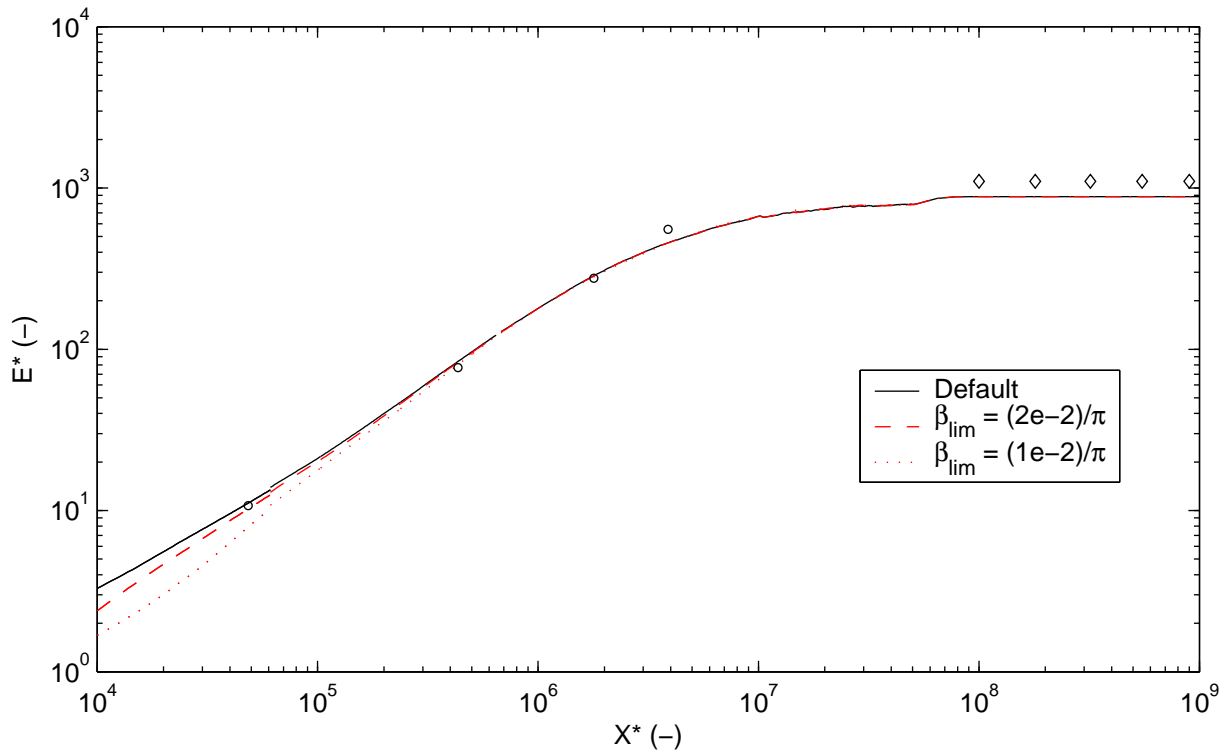
Grid lines of curvi-linear grid AZG3A (every fourth line is shown)
 outline of grid AK4A (red)
 Location of wave buoys AZB11 and AZB12

Ameland



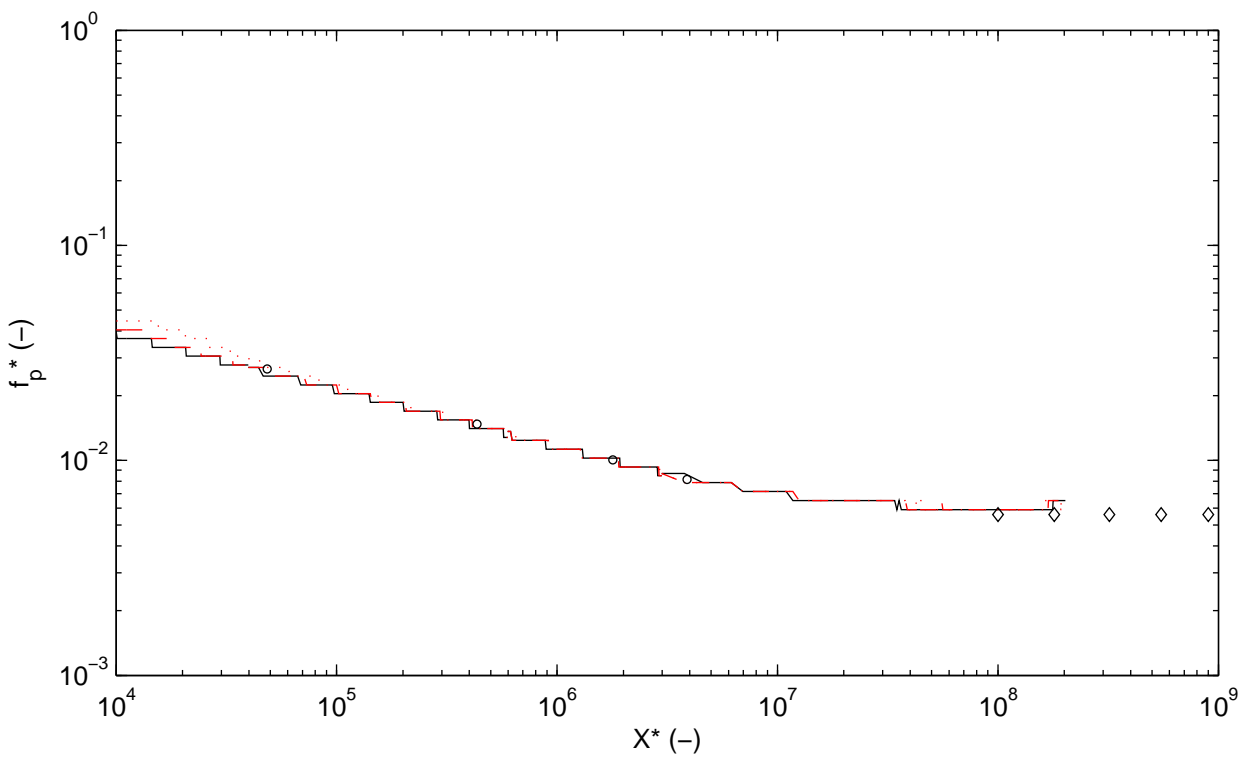
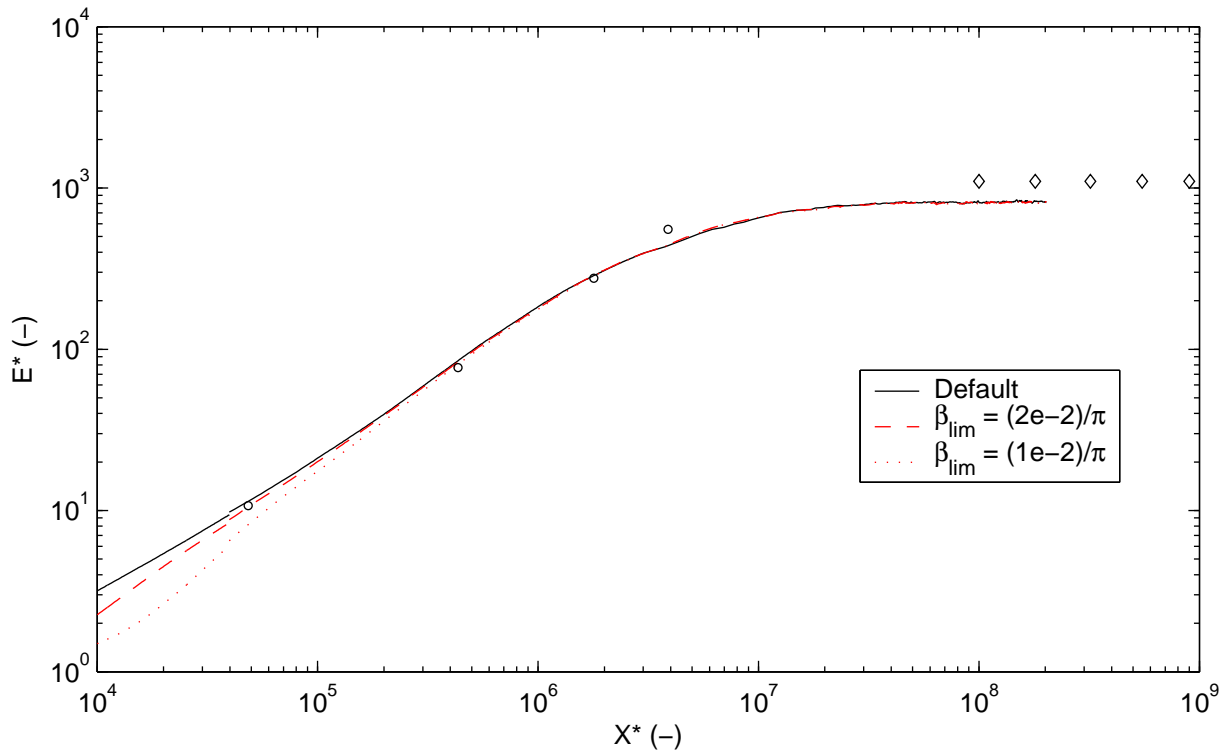
Grid lines of curvi-linear grid AK4A (every fourth line is shown)
 outline of grid AZG3A (green)
 Location of wave buoys AZB11 and AZB12

Ameland



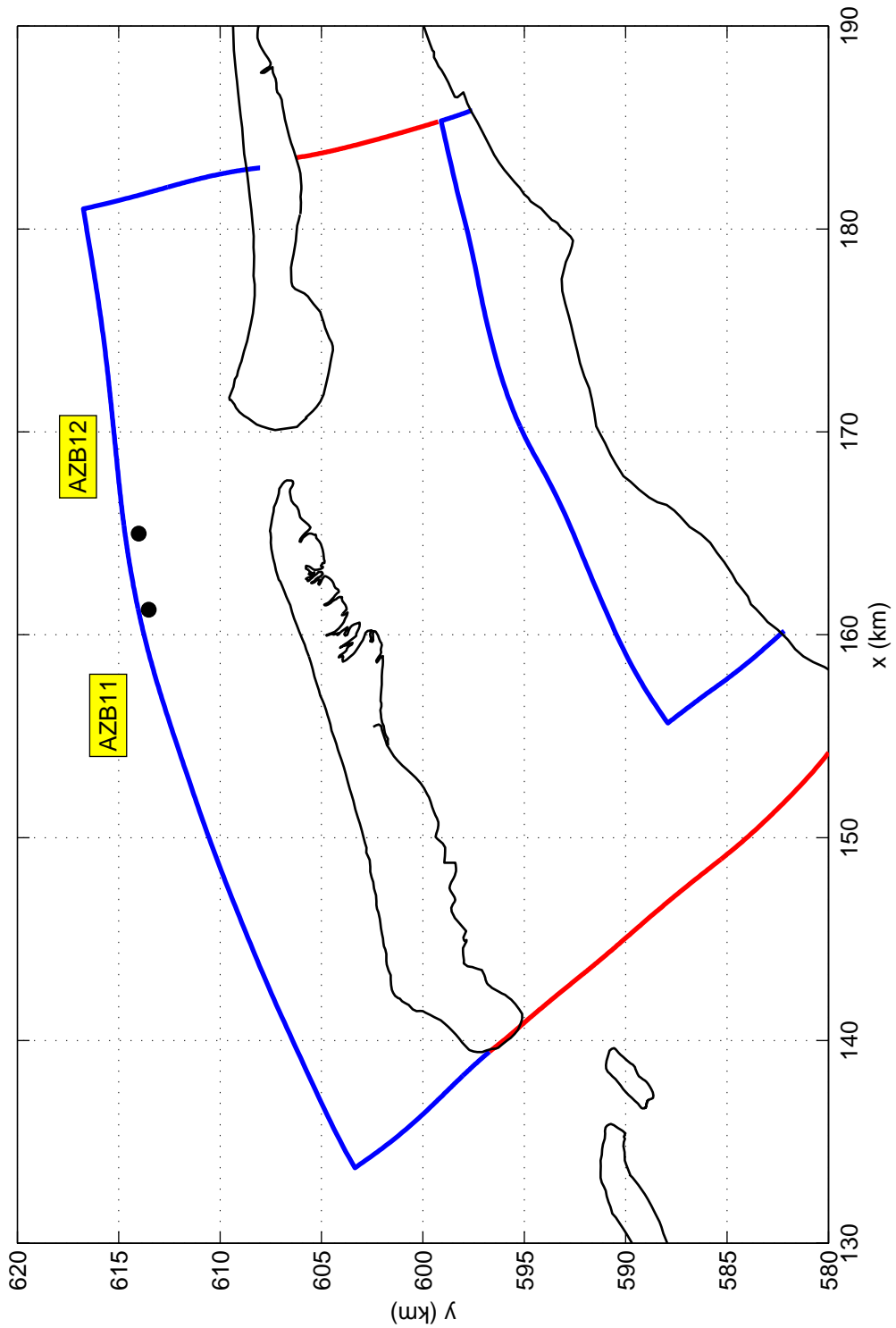
Effect of wind input limitation on fetch-limited growth curves
Results for $U_{10} = 10$ m/s

Ameland



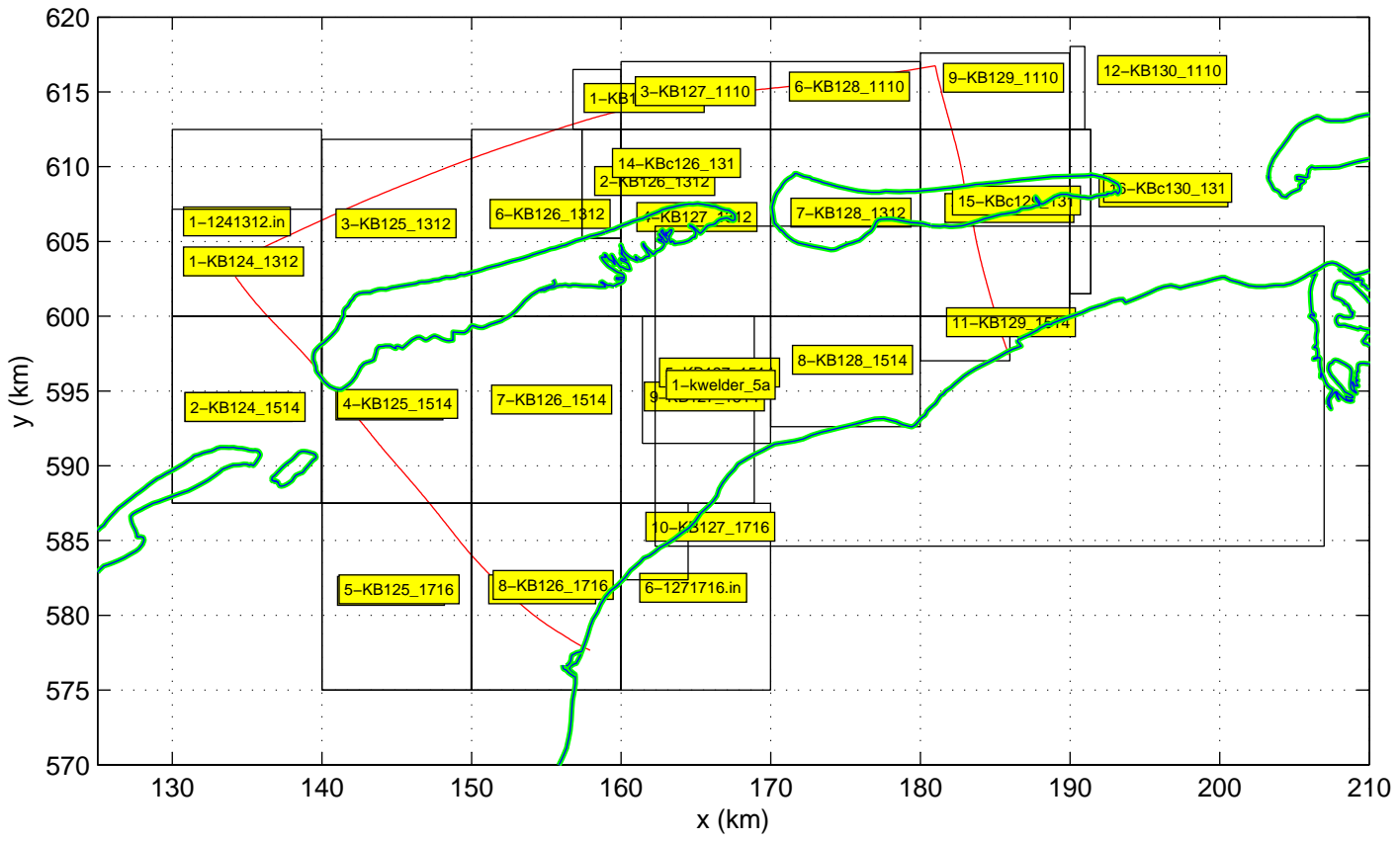
Effect of wind input limitation on fetch-limited growth curves
Results for $U_{10} = 30$ m/s

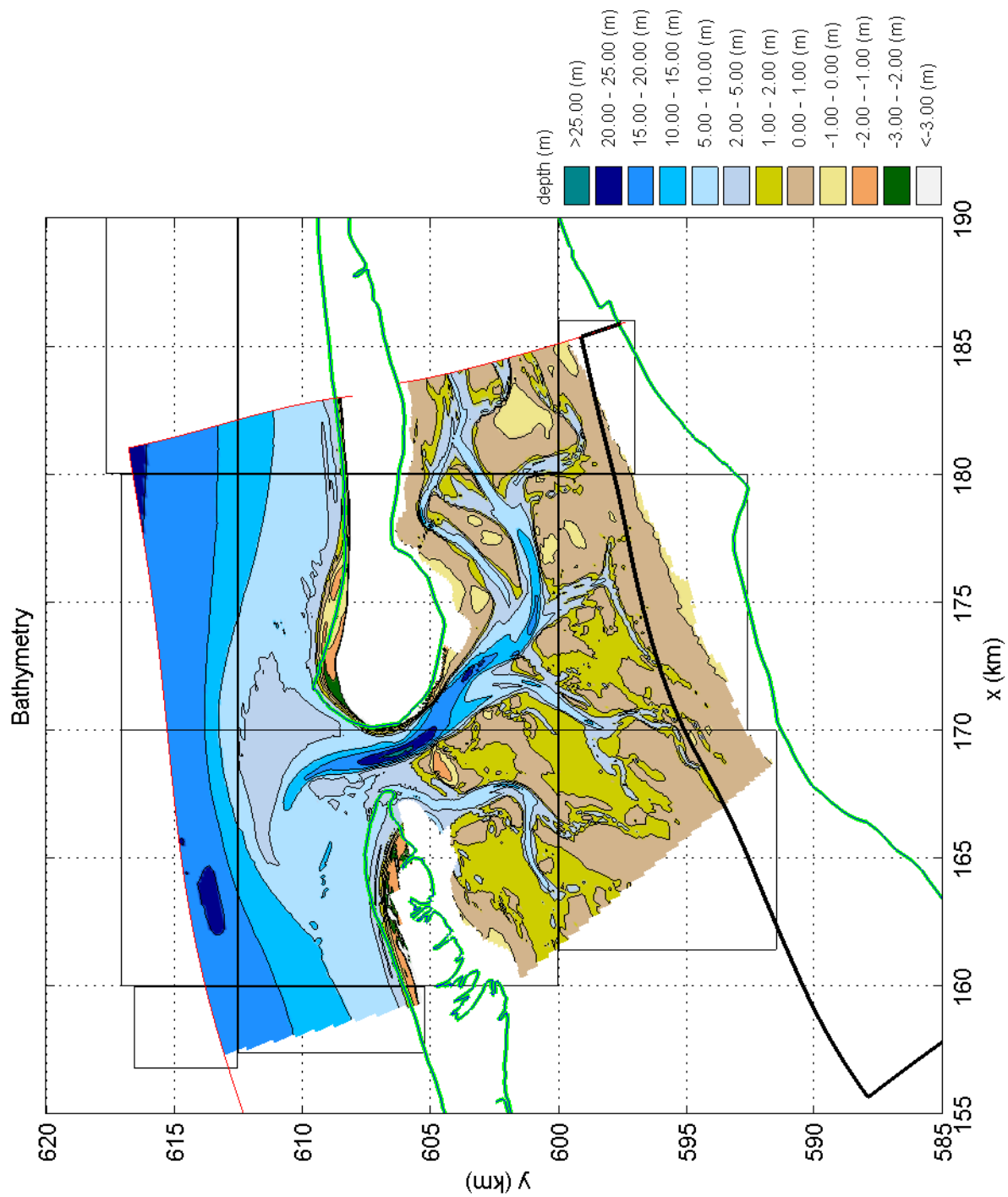
Ameland



Origin of boundary conditions for AZG3A:
 AZB11 and AZB12 (blue), and NS2 (red)

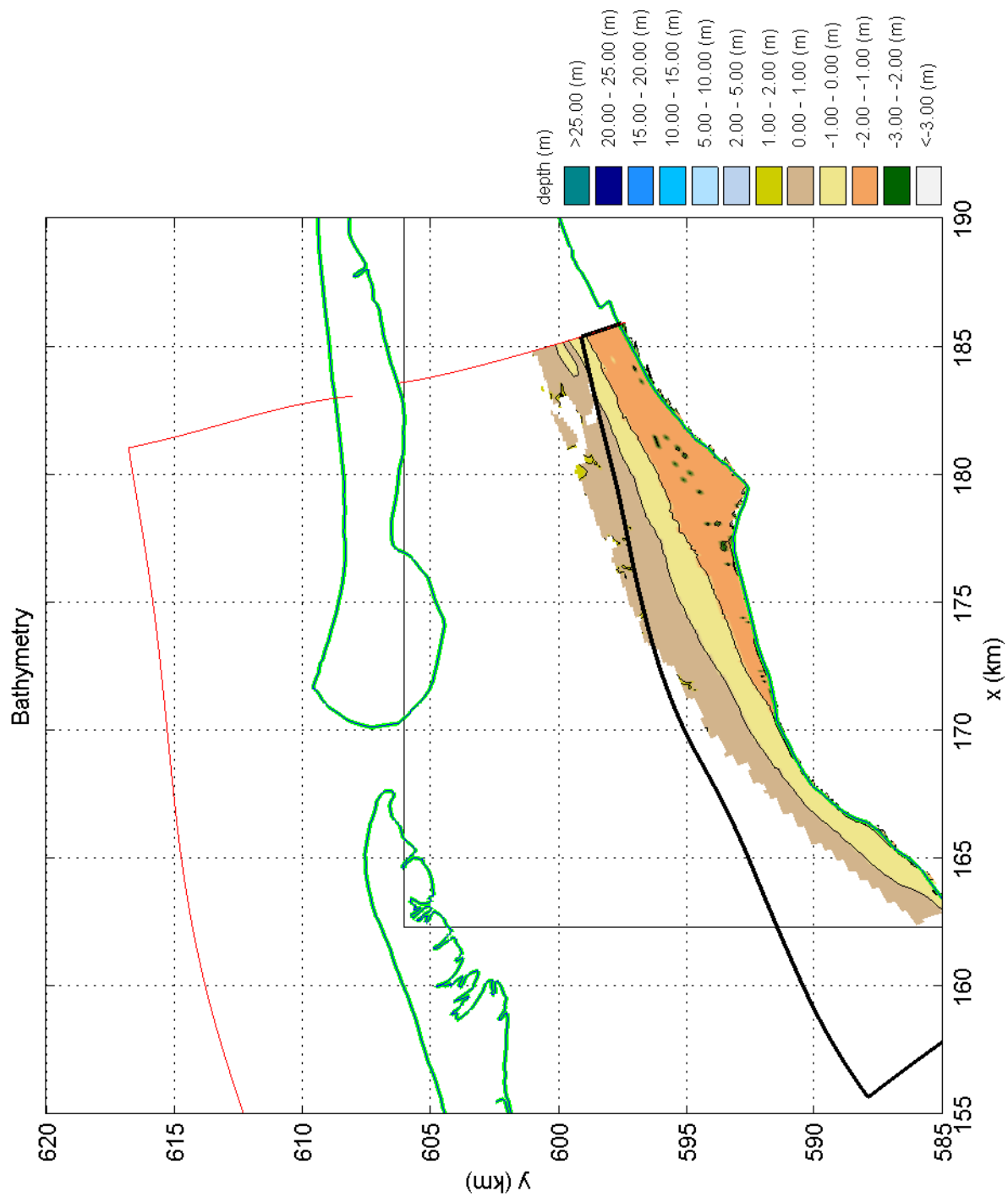
Ameland





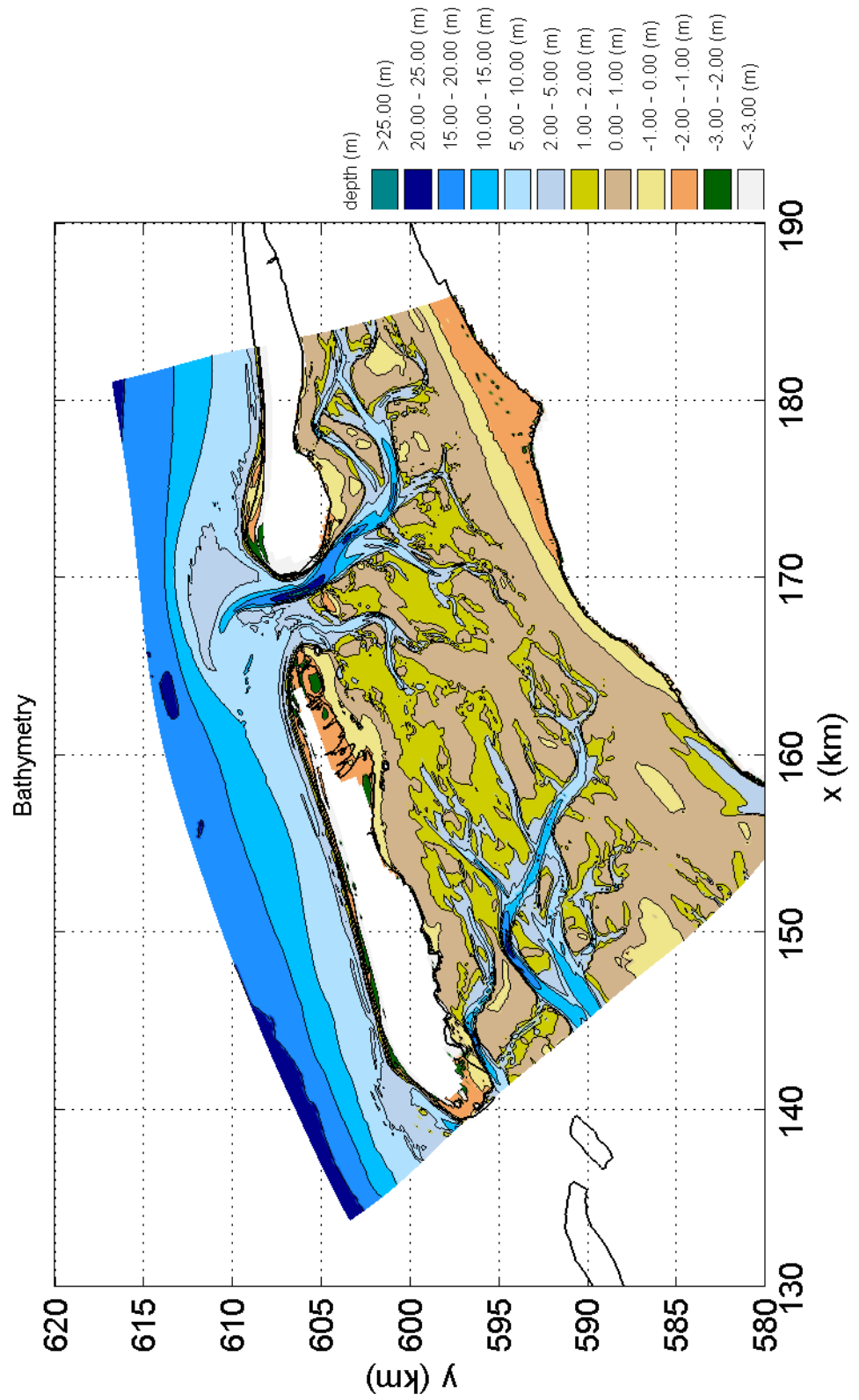
Outline of bottom data files used for construction of bathymetry for tidal inlet of Ameland based on AZG2004 data outline of grid AZG3A (red), grid AK4A (black)

Ameland



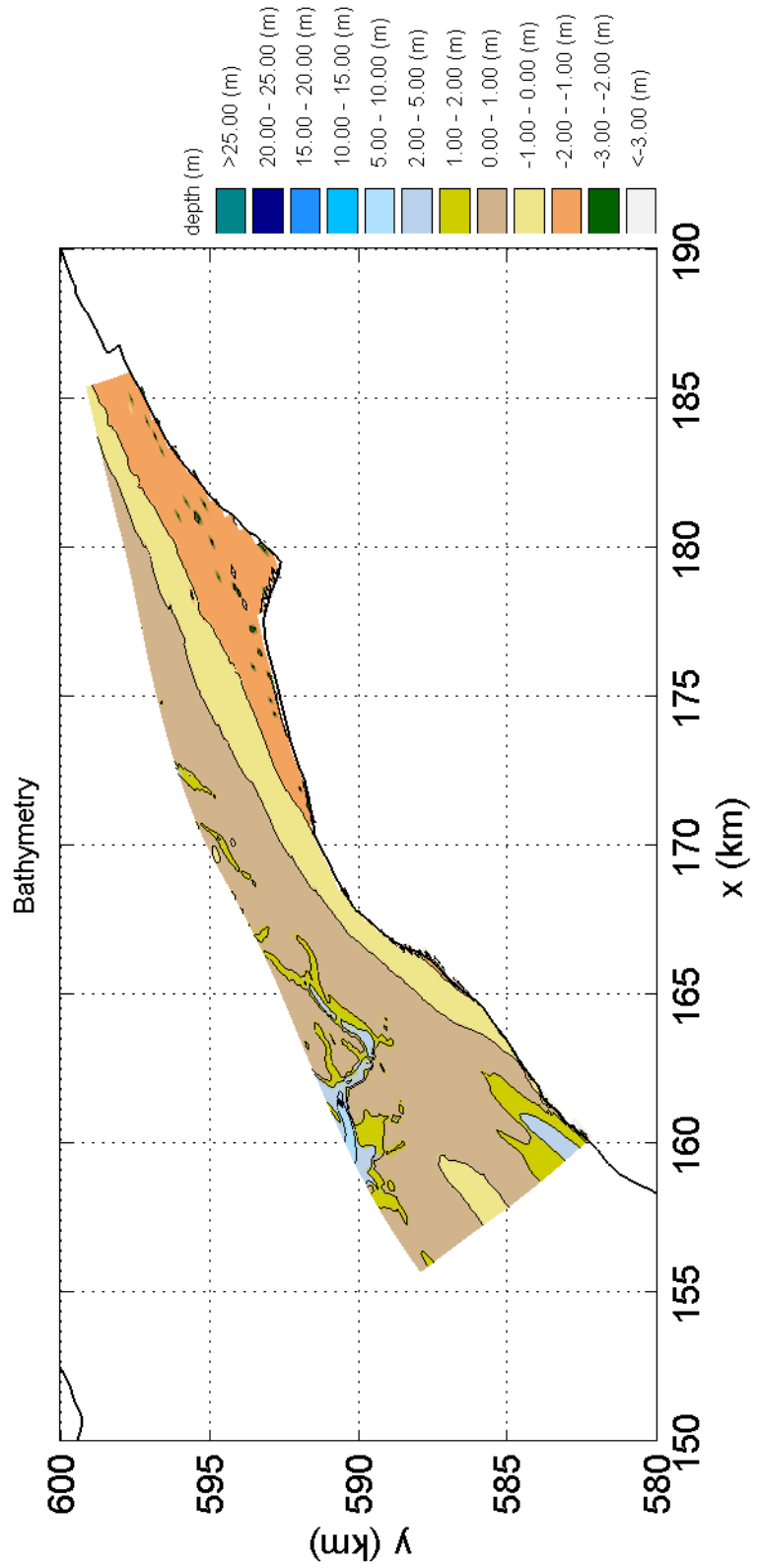
Outline of bottom data files used for construction of bathymetry for tidal inlet of Ameland based on kwelder data outline of grid AZG3A (red), grid AK4A (black)

Ameland



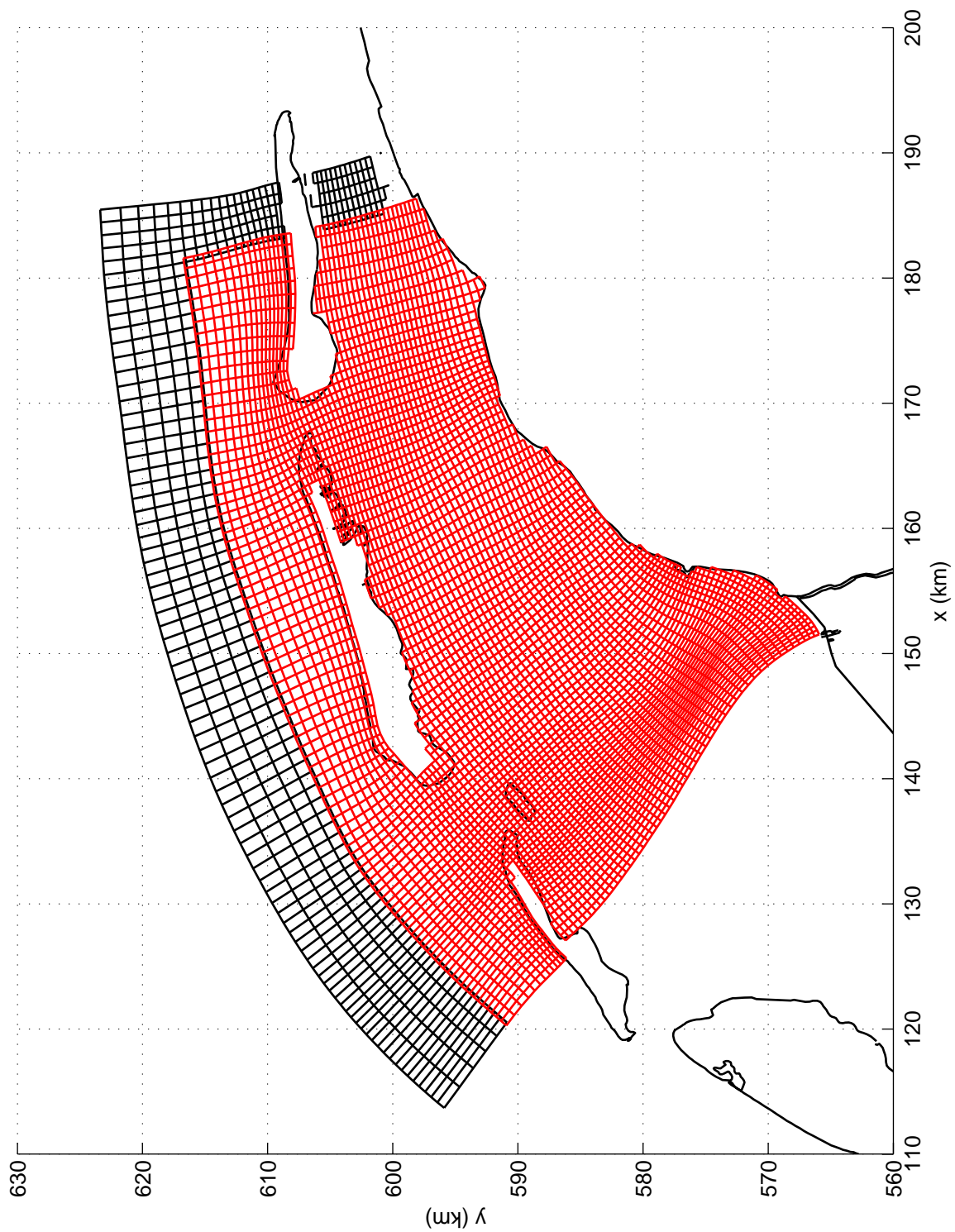
Bathymetry on computational grid AZG3A

Ameland



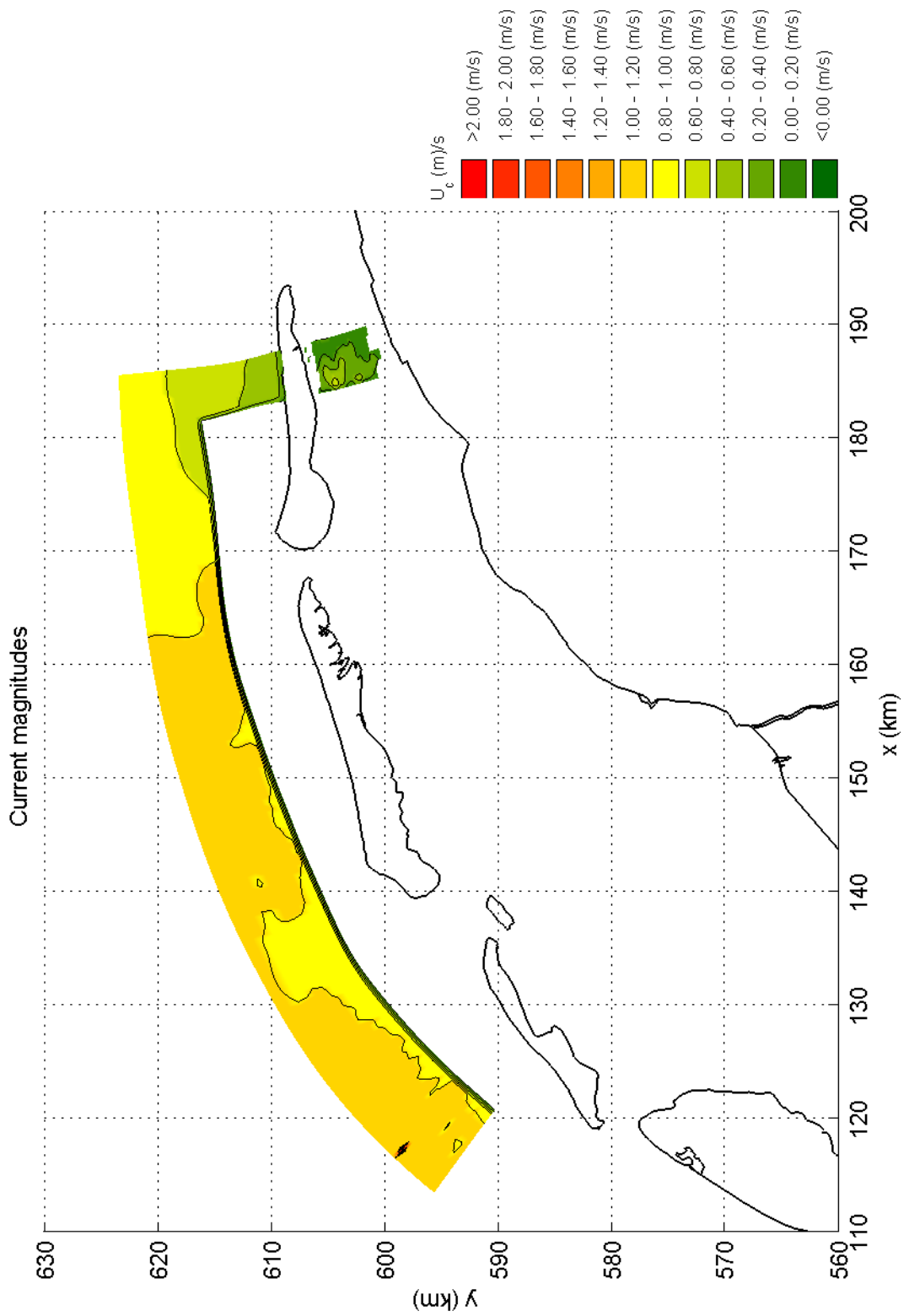
Bathymetry on computational grid AK4A

Ameland



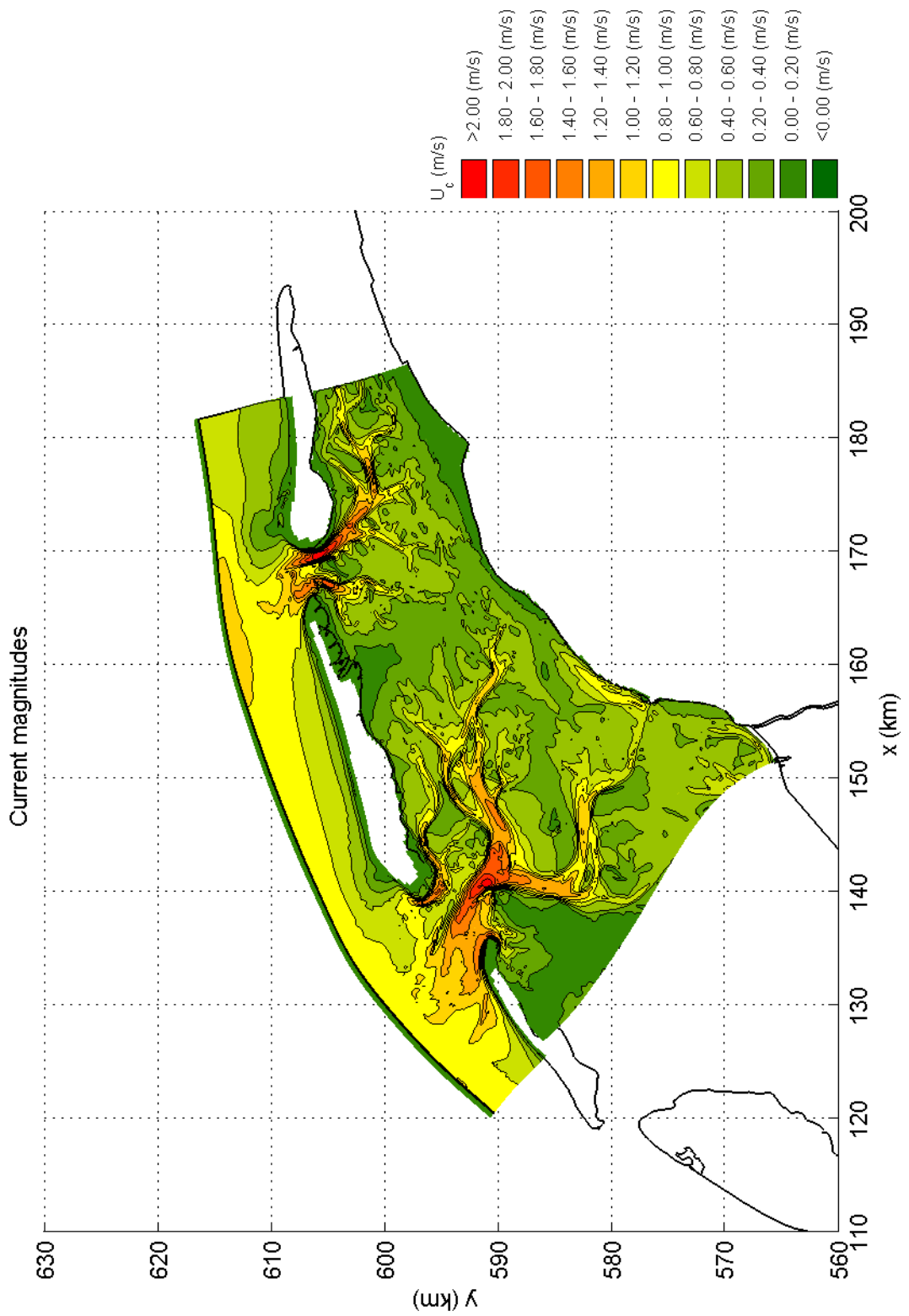
Outline of WAQUA grids
 AZG (black, every second line), WAW (red, every fifth line)

Ameland



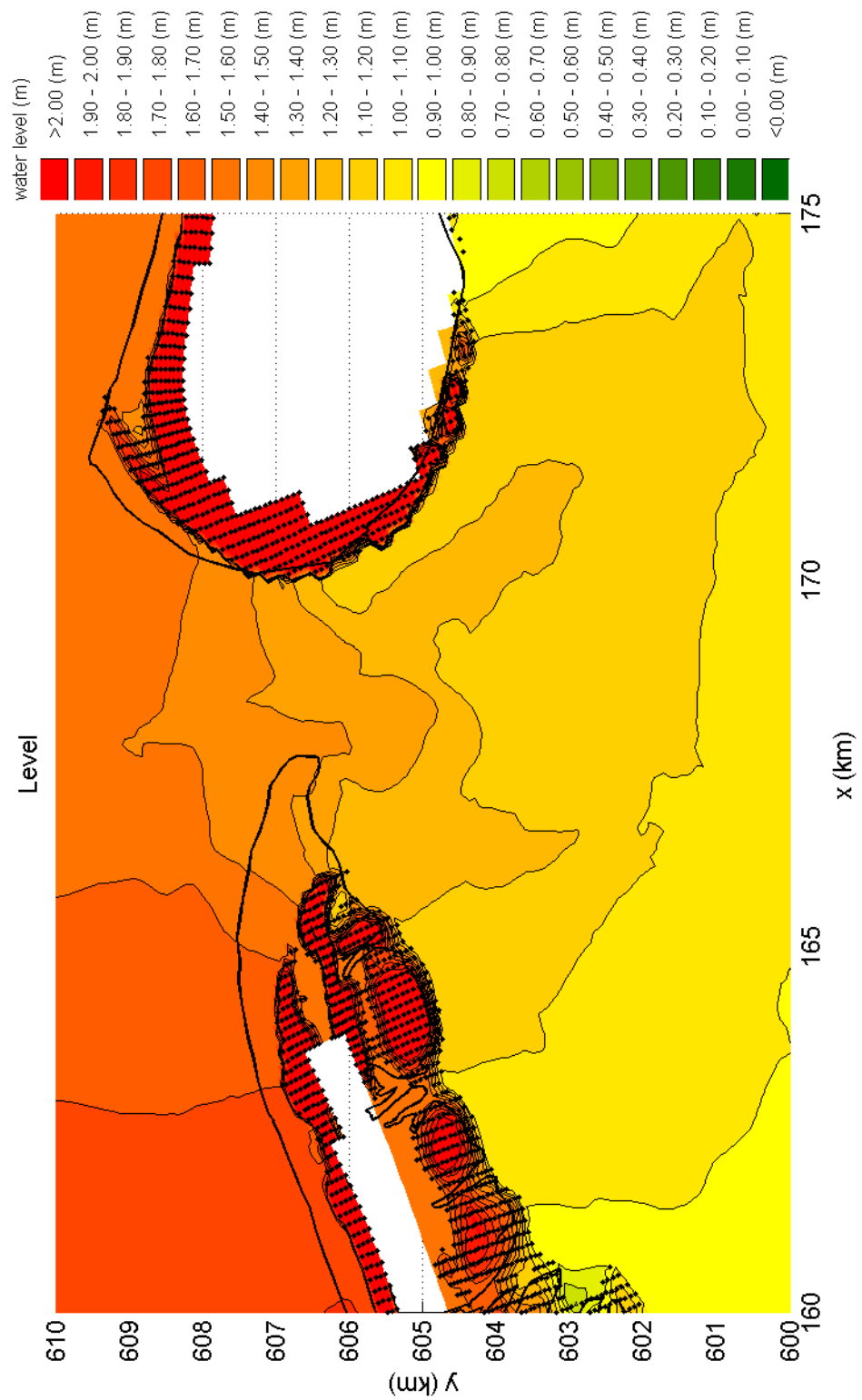
Spatial variation of current magnitude on AZG grid
for 8 Feb. 2004, 20:00 hours

Ameland



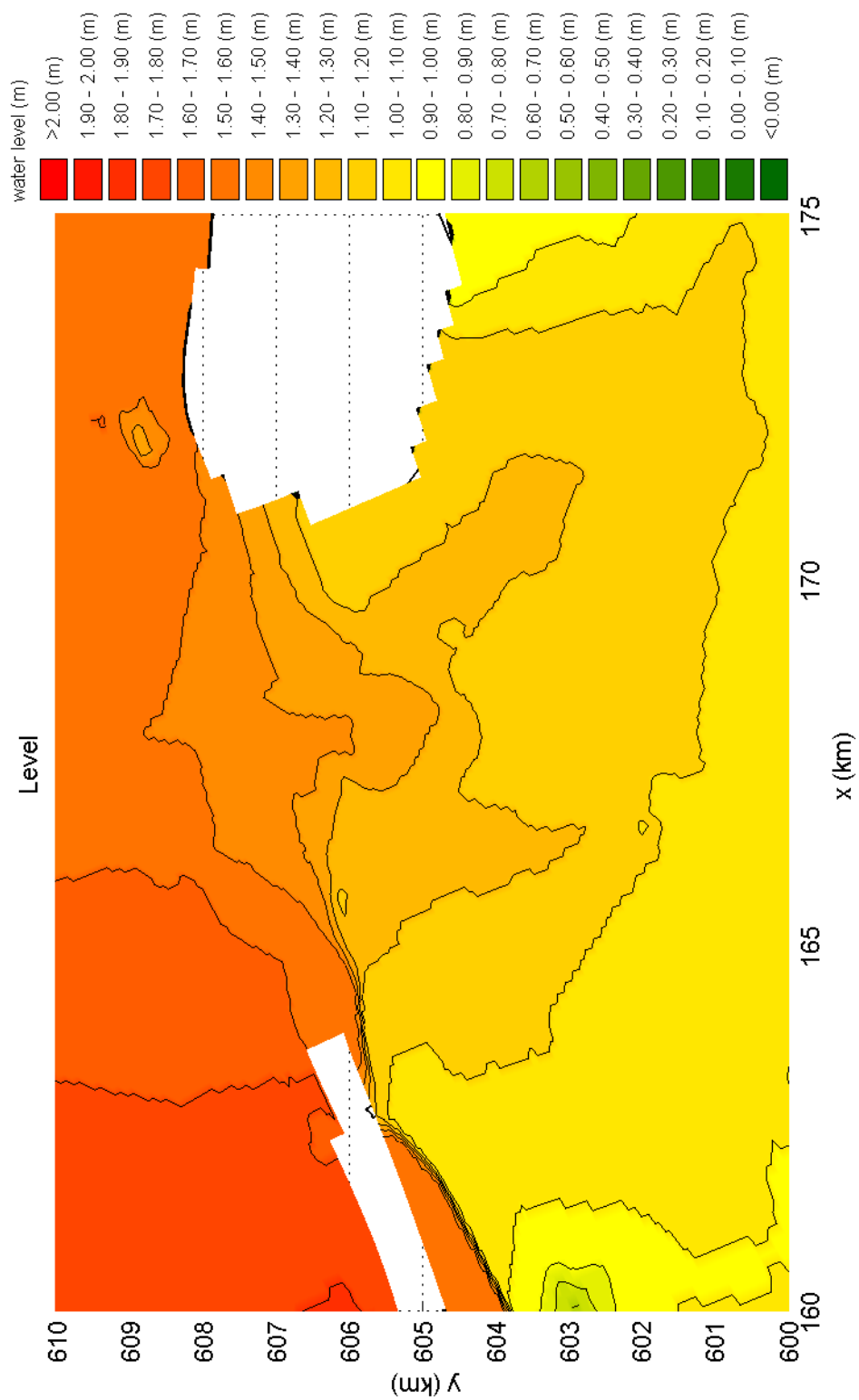
Spatial variation of current magnitude on WAW grid
for 8 Feb. 2004, 20:00 hours

Ameland



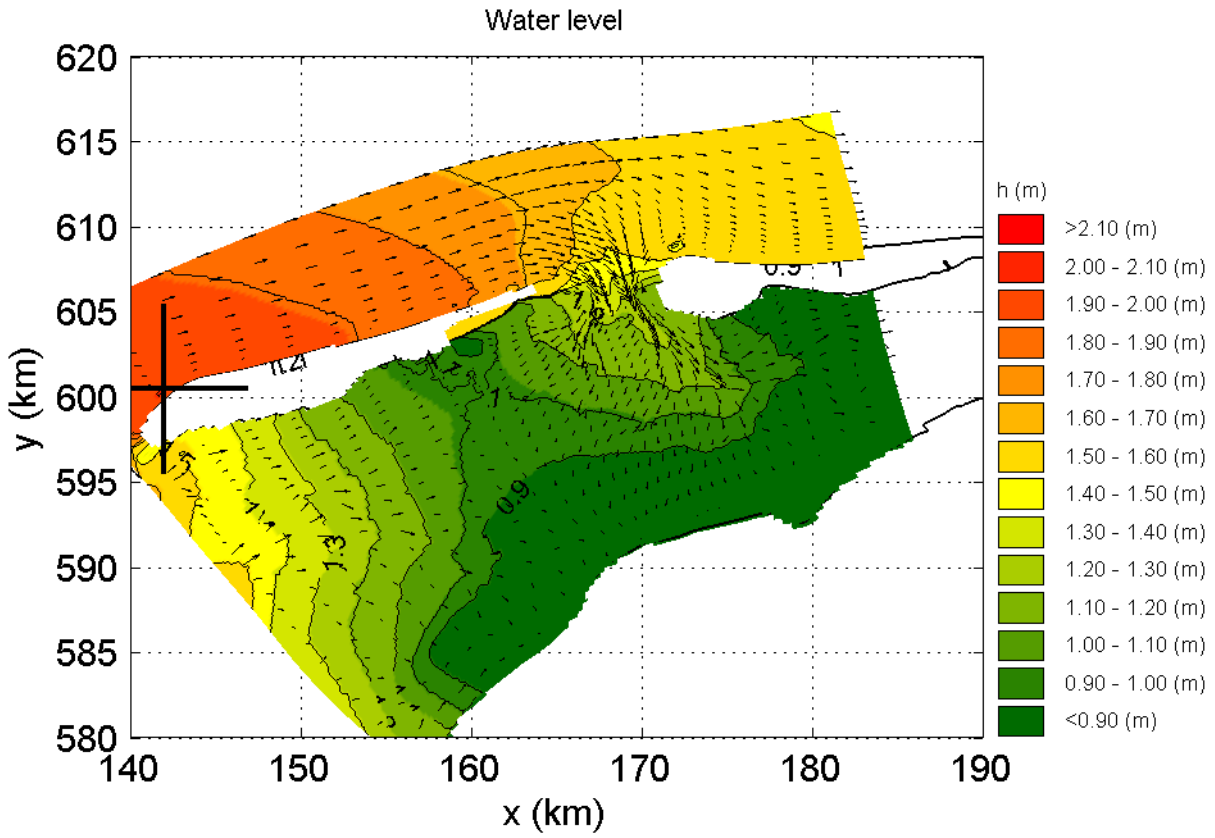
Spatial variation of the water level on WAW grid
for 8 Feb. 2004, 20:00 hours and dry points

Ameland

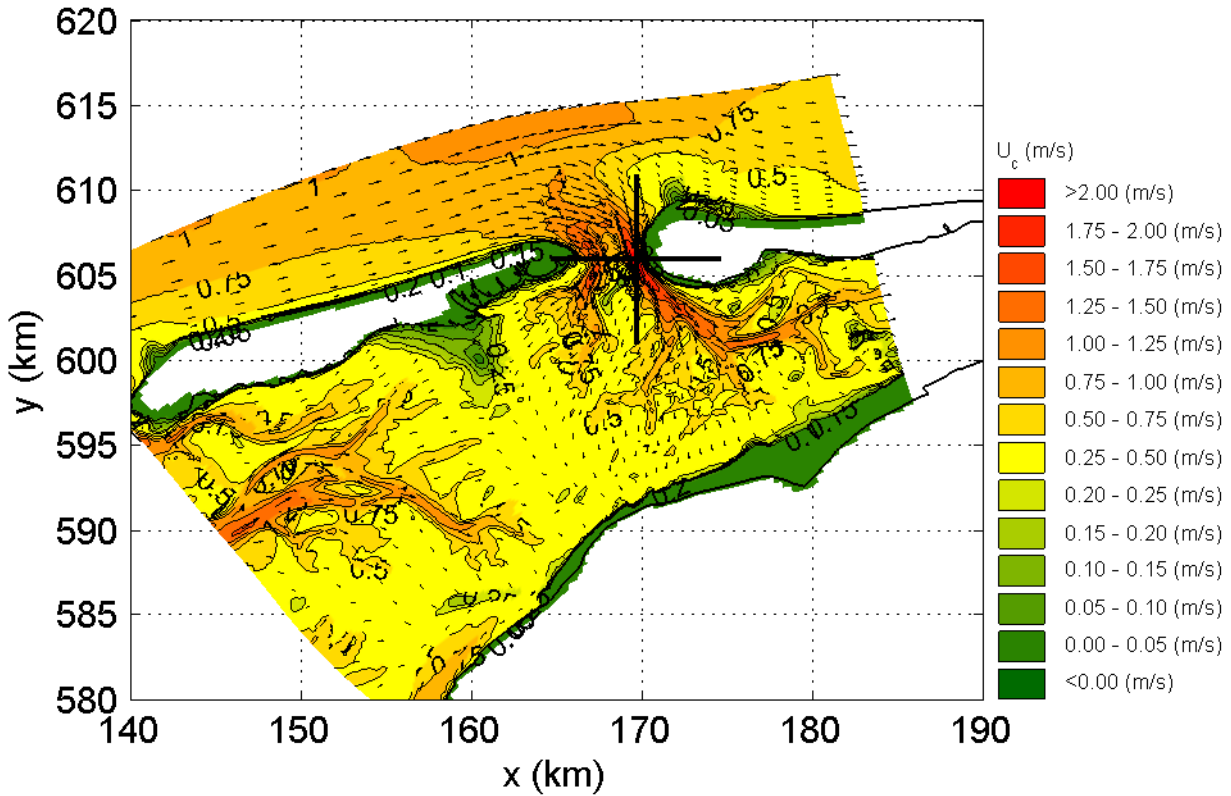


Spatial variation of the water level on WAW grid
 for 8 Feb. 2004, 20:00 hours
 after correction of dry points

Ameland

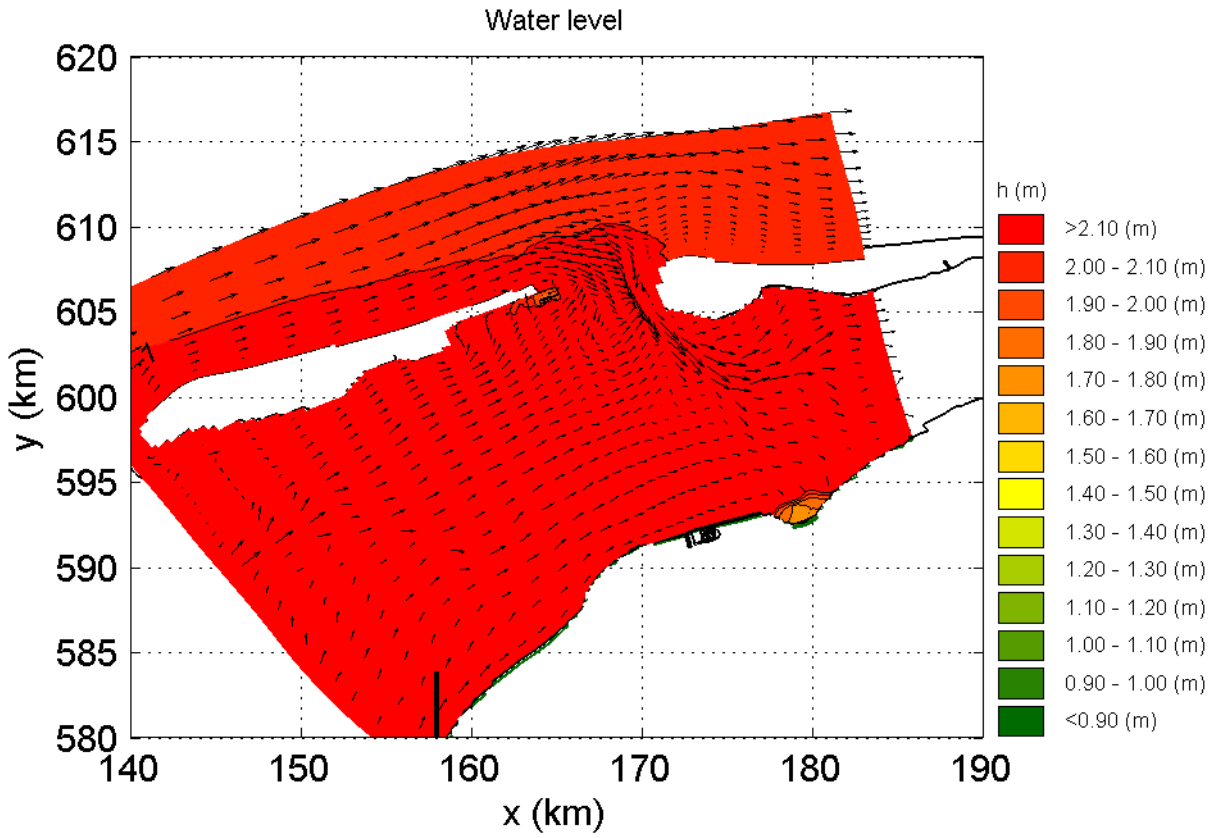


$\max(U_c) = 2.32 \text{ (m/s)}$ at $x = 169.65 \text{ (km)}$, $y = 605.93 \text{ (km)}$

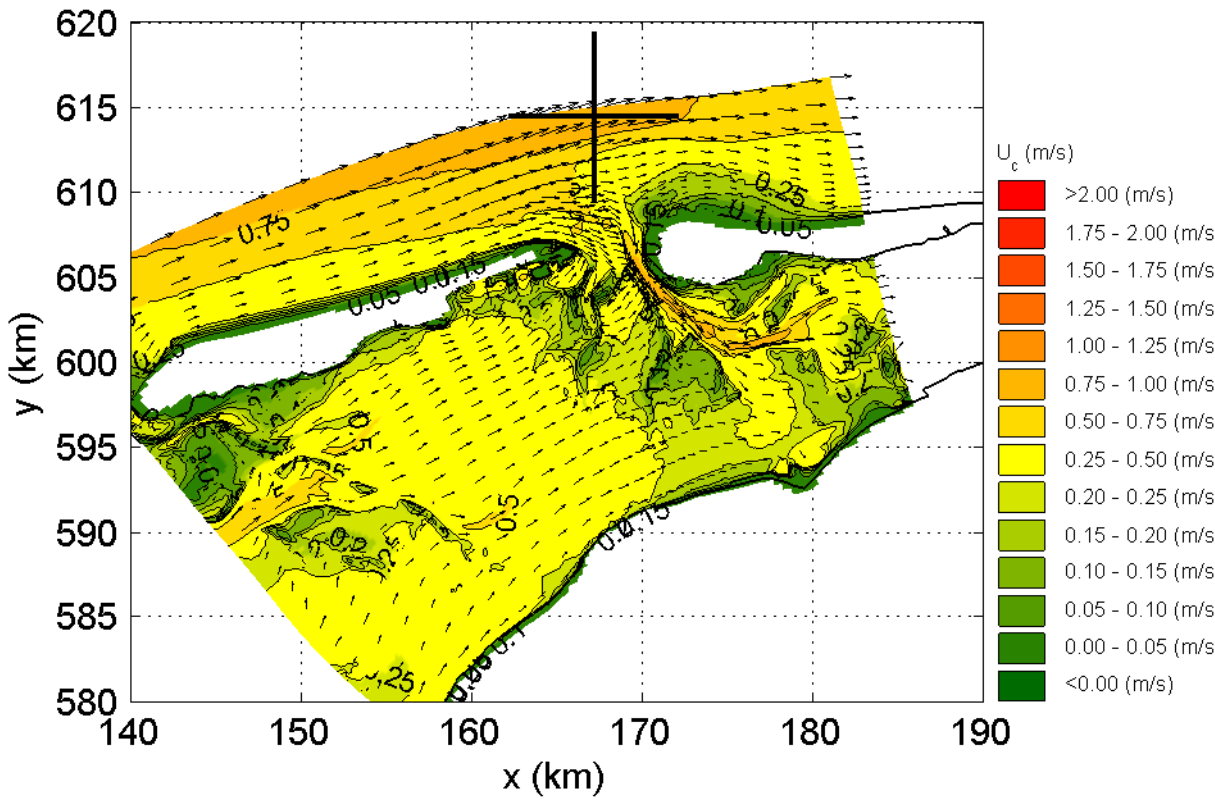


Variation of water level and current speed and direction for Grid AZG3A and for event 20040208_2000
Location of maximum current speed (black cross)

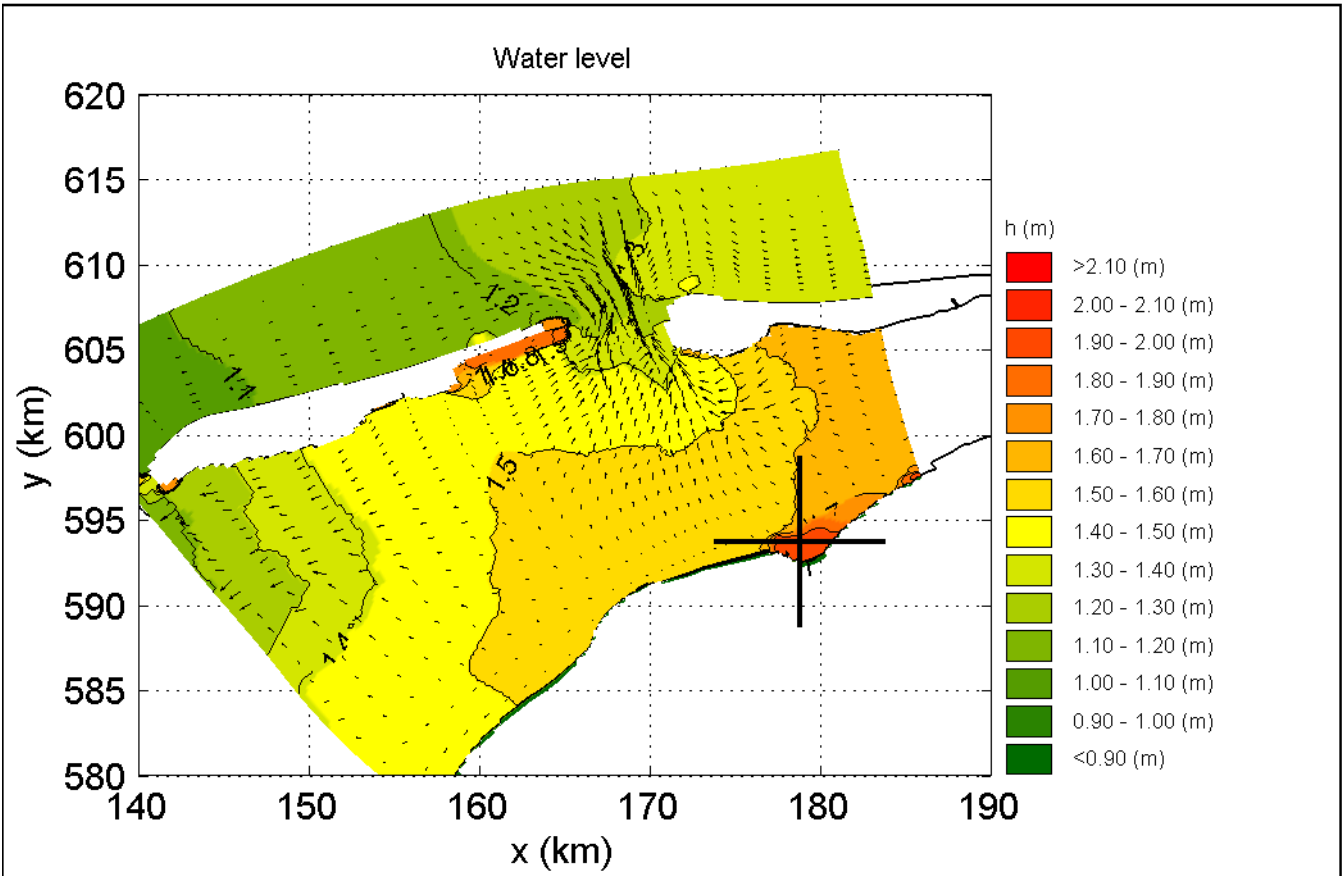
Ameland



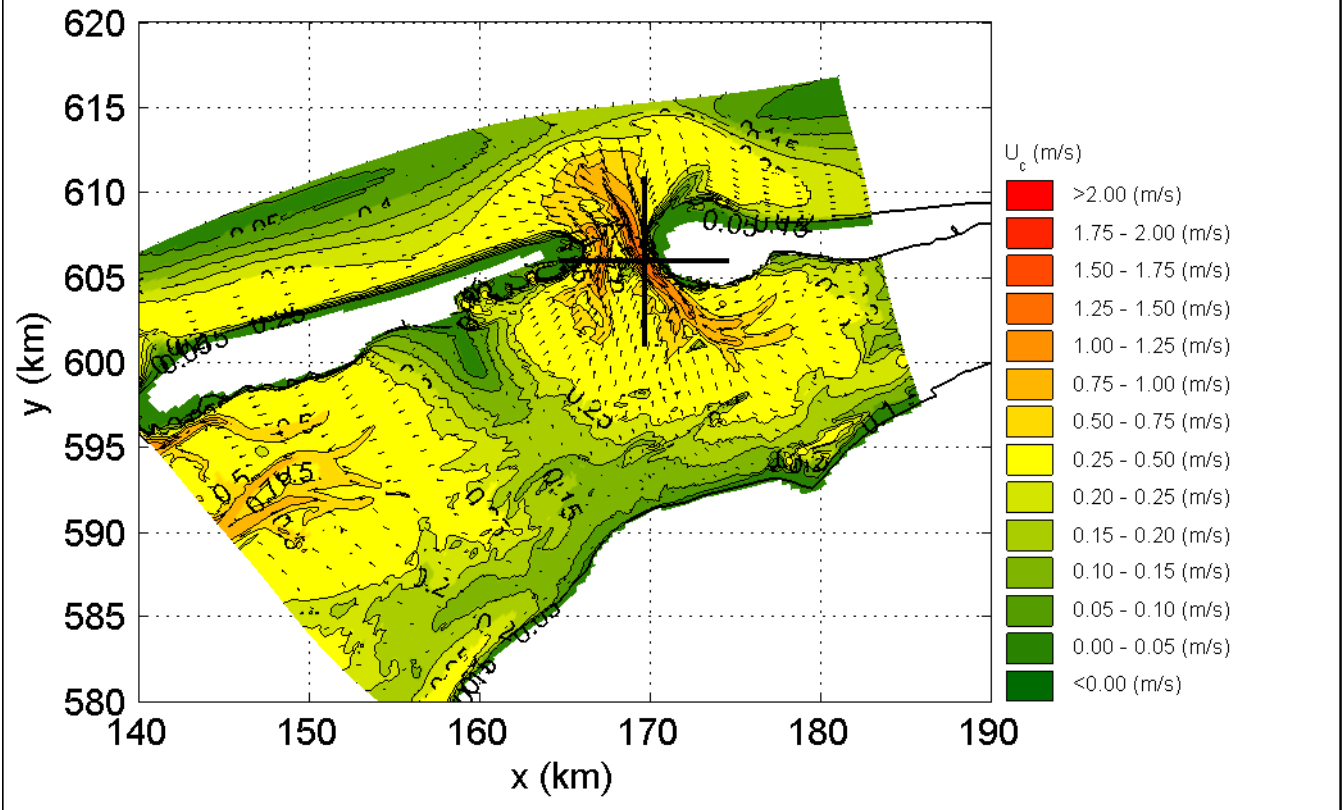
$\max(U_c) = 0.918 \text{ (m/s)}$ at $x = 167.16 \text{ (km)}$, $y = 614.41 \text{ (km)}$



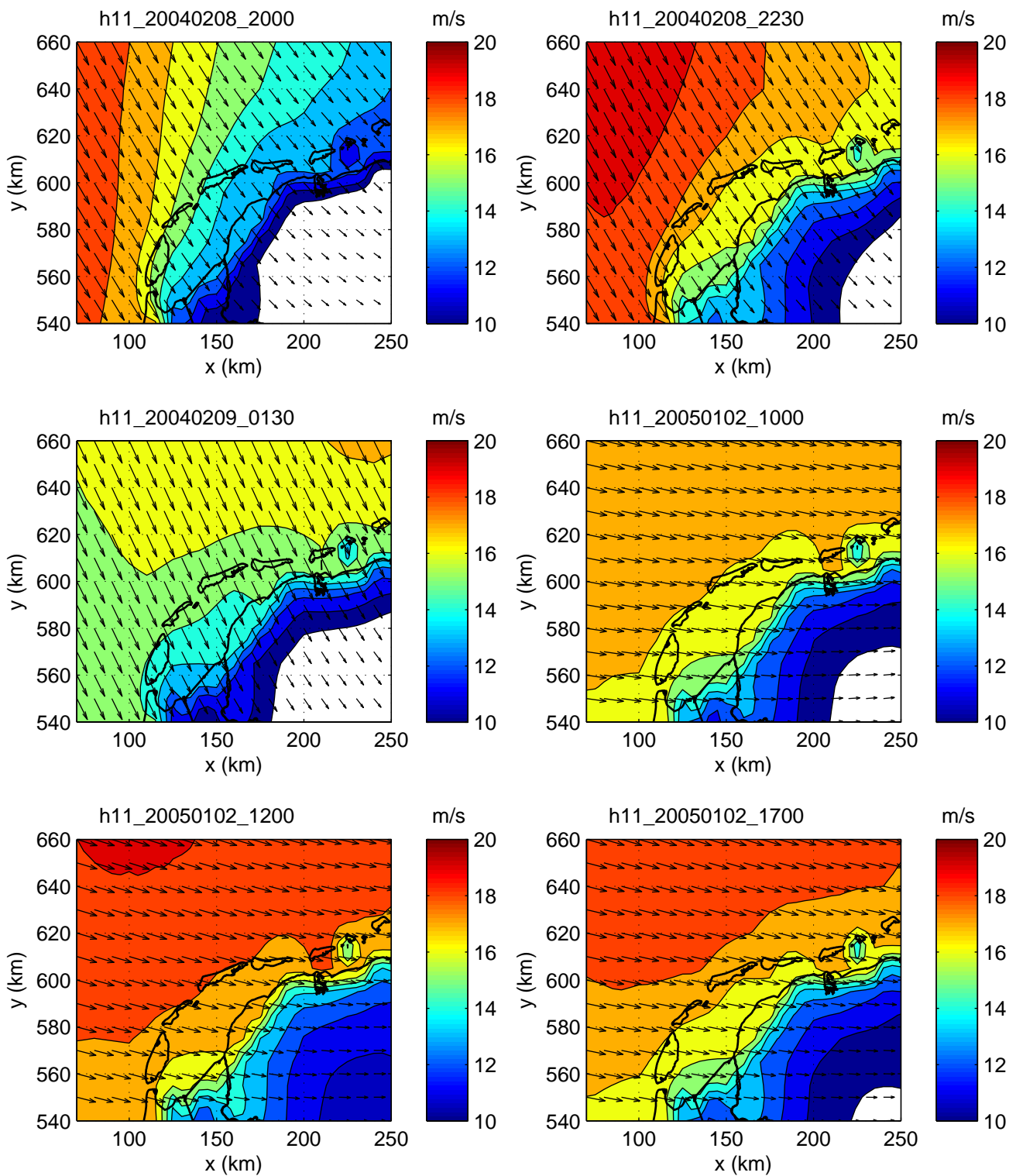
Variation of water level and current speed and direction for Grid AZG3A and for event 20040208_2230 Location of maximum current speed (black cross)		
	Ameland	
WL DELFT HYDRAULICS	H4918.20	Fig. 3.18



$\max(U_c) = 1.66 \text{ (m/s)}$ at $x = 169.65 \text{ (km)}$, $y = 605.93 \text{ (km)}$

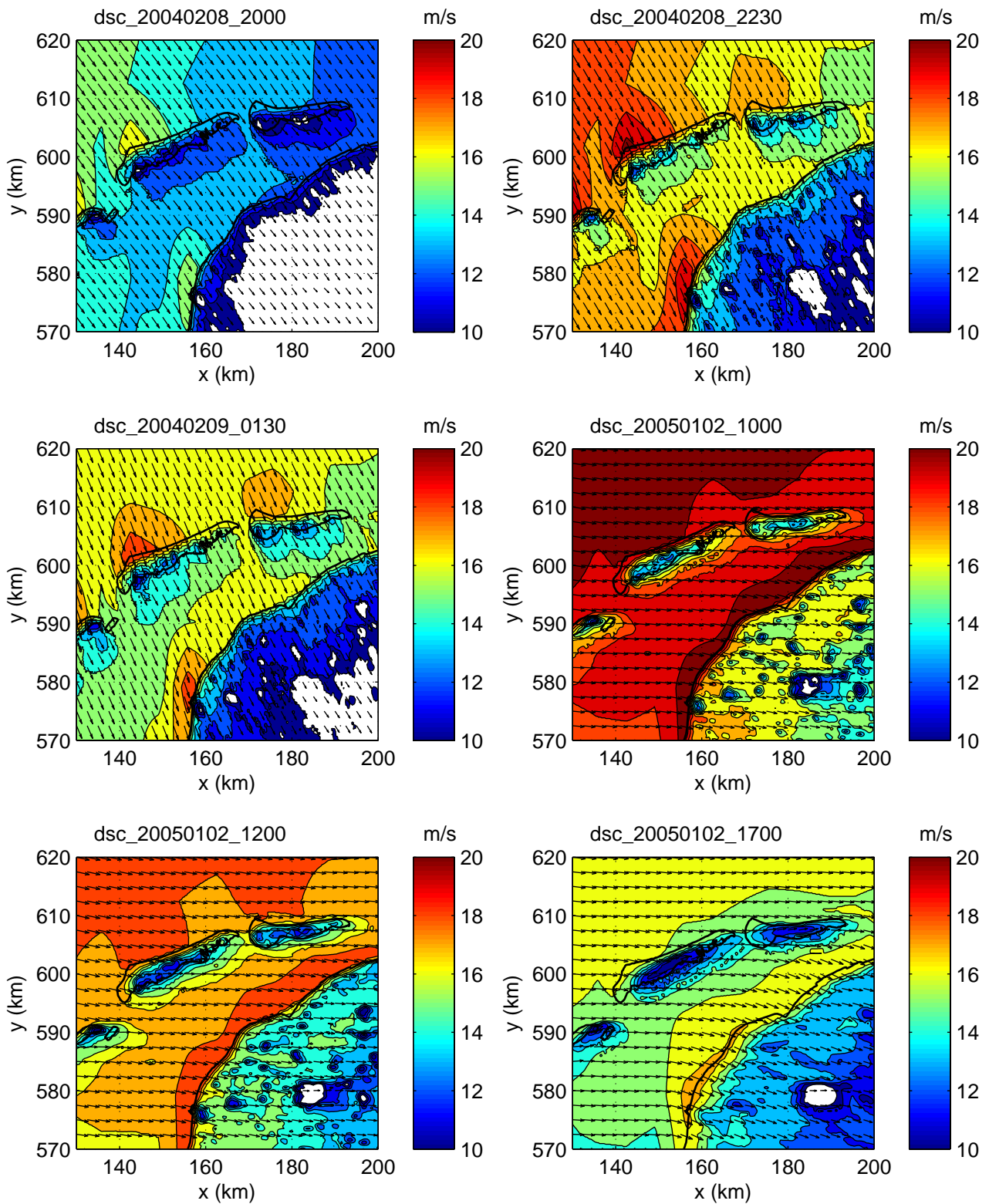


Variation of water level and current speed and direction for Grid AZG3A and for event 20040209_0130 Location of maximum current speed (black cross)		
	Ameland	
WL DELFT HYDRAULICS	H4918.20	Fig. 3.19



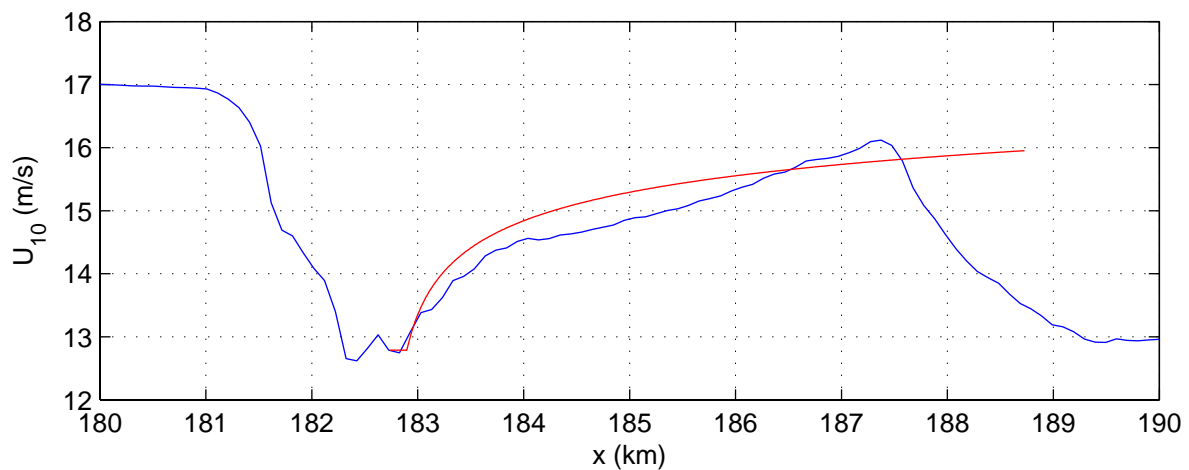
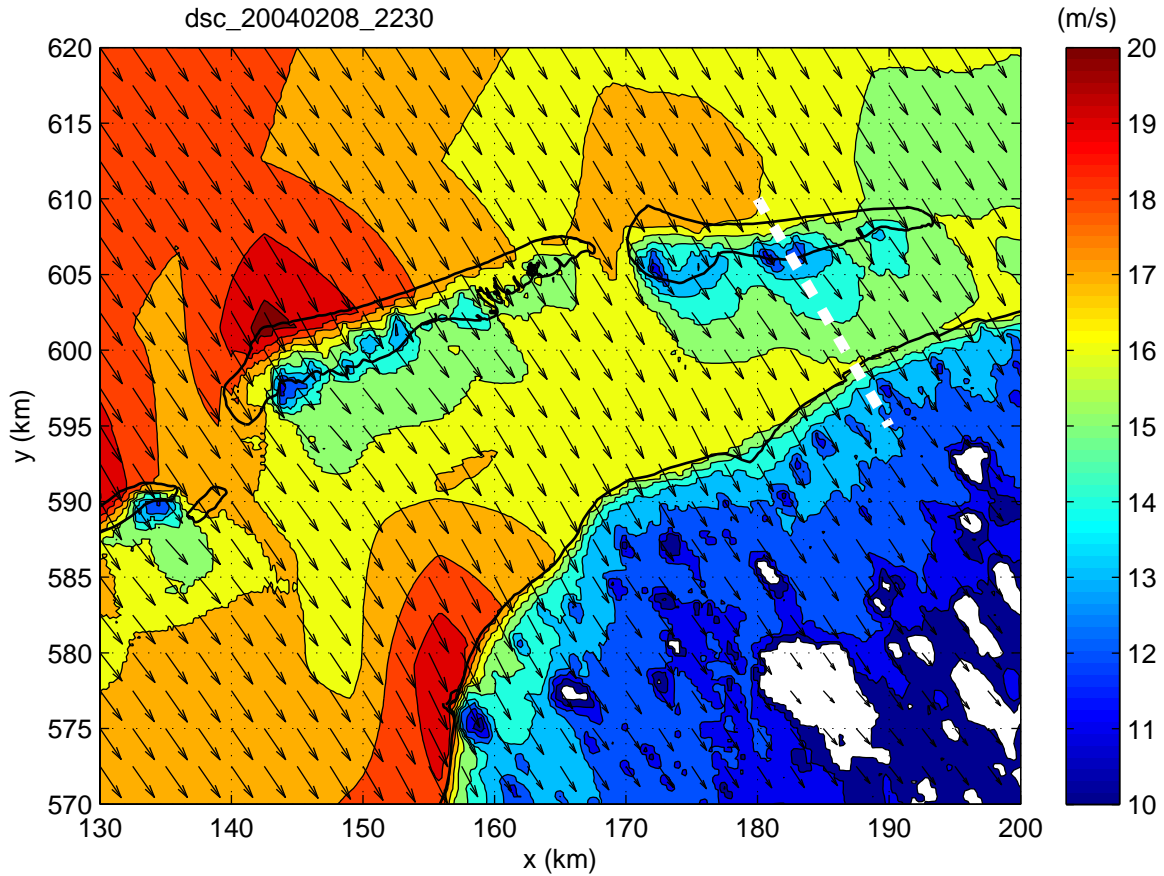
HIRLAM wind fields for the northern part of the North Sea for the six considered storm events

Ameland



Downscaled wind fields for the central part of the Wadden Sea for the six considered storm events

Ameland

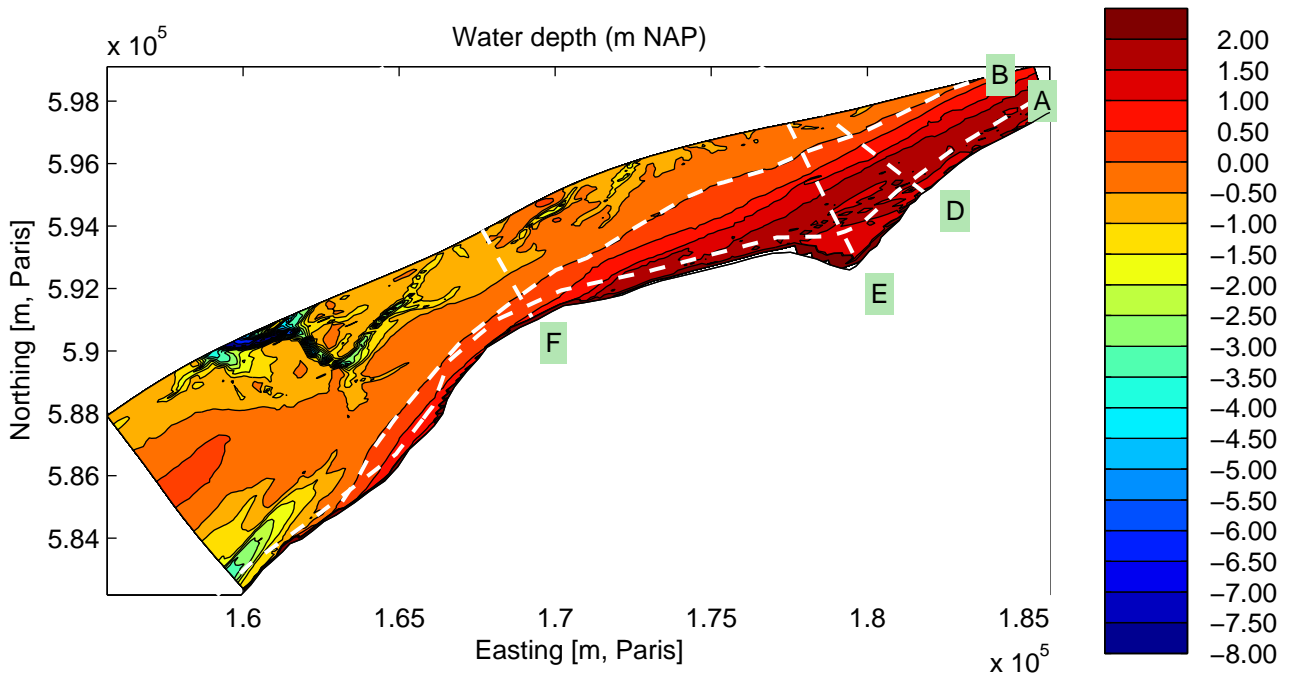
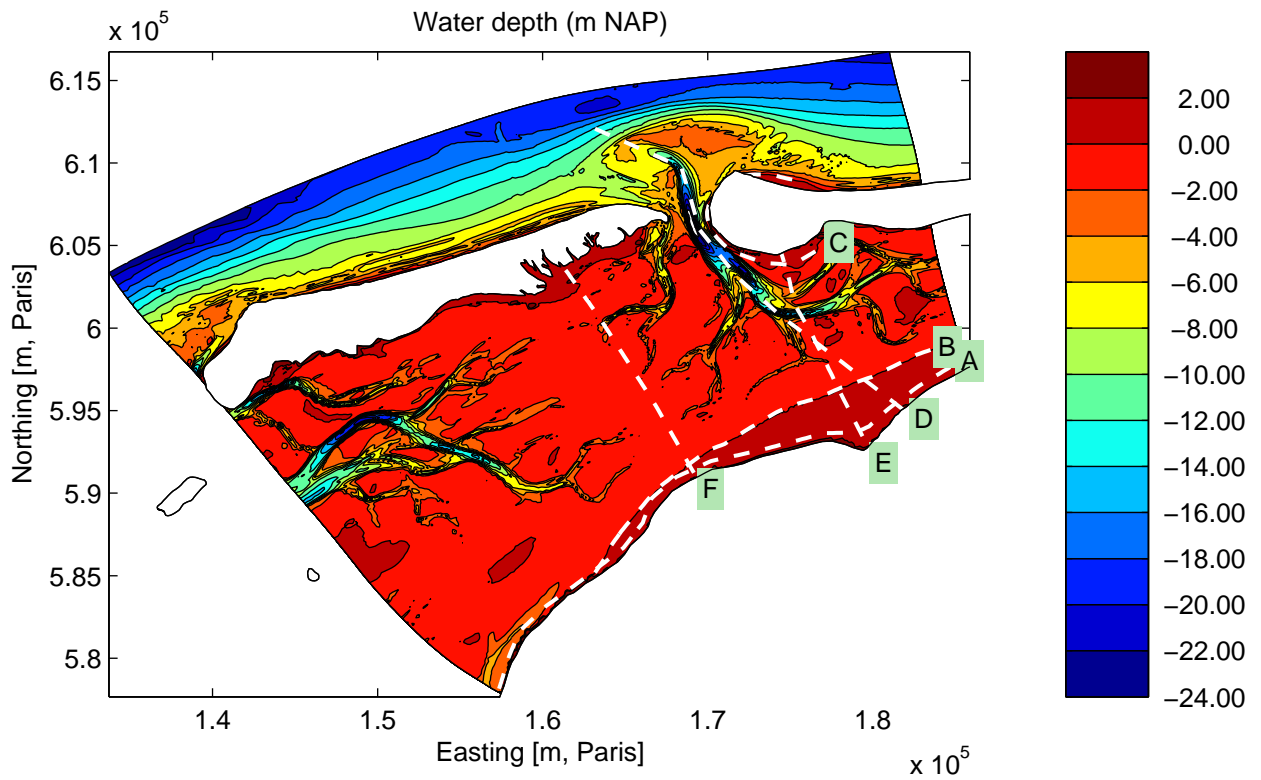


Comparison of wind speed variation from downscaling (blue line) and according to Taylor & Lee (red line) using a land roughness of 0.1 along a downwind ray from the island of Ameland (dashed white line)

8 Feb. 2004

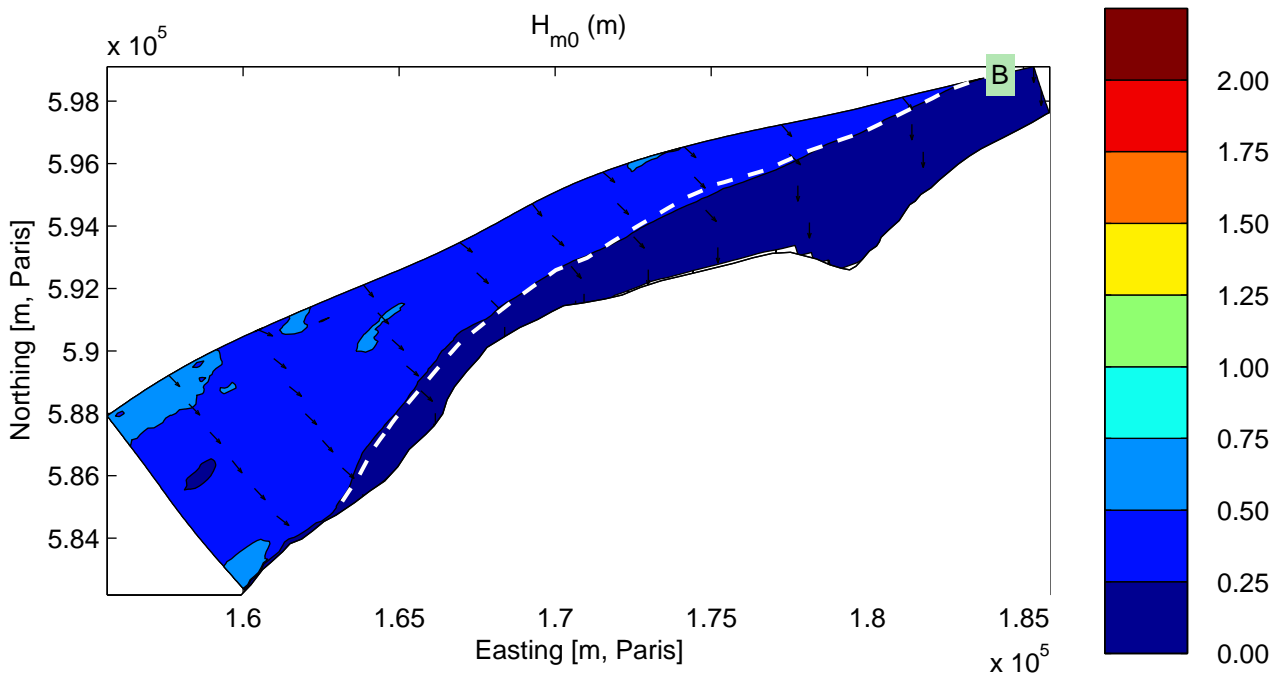
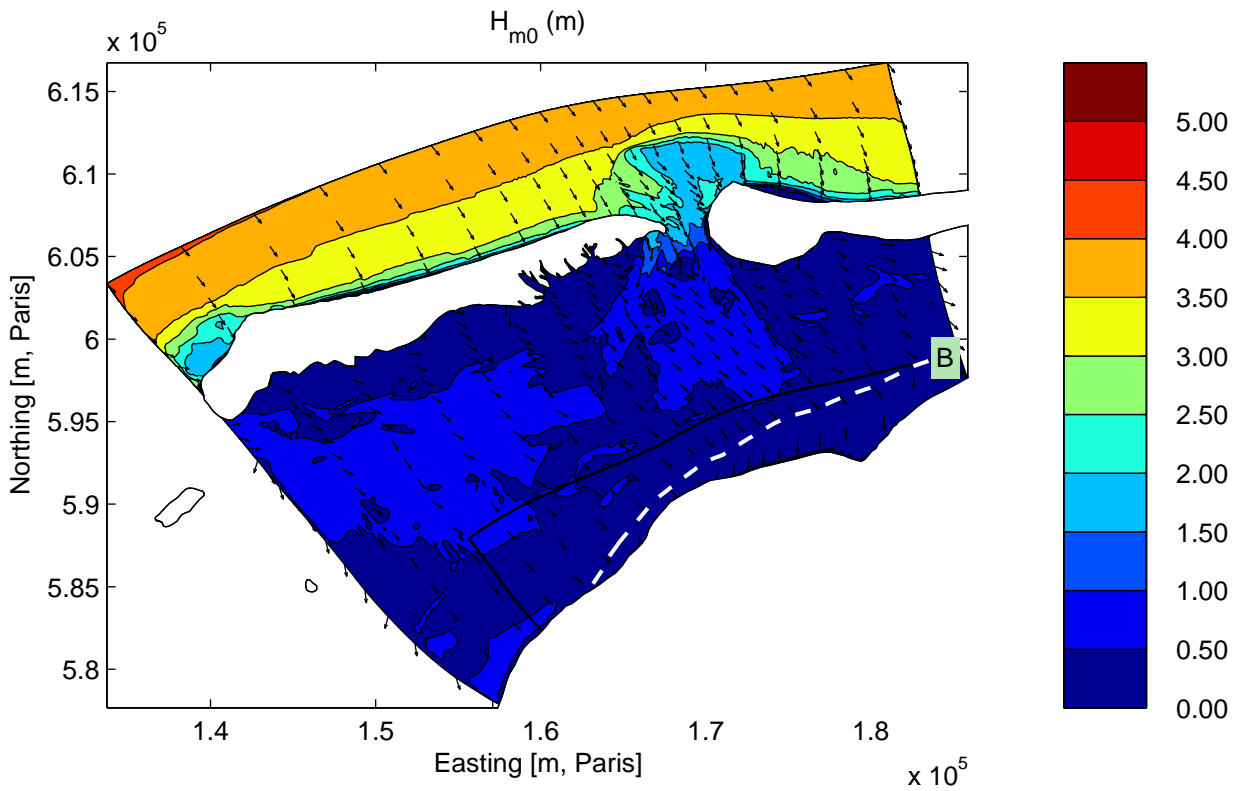
22:30 hours

Ameland



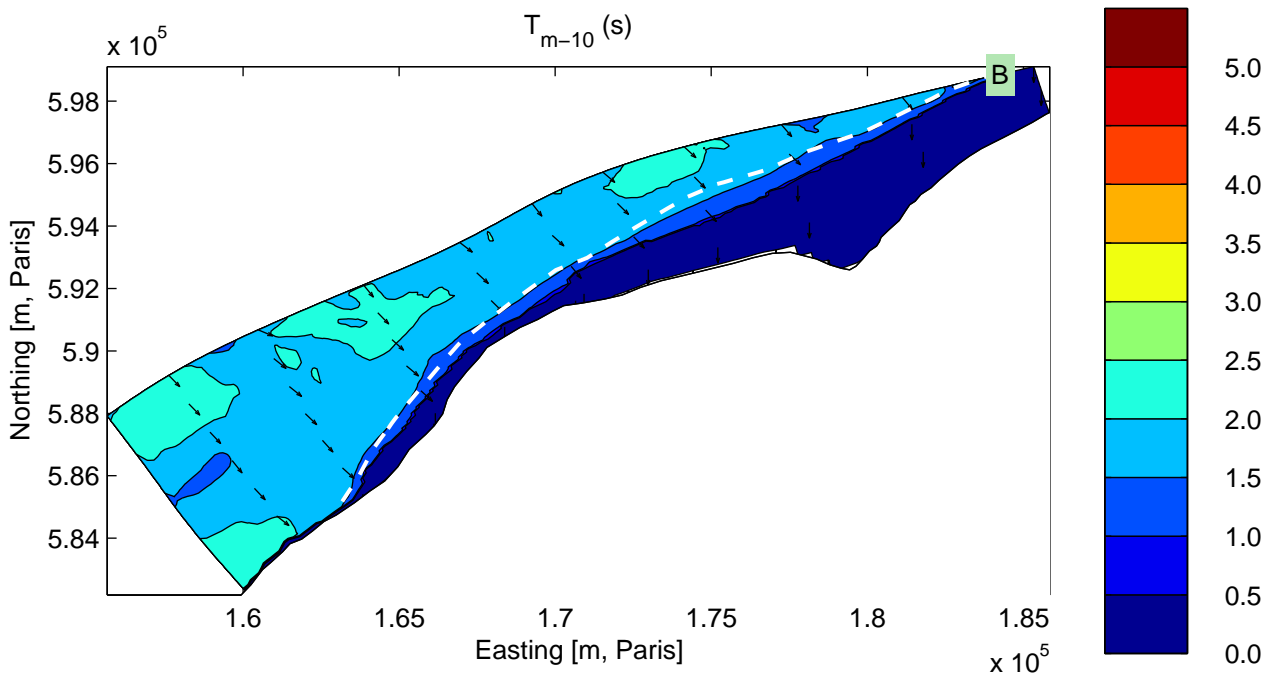
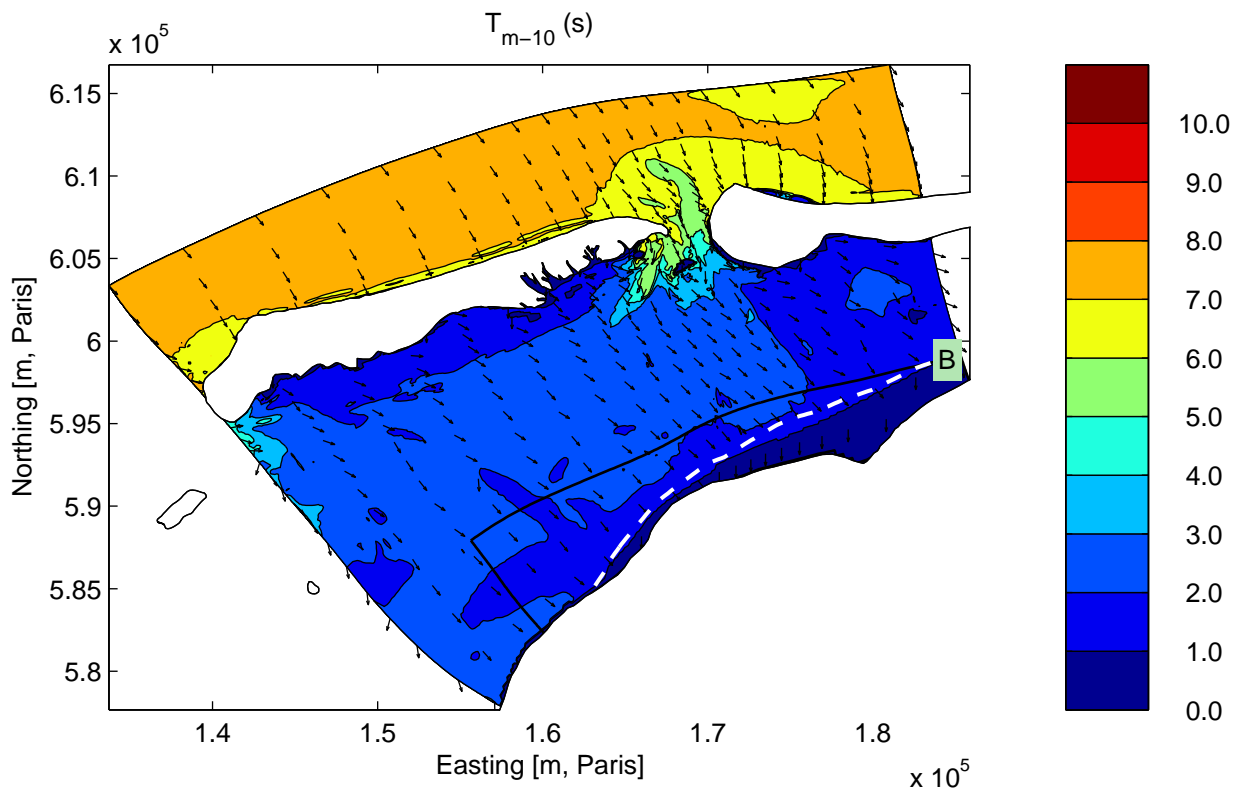
Location of output curves used in the sensitivity analysis on grid AZG3A (above) and grid AK4A (below).

Sensitivity analysis Ameland



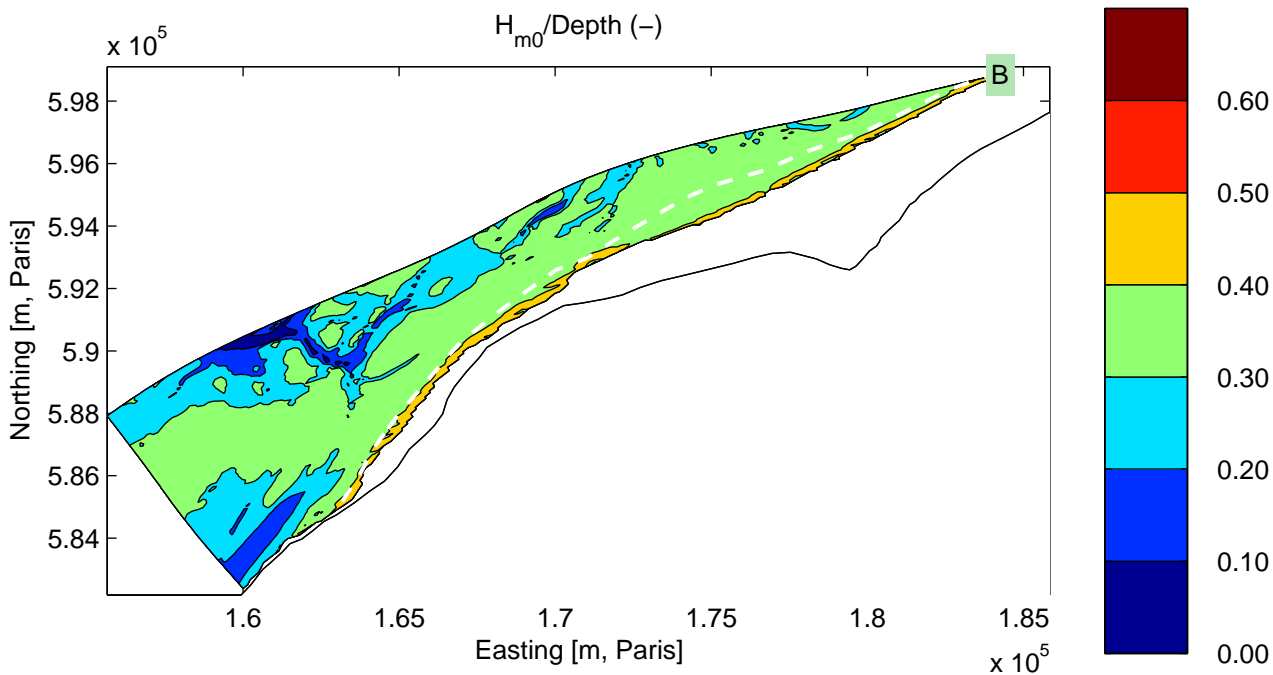
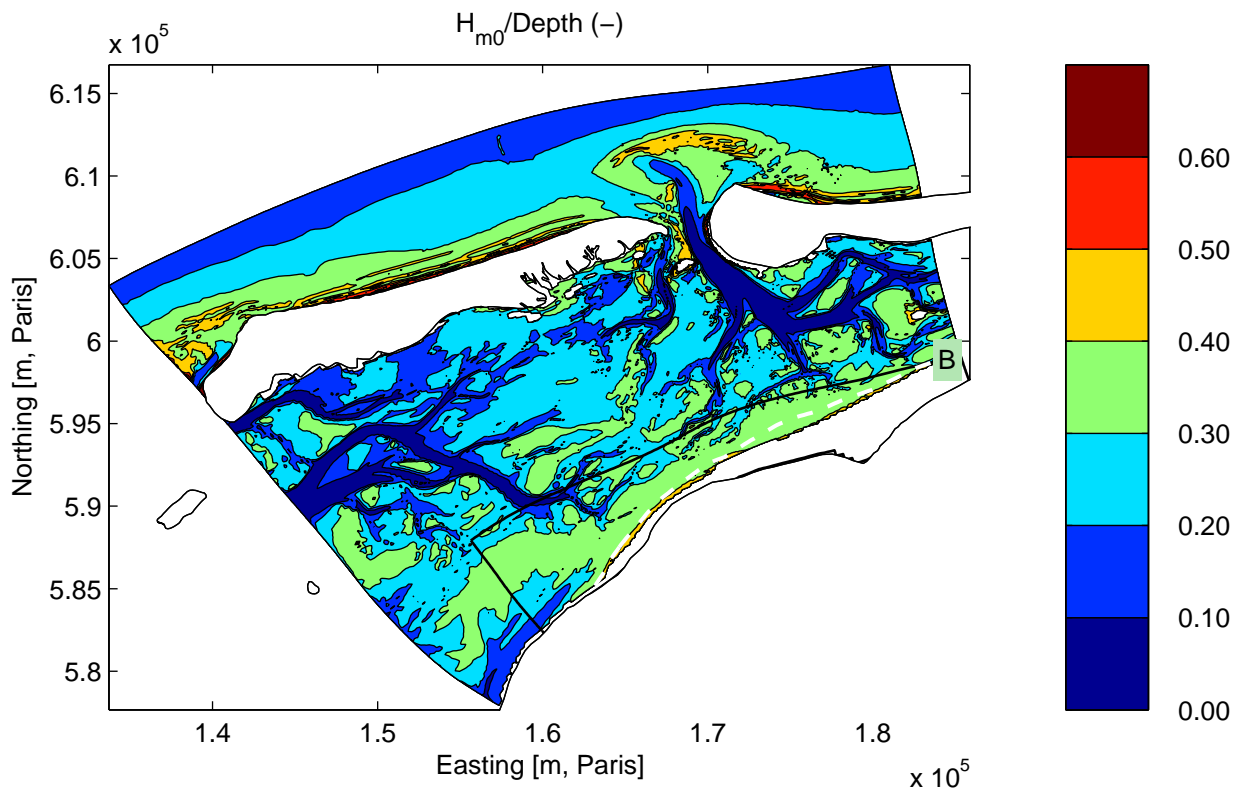
Simulation results for base case C1XXX
 Significant wave height on grids AZG3A (above) and AK4A (below).

Sensitivity analysis Ameland



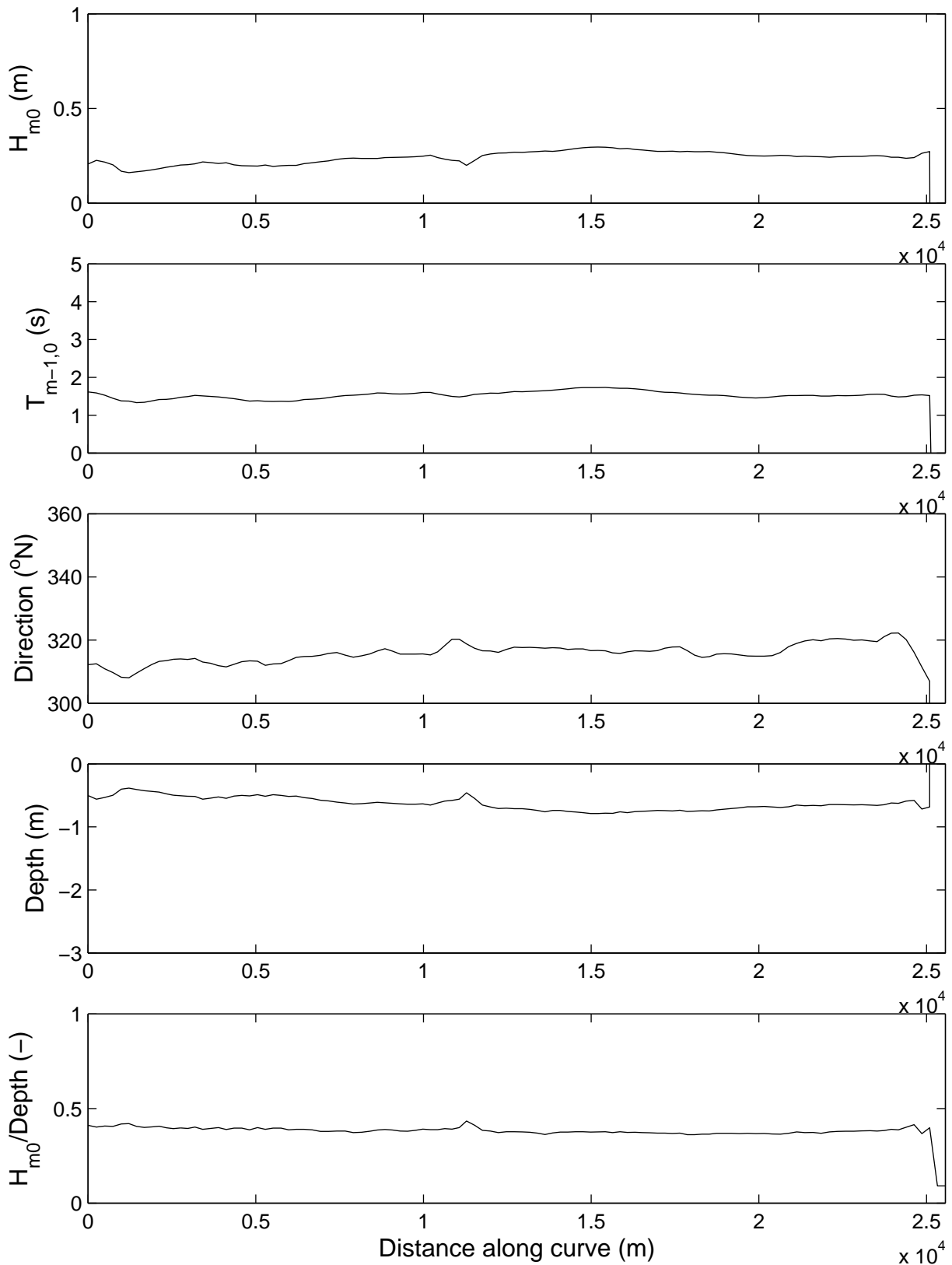
Simulation results for base case C1XXX
 Mean wave period on grids AZG3A (above) and AK4A (below).

Sensitivity analysis Ameland



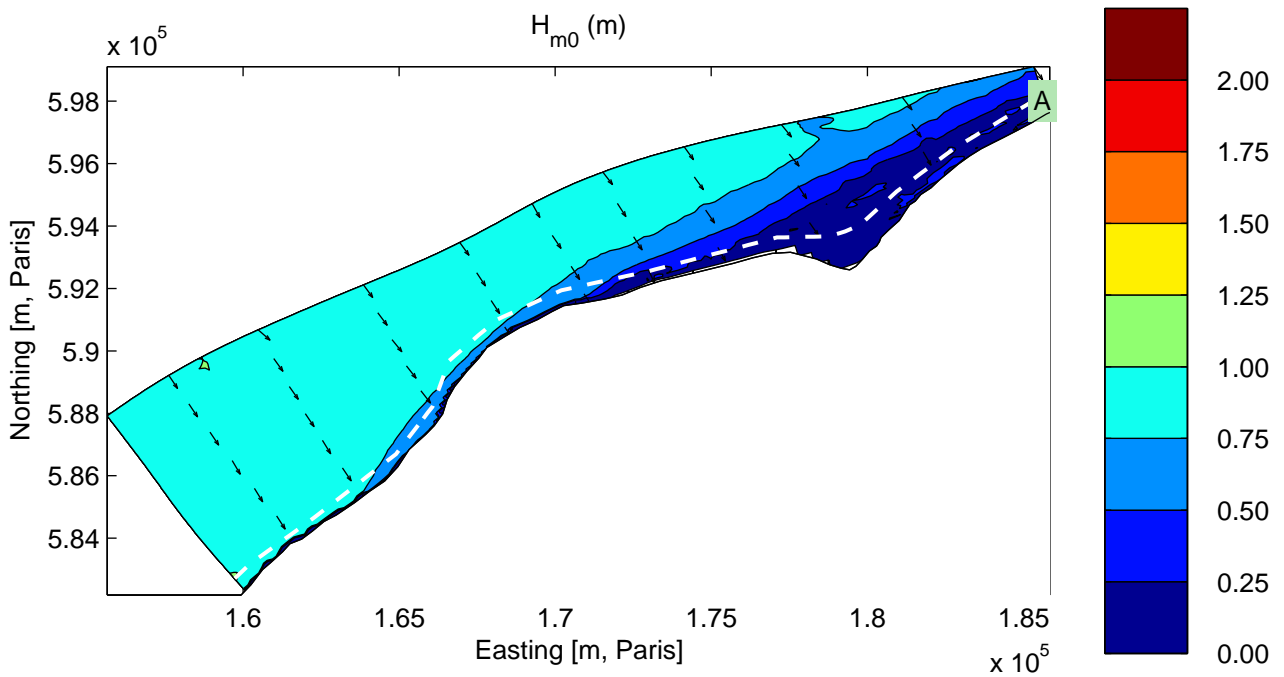
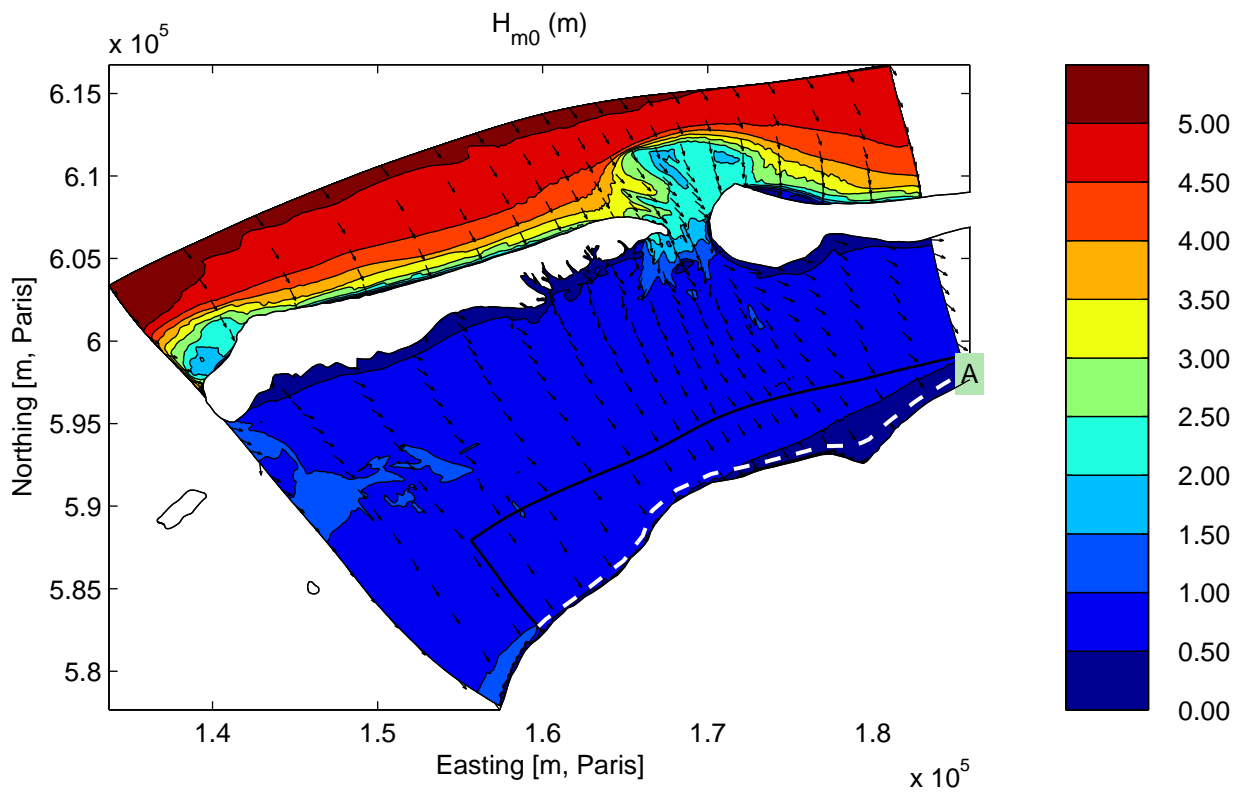
Simulation results for base case C1XXX
Ratio of H_{m0}/Depth on grids AZG3A (above) and AK4A (below).

Sensitivity analysis Ameland



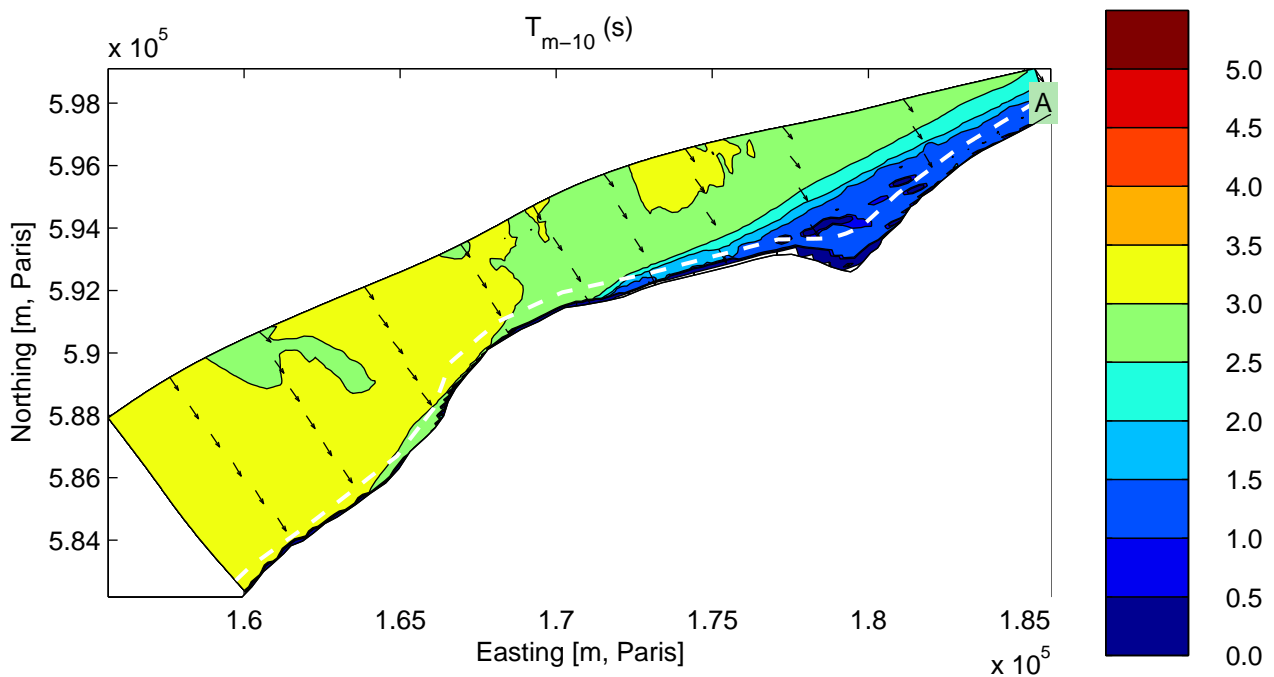
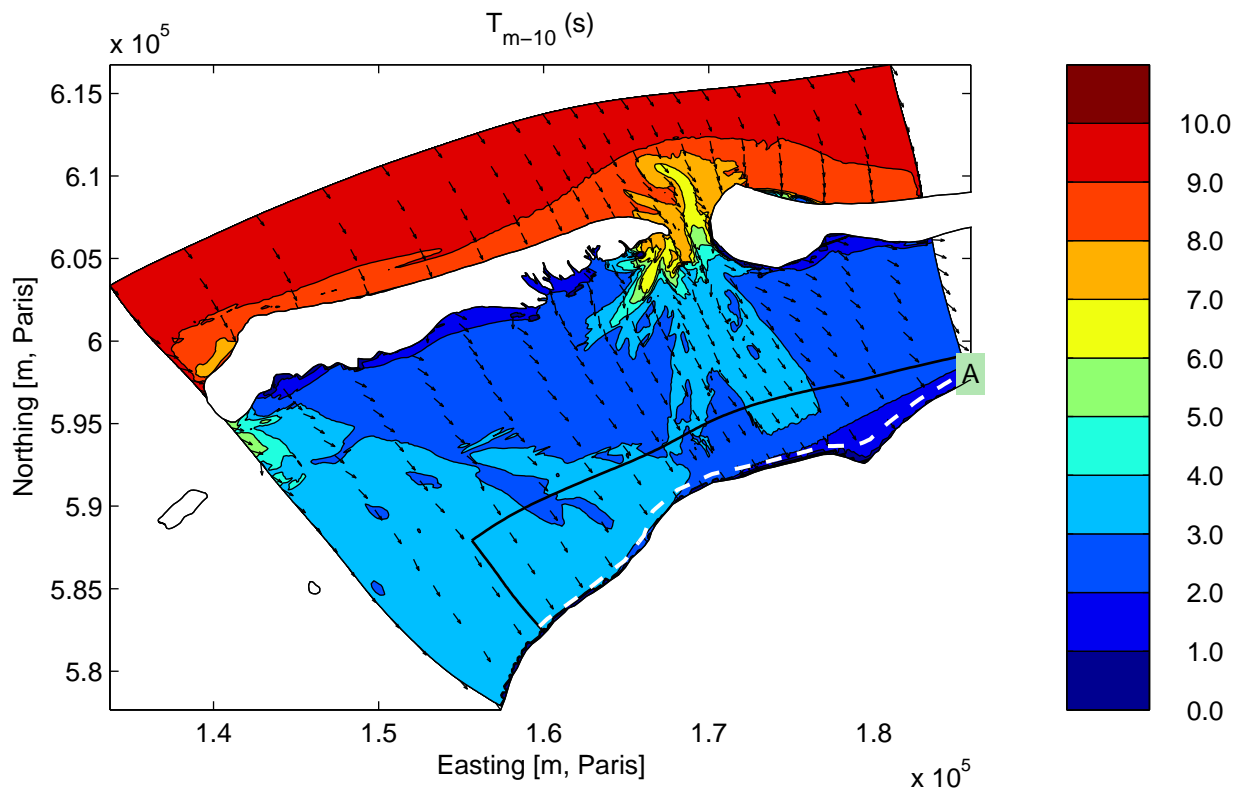
Simulation results for base case C1XXX
Integral parameters along Curve B

Sensitivity analysis Ameland



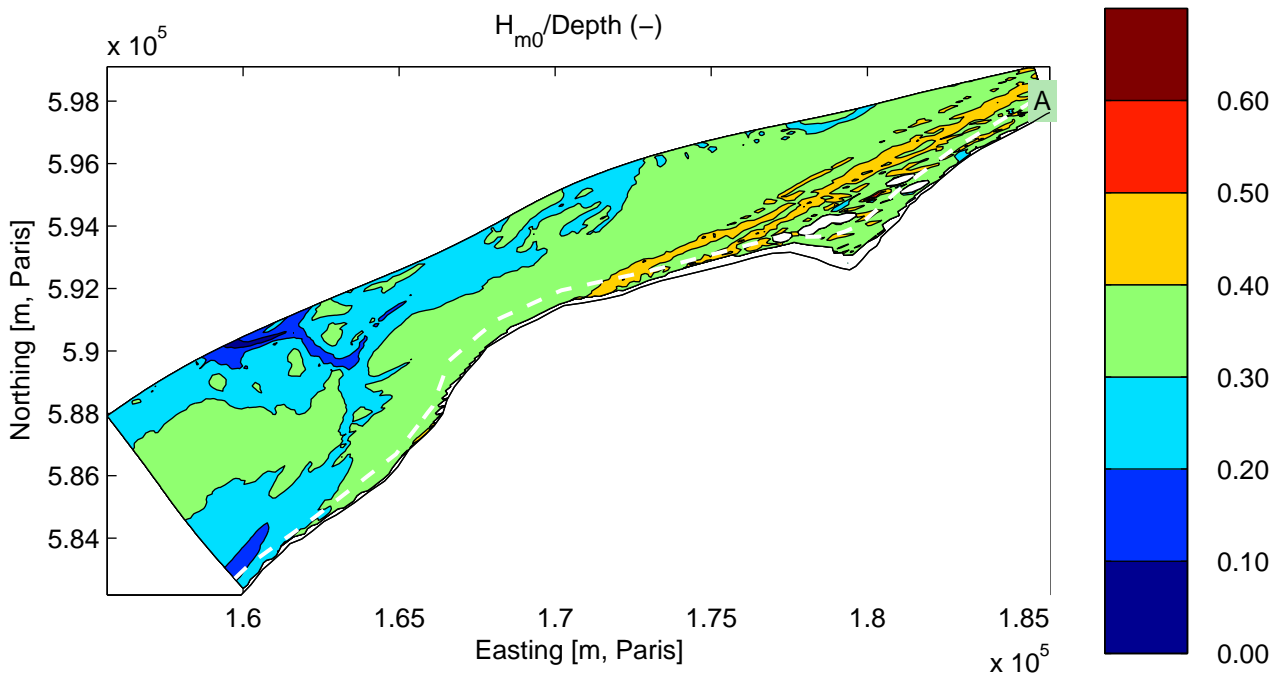
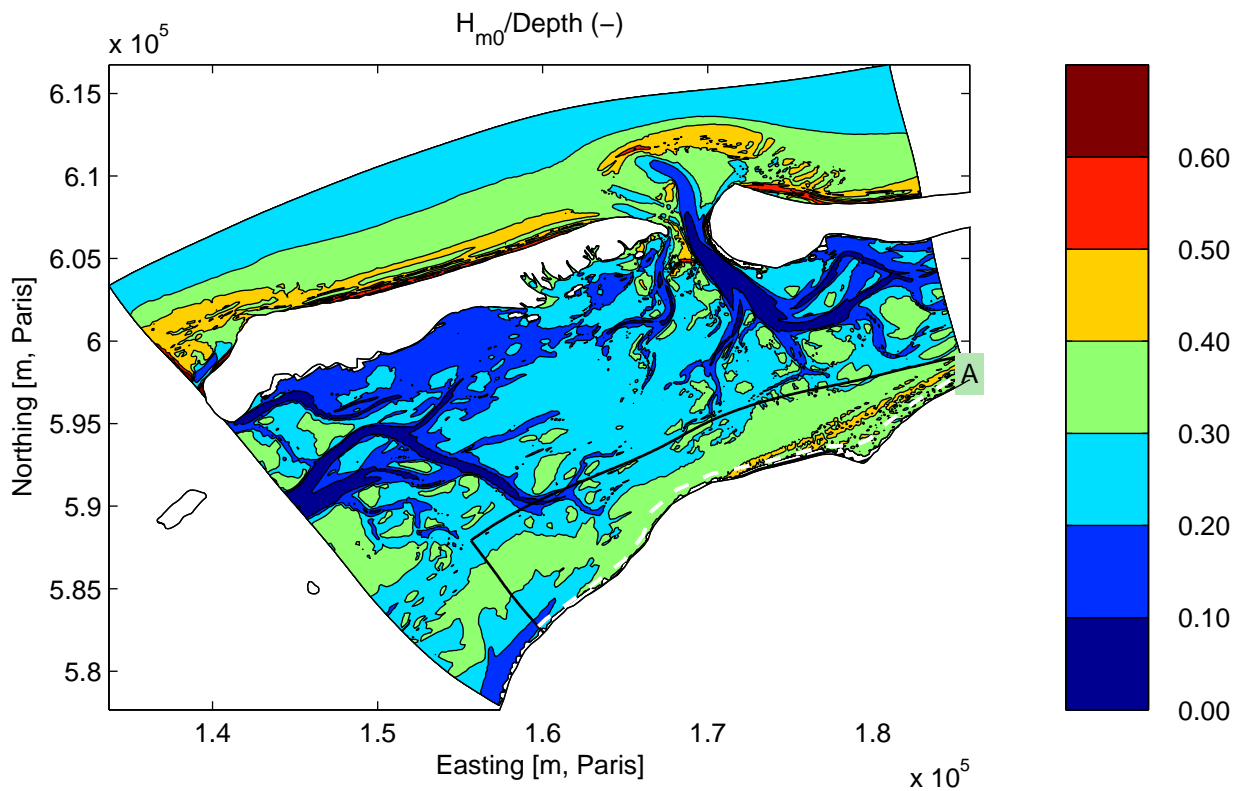
Simulation results for base case C2XXX
 Significant wave height on grids AZG3A (above) and AK4A (below).

Sensitivity analysis Ameland



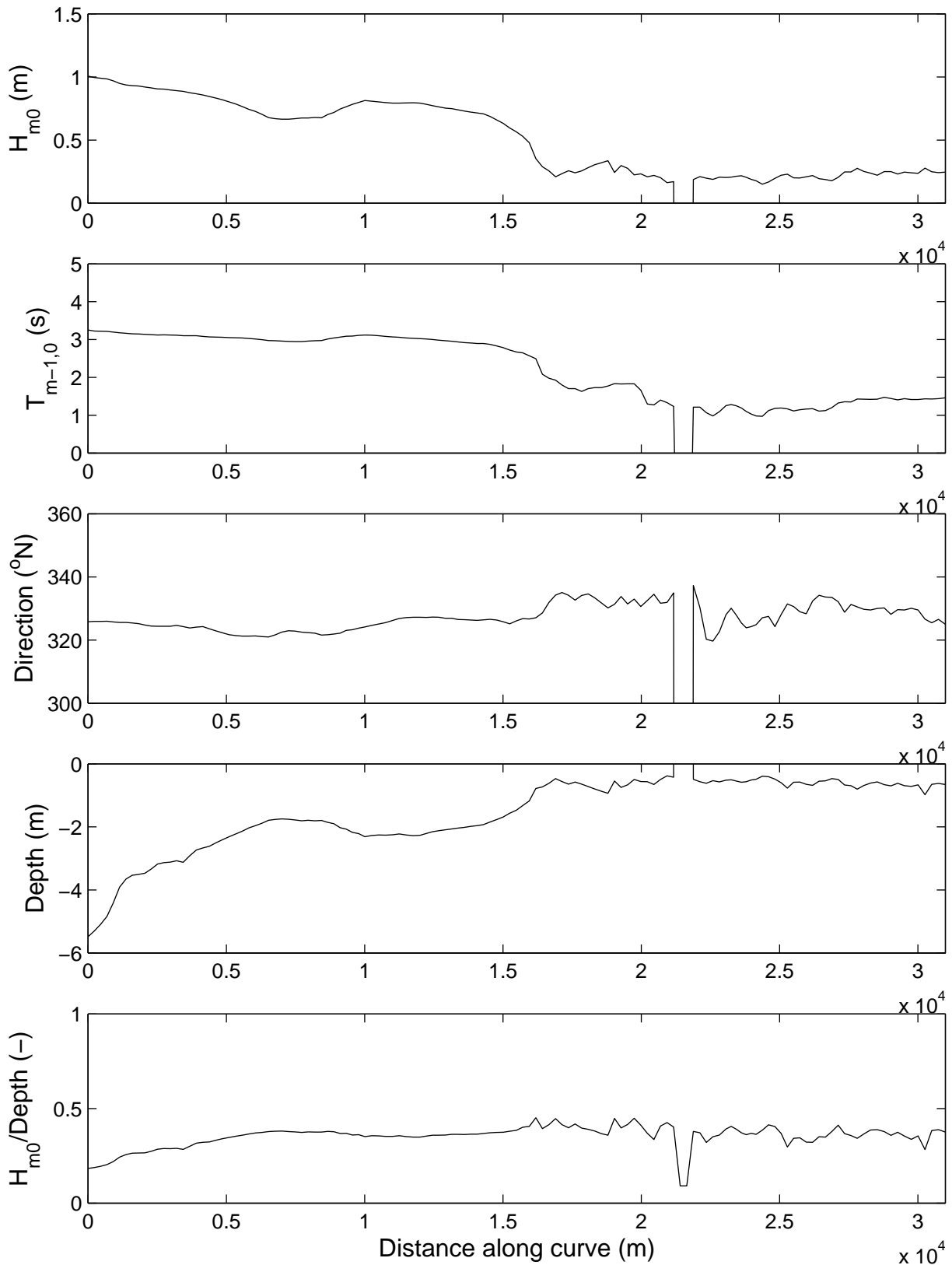
Simulation results for base case C2XXX
 Mean wave period on grids AZG3A (above) and AK4A (below).

Sensitivity analysis Ameland



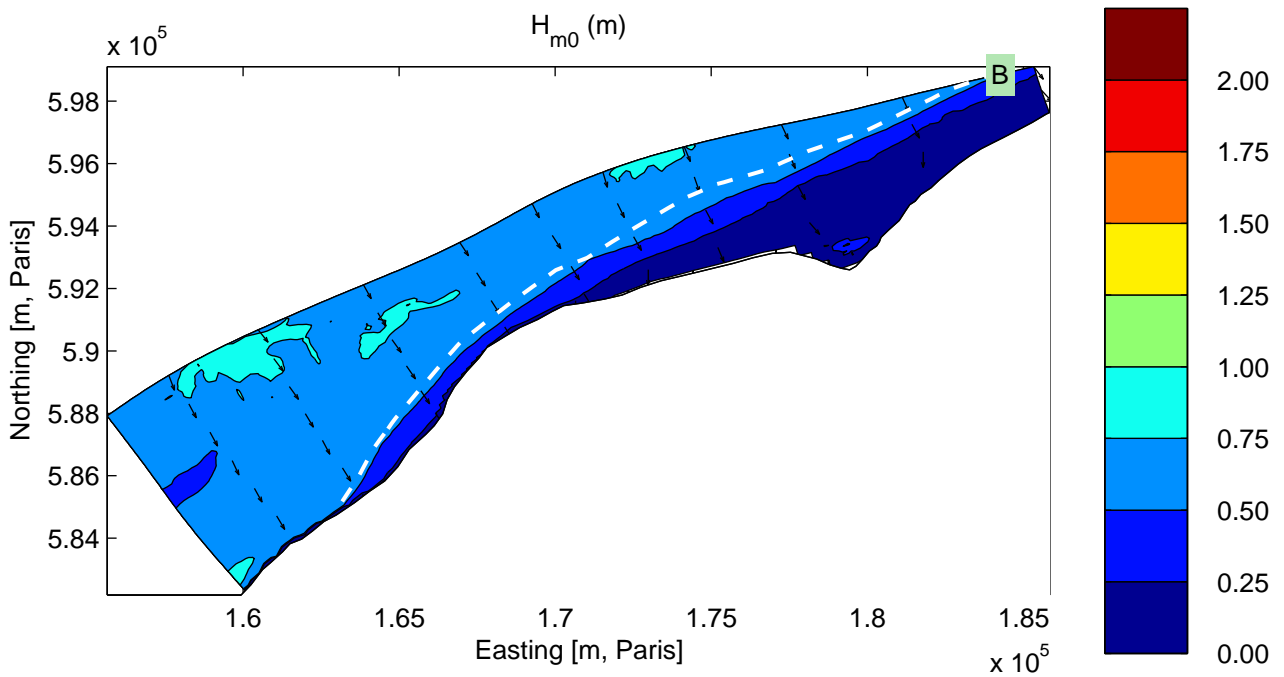
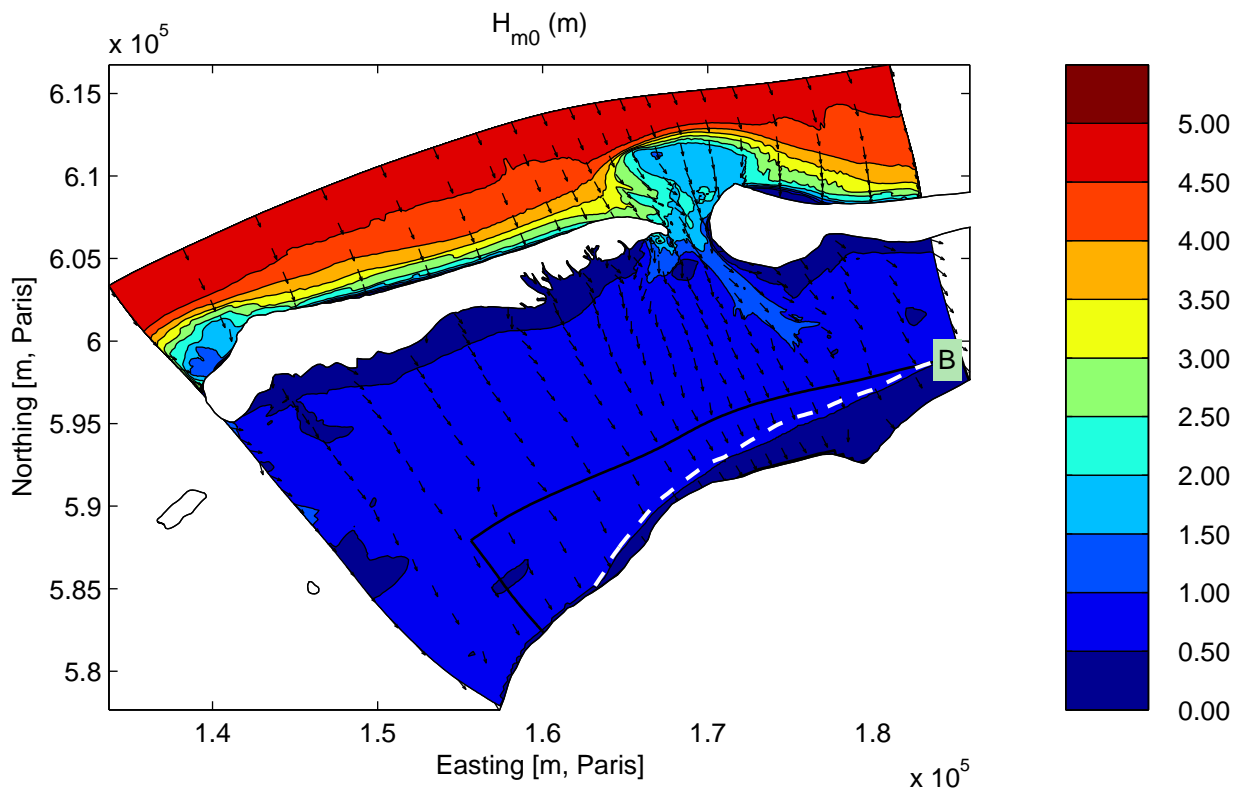
Simulation results for base case C2XXX
 Ratio of H_{m0}/Depth on grids AZG3A (above) and AK4A (below).

Sensitivity analysis Ameland



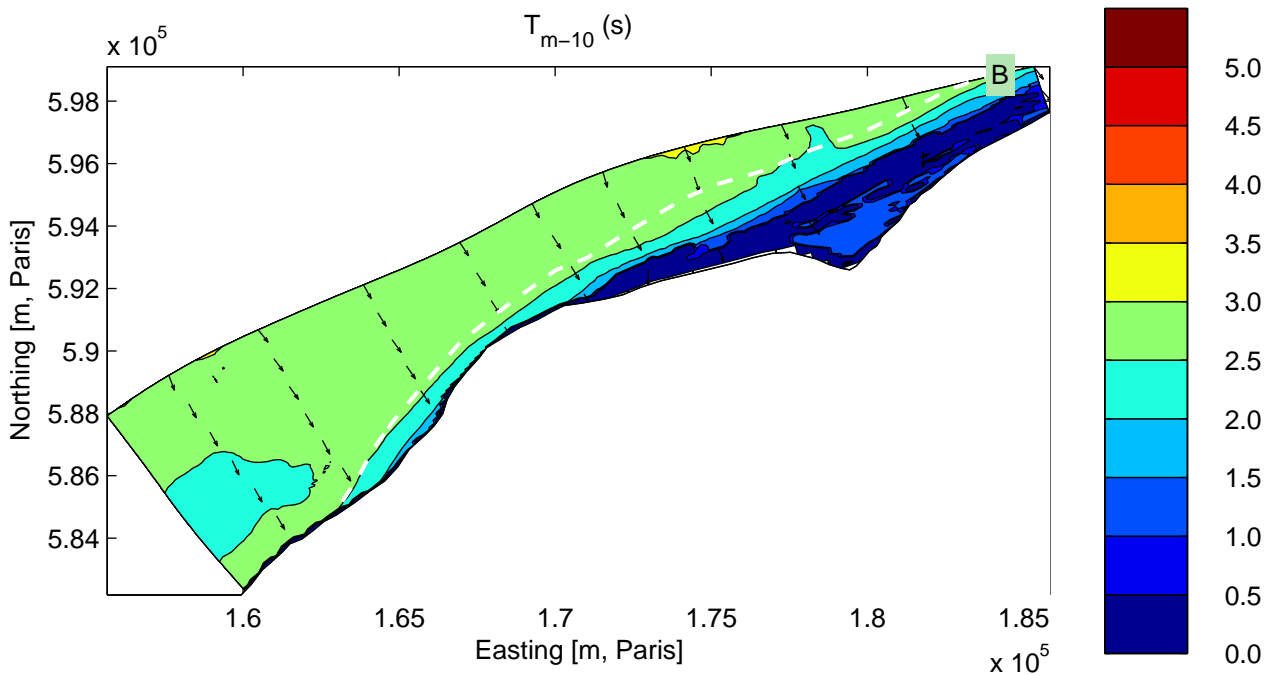
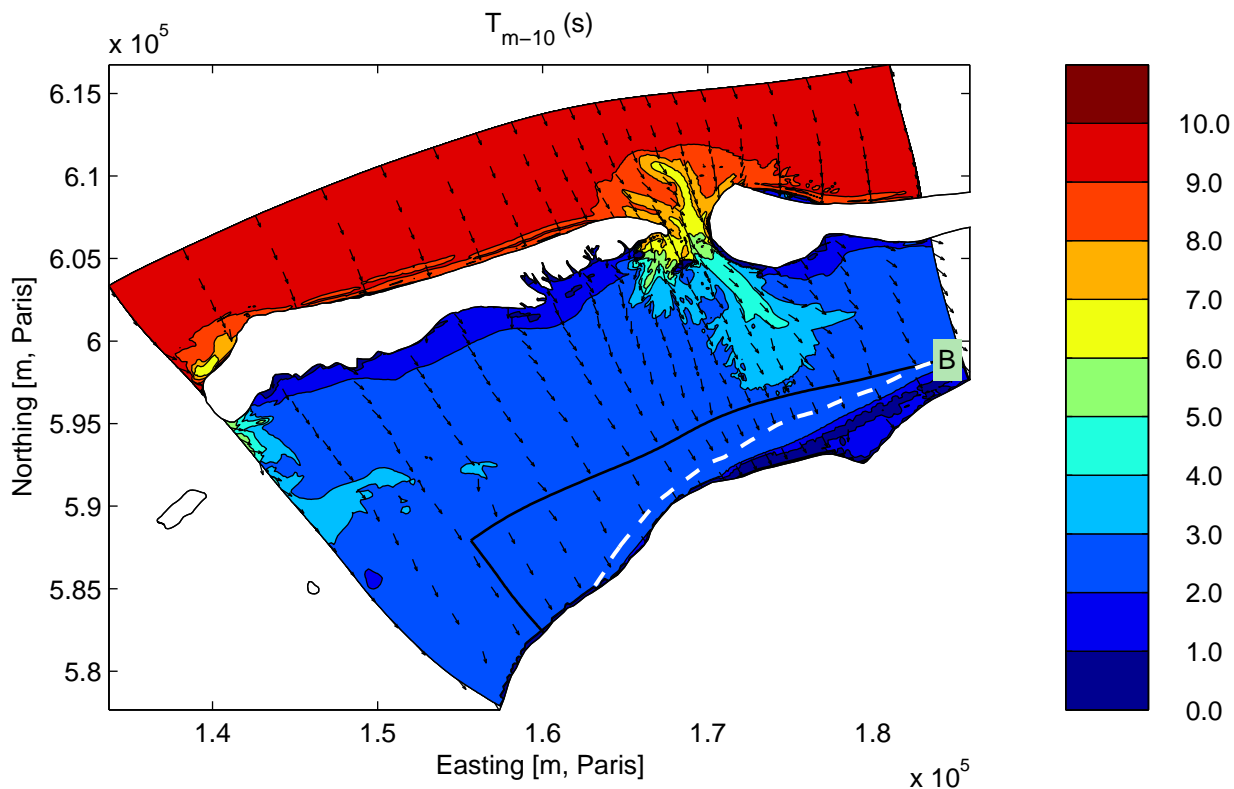
Simulation results for base case C2XXX
Integral parameters along Curve A

Sensitivity analysis Ameland



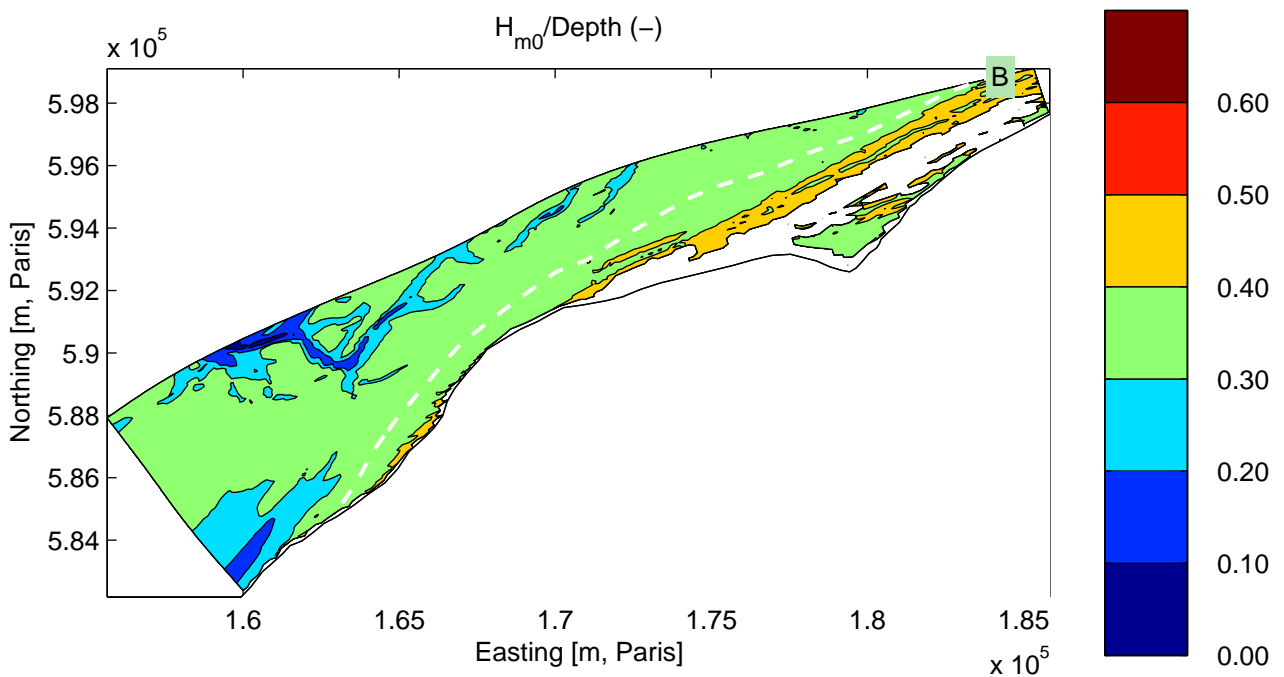
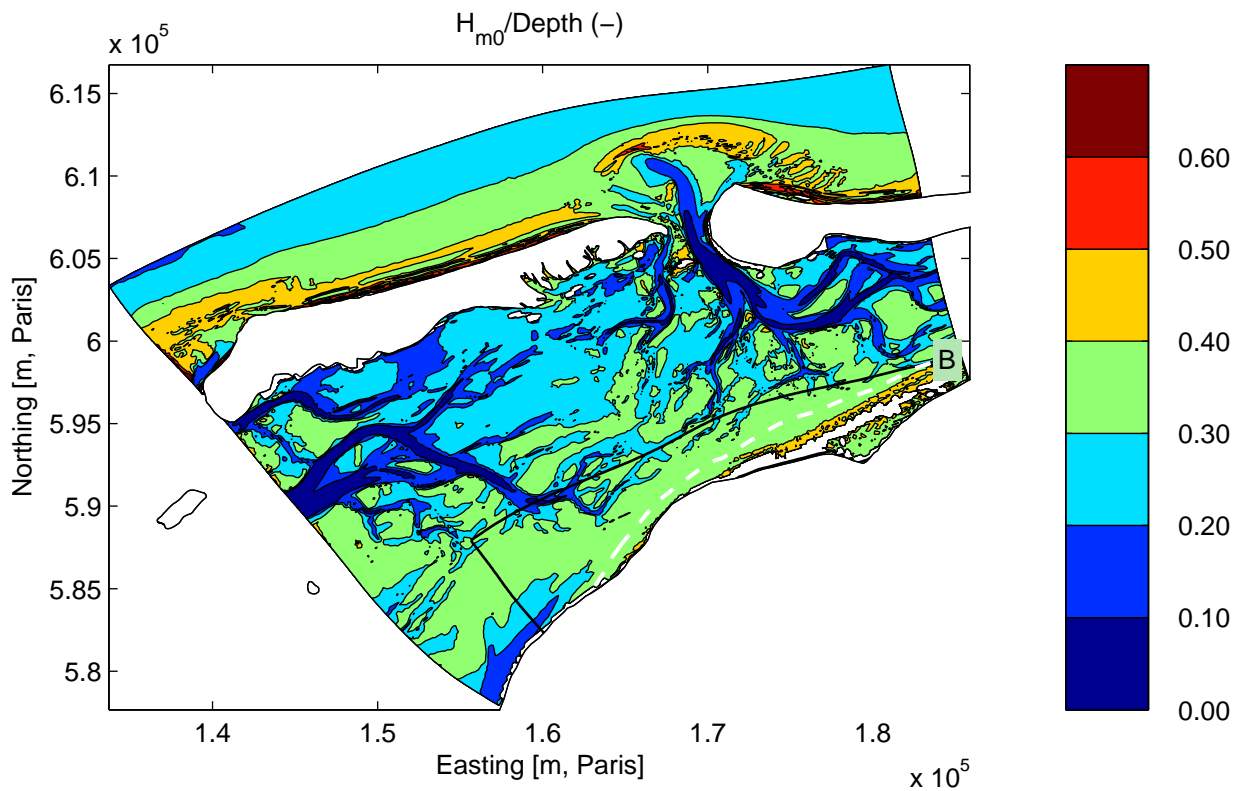
Simulation results for base case C3XXX
 Significant wave height on grids AZG3A (above) and AK4A (below).

Sensitivity analysis Ameland



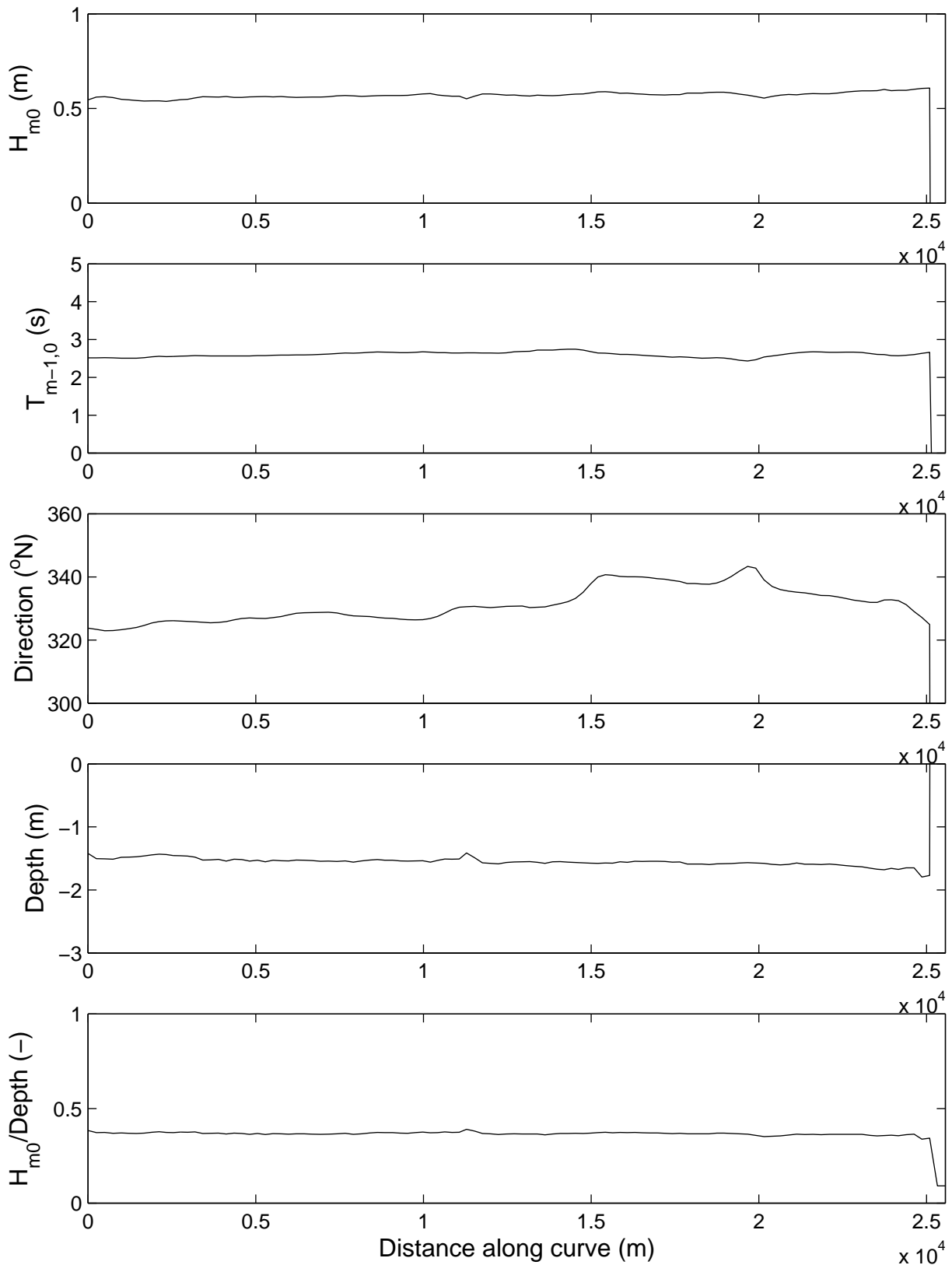
Simulation results for base case C3XXX
 Mean wave period on grids AZG3A (above) and AK4A (below).

Sensitivity analysis Ameland



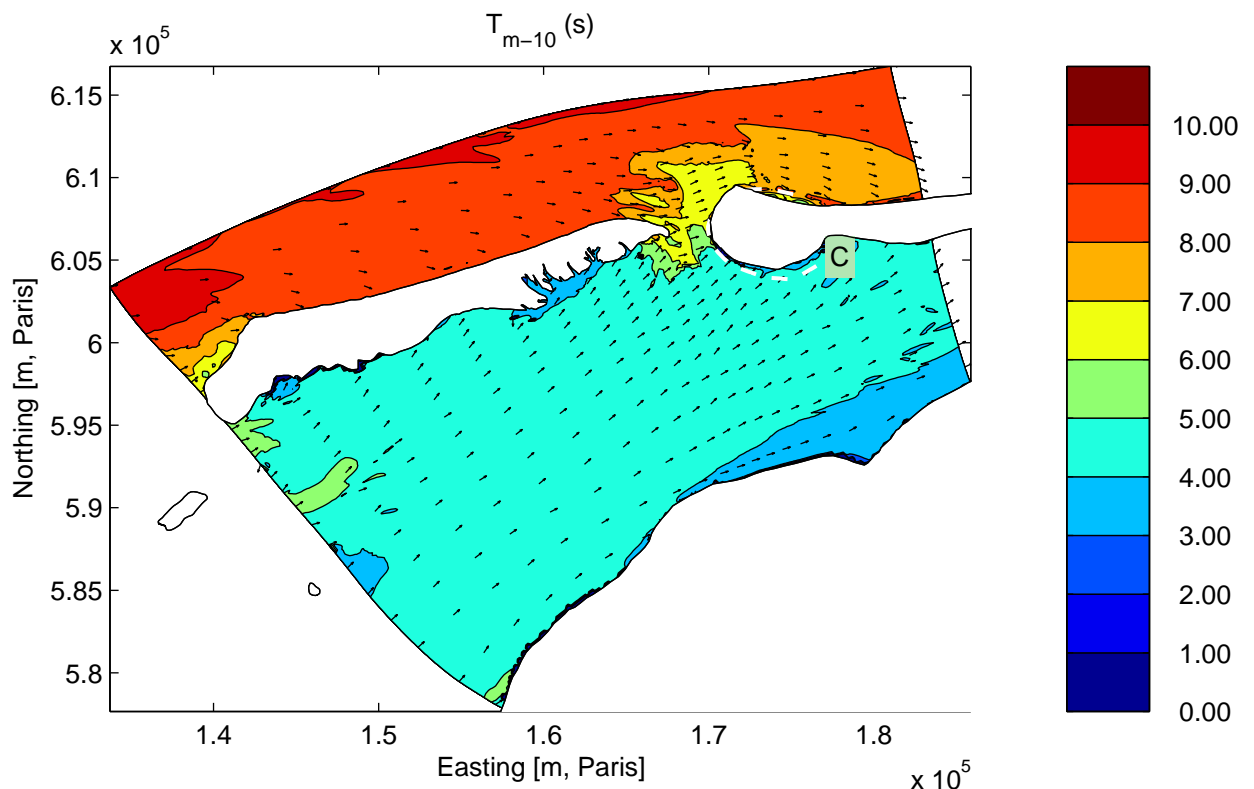
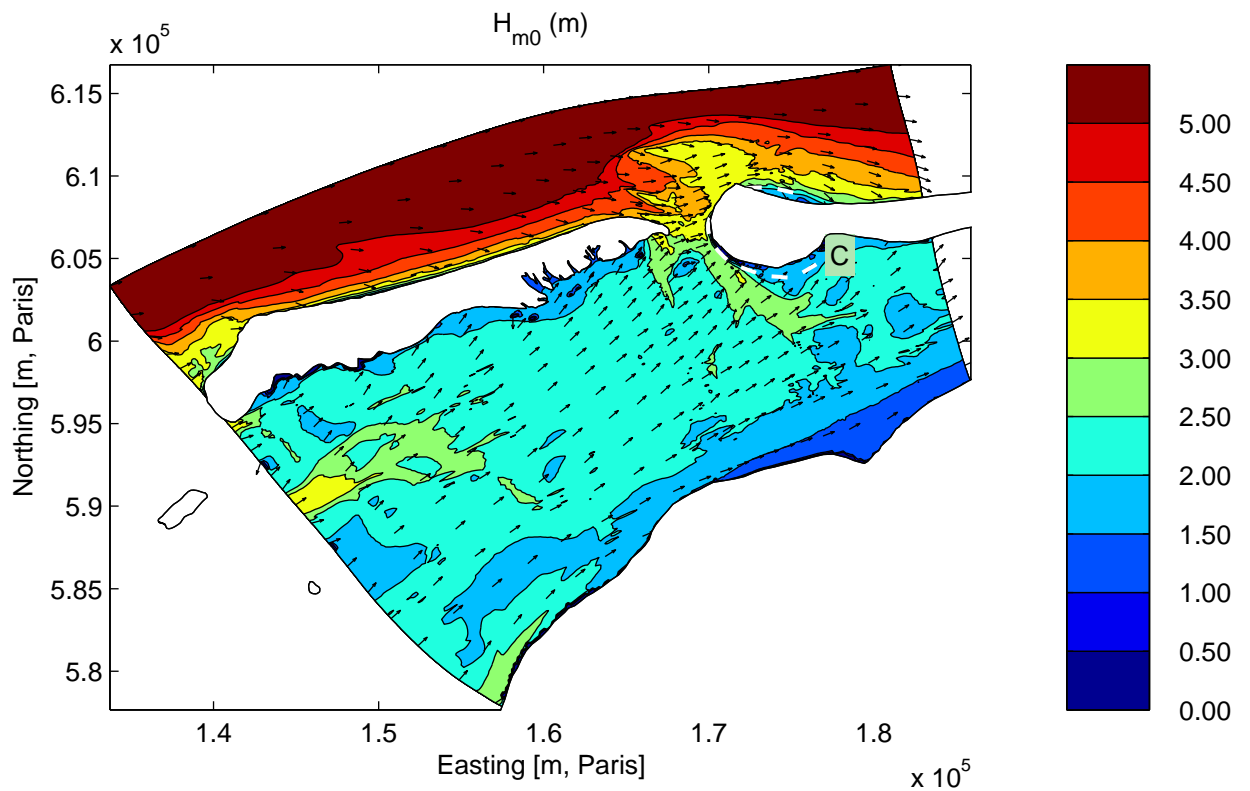
Simulation results for base case C3XXX
 Ratio of H_{m0}/Depth on grids AZG3A (above) and AK4A (below).

Sensitivity analysis Ameland



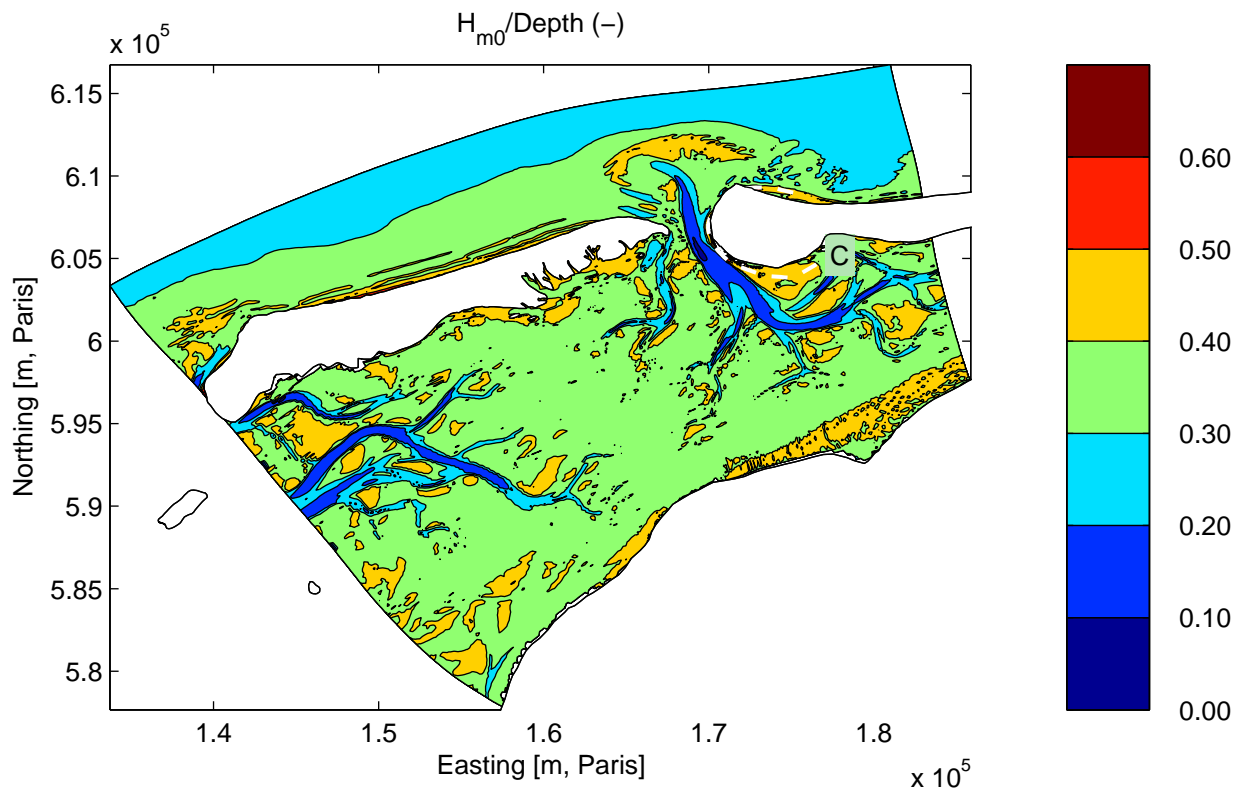
Simulation results for base case C3XXX
Integral parameters along Curve B

Sensitivity analysis Ameland



Simulation results for base case C4XXX
 Significant wave height (above) and mean wave period (below).

Sensitivity analysis Ameland



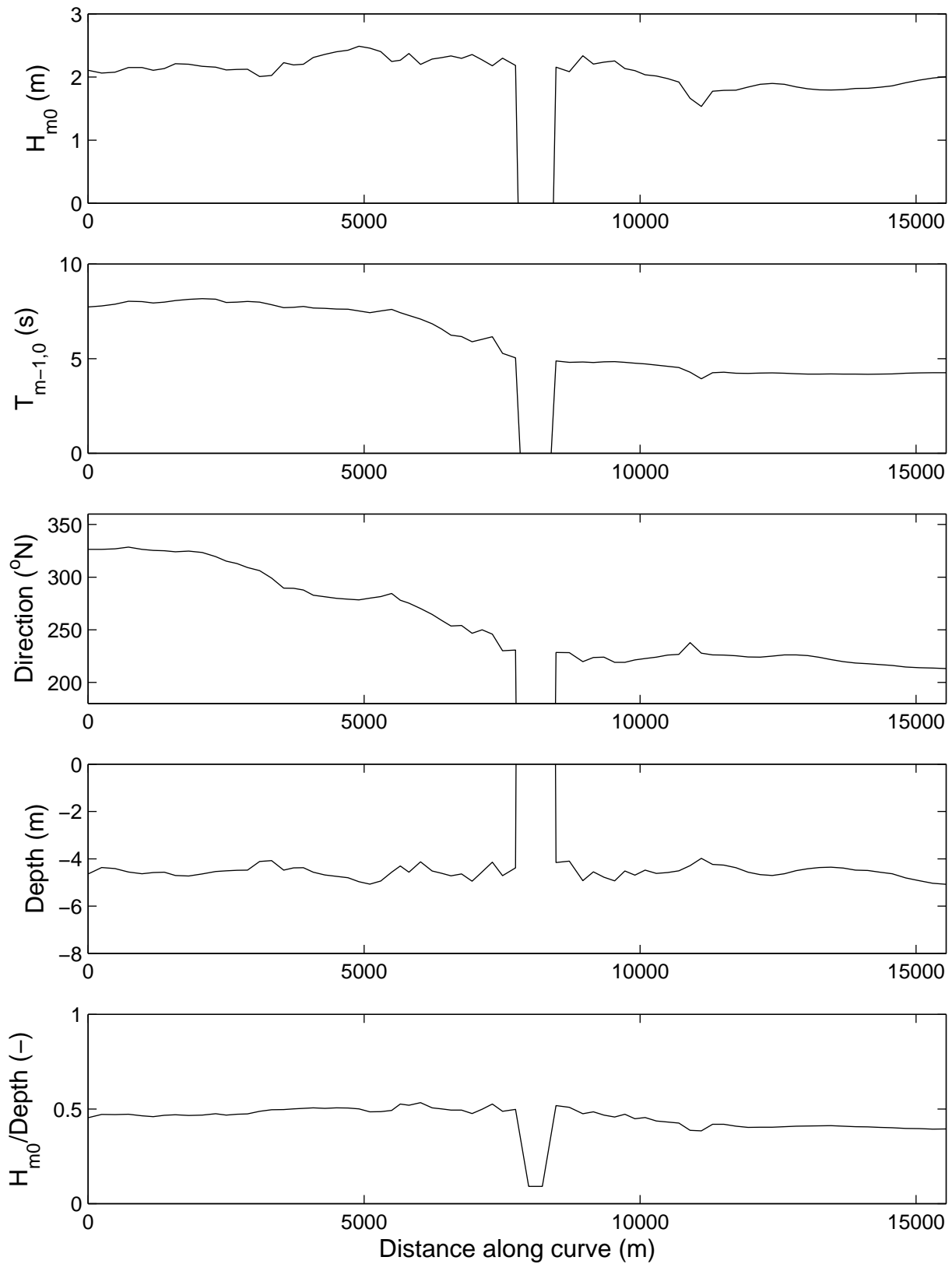
Simulation results for base case C4XXX
Ratio of H_{m0}/Depth .

Sensitivity analysis Ameland

WL | DELFT HYDRAULICS

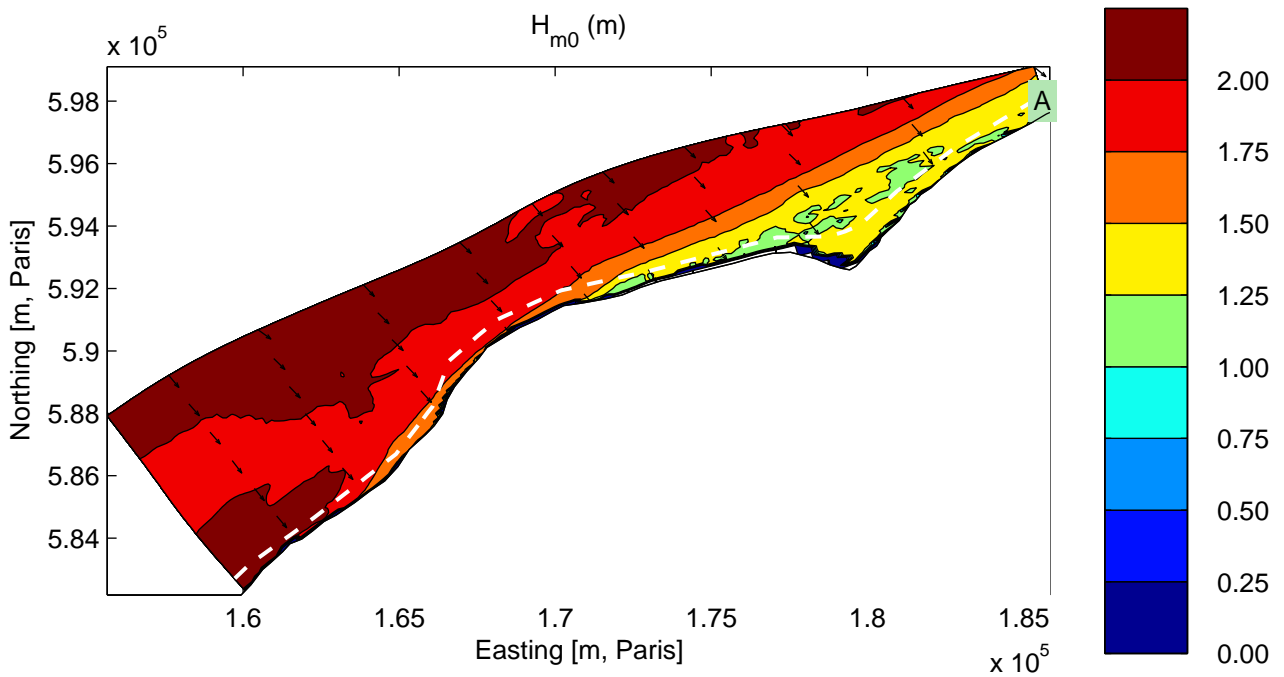
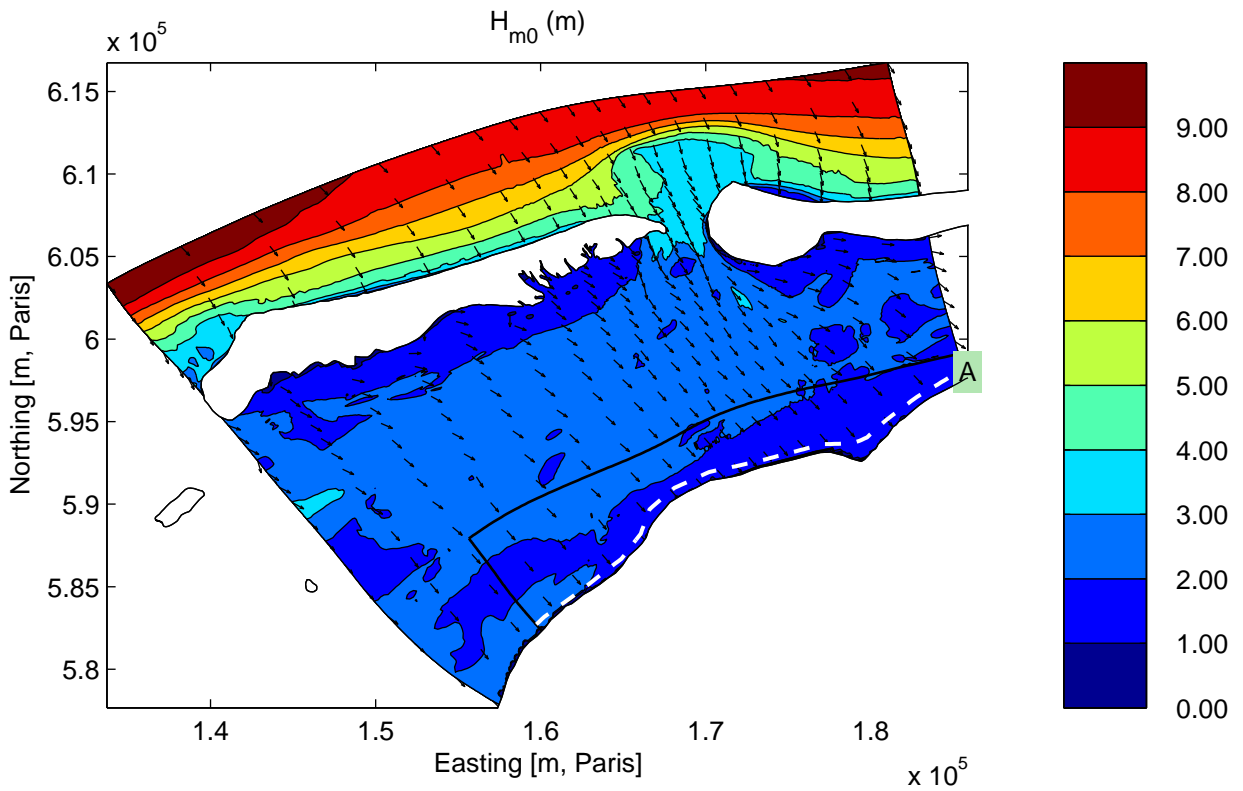
H4918.41

Fig. 4.5b



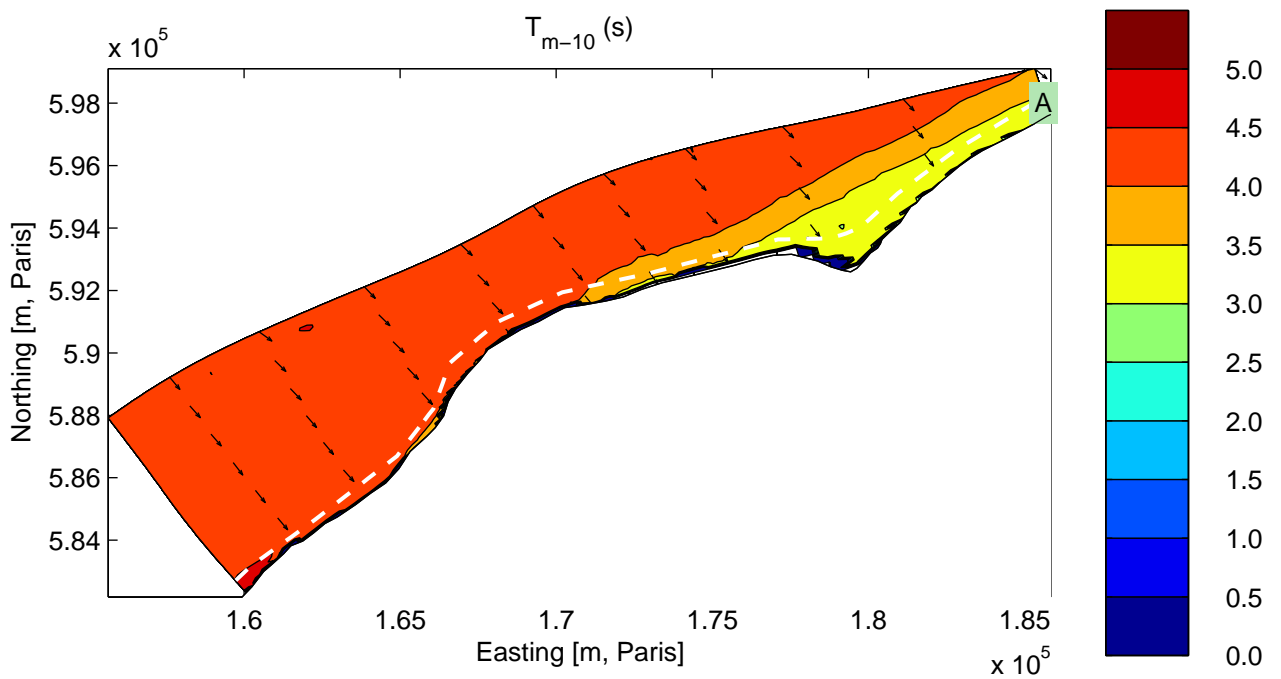
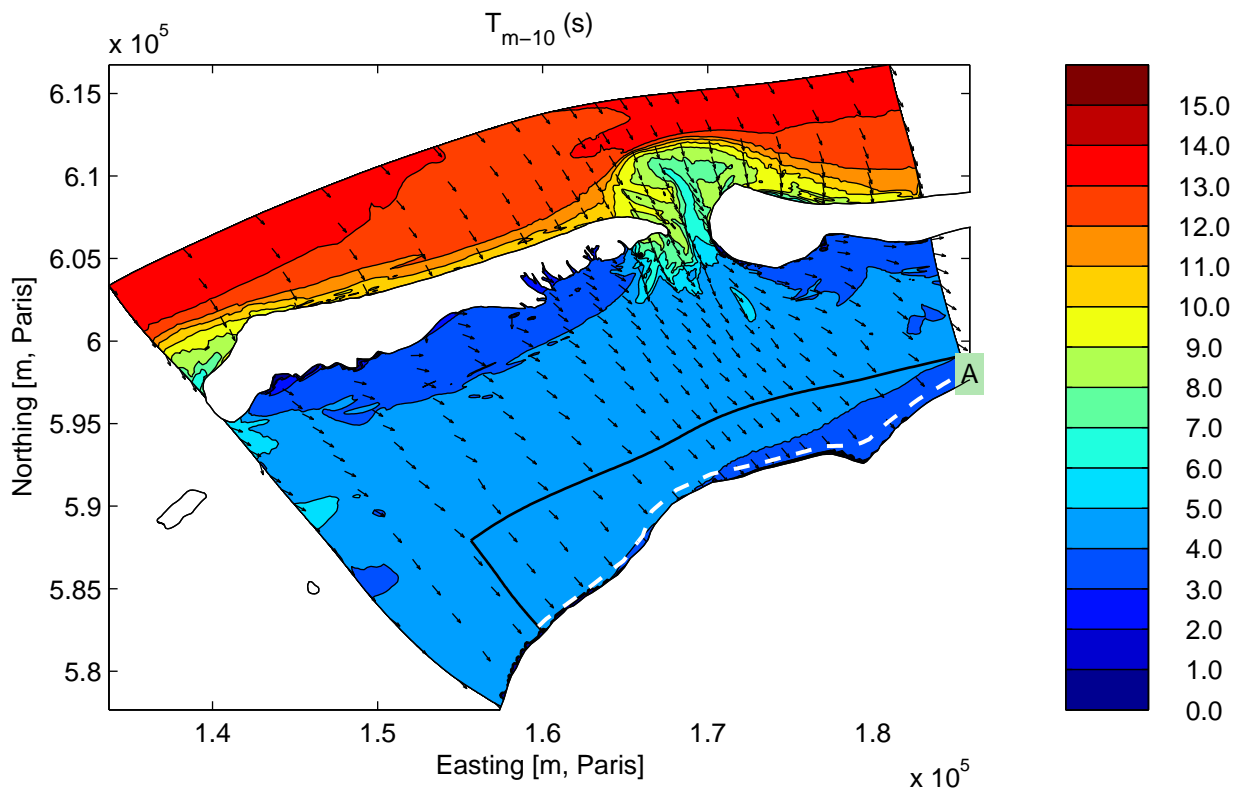
Simulation results for base case C4XXX
Integral parameters along Curve C

Sensitivity analysis Ameland



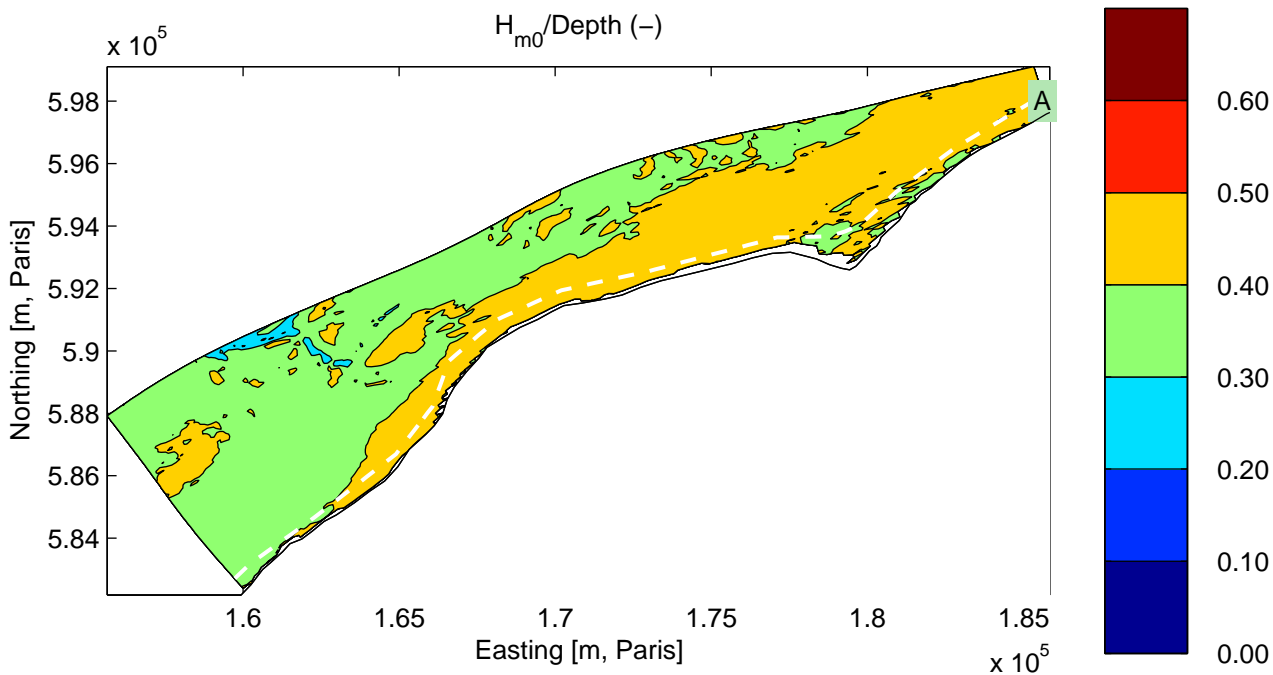
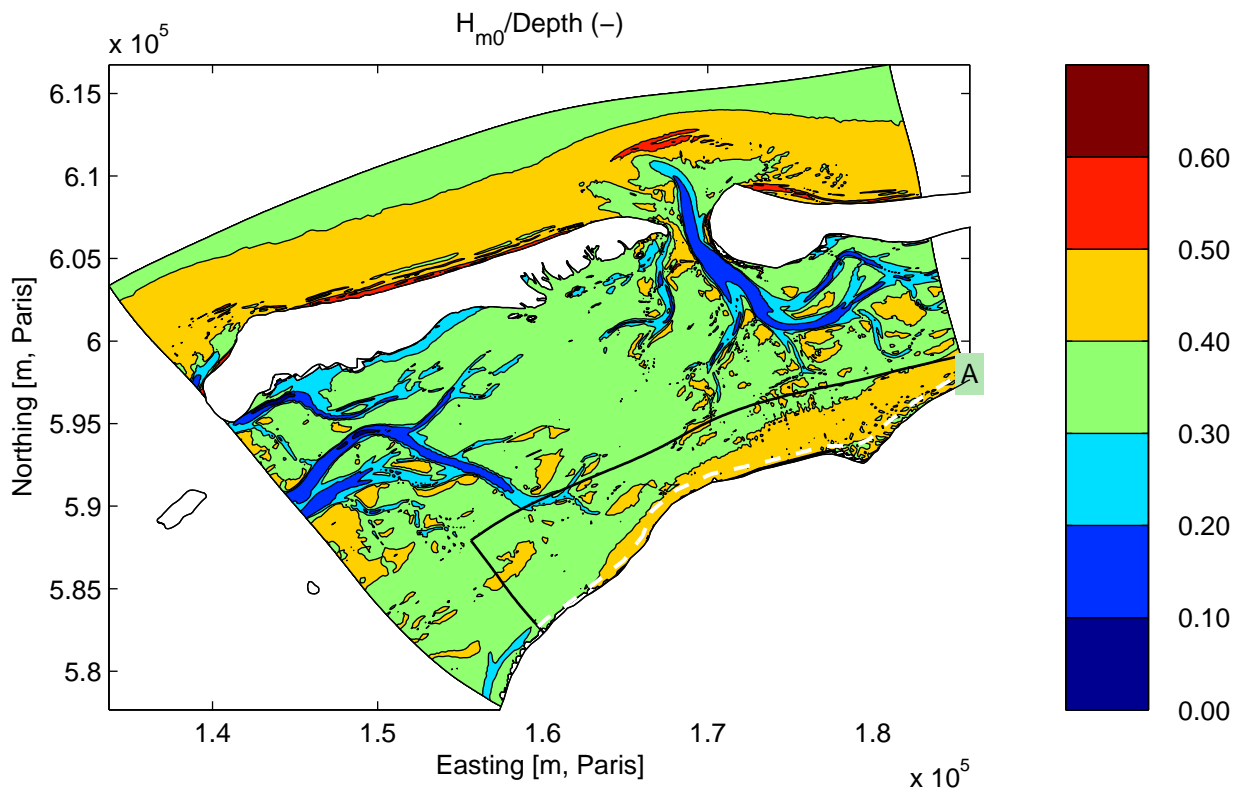
Simulation results for base case C5XXX
 Significant wave height on grids AZG3A (above) and AK4A (below).

Sensitivity analysis Ameland



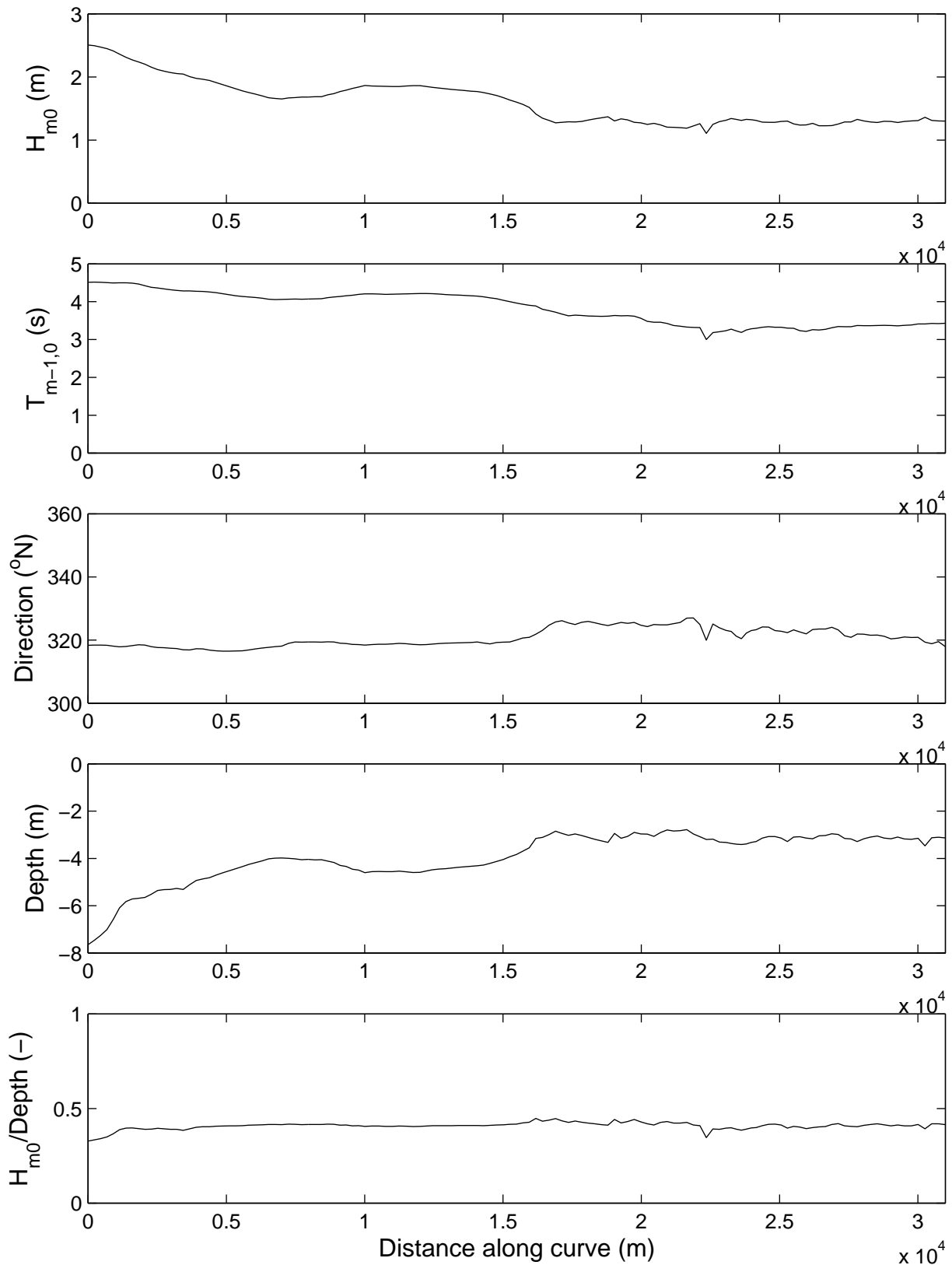
Simulation results for base case C5XXX
 Mean wave period on grids AZG3A (above) and AK4A (below).

Sensitivity analysis Ameland



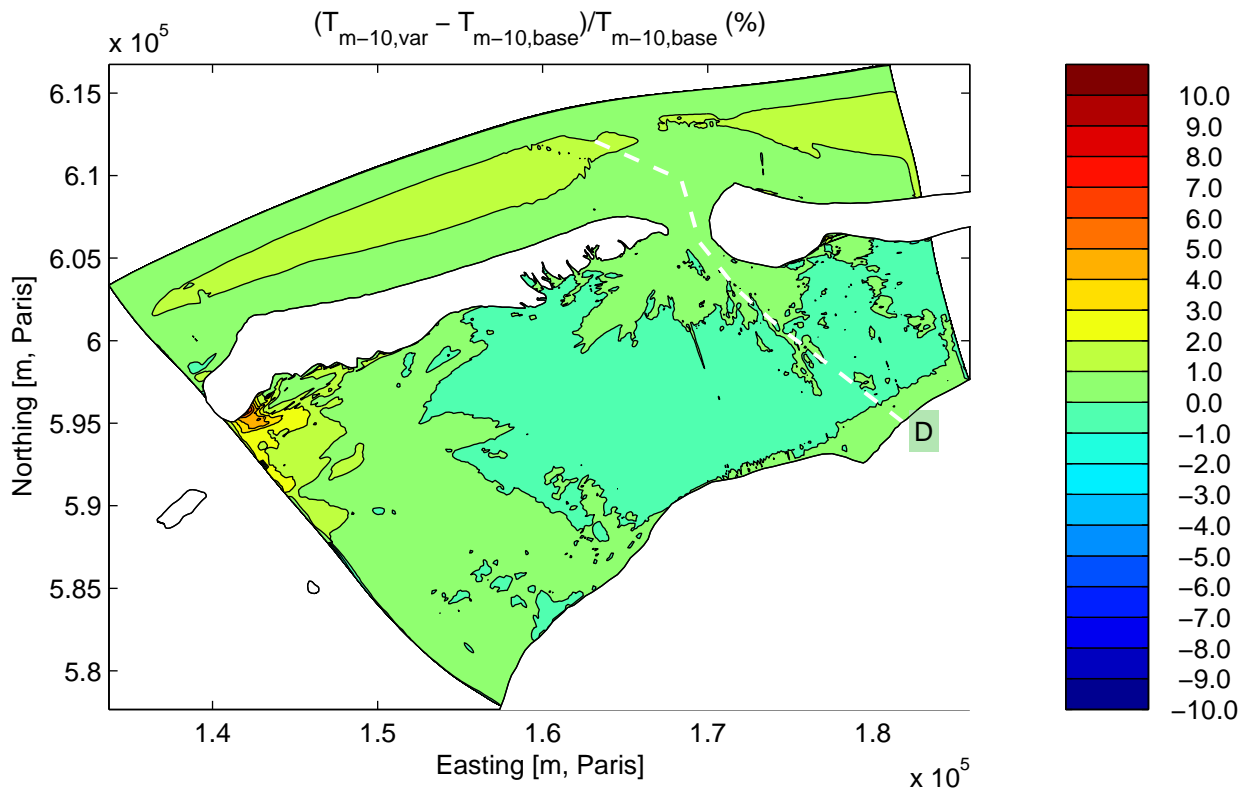
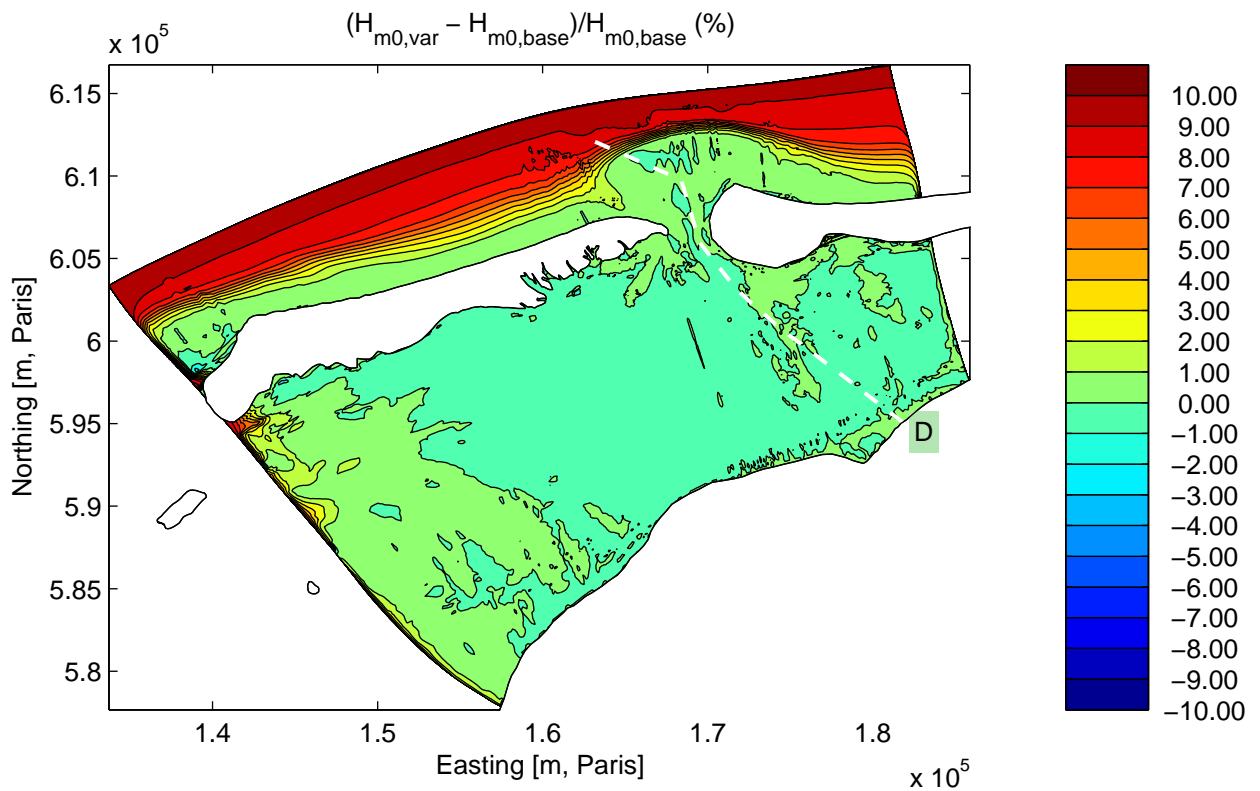
Simulation results for base case C5XXX
 Ratio of H_{m0}/Depth on grids AZG3A (above) and AK4A (below).

Sensitivity analysis Ameland



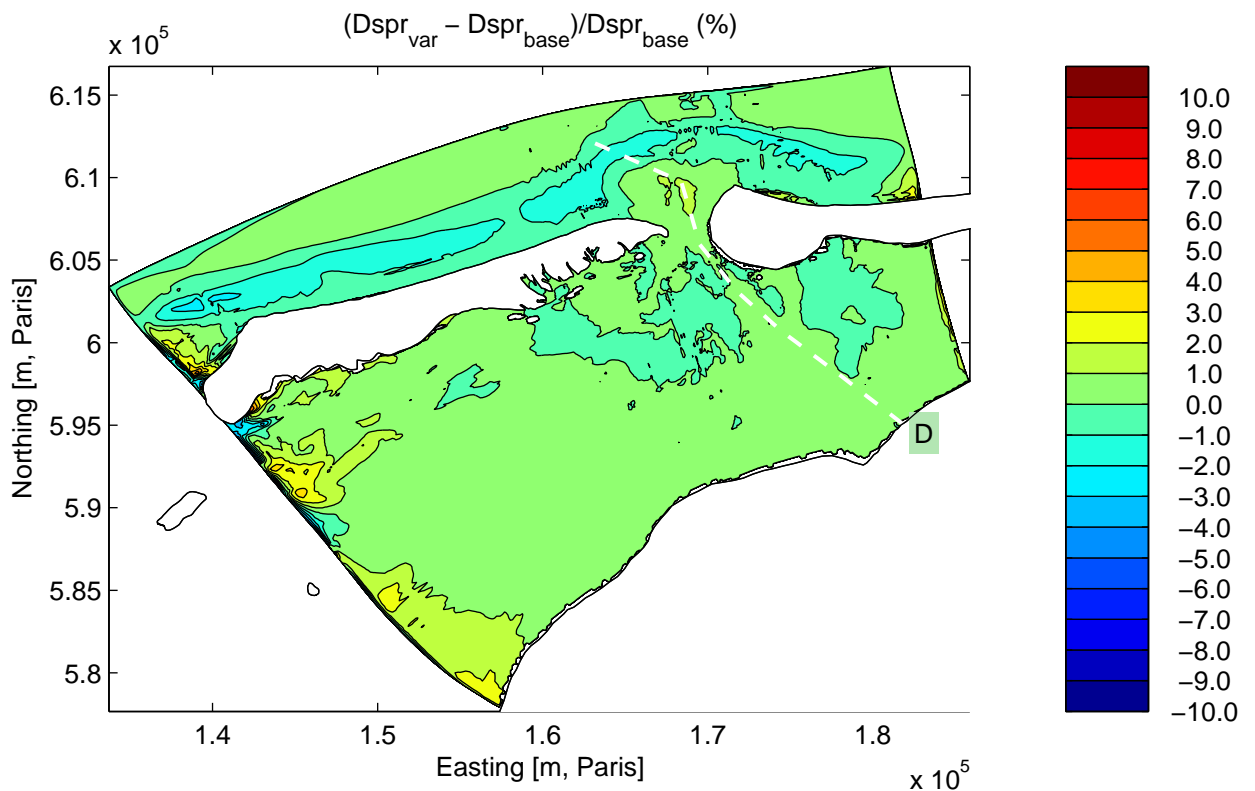
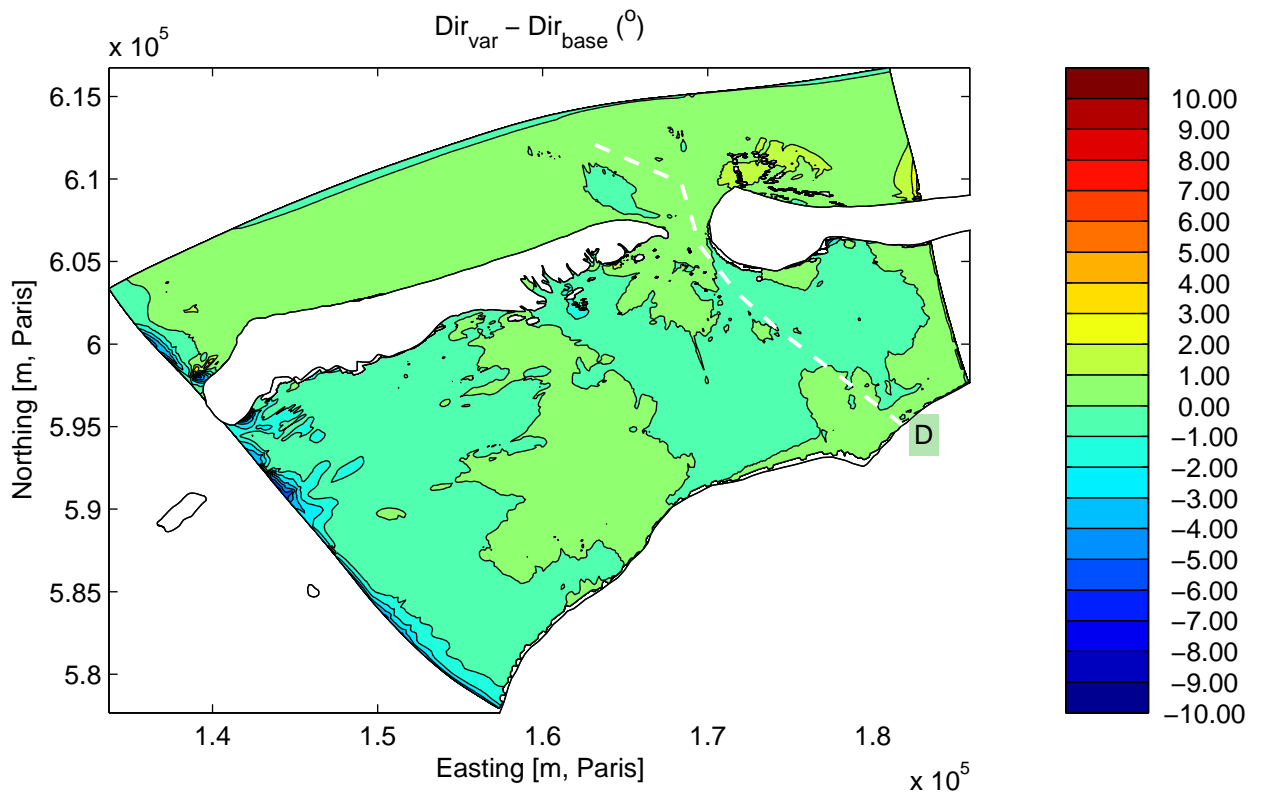
Simulation results for base case C5XXX
Integral parameters along Curve A

Sensitivity analysis Ameland



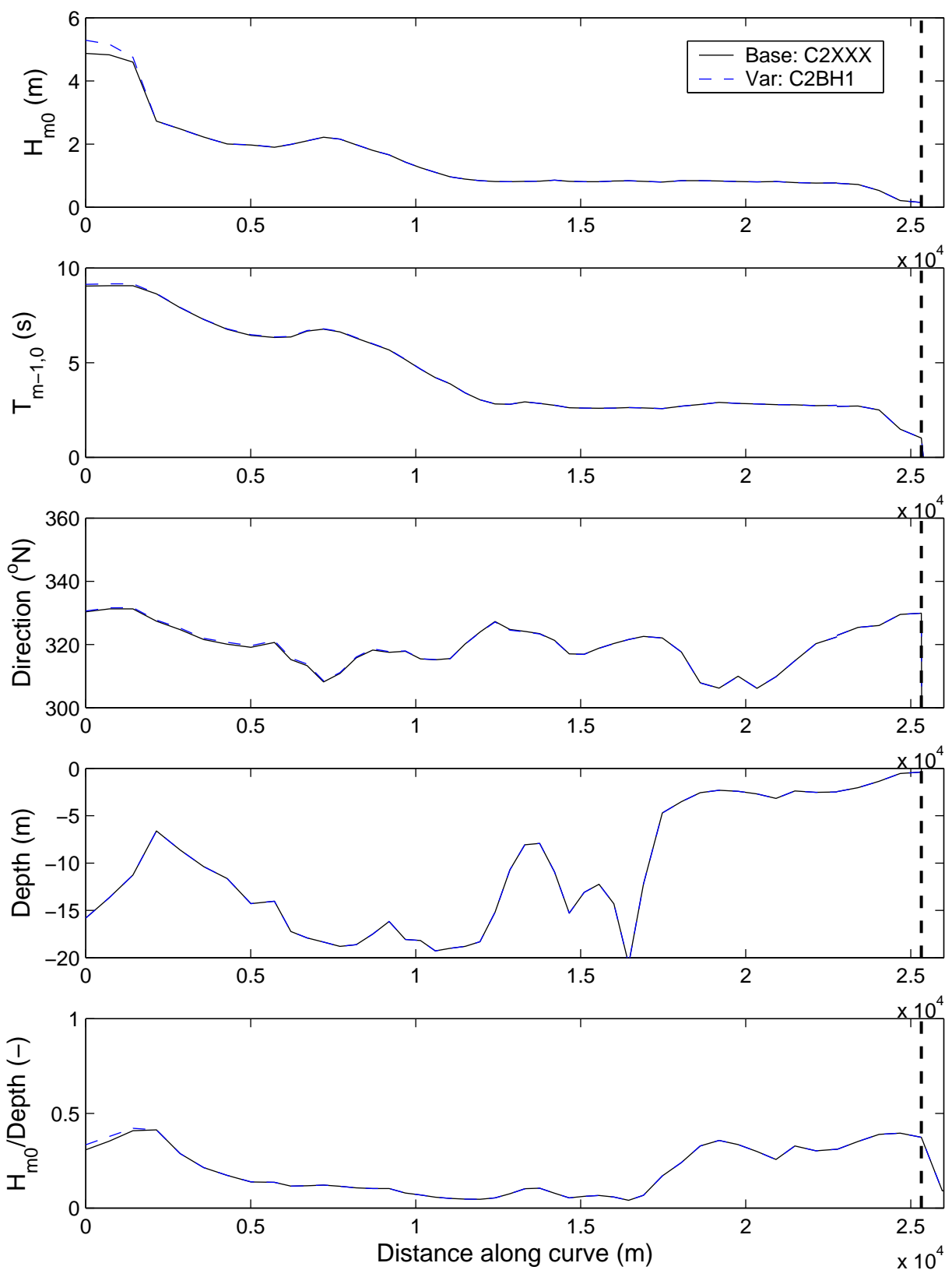
Sensitivity run C2BH1: Variation in wave height at the boundary
Differences in significant wave height (above) and mean period (below).

Sensitivity analysis Ameland



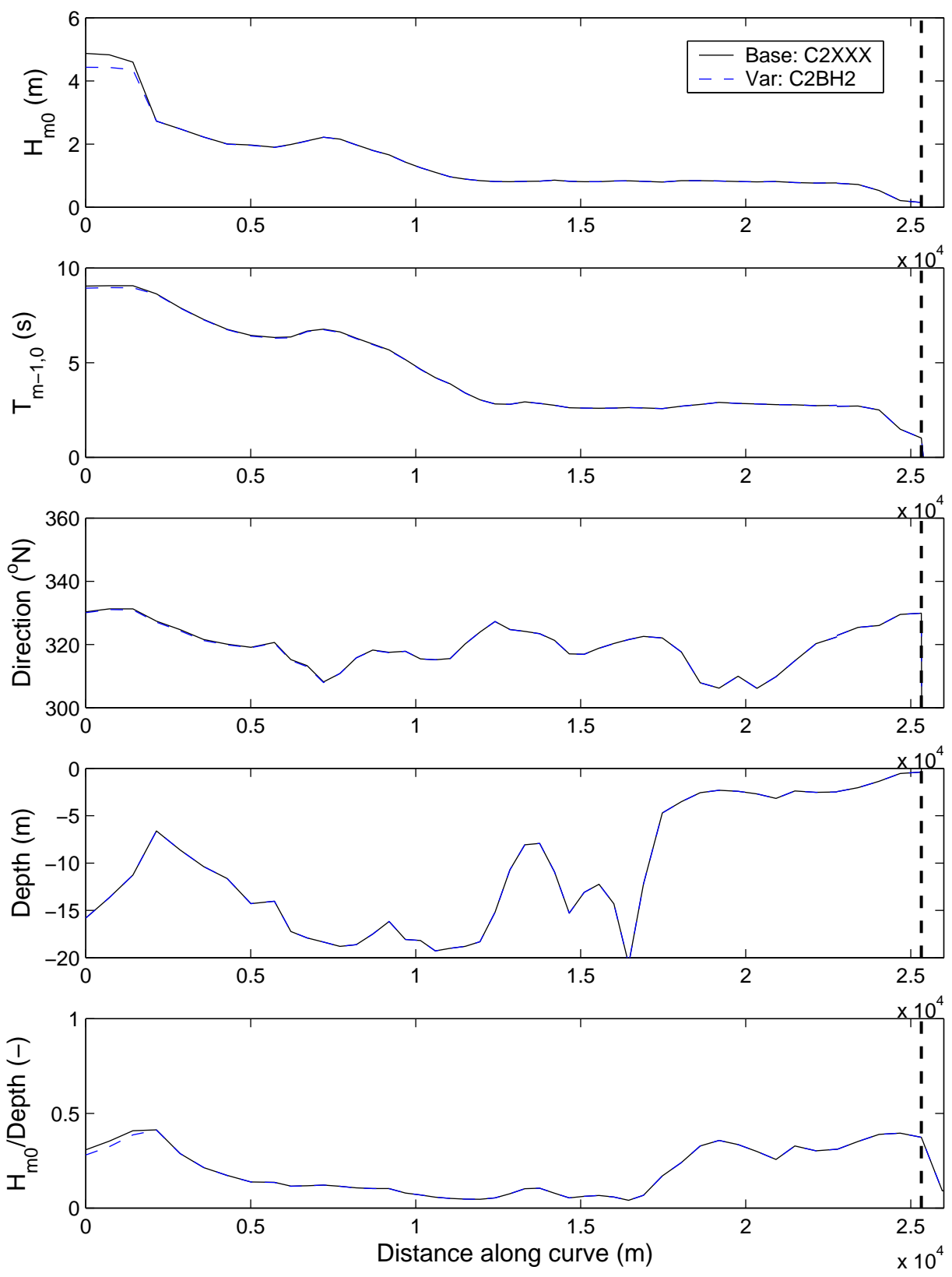
Sensitivity run C2BH1: Variation in wave height at the boundary
Differences in mean direction (above) and directional spreading (below).

Sensitivity analysis Ameland



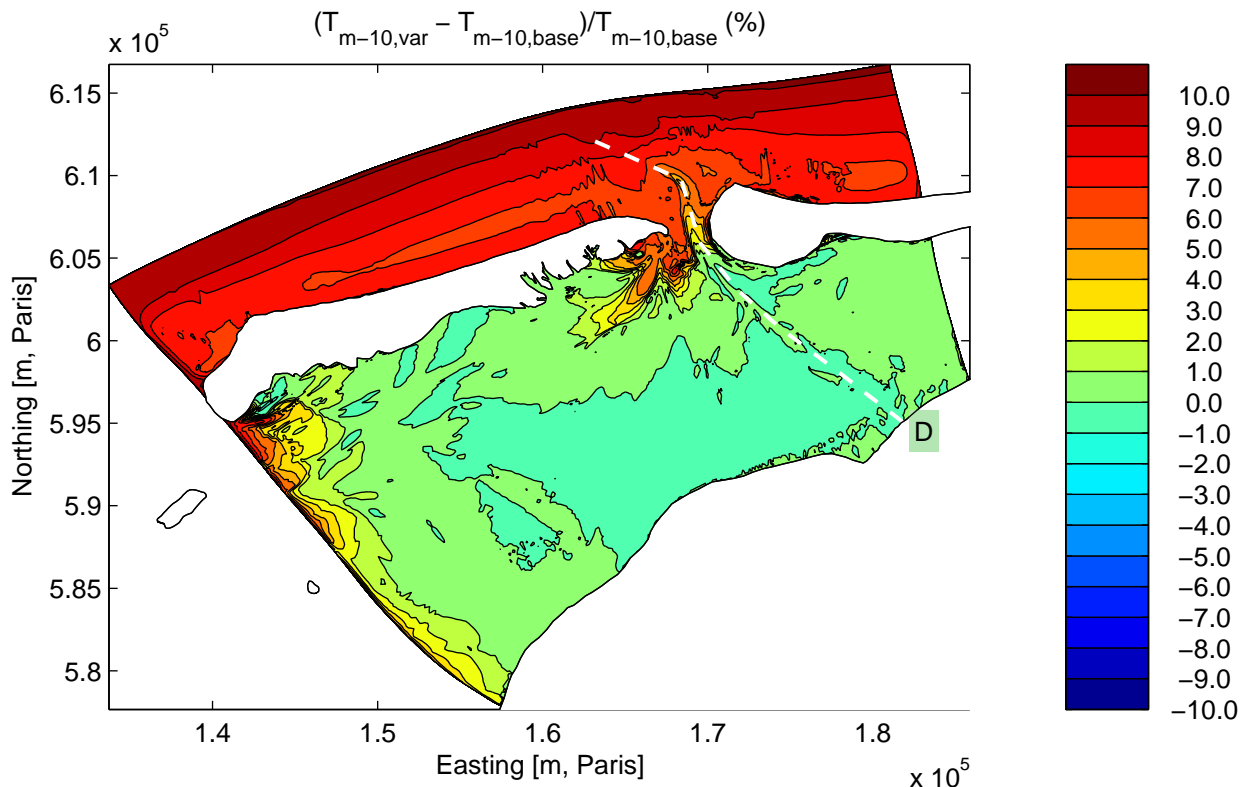
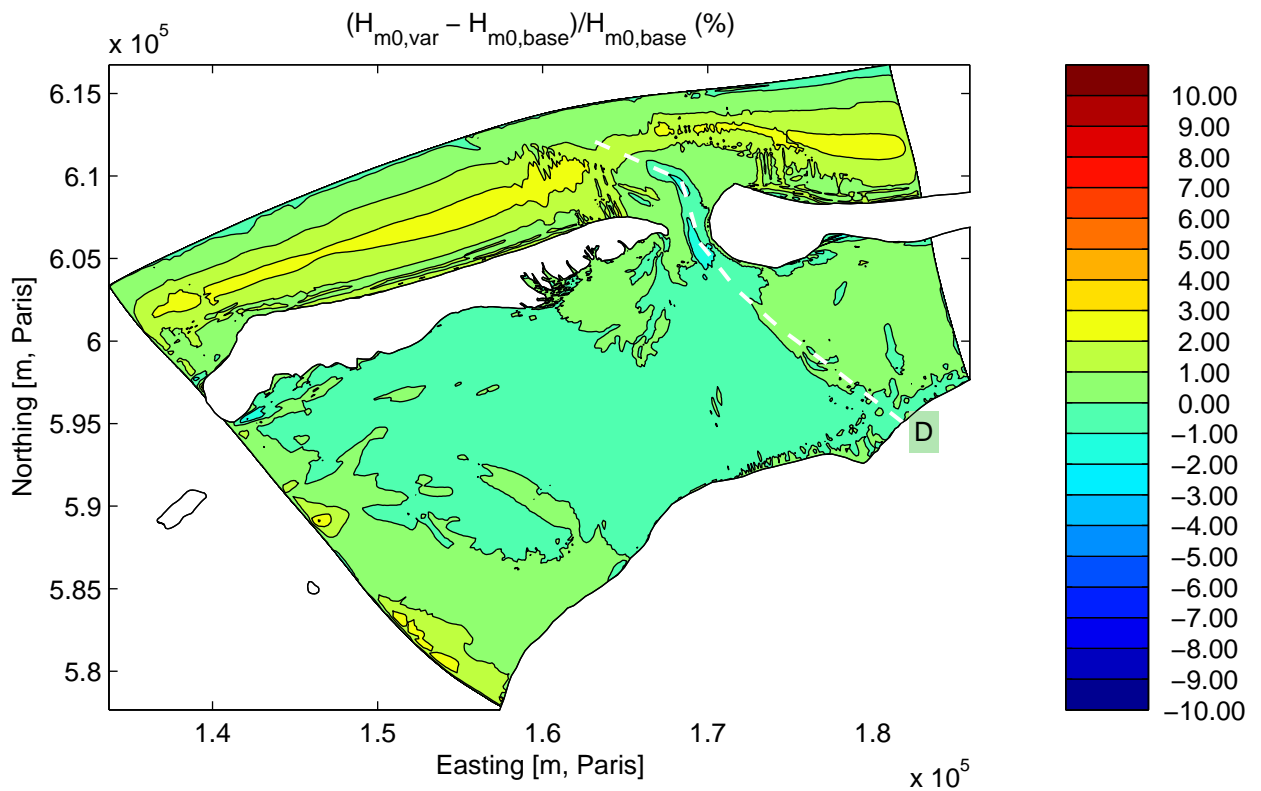
Sensitivity run C2BH1: Variation in wave height at the boundary
Integral parameters along Curve D

Sensitivity analysis Ameland



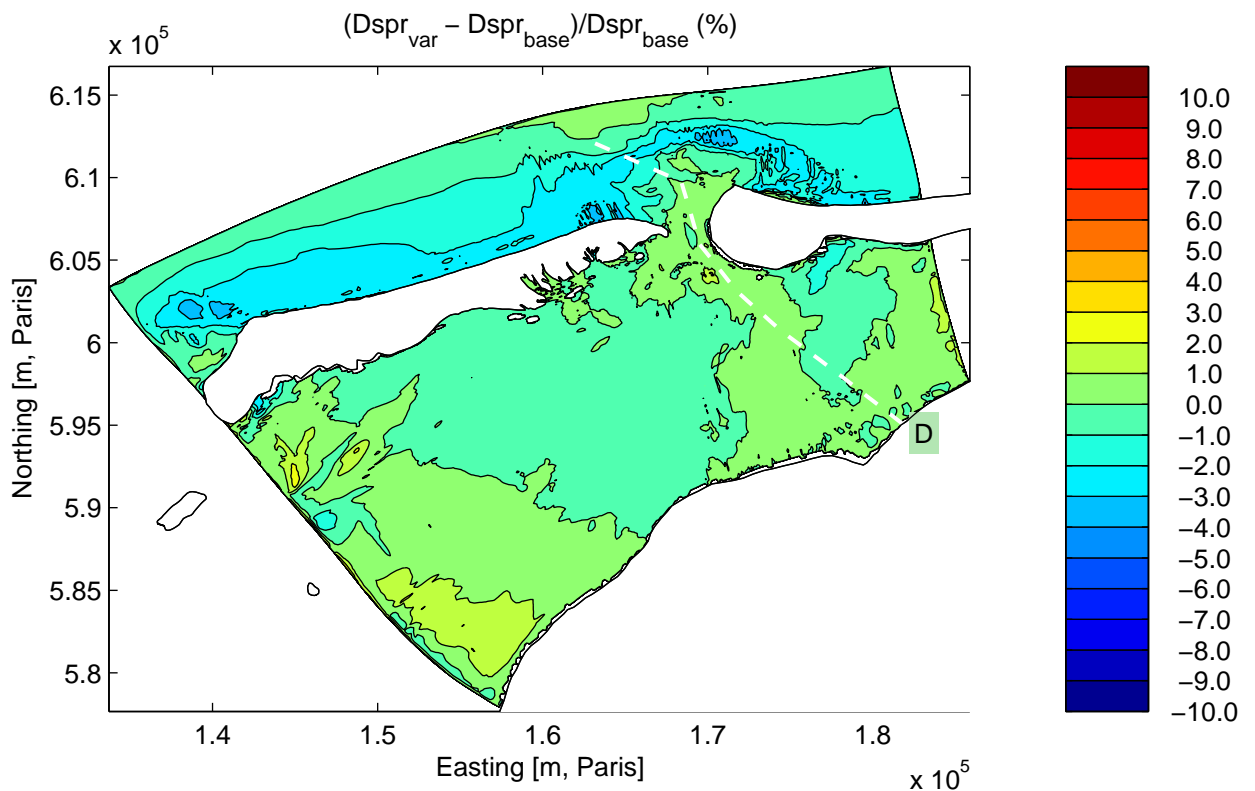
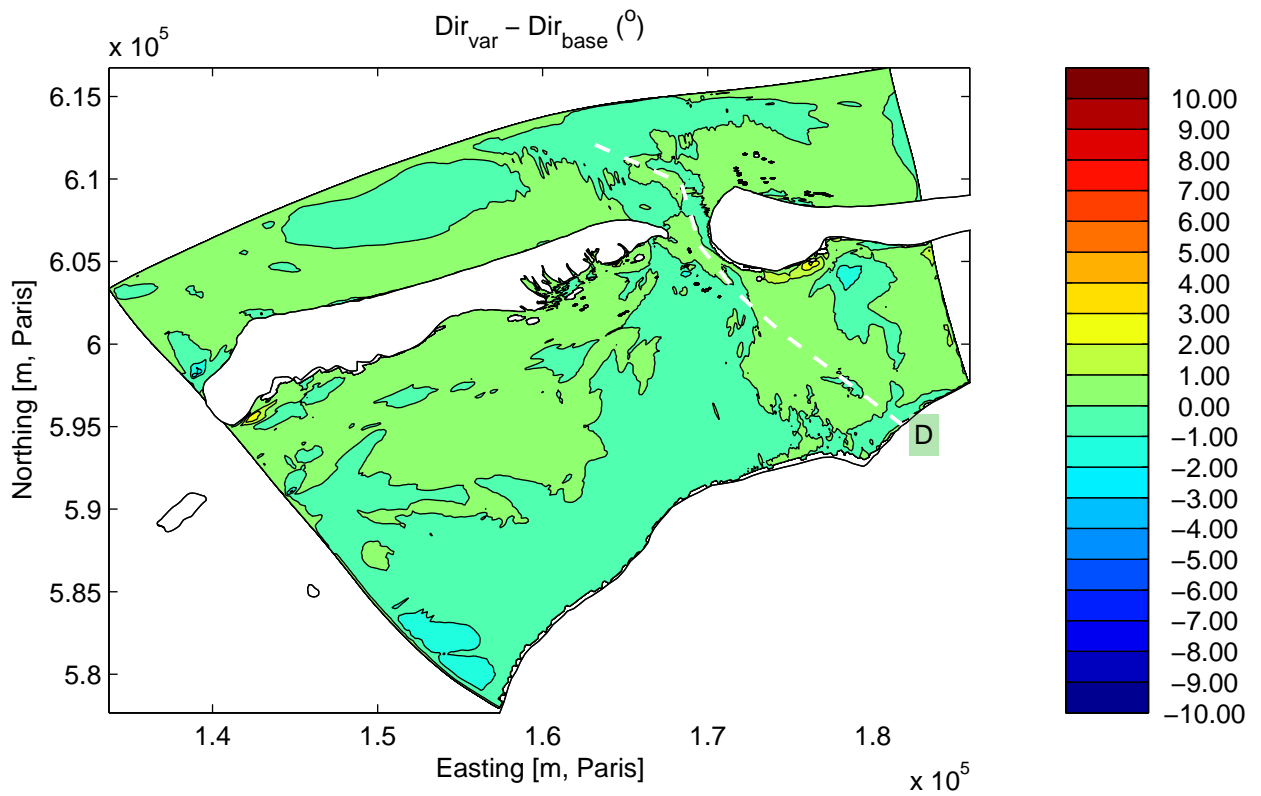
Sensitivity run C2BH2: Variation in wave height at the boundary
Integral parameters along Curve D

Sensitivity analysis Ameland



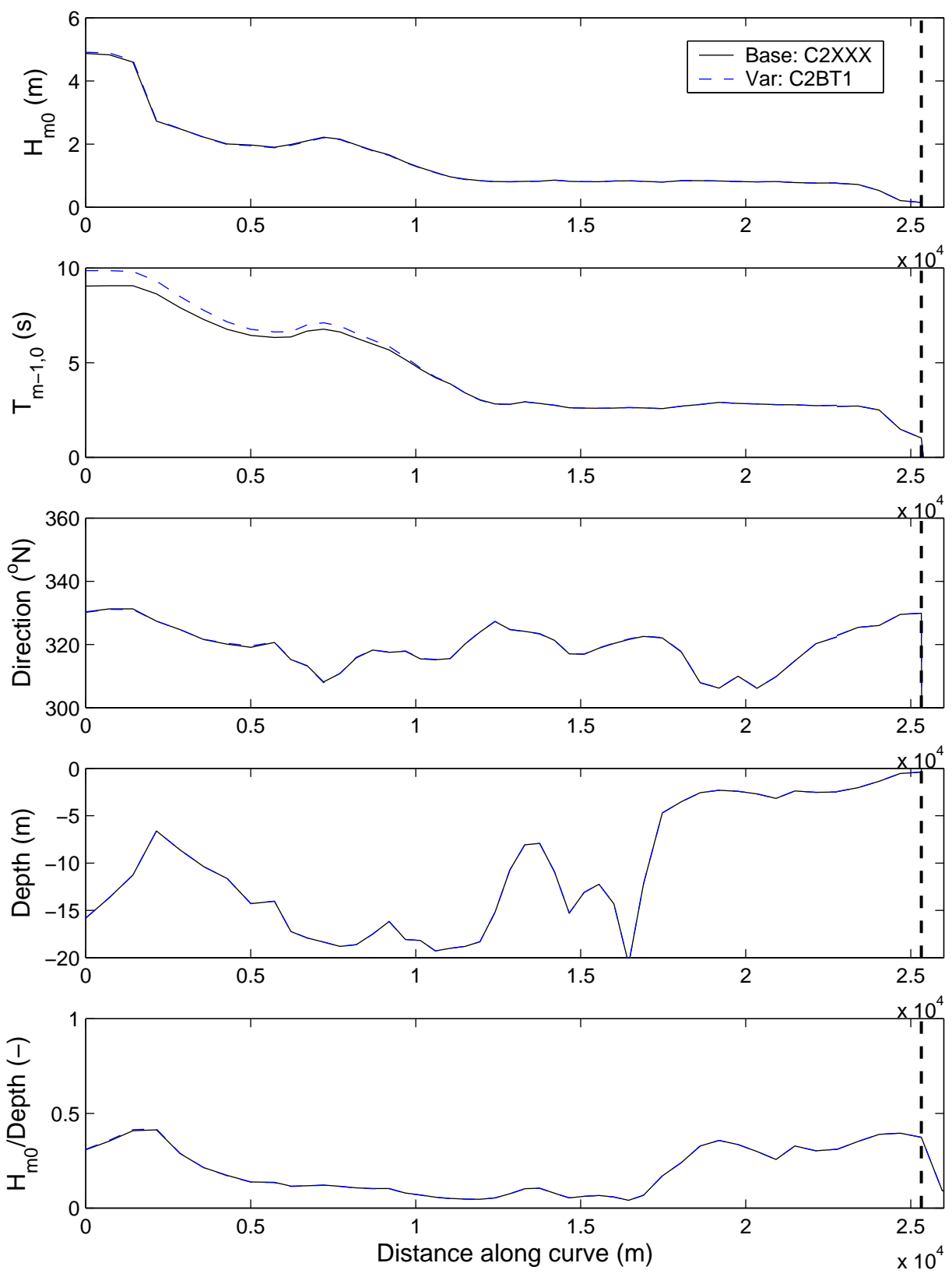
Sensitivity run C2BT1: Variation in wave period at the boundary
Differences in significant wave height (above) and mean period (below).

Sensitivity analysis Ameland



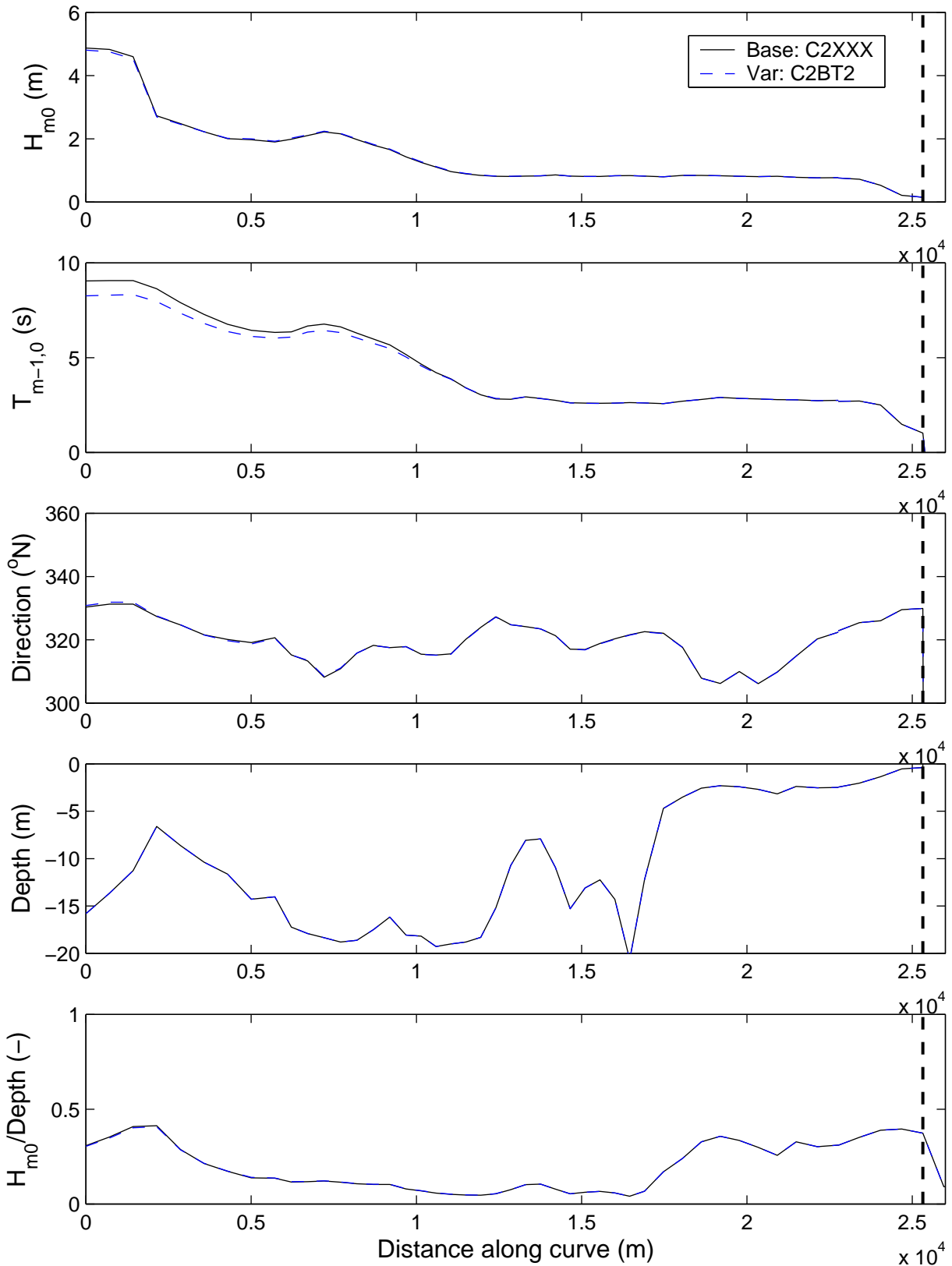
Sensitivity run C2BT1: Variation in wave period at the boundary
 Differences in mean direction (above) and directional spreading (below).

Sensitivity analysis Ameland



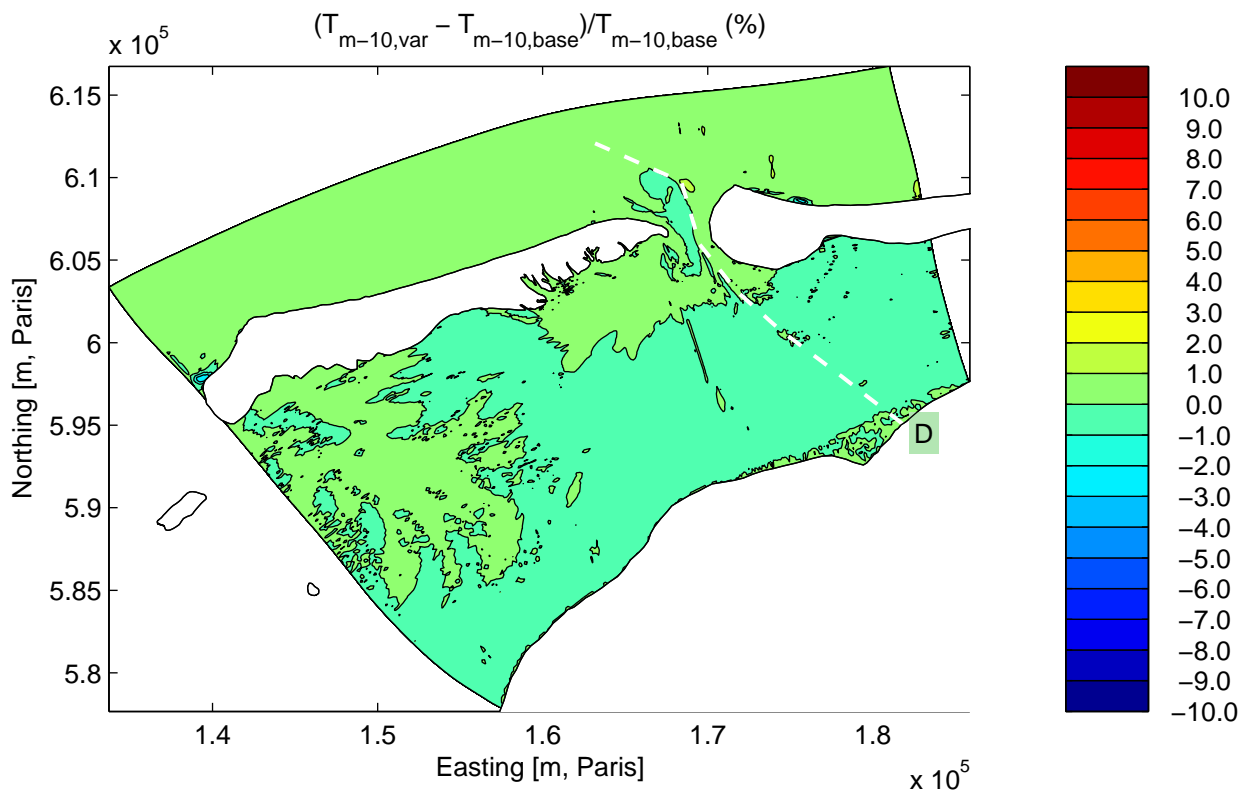
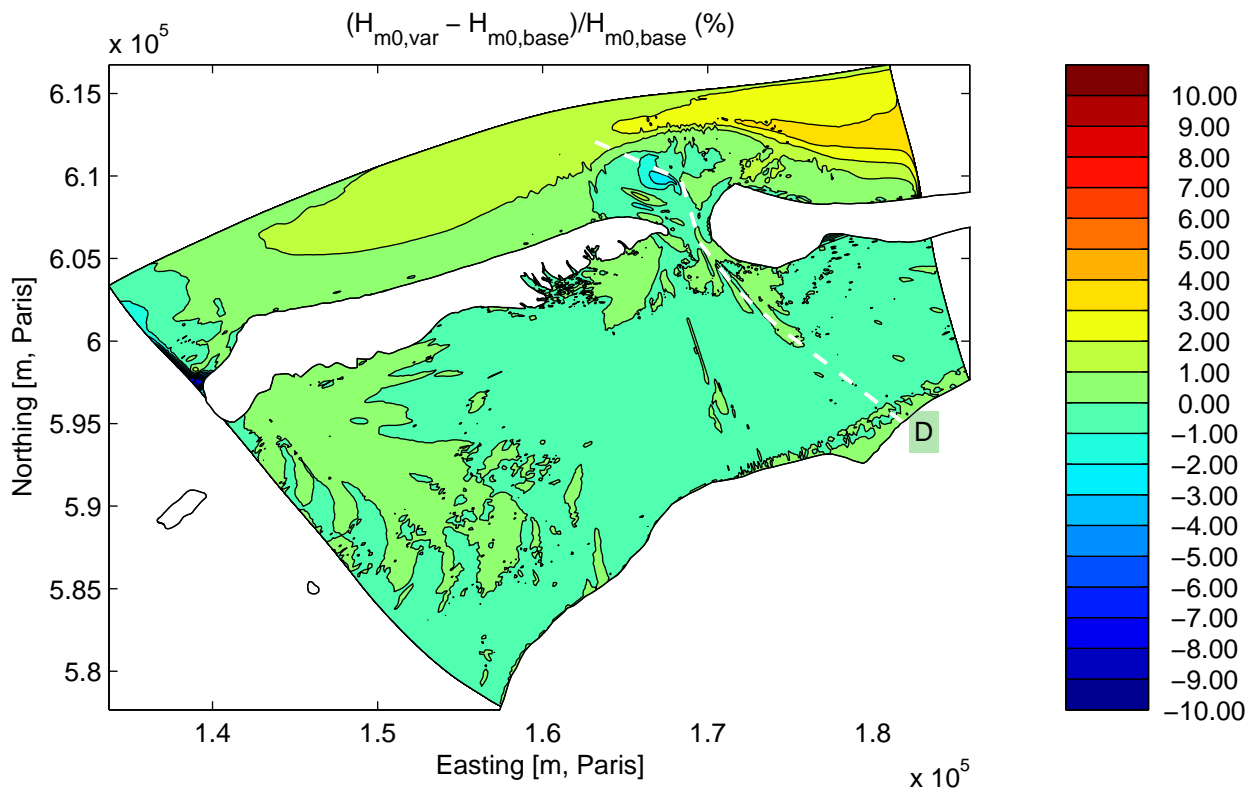
Sensitivity run C2BT1: Variation in wave period at the boundary
Integral parameters along Curve D

Sensitivity analysis Ameland



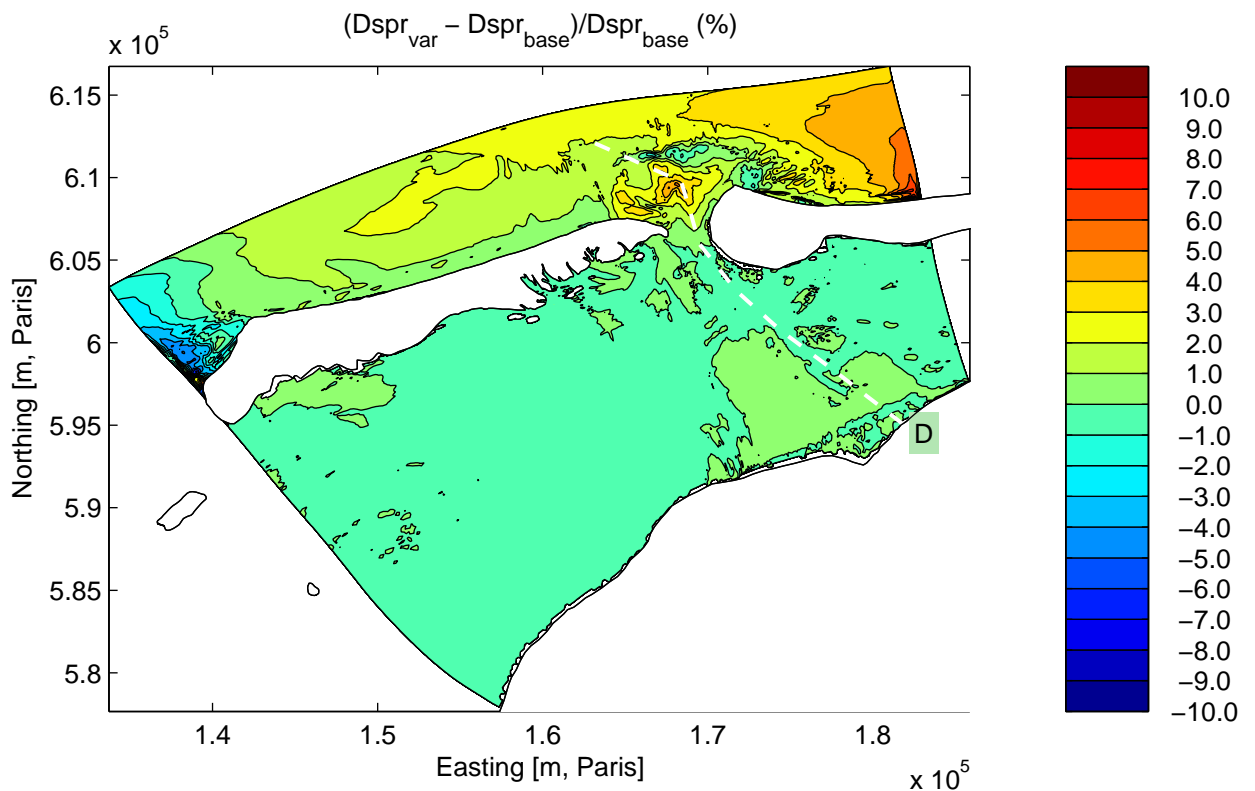
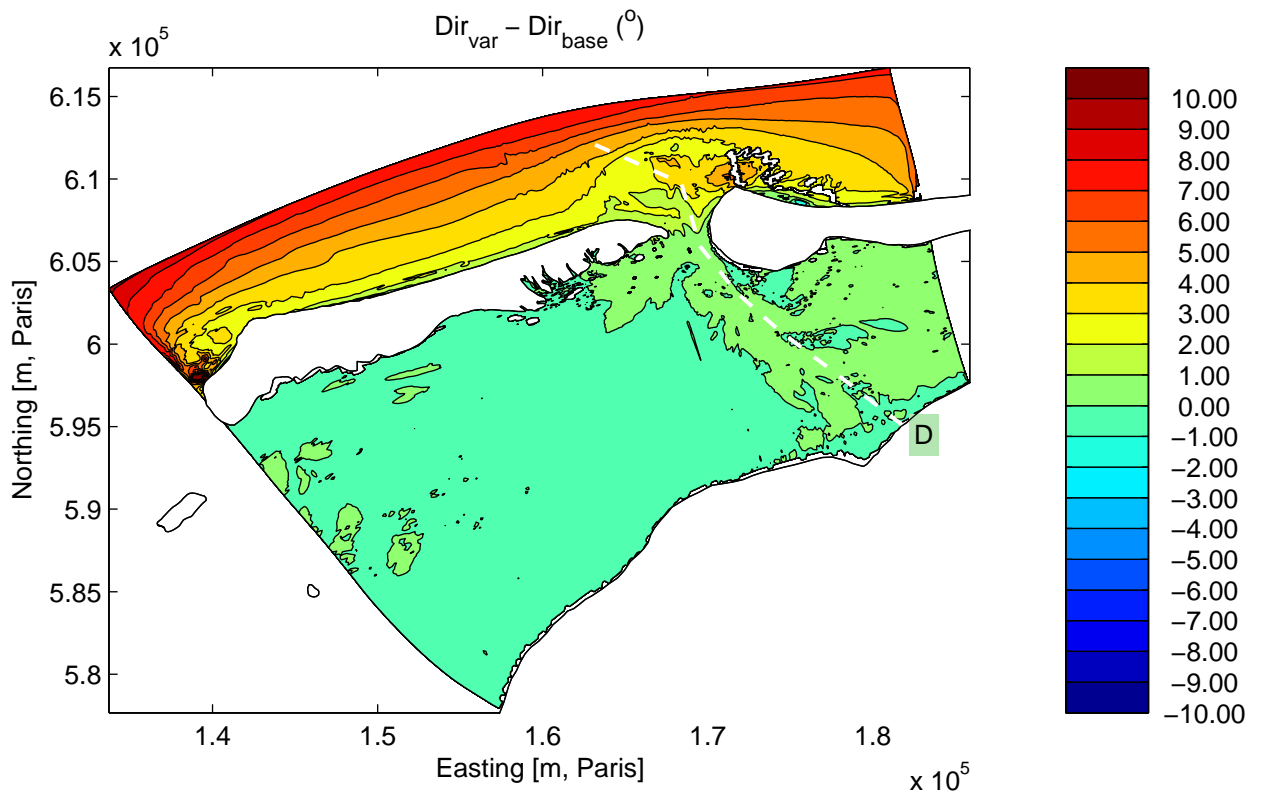
Sensitivity run C2BT2: Variation in wave period at the boundary
Integral parameters along Curve D

Sensitivity analysis Ameland



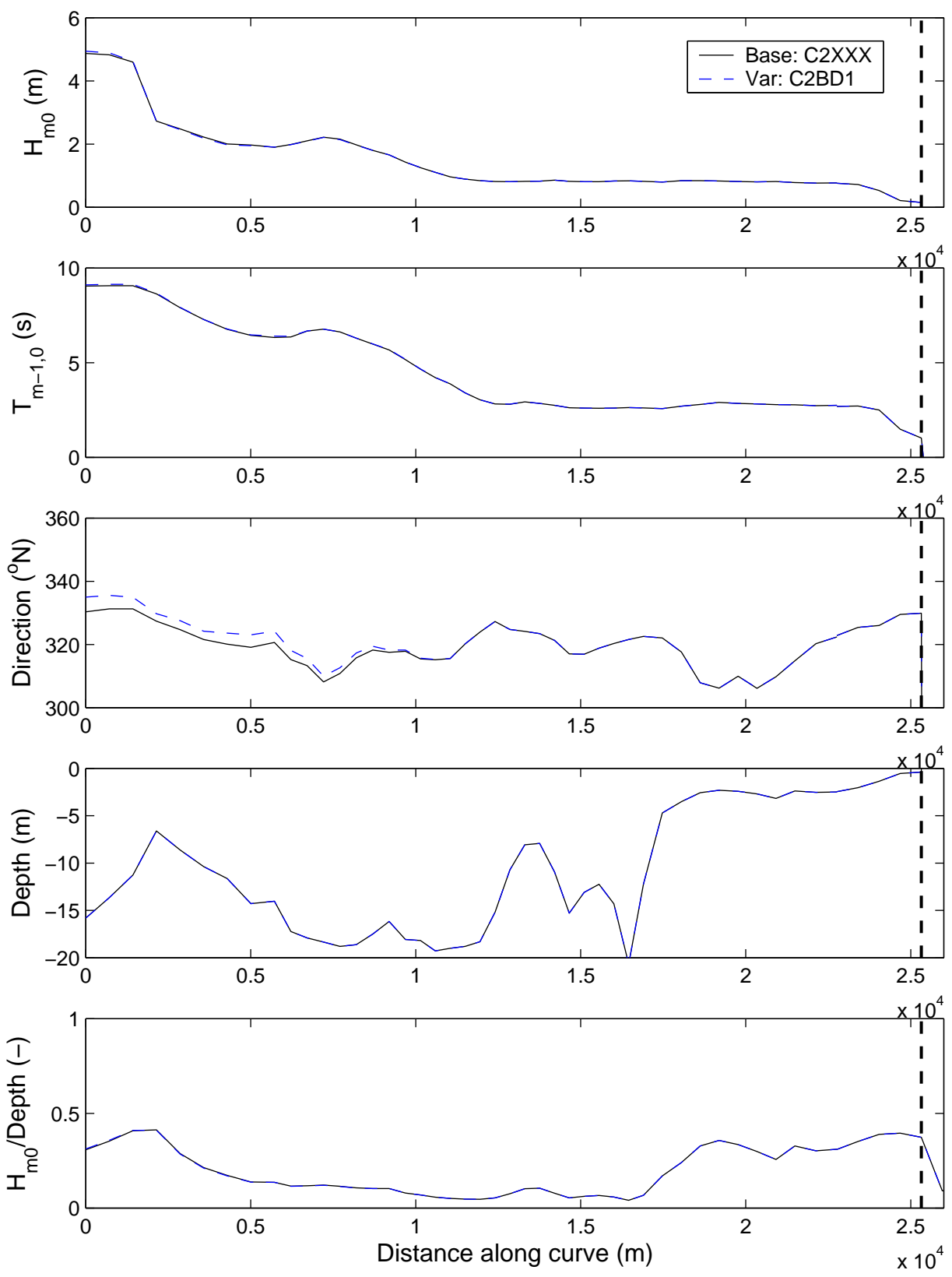
Sensitivity run C2BD1: Variation in wave direction at the boundary
Differences in significant wave height (above) and mean period (below).

Sensitivity analysis Ameland



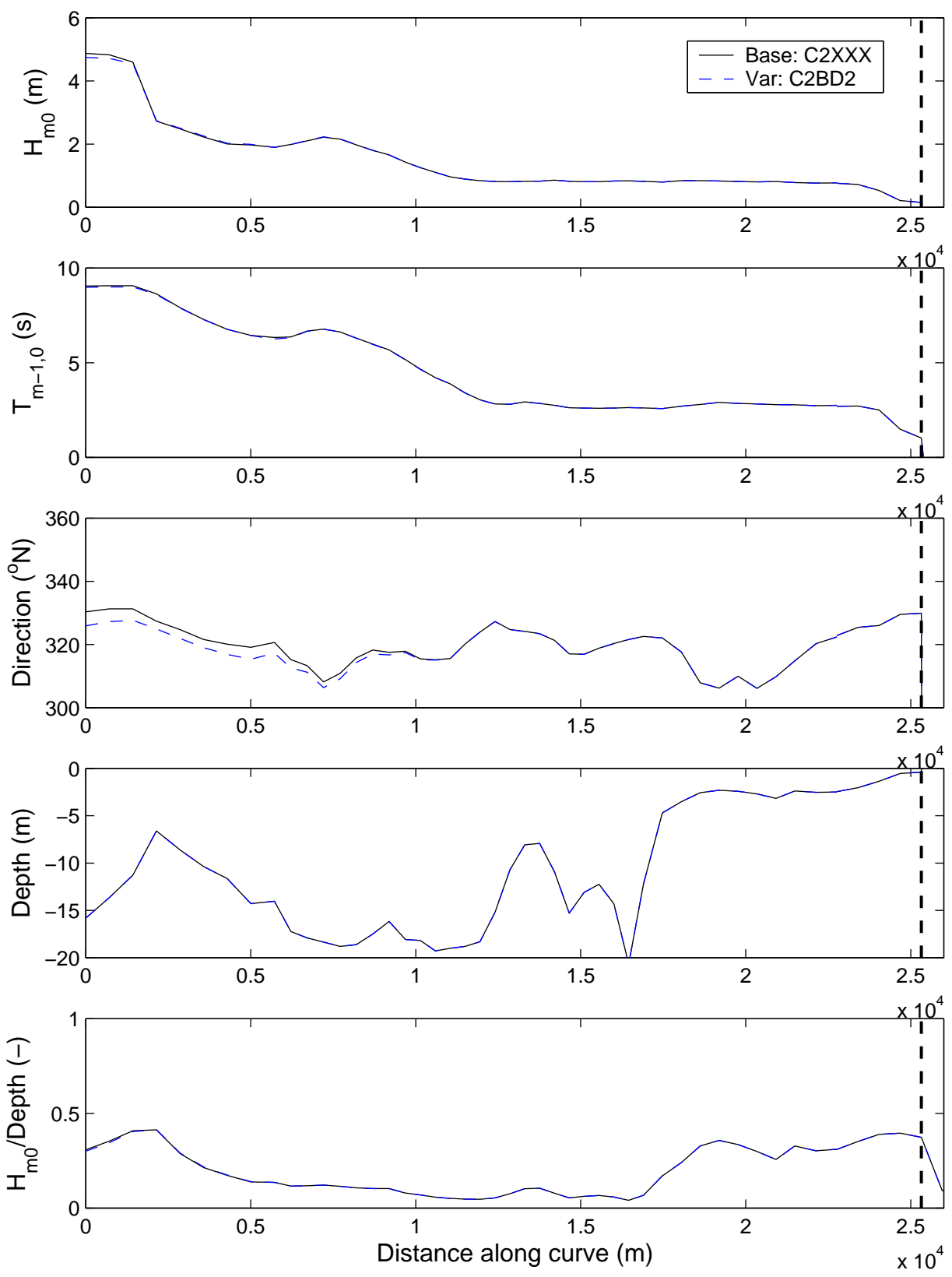
Sensitivity run C2BD1: Variation in wave direction at the boundary
 Differences in mean direction (above) and directional spreading (below).

Sensitivity analysis Ameland



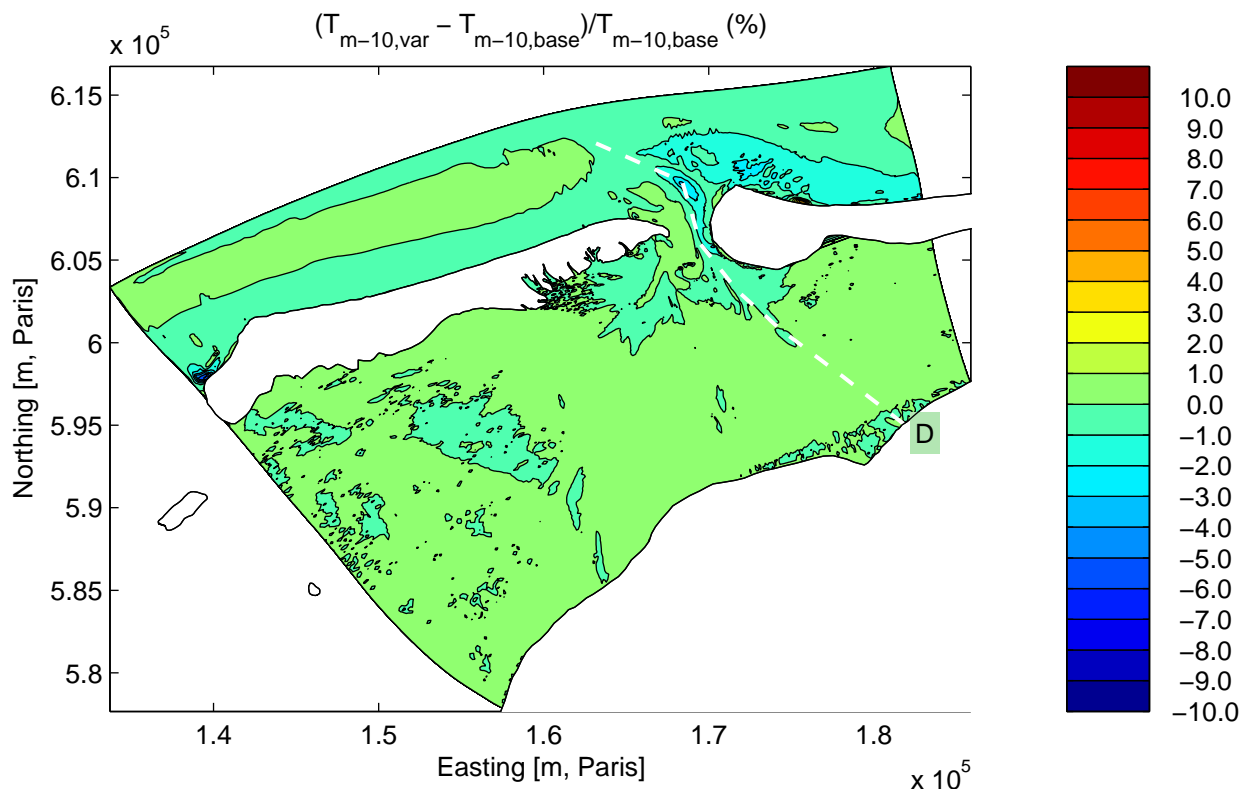
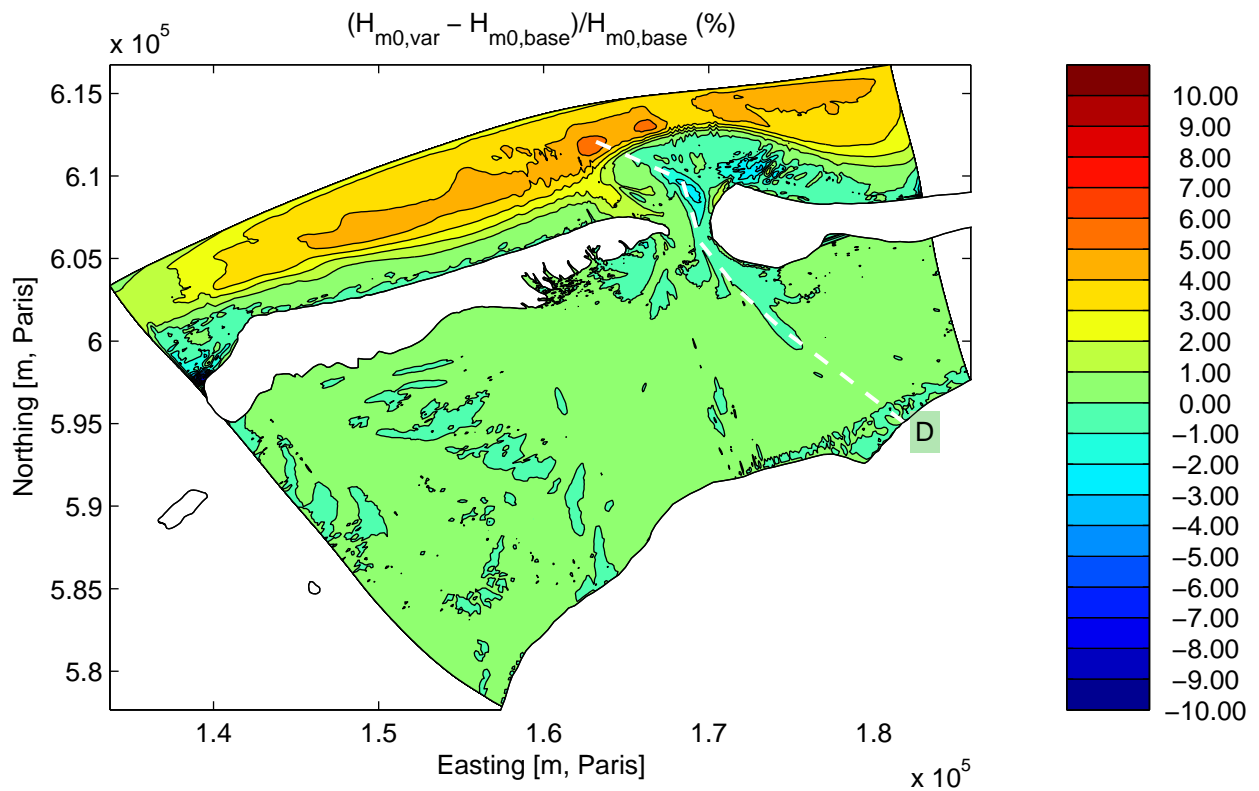
Sensitivity run C2BD1: Variation in wave direction at the boundary
Integral parameters along Curve D

Sensitivity analysis Ameland



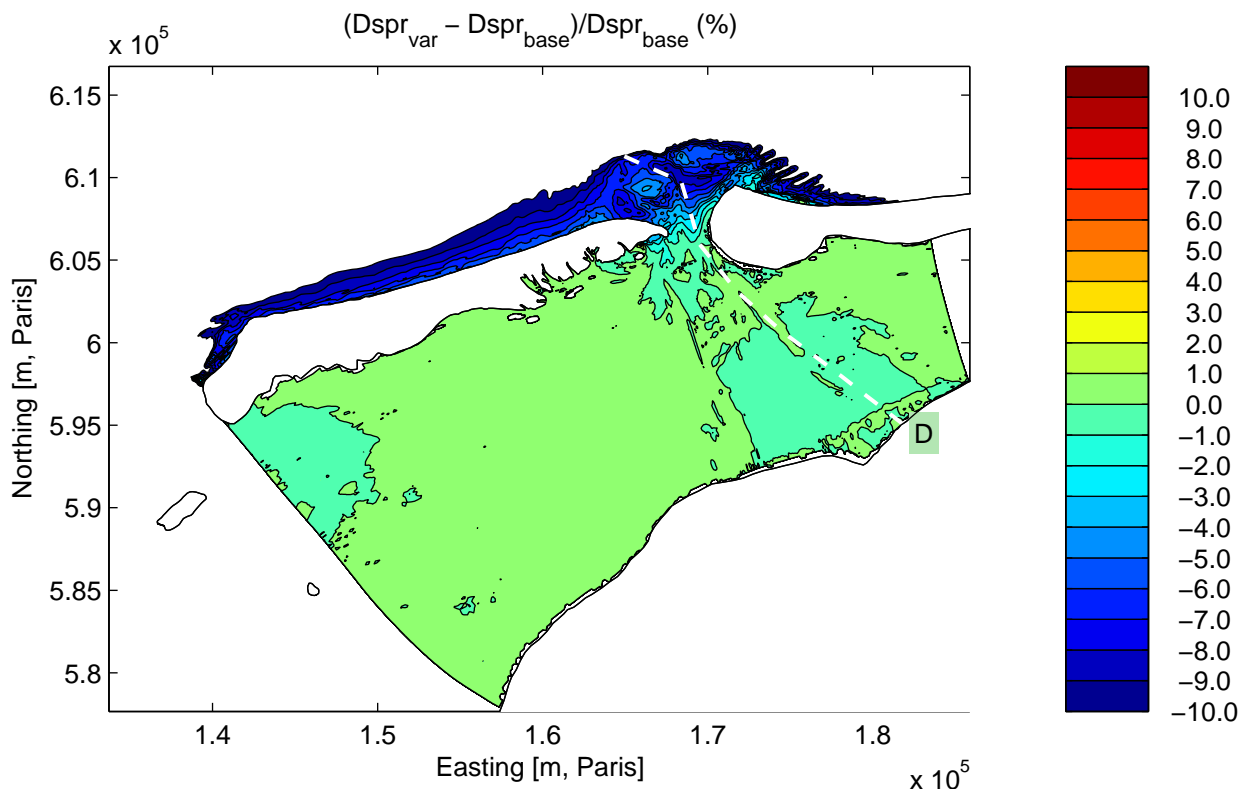
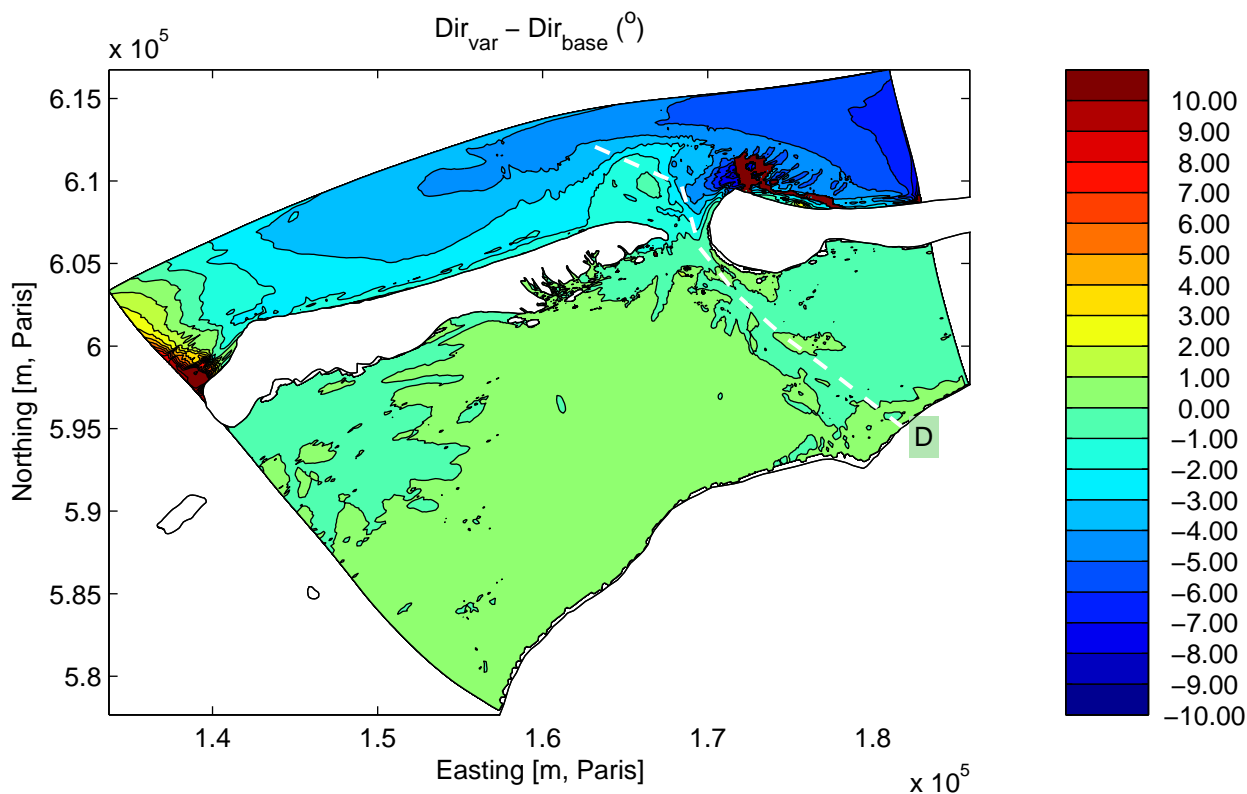
Sensitivity run C2BD2: Variation in wave direction at the boundary
Integral parameters along Curve D

Sensitivity analysis Ameland



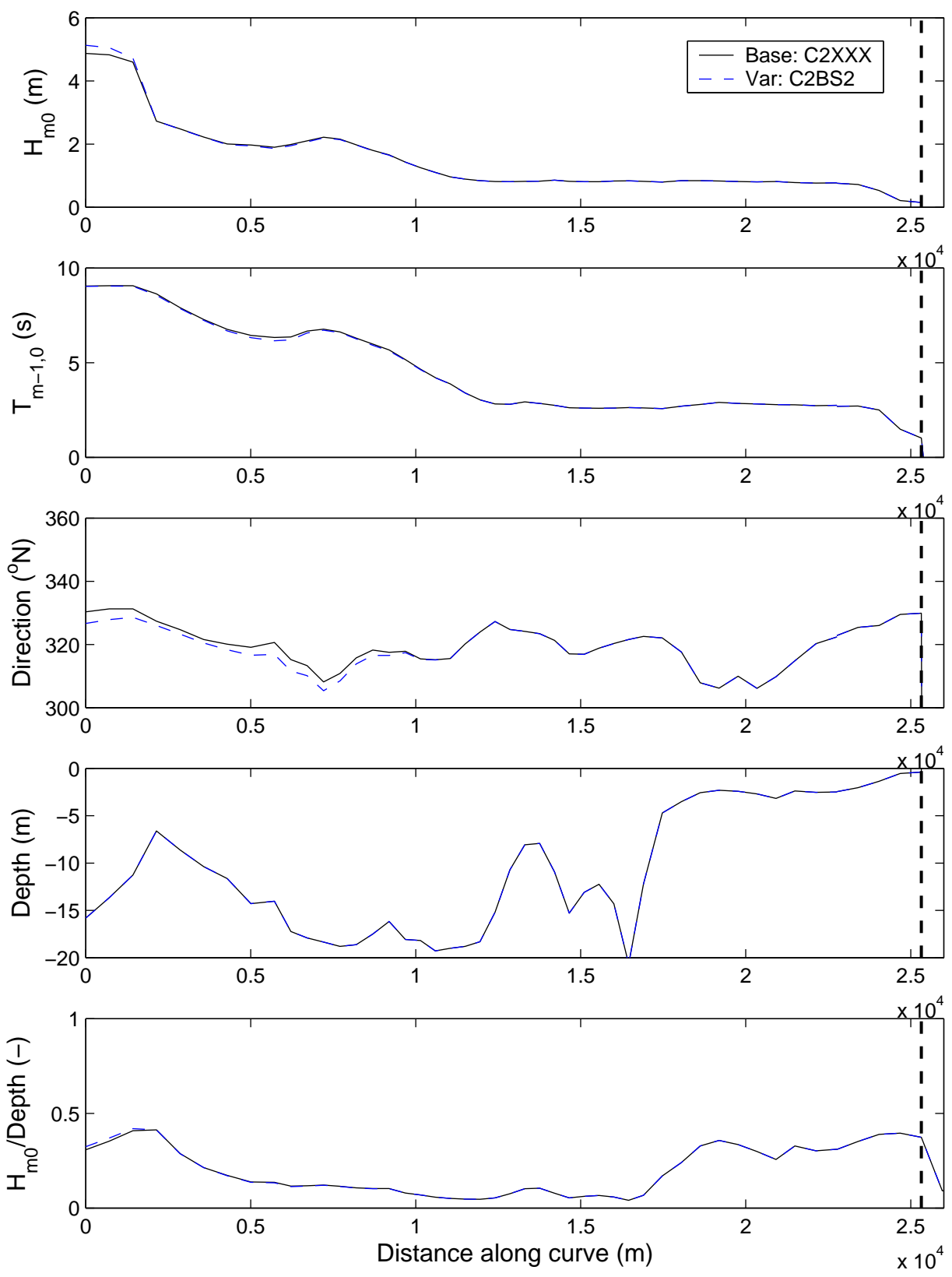
Sensitivity run C2BS2: Variation in directional spreading at the boundary
Differences in significant wave height (above) and mean period (below).

Sensitivity analysis Ameland



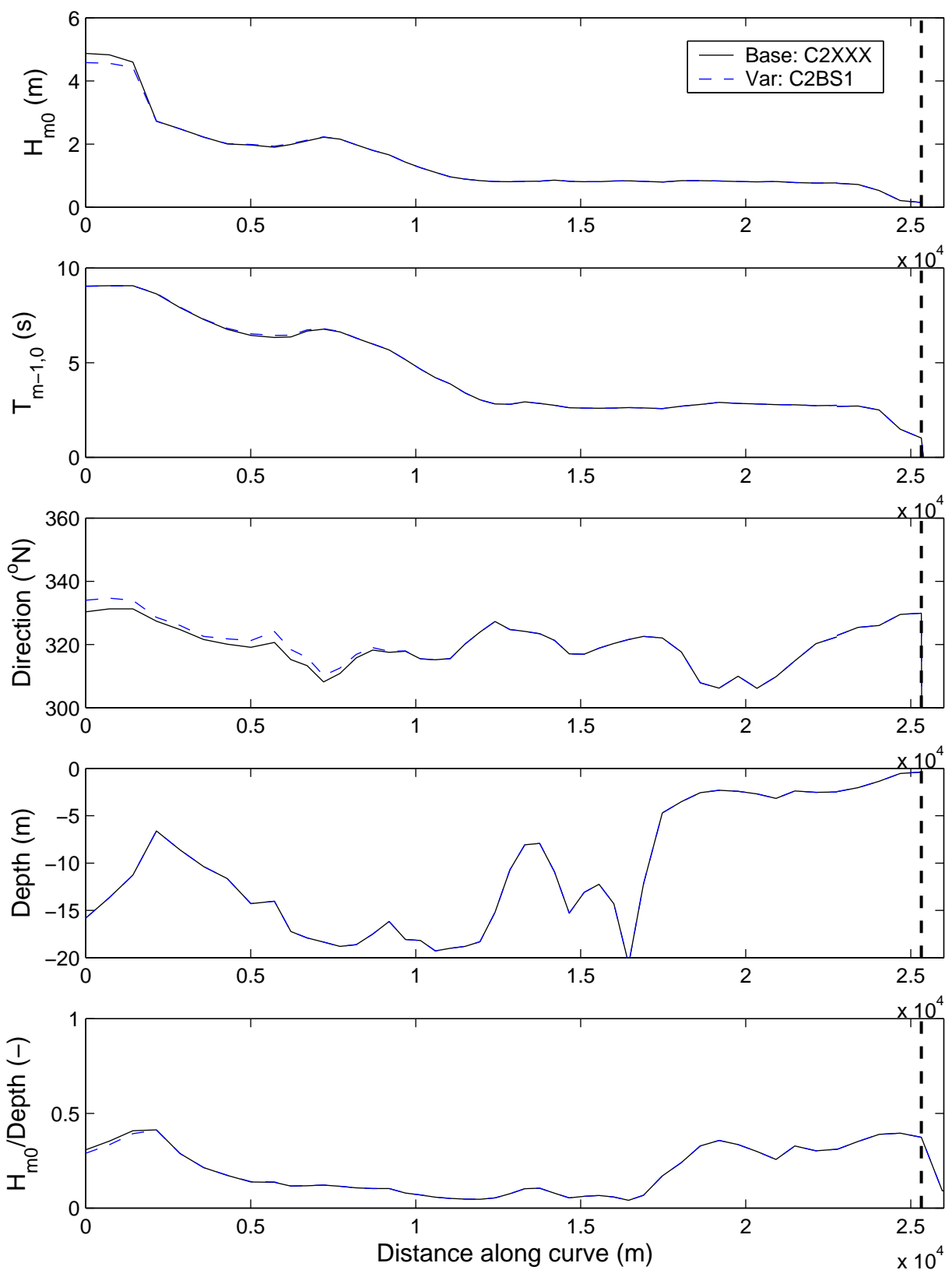
Sensitivity run C2BS2: Variation in directional spreading at the boundary
Differences in mean direction (above) and directional spreading (below).

Sensitivity analysis Ameland



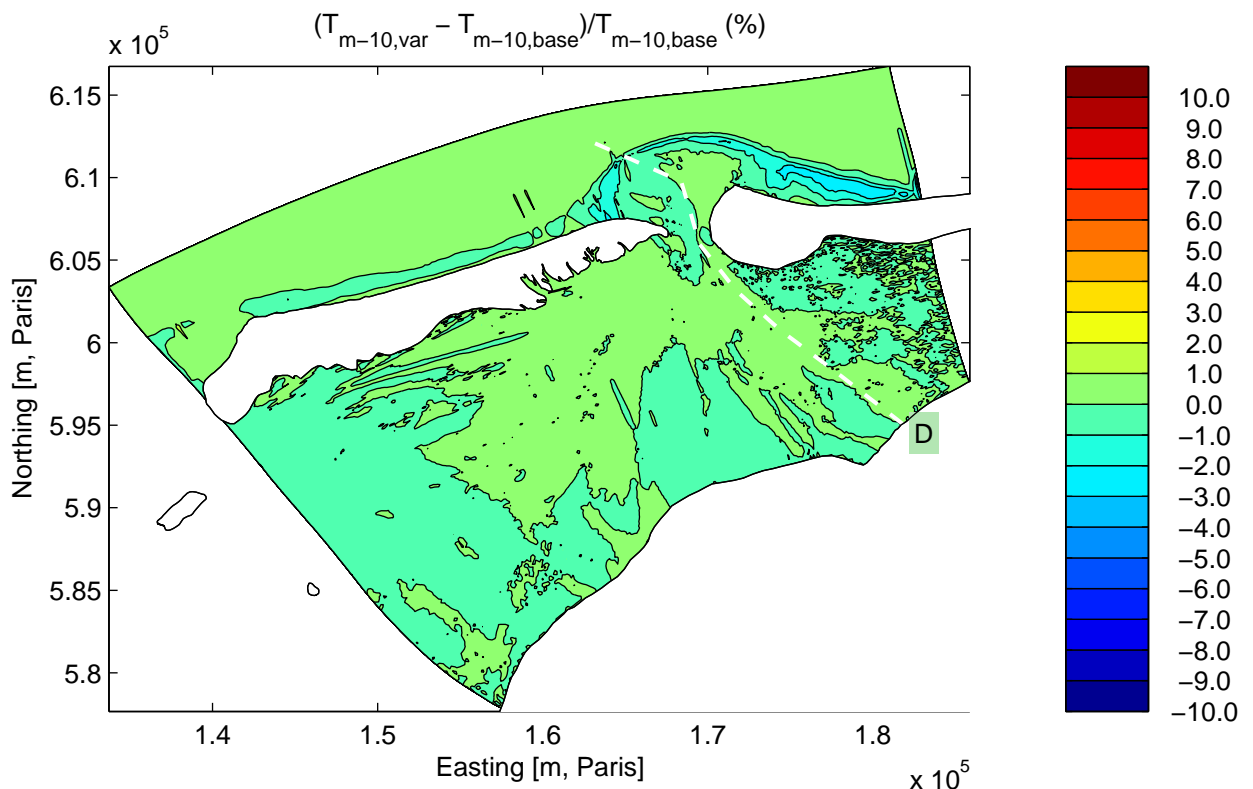
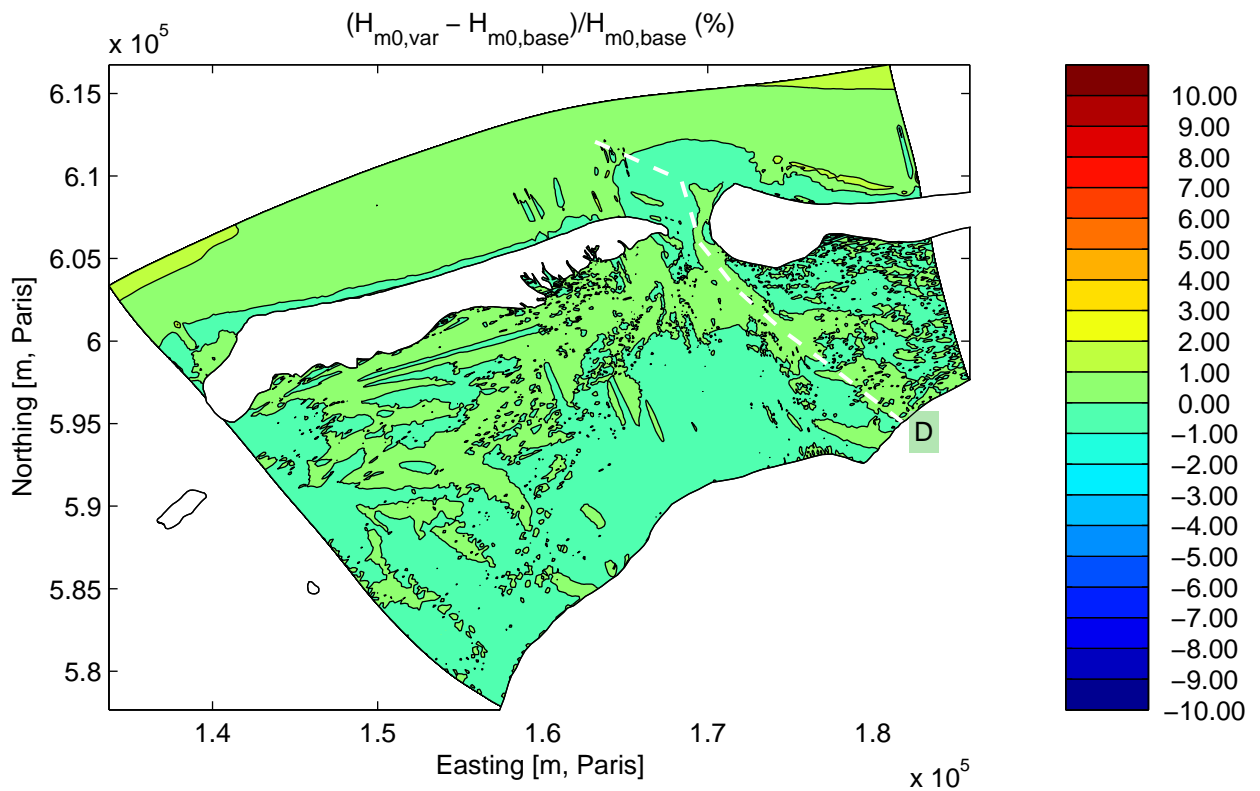
Sensitivity run C2BS2: Variation in directional spreading at the boundary
Integral parameters along Curve D

Sensitivity analysis Ameland



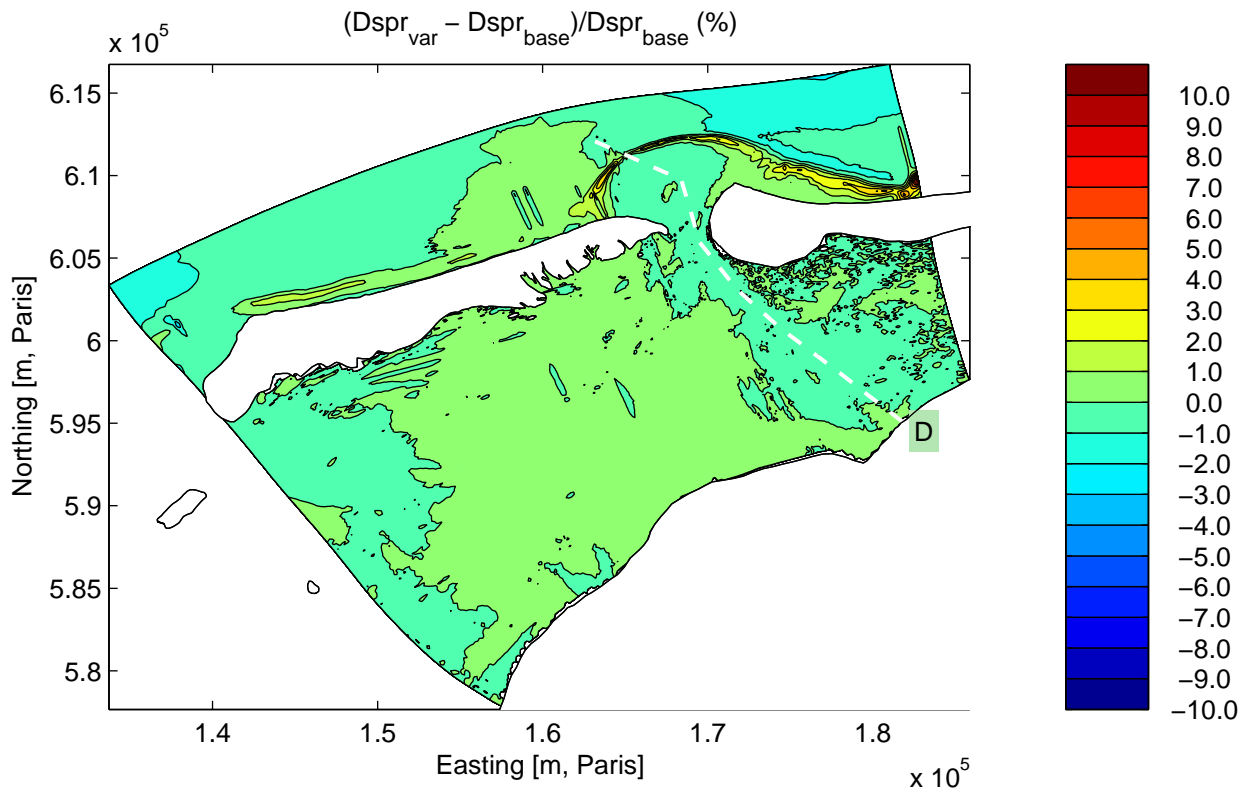
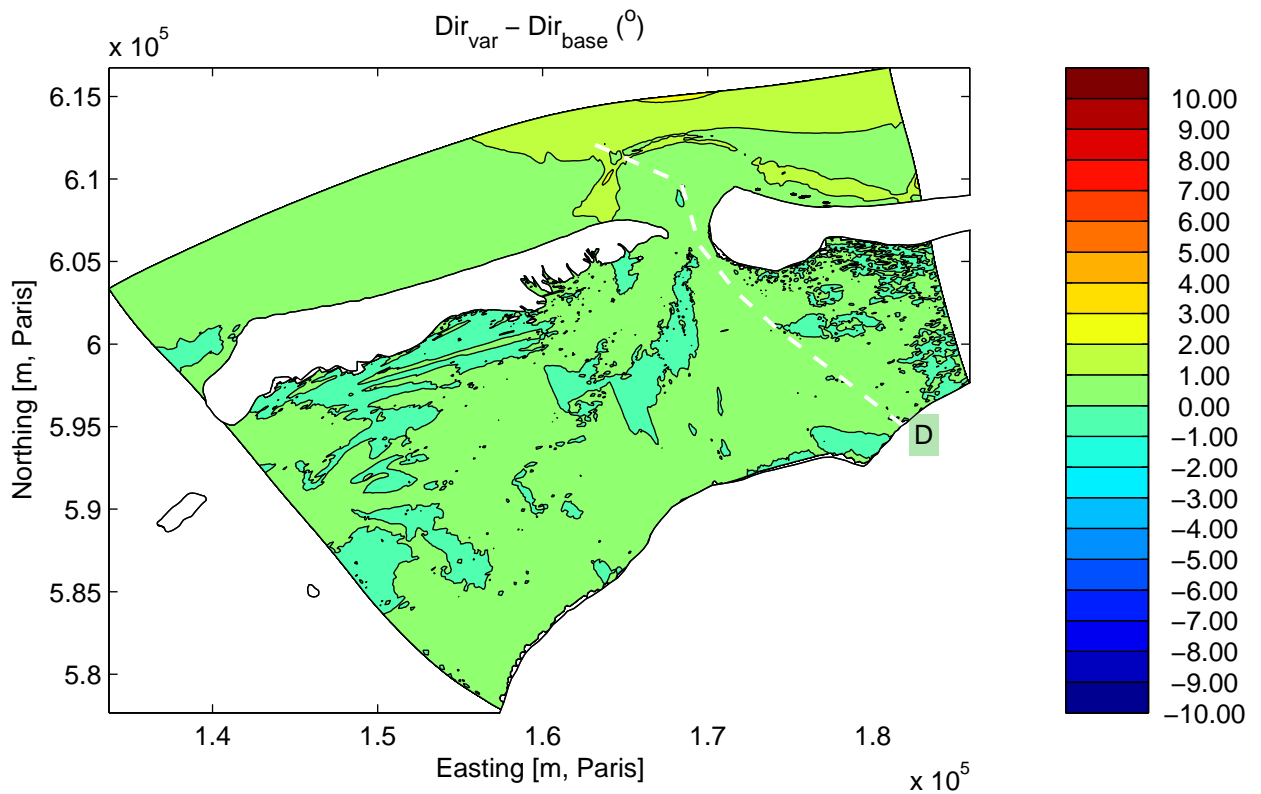
Sensitivity run C2BS1: Variation in directional spreading at the boundary
Integral parameters along Curve D

Sensitivity analysis Ameland



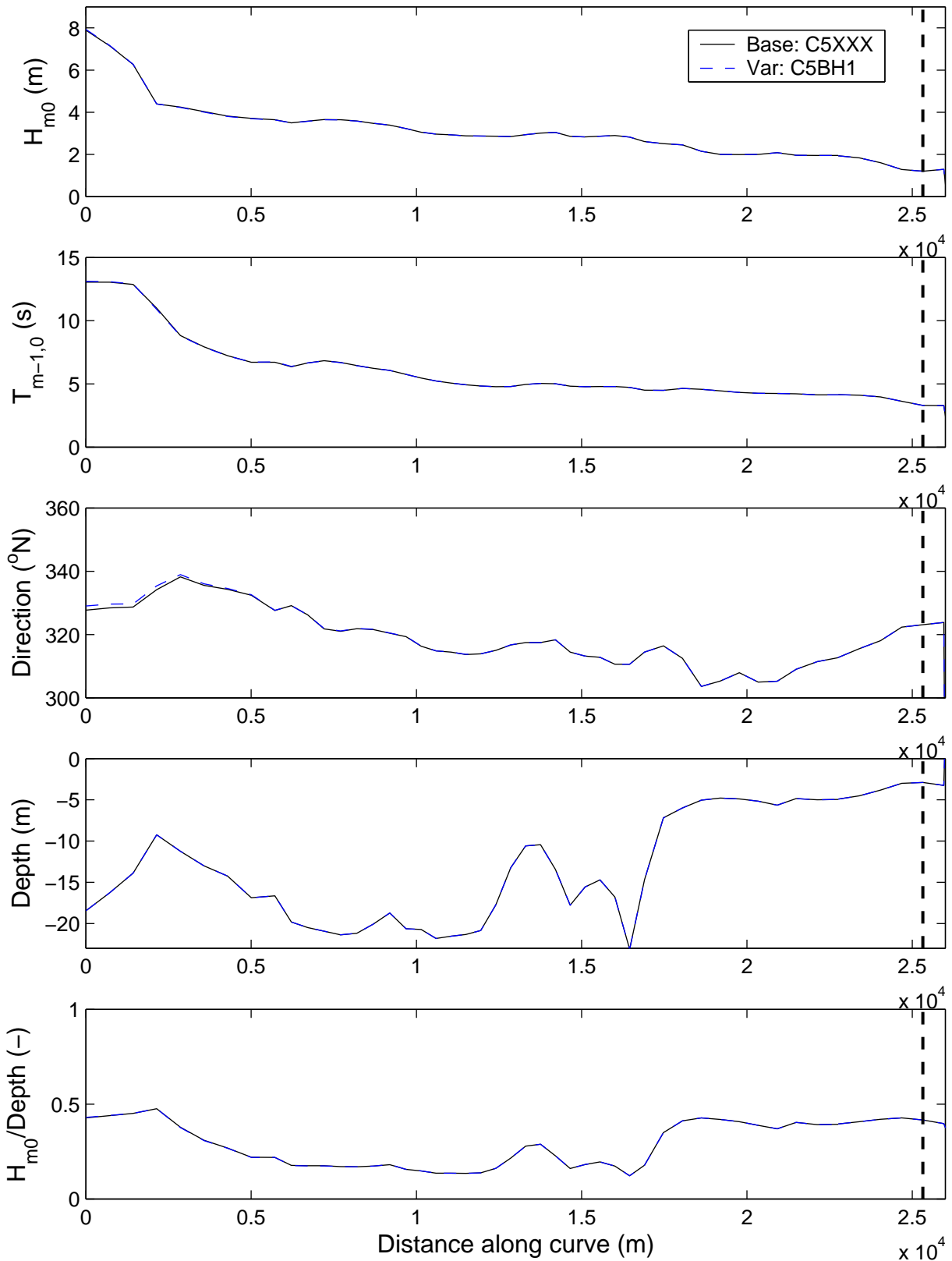
Sensitivity run C5BH1: Variation in wave height at the boundary
Differences in significant wave height (above) and mean period (below).

Sensitivity analysis Ameland



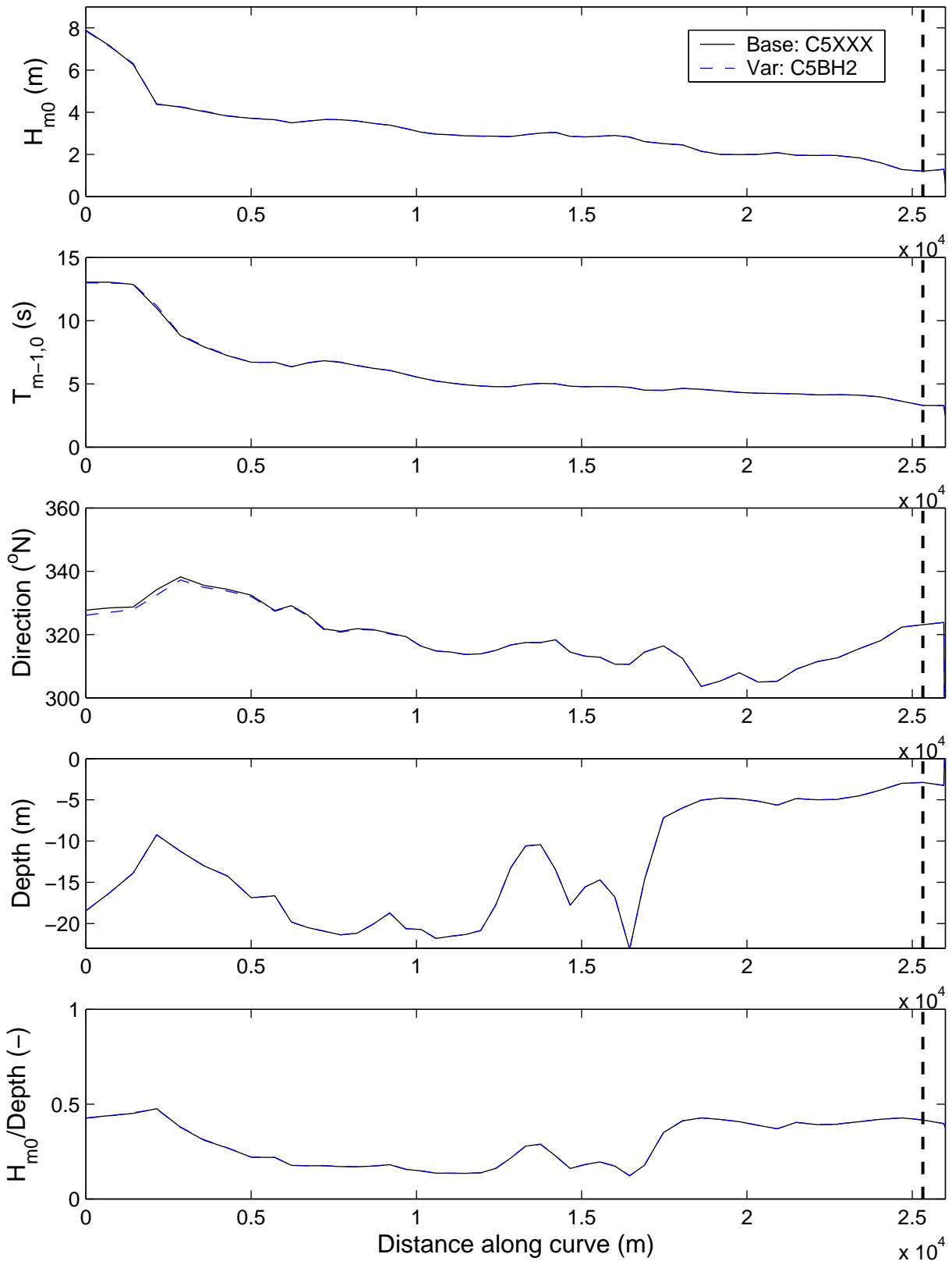
Sensitivity run C5BH1: Variation in wave height at the boundary
 Differences in mean direction (above) and directional spreading (below).

Sensitivity analysis Ameland



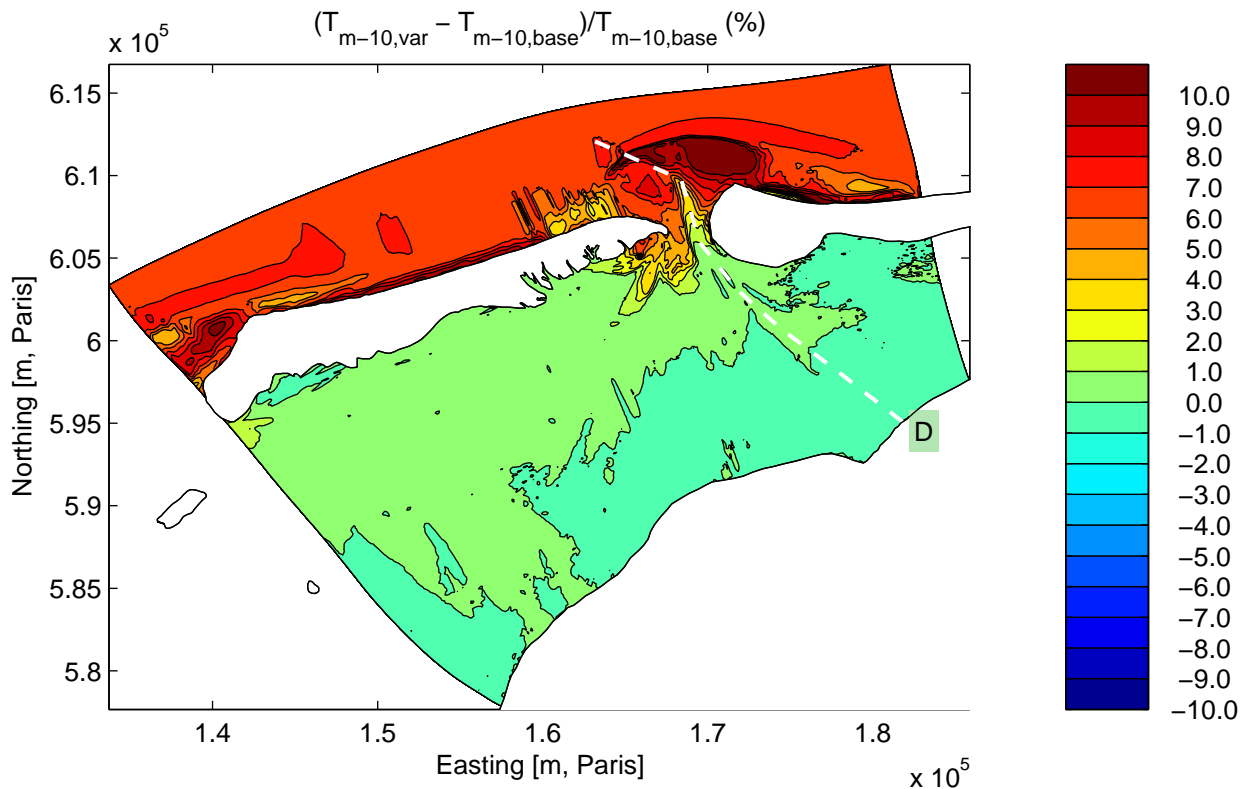
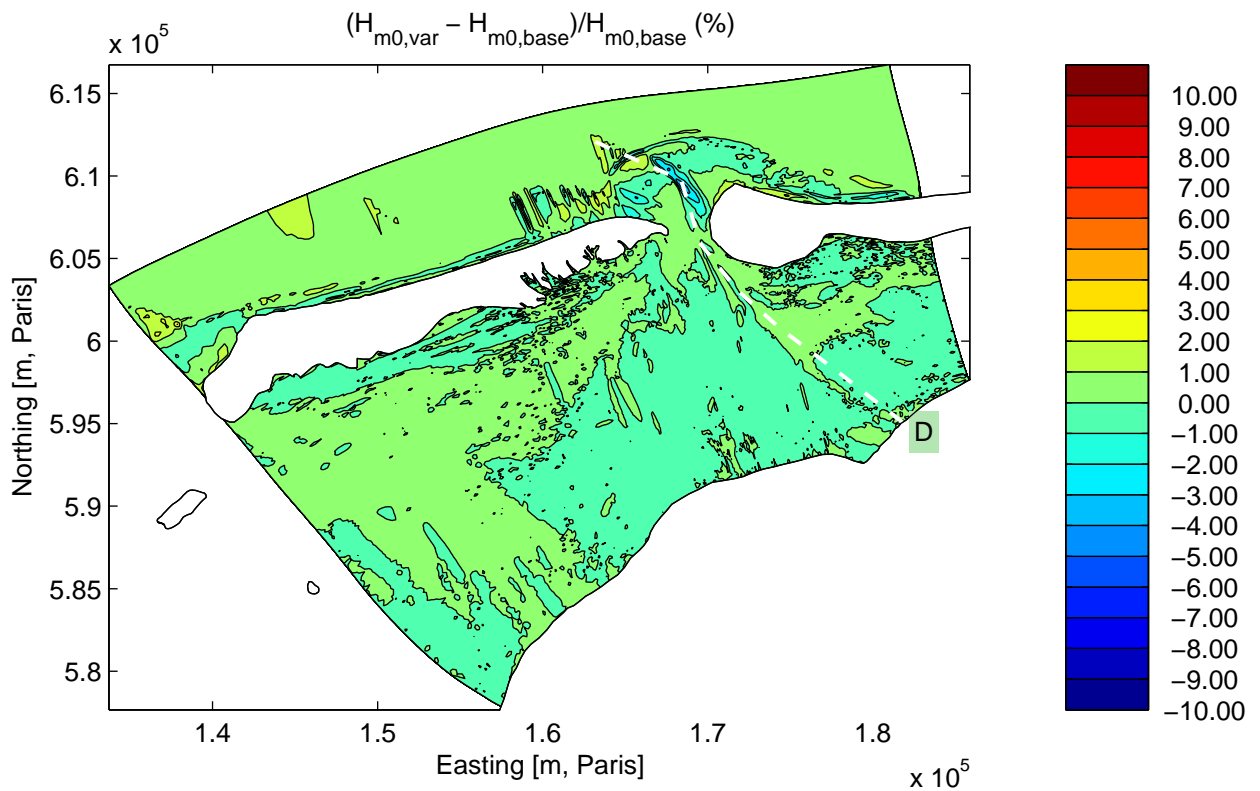
Sensitivity run C5BH1: Variation in wave height at the boundary
Integral parameters along Curve D

Sensitivity analysis Ameland



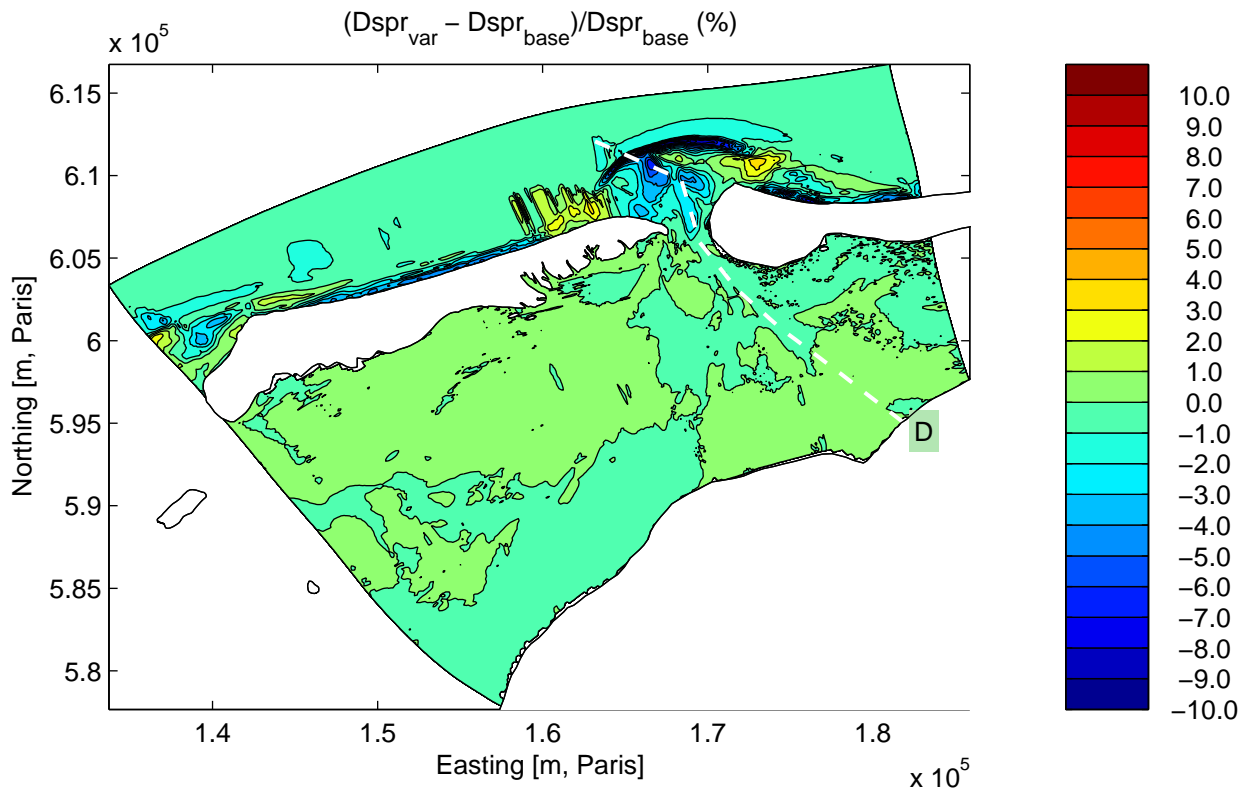
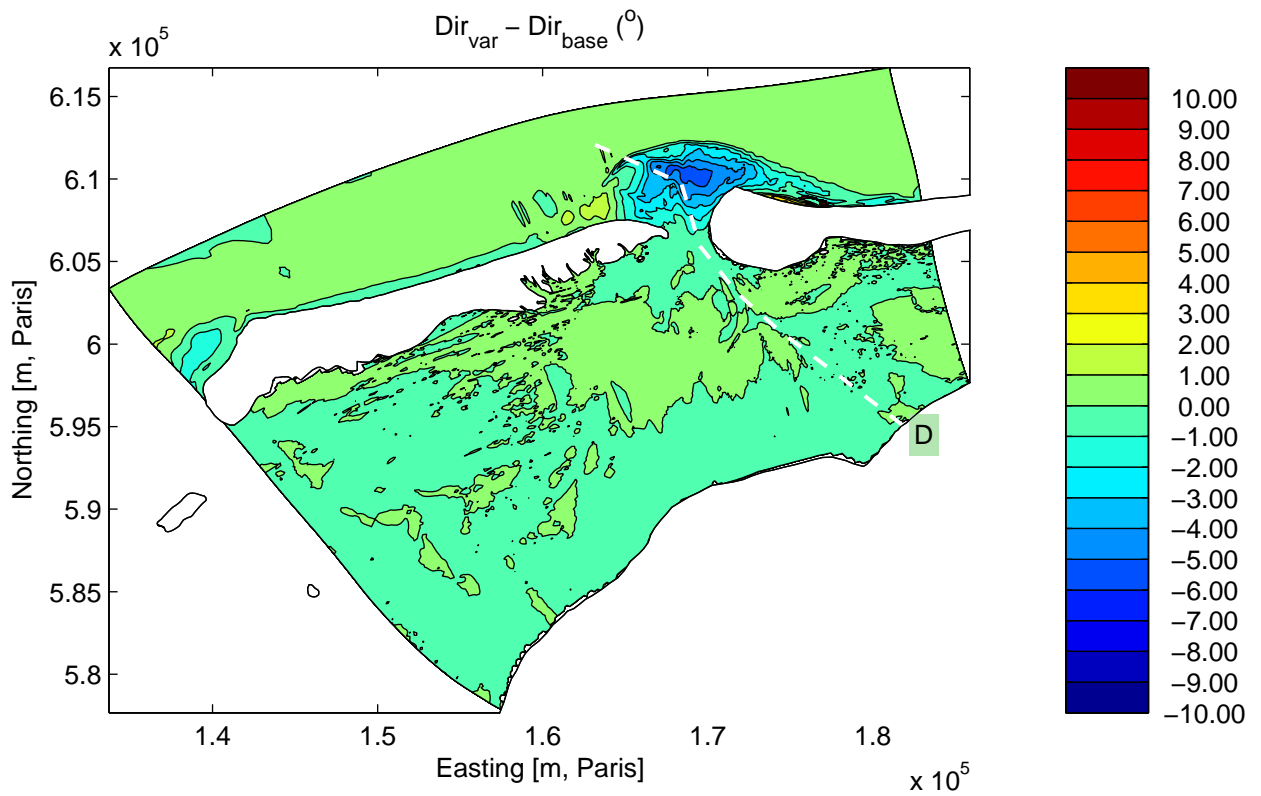
Sensitivity run C5BH2: Variation in wave height at the boundary
Integral parameters along Curve D

Sensitivity analysis Ameland



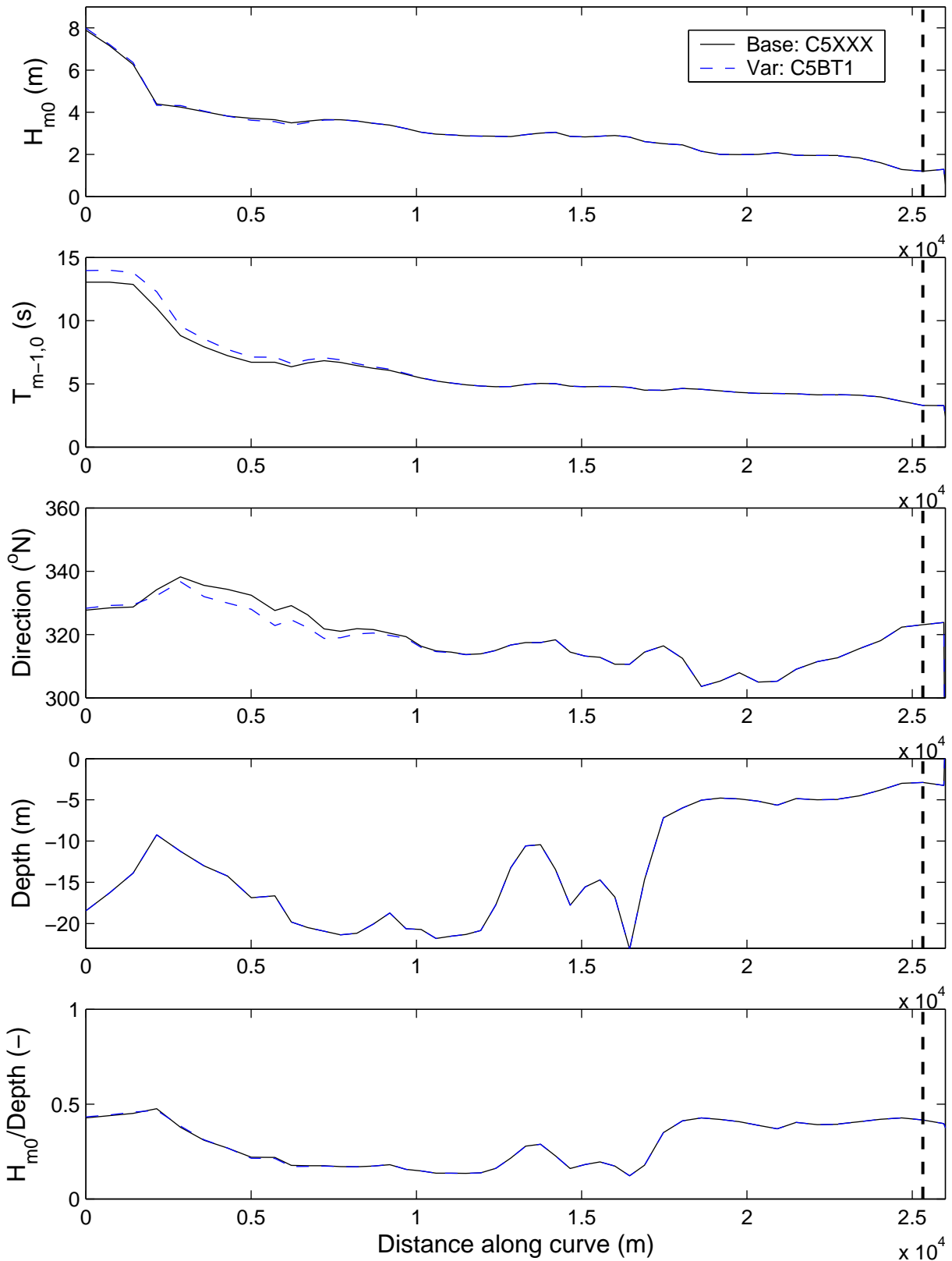
Sensitivity run C5BT1: Variation in wave period at the boundary
Differences in significant wave height (above) and mean period (below).

Sensitivity analysis Ameland



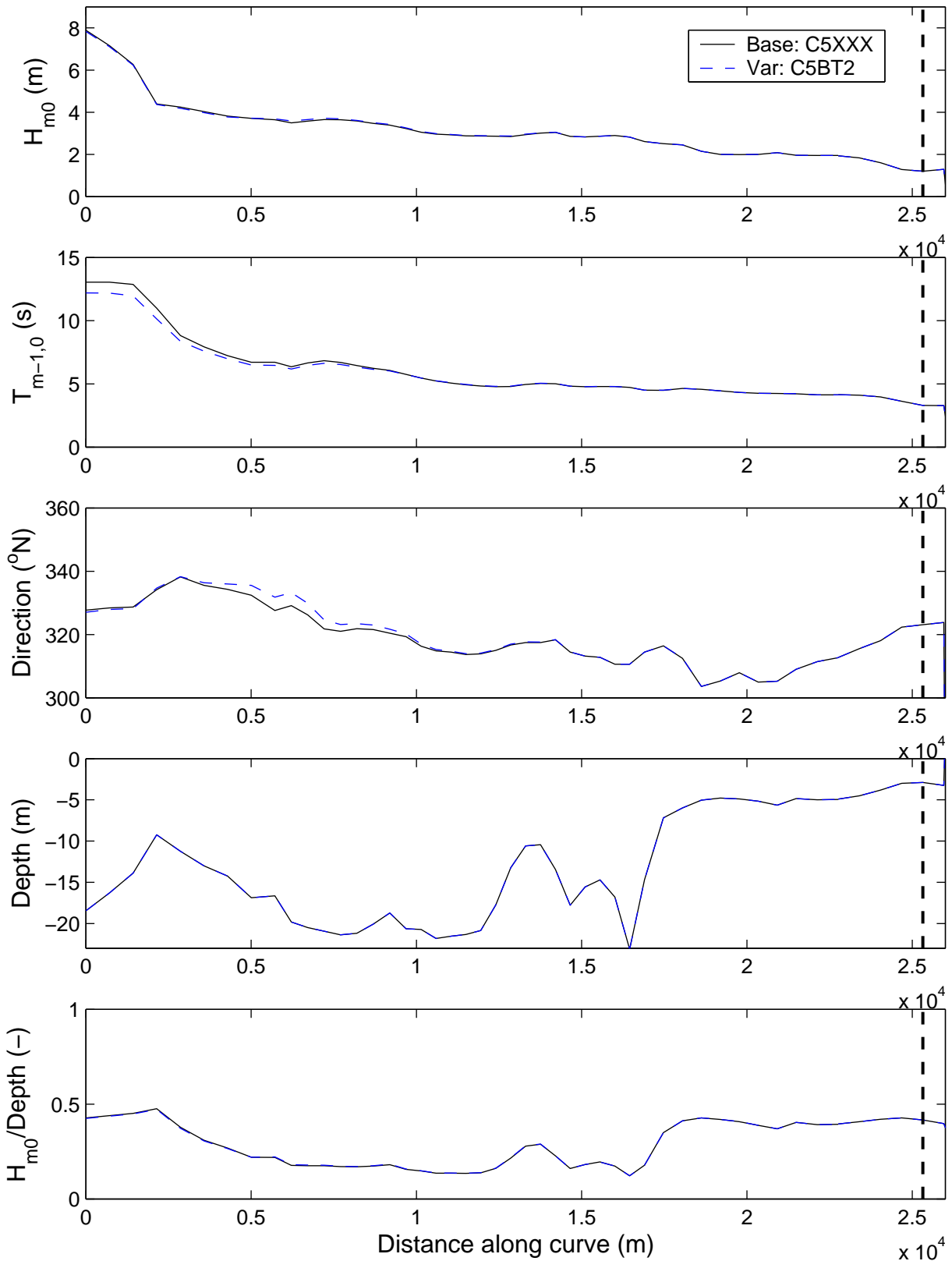
Sensitivity run C5BT1: Variation in wave period at the boundary
 Differences in mean direction (above) and directional spreading (below).

Sensitivity analysis Ameland



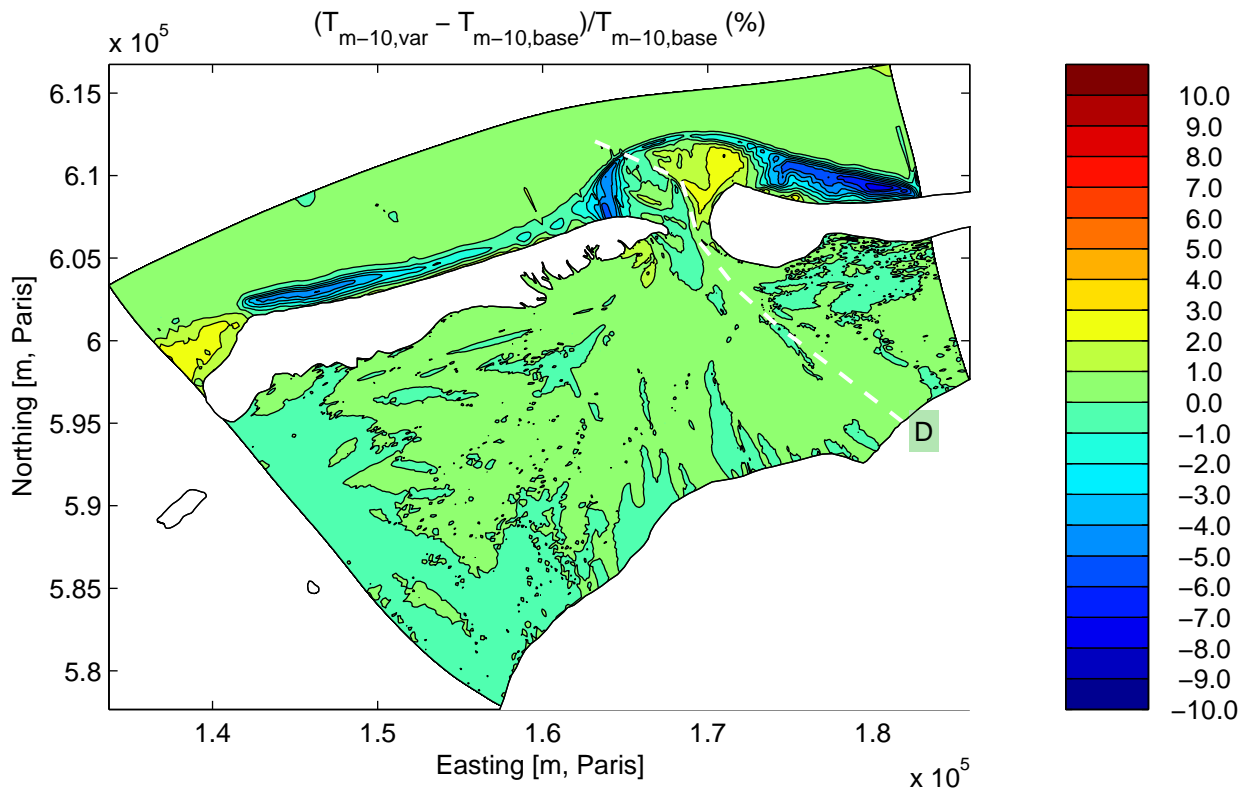
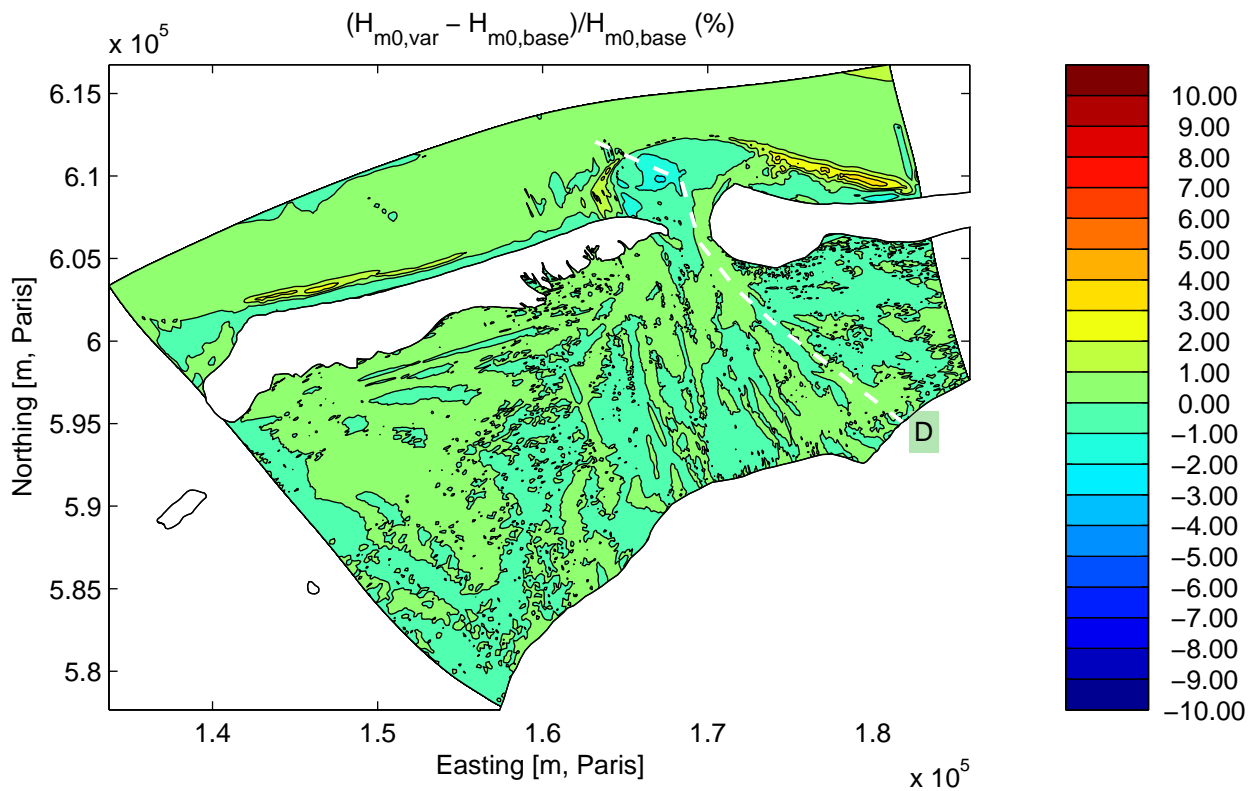
Sensitivity run C5BT1: Variation in wave period at the boundary
Integral parameters along Curve D

Sensitivity analysis Ameland



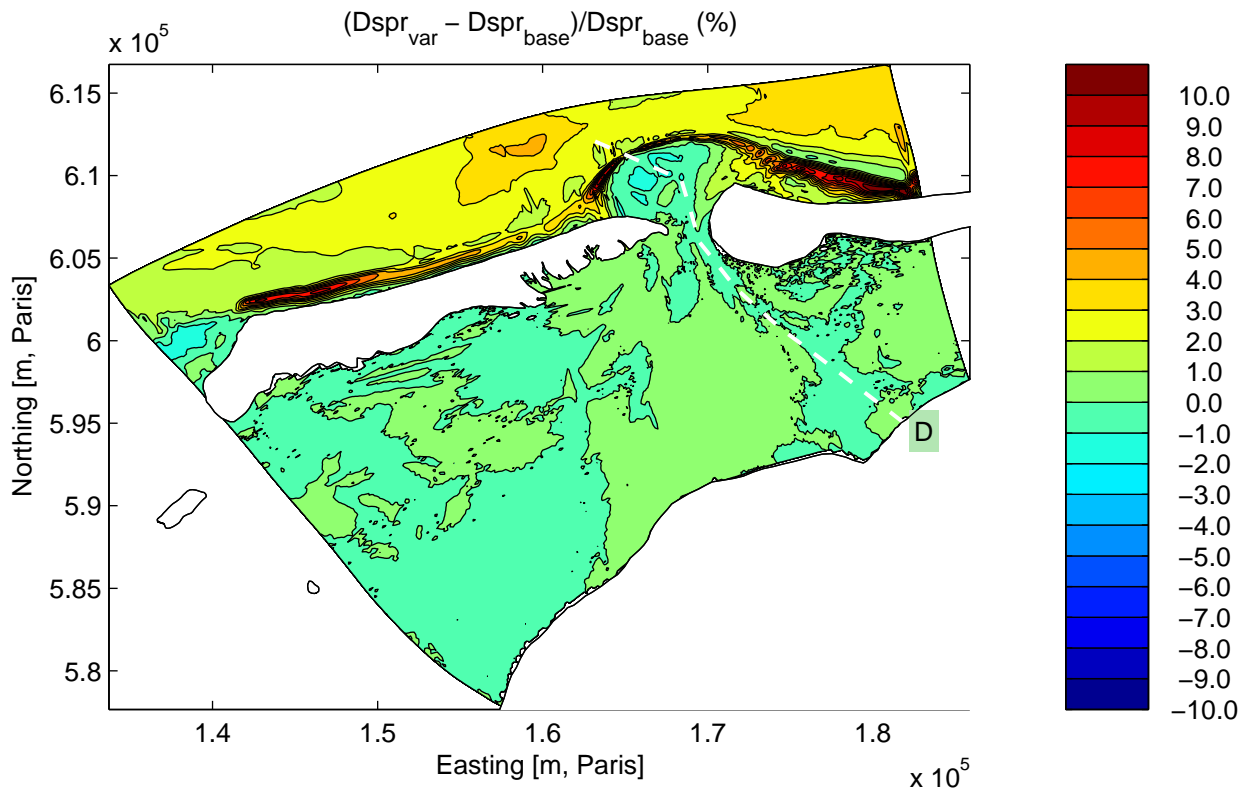
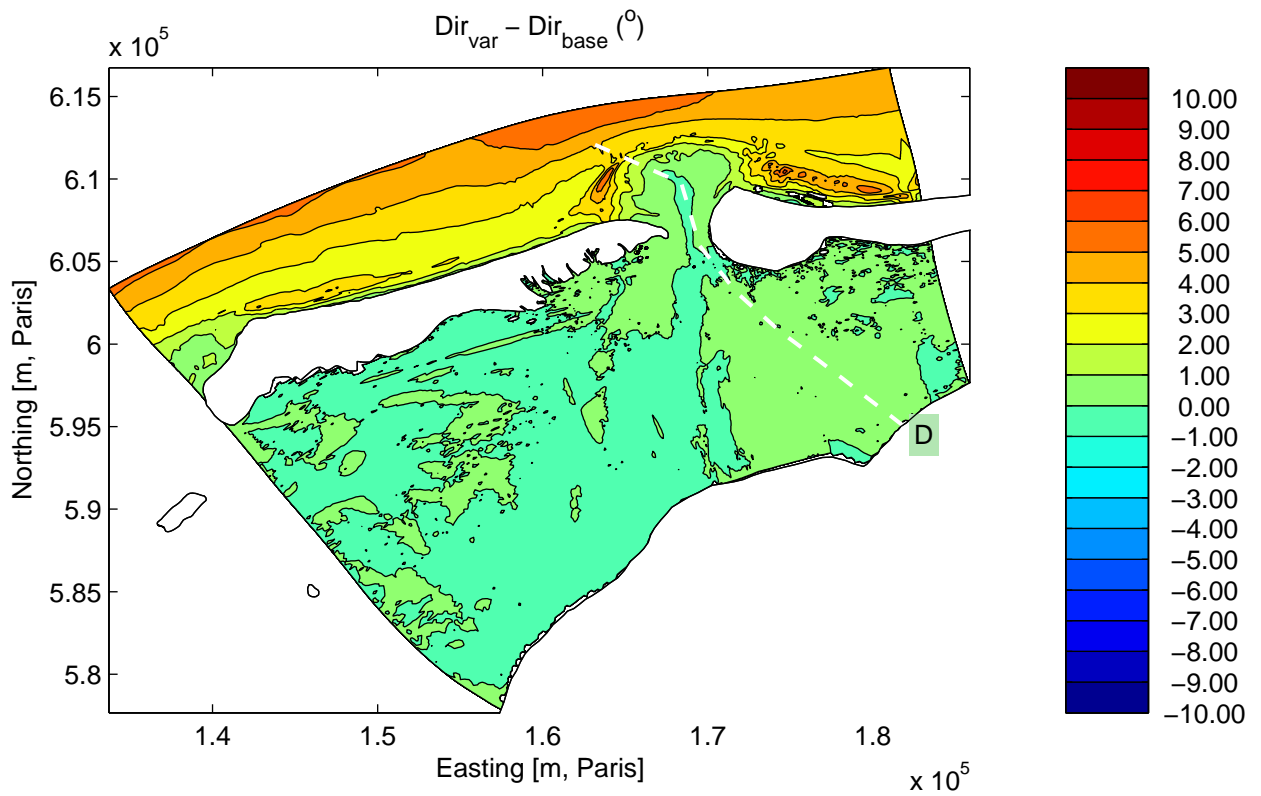
Sensitivity run C5BT2: Variation in wave period at the boundary
Integral parameters along Curve D

Sensitivity analysis Ameland



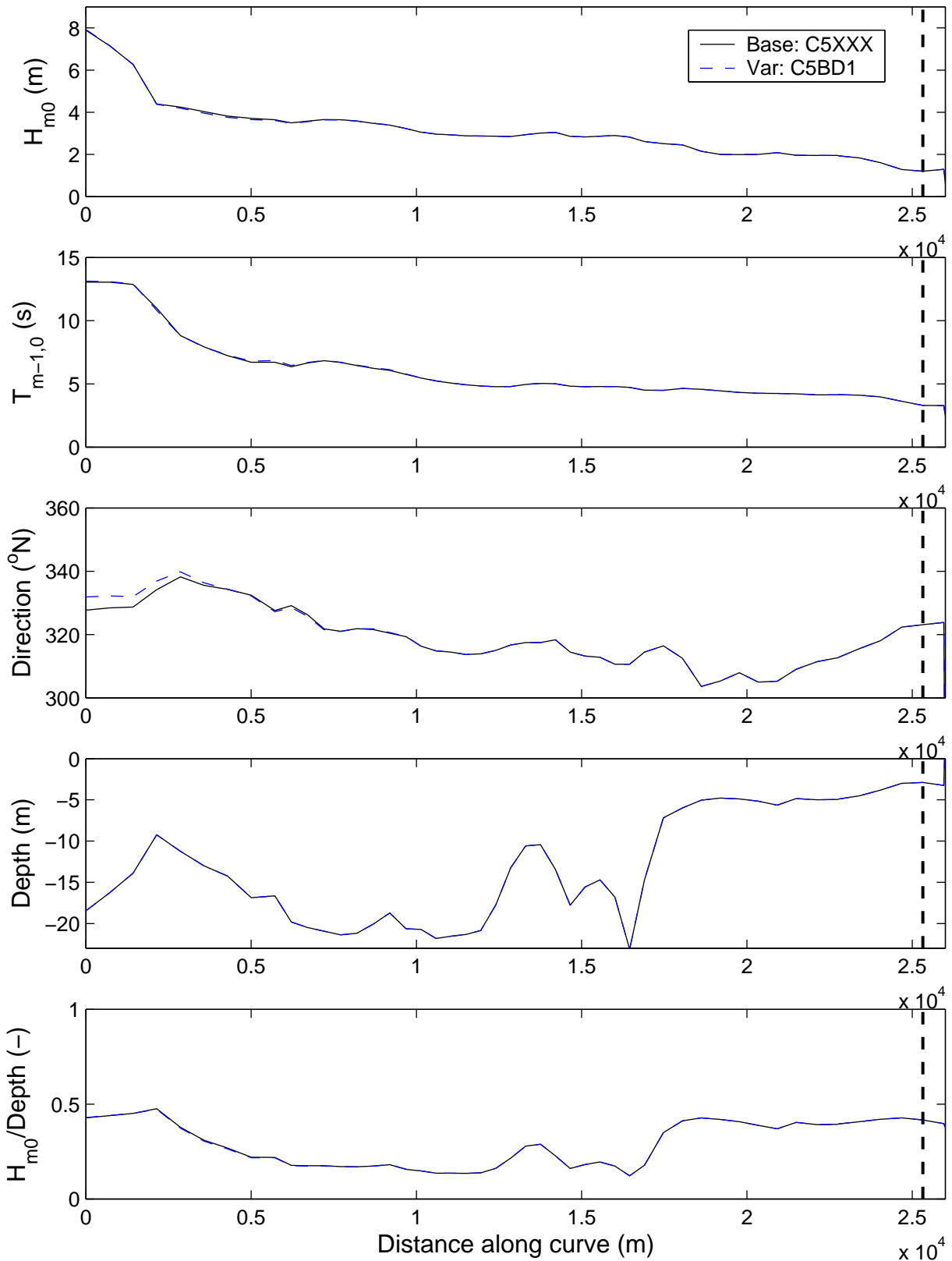
Sensitivity run C5BD1: Variation in wave direction at the boundary
Differences in significant wave height (above) and mean period (below).

Sensitivity analysis Ameland



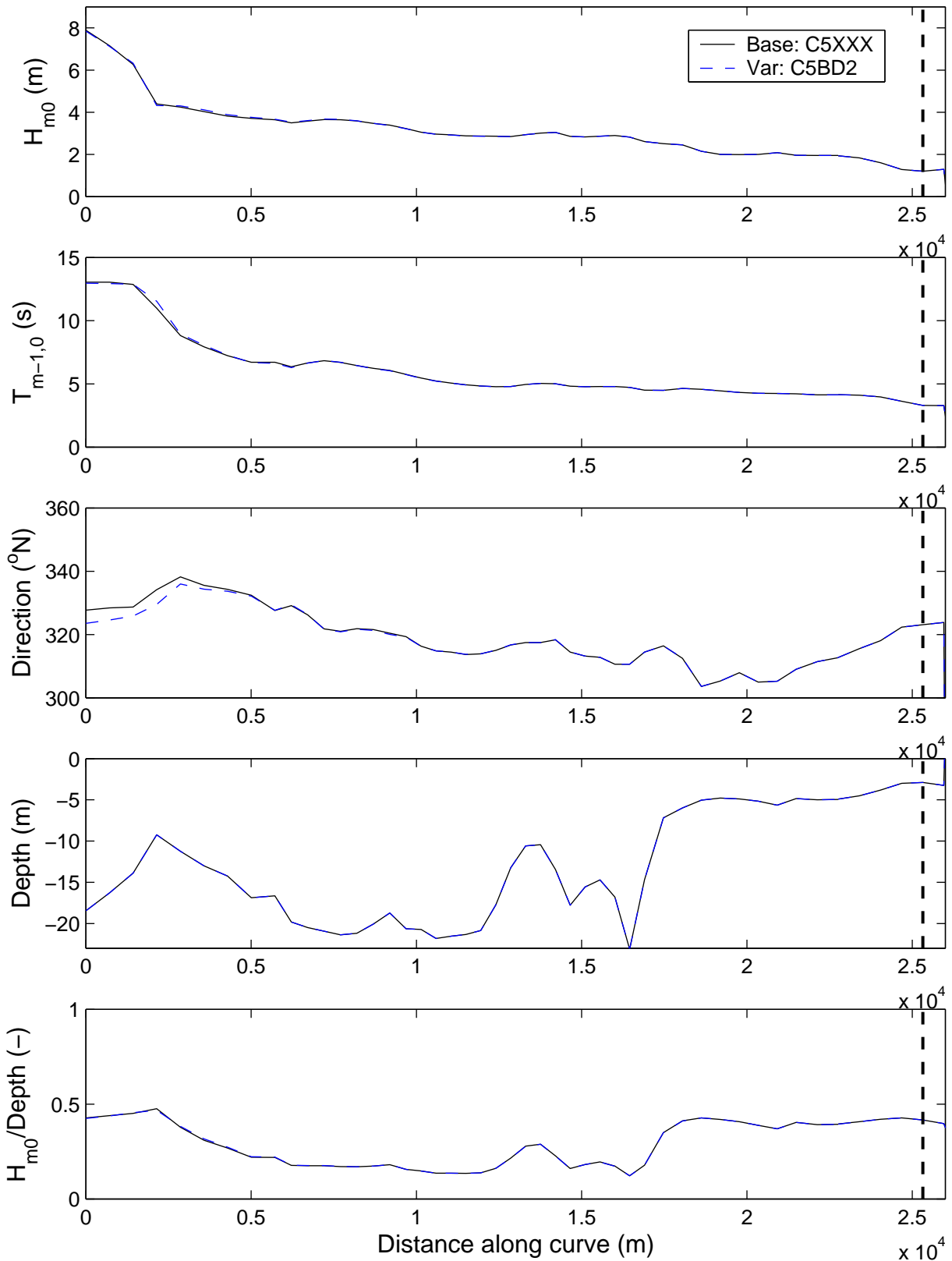
Sensitivity run C5BD1: Variation in wave direction at the boundary
 Differences in mean direction (above) and directional spreading (below).

Sensitivity analysis Ameland



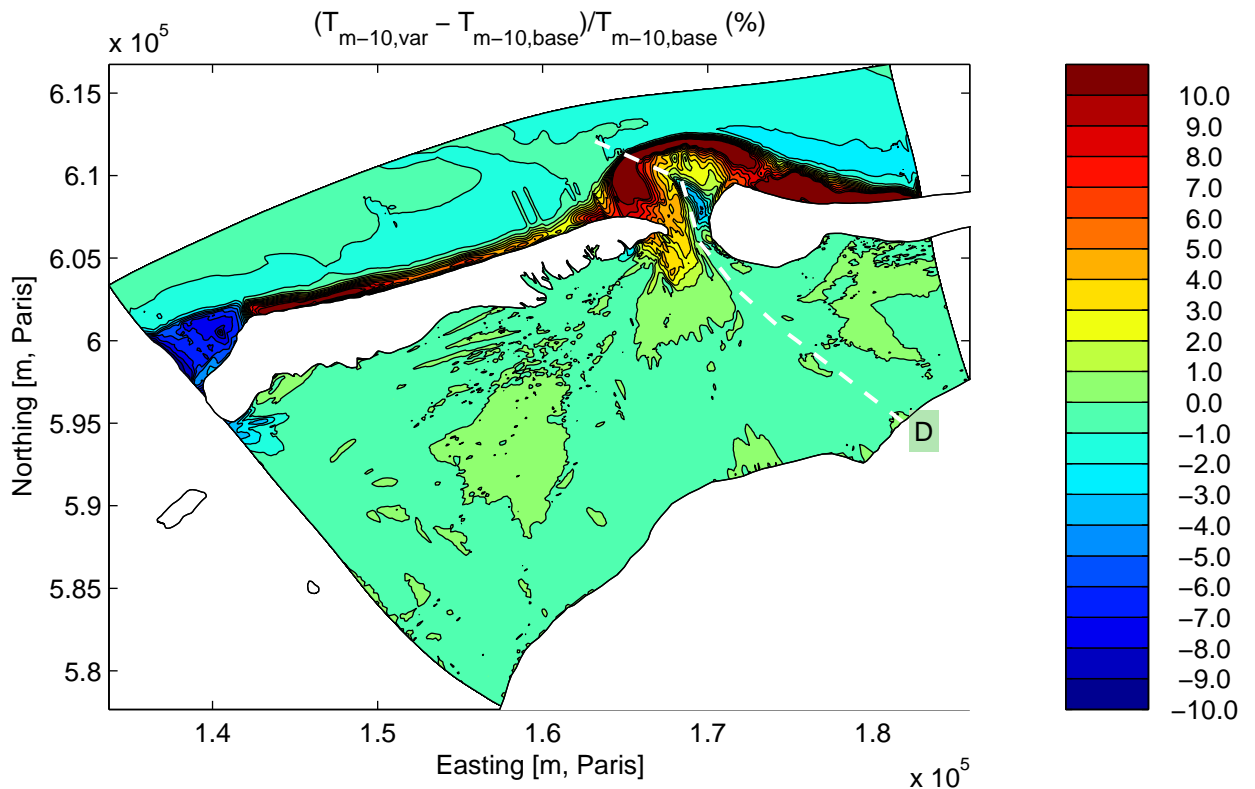
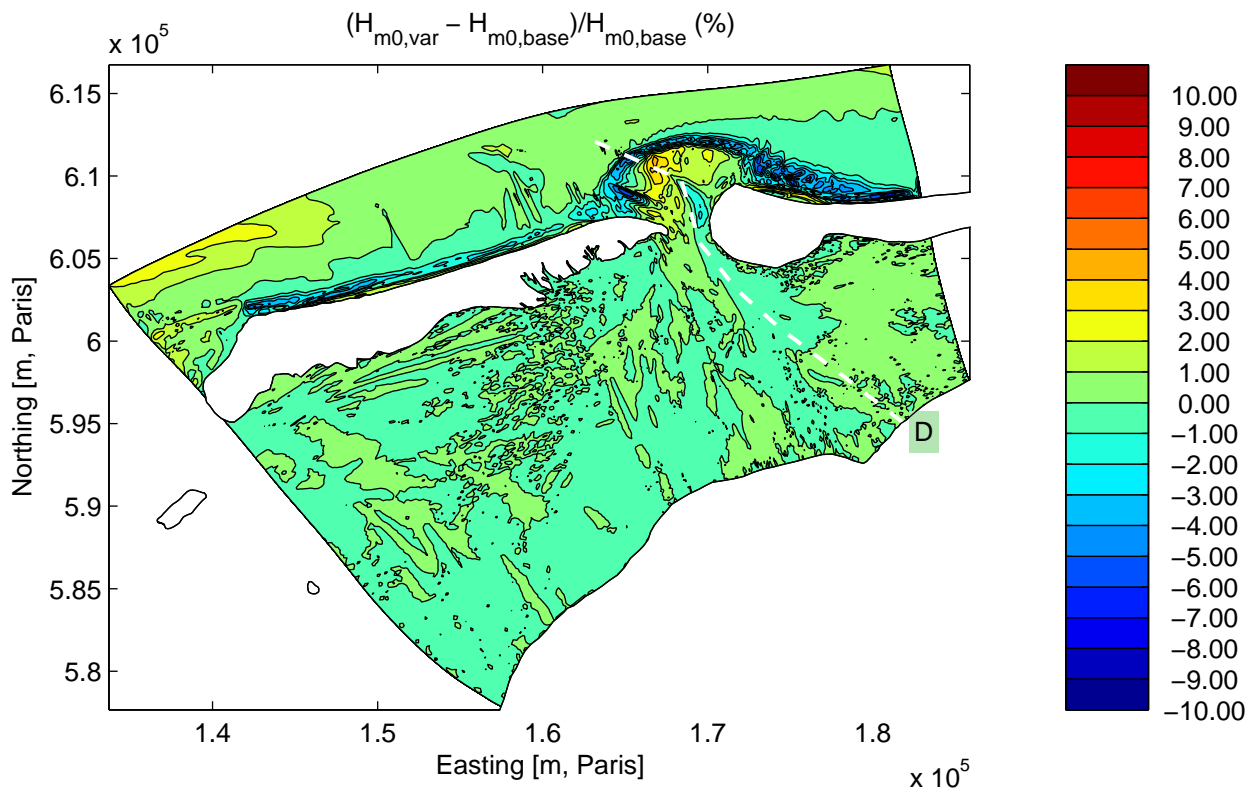
Sensitivity run C5BD1: Variation in wave direction at the boundary
Integral parameters along Curve D

Sensitivity analysis Ameland



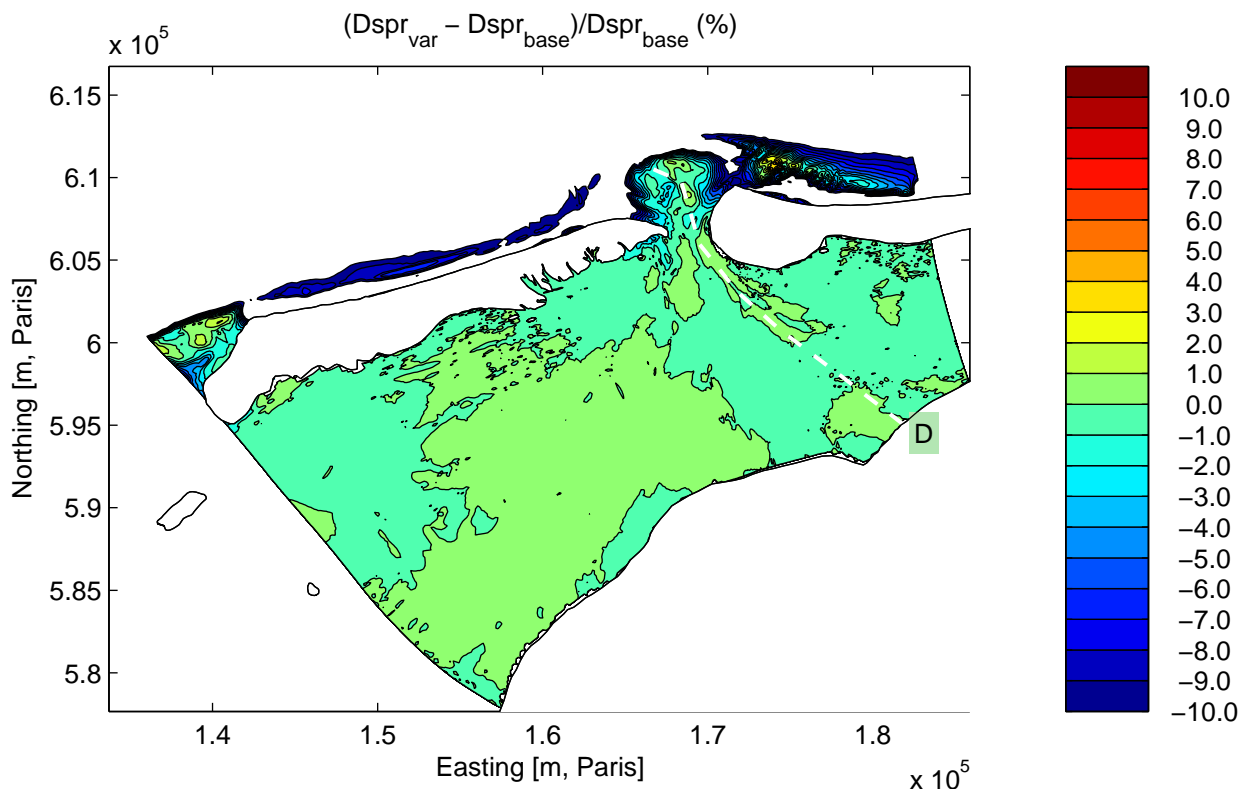
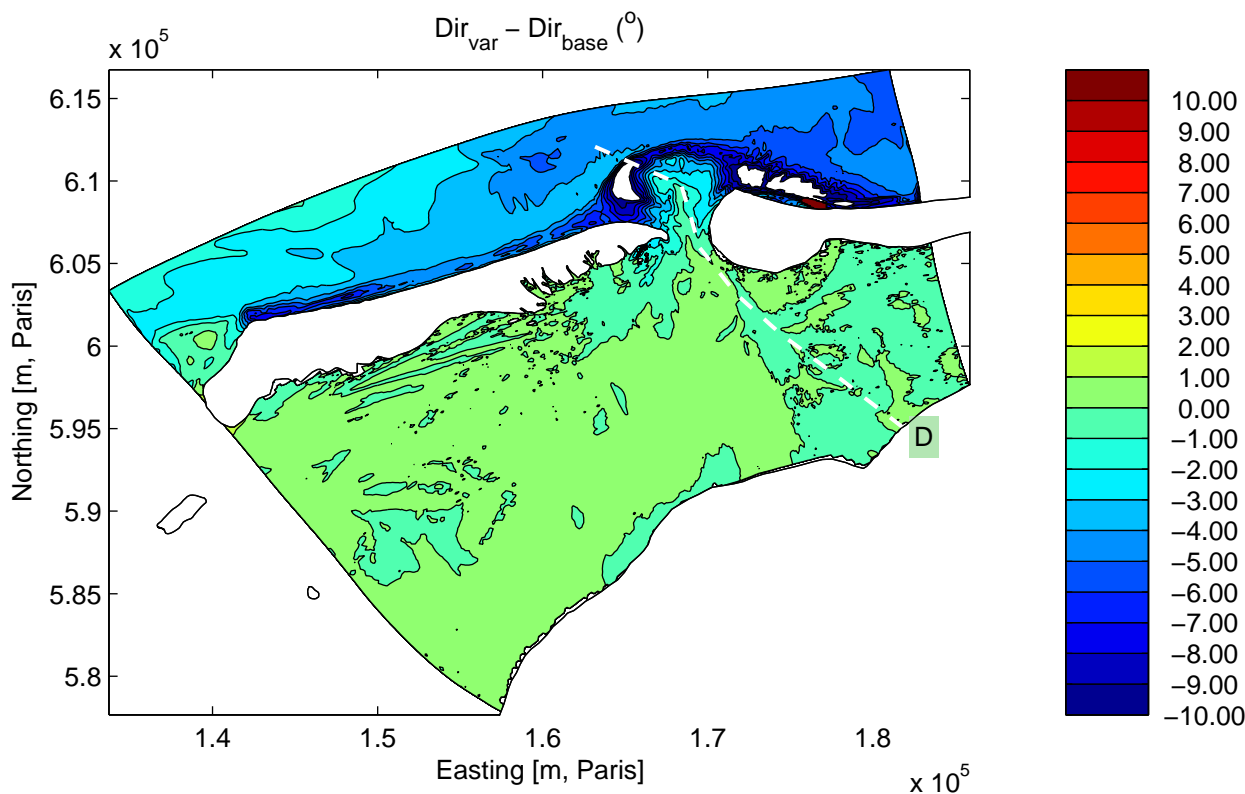
Sensitivity run C5BD2: Variation in wave direction at the boundary
Integral parameters along Curve D

Sensitivity analysis Ameland



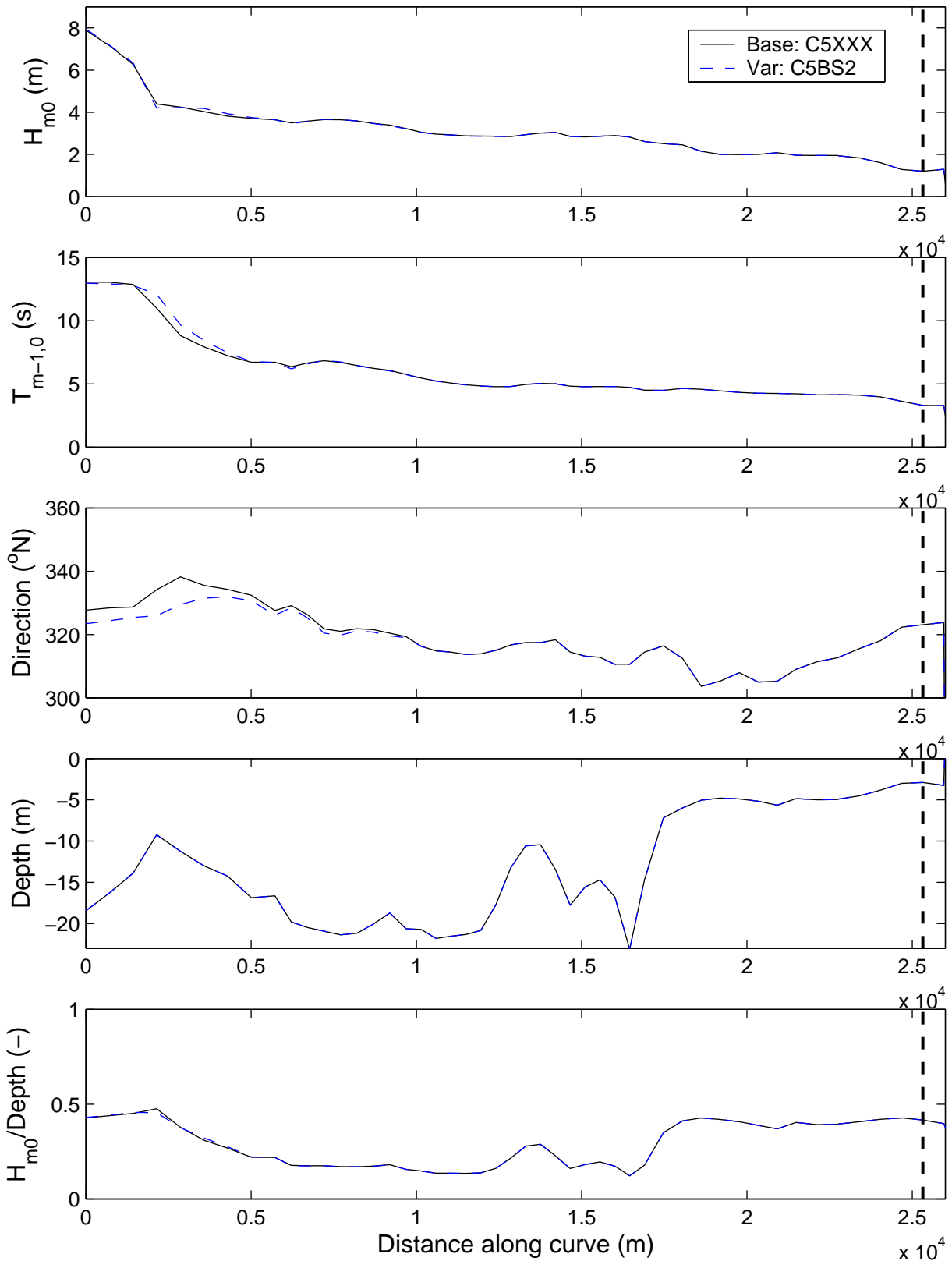
Sensitivity run C5BS2: Variation in directional spreading at the boundary
Differences in significant wave height (above) and mean period (below).

Sensitivity analysis Ameland



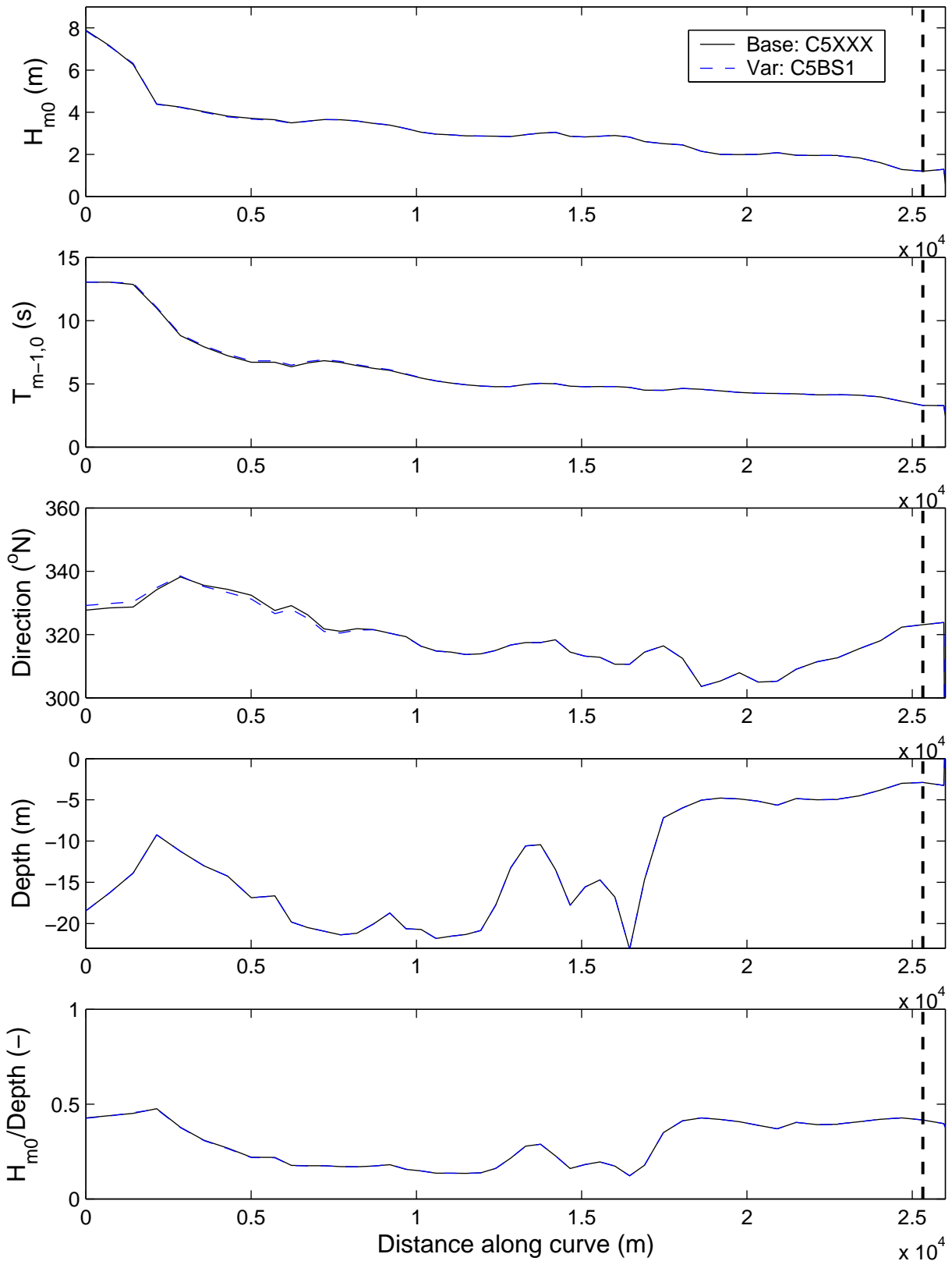
Sensitivity run C5BS2: Variation in directional spreading at the boundary
 Differences in mean direction (above) and directional spreading (below).

Sensitivity analysis Ameland



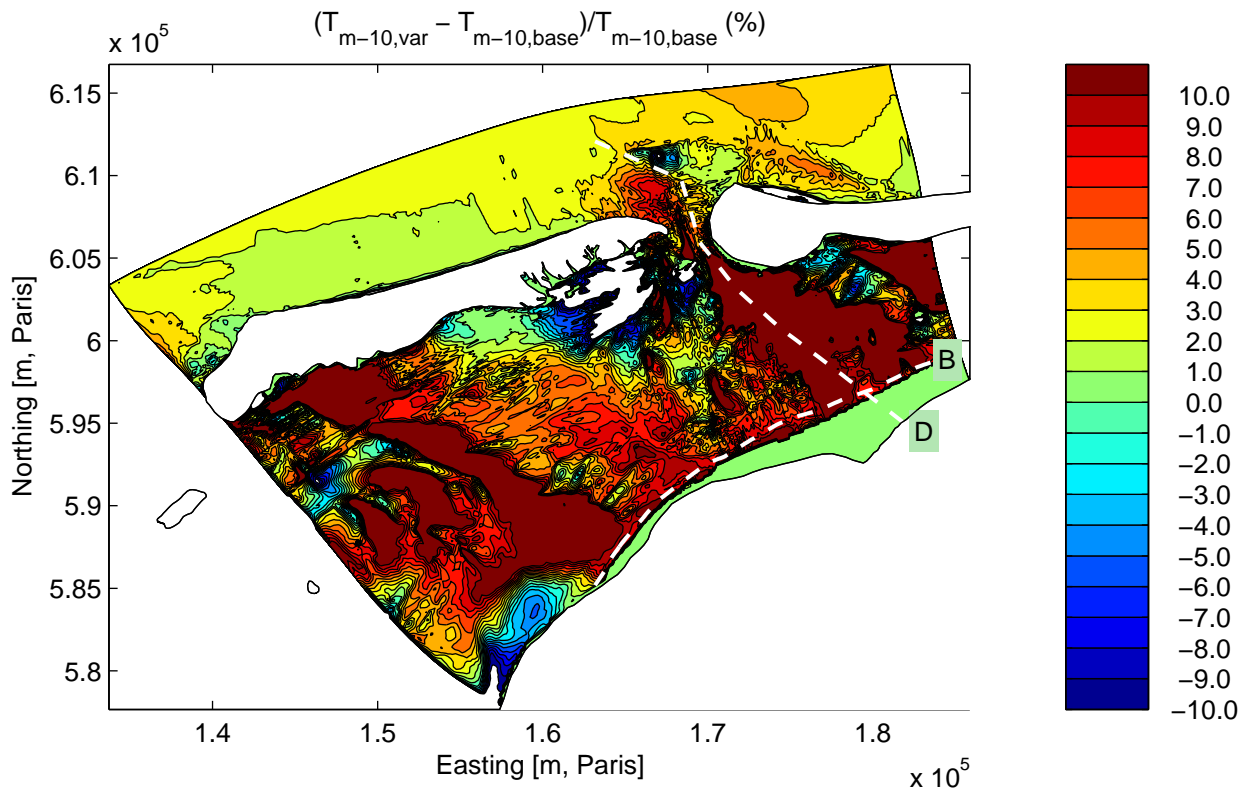
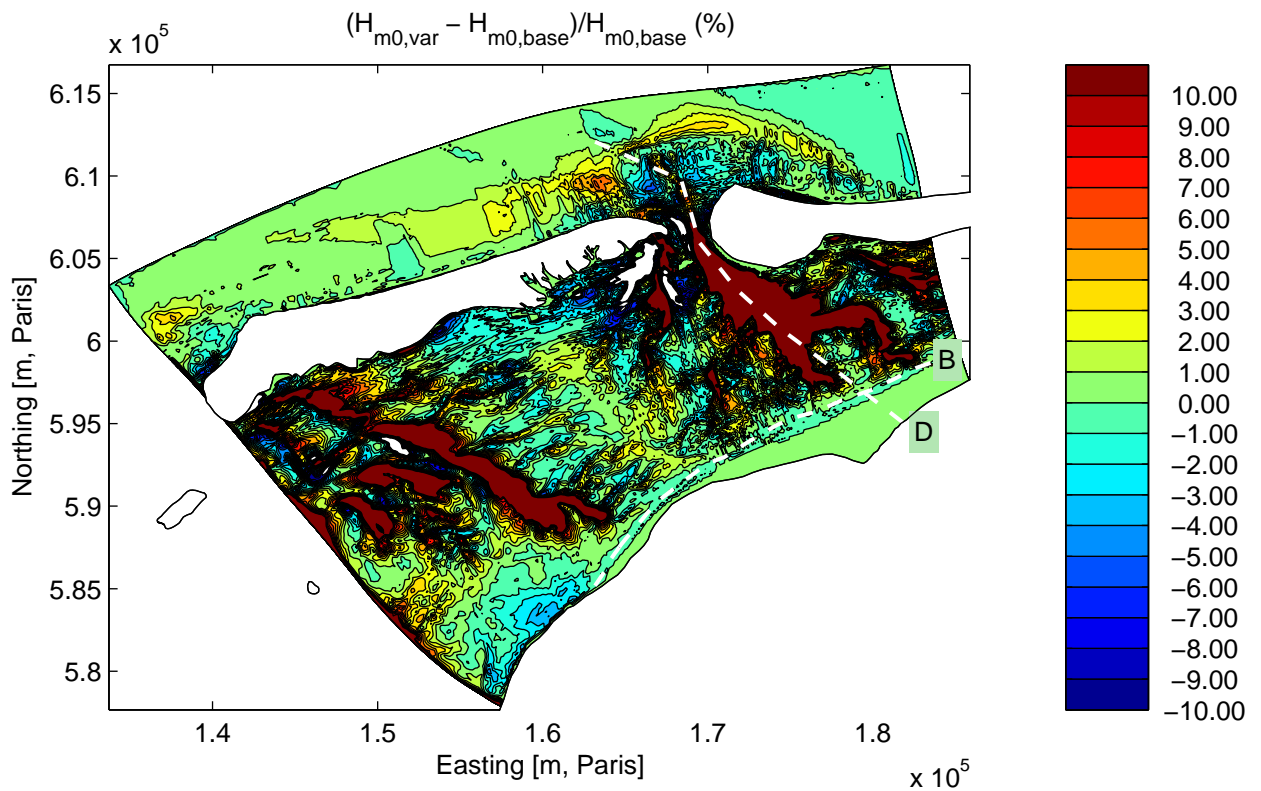
Sensitivity run C5BS2: Variation in directional spreading at the boundary
Integral parameters along Curve D

Sensitivity analysis Ameland



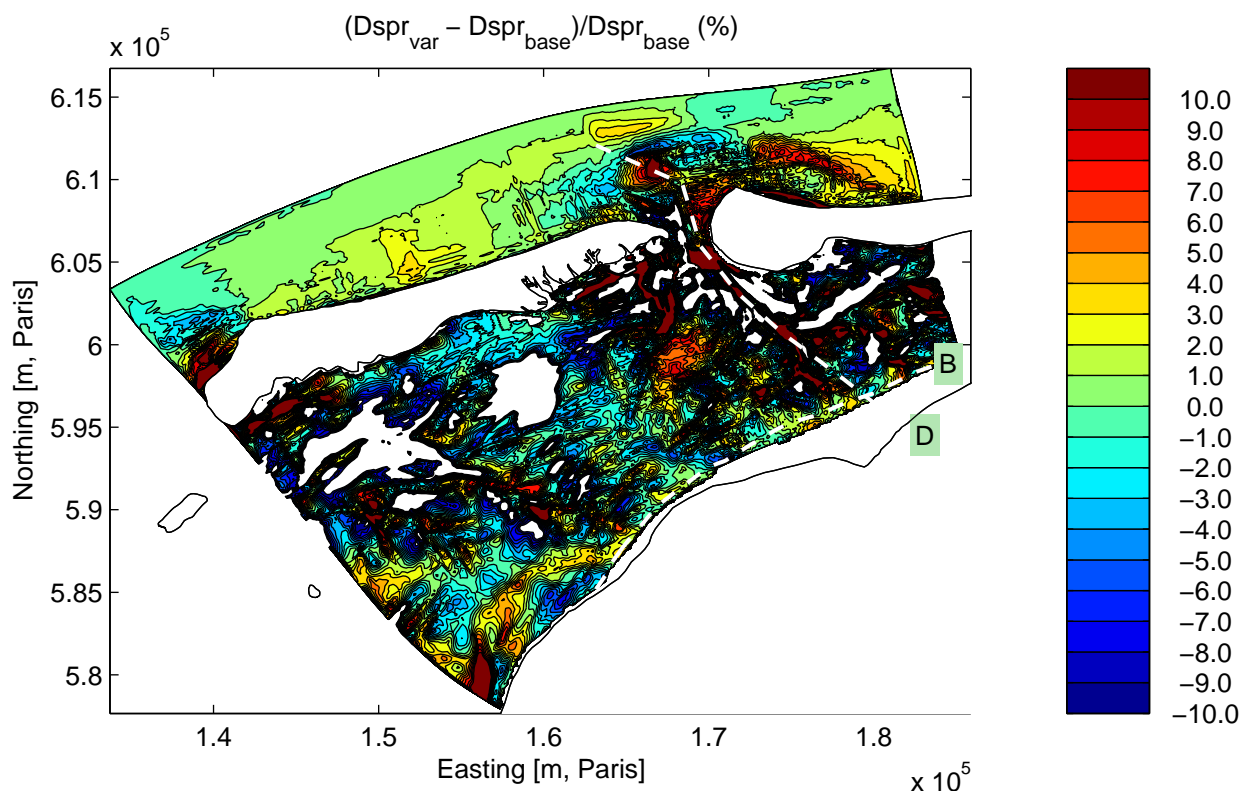
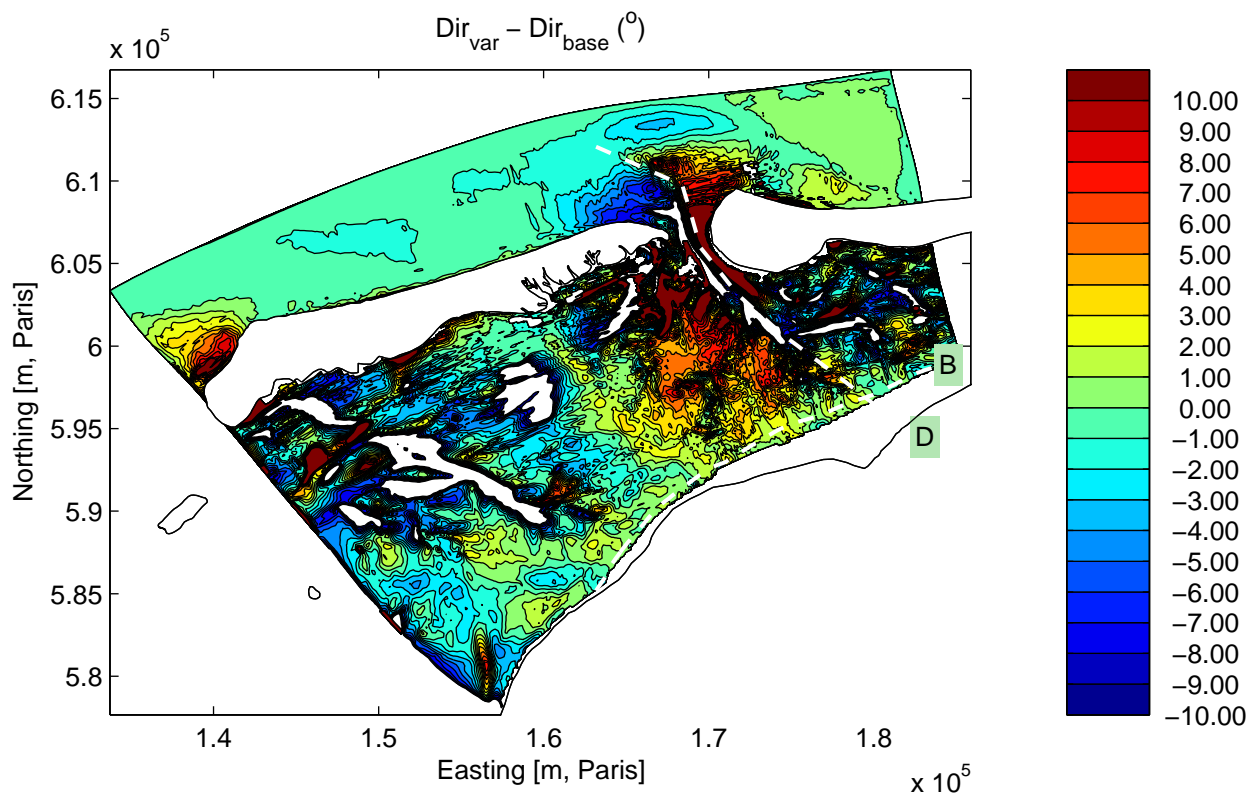
Sensitivity run C5BS1: Variation in directional spreading at the boundary
Integral parameters along Curve D

Sensitivity analysis Ameland



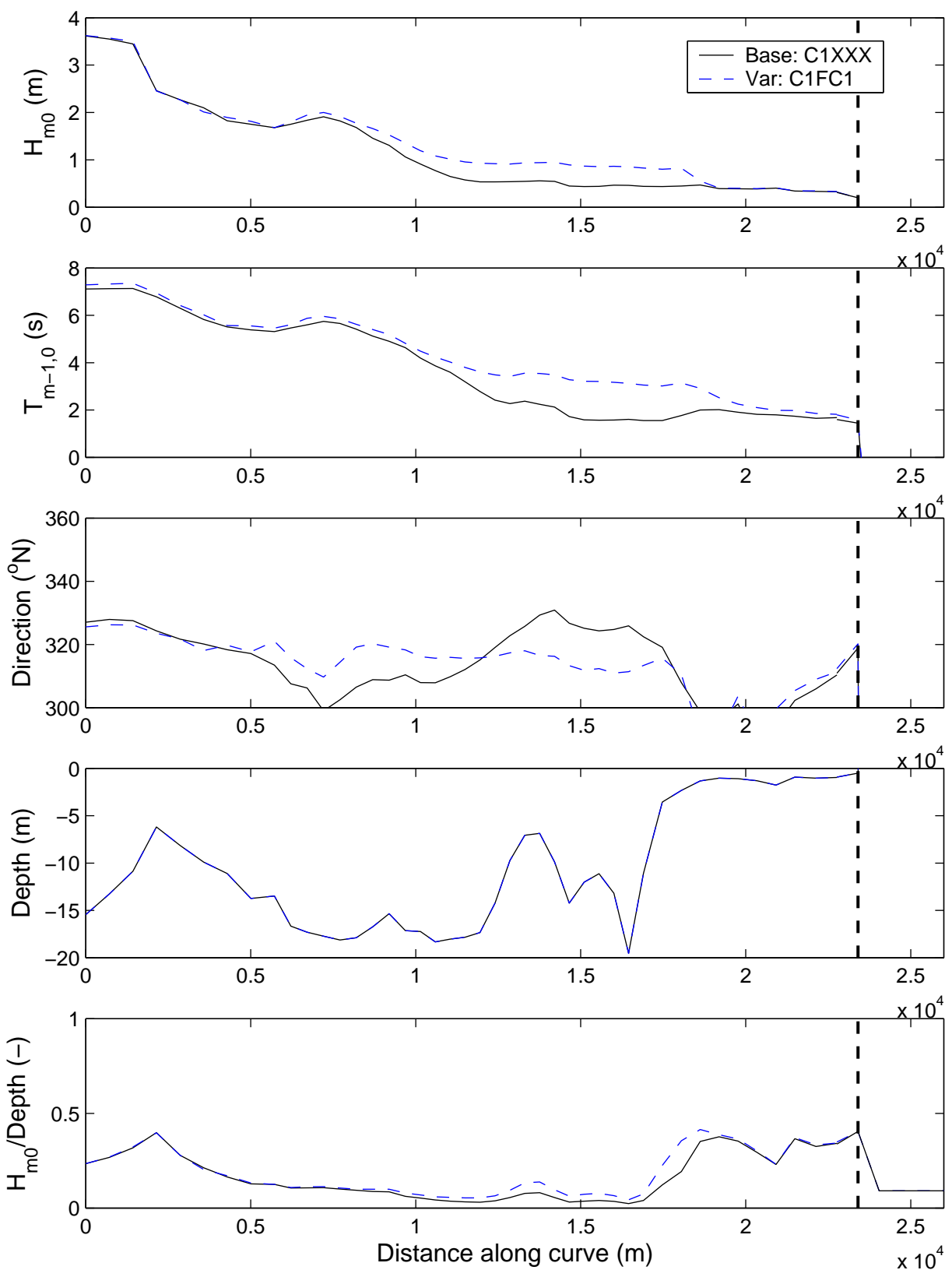
Sensitivity run C1FC1: Deactivation of flood current
Differences in significant wave height (above) and mean period (below).

Sensitivity analysis Ameland



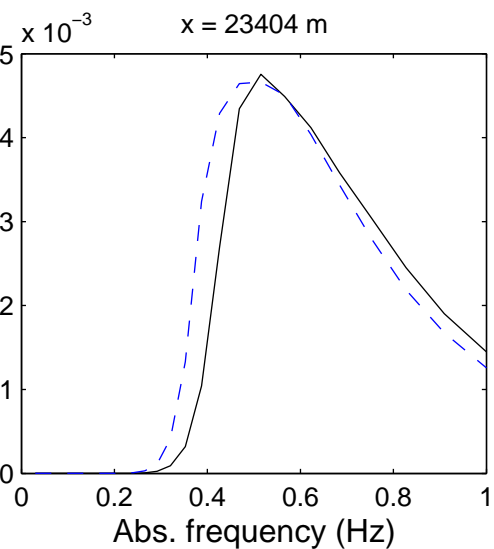
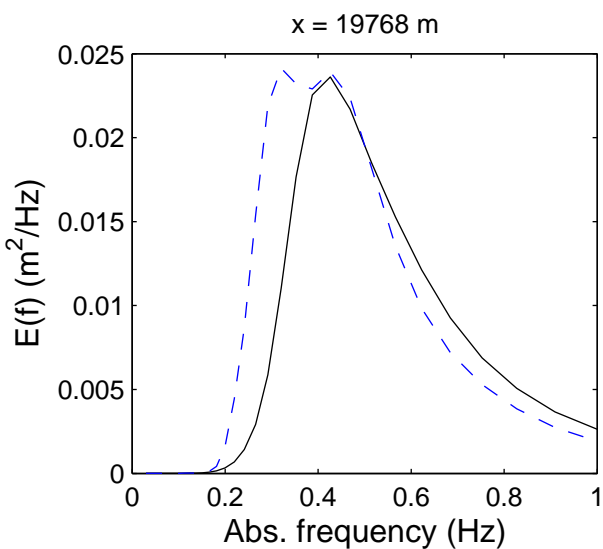
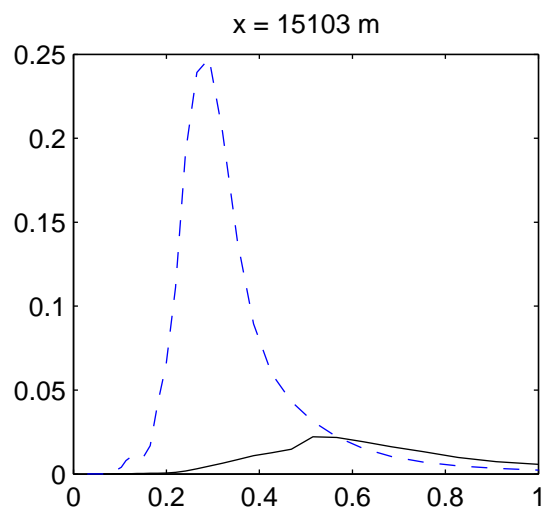
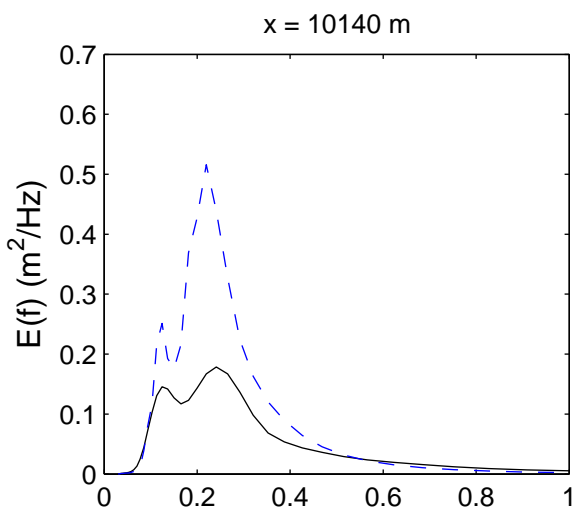
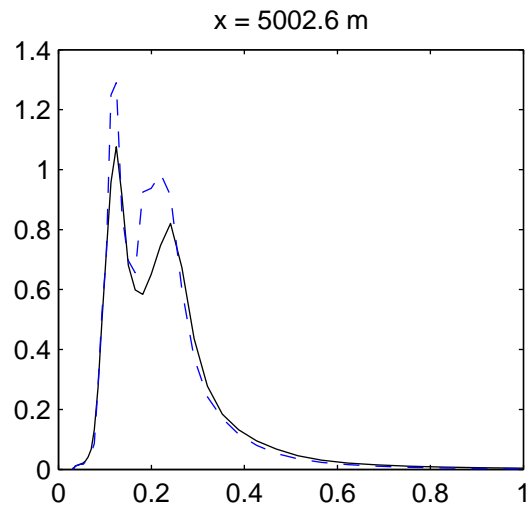
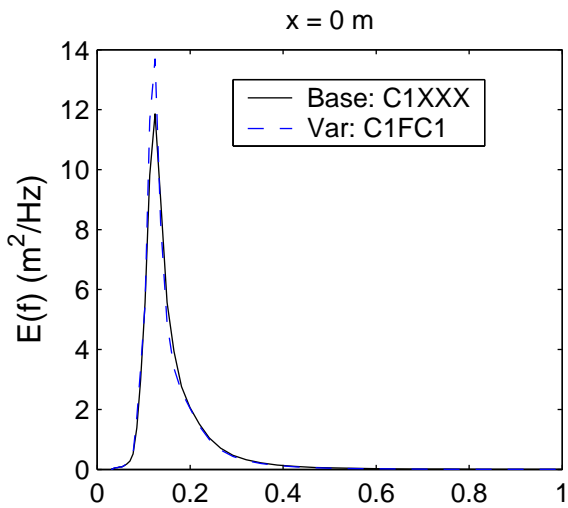
Sensitivity run C1FC1: Deactivation of flood current
Differences in mean direction (above) and directional spreading (below).

Sensitivity analysis Ameland



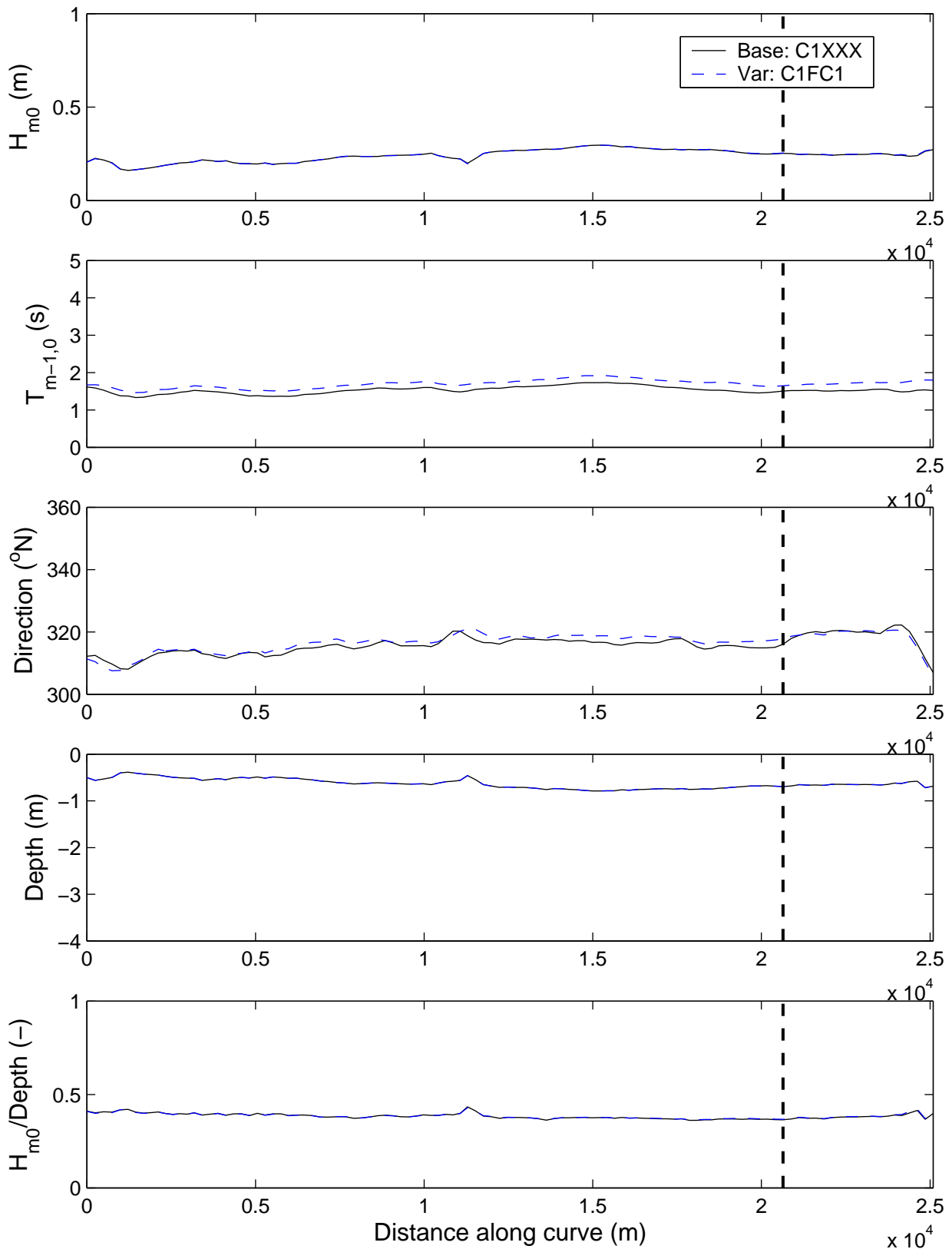
Sensitivity run C1FC1: Deactivation of flood current
Integral parameters along Curve D

Sensitivity analysis Ameland



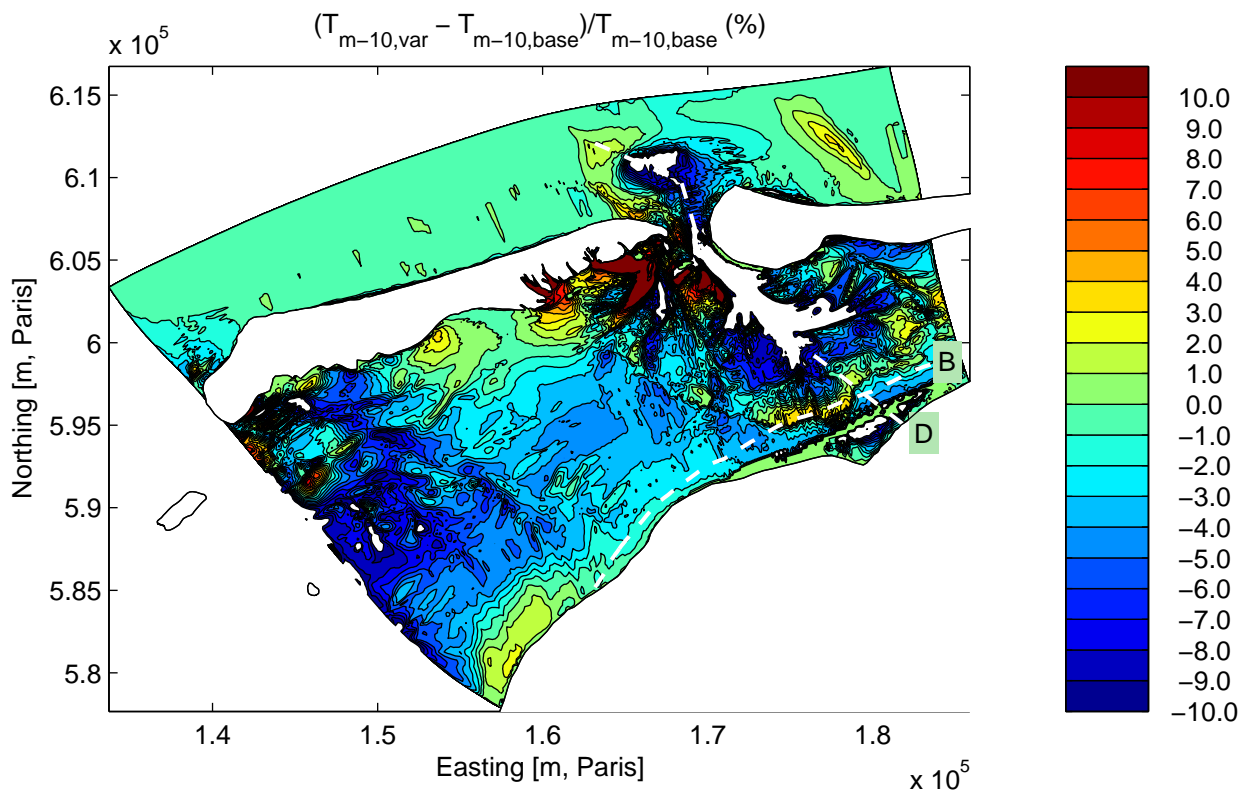
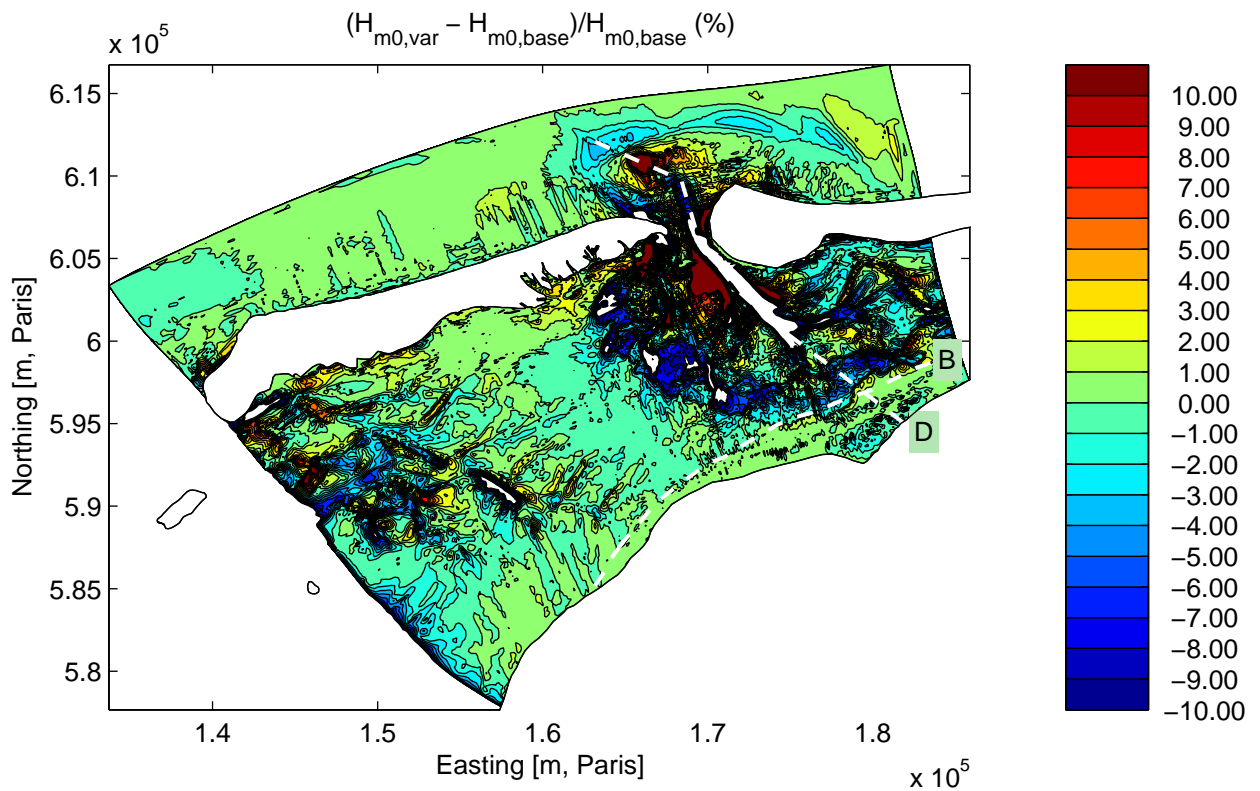
Sensitivity run C1FC1: Deactivation of flood current
 Absolute frequency spectra at various locations along Curve D

Sensitivity analysis Ameland



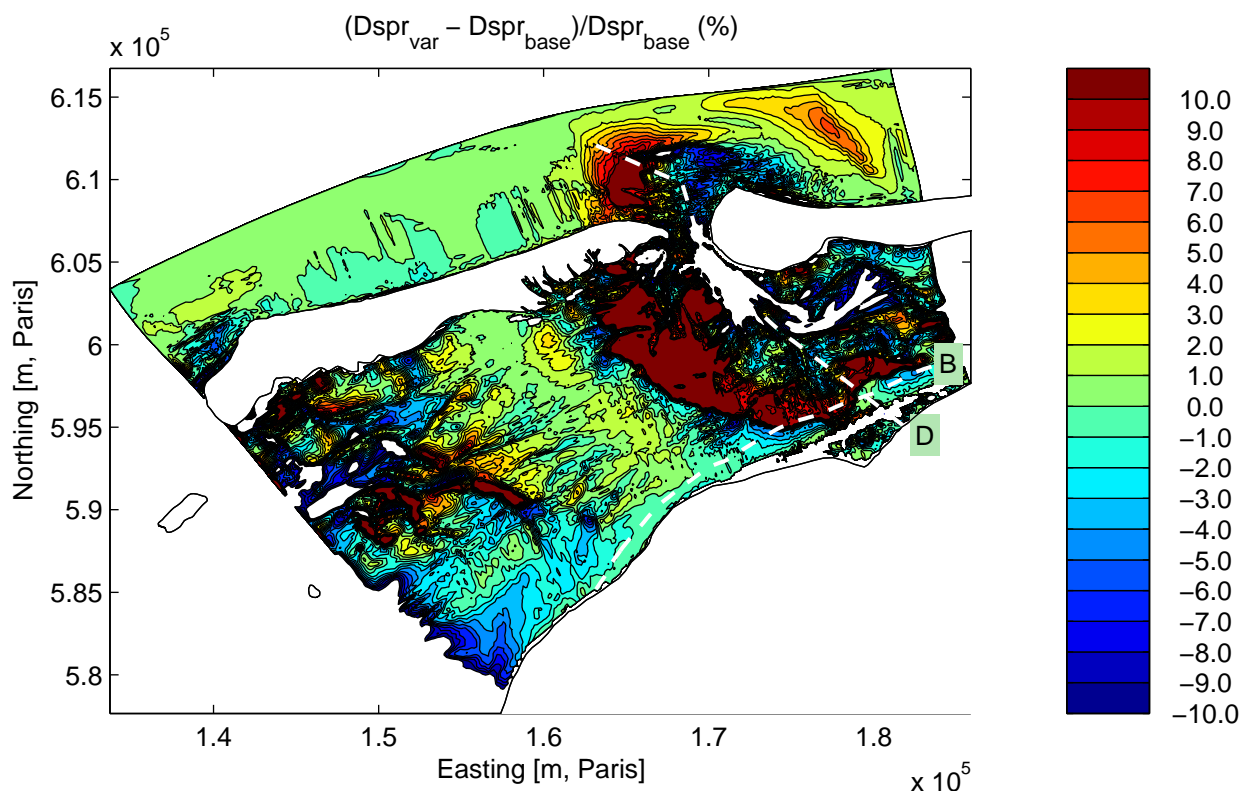
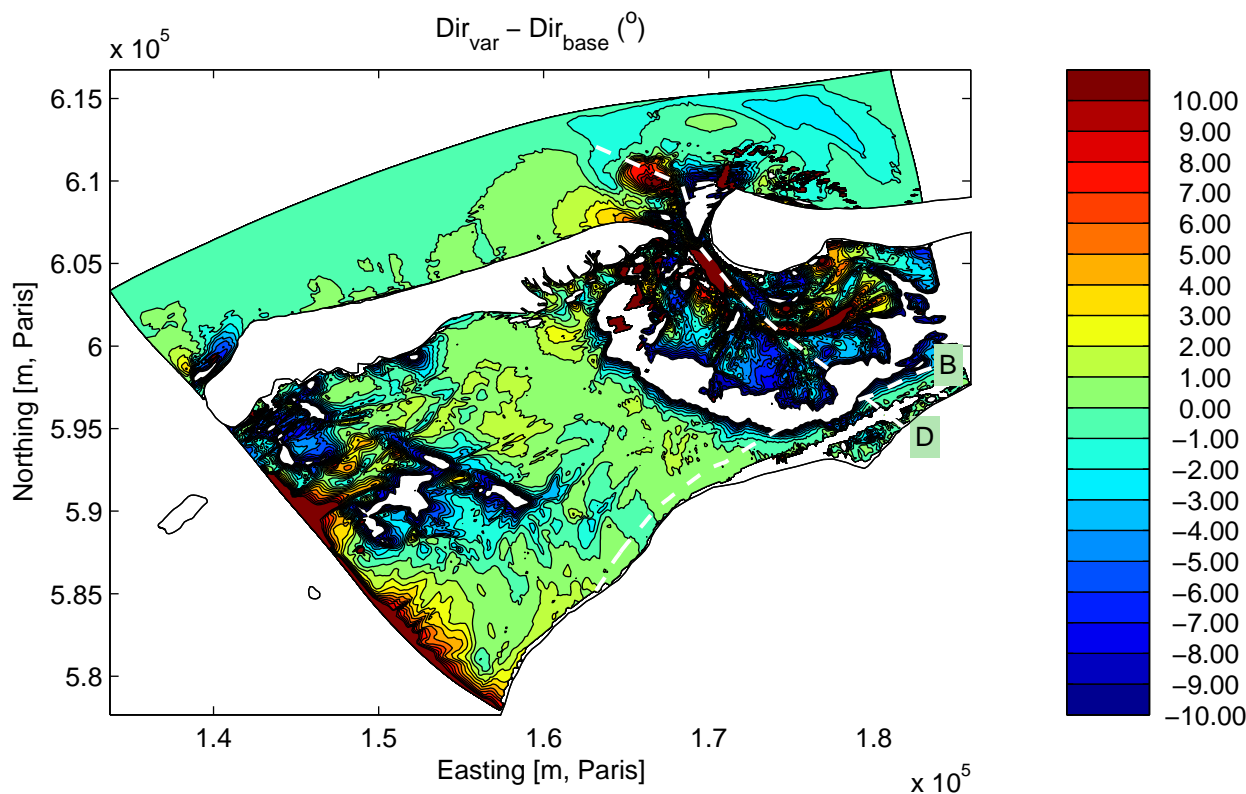
Sensitivity run C1FC1: Deactivation of flood current
Integral parameters along Curve B

Sensitivity analysis Ameland



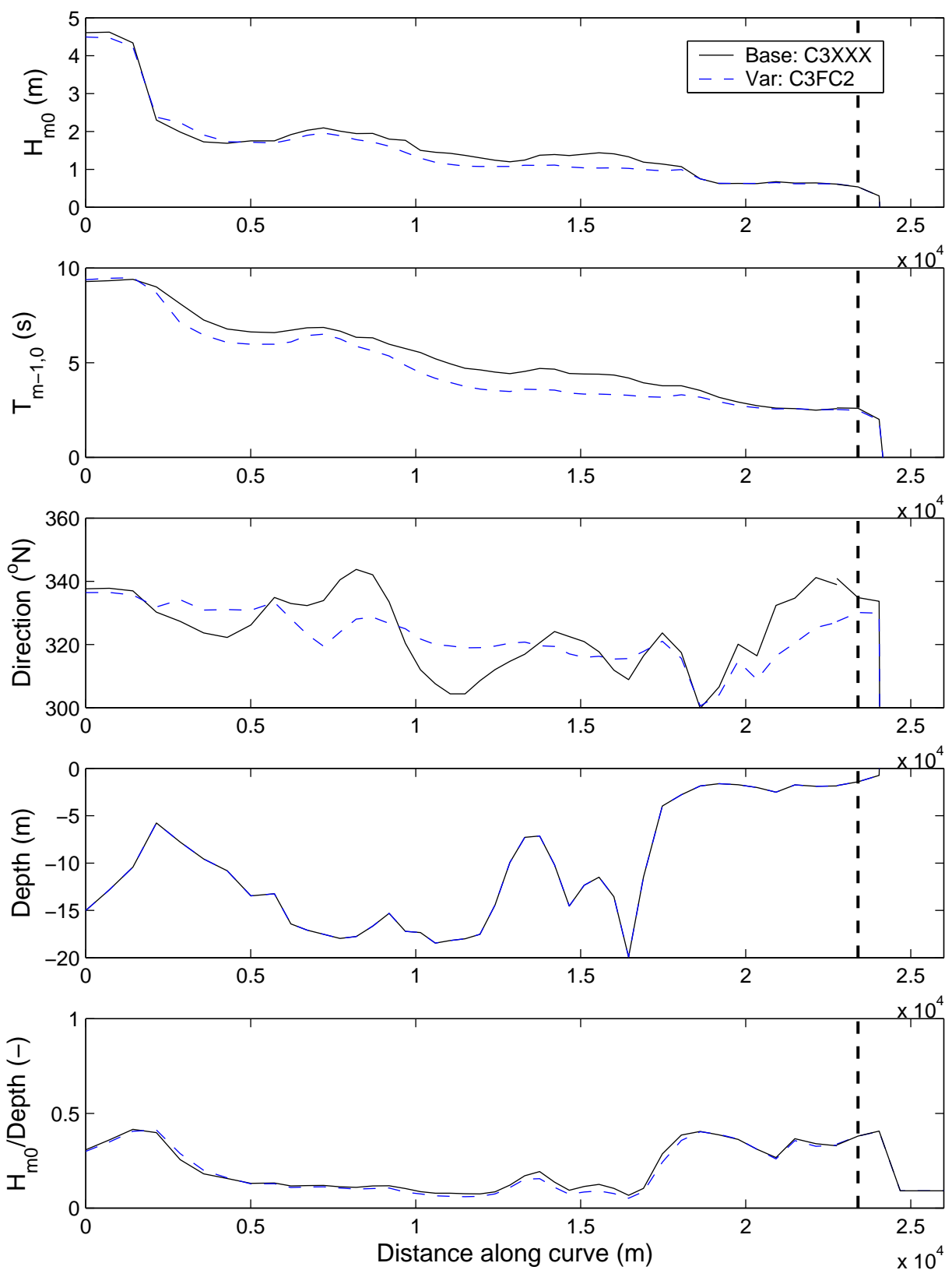
Sensitivity run C3FC2: Deactivation of ebb current
Differences in significant wave height (above) and mean period (below).

Sensitivity analysis Ameland



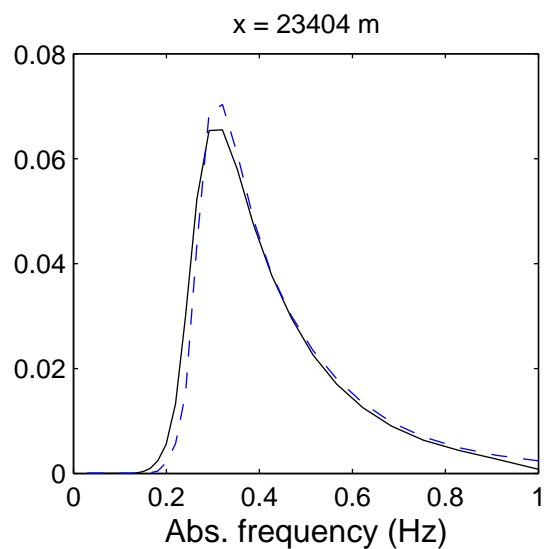
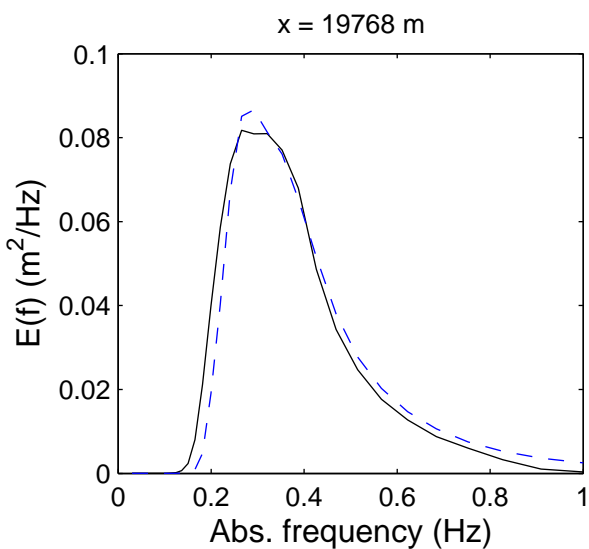
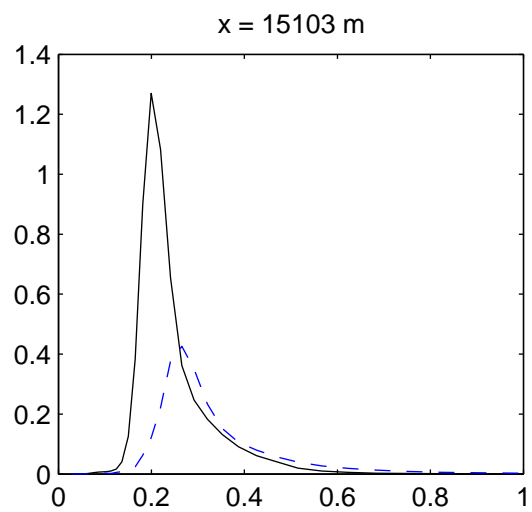
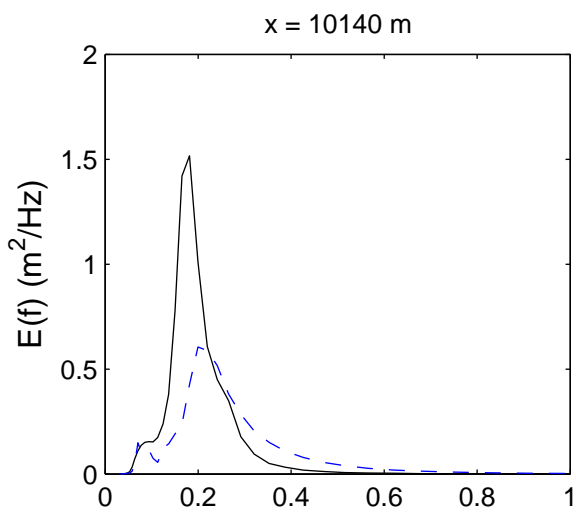
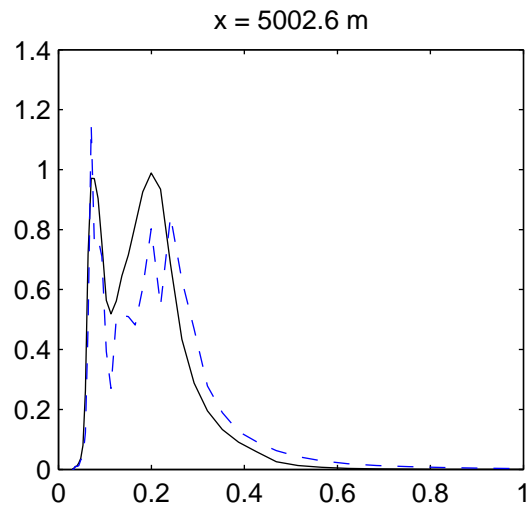
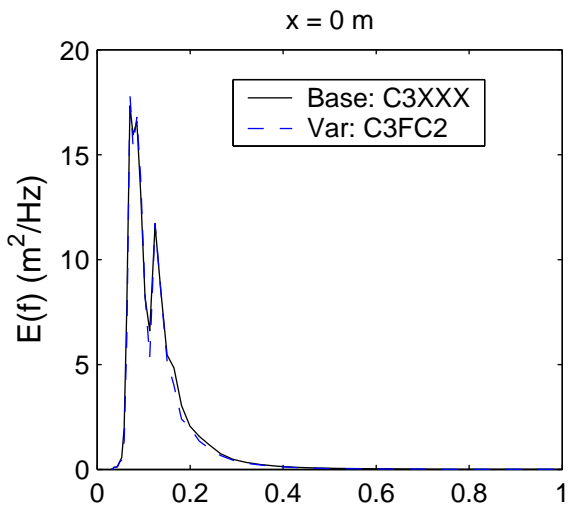
Sensitivity run C3FC2: Deactivation of ebb current
Differences in mean direction (above) and directional spreading (below).

Sensitivity analysis Ameland



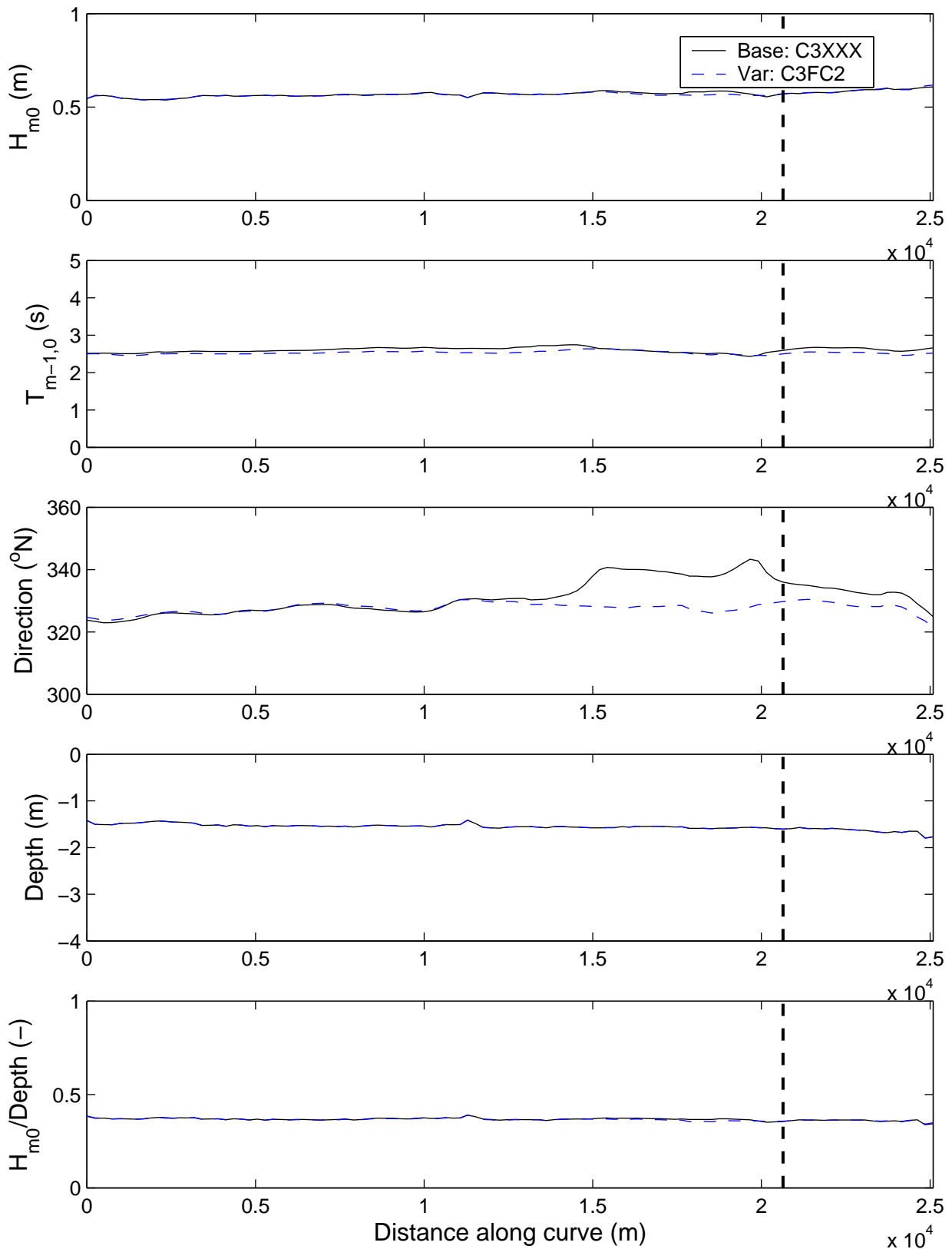
Sensitivity run C3FC2: Deactivation of ebb current
Integral parameters along Curve D

Sensitivity analysis Ameland



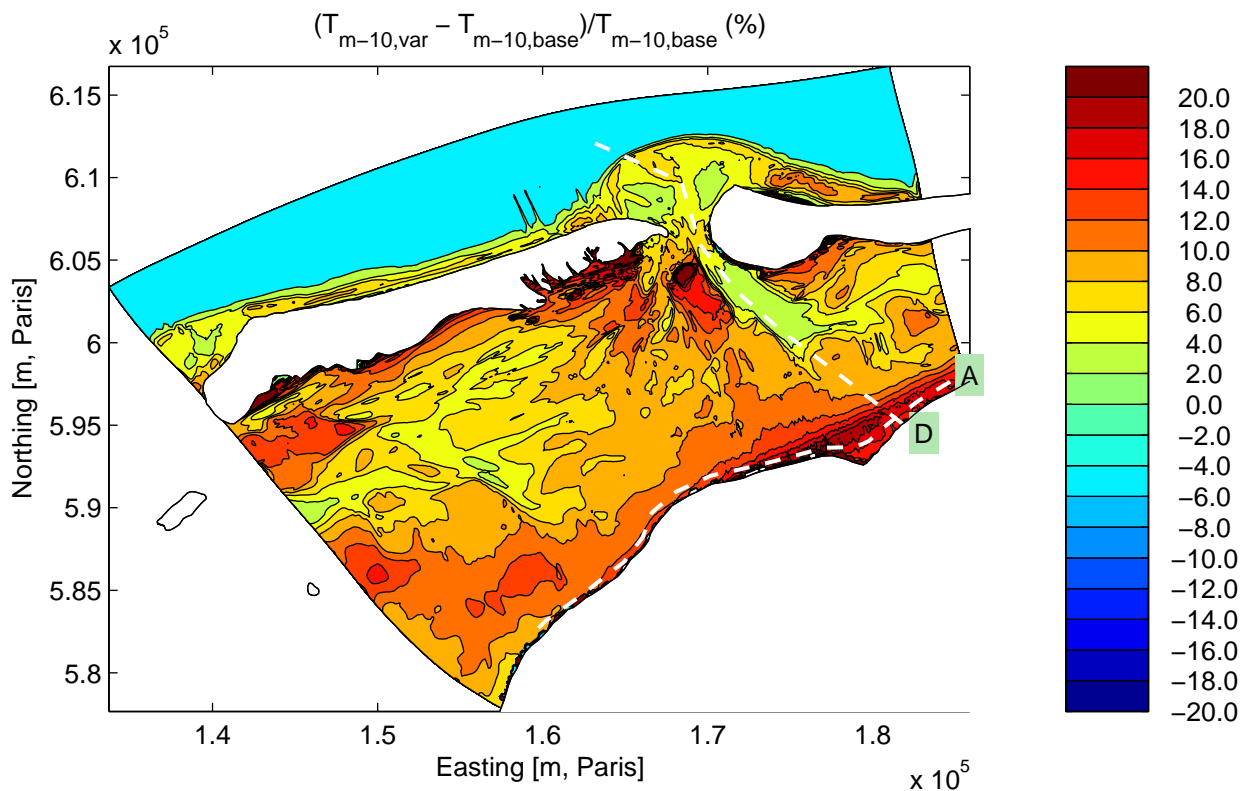
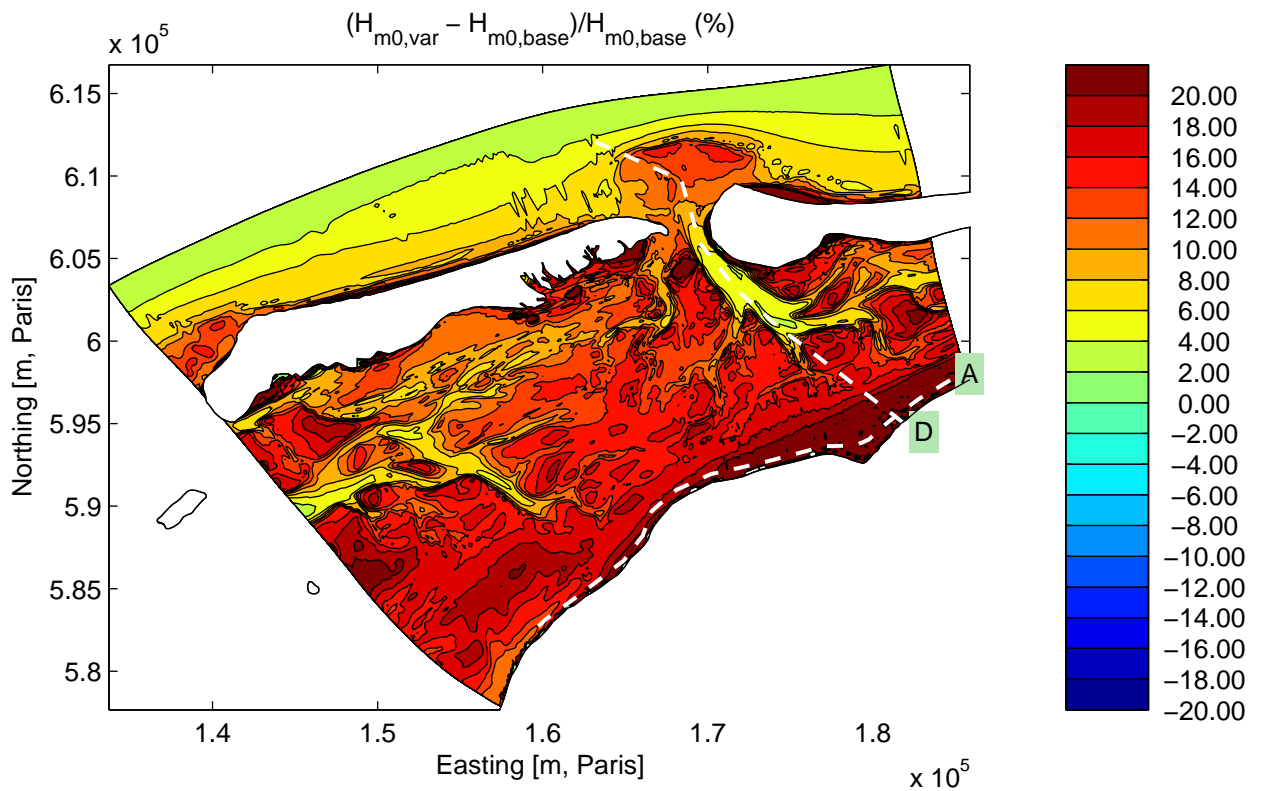
Sensitivity run C3FC2: Deactivation of ebb current
 Absolute frequency spectra at various locations along Curve D

Sensitivity analysis Ameland



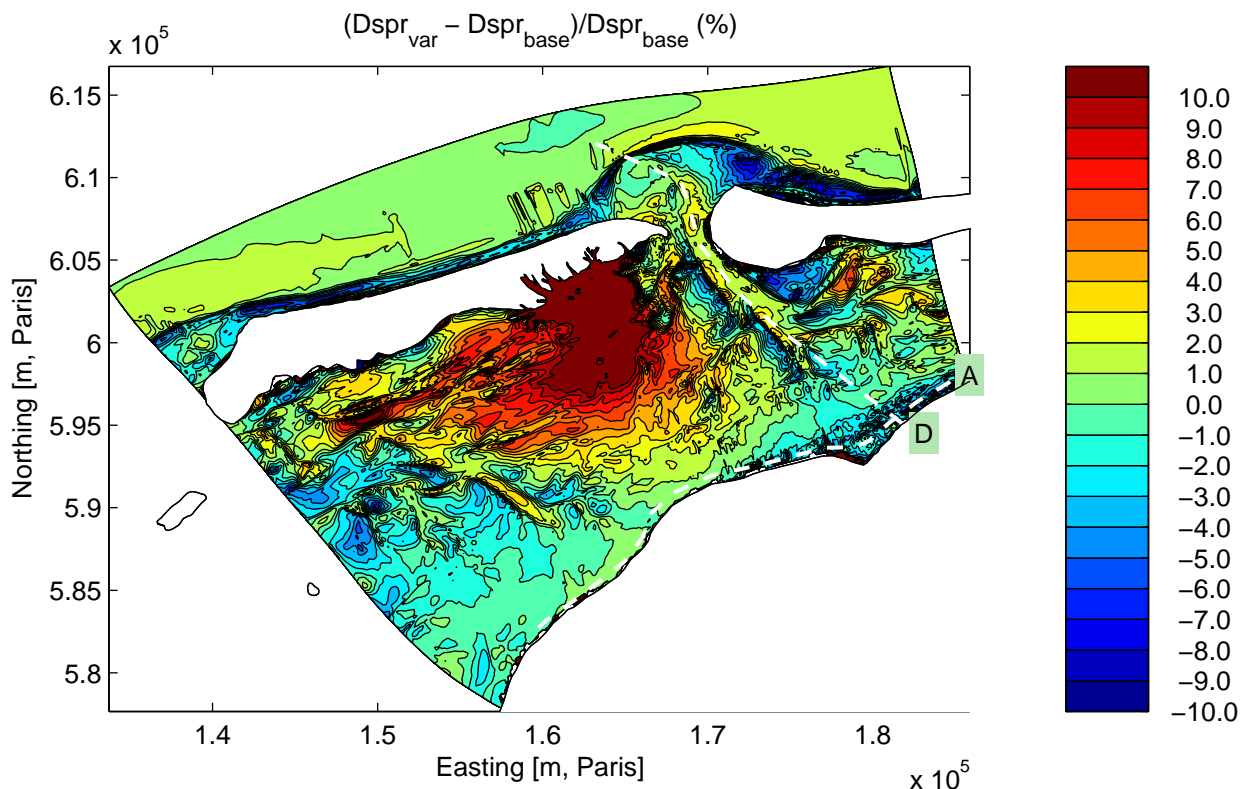
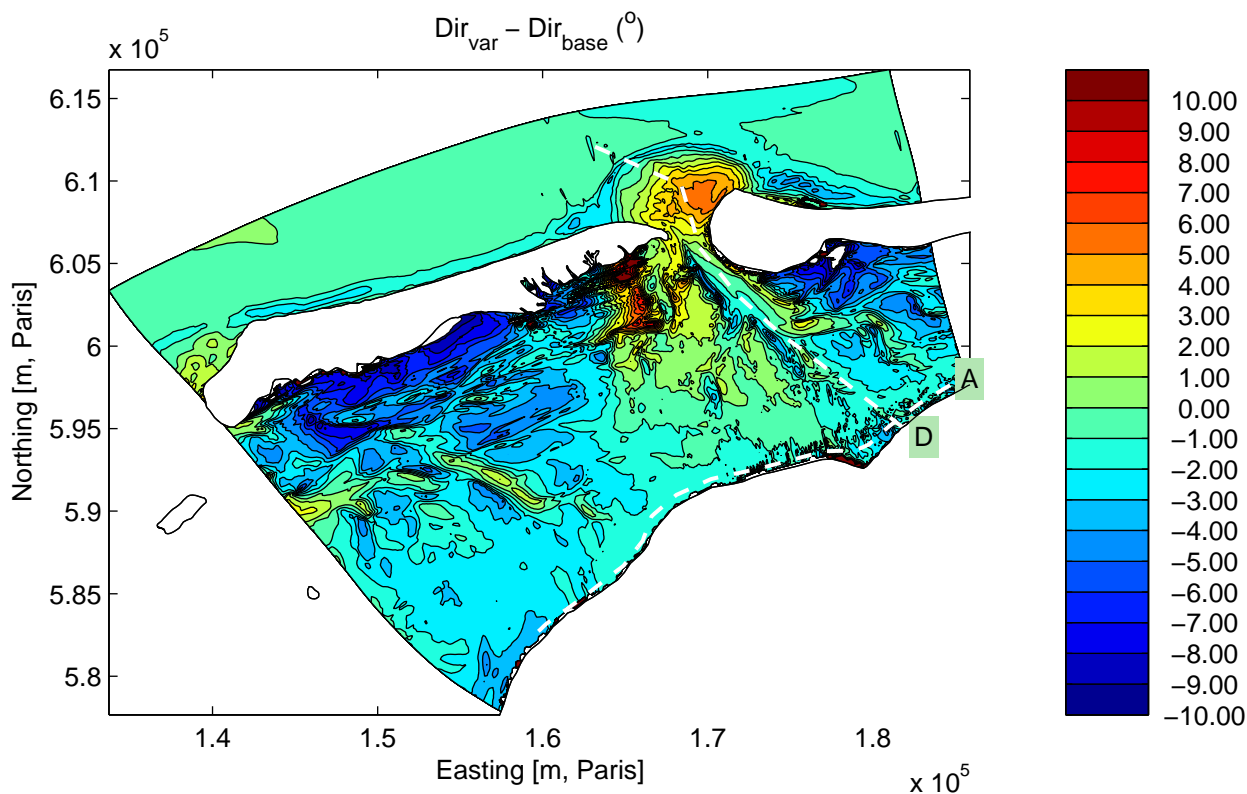
Sensitivity run C3FC2: Deactivation of ebb current
Integral parameters along Curve B

Sensitivity analysis Ameland



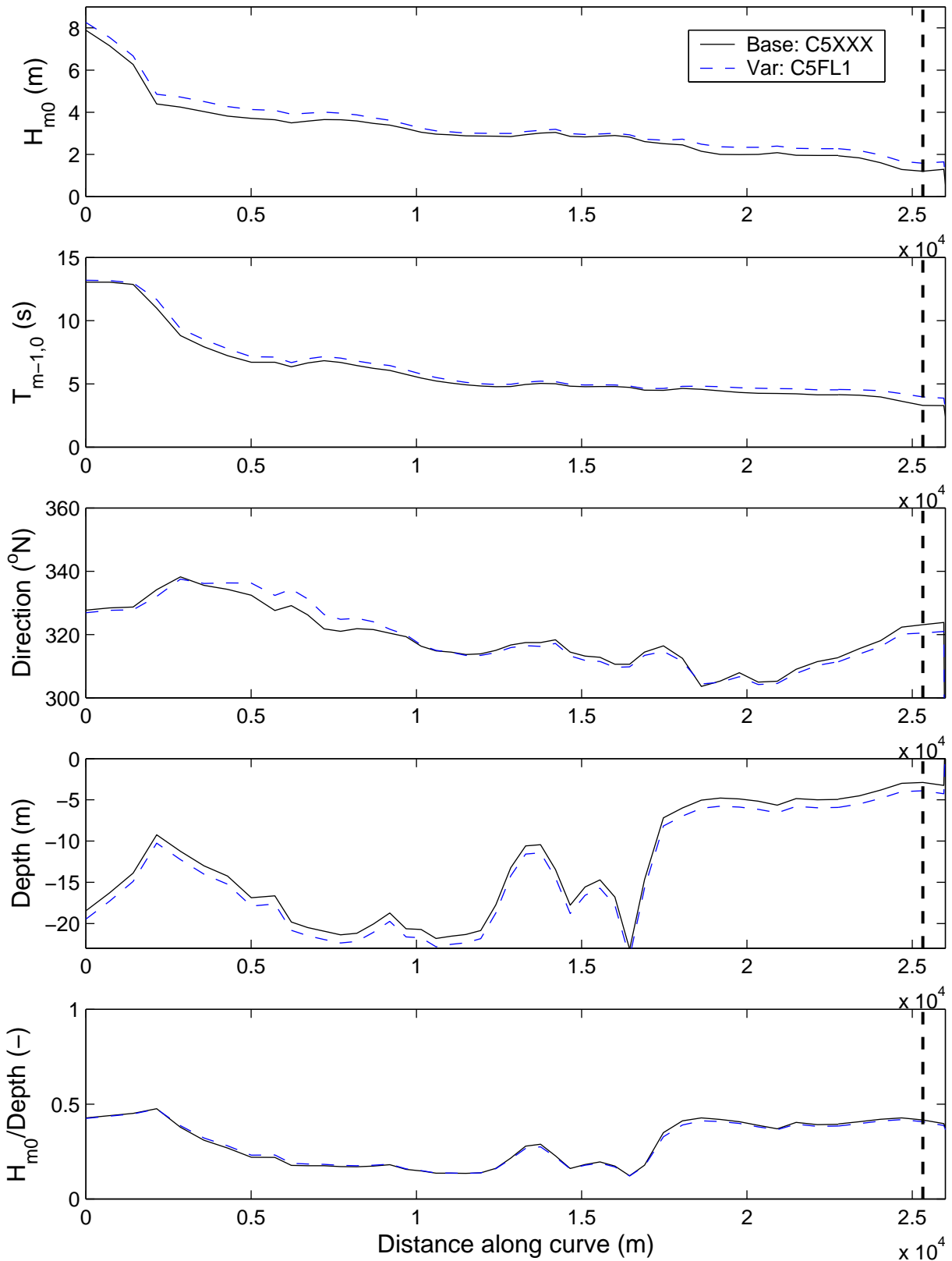
Sensitivity run C5FL1: Increase in water level
Differences in significant wave height (above) and mean period (below).

Sensitivity analysis Ameland



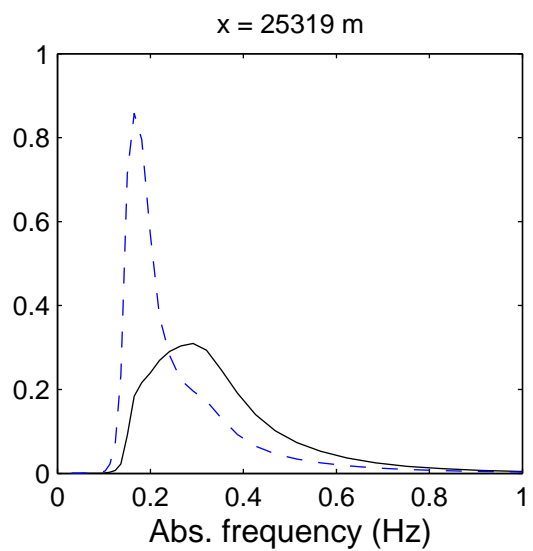
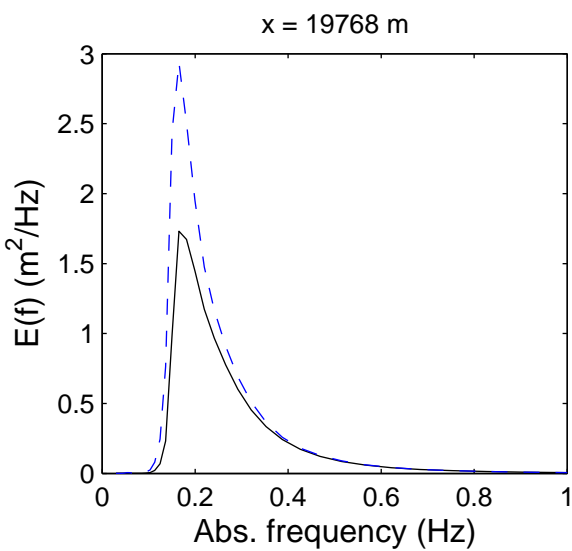
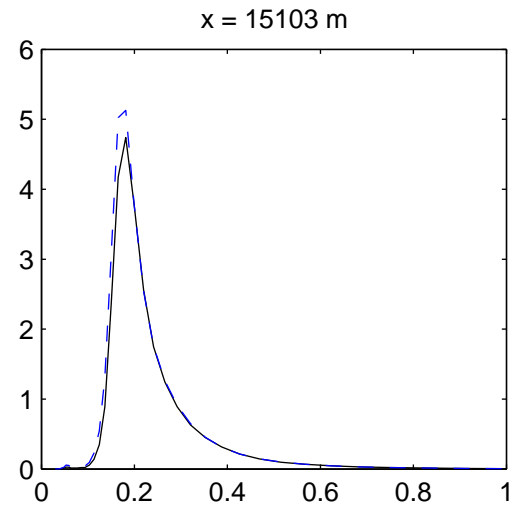
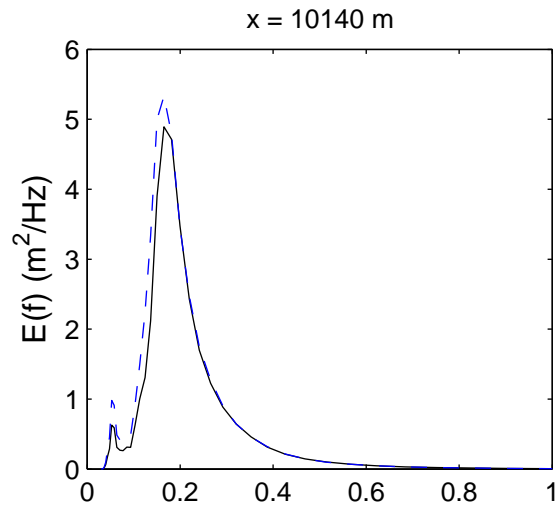
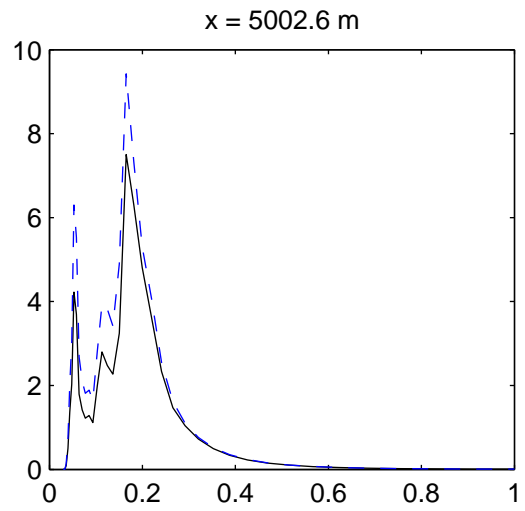
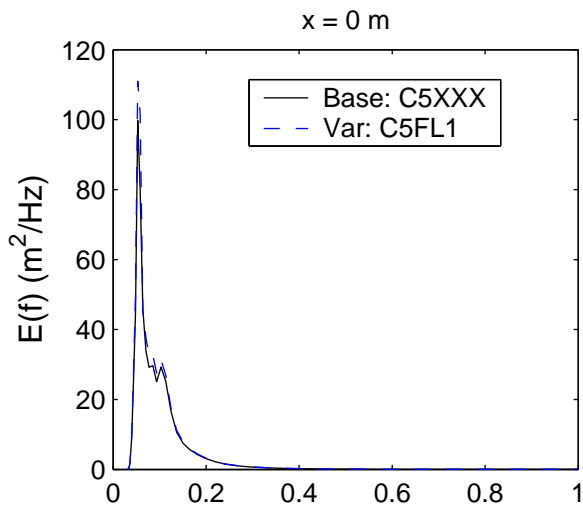
Sensitivity run C5FL1: Increase in water level
Differences in mean direction (above) and directional spreading (below).

Sensitivity analysis Ameland



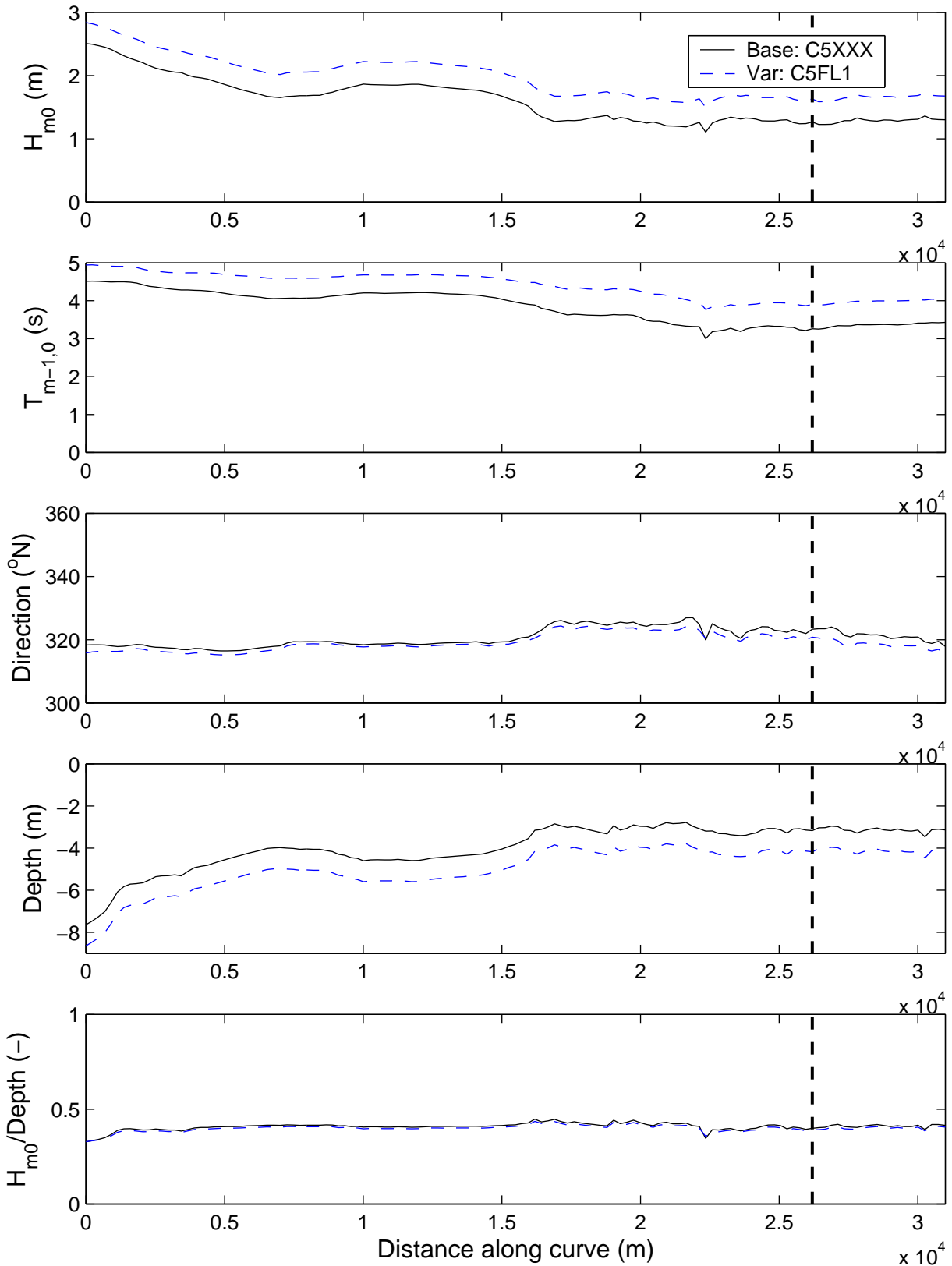
Sensitivity run C5FL1: Increase in water level
Integral parameters along Curve D

Sensitivity analysis Ameland



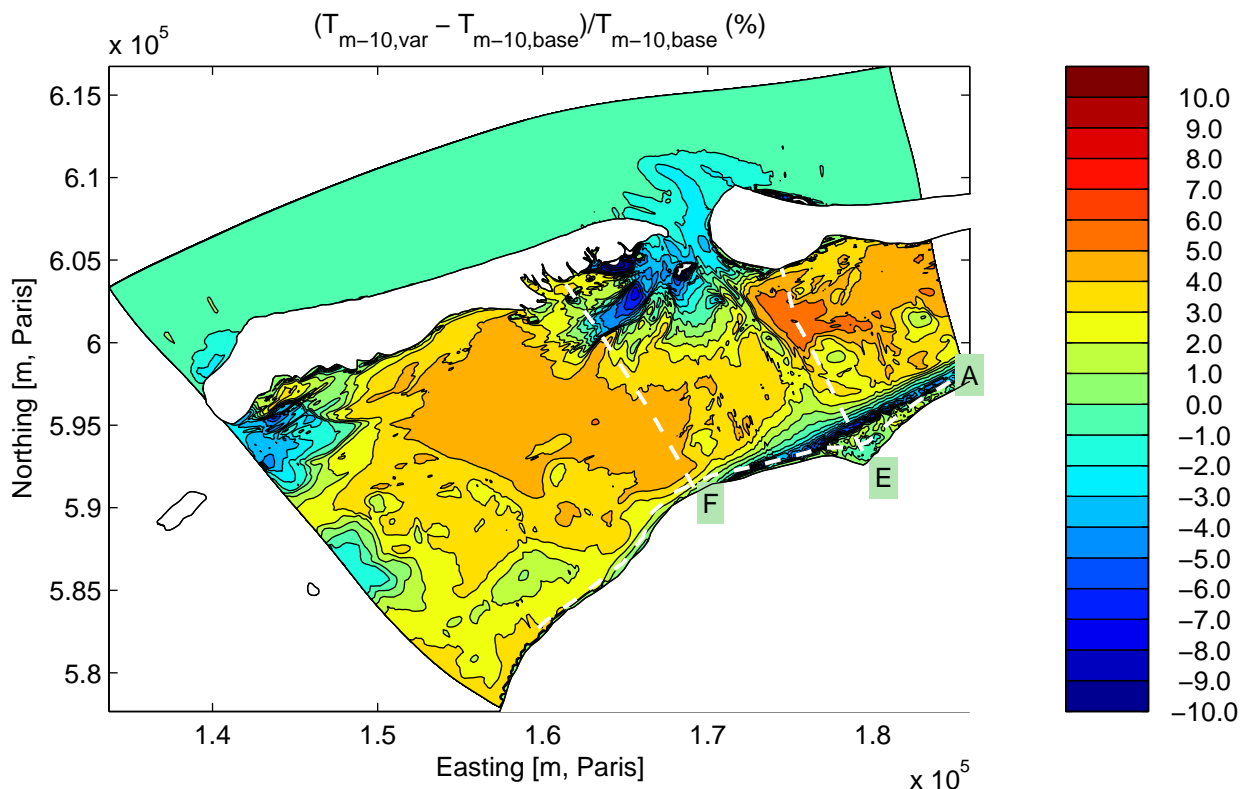
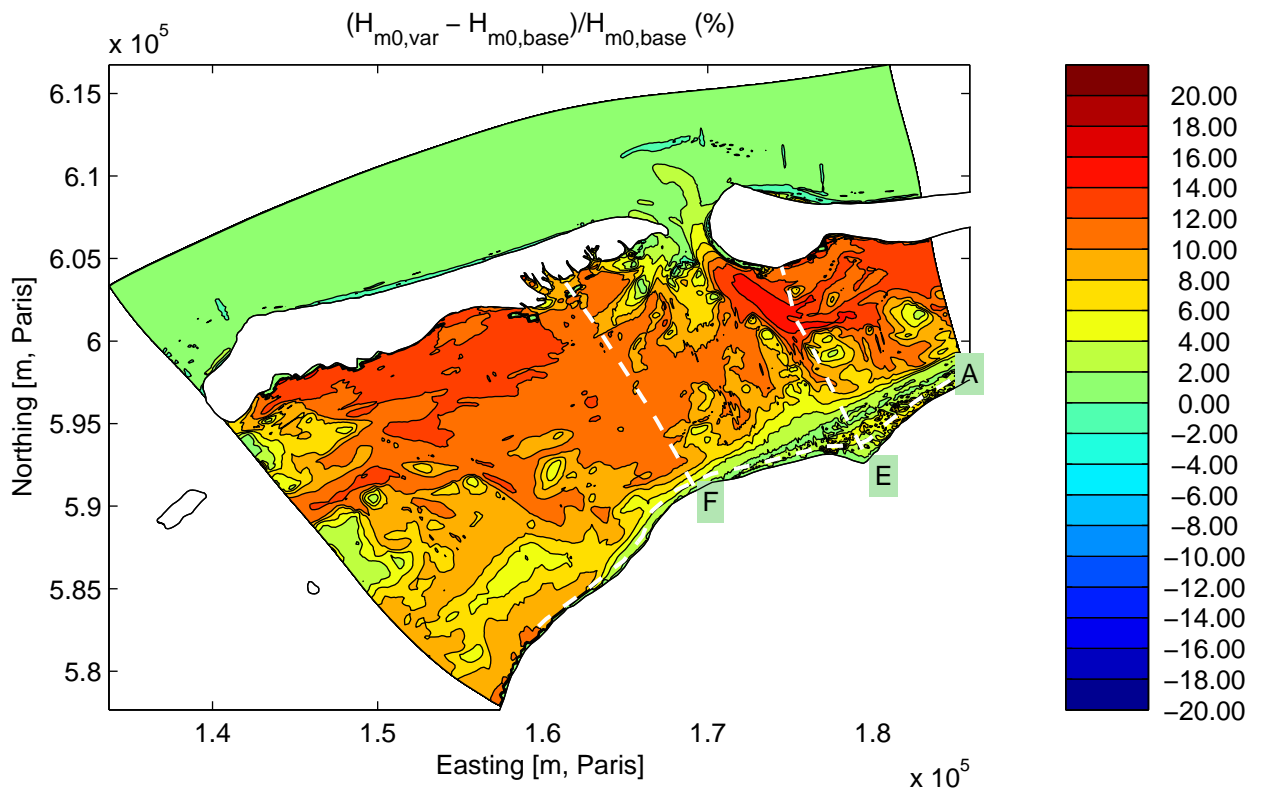
Sensitivity run C5FL1: Increase in water level
 Absolute frequency spectra at various locations along Curve D

Sensitivity analysis Ameland



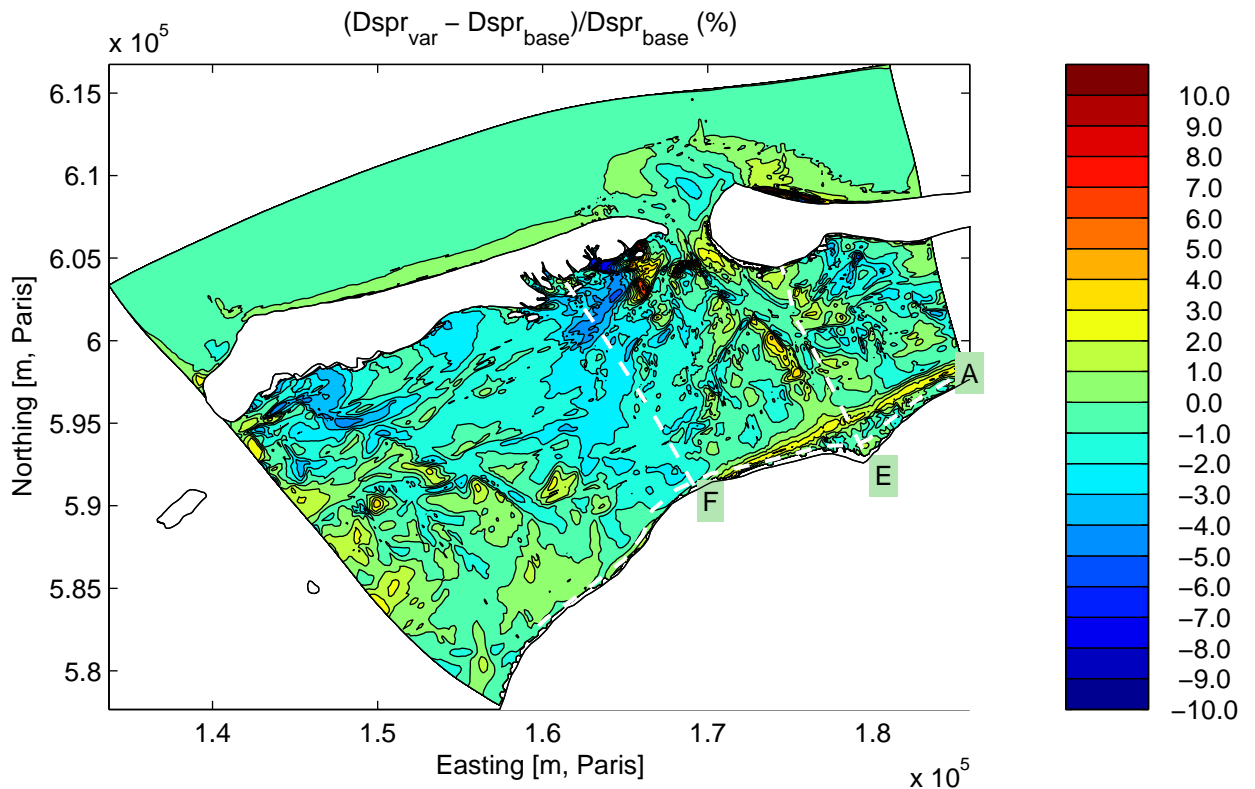
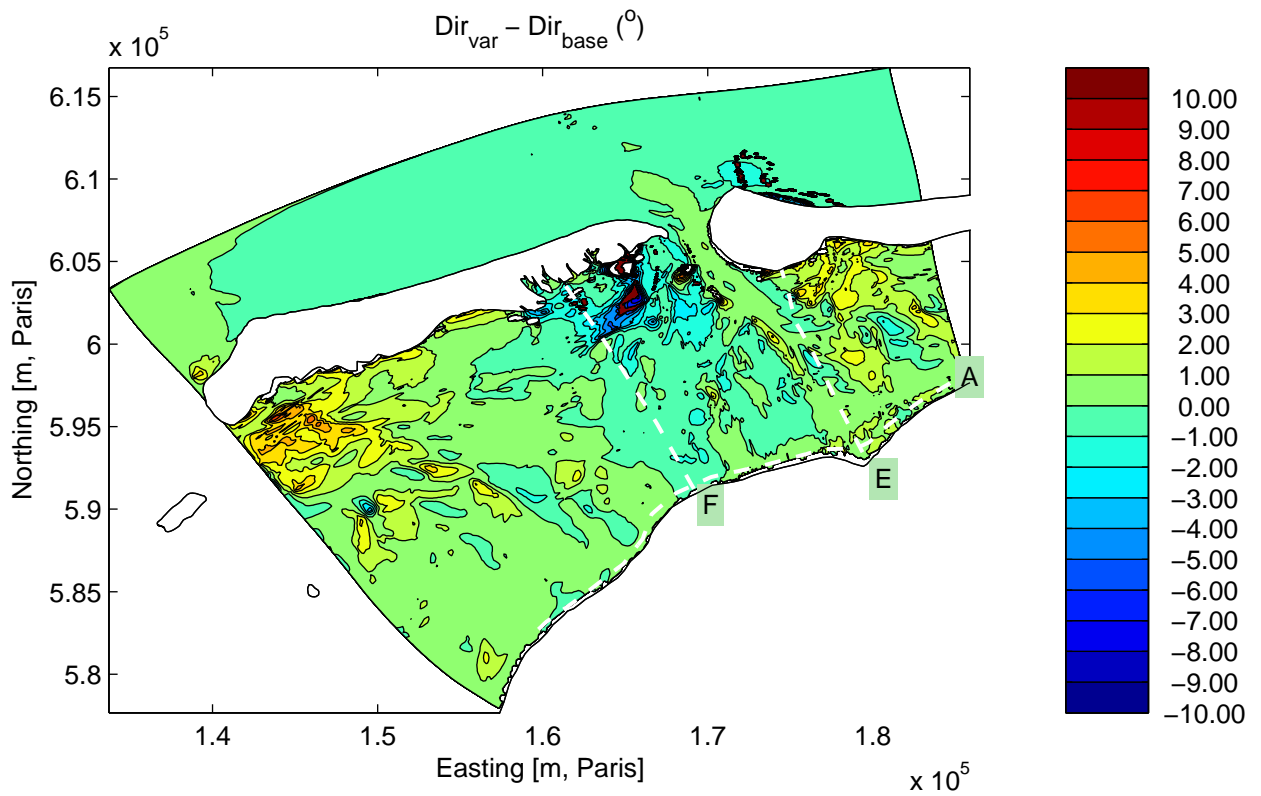
Sensitivity run C5FL1: Increase in water level
Integral parameters along Curve A

Sensitivity analysis Ameland



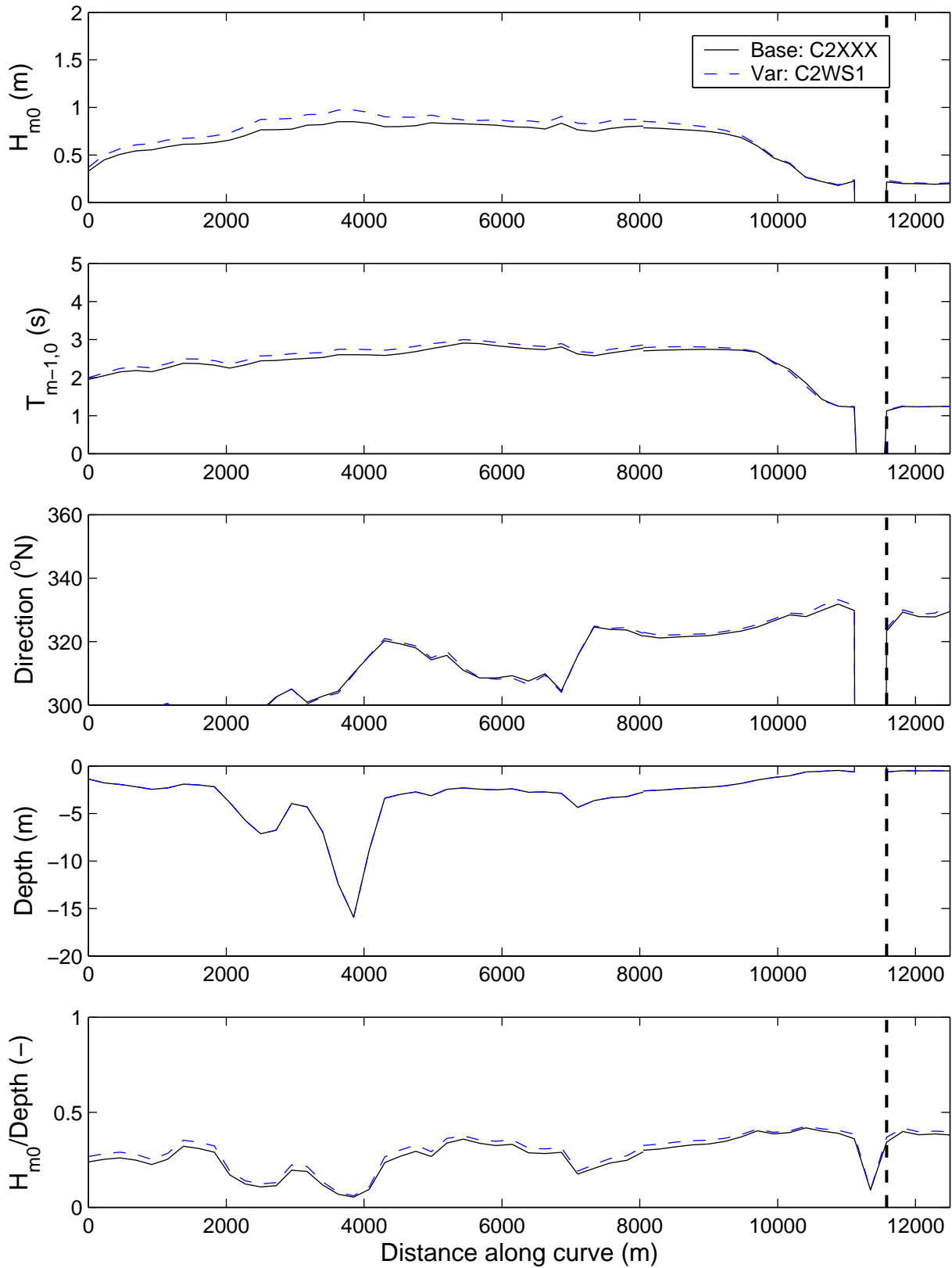
Sensitivity run C2WS1: Variation in spatially uniform wind speed
Differences in significant wave height (above) and mean period (below).

Sensitivity analysis Ameland



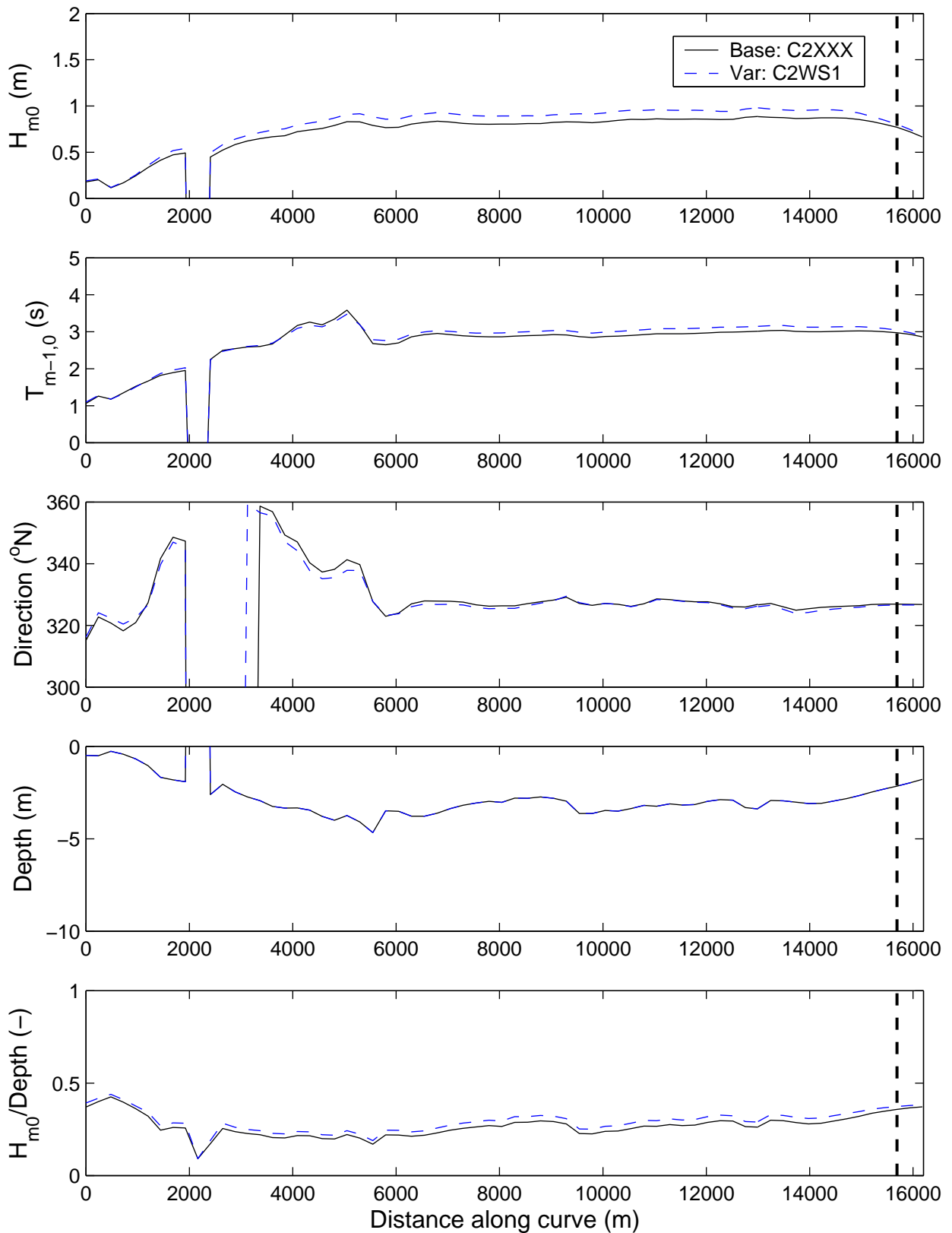
Sensitivity run C2WS1: Variation in spatially uniform wind speed
 Differences in mean direction (above) and directional spreading (below).

Sensitivity analysis Ameland



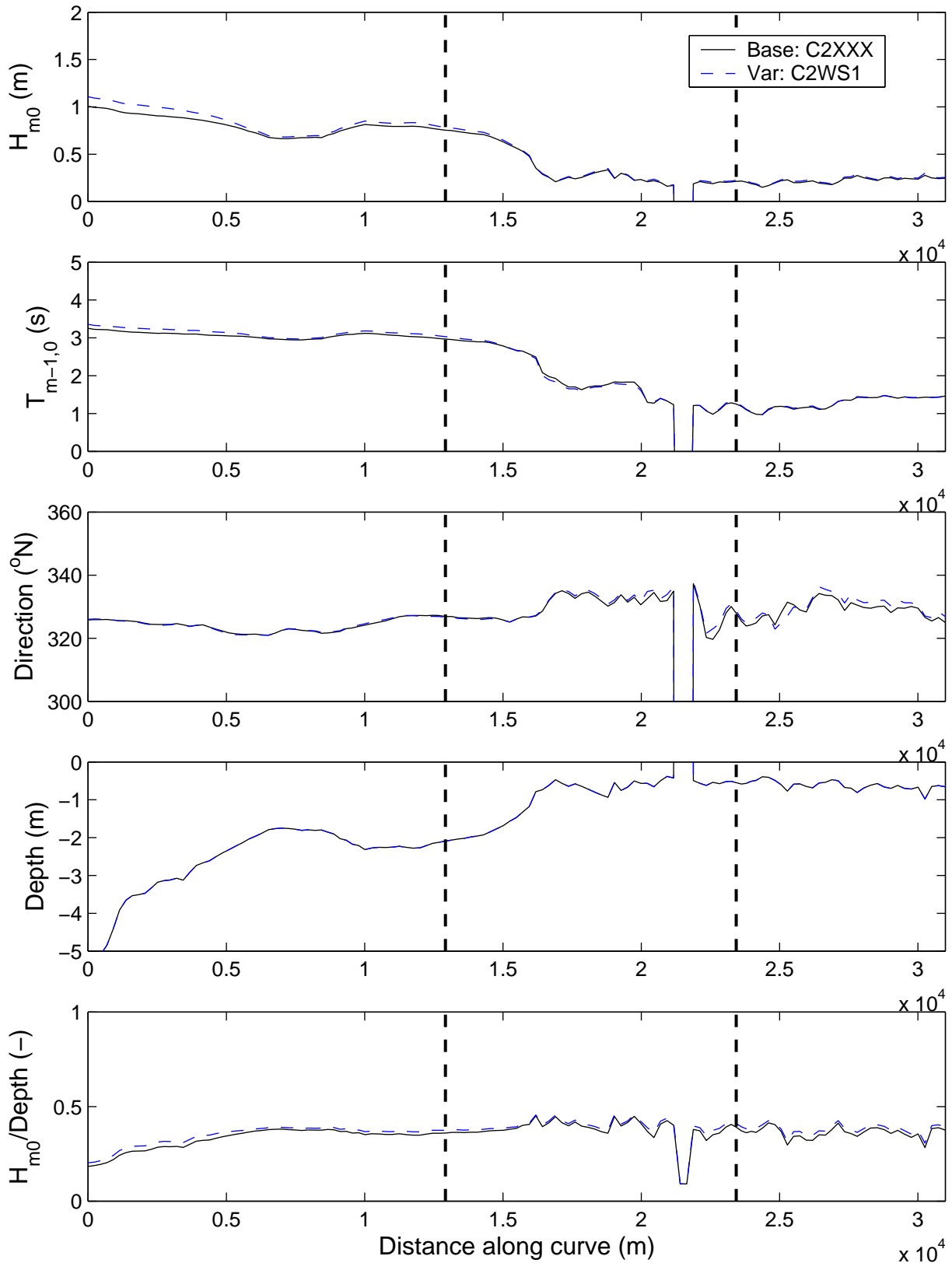
Sensitivity run C2WS1: Variation in spatially uniform wind speed
Integral parameters along Curve E

Sensitivity analysis Ameland



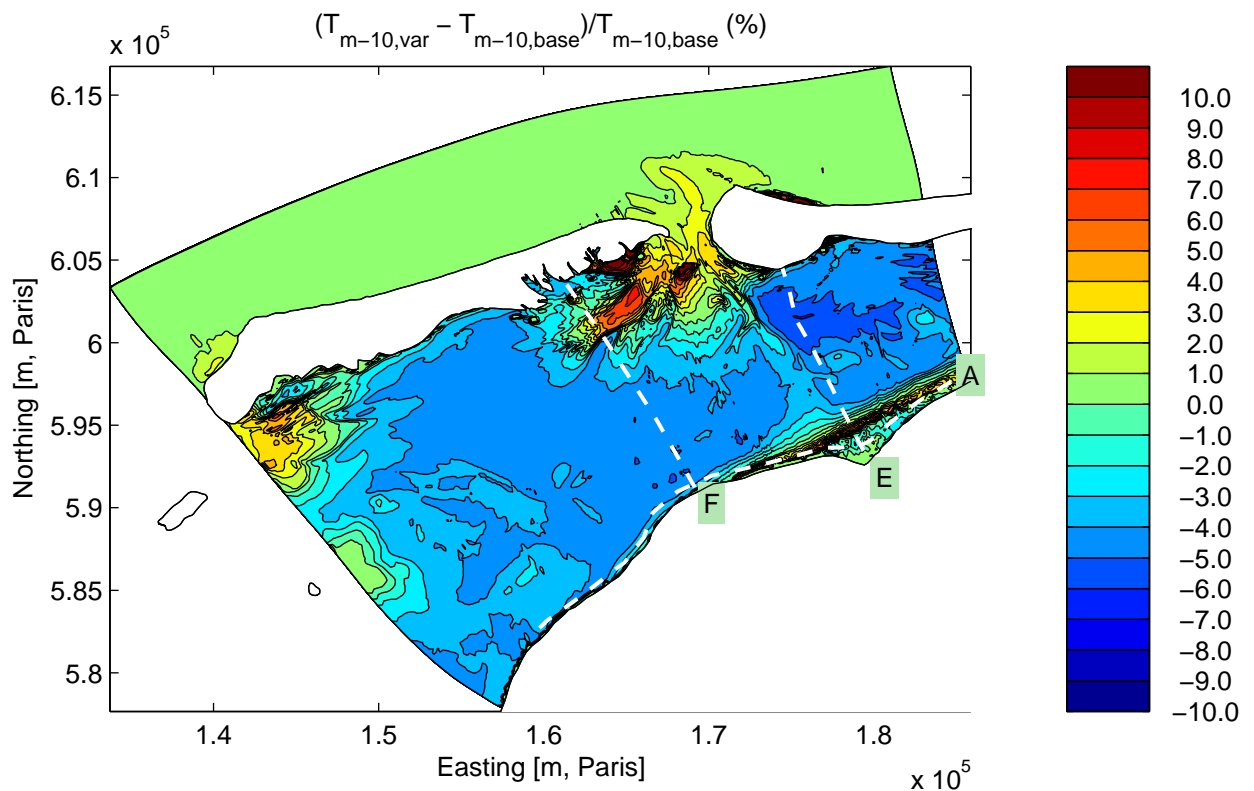
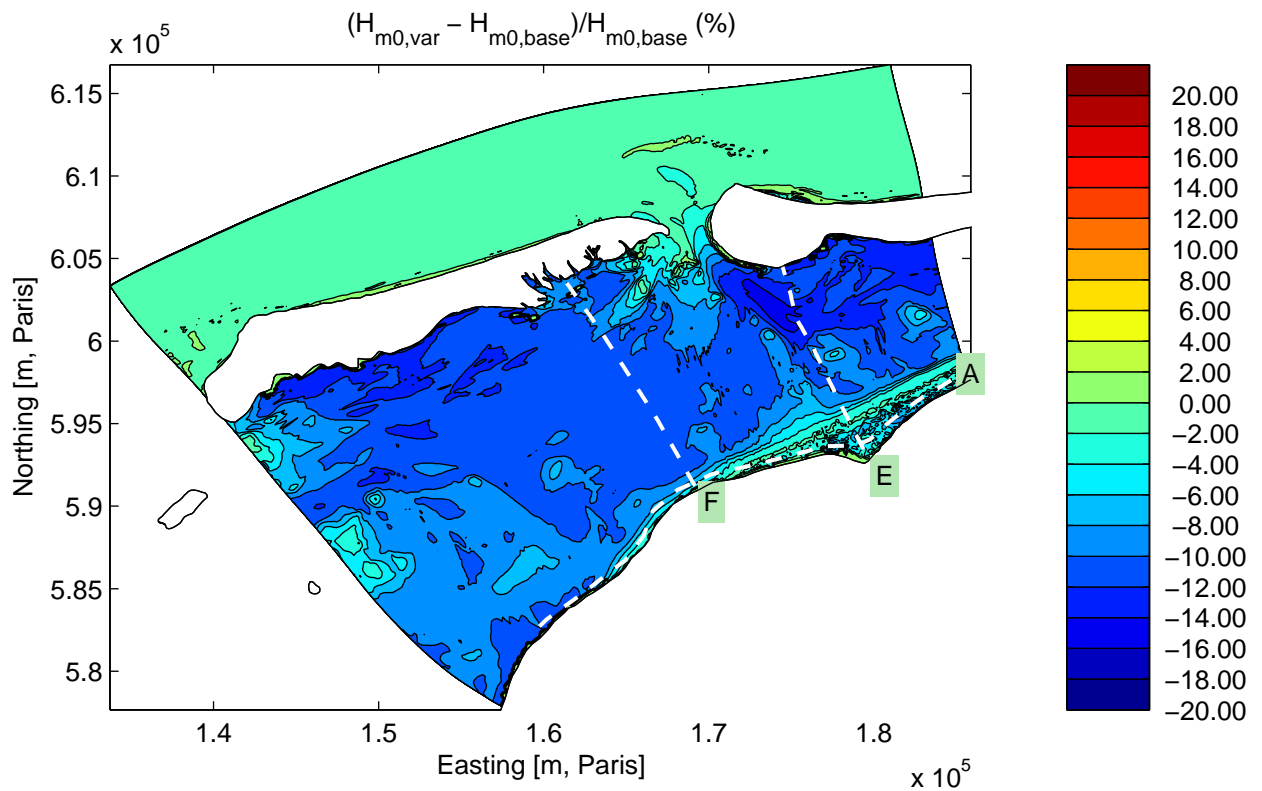
Sensitivity run C2WS1: Variation in spatially uniform wind speed
Integral parameters along Curve F

Sensitivity analysis Ameland



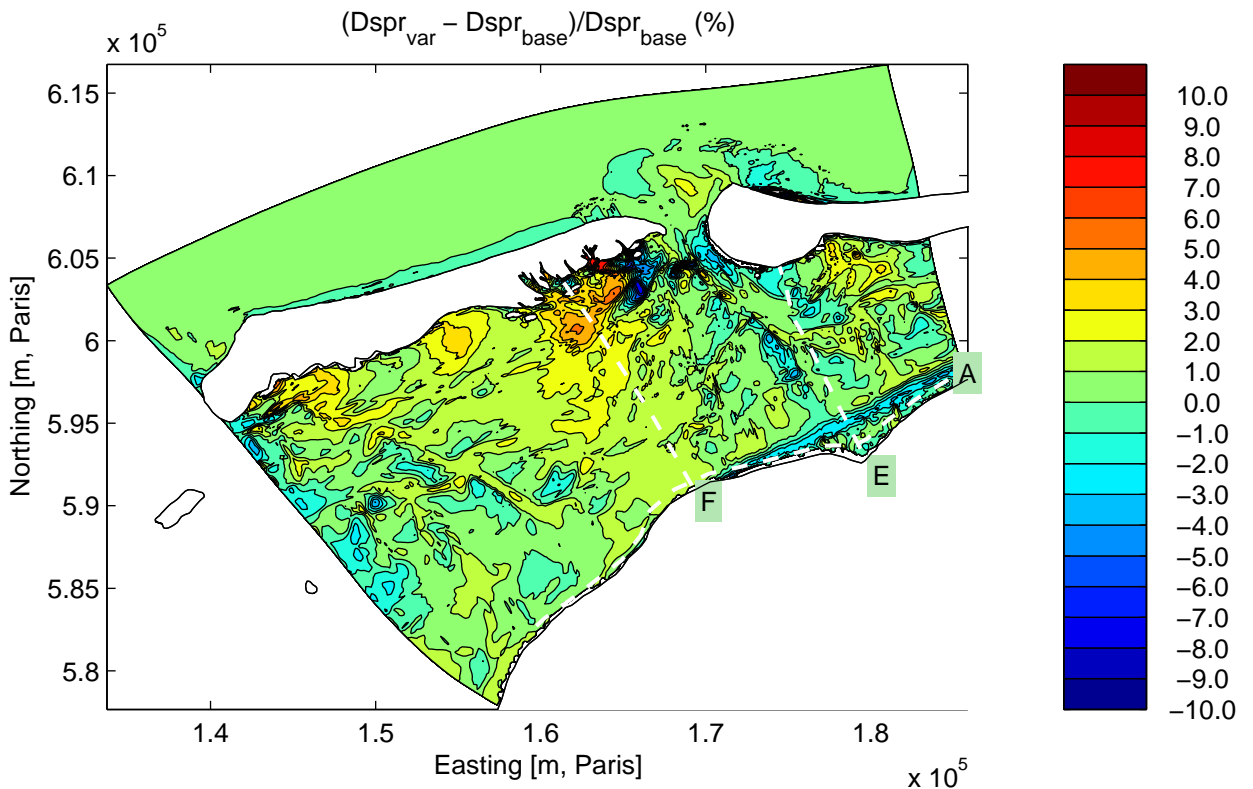
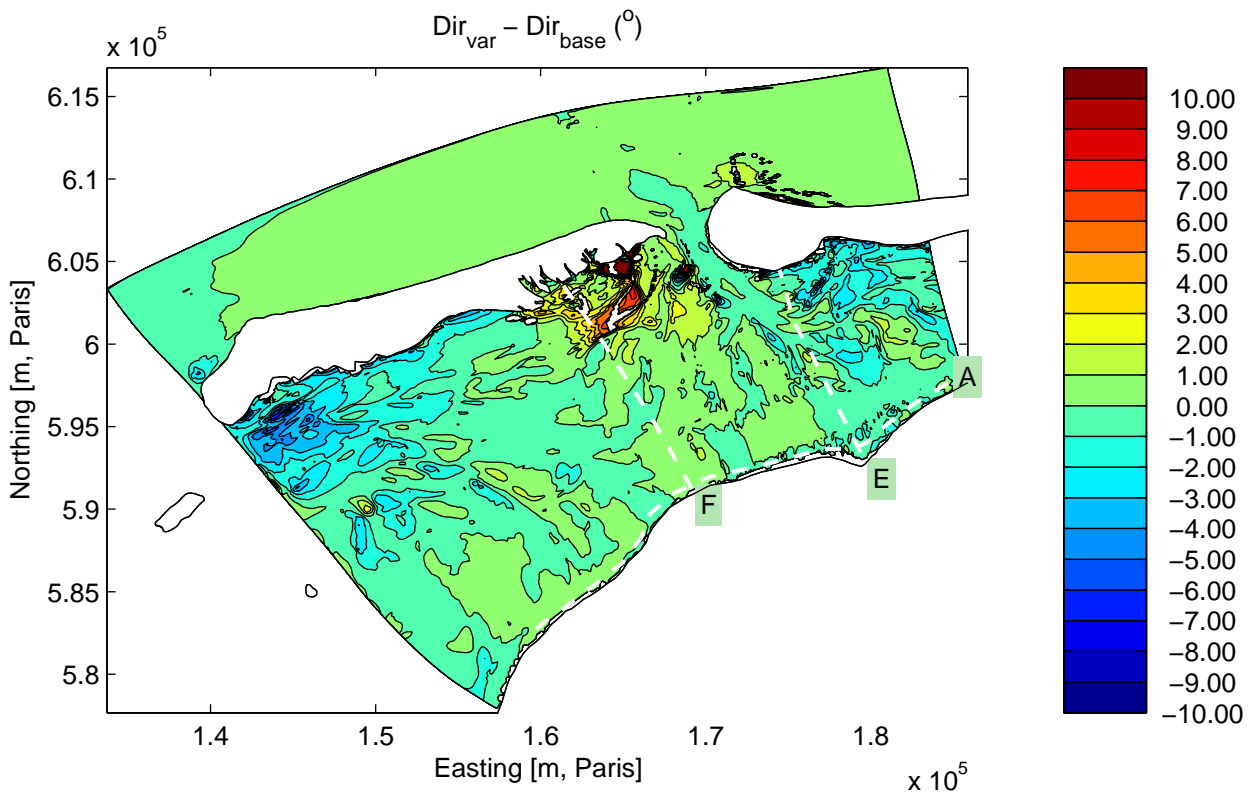
Sensitivity run C2WS1: Variation in spatially uniform wind speed
Integral parameters along Curve A

Sensitivity analysis Ameland



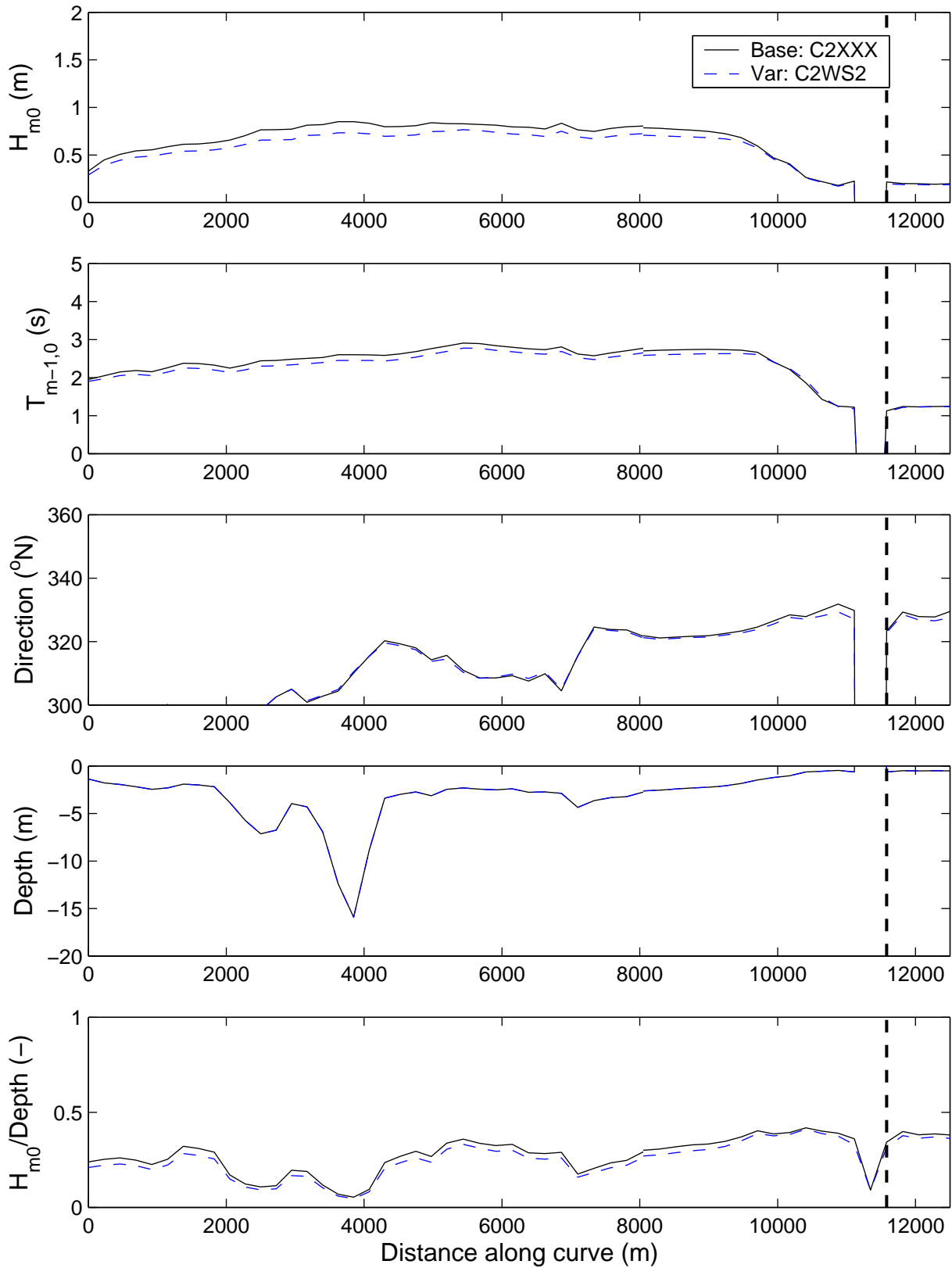
Sensitivity run C2WS2: Variation in spatially uniform wind speed
Differences in significant wave height (above) and mean period (below).

Sensitivity analysis Ameland



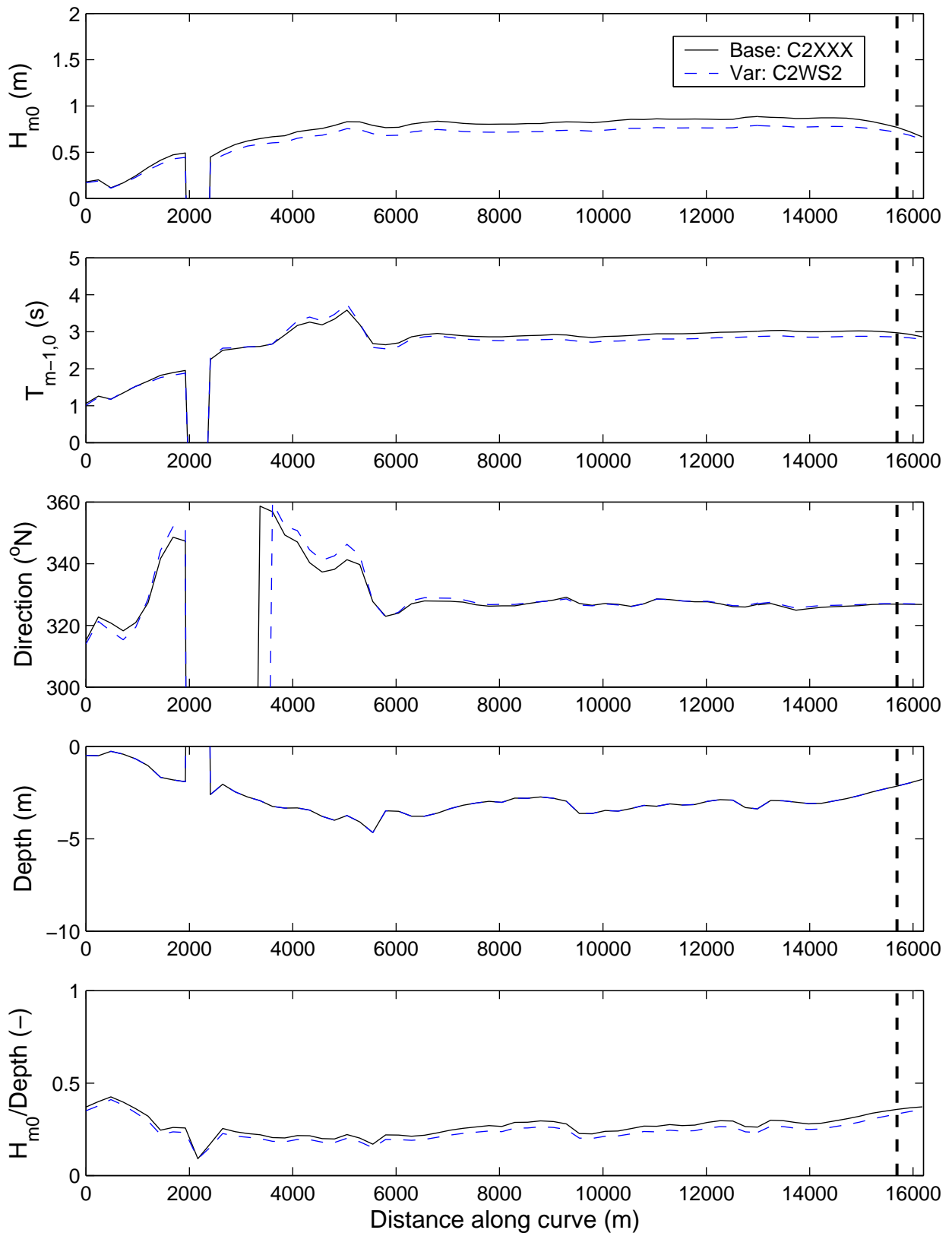
Sensitivity run C2WS2: Variation in spatially uniform wind speed
 Differences in mean direction (above) and directional spreading (below).

Sensitivity analysis Ameland



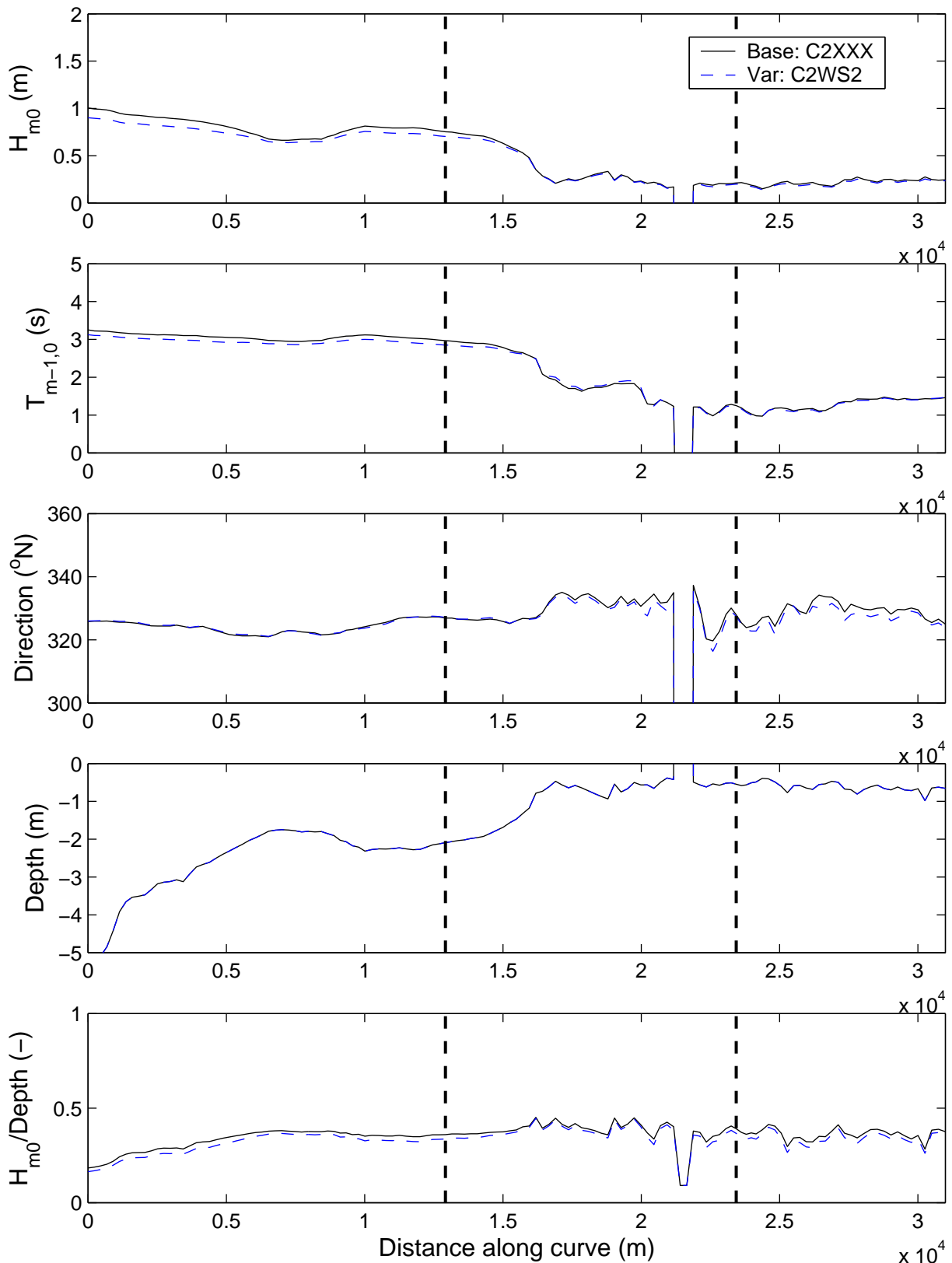
Sensitivity run C2WS2: Variation in spatially uniform wind speed
Integral parameters along Curve E

Sensitivity analysis Ameland



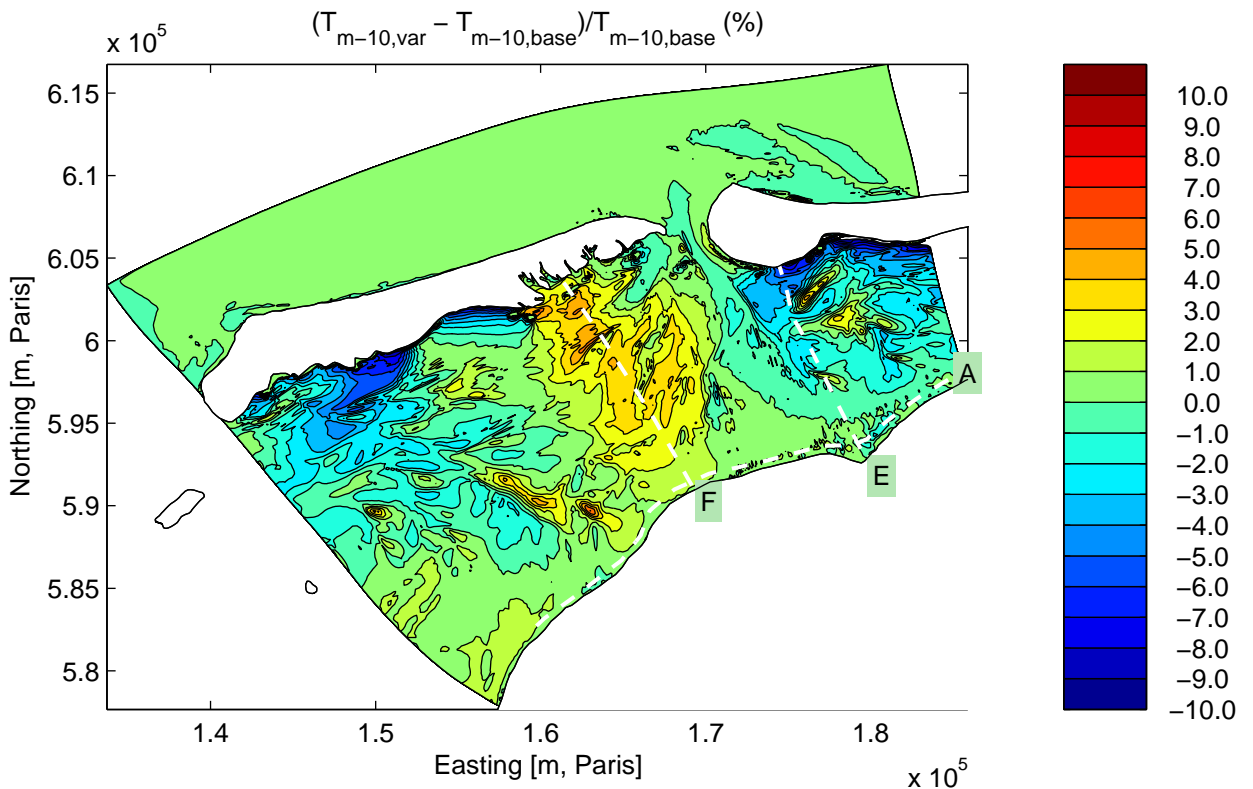
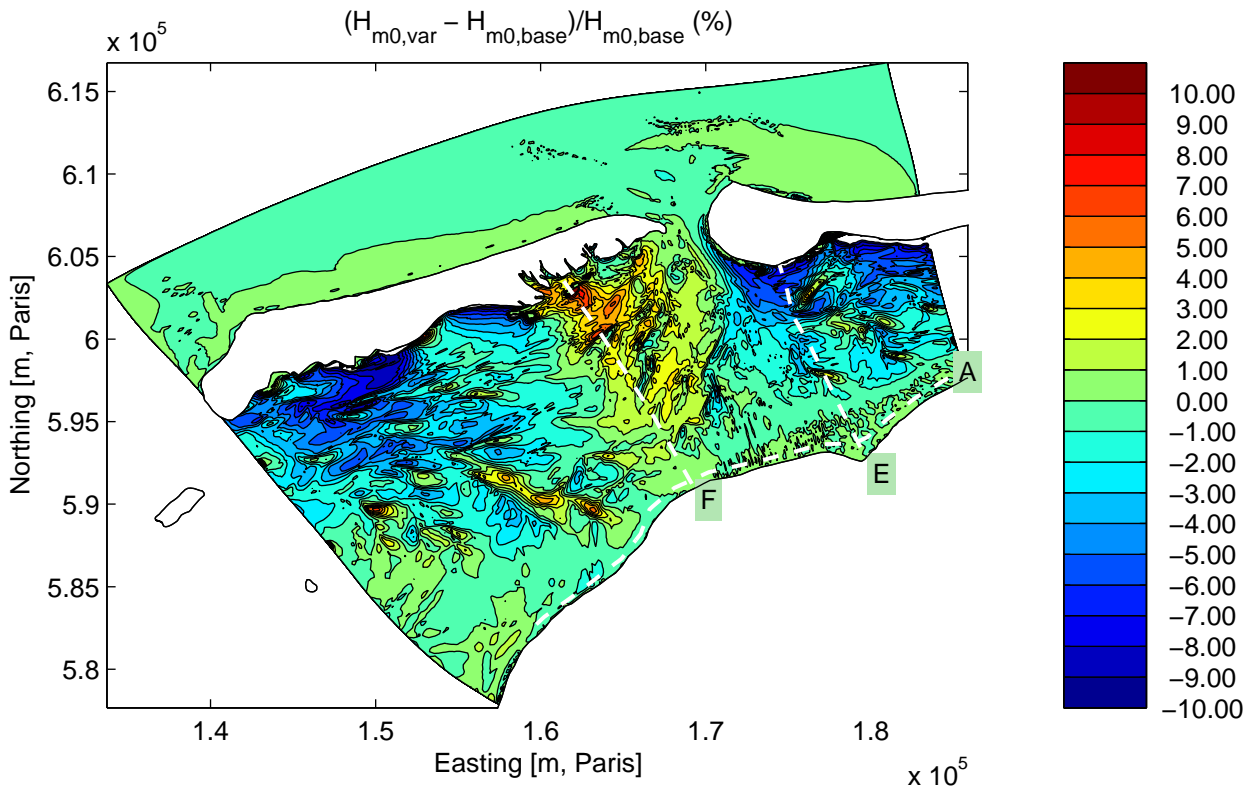
Sensitivity run C2WS2: Variation in spatially uniform wind speed
Integral parameters along Curve F

Sensitivity analysis Ameland



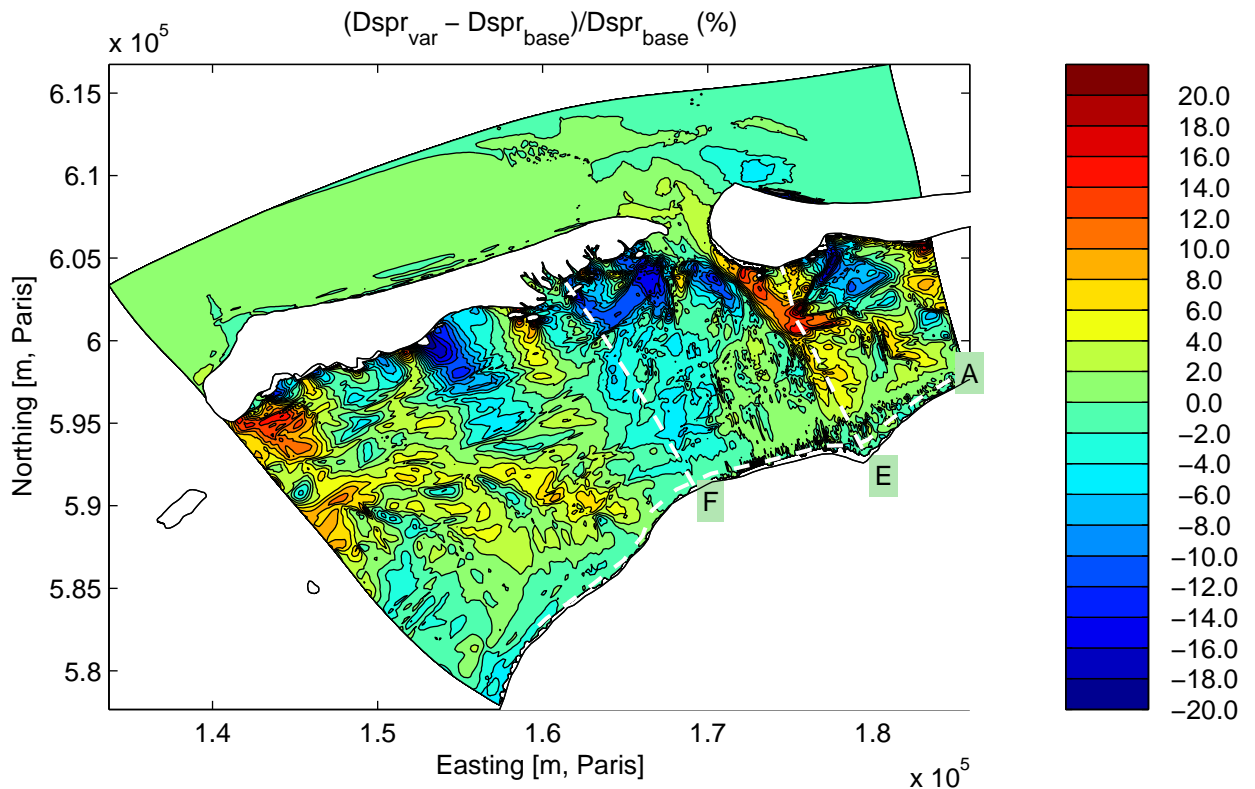
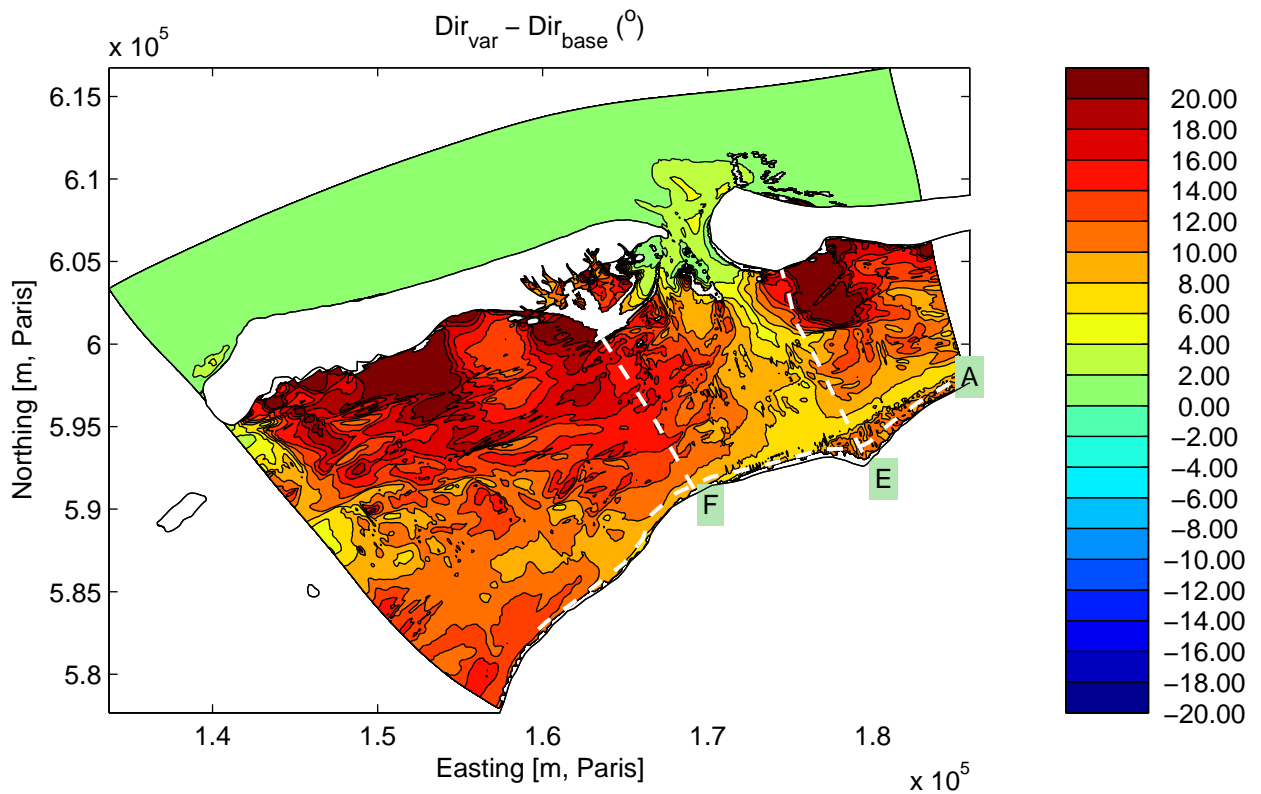
Sensitivity run C2WS2: Variation in spatially uniform wind speed
Integral parameters along Curve A

Sensitivity analysis Ameland



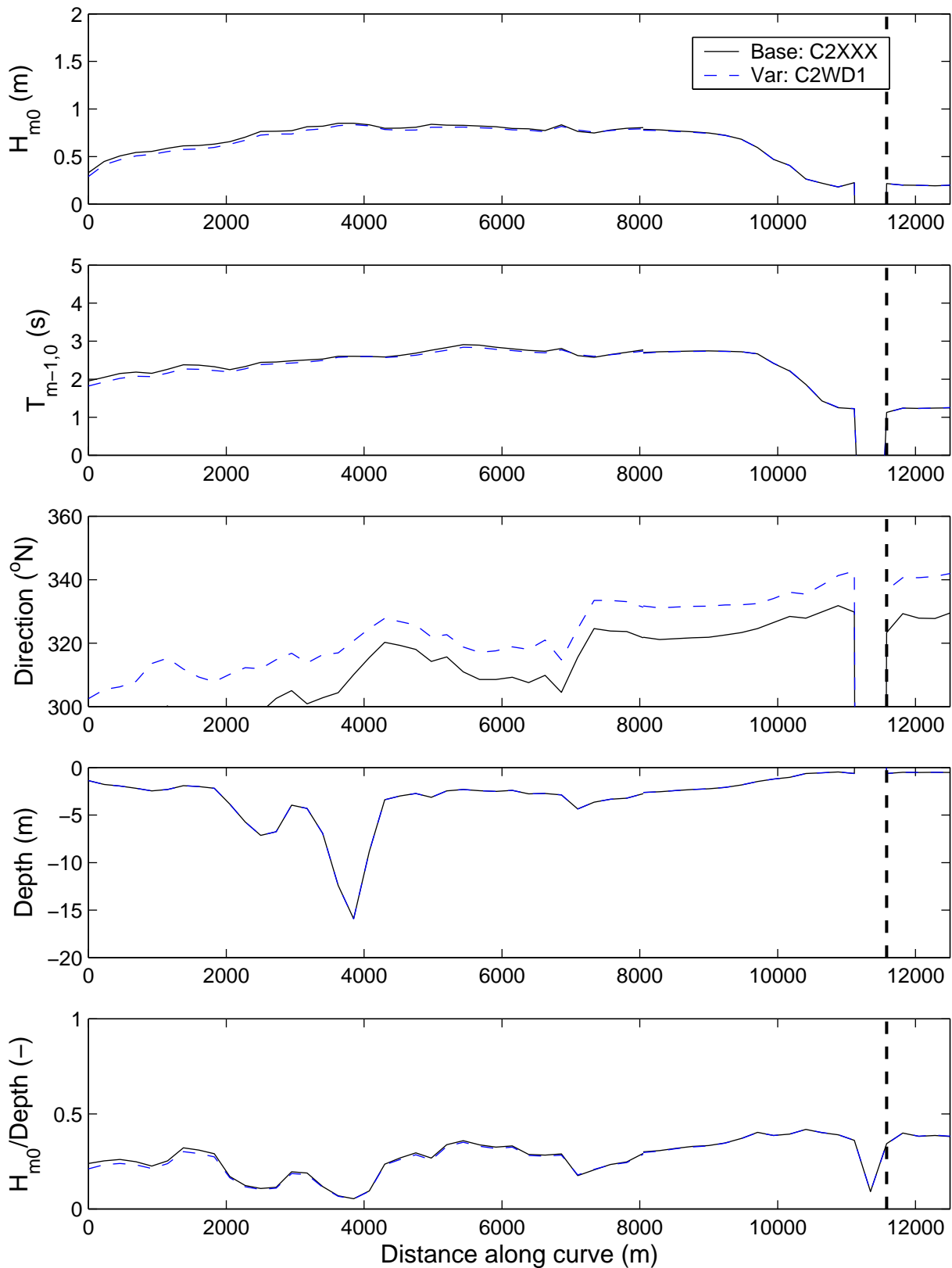
Sensitivity run C2WD1: Variation in spatially uniform wind direction
Differences in significant wave height (above) and mean period (below).

Sensitivity analysis Ameland



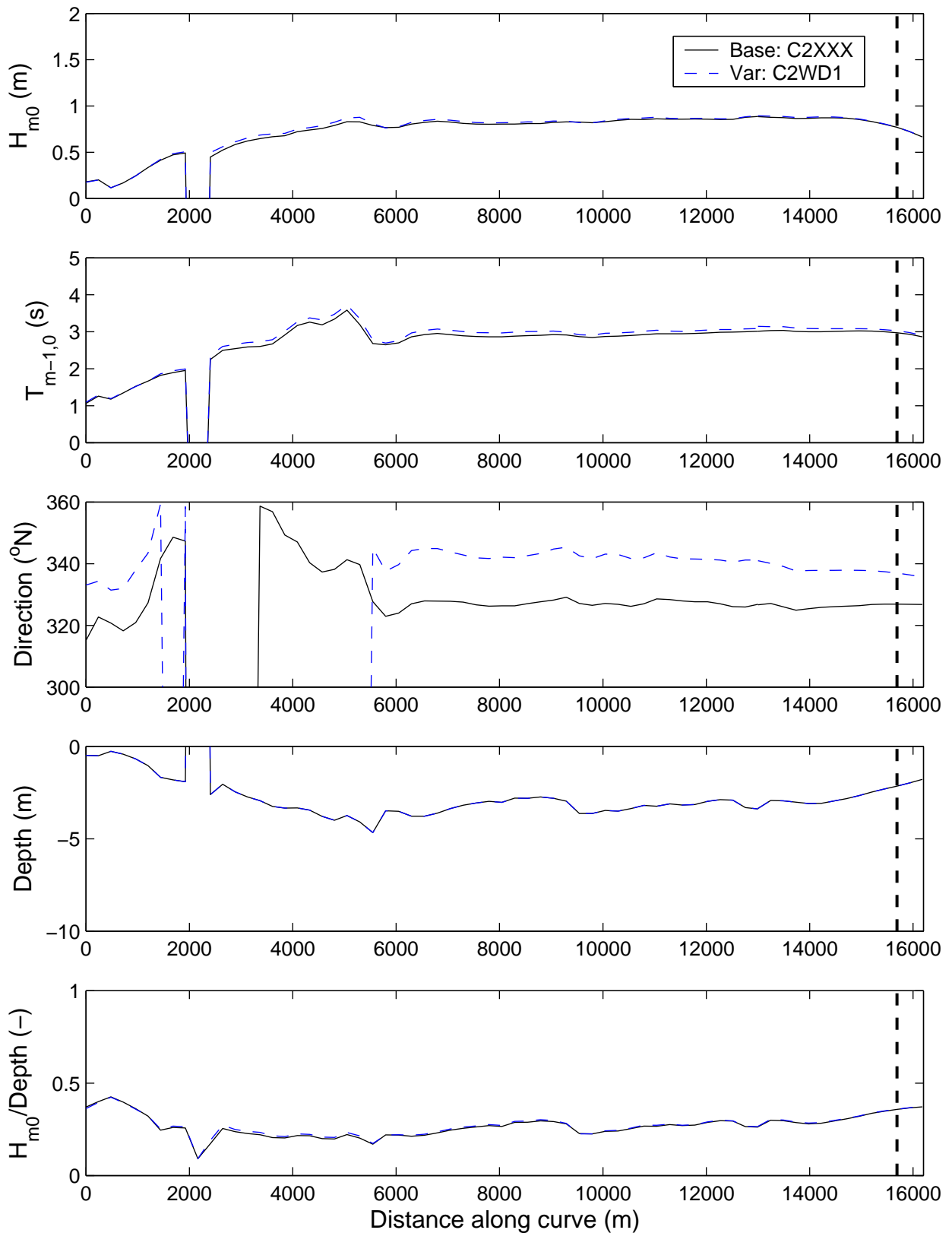
Sensitivity run C2WD1: Variation in spatially uniform wind direction
 Differences in mean direction (above) and directional spreading (below).

Sensitivity analysis Ameland



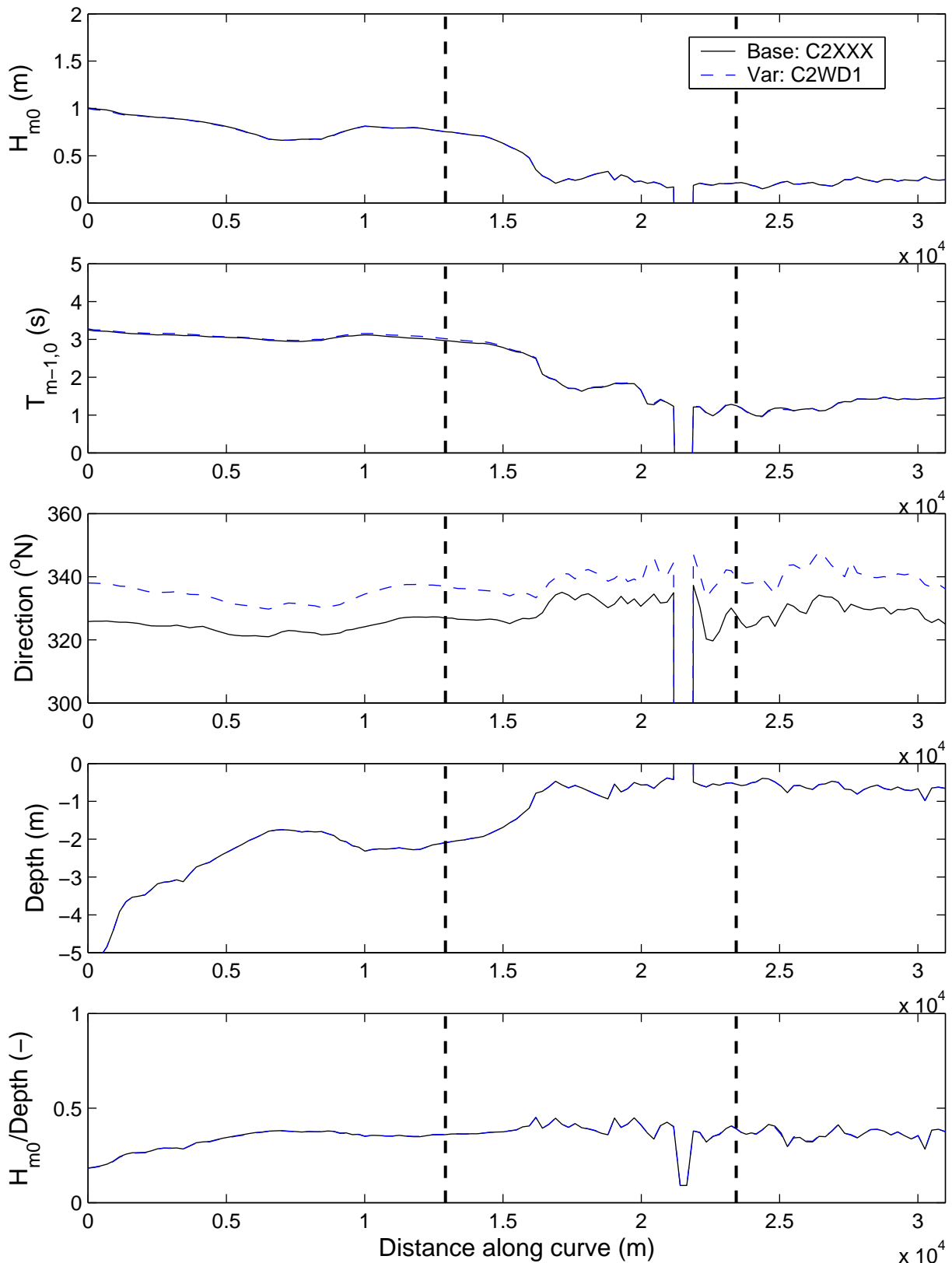
Sensitivity run C2WD1: Variation in spatially uniform wind direction
Integral parameters along Curve E

Sensitivity analysis Ameland



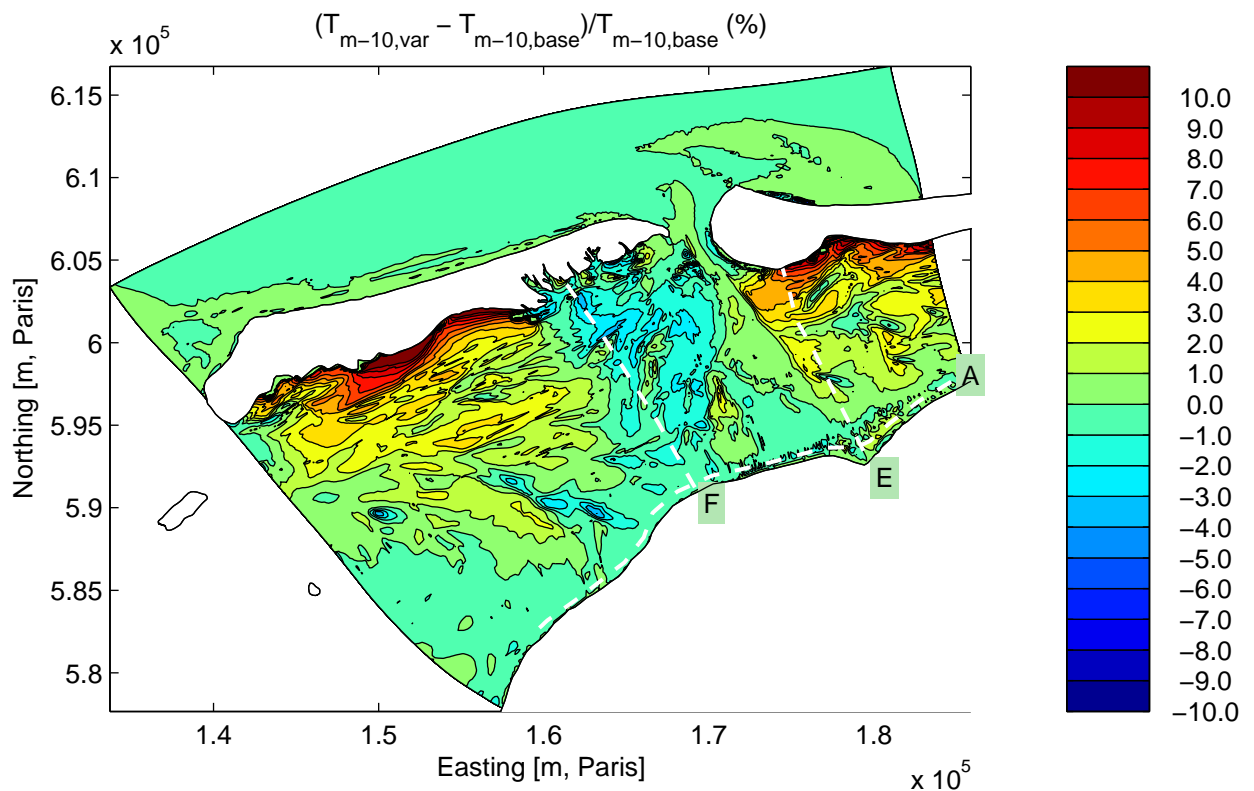
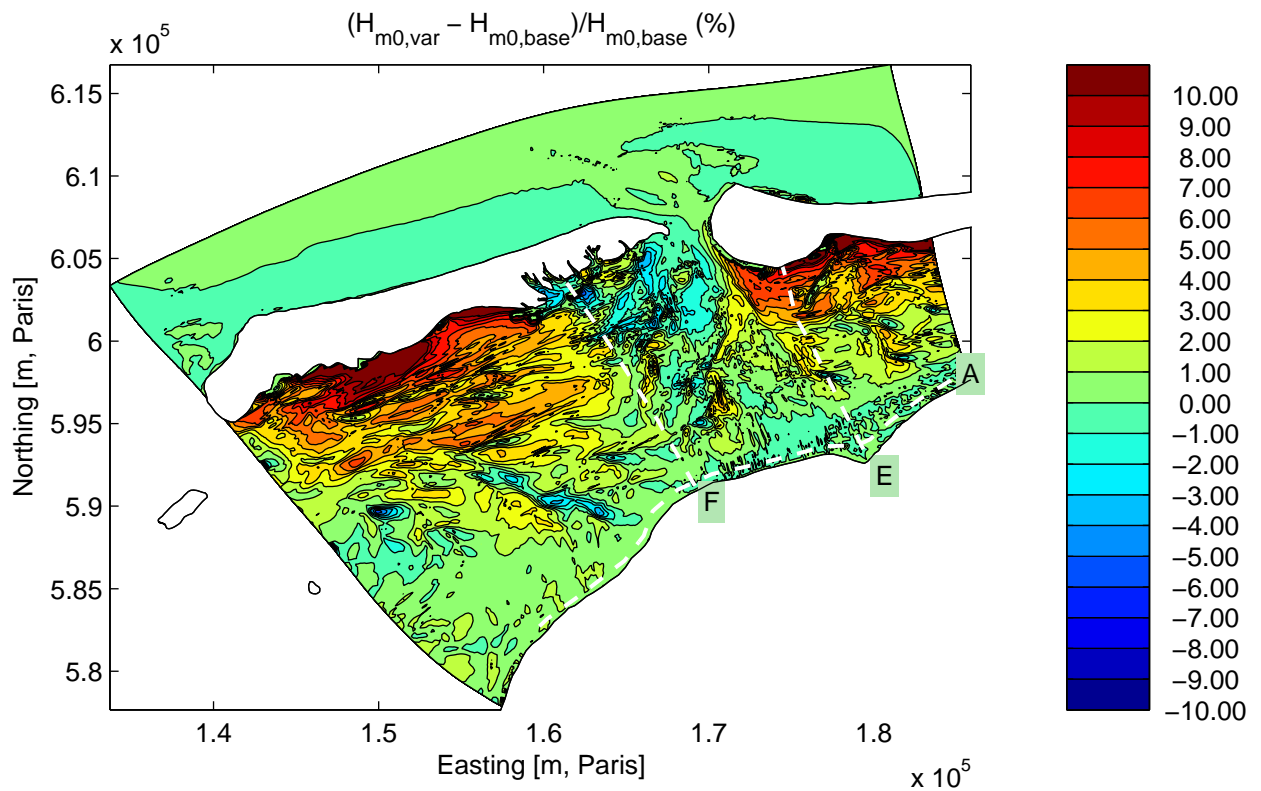
Sensitivity run C2WD1: Variation in spatially uniform wind direction
Integral parameters along Curve F

Sensitivity analysis Ameland



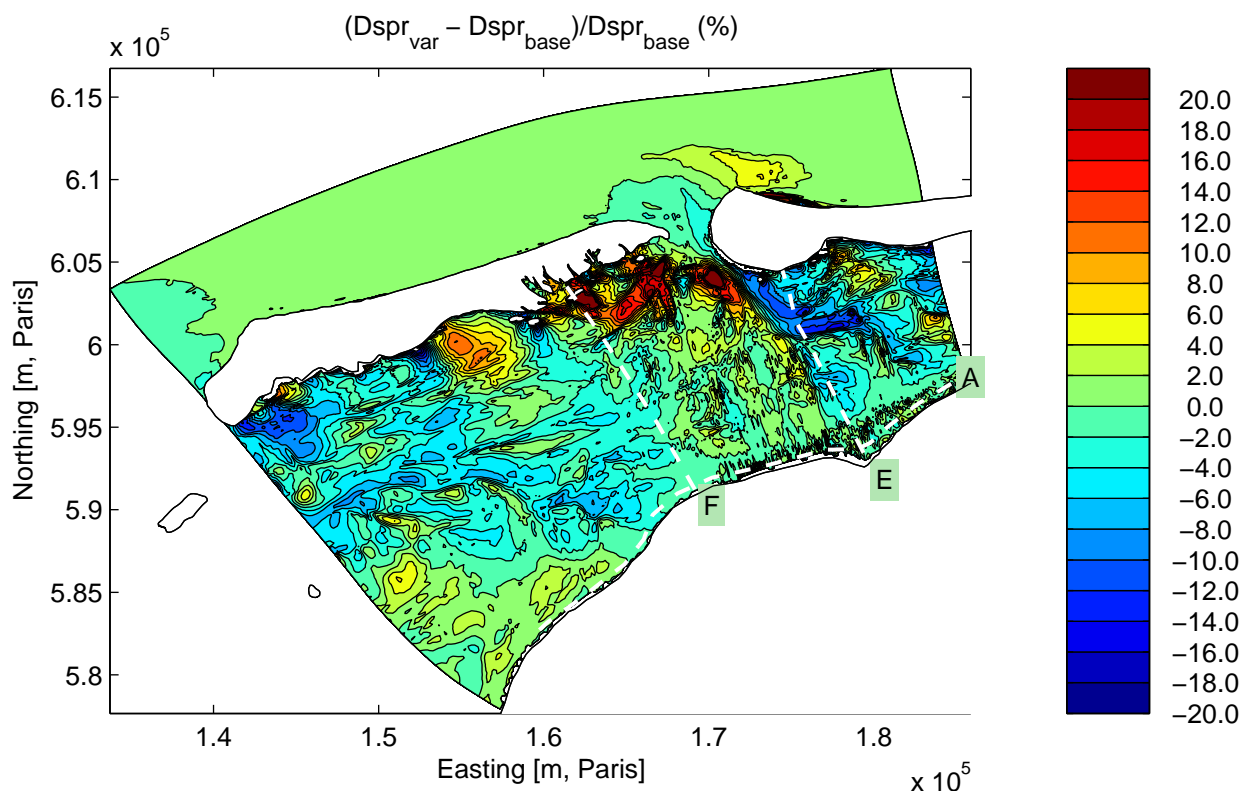
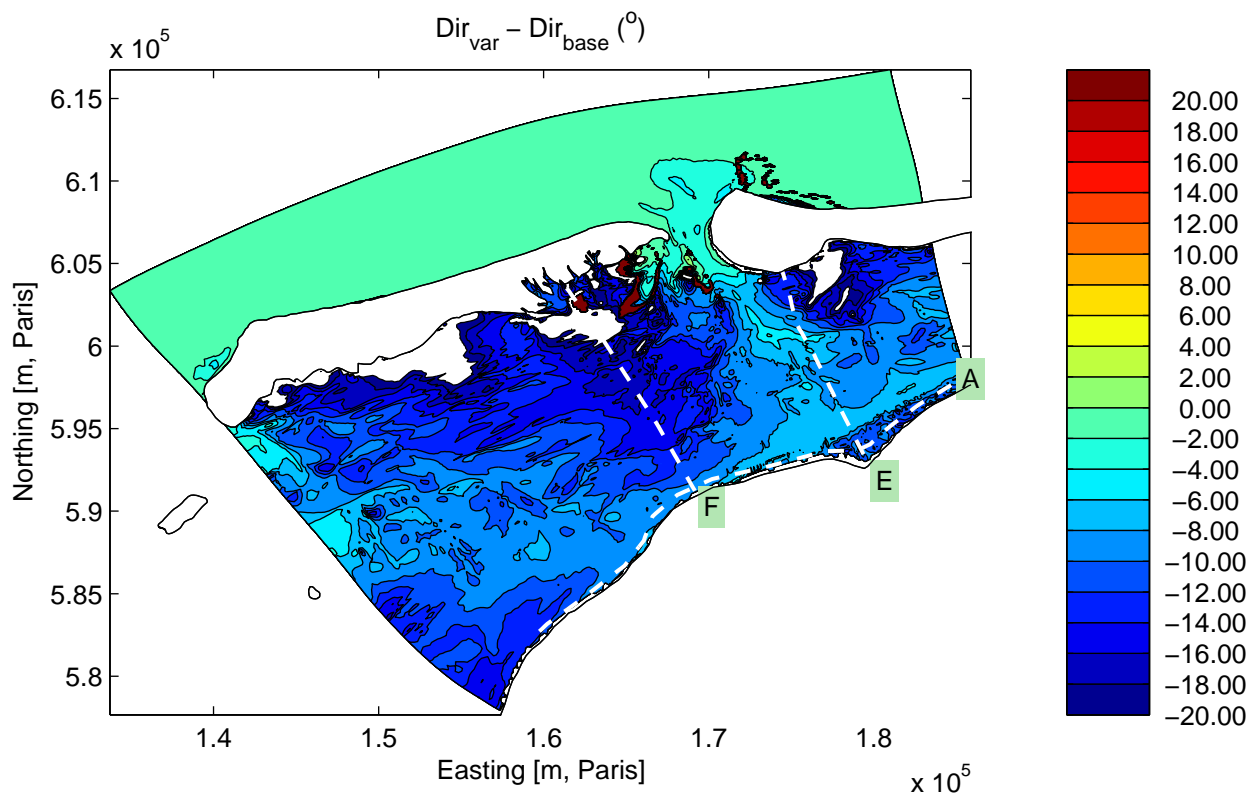
Sensitivity run C2WD1: Variation in spatially uniform wind direction
Integral parameters along Curve A

Sensitivity analysis Ameland



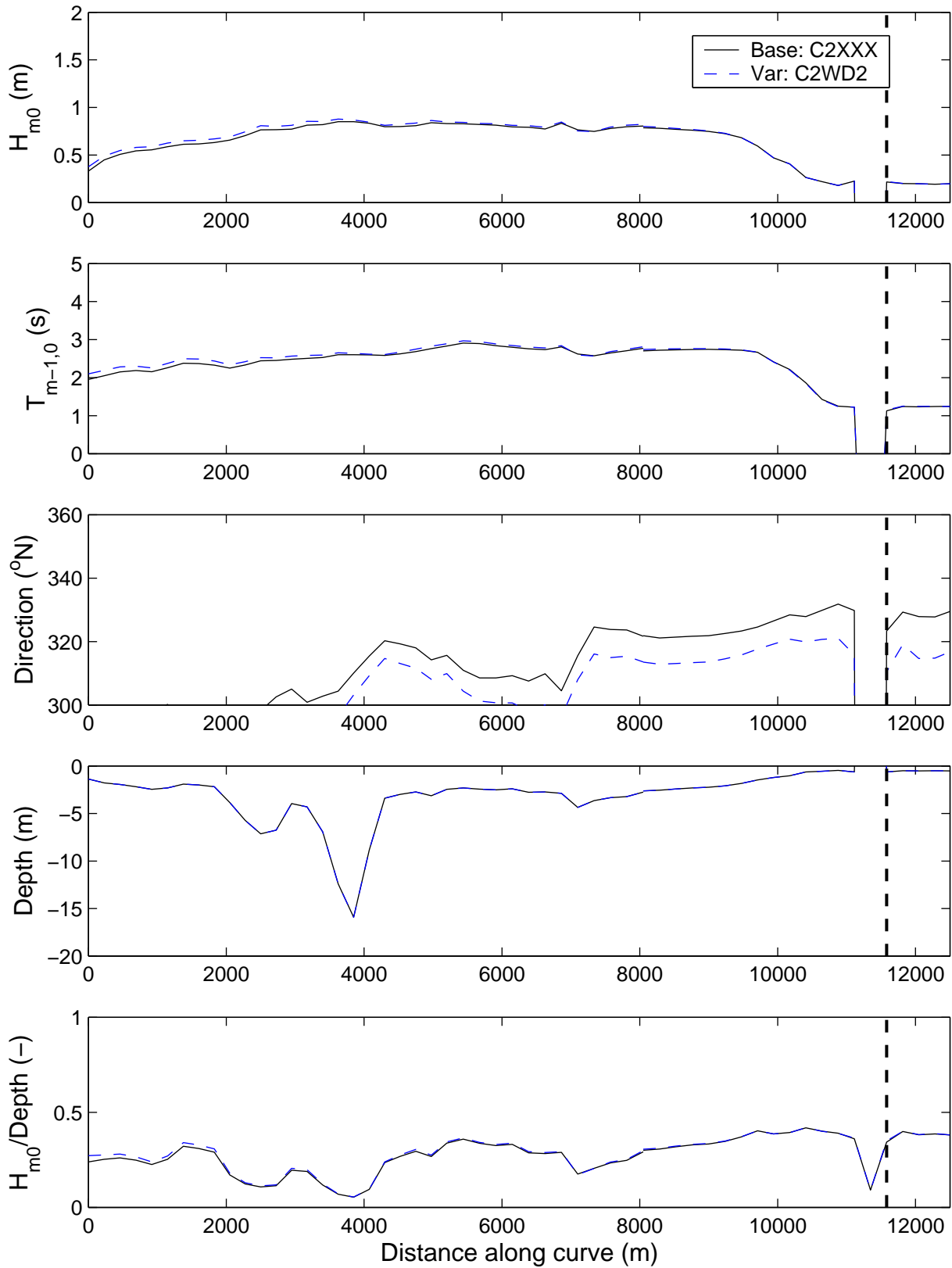
Sensitivity run C2WD2: Variation in spatially uniform wind direction
Differences in significant wave height (above) and mean period (below).

Sensitivity analysis Ameland



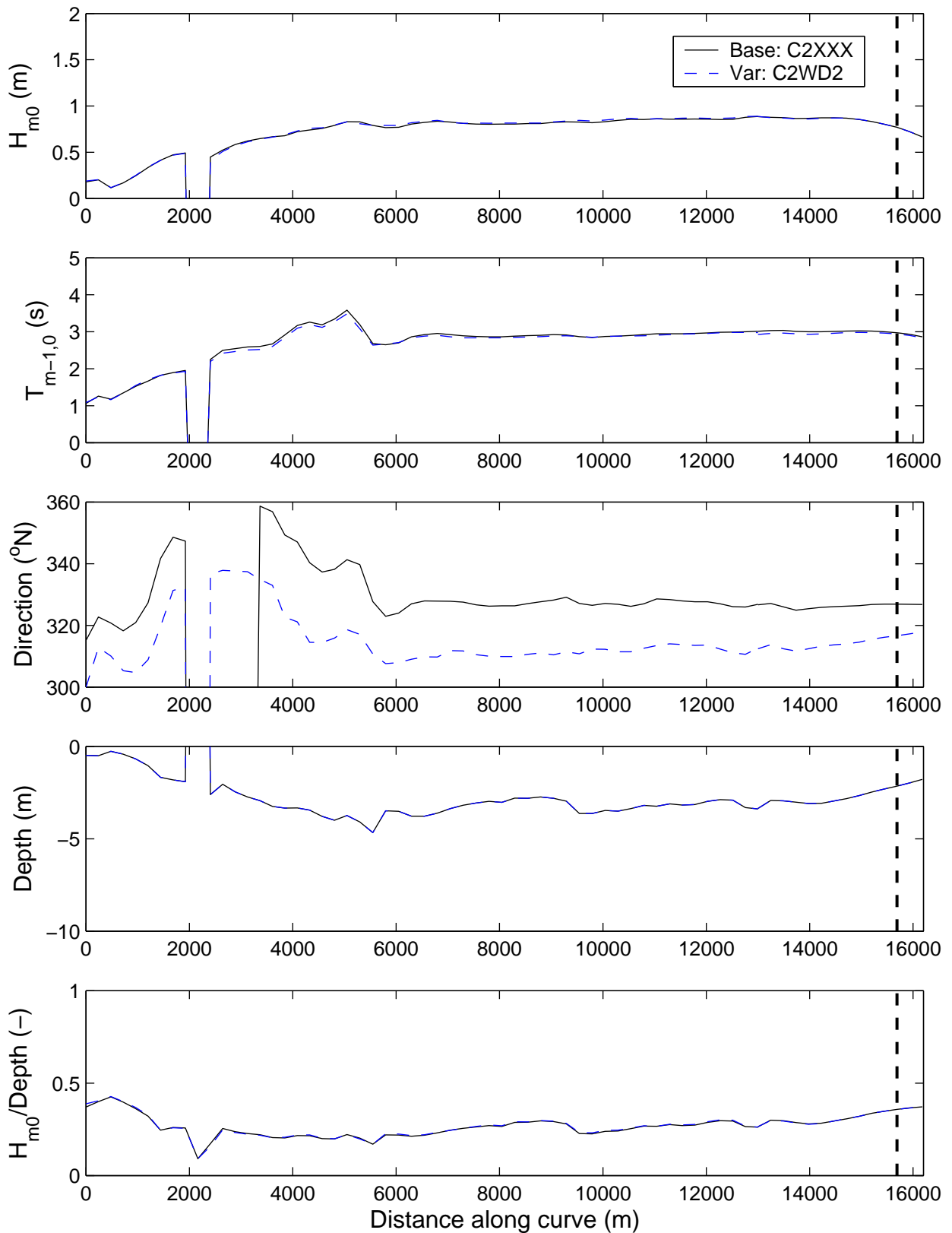
Sensitivity run C2WD2: Variation in spatially uniform wind direction
Differences in mean direction (above) and directional spreading (below).

Sensitivity analysis Ameland



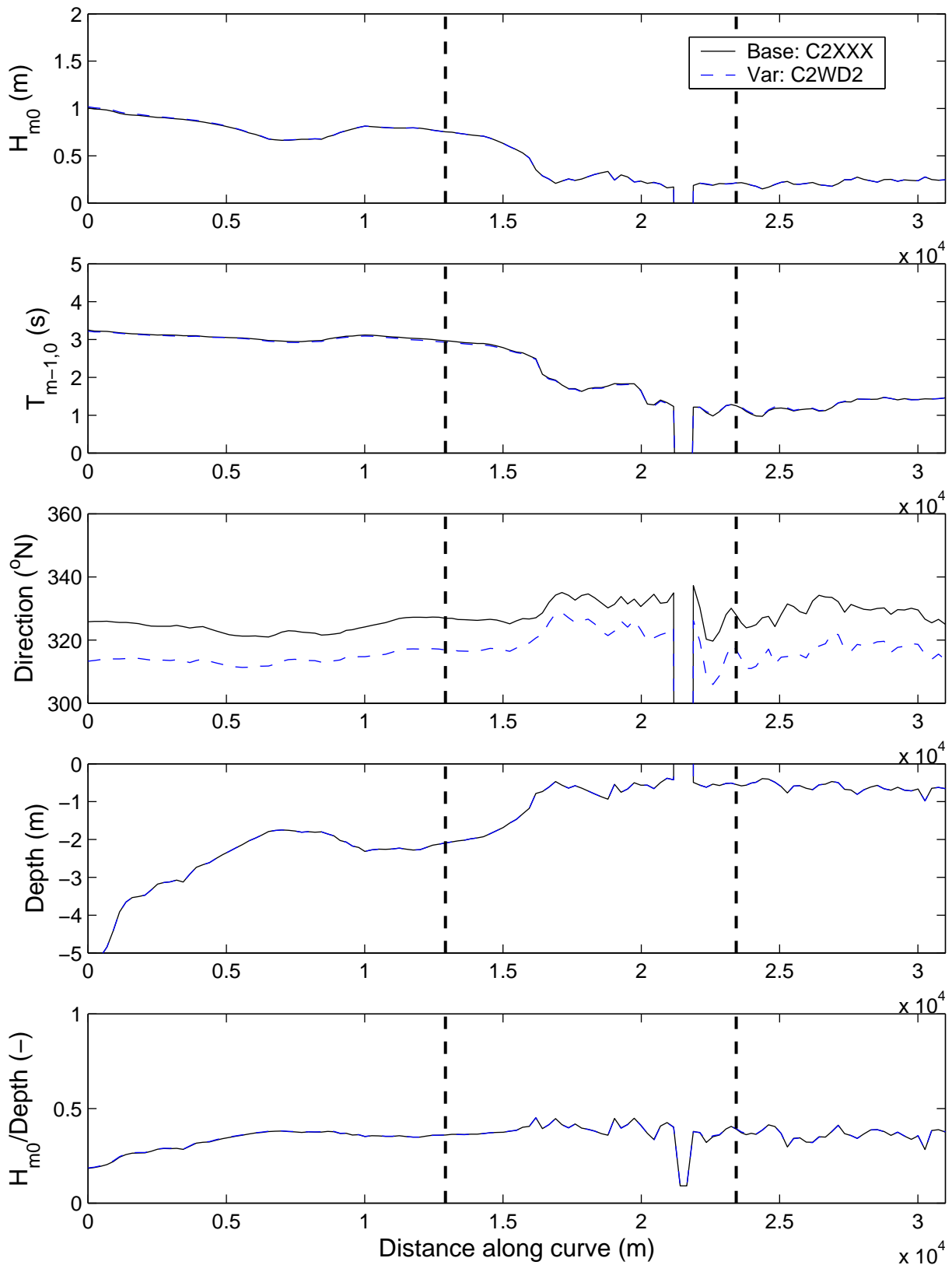
Sensitivity run C2WD2: Variation in spatially uniform wind direction
Integral parameters along Curve E

Sensitivity analysis Ameland



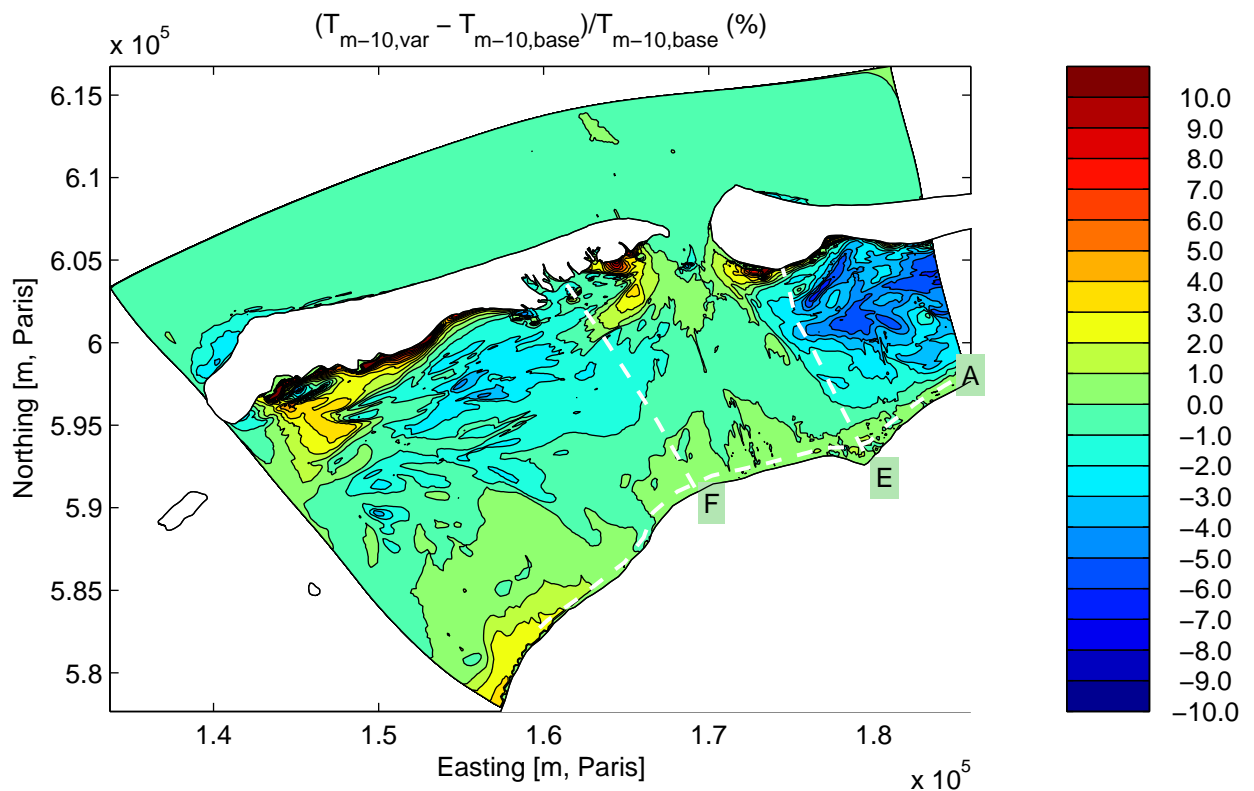
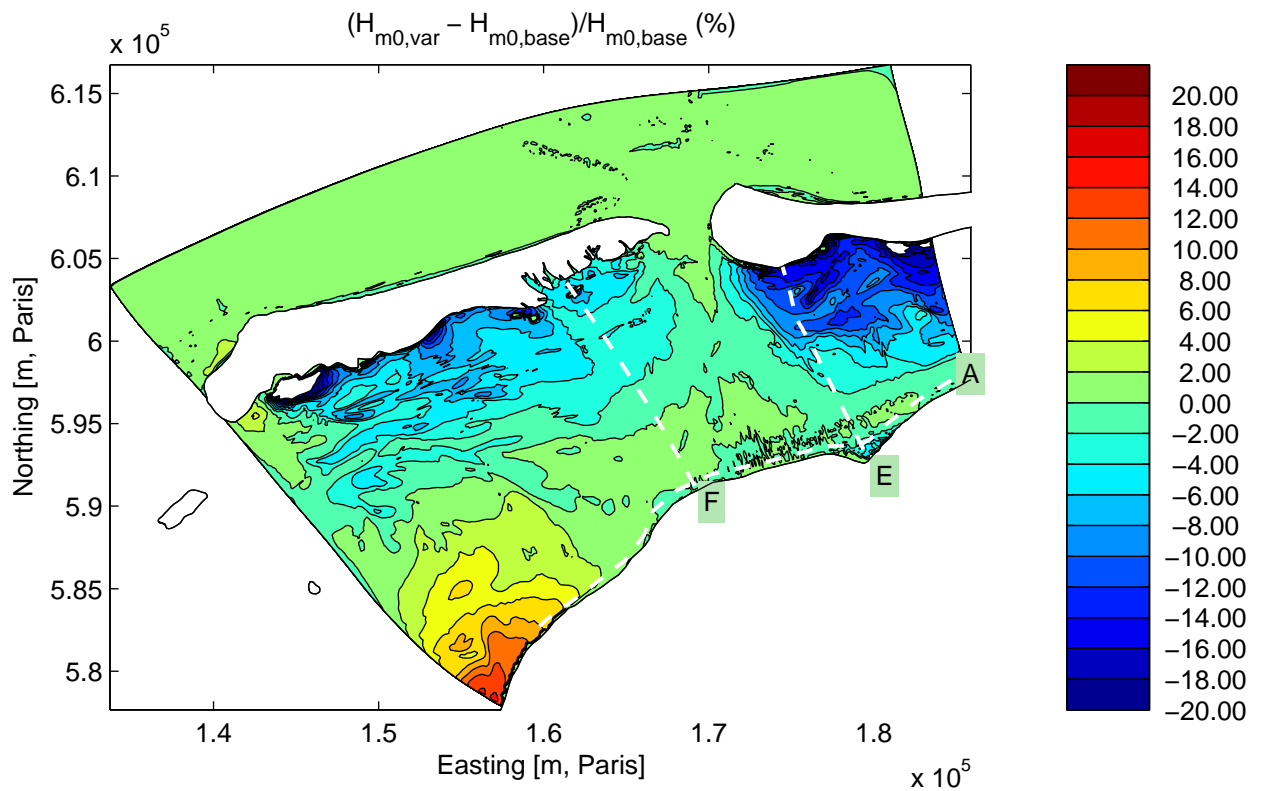
Sensitivity run C2WD2: Variation in spatially uniform wind direction
Integral parameters along Curve F

Sensitivity analysis Ameland



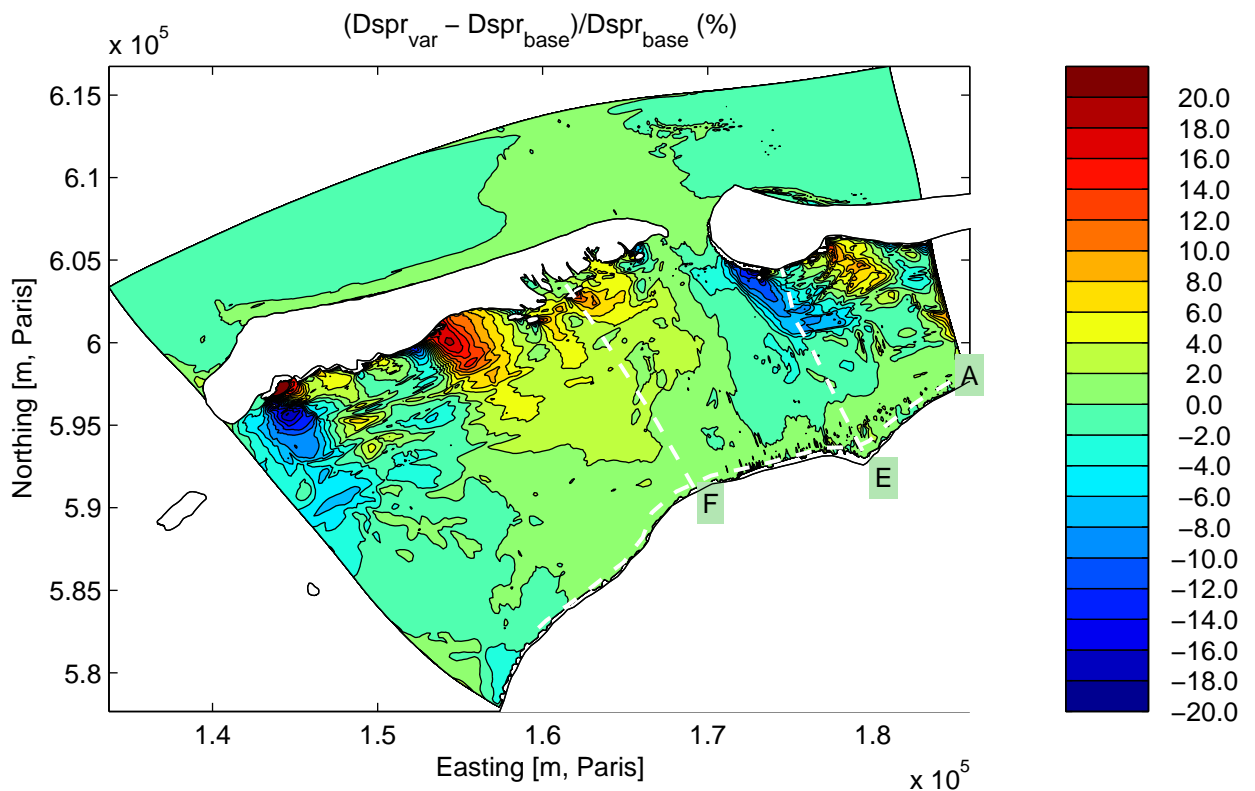
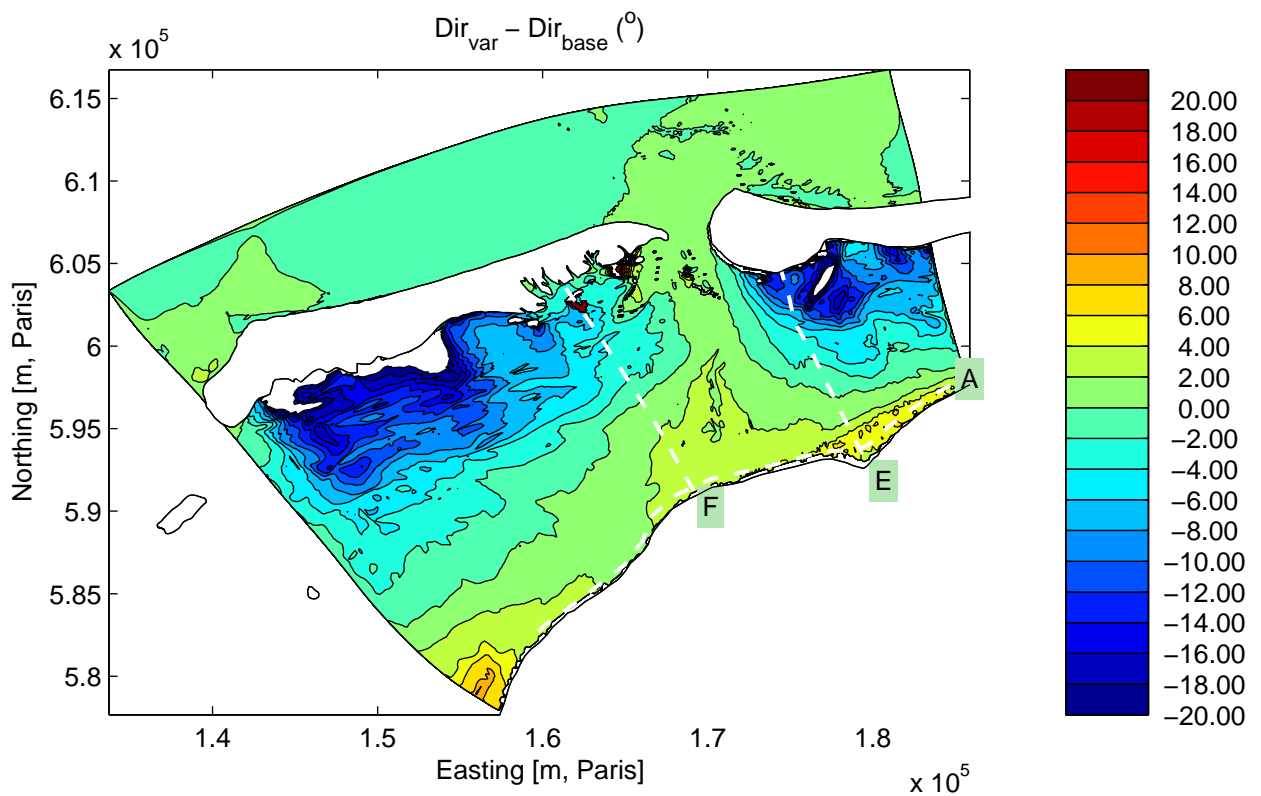
Sensitivity run C2WD2: Variation in spatially uniform wind direction
Integral parameters along Curve A

Sensitivity analysis Ameland



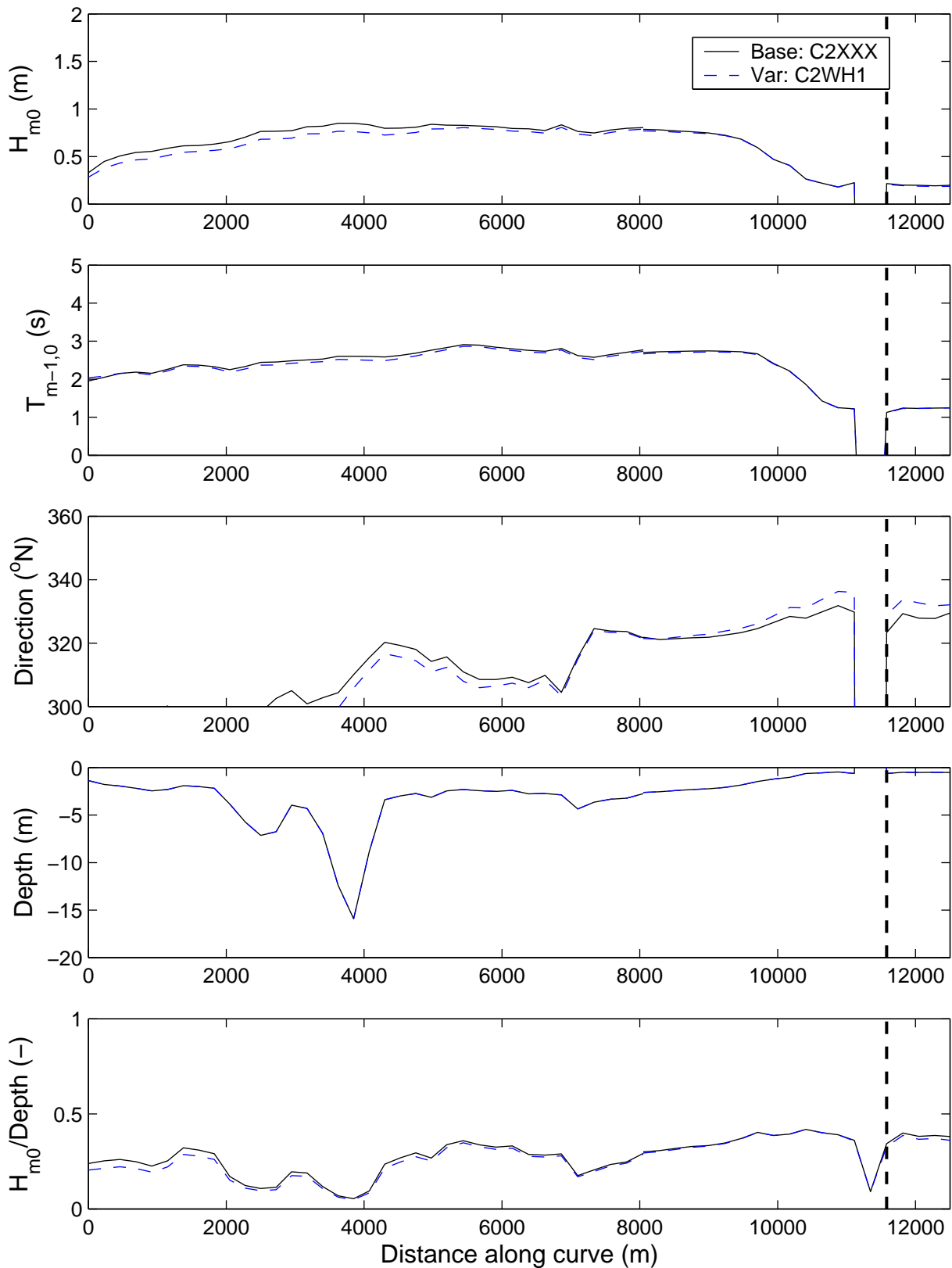
Sensitivity run C2WH1: Simulation with downscaled HIRLAM wind field
Differences in significant wave height (above) and mean period (below).

Sensitivity analysis Ameland



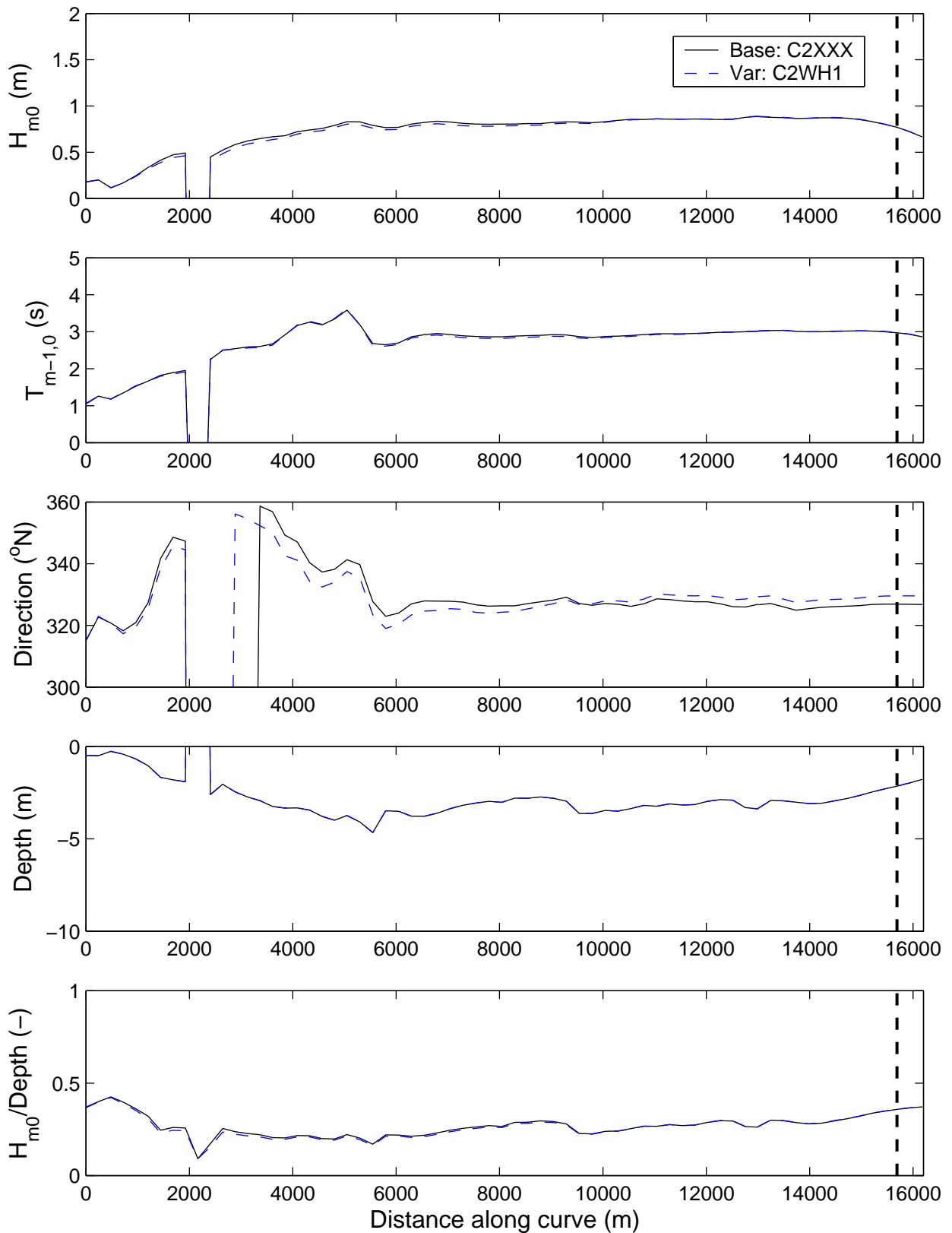
Sensitivity run C2WH1: Simulation with downscaled HIRLAM wind field
 Differences in mean direction (above) and directional spreading (below).

Sensitivity analysis Ameland



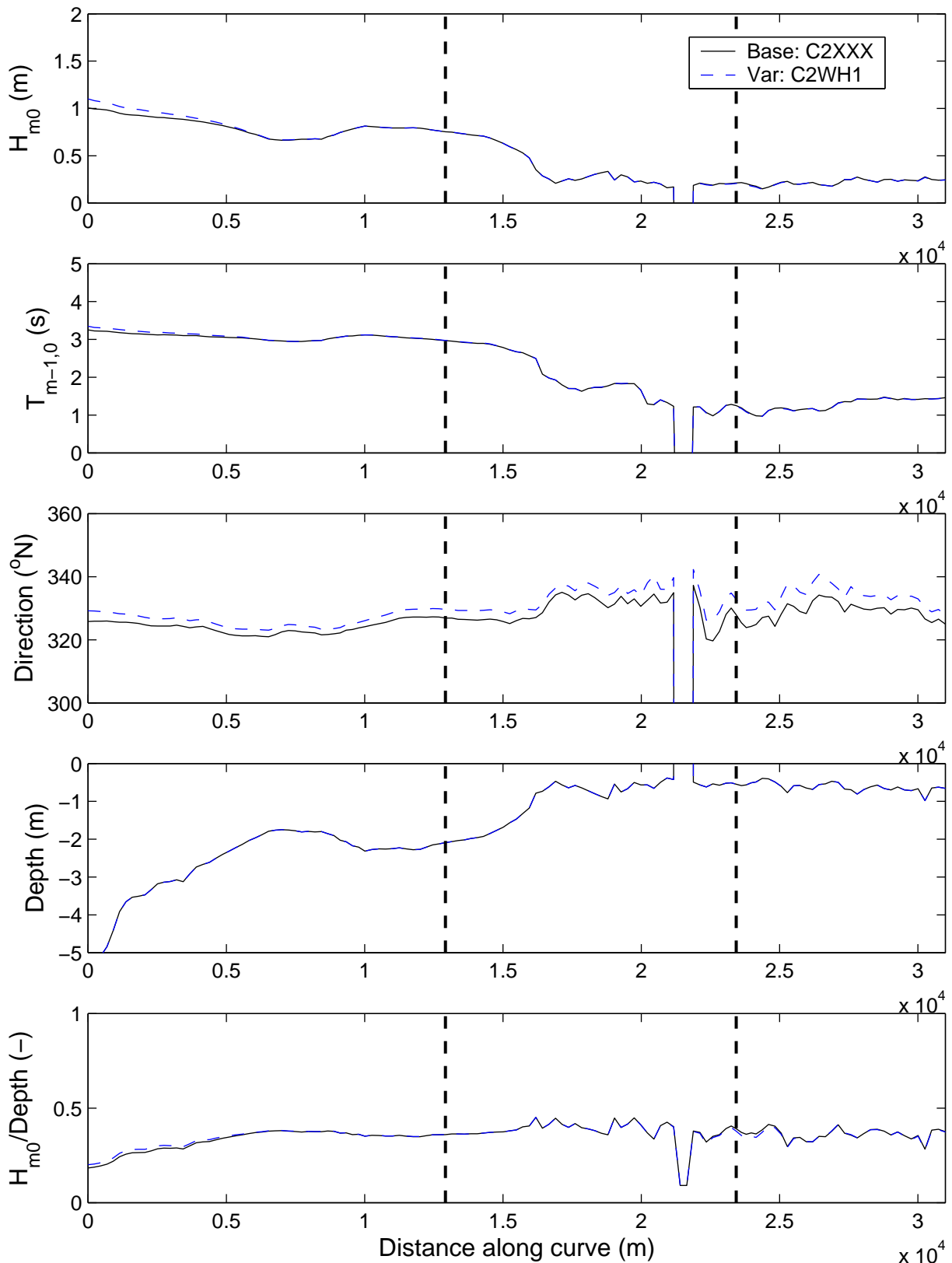
Sensitivity run C2WH1: Simulation with downscaled HIRLAM wind field
Integral parameters along Curve E

Sensitivity analysis Ameland



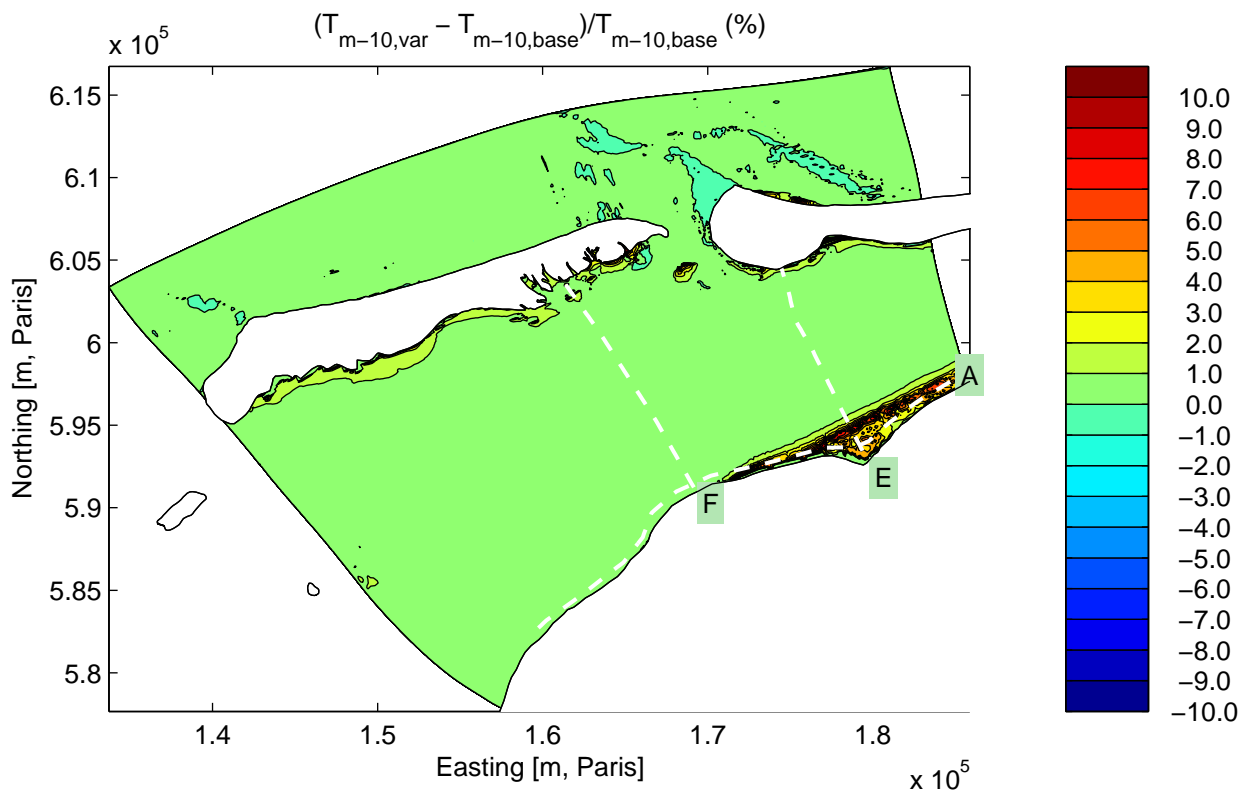
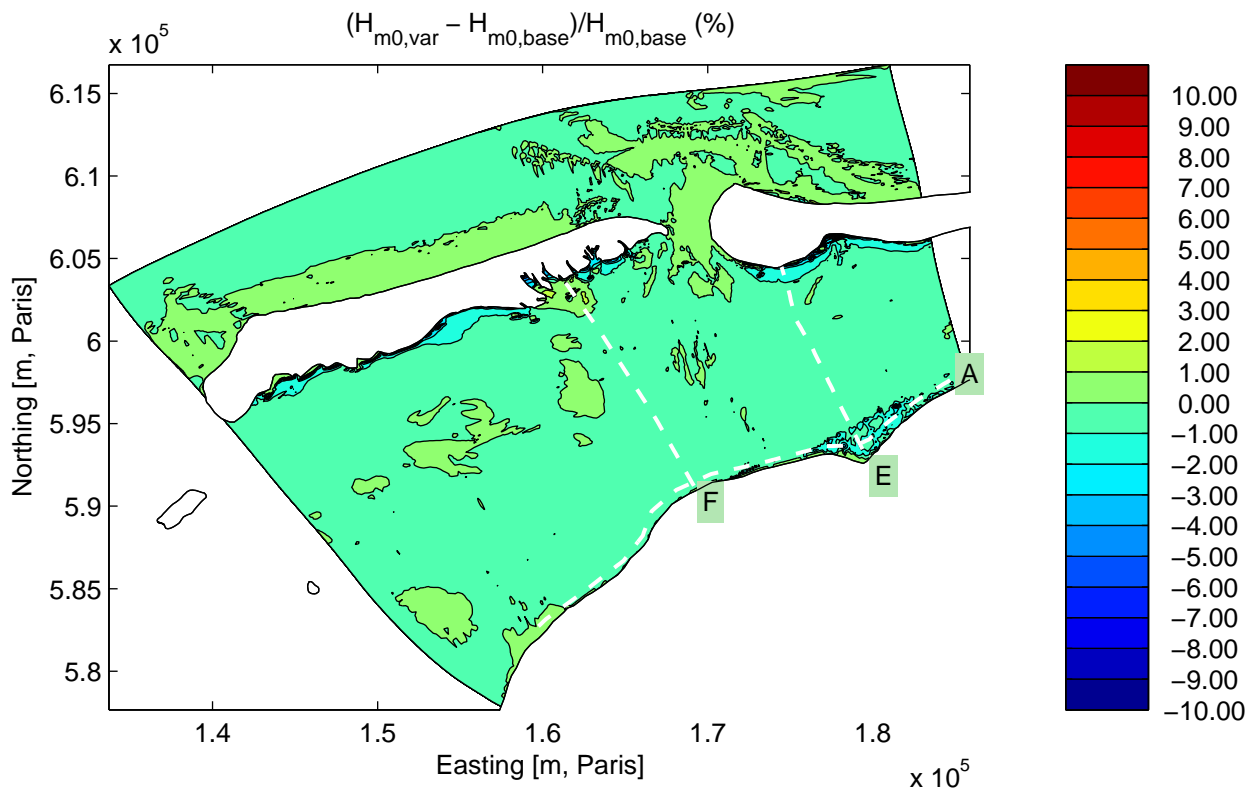
Sensitivity run C2WH1: Simulation with downscaled HIRLAM wind field
Integral parameters along Curve F

Sensitivity analysis Ameland



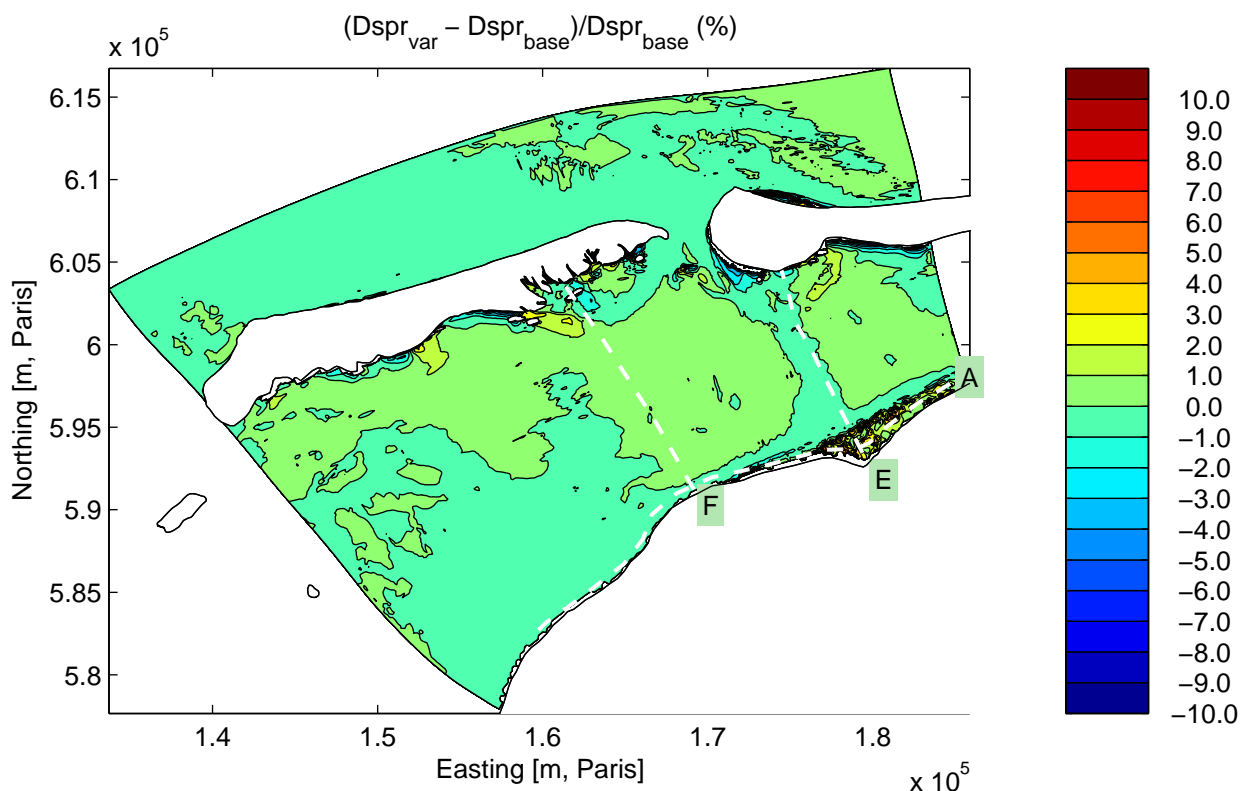
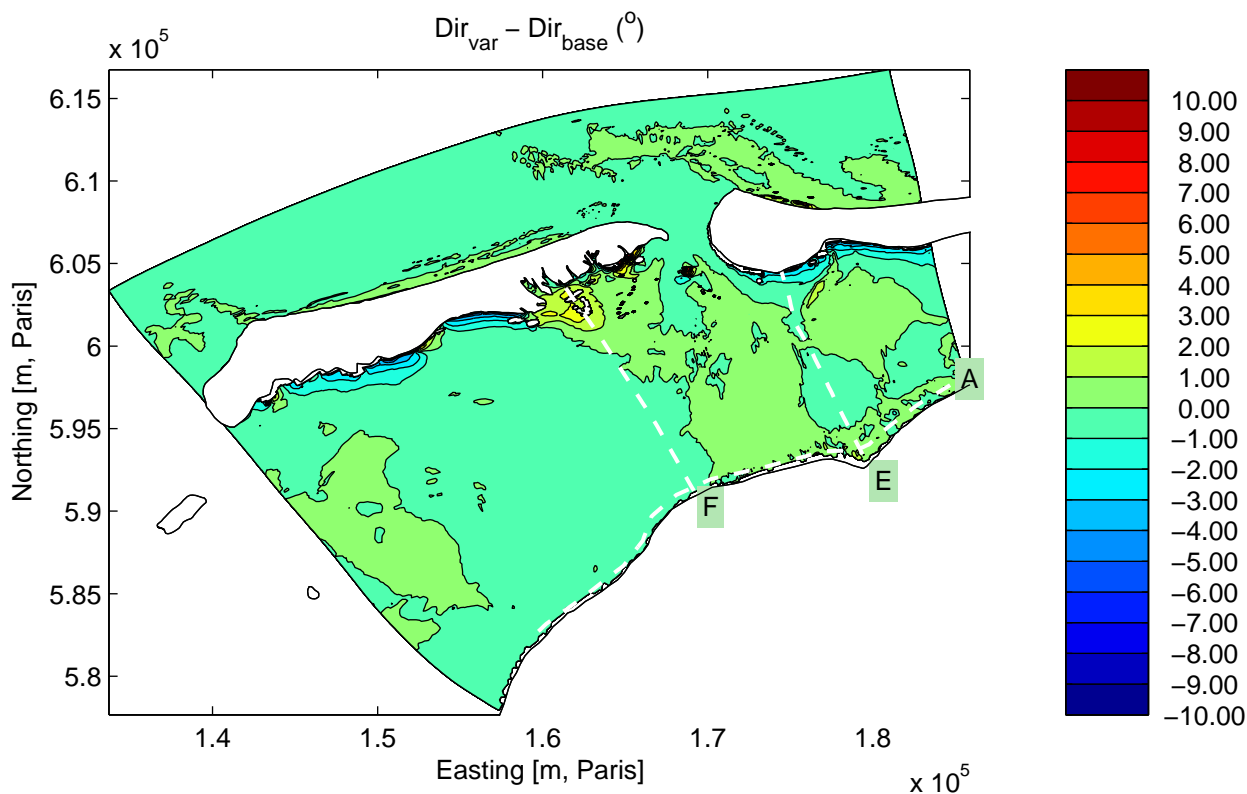
Sensitivity run C2WH1: Simulation with downscaled HIRLAM wind field
Integral parameters along Curve A

Sensitivity analysis Ameland



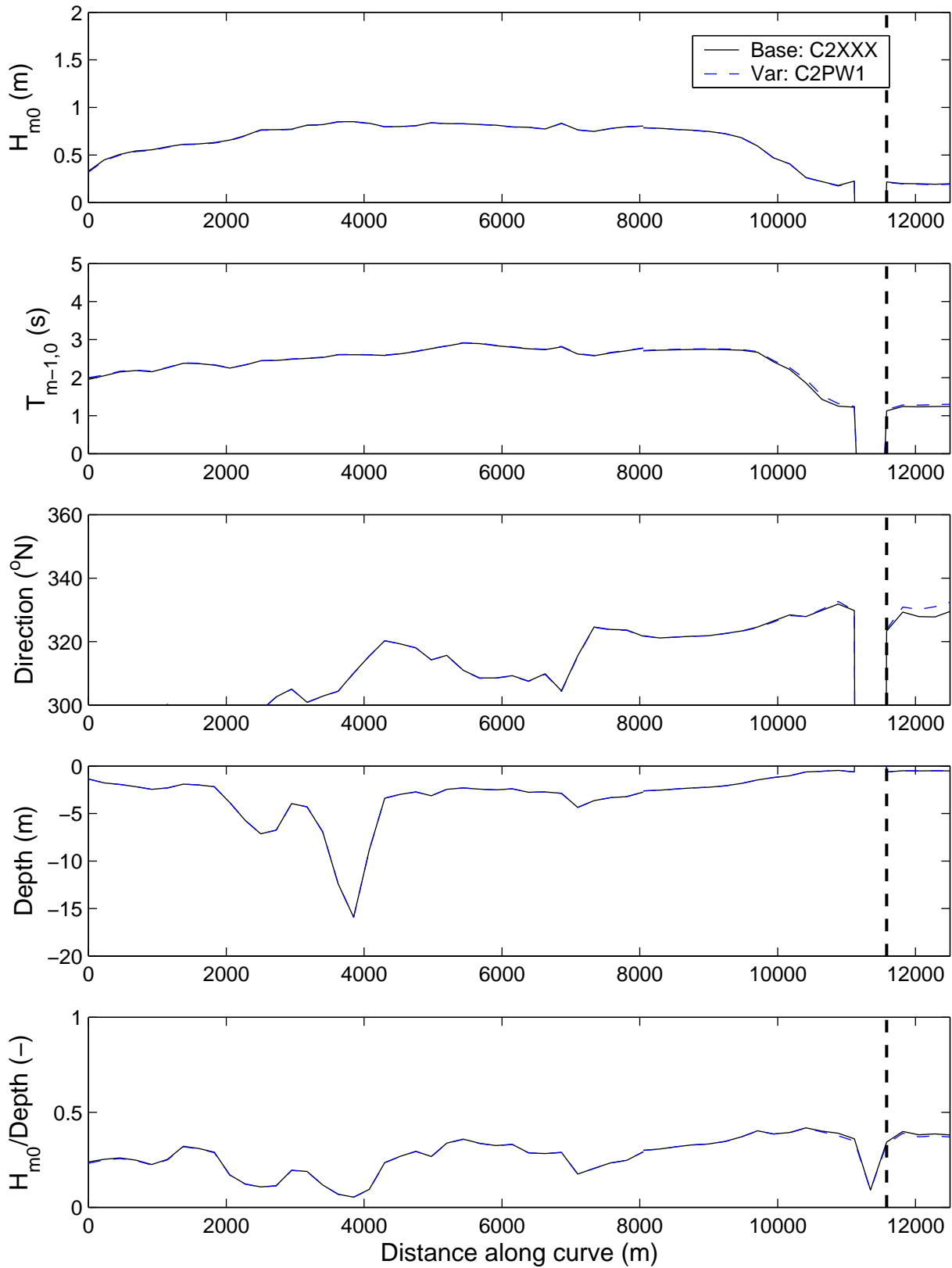
Sensitivity run C2PW1: Limiting the magnitude of wind energy transfer
Differences in significant wave height (above) and mean period (below).

Sensitivity analysis Ameland



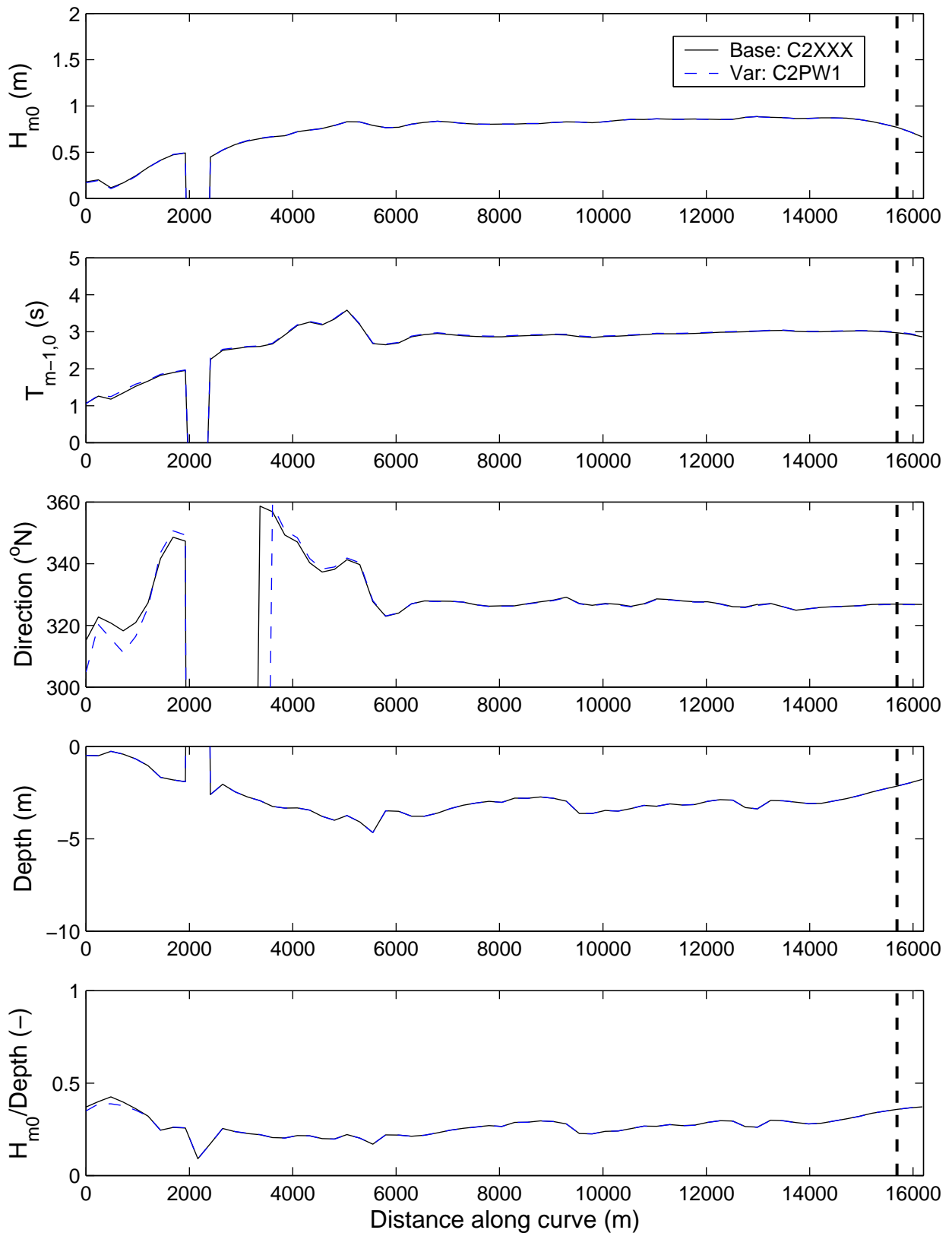
Sensitivity run C2PW1: Limiting the magnitude of wind energy transfer
Differences in mean direction (above) and directional spreading (below).

Sensitivity analysis Ameland



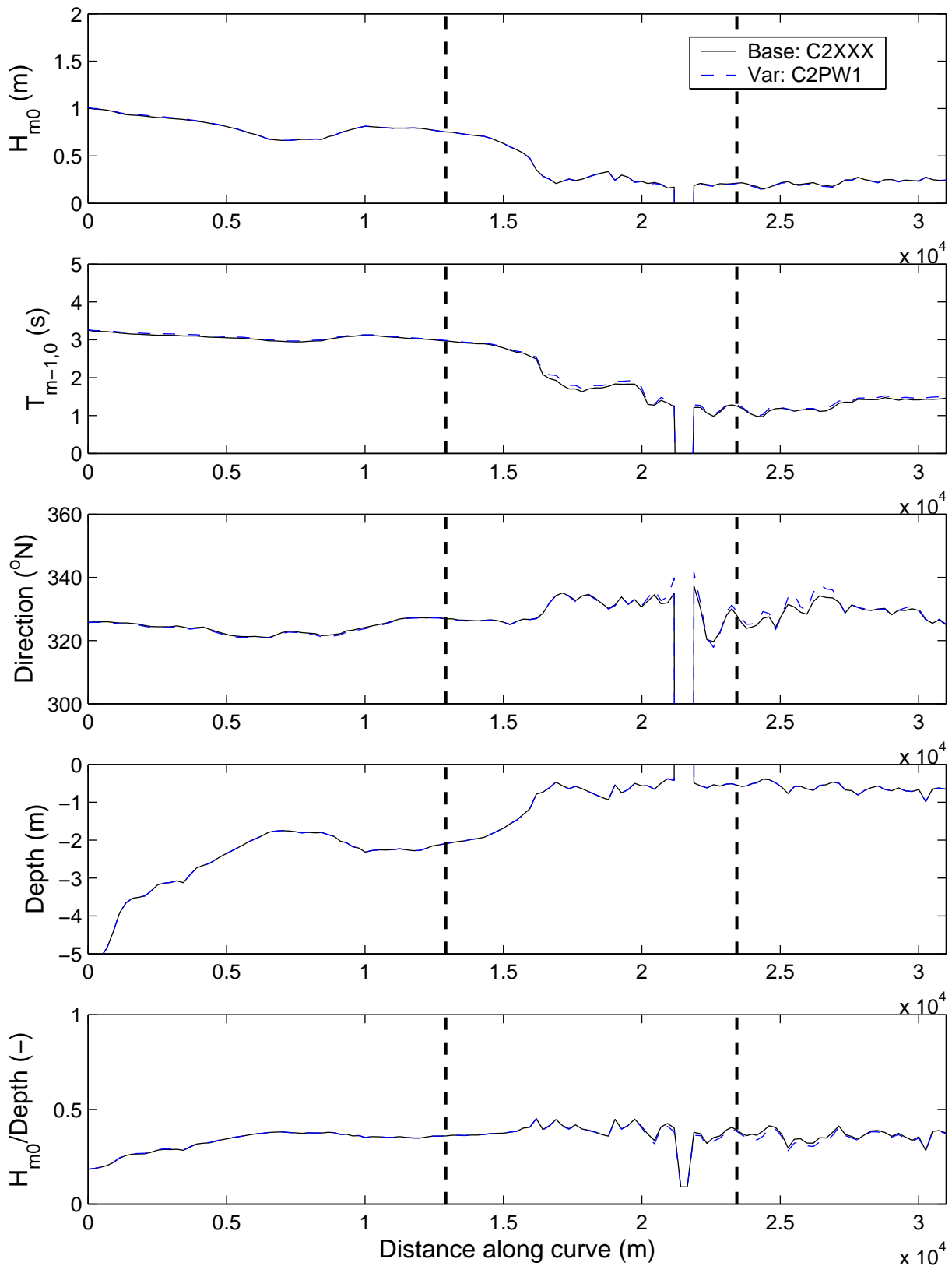
Sensitivity run C2PW1: Limiting the magnitude of wind energy transfer
Integral parameters along Curve E

Sensitivity analysis Ameland



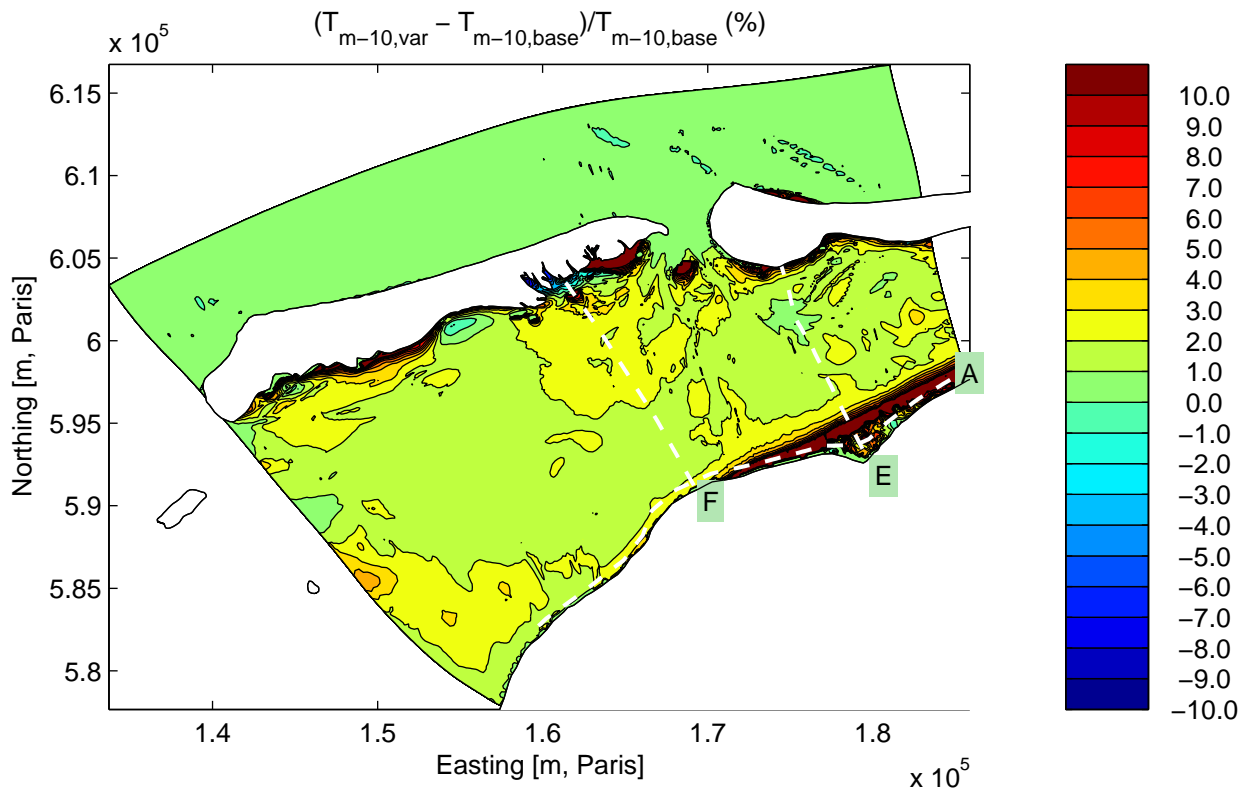
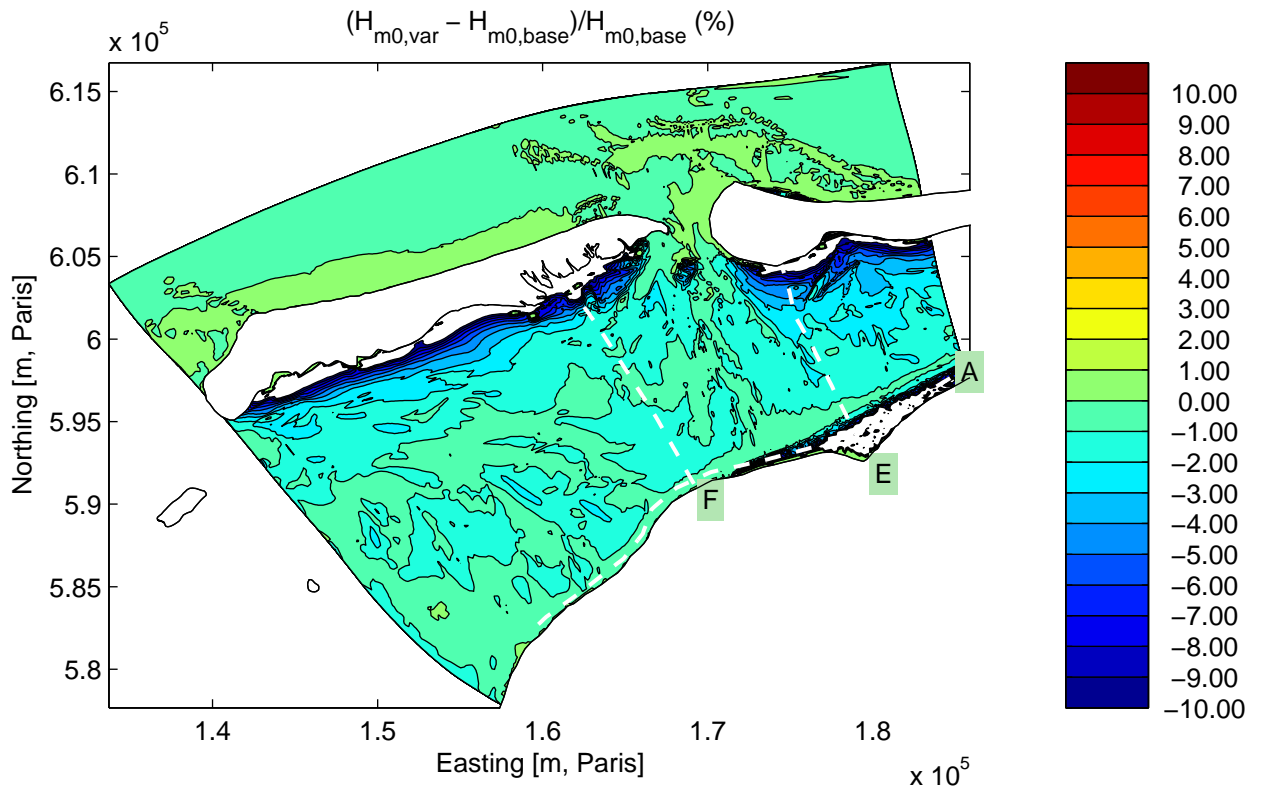
Sensitivity run C2PW1: Limiting the magnitude of wind energy transfer
Integral parameters along Curve F

Sensitivity analysis Ameland



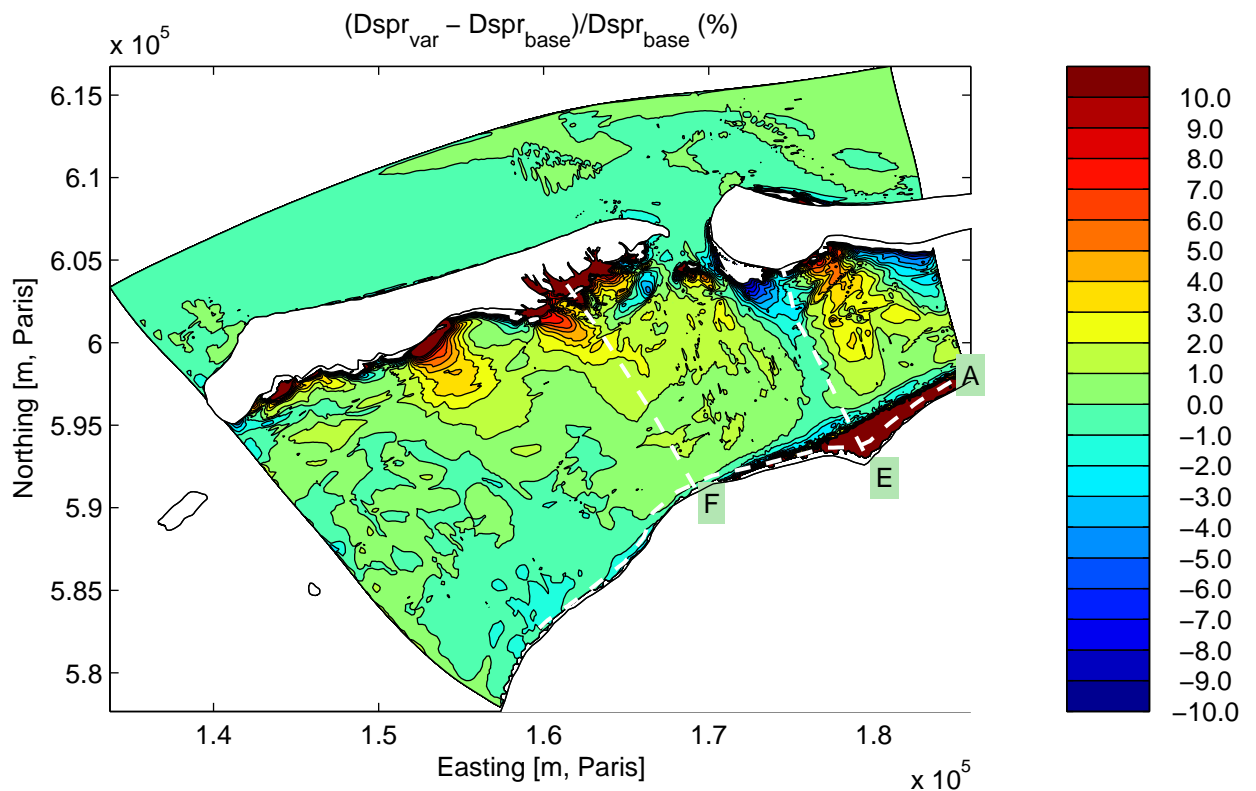
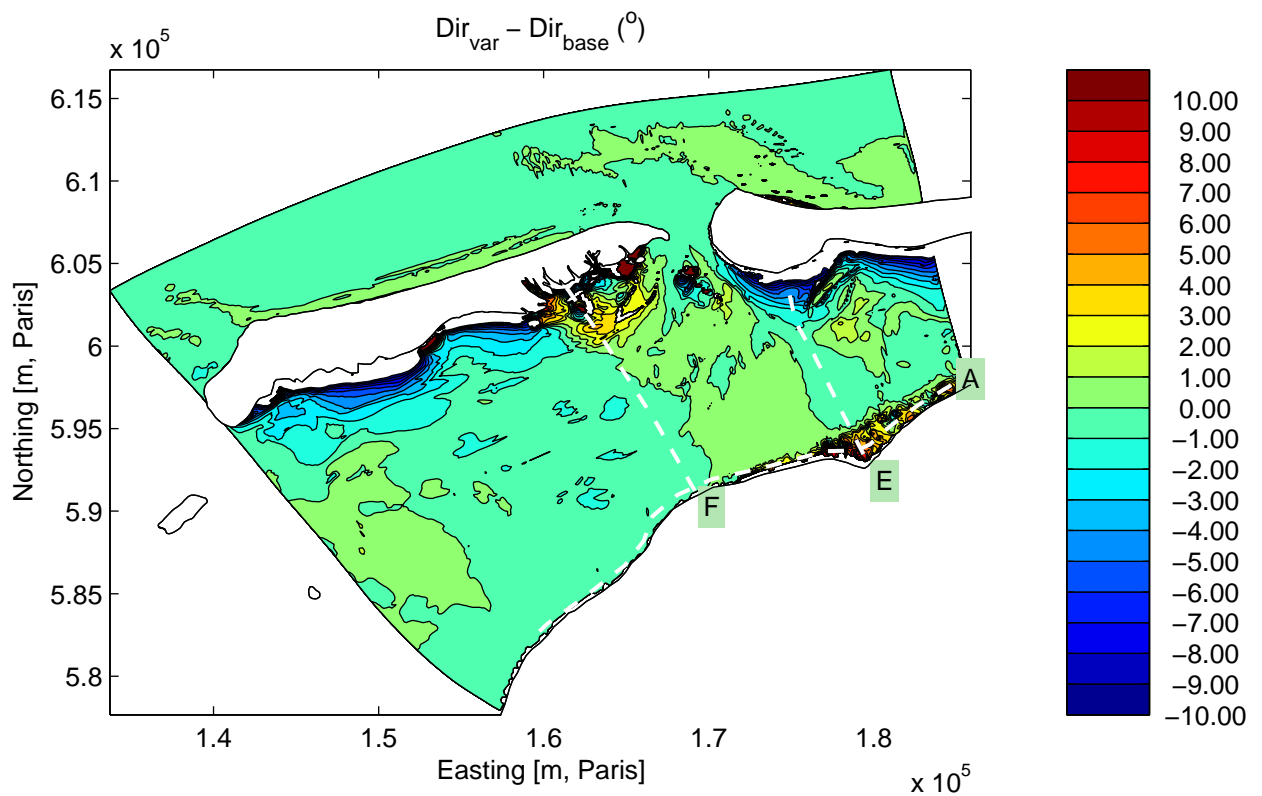
Sensitivity run C2PW1: Limiting the magnitude of wind energy transfer
Integral parameters along Curve A

Sensitivity analysis Ameland



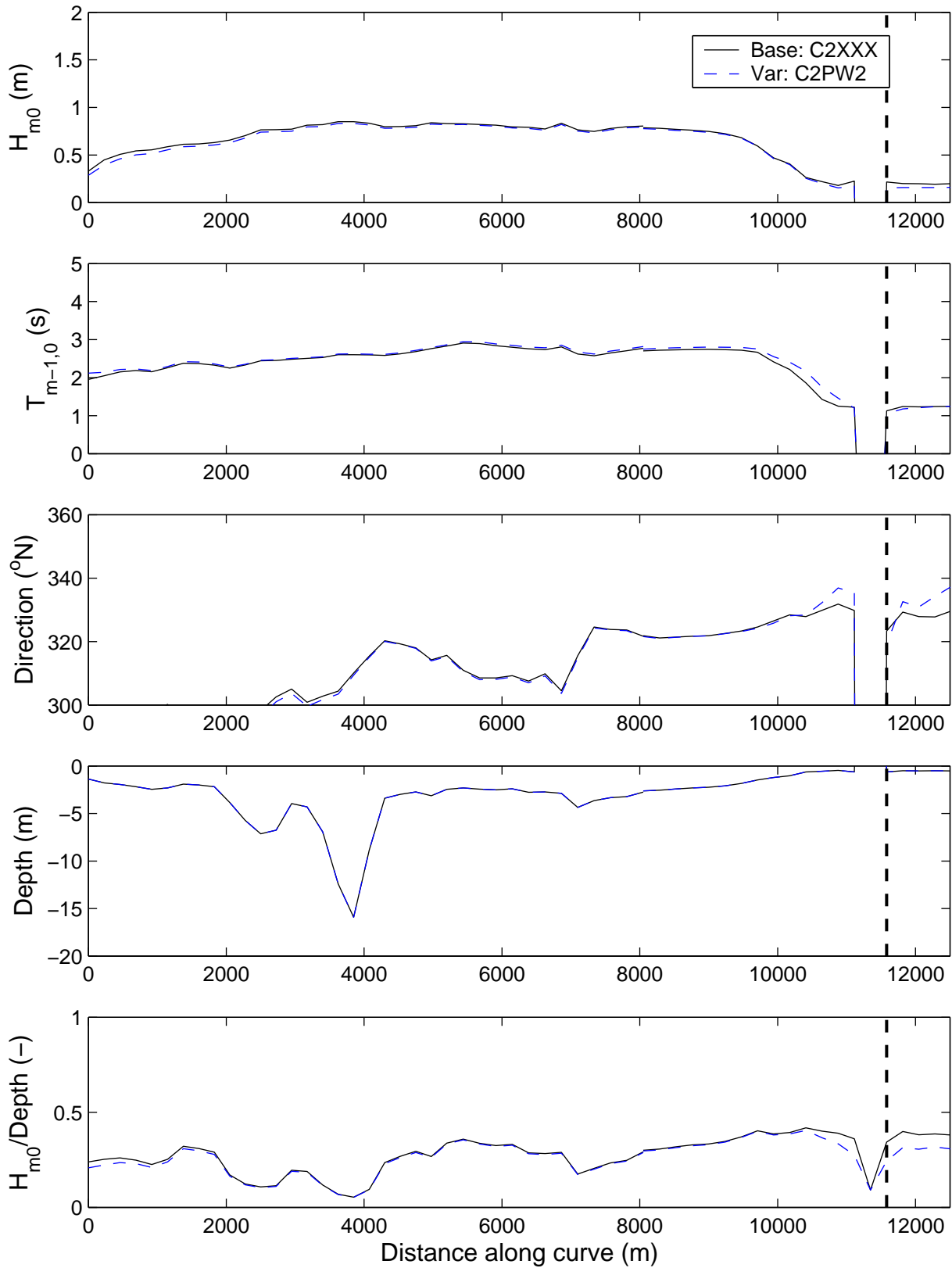
Sensitivity run C2PW2: Limiting the magnitude of wind energy transfer
Differences in significant wave height (above) and mean period (below).

Sensitivity analysis Ameland



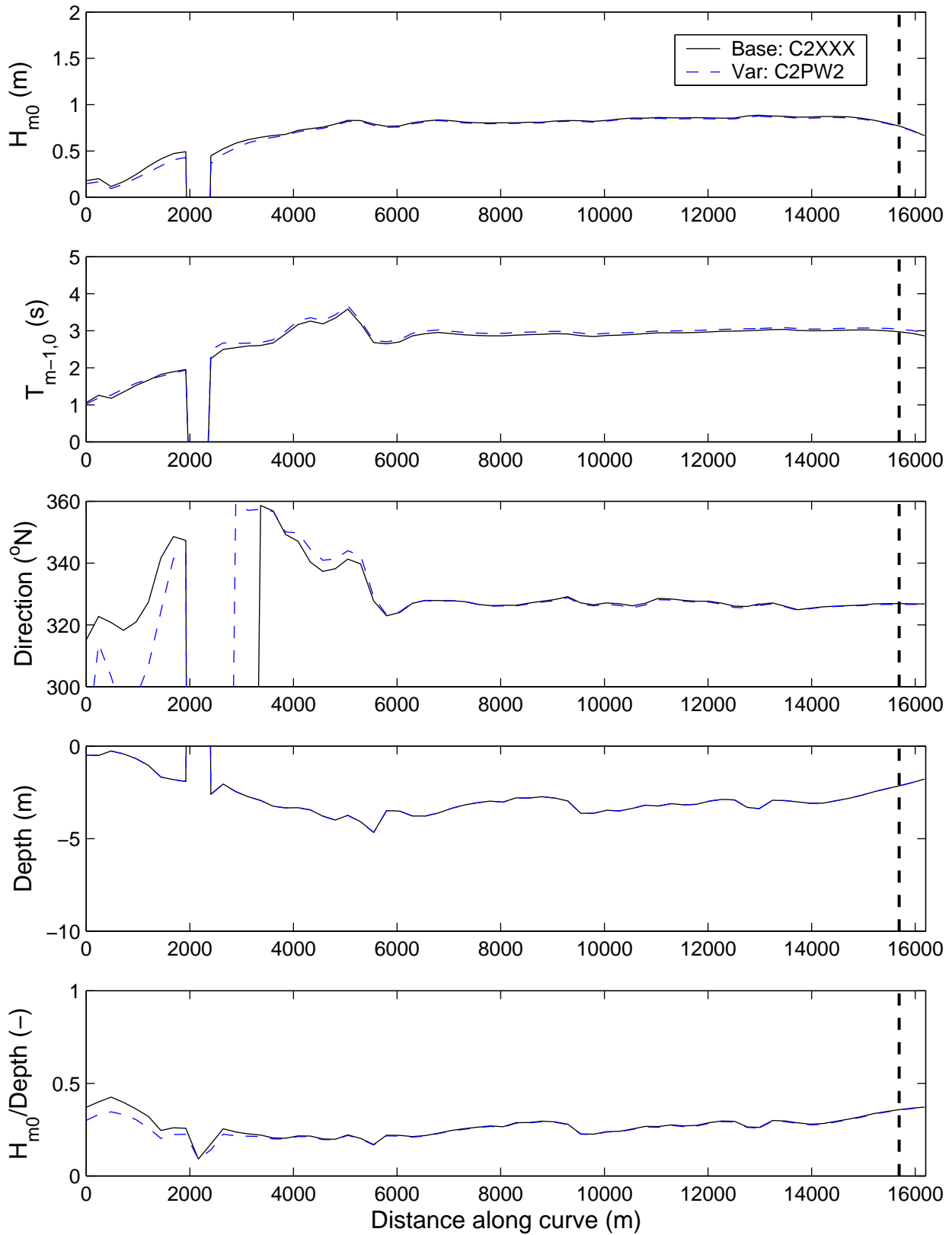
Sensitivity run C2PW2: Limiting the magnitude of wind energy transfer
 Differences in mean direction (above) and directional spreading (below).

Sensitivity analysis Ameland



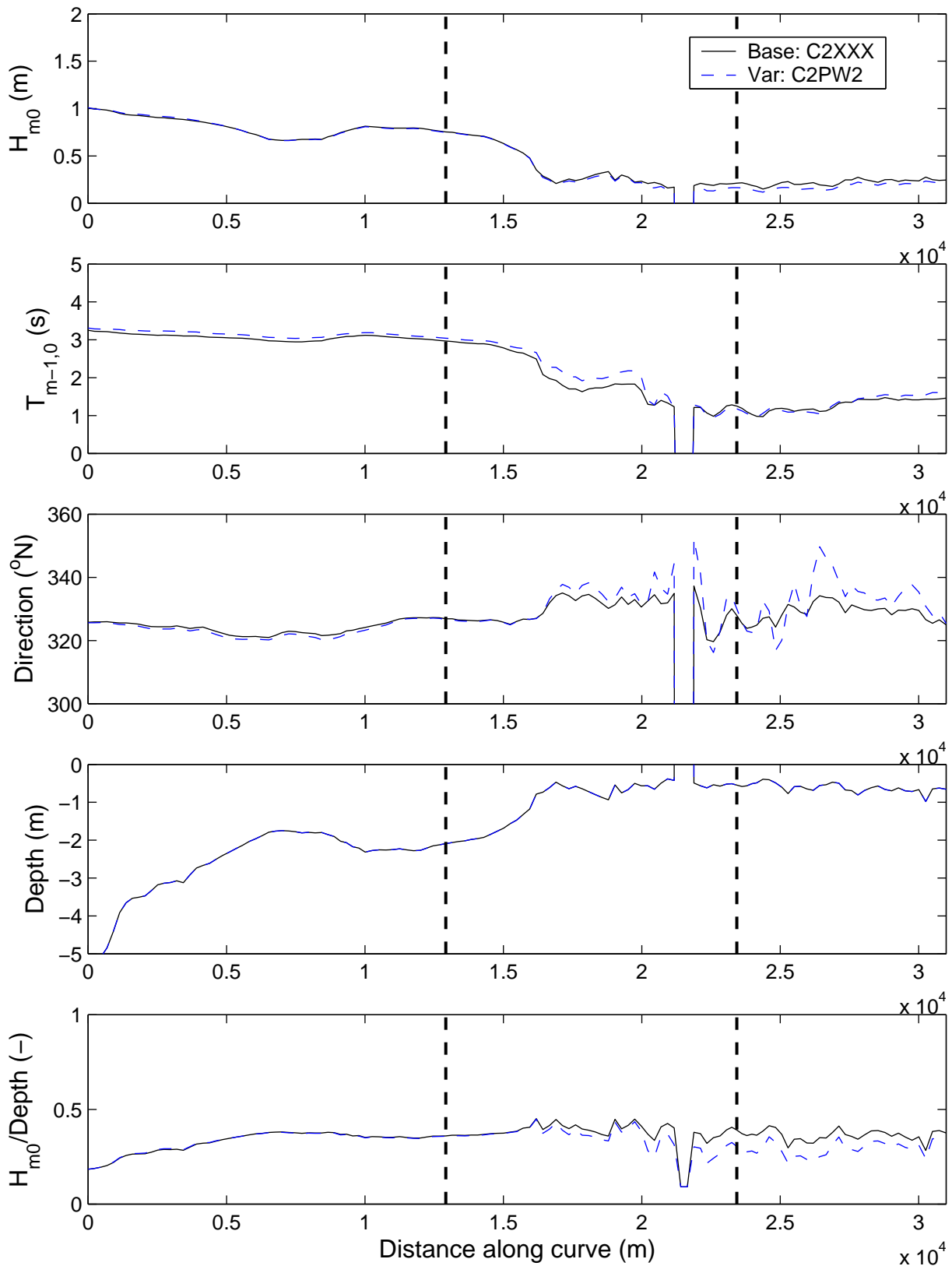
Sensitivity run C2PW2: Limiting the magnitude of wind energy transfer
Integral parameters along Curve E

Sensitivity analysis Ameland



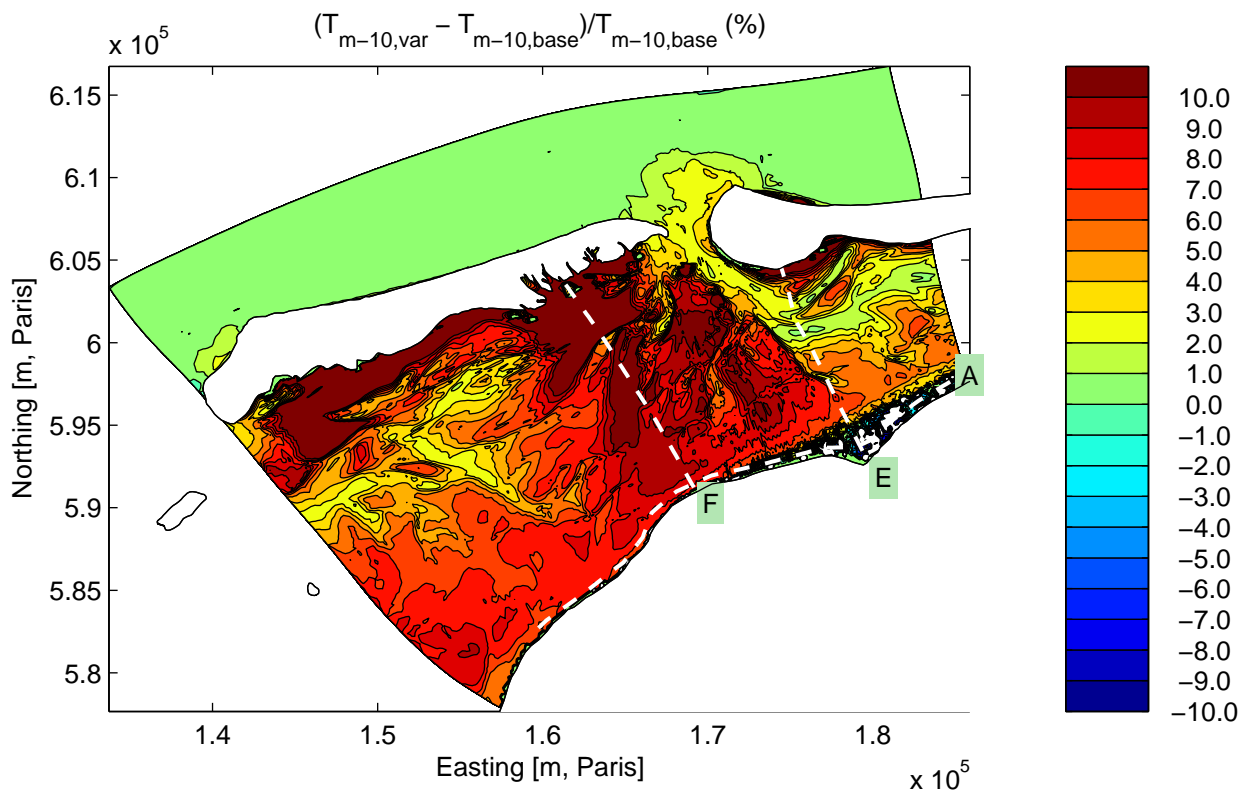
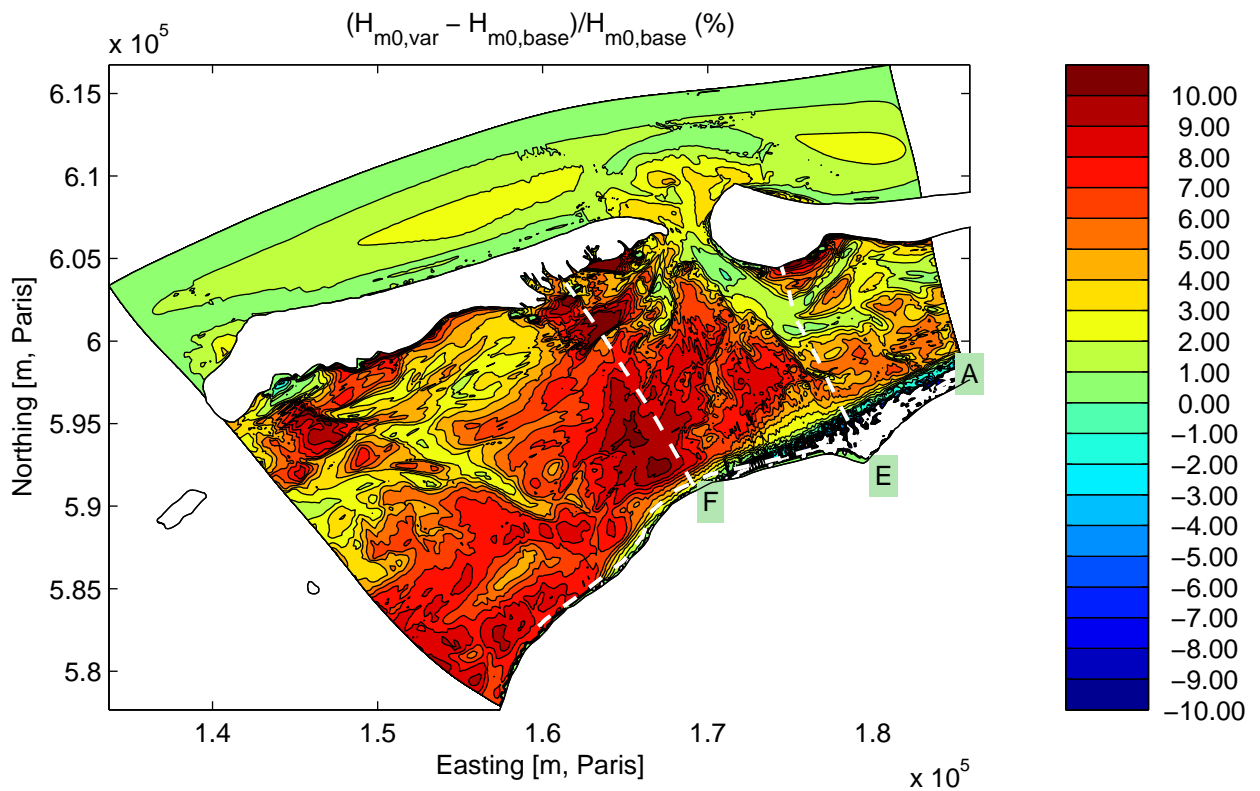
Sensitivity run C2PW2: Limiting the magnitude of wind energy transfer
Integral parameters along Curve F

Sensitivity analysis Ameland



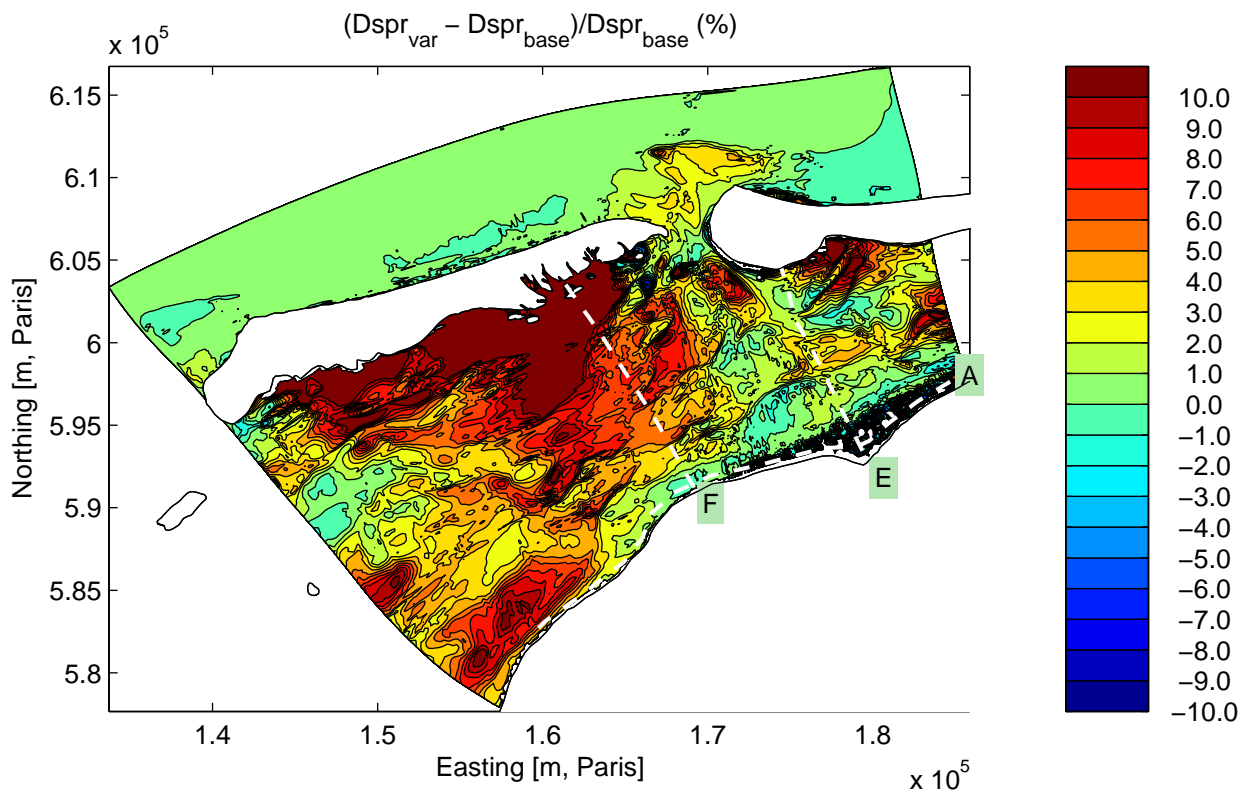
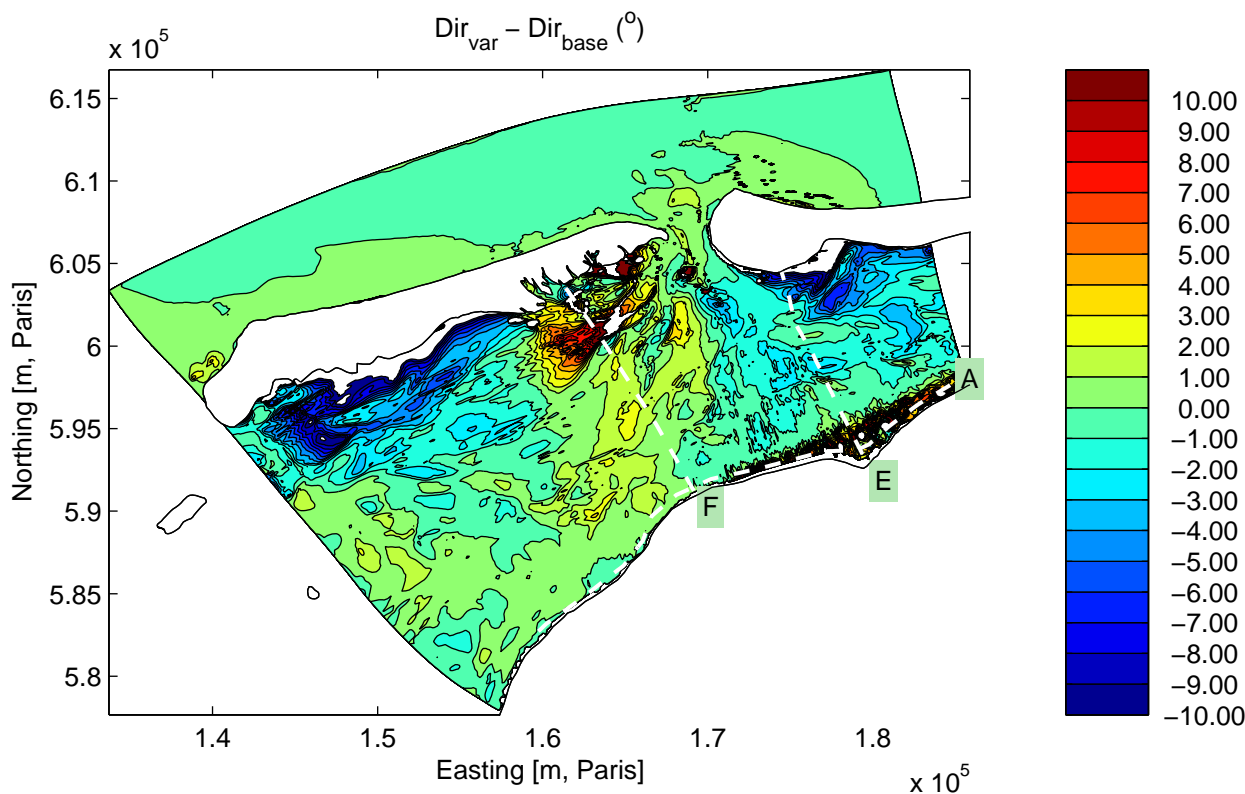
Sensitivity run C2PW2: Limiting the magnitude of wind energy transfer
Integral parameters along Curve A

Sensitivity analysis Ameland



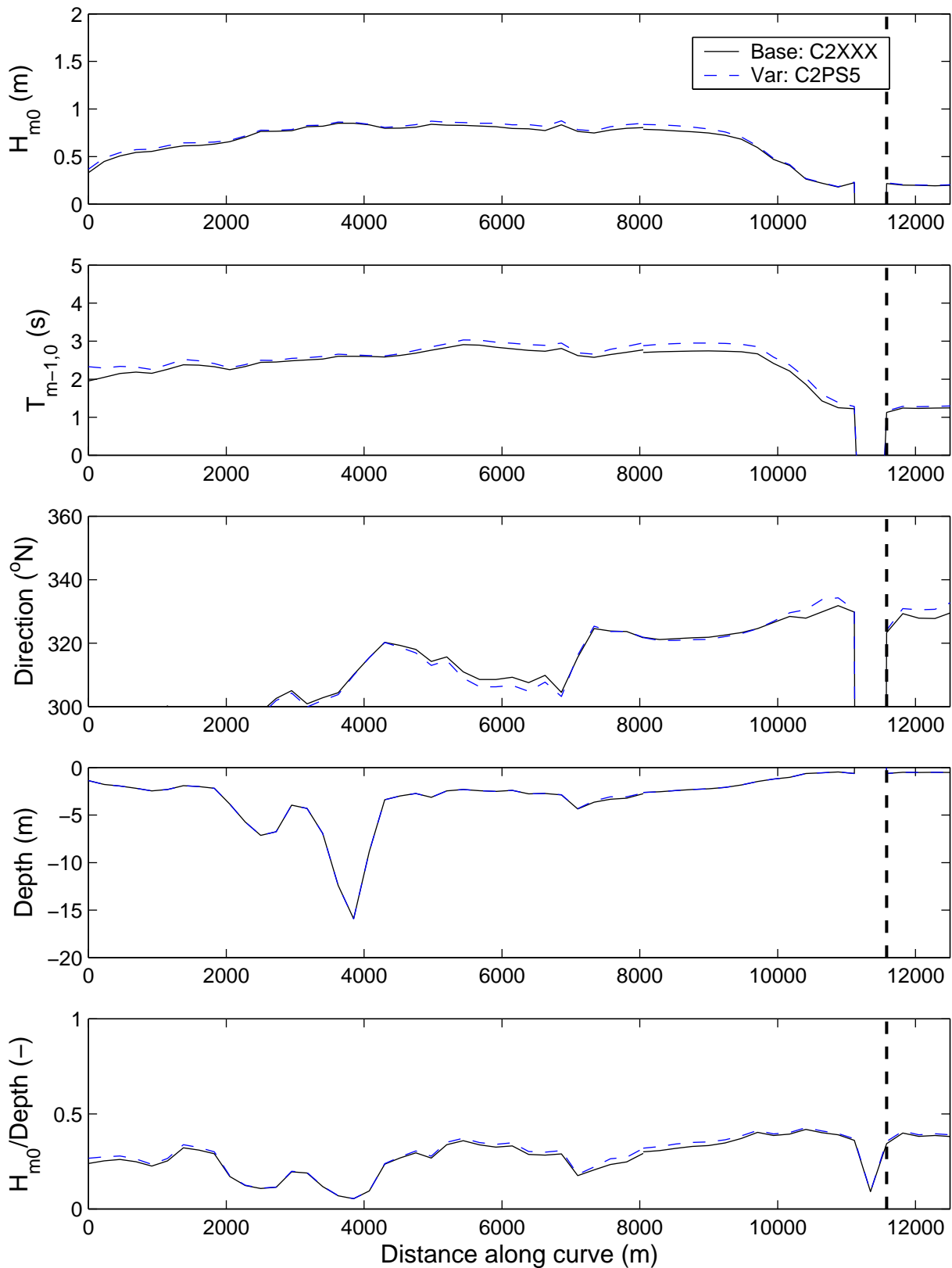
Sensitivity run C2PS5: Reduction in strength of bottom friction
Differences in significant wave height (above) and mean period (below).

Sensitivity analysis Ameland



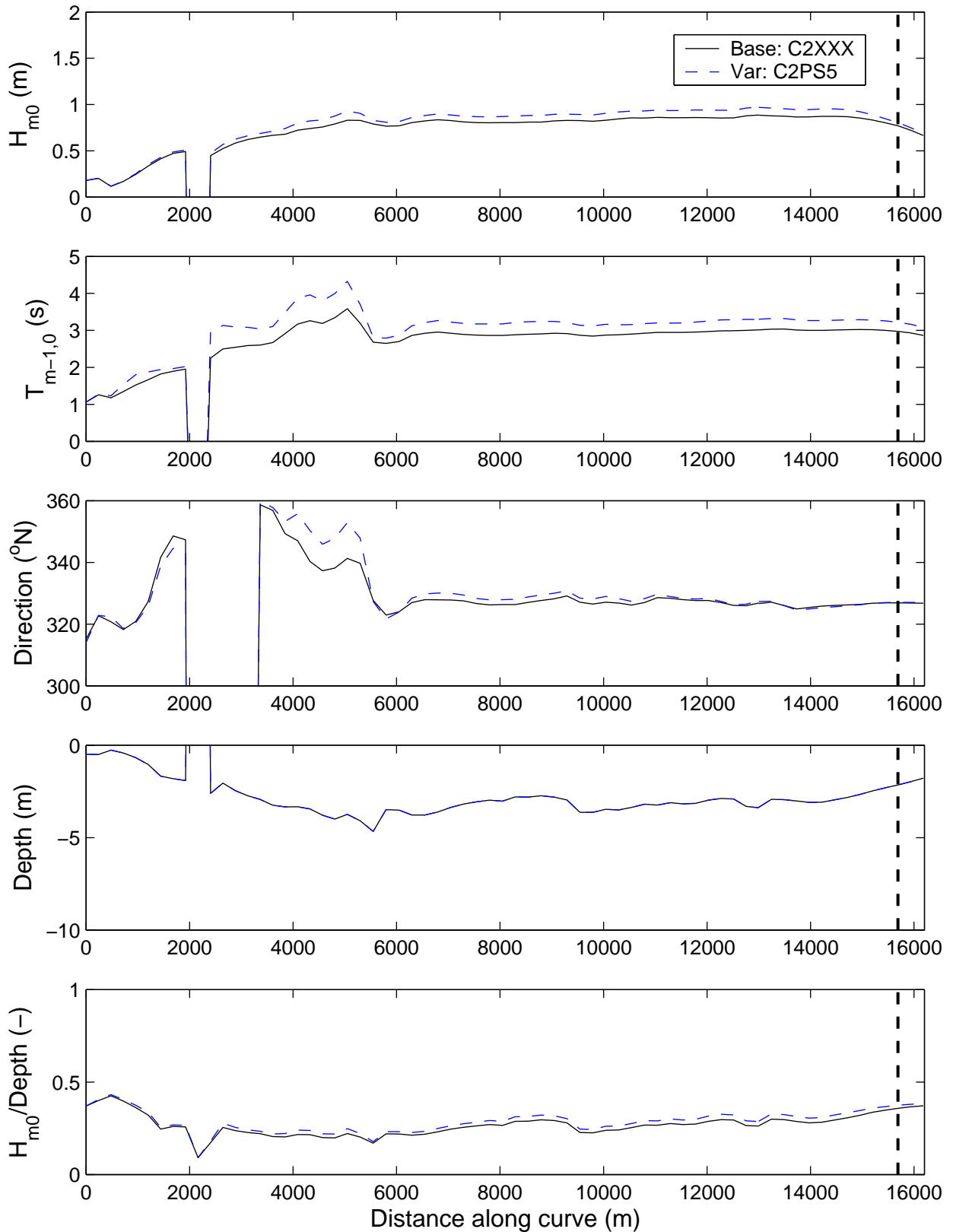
Sensitivity run C2PS5: Reduction in strength of bottom friction
 Differences in mean direction (above) and directional spreading (below).

Sensitivity analysis Ameland



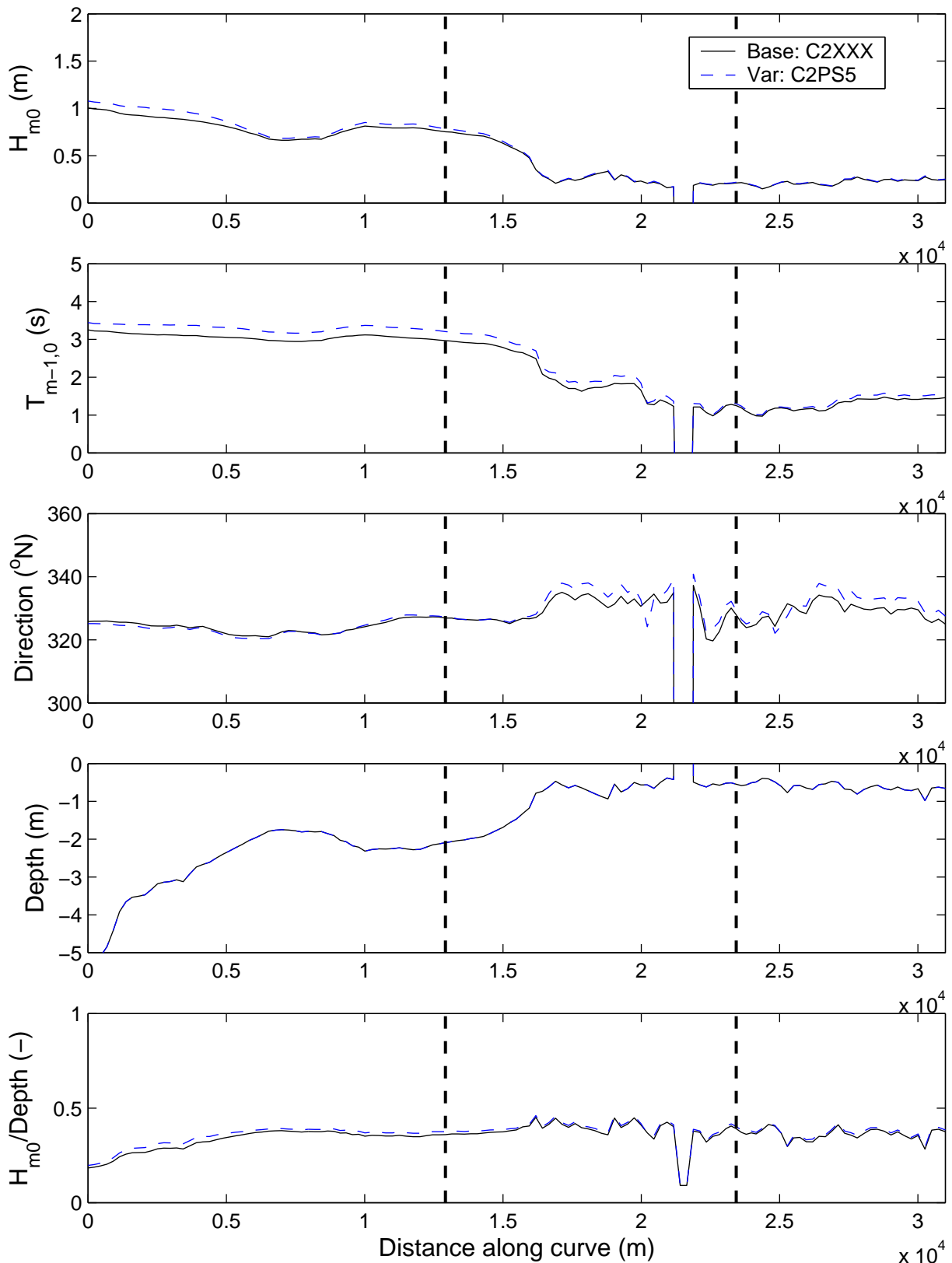
Sensitivity run C2PS5: Reduction in strength of bottom friction
Integral parameters along Curve E

Sensitivity analysis Ameland



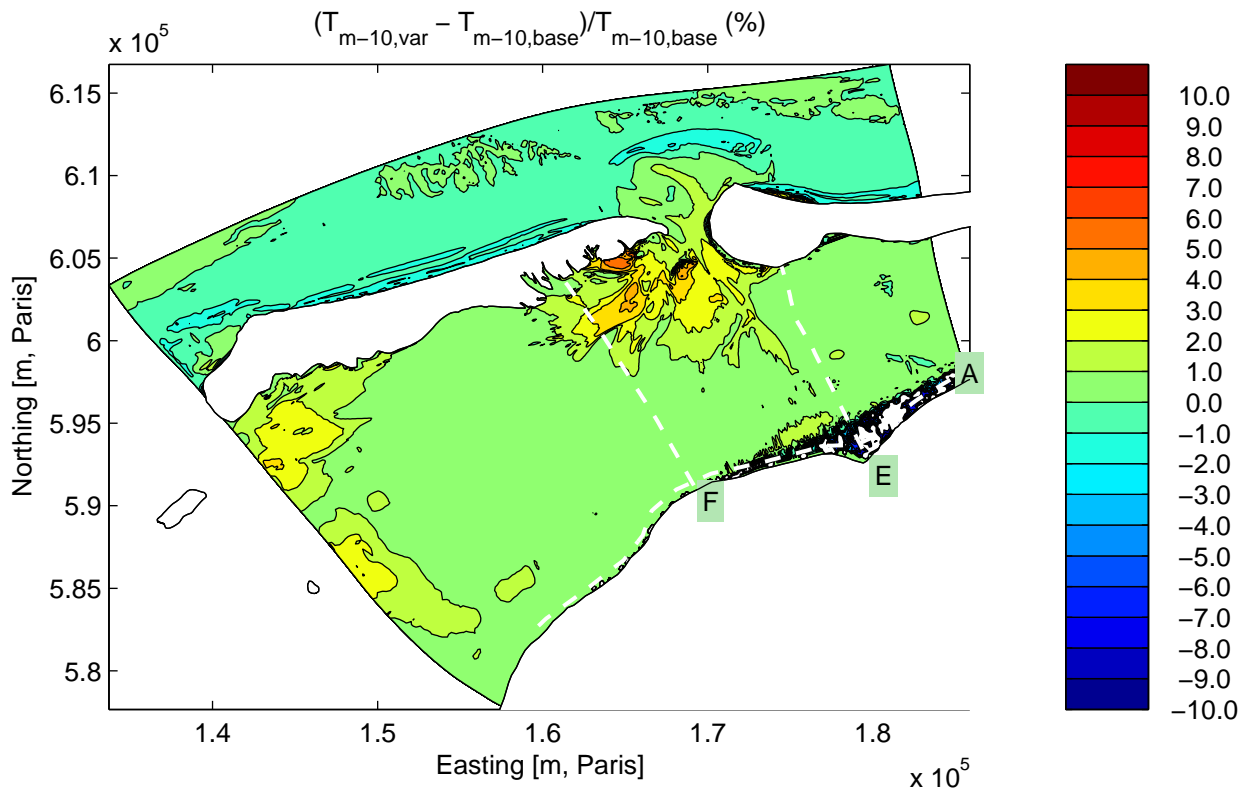
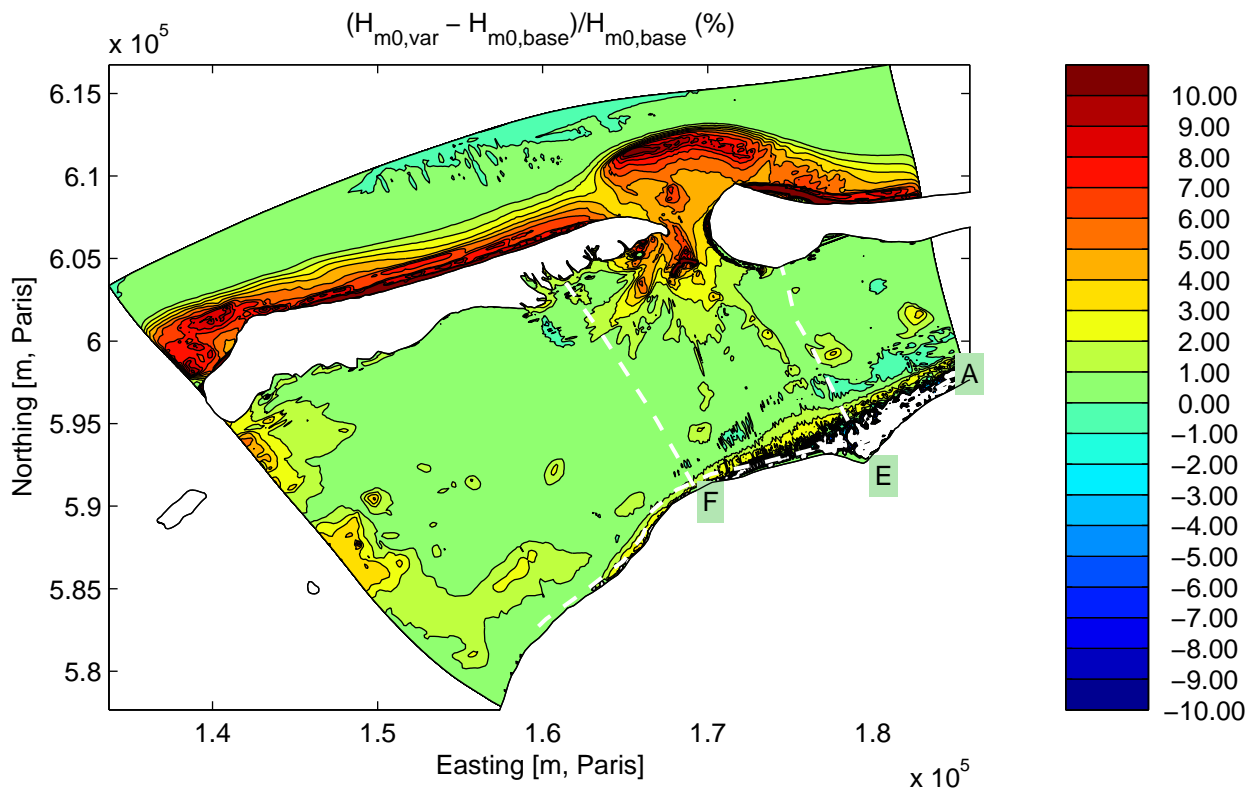
Sensitivity run C2PS5: Reduction in strength of bottom friction
Integral parameters along Curve F

Sensitivity analysis Ameland



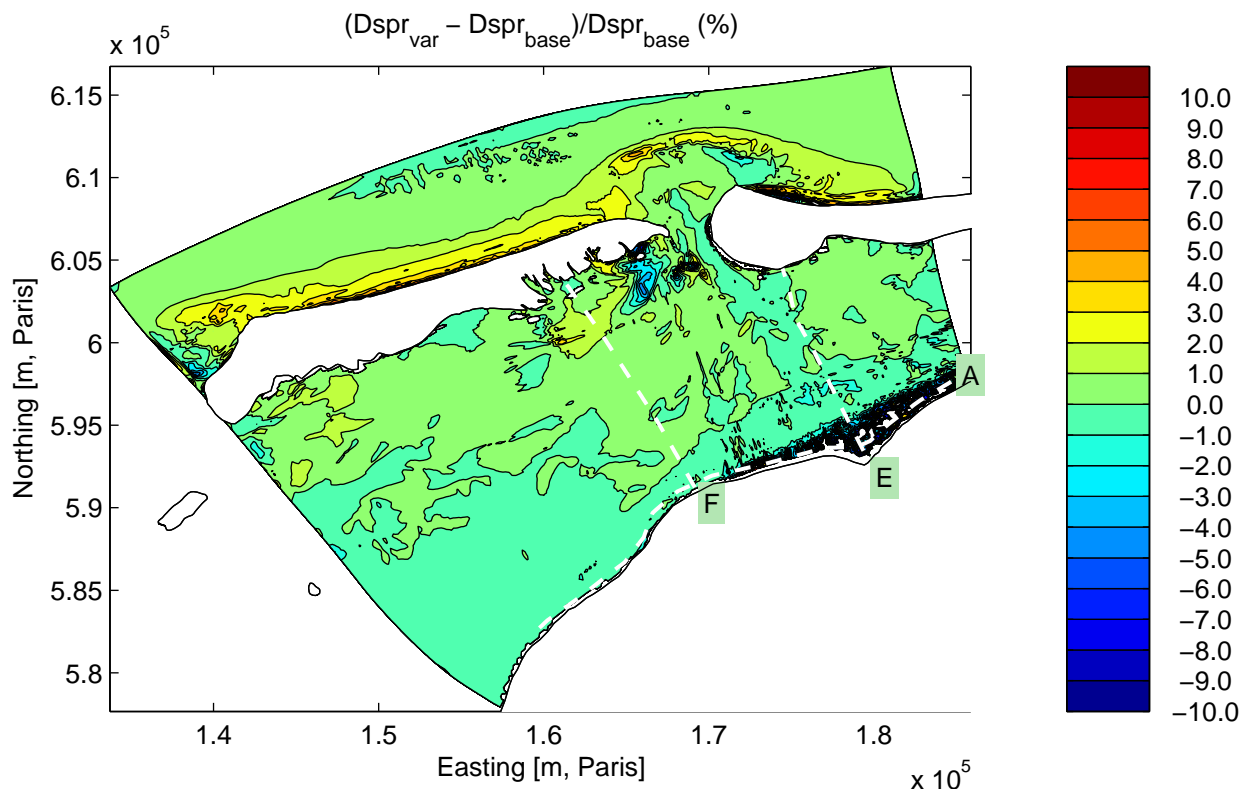
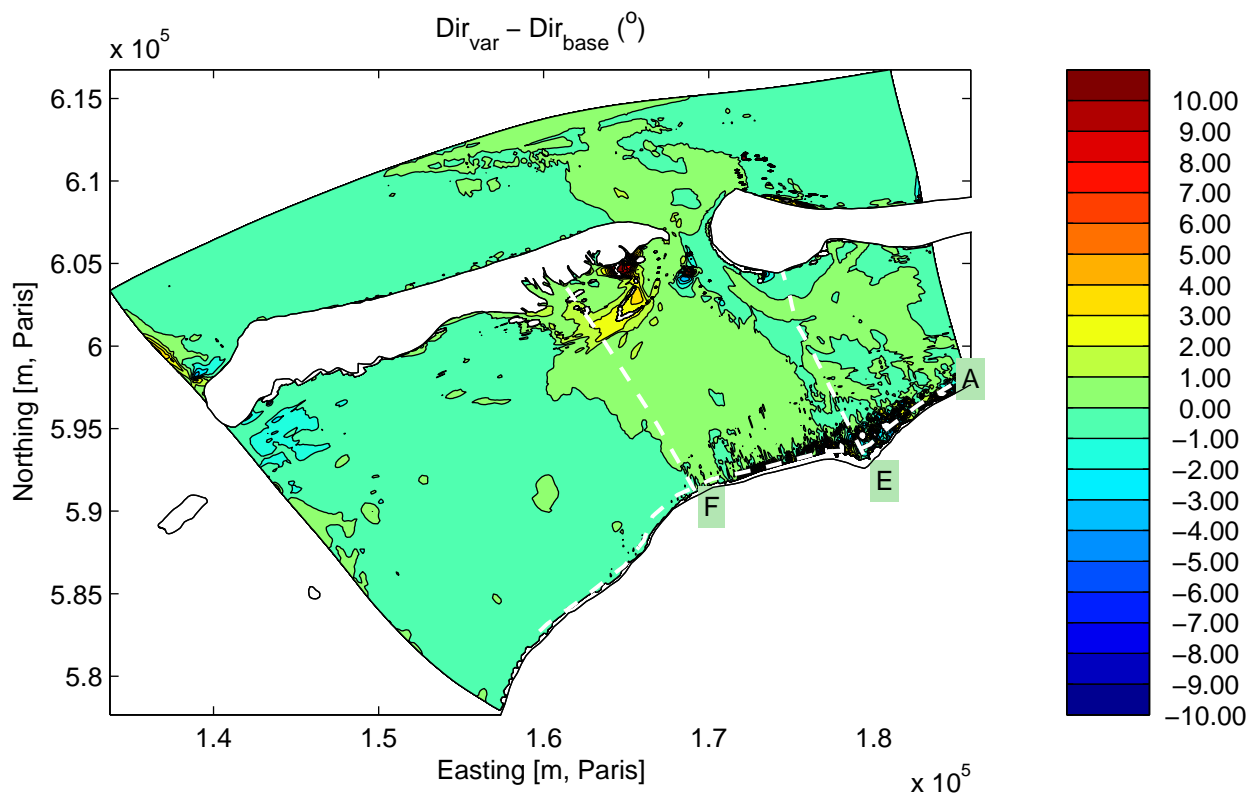
Sensitivity run C2PS5: Reduction in strength of bottom friction
Integral parameters along Curve A

Sensitivity analysis Ameland



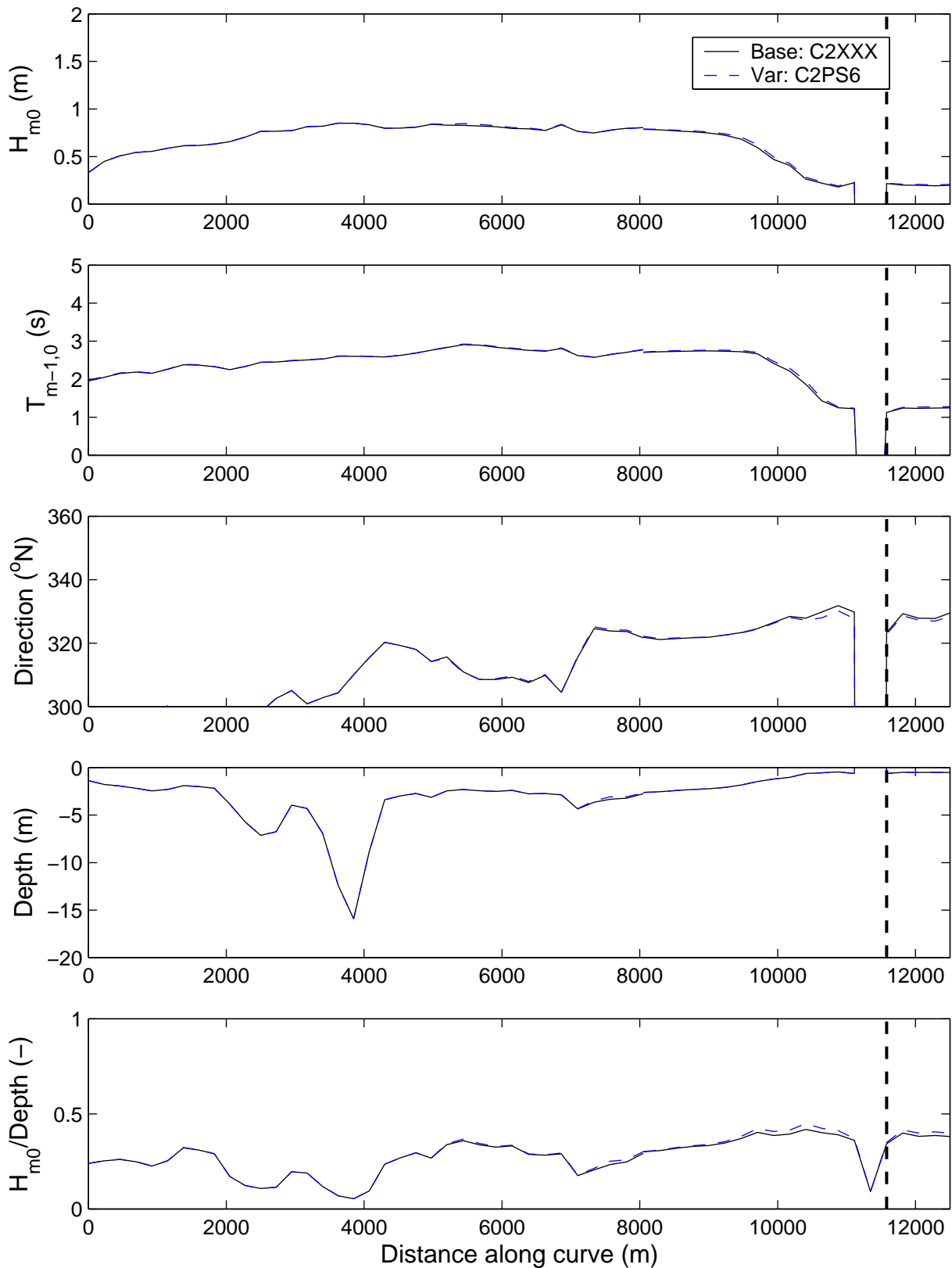
Sensitivity run C2PS6: Reduction in strength of depth-induced breaking
Differences in significant wave height (above) and mean period (below).

Sensitivity analysis Ameland



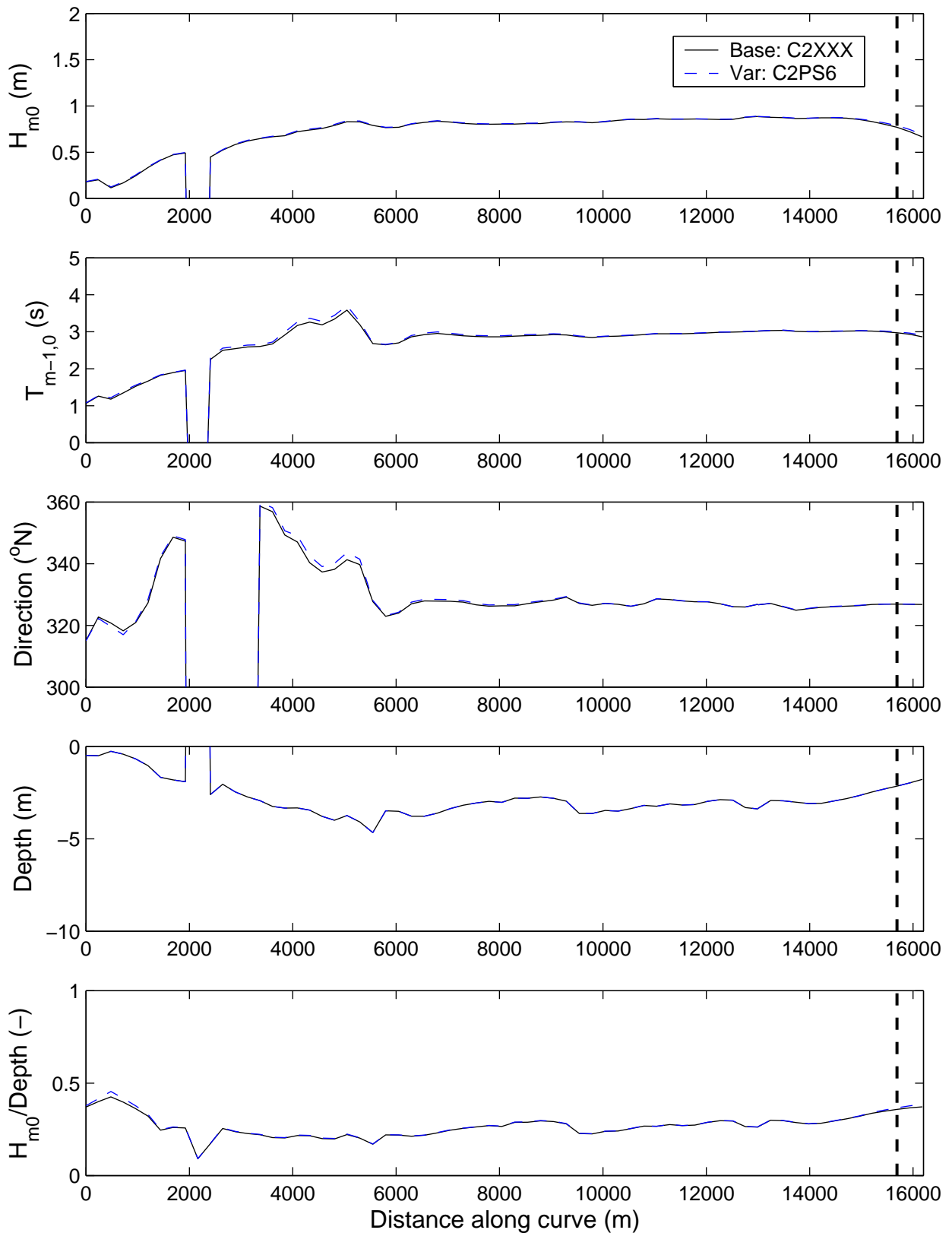
Sensitivity run C2PS6: Reduction in strength of depth-induced breaking
Differences in mean direction (above) and directional spreading (below).

Sensitivity analysis Ameland



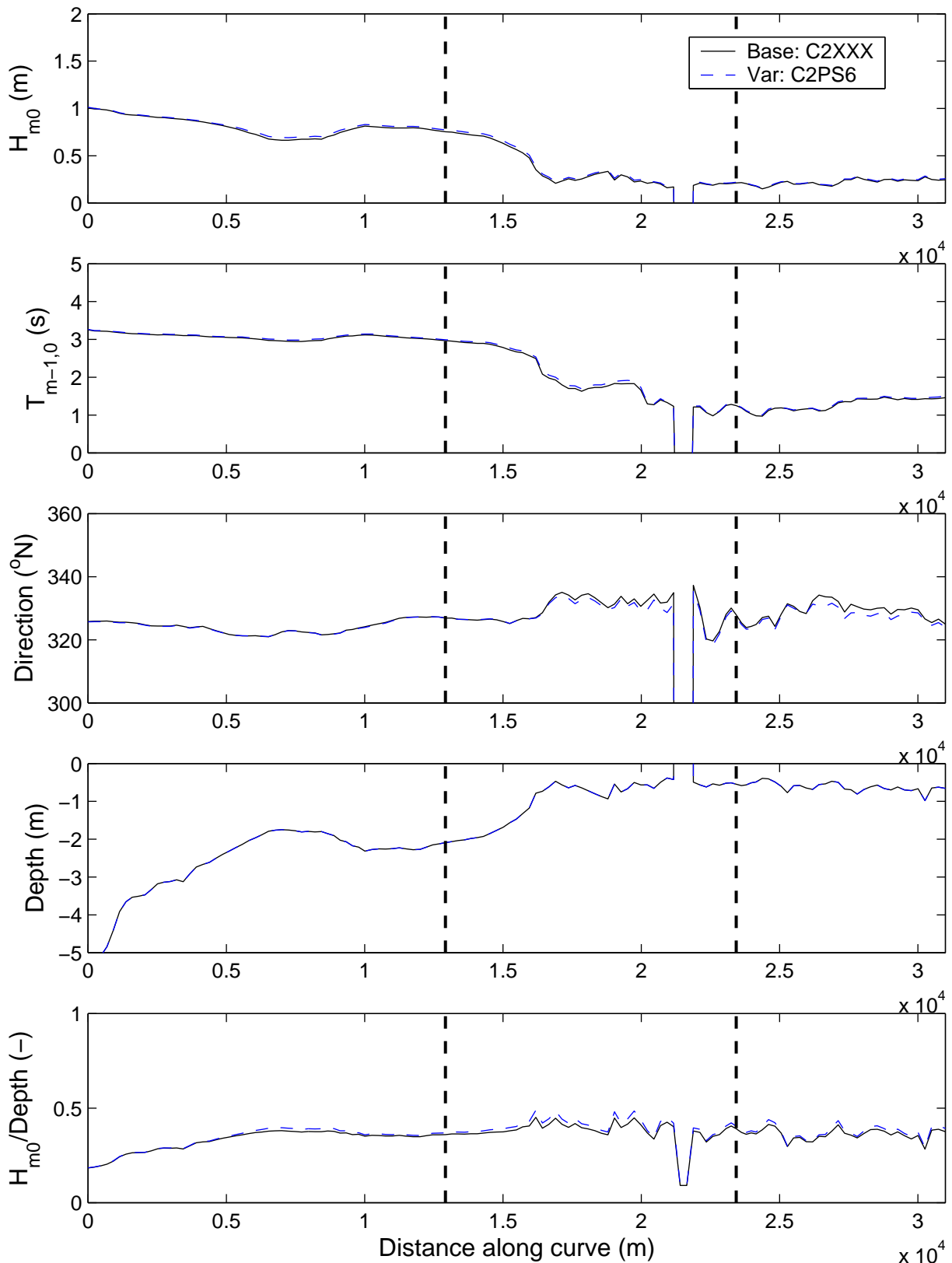
Sensitivity run C2PS6: Reduction in strength of depth-induced breaking
Integral parameters along Curve E

Sensitivity analysis Ameland



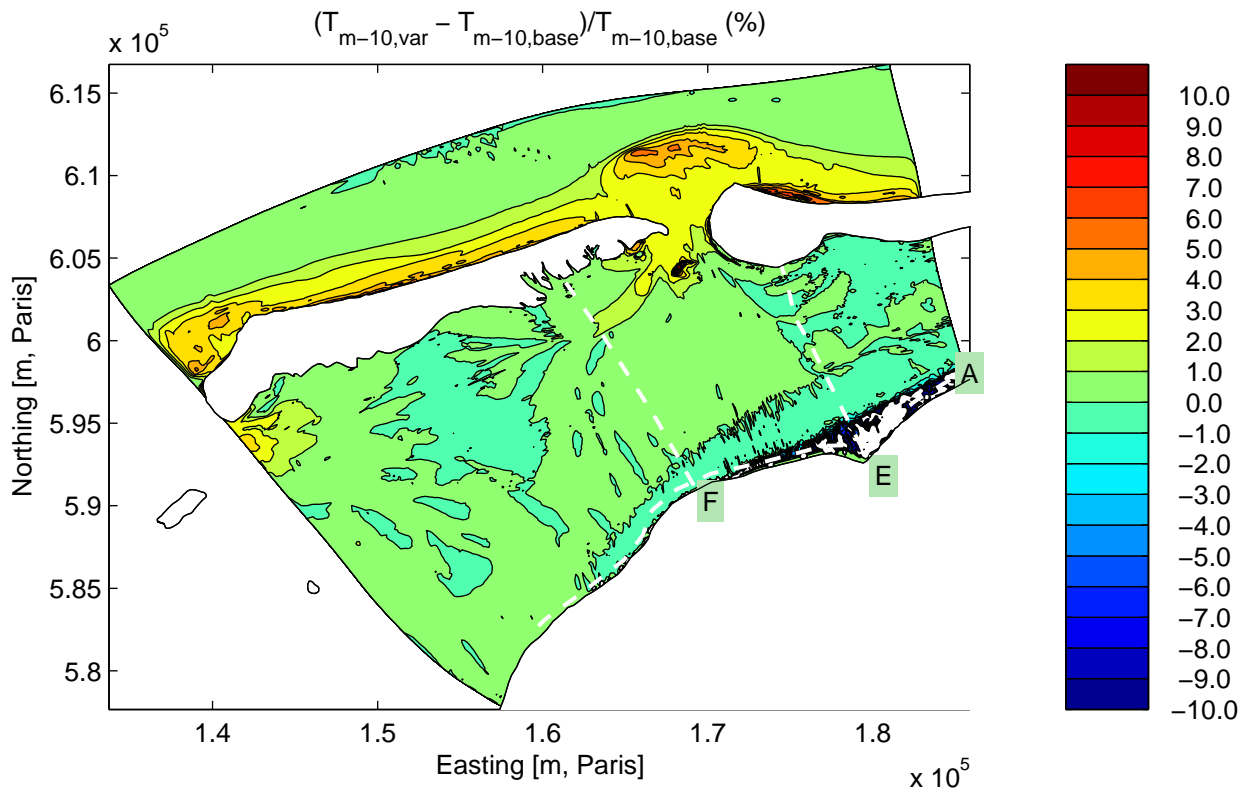
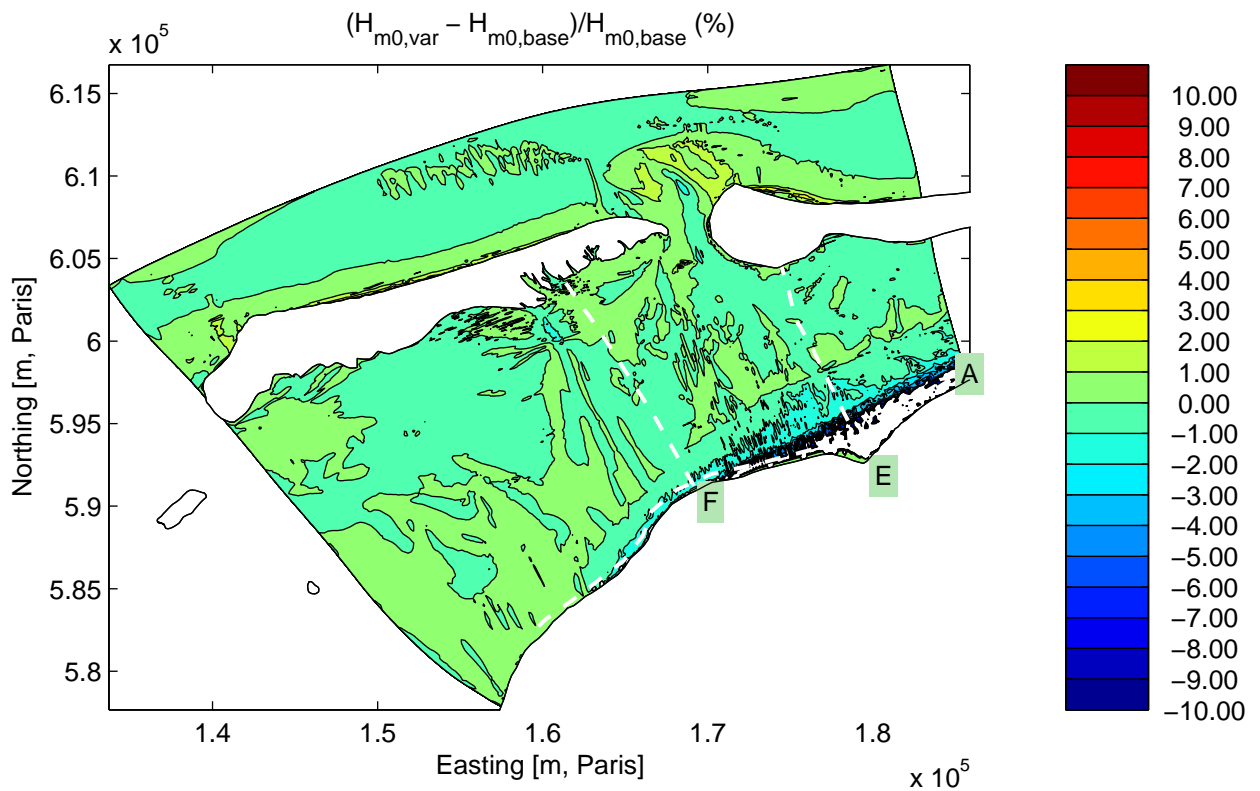
Sensitivity run C2PS6: Reduction in strength of depth-induced breaking
Integral parameters along Curve F

Sensitivity analysis Ameland



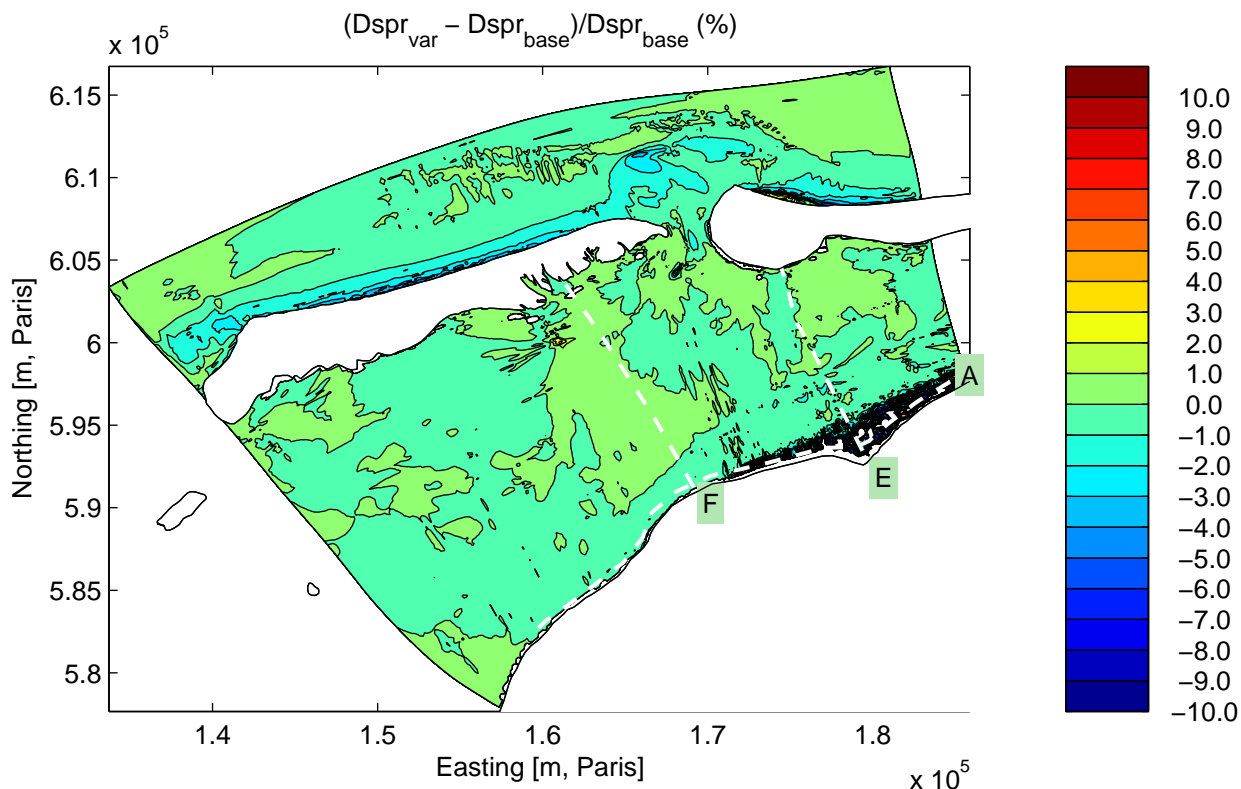
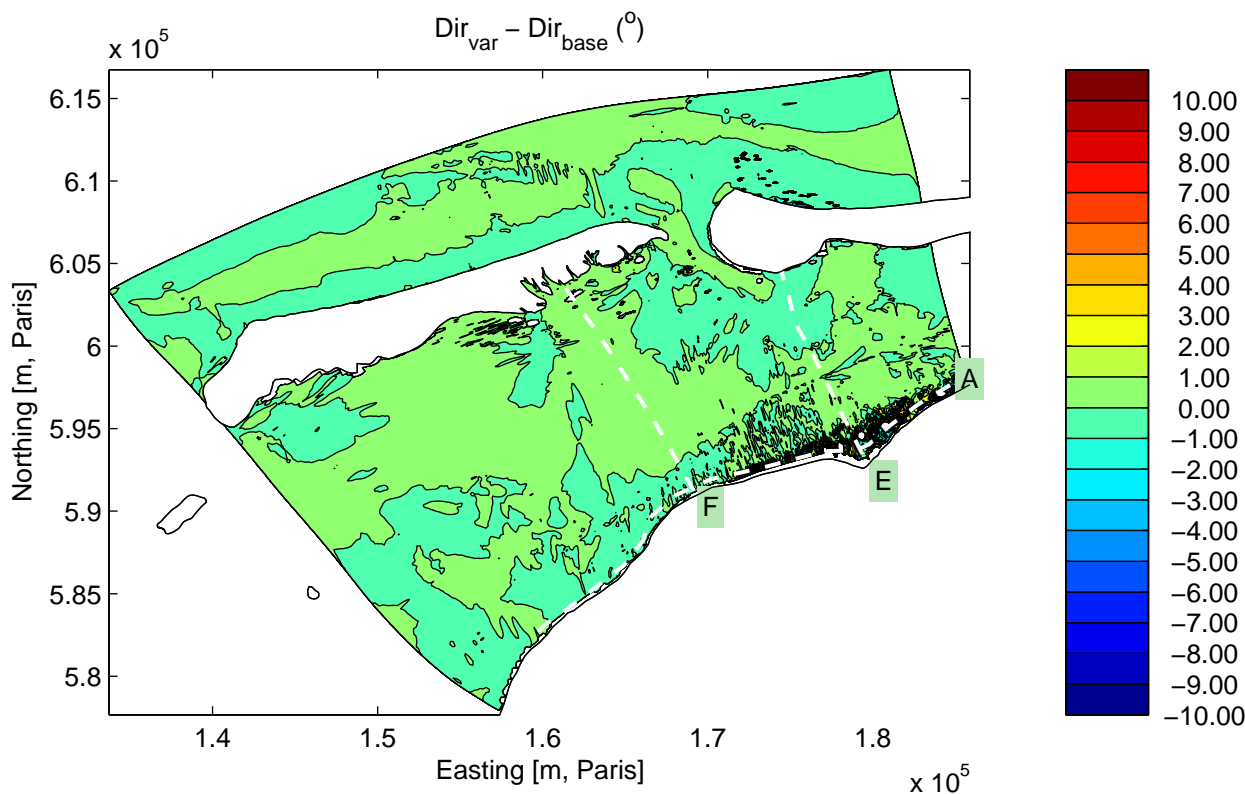
Sensitivity run C2PS6: Reduction in strength of depth-induced breaking
Integral parameters along Curve A

Sensitivity analysis Ameland



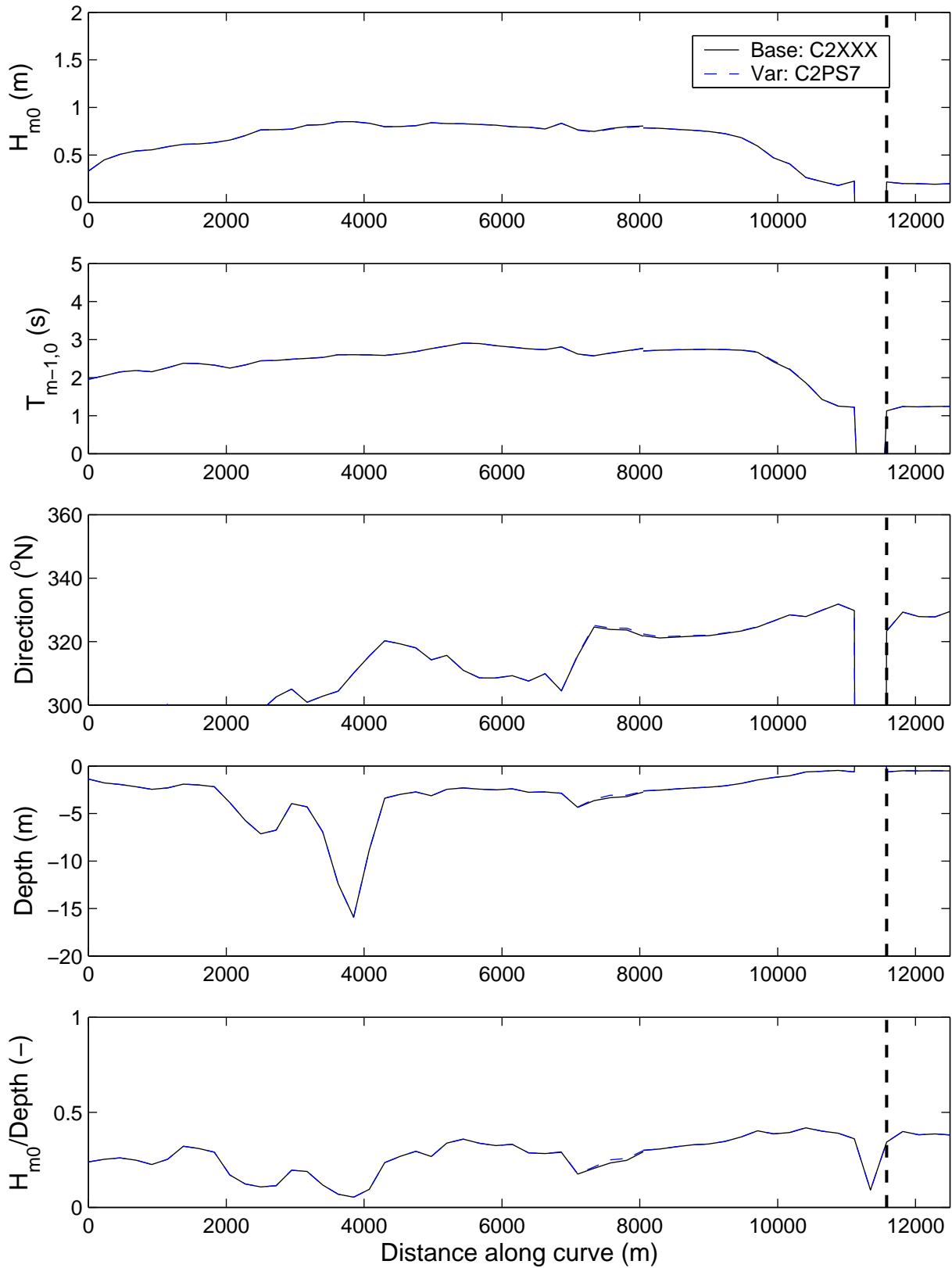
Sensitivity run C2PS7: Reduction in strength of triad interaction
Differences in significant wave height (above) and mean period (below).

Sensitivity analysis Ameland



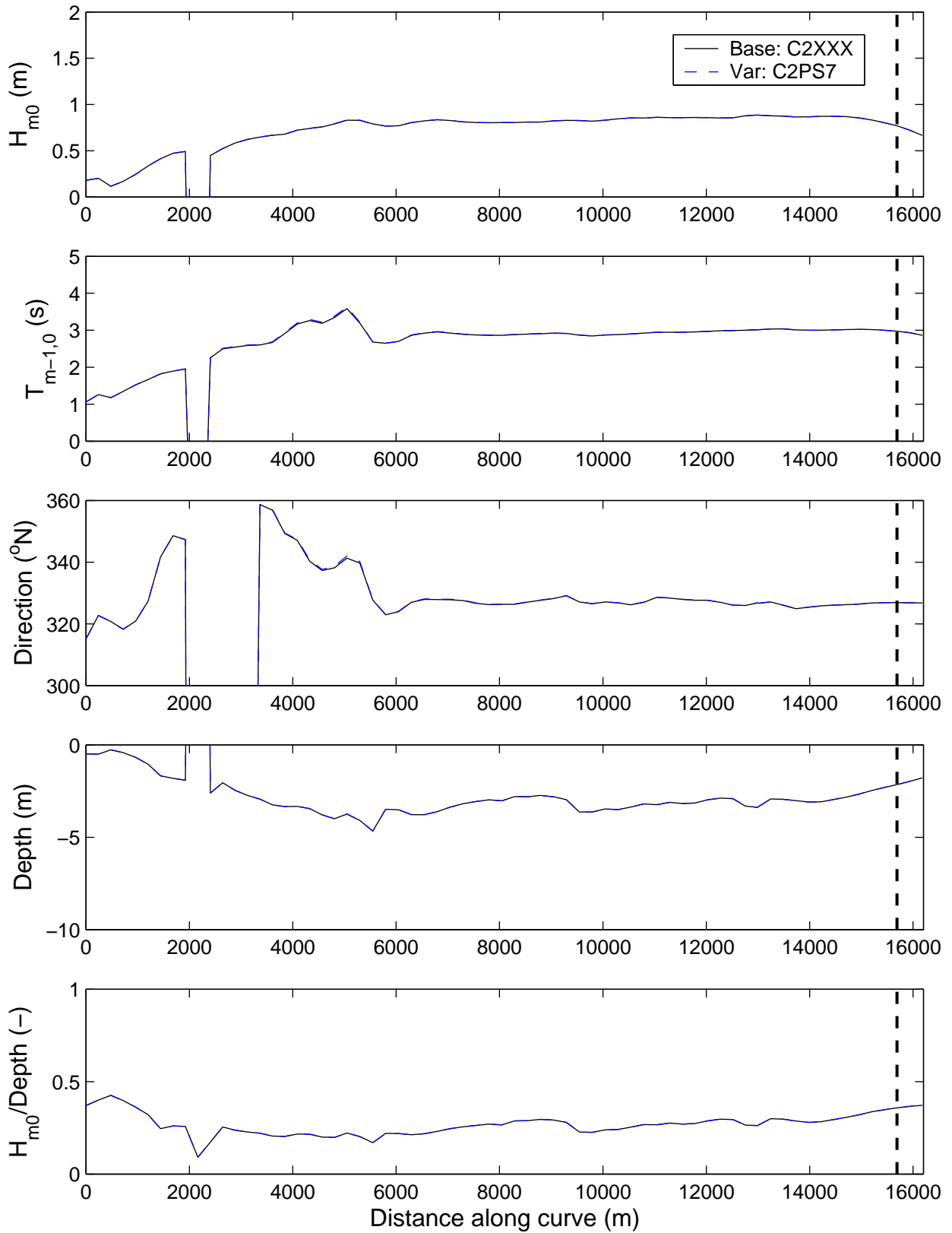
Sensitivity run C2PS7: Reduction in strength of triad interaction
Differences in mean direction (above) and directional spreading (below).

Sensitivity analysis Ameland



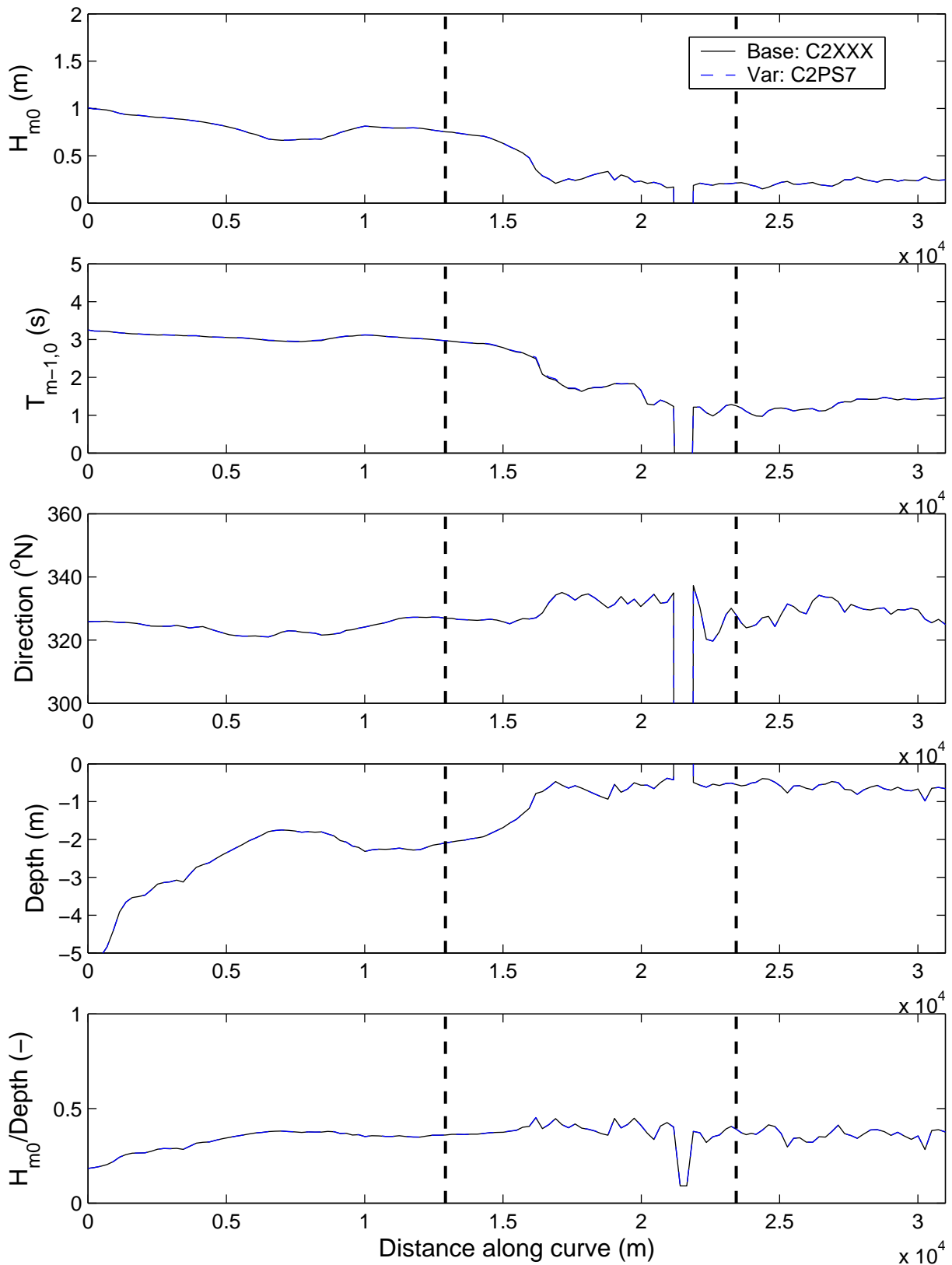
Sensitivity run C2PS7: Reduction in strength of triad interaction
Integral parameters along Curve E

Sensitivity analysis Ameland



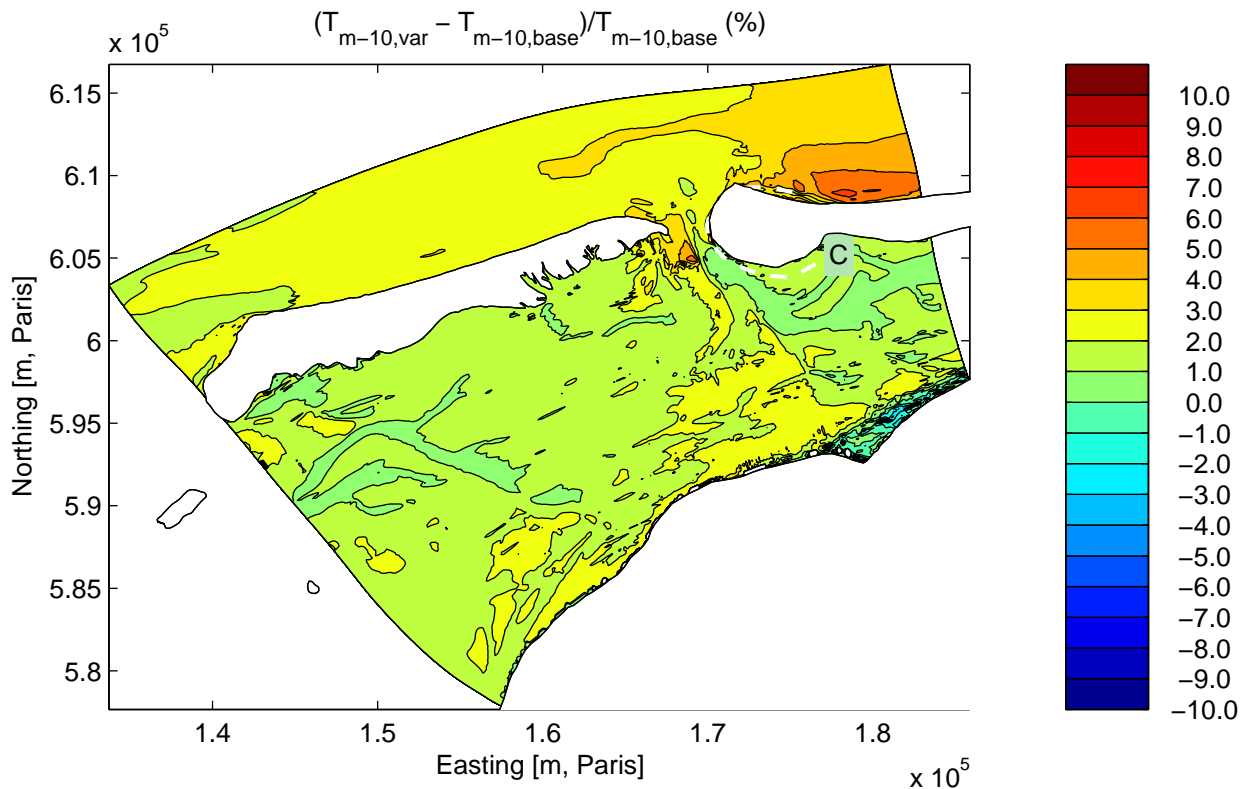
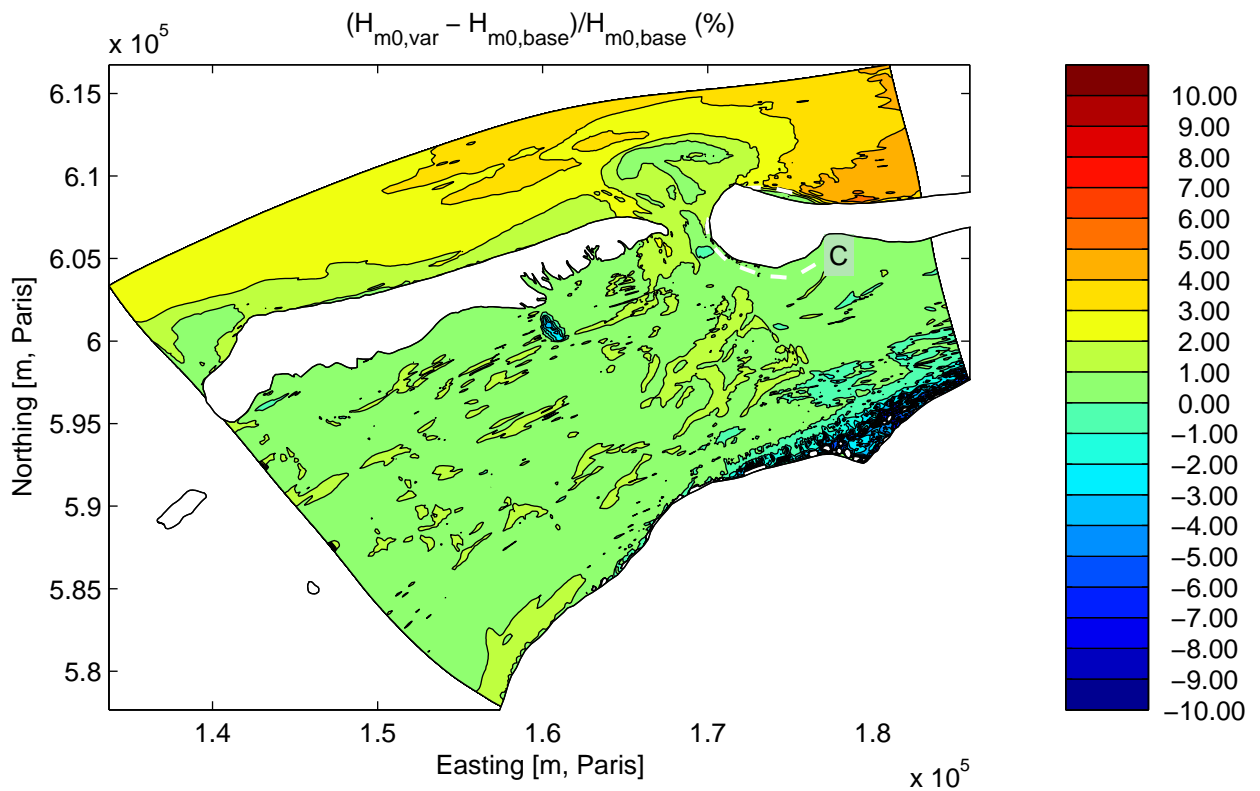
Sensitivity run C2PS7: Reduction in strength of triad interaction
Integral parameters along Curve F

Sensitivity analysis Ameland



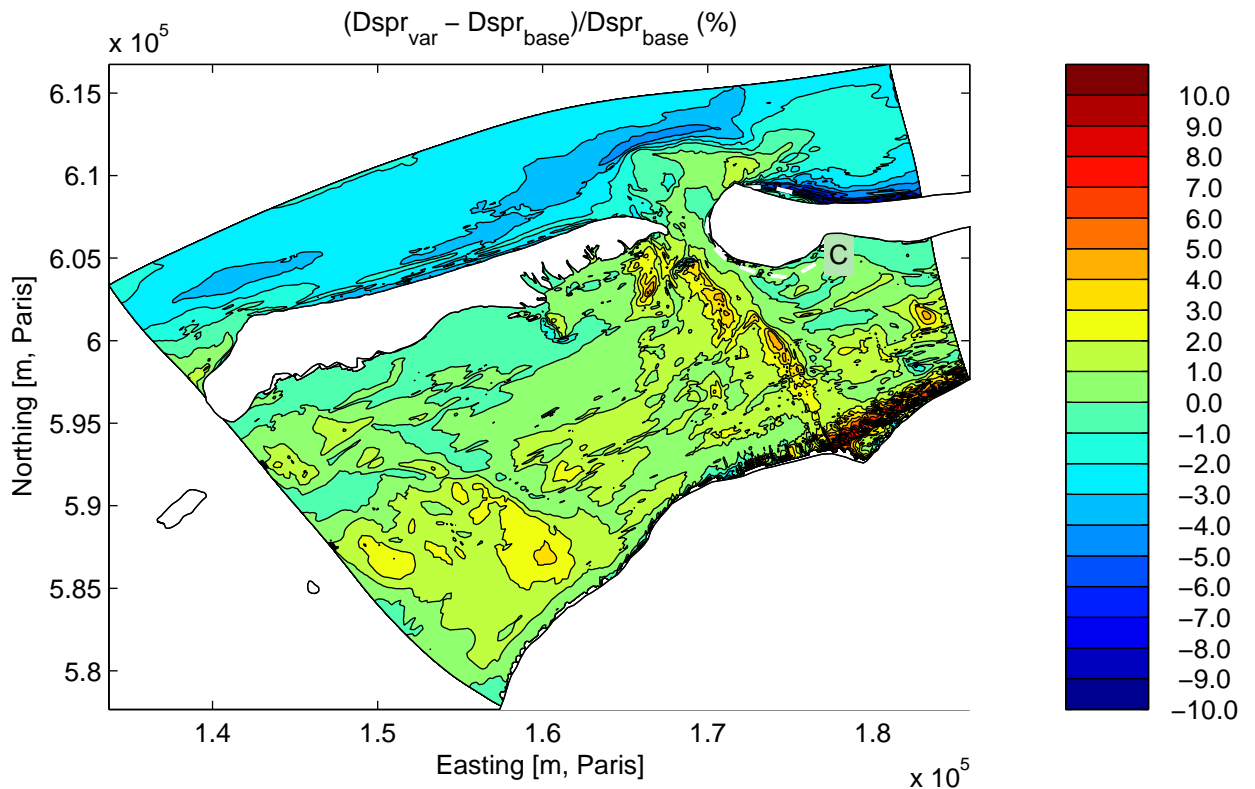
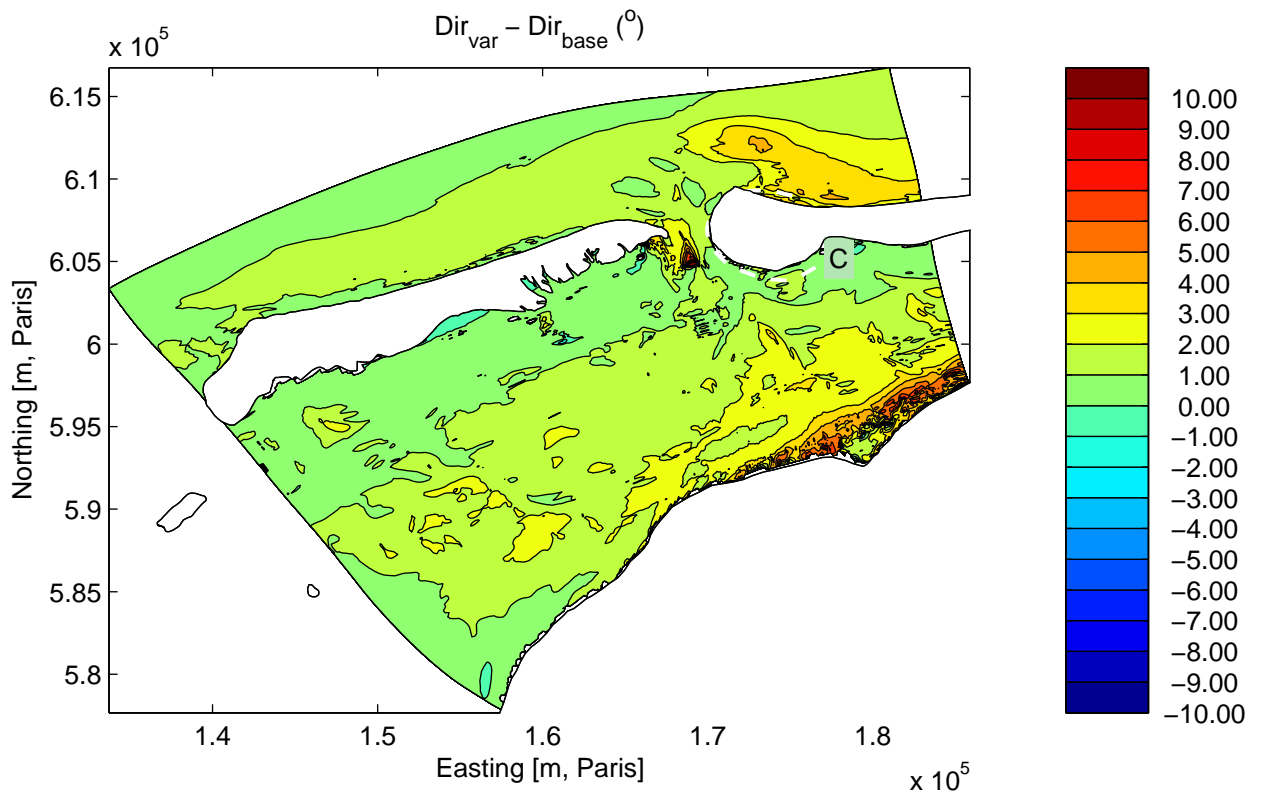
Sensitivity run C2PS7: Reduction in strength of triad interaction
Integral parameters along Curve A

Sensitivity analysis Ameland



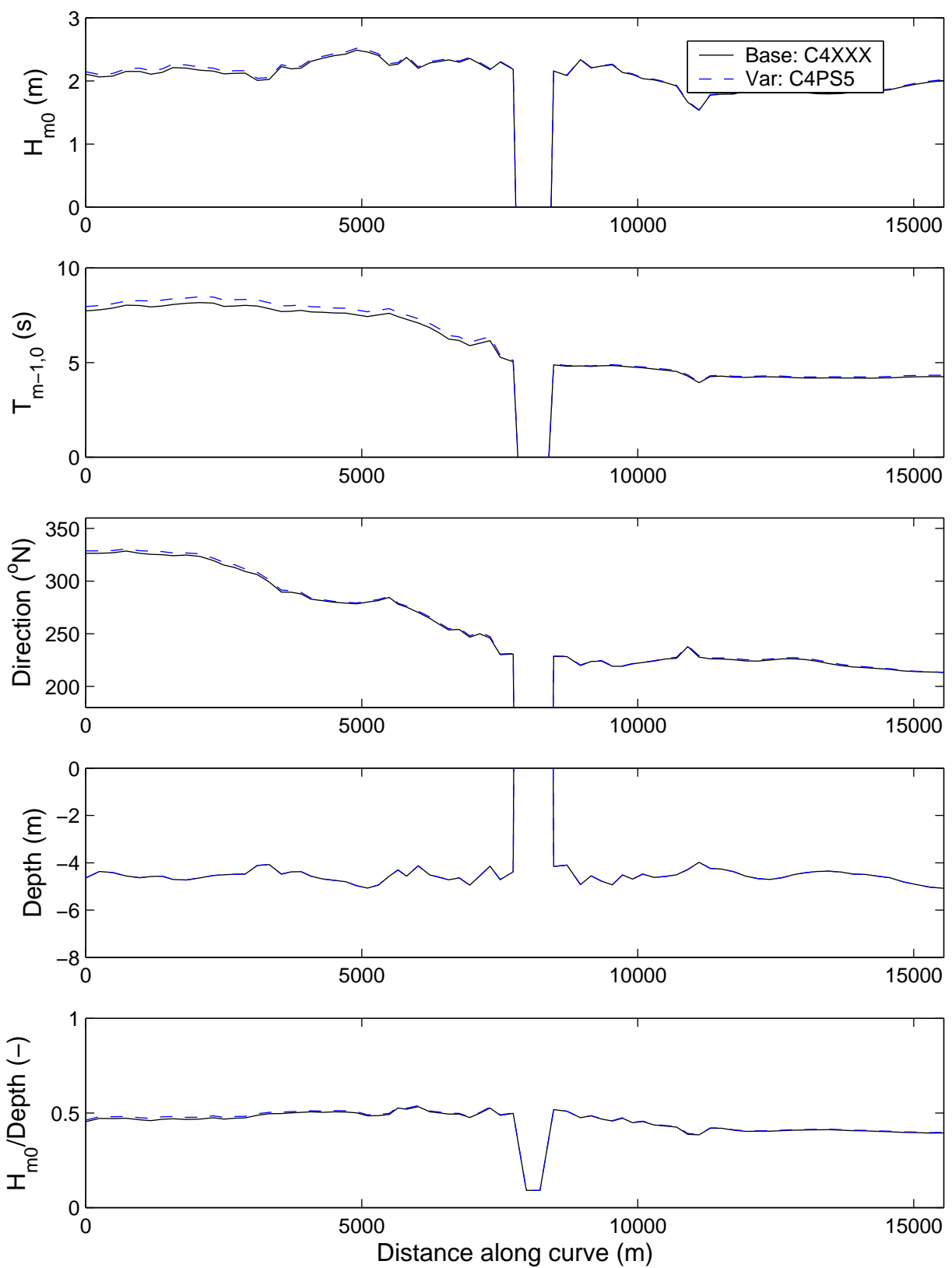
Sensitivity run C4PS5: Reduction in strength of bottom friction
Differences in significant wave height (above) and mean period (below).

Sensitivity analysis Ameland



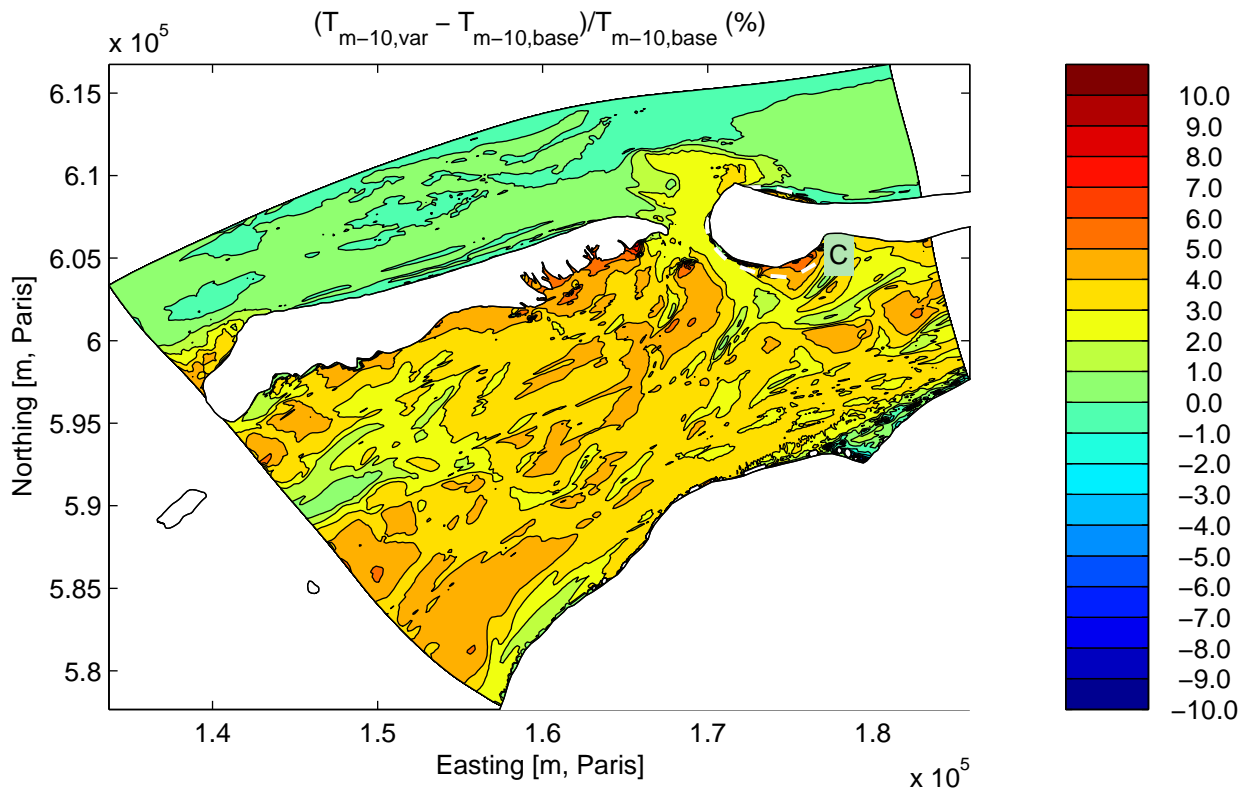
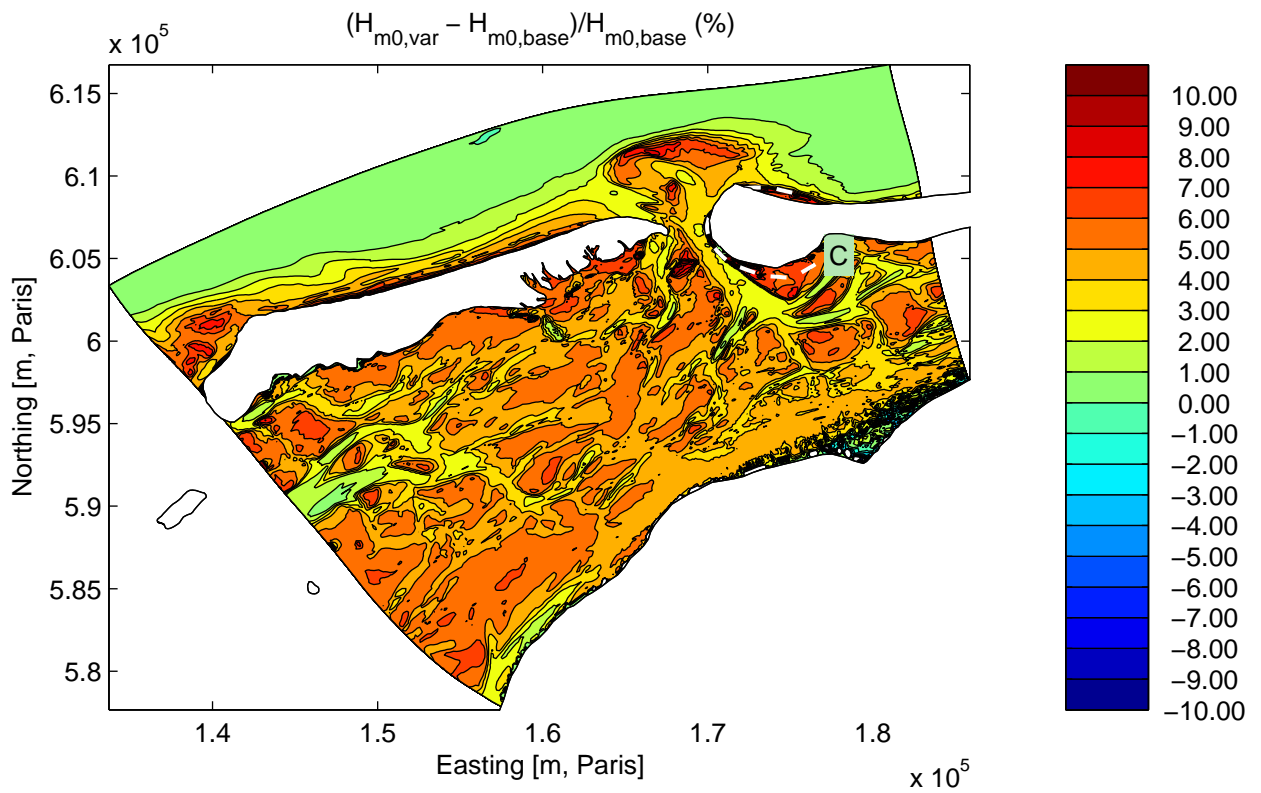
Sensitivity run C4PS5: Reduction in strength of bottom friction
 Differences in mean direction (above) and directional spreading (below).

Sensitivity analysis Ameland



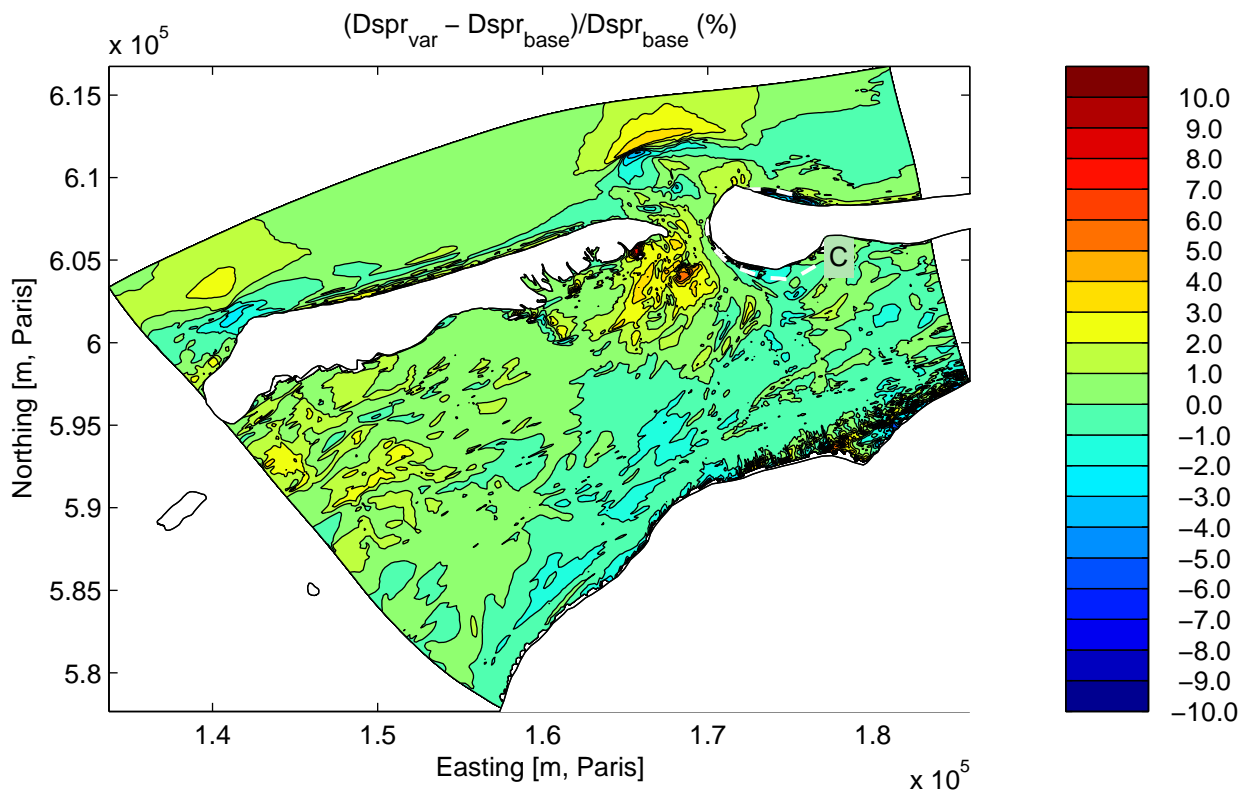
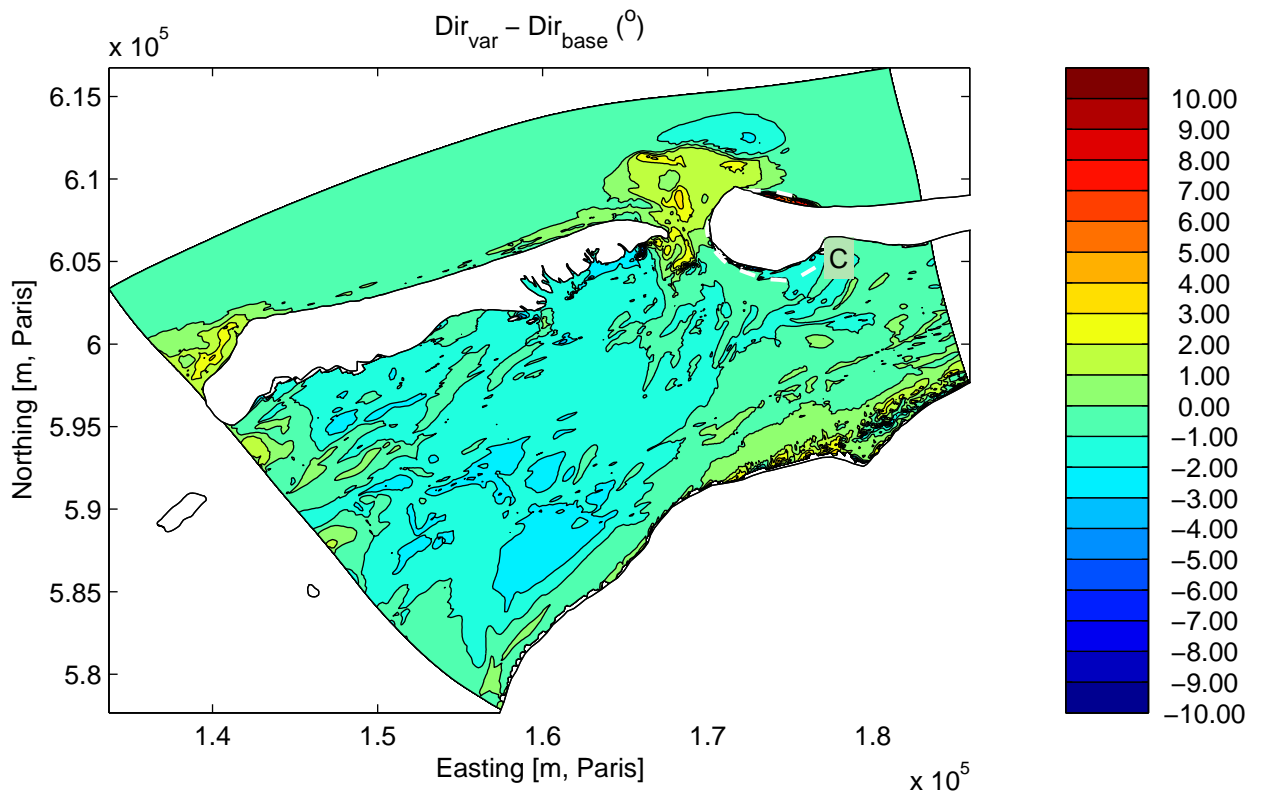
Sensitivity run C4PS5: Reduction in strength of bottom friction
Integral parameters along Curve C

Sensitivity analysis Ameland



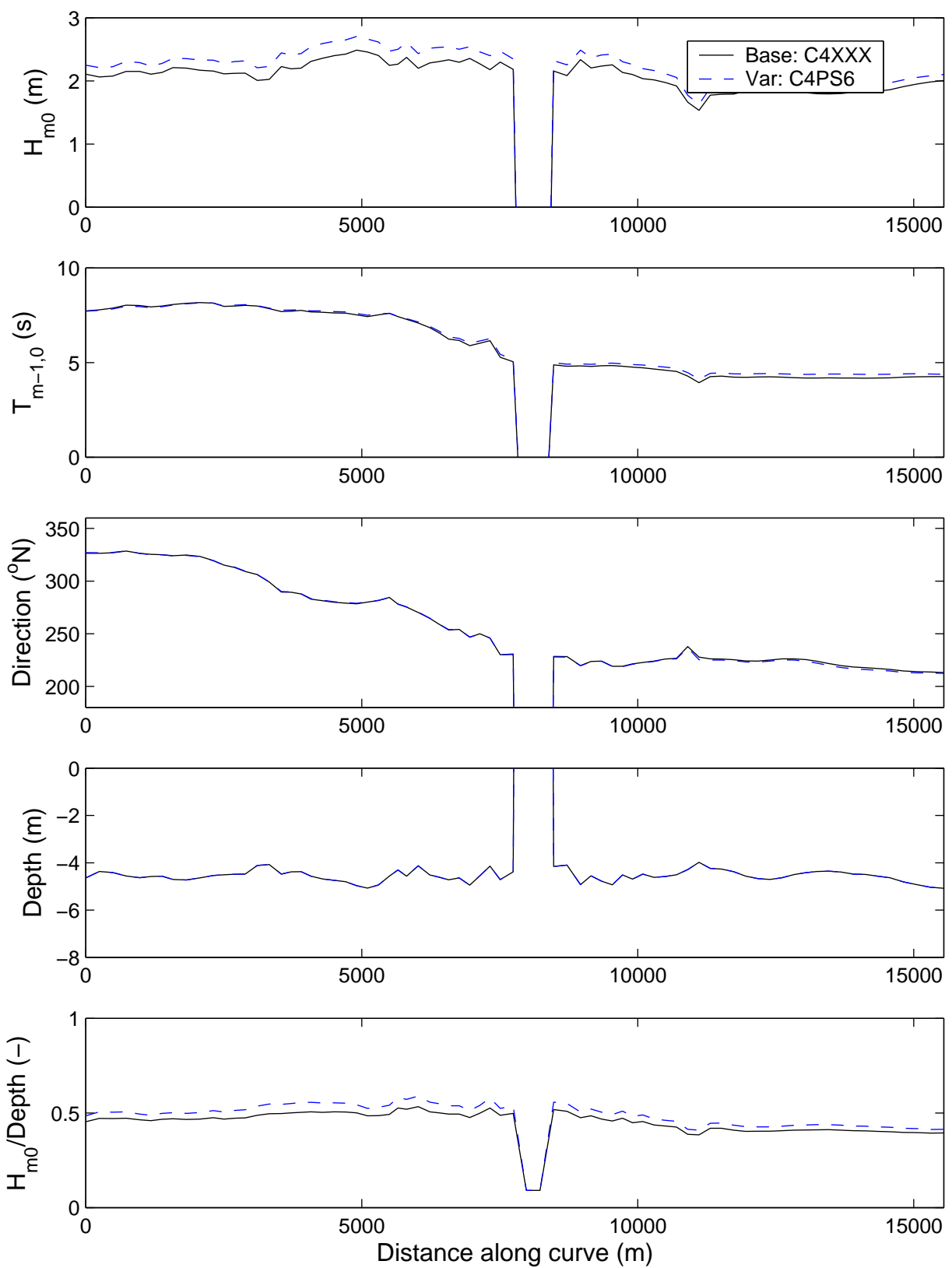
Sensitivity run C4PS6: Reduction in strength of depth-induced breaking
Differences in significant wave height (above) and mean period (below).

Sensitivity analysis Ameland



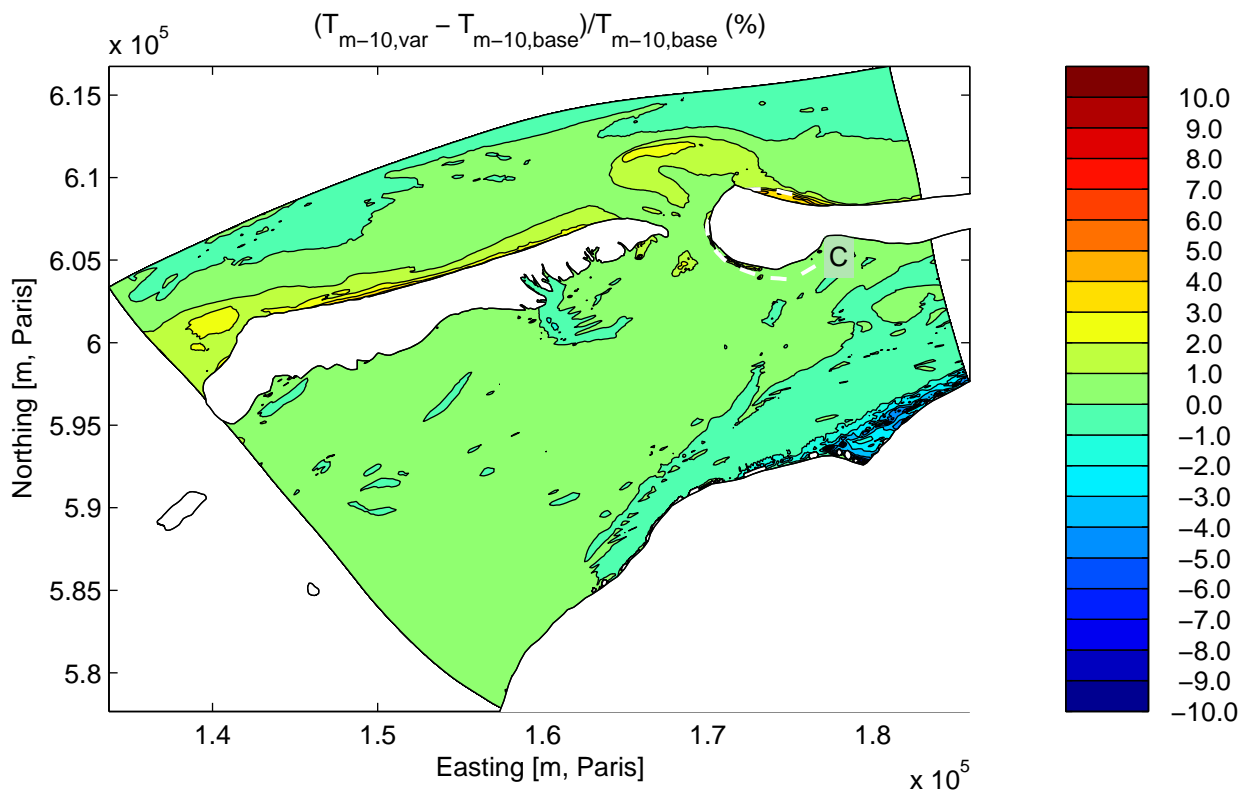
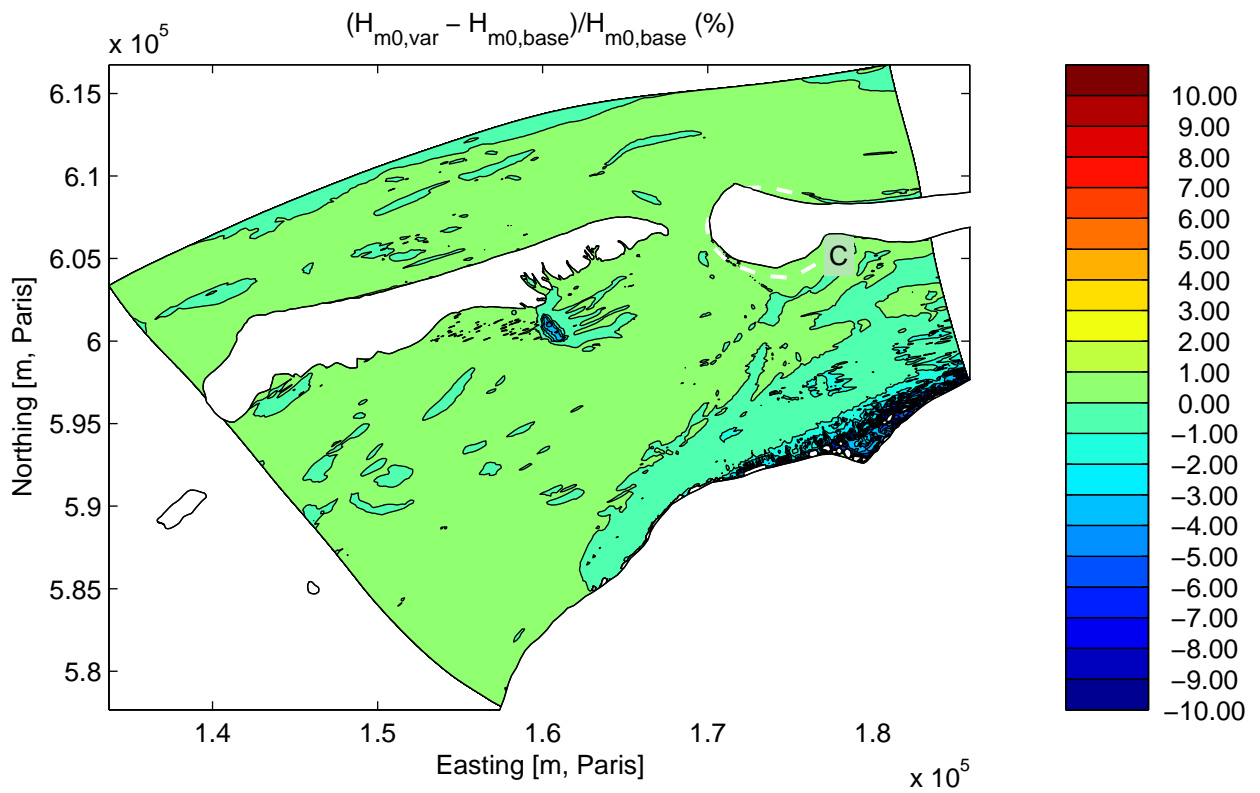
Sensitivity run C4PS6: Reduction in strength of depth-induced breaking
Differences in mean direction (above) and directional spreading (below).

Sensitivity analysis Ameland



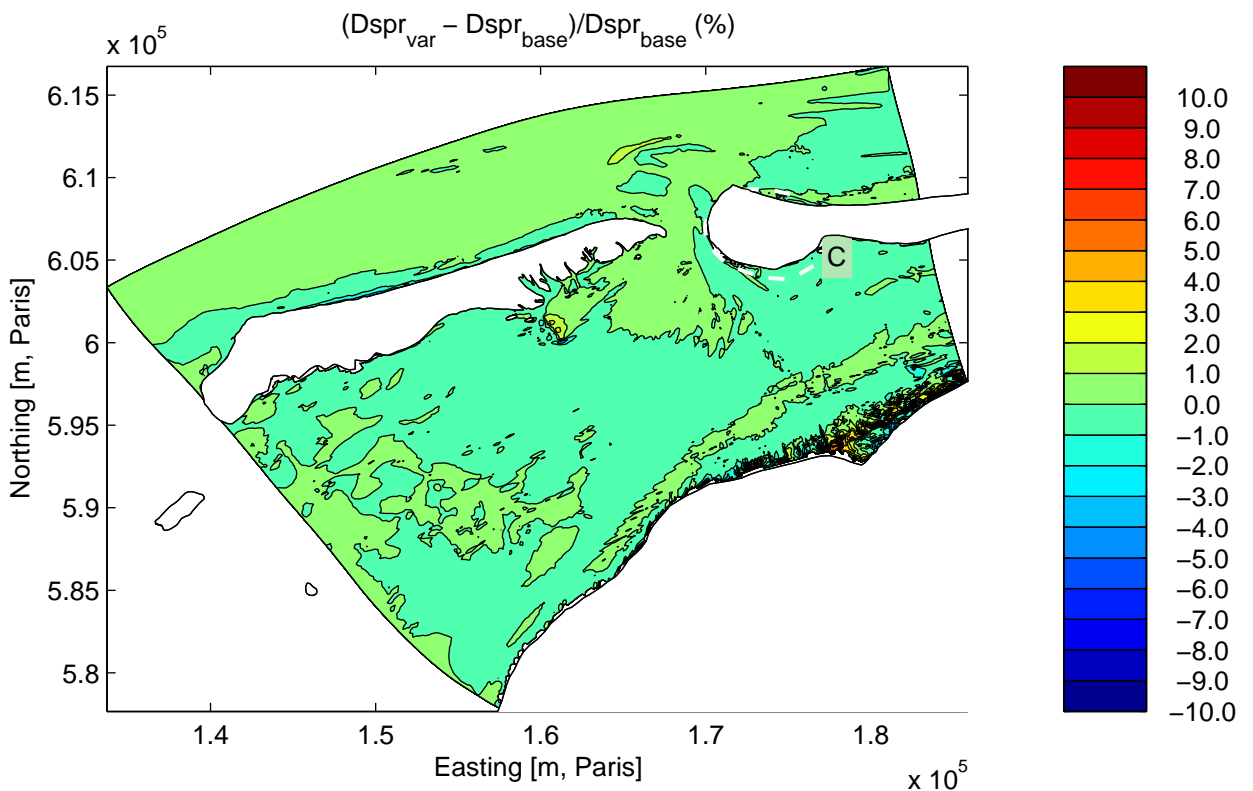
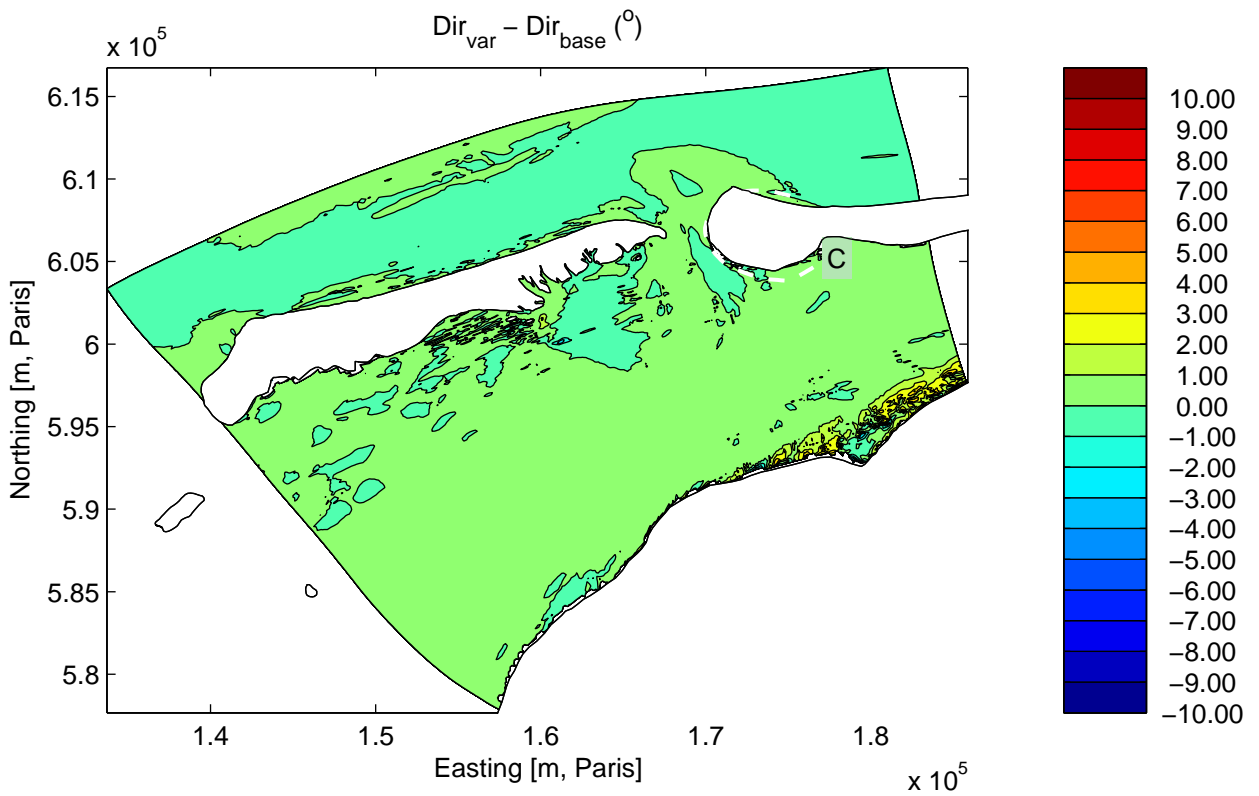
Sensitivity run C4PS6: Reduction in strength of depth-induced breaking
Integral parameters along Curve C

Sensitivity analysis Ameland



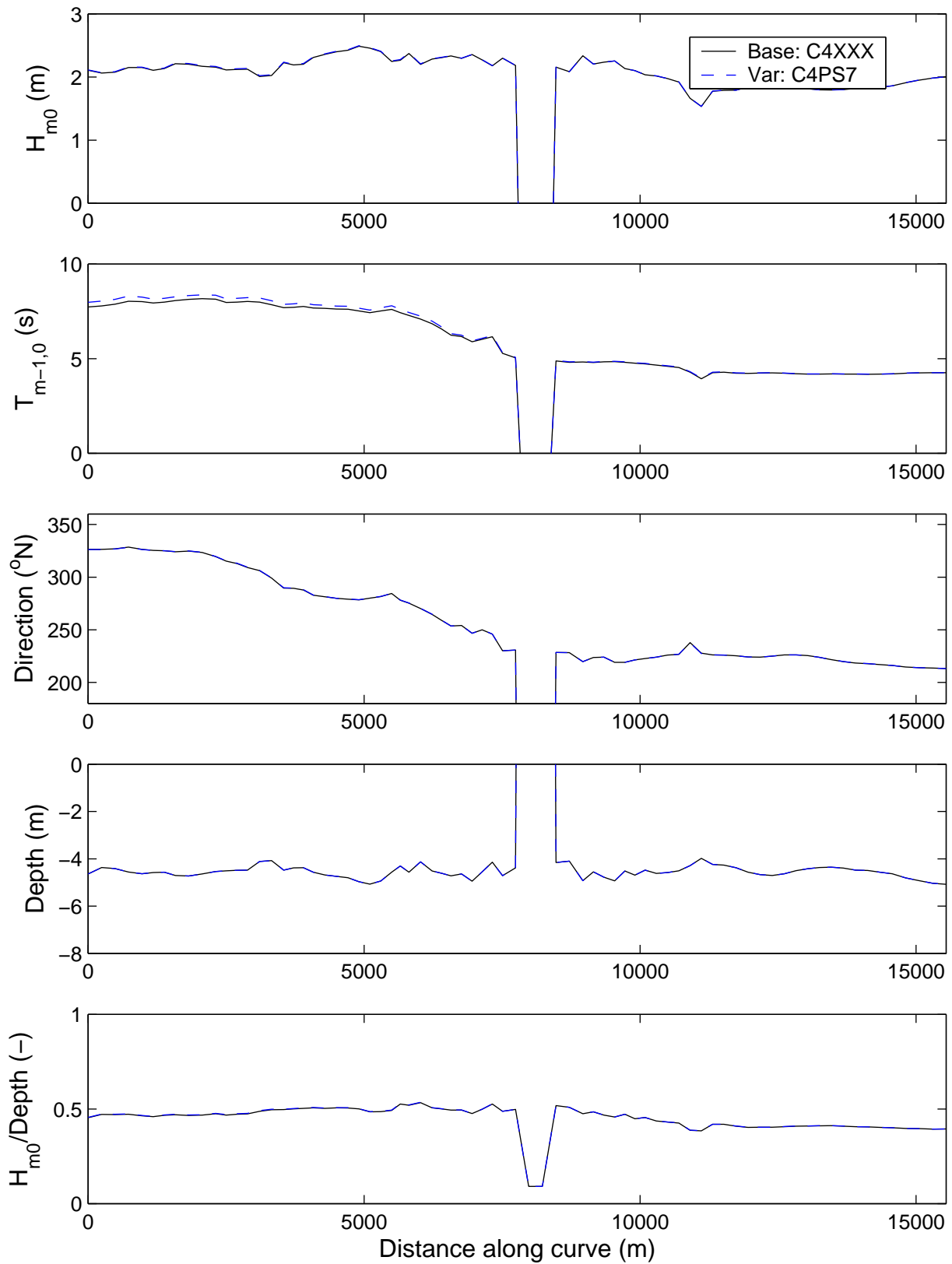
Sensitivity run C4PS7: Reduction in strength of triad interaction
Differences in significant wave height (above) and mean period (below).

Sensitivity analysis Ameland



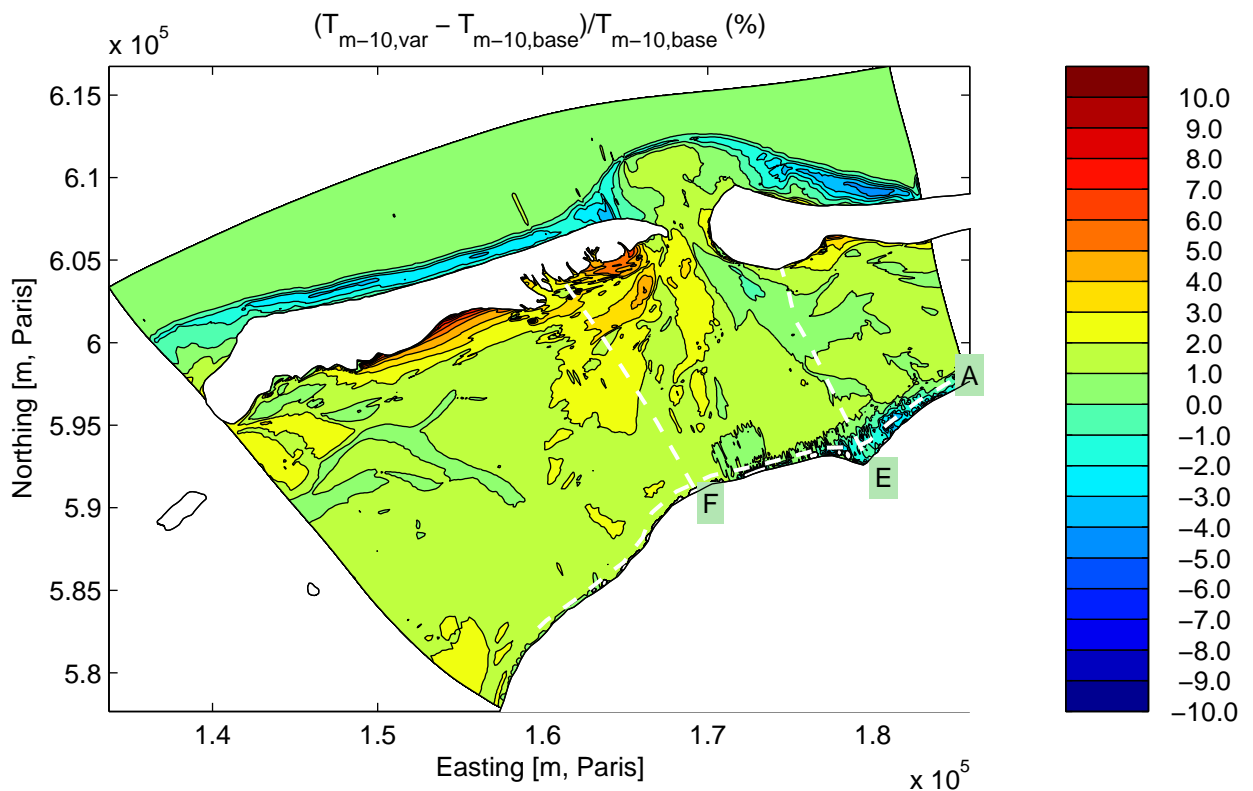
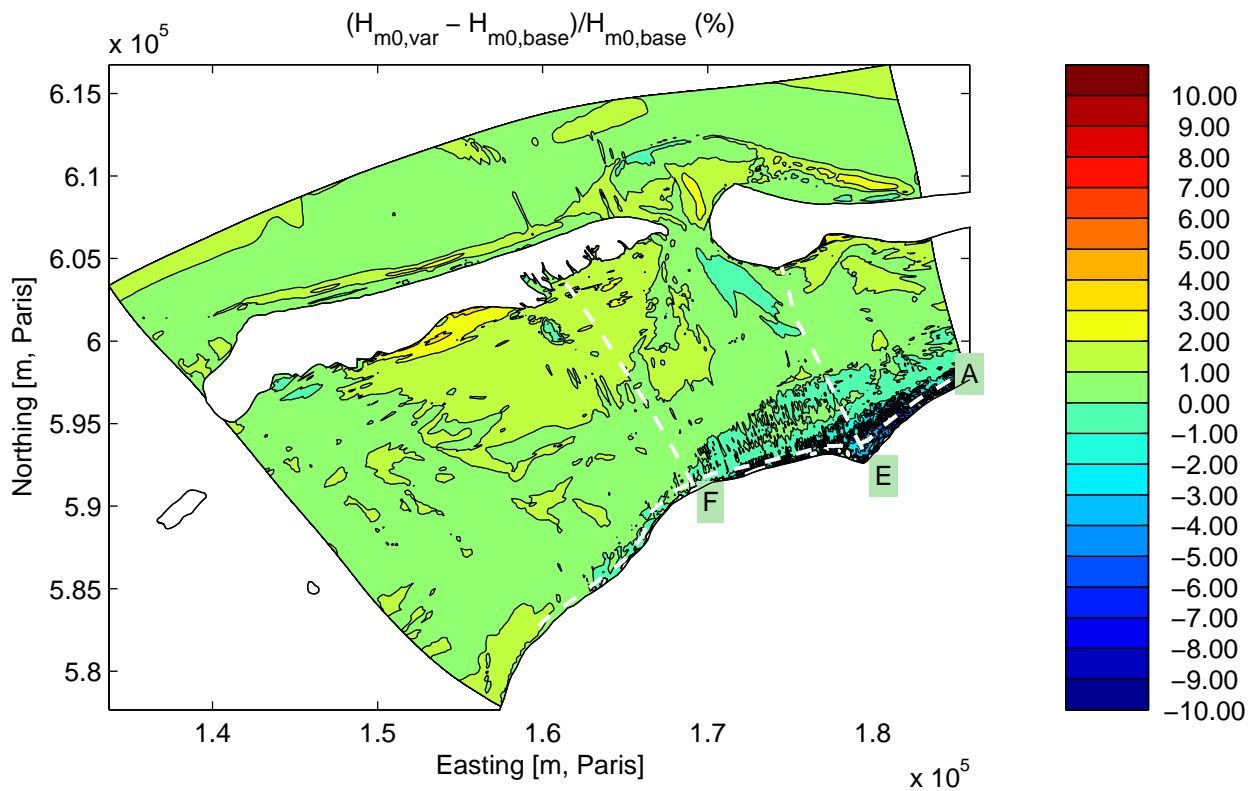
Sensitivity run C4PS7: Reduction in strength of triad interaction
Differences in mean direction (above) and directional spreading (below).

Sensitivity analysis Ameland



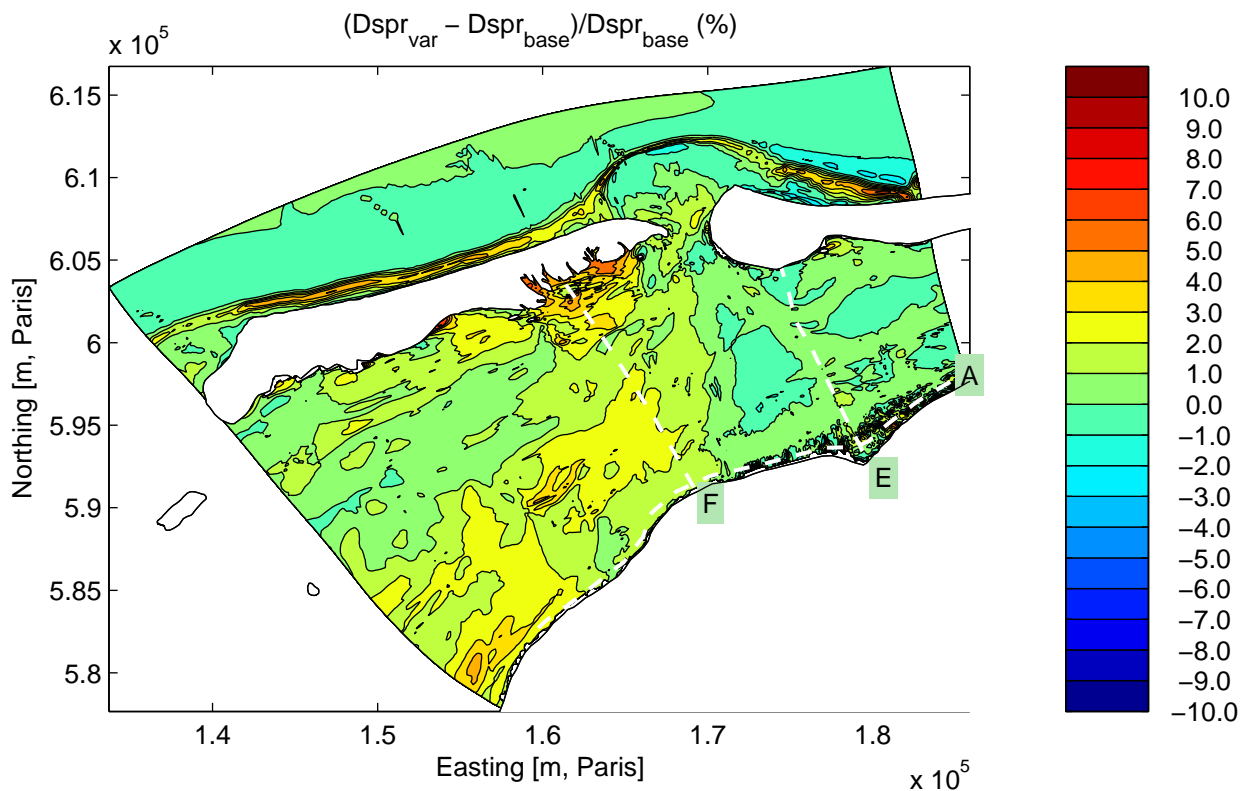
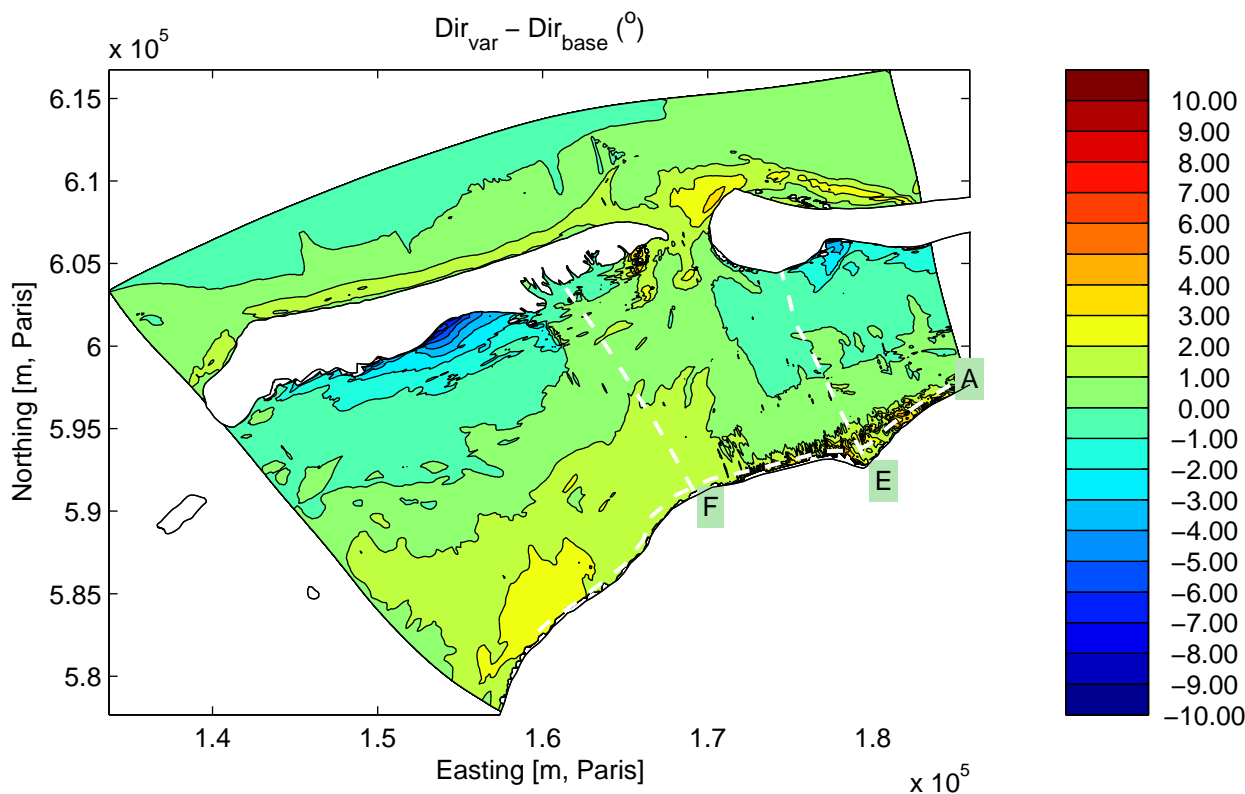
Sensitivity run C4PS7: Reduction in strength of triad interaction
Integral parameters along Curve C

Sensitivity analysis Ameland



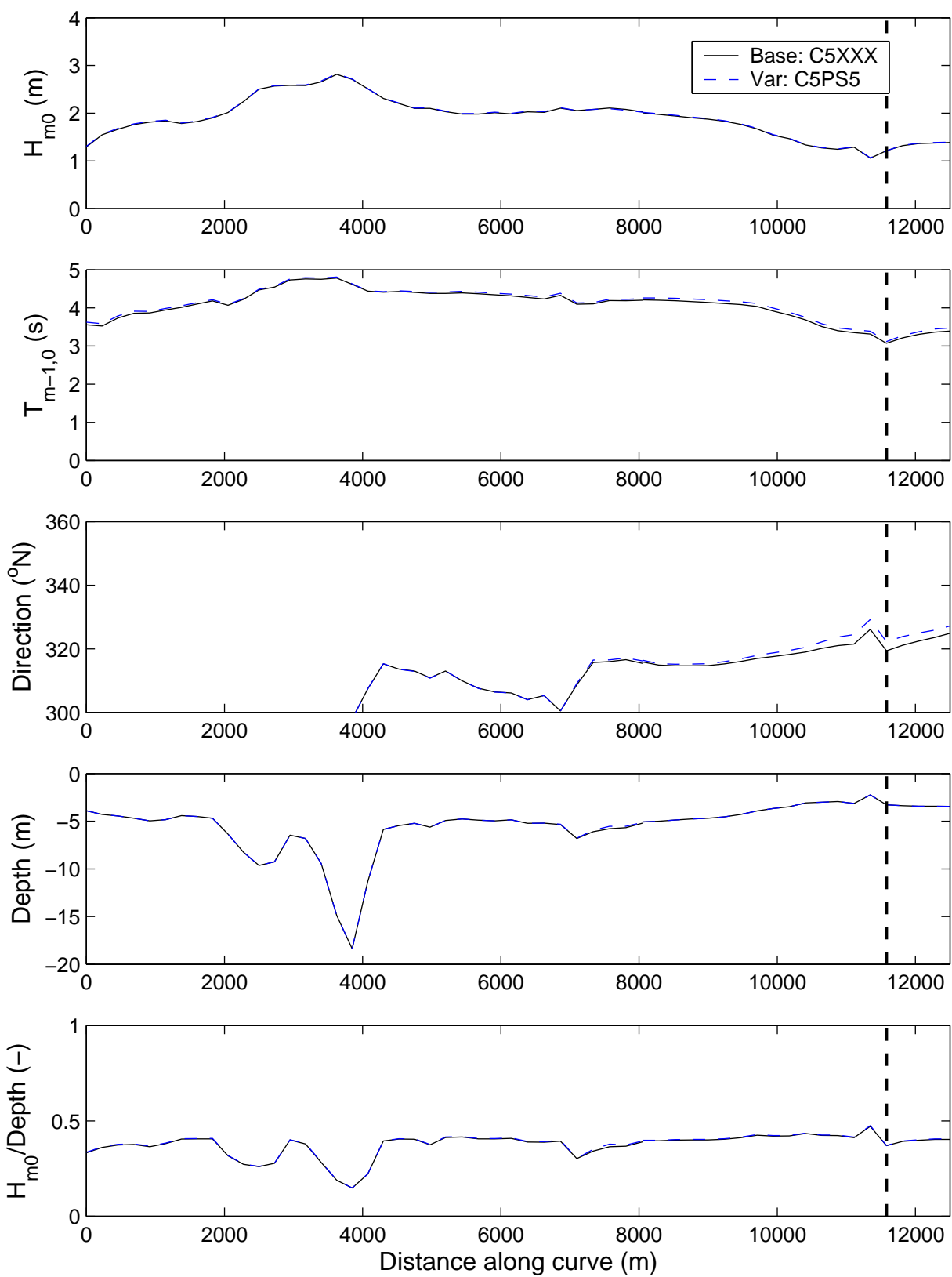
Sensitivity run C5PS5: Reduction in strength of bottom friction
Differences in significant wave height (above) and mean period (below).

Sensitivity analysis Ameland



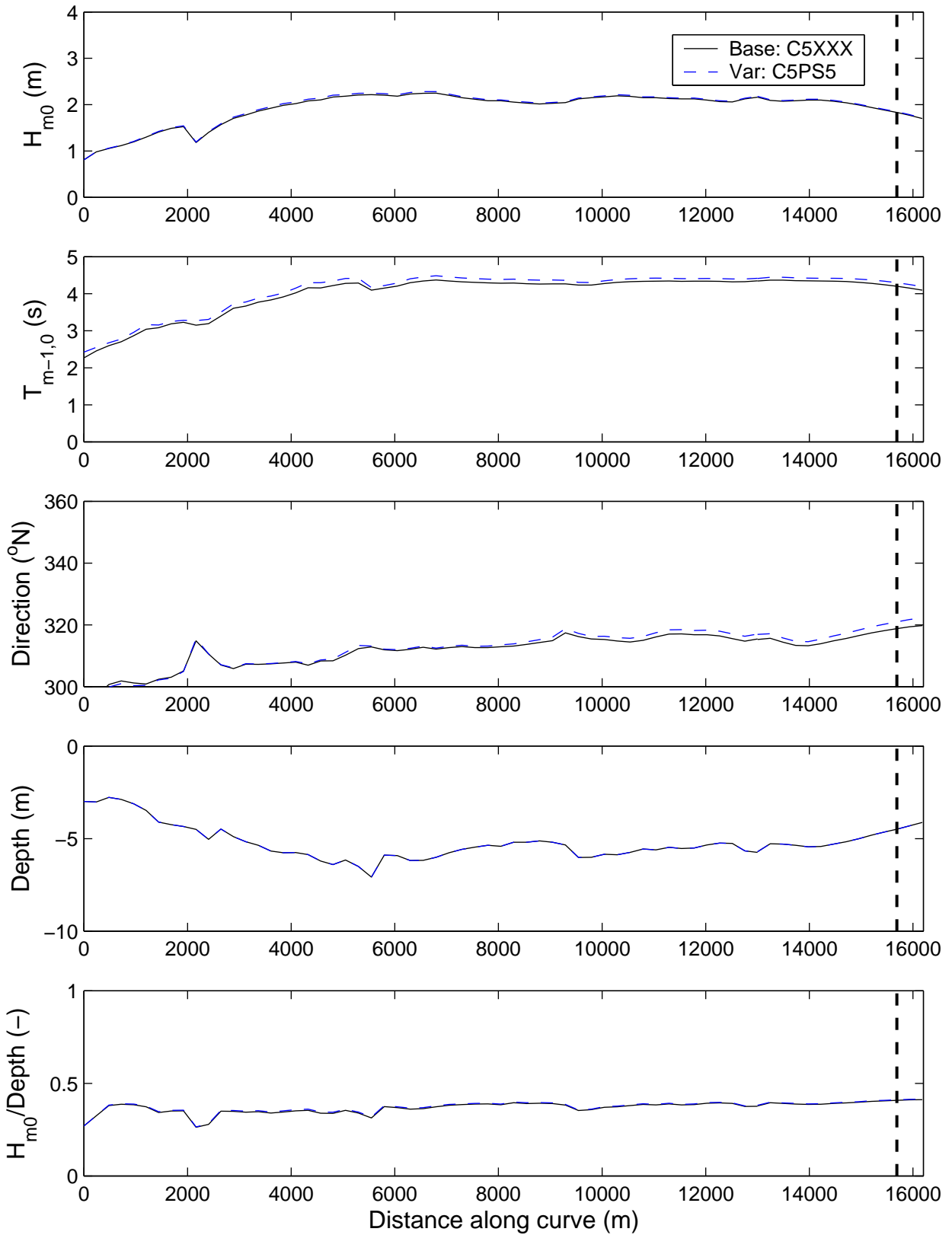
Sensitivity run C5PS5: Reduction in strength of bottom friction
 Differences in mean direction (above) and directional spreading (below).

Sensitivity analysis Ameland



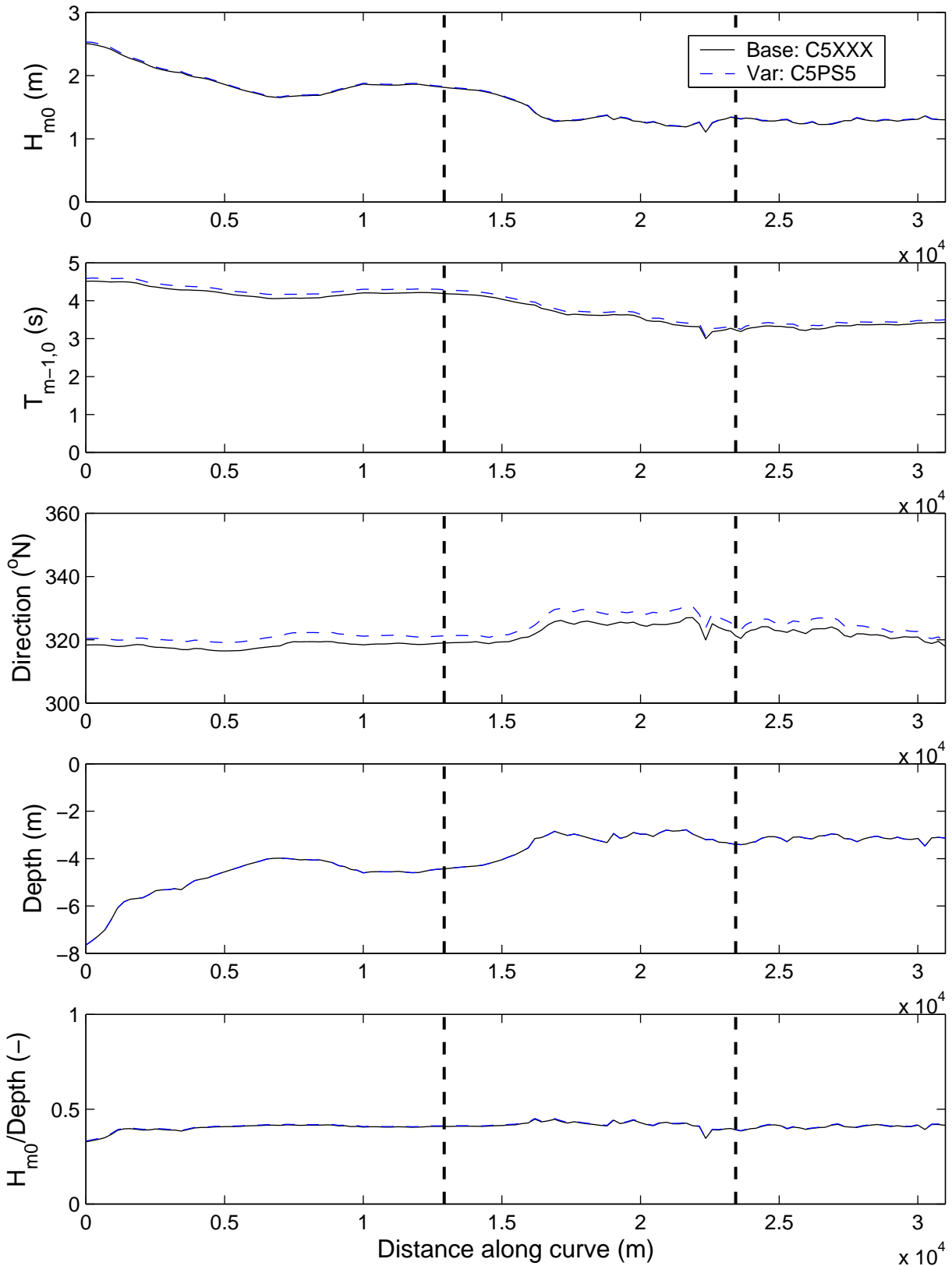
Sensitivity run C5PS5: Reduction in strength of bottom friction
Integral parameters along Curve E

Sensitivity analysis Ameland



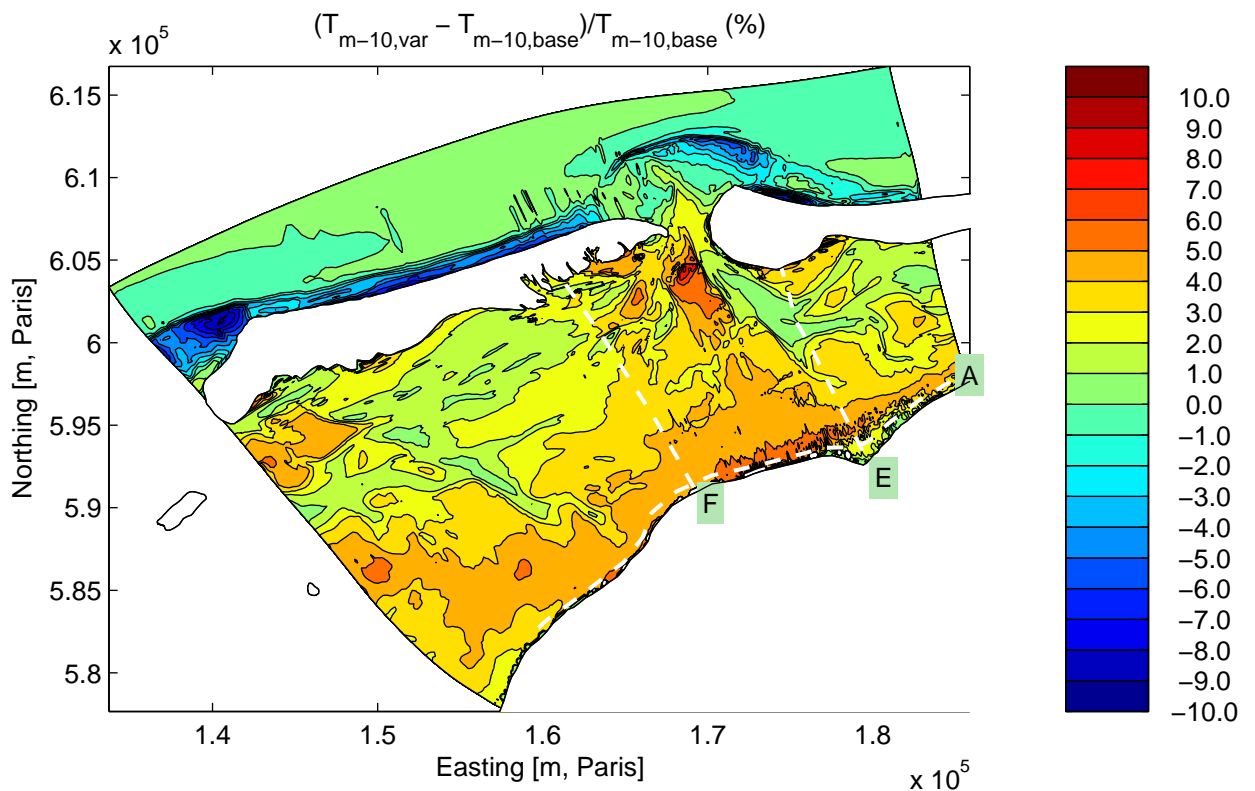
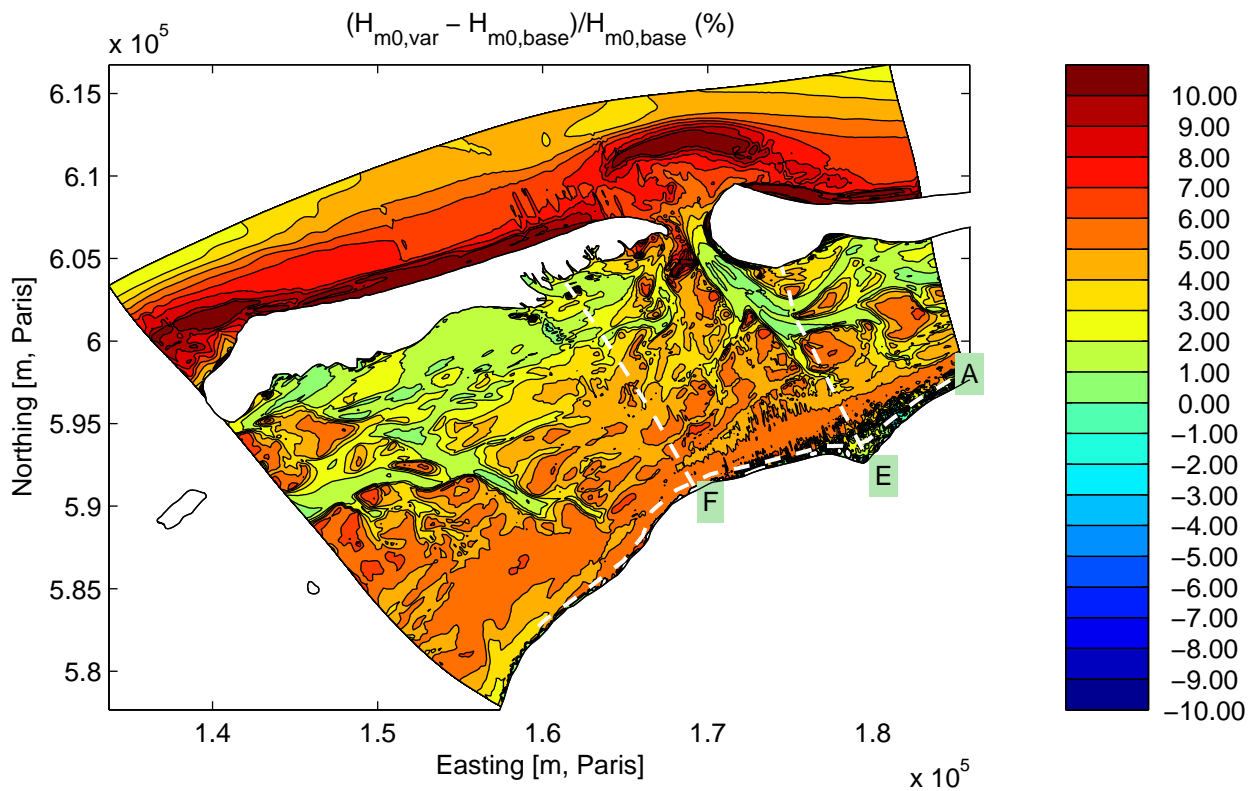
Sensitivity run C5PS5: Reduction in strength of bottom friction
Integral parameters along Curve F

Sensitivity analysis Ameland



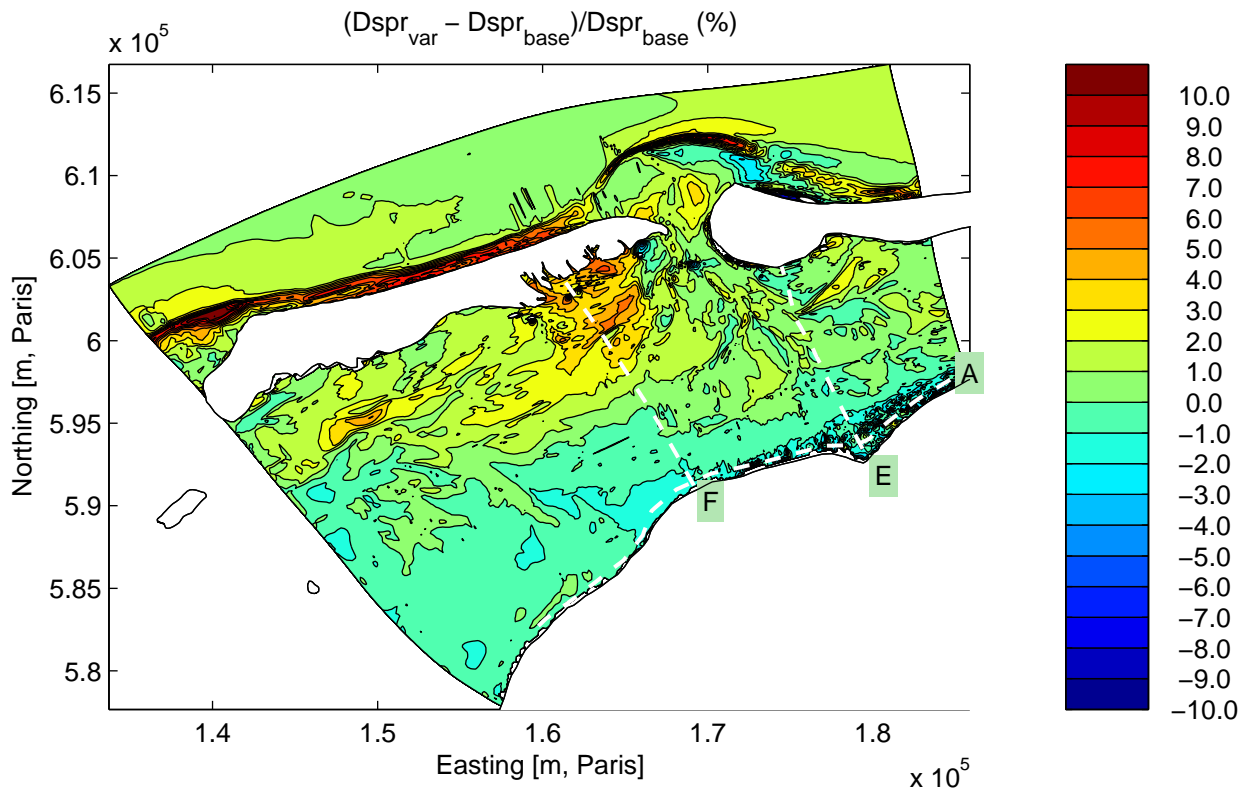
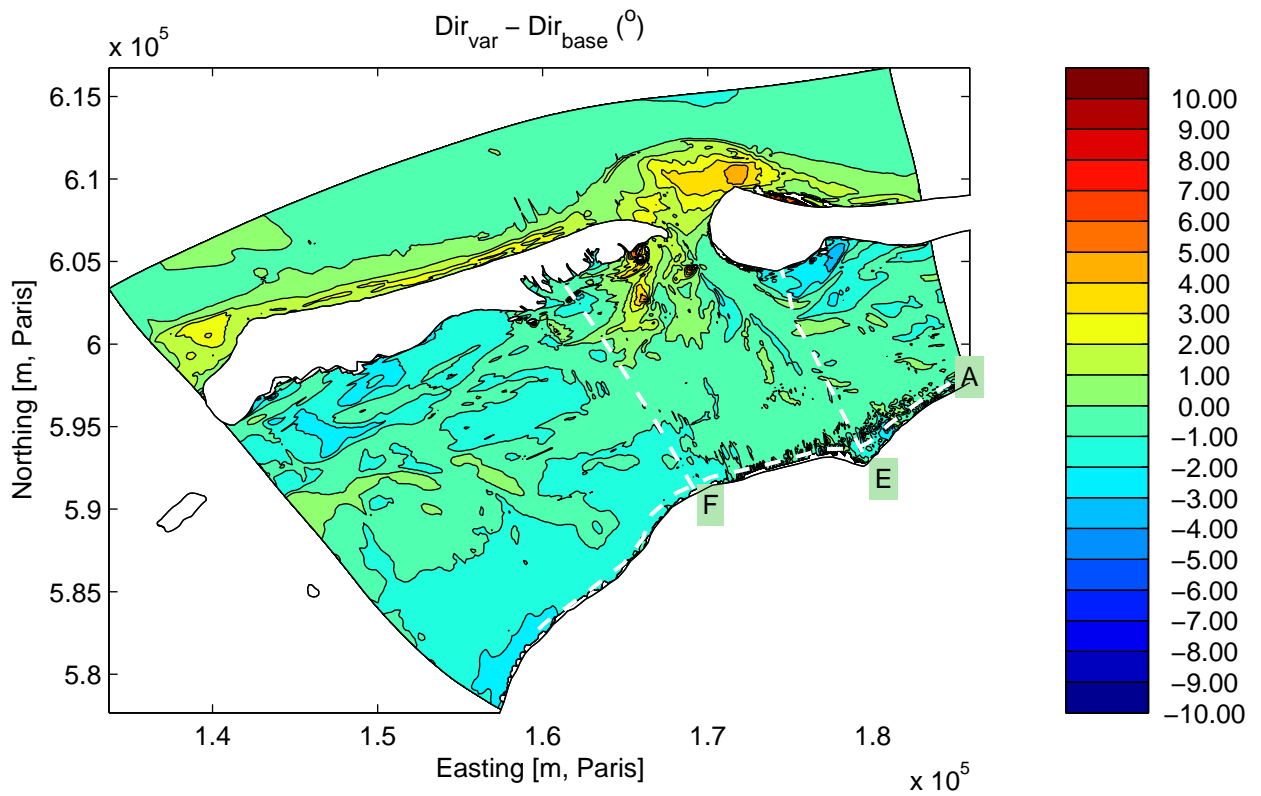
Sensitivity run C5PS5: Reduction in strength of bottom friction
Integral parameters along Curve A

Sensitivity analysis Ameland



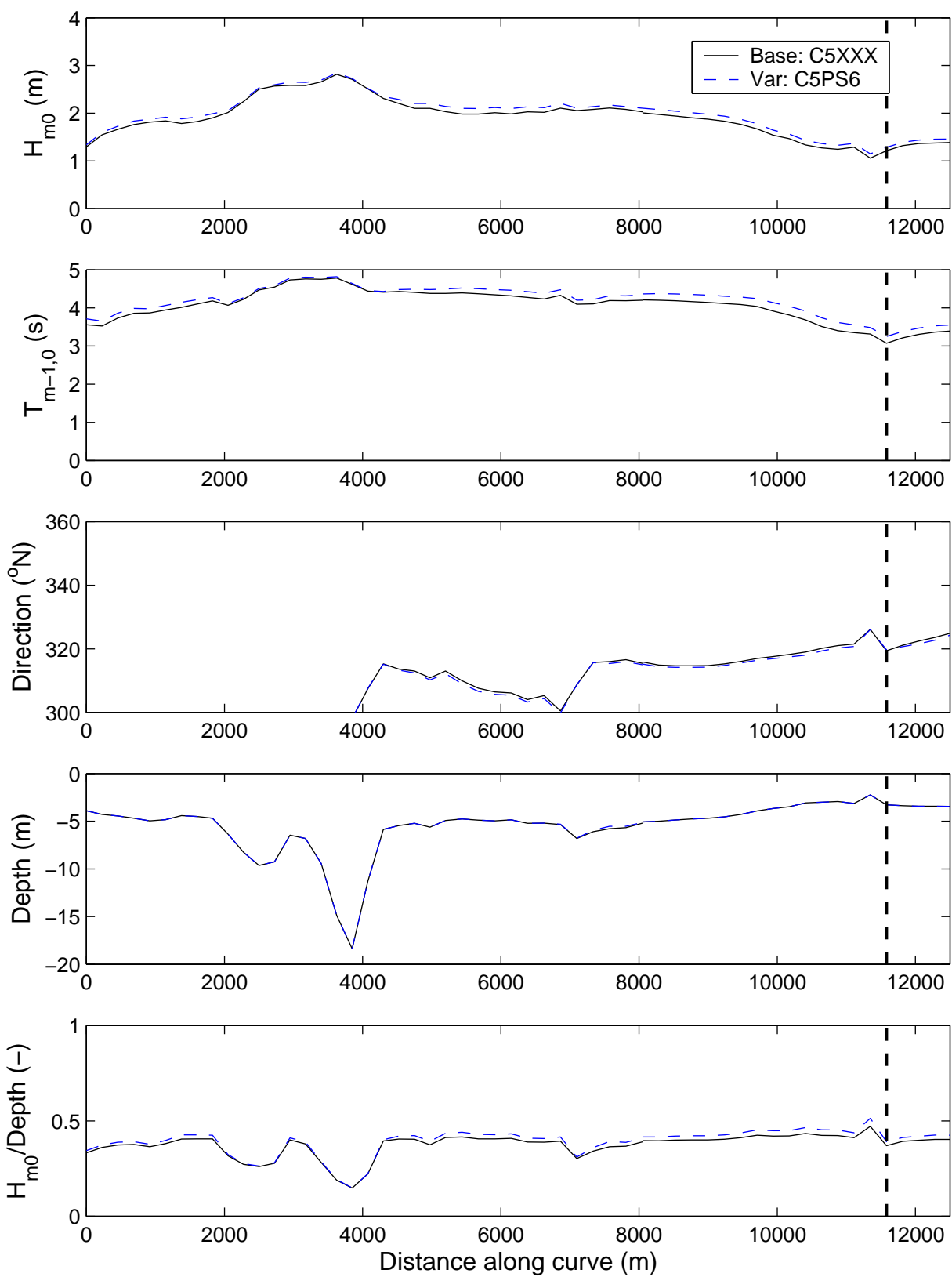
Sensitivity run C5PS6: Reduction in strength of depth-induced breaking
Differences in significant wave height (above) and mean period (below).

Sensitivity analysis Ameland



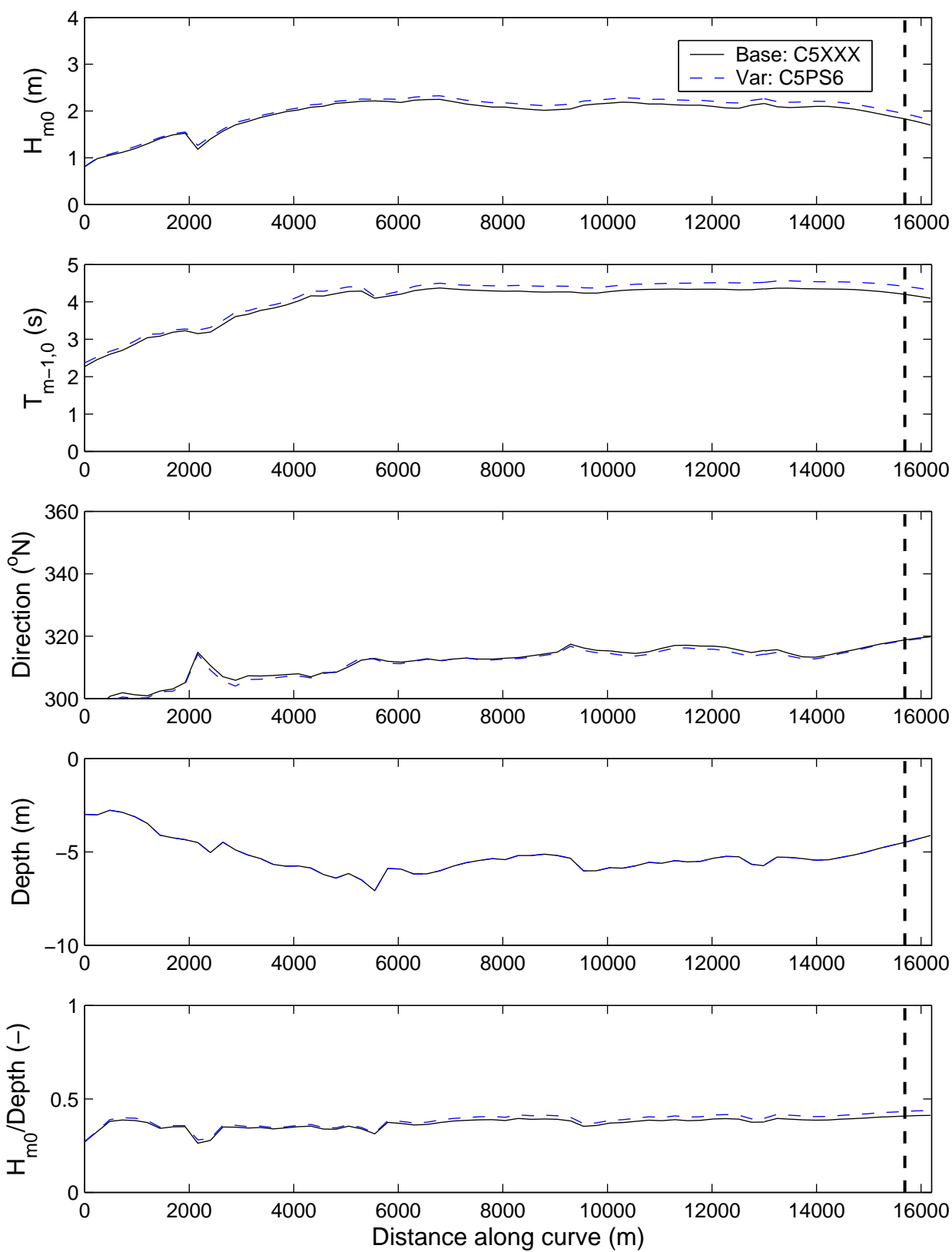
Sensitivity run C5PS6: Reduction in strength of depth-induced breaking
 Differences in mean direction (above) and directional spreading (below).

Sensitivity analysis Ameland



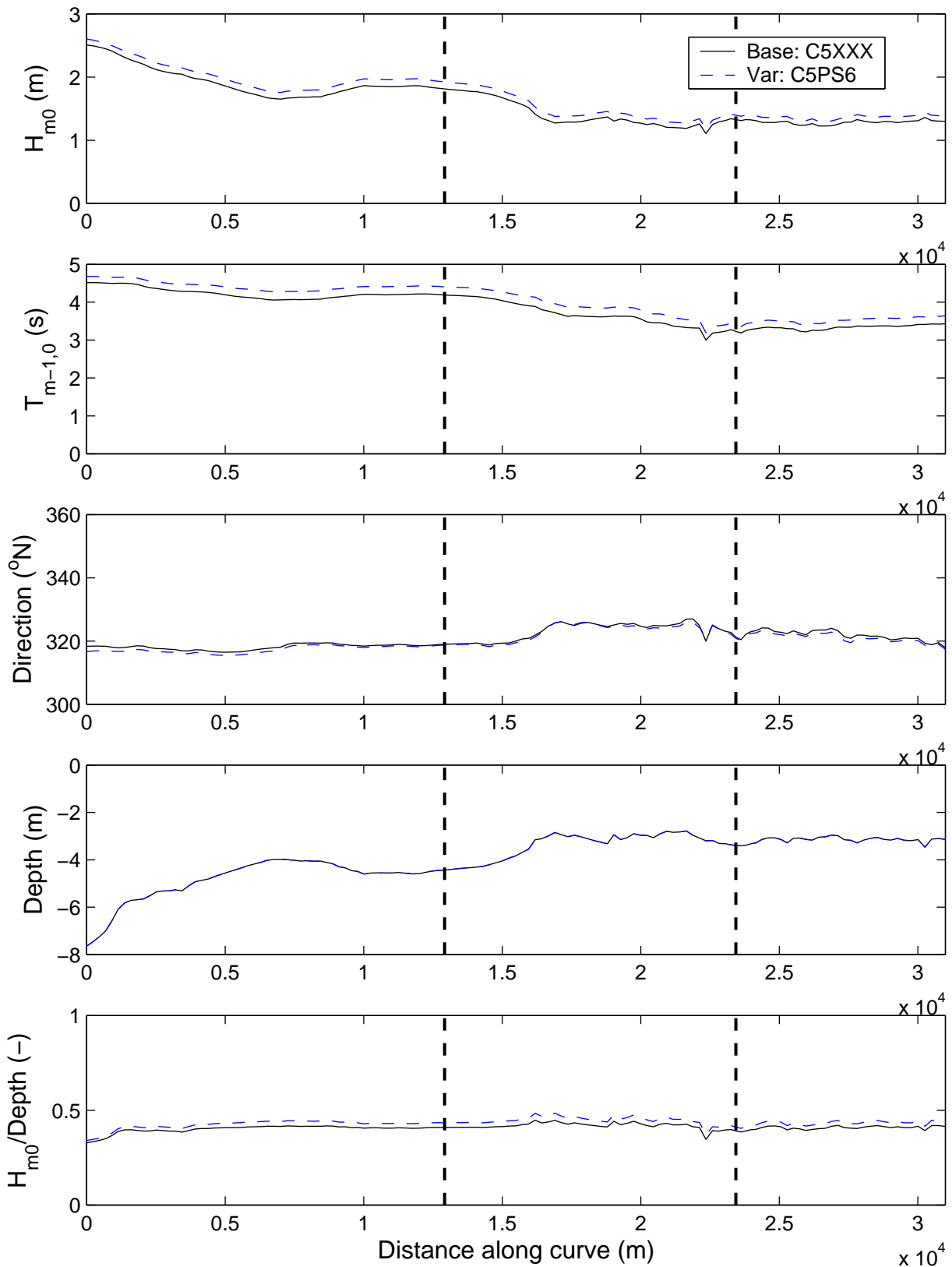
Sensitivity run C5PS6: Reduction in strength of depth-induced breaking
Integral parameters along Curve E

Sensitivity analysis Ameland



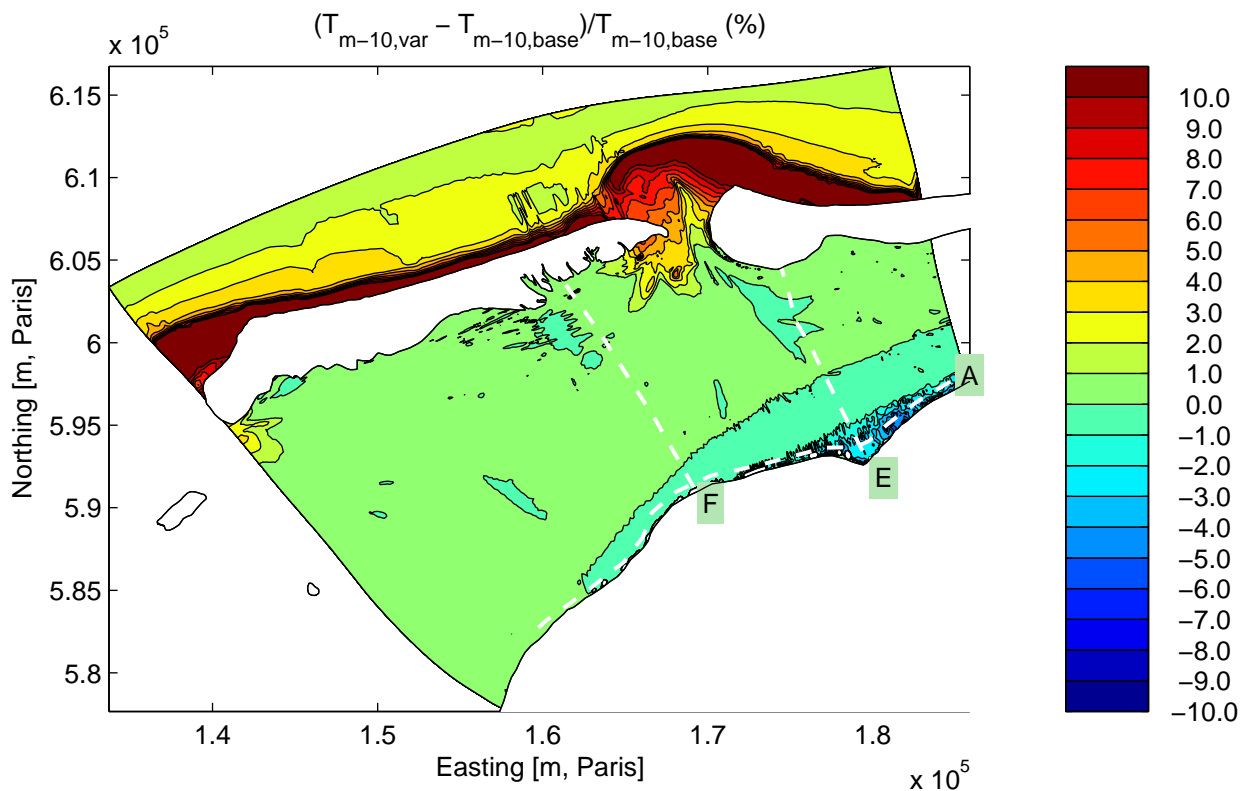
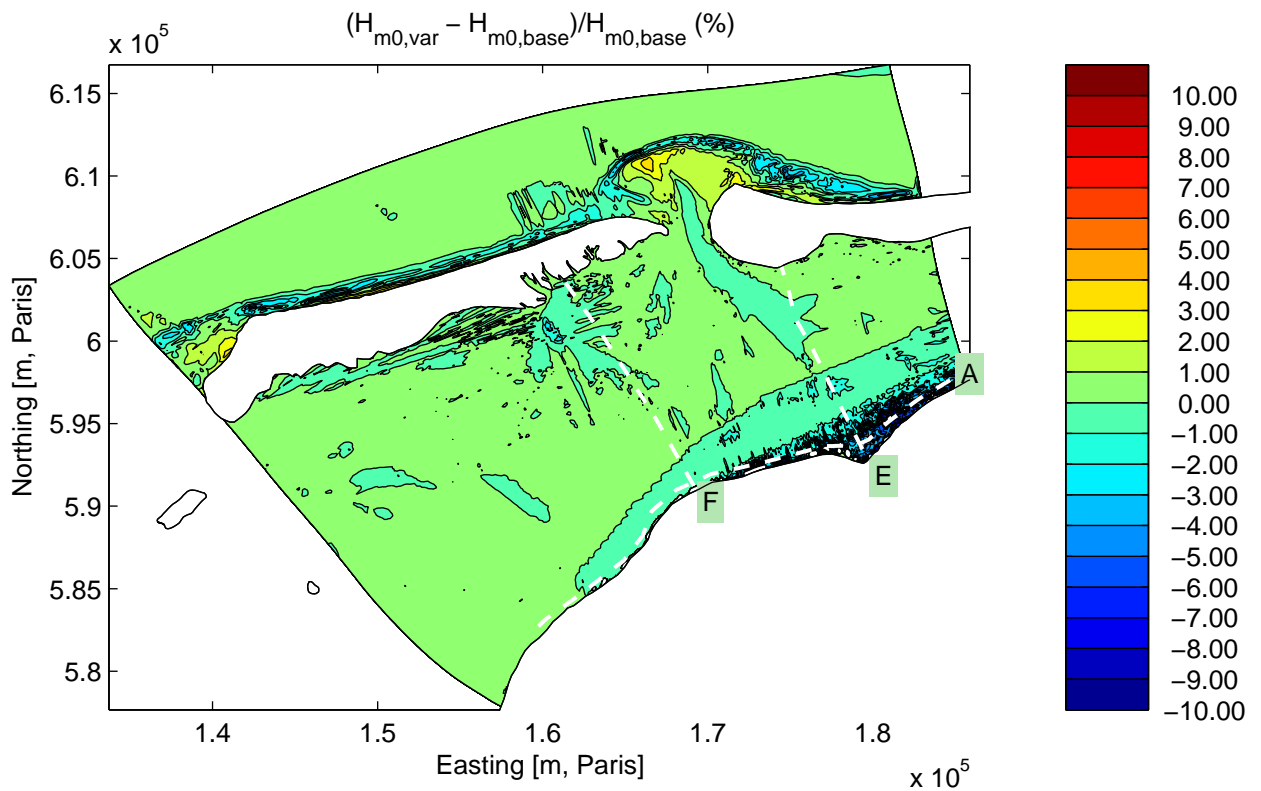
Sensitivity run C5PS6: Reduction in strength of depth-induced breaking
Integral parameters along Curve F

Sensitivity analysis Ameland



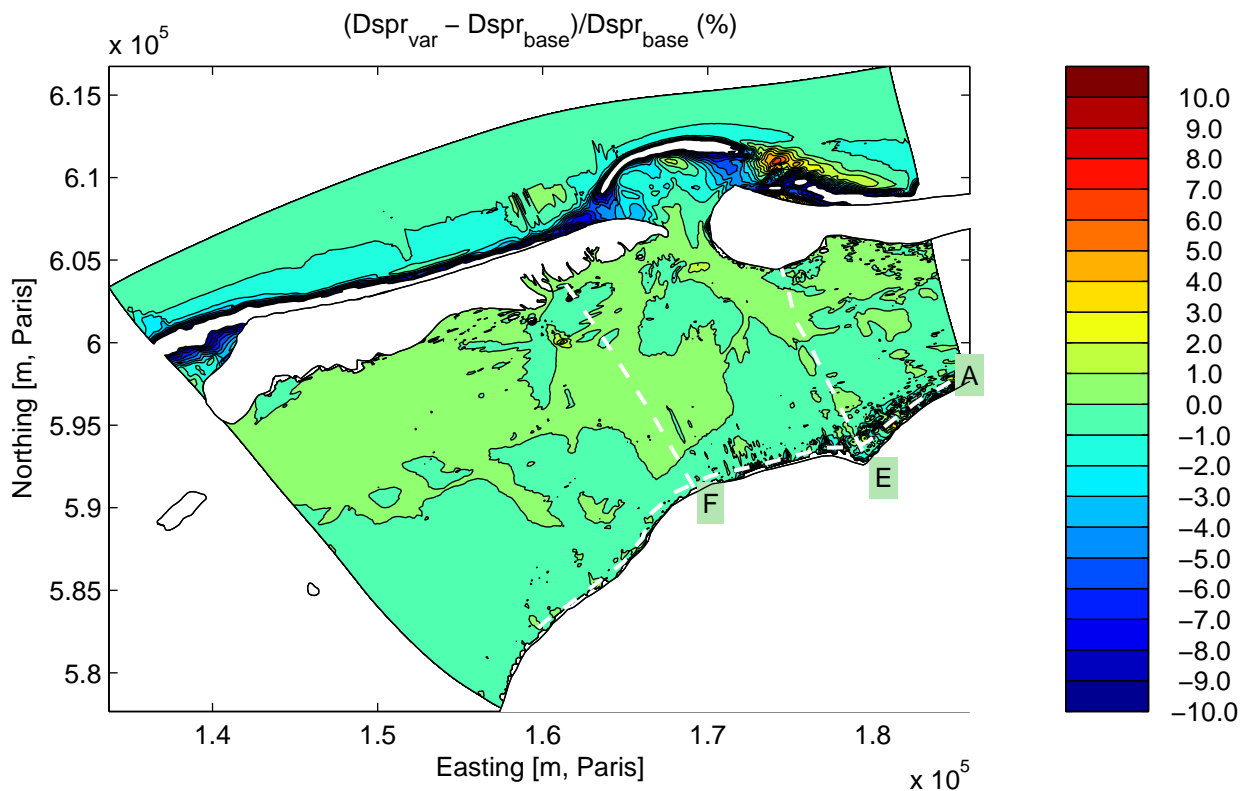
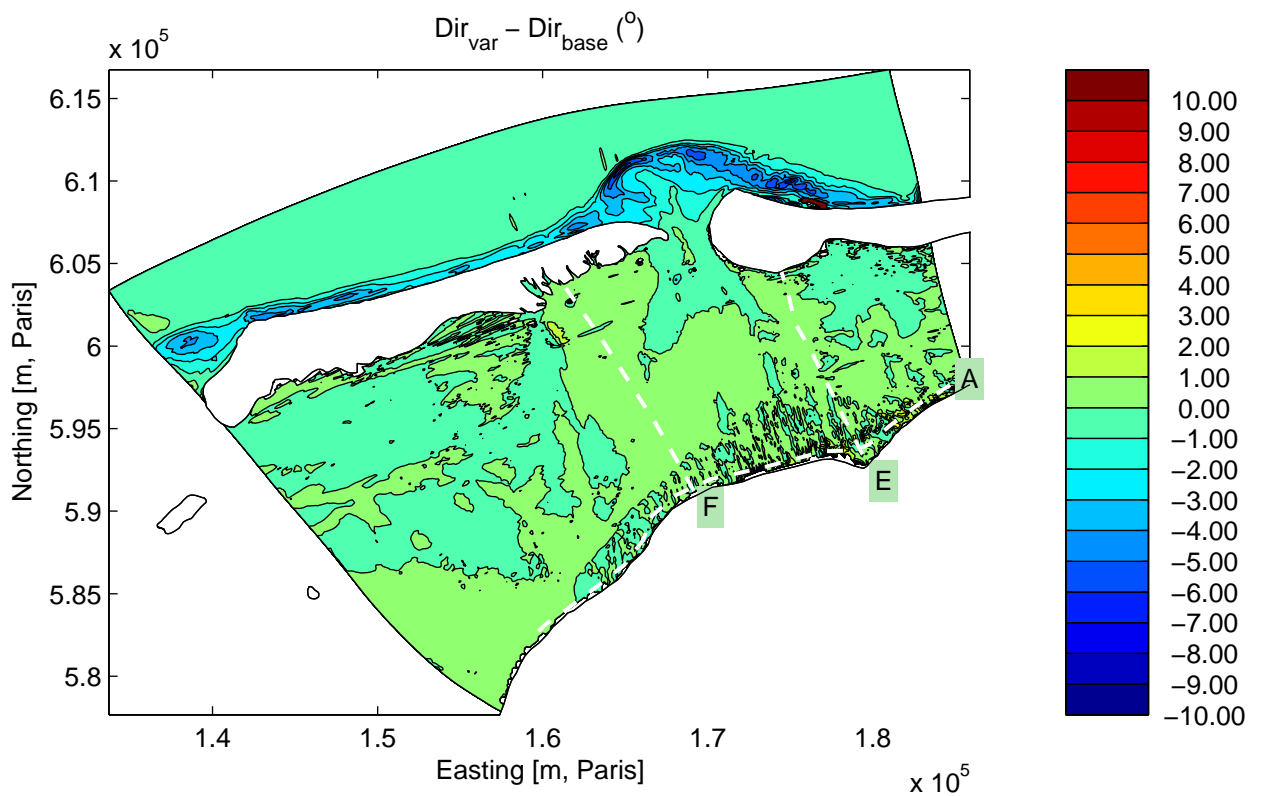
Sensitivity run C5PS6: Reduction in strength of depth-induced breaking
Integral parameters along Curve A

Sensitivity analysis Ameland



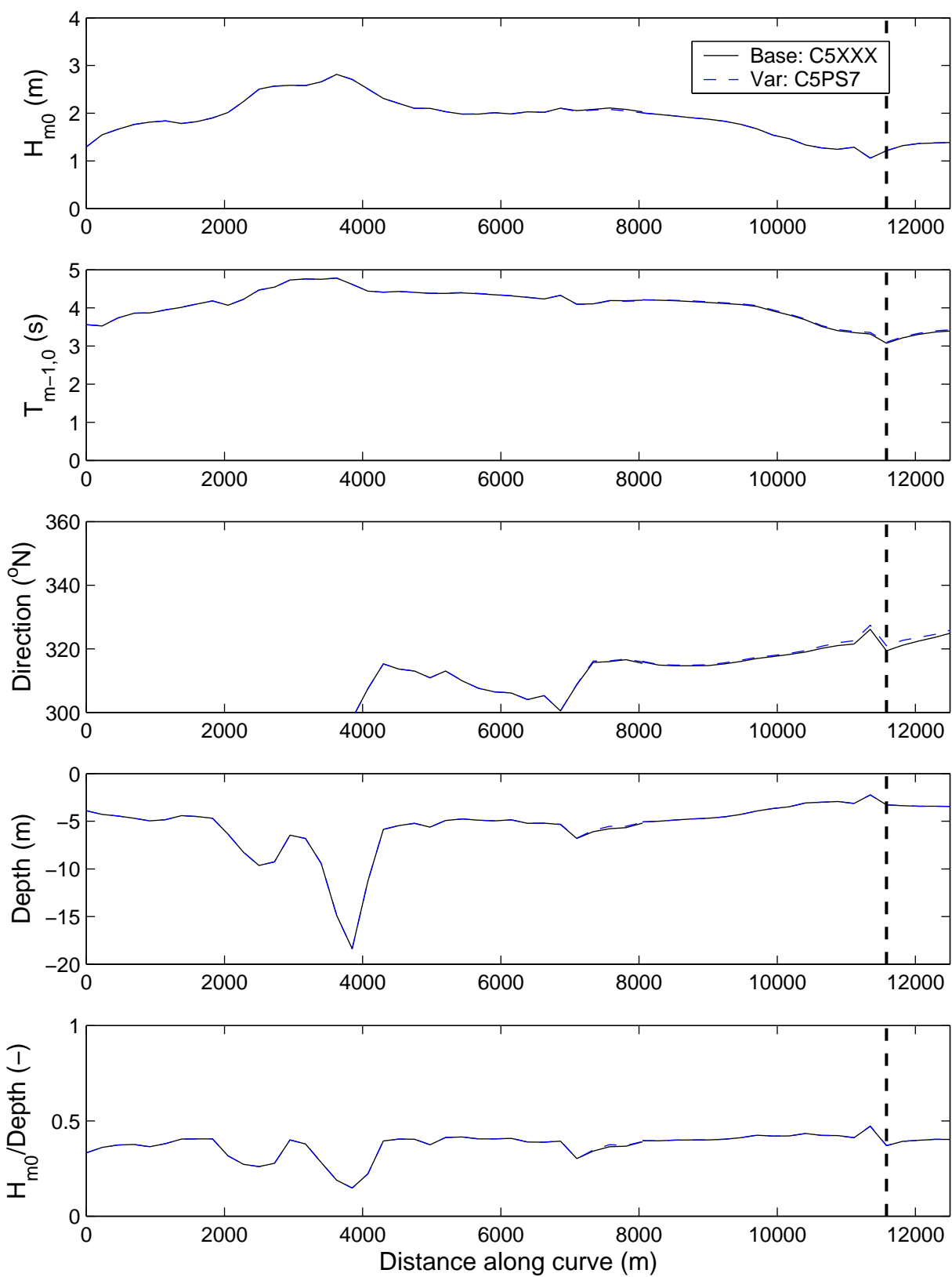
Sensitivity run C5PS7: Reduction in strength of triad interaction
Differences in significant wave height (above) and mean period (below).

Sensitivity analysis Ameland



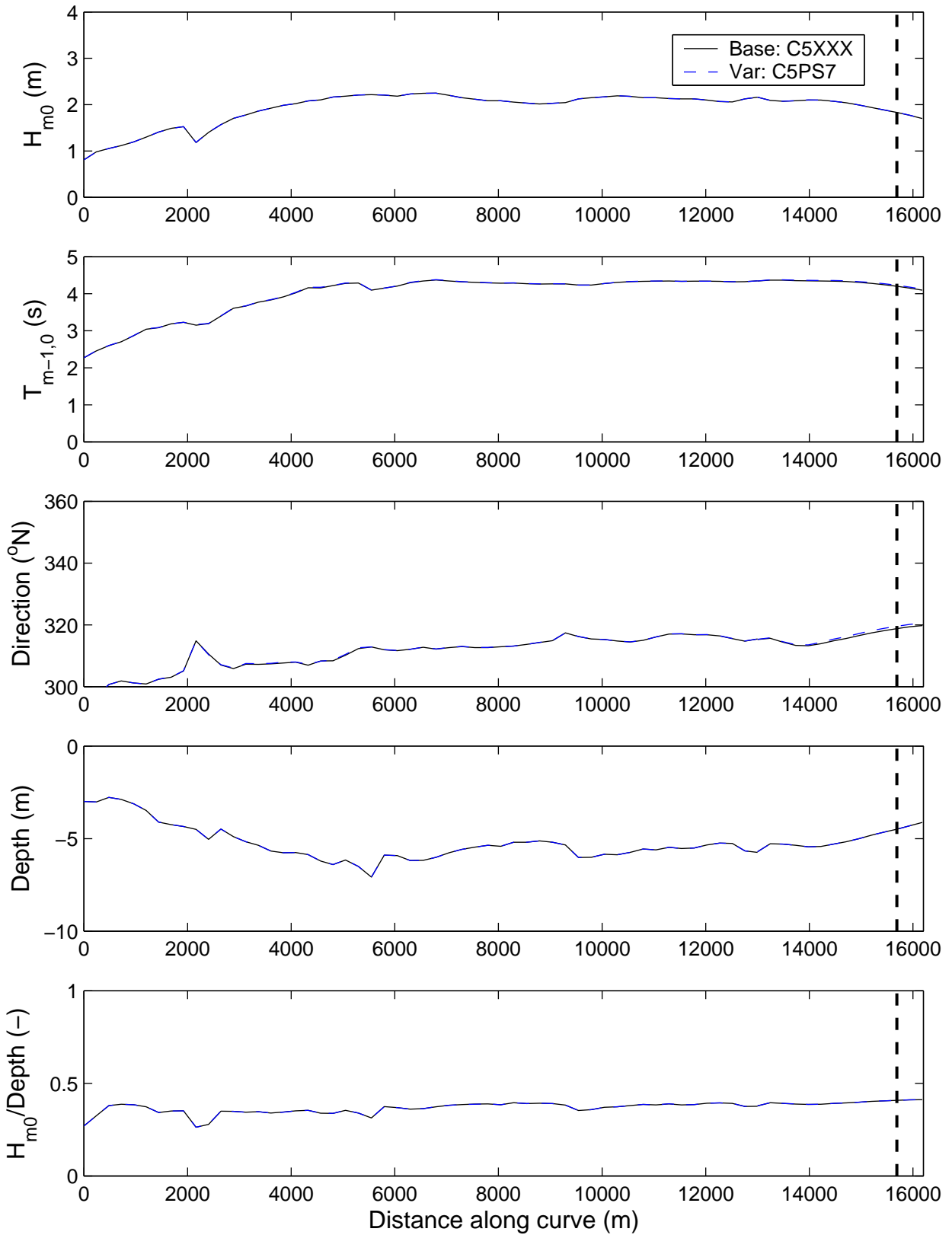
Sensitivity run C5PS7: Reduction in strength of triad interaction
Differences in mean direction (above) and directional spreading (below).

Sensitivity analysis Ameland



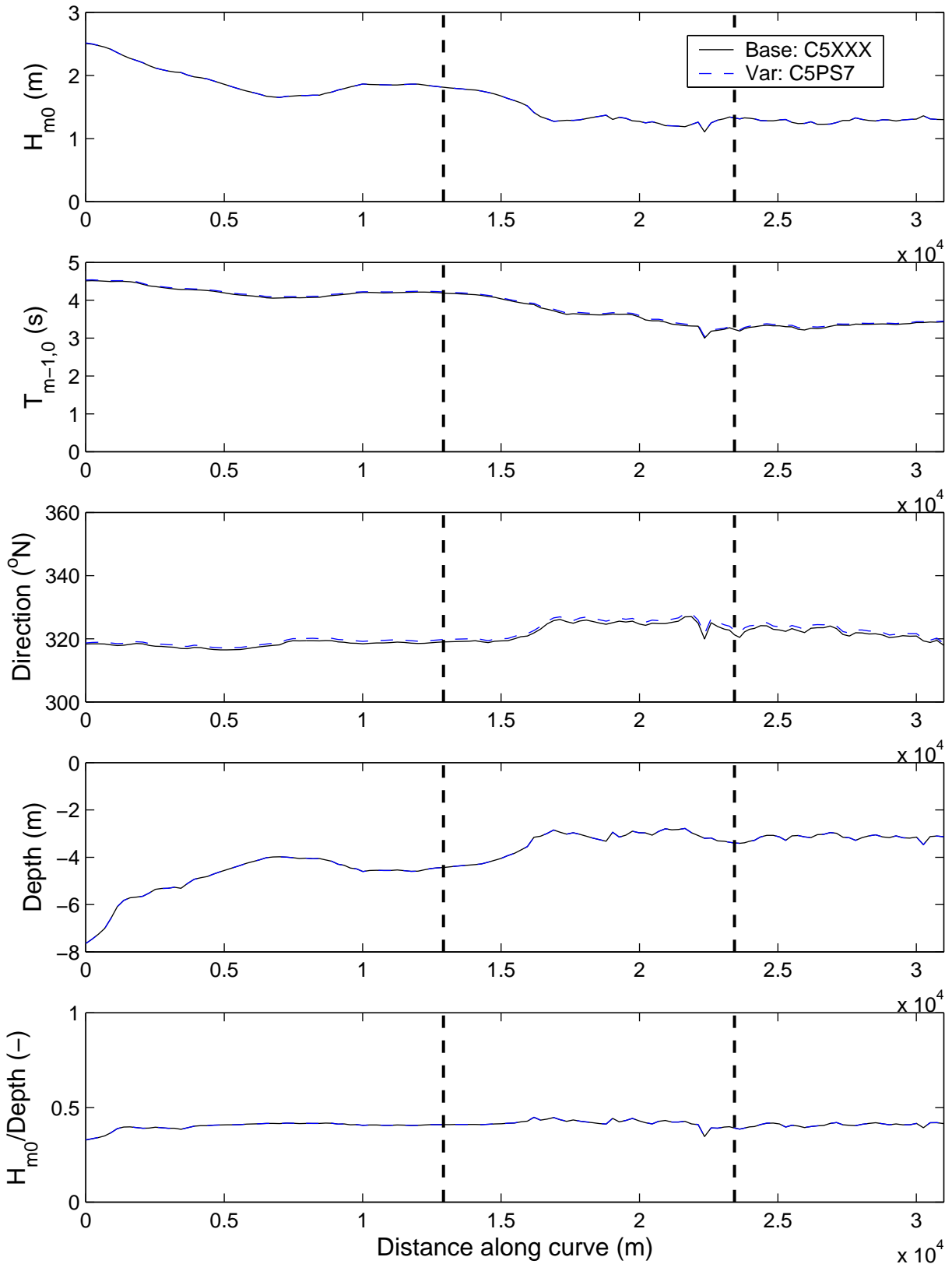
Sensitivity run C5PS7: Reduction in strength of triad interaction
Integral parameters along Curve E

Sensitivity analysis Ameland



Sensitivity run C5PS7: Reduction in strength of triad interaction
Integral parameters along Curve F

Sensitivity analysis Ameland



Sensitivity run C5PS7: Reduction in strength of triad interaction
Integral parameters along Curve A

Sensitivity analysis Ameland



WL | Delft Hydraulics

Rotterdamseweg 185
postbus 177
2600 MH Delft
telefoon 015 285 85 85
telefax 015 285 85 82
e-mail info@wldelft.nl
internet www.wldelft.nl

Rotterdamseweg 185
p.o. box 177
2600 MH Delft
The Netherlands
telephone +31 15 285 85 85
telefax +31 15 285 85 82
e-mail info@wldelft.nl
internet www.wldelft.nl

